ISTANBUL TECHNICAL UNIVERSITY ★ GRADUATE SCHOOL OF SCIENCE ENGINEERING AND TECHNOLOGY

NUMERICAL MODELLING OF STRATIFIED DAM RESERVOIRS AND LAKES

Ph.D. THESIS

Redvan GHASEMLOUNIA

Department of Civil Engineering

Hydraulic and Water Resources Engineering Programme

August 2016

ISTANBUL TECHNICAL UNIVERSITY ★ GRADUATE SCHOOL OF SCIENCE ENGINEERING AND TECHNOLOGY

NUMERICAL MODELLING OF STRATIFIED DAM RESERVOIRS AND LAKES

Ph.D. THESIS

Redvan GHASEMLOUNIA
(501092505)

Department of Civil Engineering

Hydraulic and Water Resources Engineering Programme

Thesis Advisor: Prof. Dr. M.Sedat KABDAŞLI

August 2016

İSTANBUL TEKNİK ÜNİVERSİTESİ ★ FEN BİLİMLERİ ENSTİTÜSÜ

TABAKALI HAZNELİ BARAJLAR VE GÖLLERİN NÜMERİK OLARAK ARAŞTIRILMASI

DOKTORA TEZİ

Redvan GHASEMLOUNIA
(501092505)

İnşaat Mühendisliği Anabilim Dalı

Hidrolik ve Su Kaynakları Mühendisliği Programı

Tez Danışmanı: Prof. Dr. M.Sedat KABDAŞLI

Ağustos 2016

Redvan GHASEMLOUNIA, a Ph.D. student of ITU Graduate School of Science Engineering and Technology student ID 501092505, successfully defended the thesis entitled " NUMERICAL MODELLING OF STRATIFIED DAM RESERVOIRS AND LAKES", which he prepared after fulfilling the requirements specified in the associated legislations, before the jury whose signatures are below.

Thesis Advisor :	**Prof. Dr. M.Sedat KABDAŞLI** Istanbul Technical University	.....
Jury Members :	**Prof. Dr. Bihrat Önöz** Istanbul Technical University	.....
	Prof. Dr. Emel İRTEM Balikesir University	.....
	Prof. Dr. Hafzullah AKSOY Istanbul Technical University	.....
	Assoc. Prof. Dr. Ahmet DOĞAN Yildiz Technical University	.....

Date of Submission : 27 July 2016
Date of Defense : 11 August 2016

To my family, spouse and Neshtiman

FOREWORD

First of all I would like to thank my advisor Prof.Dr.M.Sedat KABDASLI for his gentle nudging and support and supervising this thesis and making it possible for me to write this thesis and contributing with his expertise, as well as for giving me the freedom to pursue my interests.

I would like to acknowledge and thank the members of my thesis jury Prof.Dr.Bihrat ONOZ and Prof.Dr.Emel IRTEM. I am very thankful to have been able to get this great research environment, education and to freely unfold my interests and life without hurdles. Therefore and for their openness and support, I want to truly thank my parents Mina and Naser. Without their support and encouragement, I may never reach where I am today. Further, I would like to thank my father for his special contribution to this work, his great helpfulness and support with his deep knowledge and experiences as an civil engineer. Finally, I would like to thank my wife Elham for her great support, encouragement and patience for this thesis and for pushing me forward in times of stagnation. I want to dedicate this thesis to Neshtiman, my late sister, who will be in my heart forever.

August 2016

Redvan Ghasemlounia
(Civil Engineer)

TABLE OF CONTENTS

Page

FOREWORD ..... **ix**
TABLE OF CONTENTS ..... **xi**
ABBREVIATIONS ..... **xv**
LIST OF TABLES ..... **xvii**
LIST OF FIGURES ..... **xix**
SYMBOLS ..... **xxxix**
SUMMARY ..... **xxxiii**
ÖZET ..... **xxxv**
1. INTRODUCTION **1**
1.1 Thermal Stratification 3
1.2 Density Stratification (Caused by Concentration of Suspended Sediments) 4
1.3 Sediment Transport 5
1.3.1 Hyperpycnal Flow 7
1.3.2 Hypopycnal Flow 8
1.3.3 Homopycnal Flow 9
1.3.4 Mesopycnal 9
1.4 Purpose of Thesis 10
1.5 Literature Review 12
1.5.1 Sediment transport 12
1.5.2 Thermal stratification studies 13
1.5.3 Density stratification (Caused by Concentration of Sediments and Salinity) 15
2. PHYSICS OF FLUID DYNAMICS **17**
2.1 Governing Equations 17
2.1.1 Continuity Equation 18
2.1.2 Momentum Equation 21
2.1.3 Energy Equation 26
2.1.4 Suspended Sediment Transport Equation 27
2.1.5 Non-dimensional Navier-Stokes Equations 28
2.1.6 Reynolds Average Navier-Stokes Equations 29
2.2 Boussinesq Assumption 32
2.3 Fick's First and Second Laws of Diffusion 34
2.4 Types of Turbulence Models 36
2.4.1 Algebraic Models (Zero-Equation Models) 36
2.4.2 One-Equation Models 37
2.4.3 Two-Equation Models 37
2.4.4 Renormalizeds Group Models 38
2.4.5 Large Eddy Simulation Models (LES) 38

3. COMPUTATIONAL FLUID DYNAMICS (CFD), CE-qual-W2 and FLOW3D 41
3.1 Introduction of CE-qual-W2 42
3.2 Introduction of FLOW3D 43
3.3 Previous studies using FLOW 3D 45
3.4 Significant features of FLOW 3D (From FLOW3D Manual Book) 46
3.4.1 Volume of fluid (VOF) 46
3.4.2 Fractional area-volume obstacle representation 48
3.5 Coordinate systems used in FLOW3D 49
3.6 Governing equations used in FLOW 3D 50
3.6.1 Continuity equation 50
3.6.2 Momentum Equation 51
3.6.3 Fluid Energy Equation 54
3.6.4 Sediment Transport Equations 54
3.7 Turbulence Solution Models 62
3.8 Turbulence models used in FLOW 3D 62
3.8.1 Prandtl Mixing-Length Model 63
3.8.2 Turbulence Transport Models 64
4. NUMERICAL MODELING 67
4.1 Numerical Approximation 67
4.2 Description of Models and Sensivity of Simulations 71
4.3 Input Data 71
4.3.1 Fluid Type 72
4.3.2 Reservoir Dimensions 74
4.3.3 Seasons 74
4.3.4 Discharges 75
4.3.5 Temperature 75
4.3.6 Suspended Sediment Types and Concentrations 75
4.4 Geometry of Models 76
4.5 Meshes and Grids of Models 77
4.6 Boundary Conditions of Models 79
4.7 Selected Turbulence Models 80
4.8 Computational Modeling Scenarios 81
4.9 Results of Simulations 82
4.10 Results for Reservoir with Spillway outlet (S Type Simulations) 83
4.11 Results for Reservoir with Bottom outlet (B Type Simulations) 126
5. CASE STUDY: Lake Köyceğiz 169
5.1 Mugla Province 170
5.2 Lake Köyceğiz 173
5.3 Namnam River 196
5.4 Yuvarlak River 202
5.5 Kargıcak and Yangi River 203
5.6 Result of Simulations of Lake Köyceğiz 205
5.7 Thermal Stratification Modeling in Lake Köyceğiz using CE-qual-W2 260
5.8 Formation of Stratification in Lake Köyceğiz For Pre and Post dam Construction on Namnam River 268
5.8.1 Effect of Namnam Stream on Lake Stratification in Pre-dam Conditions 268
5.8.2 Effect of Namnam Stream on Lake Stratification in Post-dam Conditions 269

6. CONCLUSIONS 271
REFERENCES 277
APPENDICES 293
APPENDIX A 295
APPENDIX B 343
CURRICULUM VITAE 345

ABBREVIATIONS

AME : Absolute Mean Error
CFD : Computational Fluid Dynamics
DSI : Devlet Su İşleri (Governmental Water Affairs of Turkey)
FAVOR : Fractional Area Volume Obstacle Representation
ICOLD : International Commission on Large Dams
LES : Large Eddy Simulation Models
MSE : Mean Squared Error
RAE : Research Assessment Exercise
REM : Relative Error of the Mean
RMSE : Root Mean Square Error
RNG : Renormalizeds Group
SSC : Suspended Sediment Concentration
TSS : Total Suspended Solids
USGS : United States Geological Survey
VOF : Volume of Fluid
WSC : Wind-sheltering Coefficient

LIST OF TABLES

Page

Table 4.1 : Flag Values ($NF_{i,j,k}$) 70
Table 4.2 : Sediment Classification. 76
Table 4.3 : The Selected Dimensions for the Models 77
Table 4.4 : Grid Information of Each Mesh Block 79
Table 4.5 : Matrix of Simulations (Scenarios) of Reservoir Operating with Spillway 81
Table 4.6 : Matrix of Simulations (Scenarios) of Reservoir Operating with Bottom Outlet 82
Table 4.7 : Comparing Results for S3, S6, S9 and S12 97
Table 5.1 : Monthly Stream Flows for Köyceğiz Sub-basin (Mm^3/month)..... 174
Table 5.2 : Seasonally and Monthly Long-term precipitation for Köyceğiz 179
Table 5.3 : Long-term Evaporation for Köyceğiz (1981-2010)..... 180
Table 5.4 : Area-Volume-Depth Relation in Lake Köyceğiz 191
Table 5.5 : Measured Parameters of Namnam River at Connection Point with Lake Köyceğiz 199
Table 5.6 : Temperature Calibration Coefficients Values 261
Table 5.7 : Approximate Thickness of Thermal Layers in Lake Köyceğiz..... 265
Table 5.8 : REM and RAE Values for Temperature Modeled and Observed data. 267
Table 5.9 : MSE, RMSE and AME Criterias for Modeled and Observed Values of Thermal Stratification in Lake Köyceğiz 267

LIST OF FIGURES

Page

Figure 1.1 : Distribution of Water on the Earth 1
Figure 1.2 : Thermal Stratification and temperature changes through the depth in a)Spring, b)Summer, c) Autumn and d)Winter 4
Figure 1.3 : Sediment transport modes 6
Figure 1.4 : Behavior of river water meets reservoir/lake 7
Figure 1.5 : Hyperpycnal flows (waxing flow) 8
Figure 1.6 : Hyperpycnal flows (early waning flow) 8
Figure 1.7 : Hypopycnal flow in a reservoir/lake 8
Figure 1.8 : Homopycnal flows in a reservoir/lake 9
Figure 1.9 : Mesopycnal flow in reservoir/lake 9
Figure 2.1 : Selected infinitesimal fixed control volume 18
Figure 2.2 : Selected infinitesimal fixed control volume 21
Figure 2.3 : Stresses on the surface of the differential control volume in the x direction 22
Figure 2.4 : Turbulent velocity fluctuation and mean values. 30
Figure 2.5 : Diffusion of fluid's mulecules. 34
Figure 2.6 : Example of changes of concentration through time and x according to fick's second law. 36
Figure 3.1 : Values of funcion F in volume of fluid method (FLOW3D user manual). 47
Figure 3.2 : FAVOR Method (Flow 3D user manual, 2008). 49
Figure 3.3 : Cartesian and cylindrical coordinates. 49
Figure 4.1 : Mesh elements. 67
Figure 4.2 : Mesh arrangement and labeling convention. 68
Figure 4.3 : Location of variables in a mesh cell. 68
Figure 4.4 : Density-Temperature relation of water. 73
Figure 4.5 : Dynamic (μ) /Kinematik (υ) viscosity of water with temperature changes. 73
Figure 4.6 : Thermal conductivity-Temperature relation of water. 74
Figure 4.7 : Mesh structure of models. 78
Figure 4.8 : Number and position of blocks in all models 78
Figure 4.9 : Body of dam, reservoir, outlets and boundary conditions 80
Figure 4.10 : Temperature and SSC Contours of Simulation S1 84
Figure 4.11 : Temperature and SSC Contours of Simulation S2 85
Figure 4.12 : Temperature and SSC Contours of Simulation S3 86
Figure 4.13 : Structure of Turbidity Current Formed in Simulations 87
Figure 4.14 : Temperature and SSC Contours of Simulation S4 88
Figure 4.15 : Temperature and SSC Contours of Simulation S5 89
Figure 4.16 : Temperature and SSC Contours of Simulation S6 90
Figure 4.17 : SSC Contours of Simulations S7, S8 and S9 92

Figure 4.18 : Temperature and SSC Contours of Simulation S10 93
Figure 4.19 : Temperature and SSC Contours of Simulation S11 94
Figure 4.20 : Temperature and SSC Contours of Simulation S12 95
Figure 4.21 : Structure of Turbidty Flow 96
Figure 4.22 : Plunge points of Simulations S3, S6, S9 and S12 96
Figure 4.23 : Location of the Circulation Flow 97
Figure 4.24 : Velocity Vectors Colored by 2D Velocity Magnitude for S3 98
Figure 4.25 : Velocity Vectors Colored by 2D Velocity Magnitude for S6 98
Figure 4.26 : Velocity Vectors Colored by 2D Velocity Magnitude for S9 99
Figure 4.27 : Velocity Vectors Colored by 2D Velocity Magnitude for S12 99
Figure 4.28 : Circulation and the Reverse Current of the simulations S1 to S12 ... 100
Figure 4.29 : B/W contours of temperature and concentration (S3) 100
Figure 4.30 : B/W contours of temperature and concentration (S6) 101
Figure 4.31 : B/W contours of temperature and concentration (S9) 101
Figure 4.32 : B/W contours of temperature and concentration (S12) 101
Figure 4.33 : Inter and under flow condition (Velocity vectors) 102
Figure 4.34 : Velocity vectors and flow direction when spillway starts to operate 102
Figure 4.35 : Selected sections for comparing results 102
Figure 4.36 : Temperature variations during time in section 1 (S1-S12) 103
Figure 4.37 : SSC variations during time in section 1 (S1-S12) 103
Figure 4.38 : Temperature variations during time in section 2 (S1-S12) 104
Figure 4.39 : SSC variations during time in section 2 (S1-S12) 104
Figure 4.40 : Temperature and SSC Contours of Simulation S13 106
Figure 4.41 : Temperature and SSC Contours of Simulation S14 107
Figure 4.42 : Temperature and SSC Contours of Simulation S15 108
Figure 4.43 : Temperature and SSC Contours of Simulation S16 110
Figure 4.44 : Temperature and SSC Contours of Simulation S17 111
Figure 4.45 : Temperature and SSC Contours of Simulation S18 112
Figure 4.46 : SSC Contours of Simulation S19, S20 and S21 113
Figure 4.47 : Temperature and SSC Contours of Simulation S22 115
Figure 4.48 : Temperature and SSC Contours of Simulation S23 116
Figure 4.49 : Temperature and SSC Contours of Simulation S24 117
Figure 4.50 : Thickness of the upper layer of SSC at bed slope change area 118
Figure 4.51 : Velocity Vectors and flow directions of simulations S13 to S18 118
Figure 4.52 : Velocity Vectors and flow directions of simulations S19 to S24 118
Figure 4.53 : B/W contours of temperature and concentration (S15) 119
Figure 4.54 : B/W contours of temperature and concentration (S18) 119
Figure 4.55 : B/W contours of temperature and concentration (S21) 120
Figure 4.56 : B/W contours of temperature and concentration (S24) 120
Figure 4.57 : Temperature variations during time in section 1 (S13-S24) 121
Figure 4.58 : SSC variations during time in section 1 (S13-S24) 121
Figure 4.59 : Temperature variations during time in section 2 (S13-S24) 122
Figure 4.60 : SSC variations during time in section 2 (S13-S24) 122
Figure 4.61 : Velocity Vectors Colored by 2D Velocity Magnitude for S15 123
Figure 4.62 : Velocity Vectors Colored by 2D Velocity Magnitude for S18 123
Figure 4.63 : Velocity Vectors Colored by 2D Velocity Magnitude for S21 124
Figure 4.64 : Velocity Vectors Colored by 2D Velocity Magnitude for S24 124
Figure 4.65 : Temperature and SSC Contours of Simulation B1 127
Figure 4.66 : Temperature and SSC Contours of Simulation B2 128
Figure 4.67 : Temperature and SSC Contours of Simulation B3 129

Figure 4.68 : Temperature and SSC Contours of Simulation B4 131
Figure 4.69 : Temperature and SSC Contours of Simulation B5 132
Figure 4.70 : Temperature and SSC Contours of Simulation B6 133
Figure 4.71 : SSC Contours of Simulation B7, B8 and B9 134
Figure 4.72 : Temperature and SSC Contours of Simulation B10 136
Figure 4.73 : Temperature and SSC Contours of Simulation B11 137
Figure 4.74 : Temperature and SSC Contours of Simulation B12 138
Figure 4.75 : B/W contours of temperature and concentration (B3) 140
Figure 4.76 : B/W contours of temperature and concentration (B6) 140
Figure 4.77 : B/W contours of temperature and concentration (B9) 140
Figure 4.78 : B/W contours of temperature and concentration (B12) 141
Figure 4.79 : Temperature variations during time in section 1 (B1-B12) 142
Figure 4.80 : SSC variations during time in section 1 (B1-B12)..... 142
Figure 4.81 : Temperature variations during time in section 2 (B1-B12) 143
Figure 4.82 : SSC variations during time in section 2 (B1-B12)..... 143
Figure 4.83 : Velocity Vectors Colored by 2D Velocity Magnitude for B3..... 144
Figure 4.84 : Velocity Vectors Colored by 2D Velocity Magnitude for B6..... 144
Figure 4.85 : Velocity Vectors Colored by 2D Velocity Magnitude for B9..... 145
Figure 4.86 : Velocity Vectors Colored by 2D Velocity Magnitude for B12..... 145
Figure 4.87 : Velocity Vectors and direction of the flow (B1 to B12) 146
Figure 4.88 : Reverse and circulation current, which occurred in first 12 simulations of reservoir with bottom outlet (B models)..... 146
Figure 4.89 : Wall jet current..... 147
Figure 4.90 : Temperature and SSC Contours of Simulation B13 148
Figure 4.91 : Temperature and SSC Contours of Simulation B14 149
Figure 4.92 : Temperature and SSC Contours of Simulation B15 150
Figure 4.93 : Temperature and SSC Contours of Simulation B16 152
Figure 4.94 : Temperature and SSC Contours of Simulation B17 153
Figure 4.95 : Temperature and SSC Contours of Simulation B18 154
Figure 4.96 : SSC Contours of Simulation B19, B20 and B21 155
Figure 4.97 : Changes in thickness of SSC layers with temperature after 3000s for simulations B15, B18 and B21 155
Figure 4.98 : Temperature and SSC Contours of Simulation B22 157
Figure 4.99 : Temperature and SSC Contours of Simulation B23 158
Figure 4.100 : Temperature and SSC Contours of Simulation B24 159
Figure 4.101 : B/W contours of temperature and concentration (B15) 160
Figure 4.102 : B/W contours of temperature and concentration (B18) 160
Figure 4.103 : B/W contours of temperature and concentration (B21) 161
Figure 4.104 : B/W contours of temperature and concentration (B24) 161
Figure 4.105 : Temperature variations during time in section 1 (B13-B24) 162
Figure 4.106 : SSC variations during time in section 1 (B13-B24)..... 162
Figure 4.107 : Temperature variations during time in section 2 (B13-B24) 163
Figure 4.108 : SSC variations during time in section 2 (B13-B24)..... 163
Figure 4.109 : Velocity Vectors Colored by 2D Velocity Magnitude for B15..... 165
Figure 4.110 : Velocity Vectors Colored by 2D Velocity Magnitude for B18..... 165
Figure 4.111 : Velocity Vectors Colored by 2D Velocity Magnitude for B21..... 166
Figure 4.112 : Velocity Vectors Colored by 2D Velocity Magnitude for B24..... 166
Figure 4.113 : Changes in thickness of stratification layers for suspended sediment concentration..... 167

Figure 4.114 : Changes in thickness of stratification layers for suspended sediment concentration 168
Figure 5.1: Basin Map of Turkey 169
Figure 5.2: Selected Area 169
Figure 5.3: Köyceğiz -Dalyan Sub-Basin 170
Figure 5.4: Elevation of Köyceğiz Watershed Region 170
Figure 5.5: Average Values of Temperature, Max temperature, Min Temperature, Sunshine hours and Number of Days with Precipitation (T.C. forestry and water affairs minister) 171
Figure 5.6: Total Amount of Monthly Precipitation for Years 1950 to 2014. 171
Figure 5.7: The Annual Precipitation (mm) (T.C. forestry and water affairs minister) 172
Figure 5.8: Highest and the Lowest Values of Temperature for the Months of the Years Beetween 1950 and 2014 172
Figure 5.9: Location of the Lake Köyceğiz 173
Figure 5.10: Position of Dalyan Canal 174
Figure 5.11: Monthly Stream flows for Köyceğiz Sub-basin (Mm^3/month) 175
Figure 5.12: Total Yearly Stream Flows of the Köyceğiz Sub-basin 175
Figure 5.13: Percentage of Distribution of Average Monthly Stream Flows in Köyceğiz Watershed 176
Figure 5.14: Weather Temperature of Köyceğiz Meteorological Station 176
Figure 5.15: The Average Number of Days With Precipitation and Snow 177
Figure 5.16: The Monthly and the Annual Average Precipitations 177
Figure 5.17: Annualy Total Precipitation 178
Figure 5.18: Long Term Monthly Precipitation Averages (mm) of Köyceğiz Meteorological Station (1975- 2013) 178
Figure 5.19: Long Term Amount of Monthly Total Evaporation (mm), Average Temperature (^oC) and Average Relative Humidity (%) 179
Figure 5.20: Monthly ETo Maps for Köyceğiz Area 181
Figure 5.21: Monthly Average Wind Velocities (m/s) 182
Figure 5.22: Monthly Number of Winds from Different Directions 183
Figure 5.23: An Approximate Number and Directions of the Winds in a Year 184
Figure 5.24: The Number and Direction of Winds by Season 184
Figure 5.25: Average Monthly Velocity of Wind (m/s) 185
Figure 5.26: A schematic map for the study area (Lake Köyceğiz) 186
Figure 5.27: The Schematic Longitudinal Section View of the Lake 187
Figure 5.28: Cross-sections of Köyceğiz and Sultaniye Parts of the Lake 187
Figure 5.29: The Bathymetric Map of Lake Köyceğiz 188
Figure 5.30: The Drawn Point Map 188
Figure 5.31: Bathymetric Map of Lake Köyceğiz From Surfer8 189
Figure 5.32: Wireframe and Vector Map of Lake Köyceğiz 189
Figure 5.33: Bathymetric Map of Lake Köyceğiz From Surfer8 190
Figure 5.34: The Three Dimensional Surface of Bathymetry of the Lake Köyceğiz 190
Figure 5.35: The Area-Depth Relation of the Lake Köyceğiz (Maktav-1998) 192
Figure 5.36: The Volume-Depth Relation of the Lake Köyceğiz (Maktav-1998) 192
Figure 5.37: Thermal Stratification of Lake Köyceğiz (Kazanci 1992) 193
Figure 5.38: Measured Salinity and Calculated Densities of Each Part of the lake 194
Figure 5.39: Position of Namnam River 196
Figure 5.40: The Daily Discharges for the Time Period of 1990 to 1999 196

Figure 5.41: The average monthly discharges for the 1990-1999 197
Figure 5.42: Total annual discharges of this river (Mm^3)..... 197
Figure 5.43: The Long Term Average Monthly Discharges (m^3/s) and the Monthly Precipitation (mm) of Namnam River (1990-1999) 198
Figure 5.44: The Long Term Average Monthly Discharges for Namnam River By Adding the Years 1981 To 1986 (DSI) 198
Figure 5.45: The Measured Average Monthly Temperatures..... 199
Figure 5.46: The Measured Salinity of Namnam River..... 200
Figure 5.47: The Measured TSS (mg/l) 200
Figure 5.48: Erosion Situation of Study Area (Anonym, 2007a) 201
Figure 5.49: Location of Yuvarlak River..... 202
Figure 5.50: The Long-term Average Discharges of Yuvarlak River 202
Figure 5.51: Average monthly temperatures of Yuvarlak River (1991-1993) 203
Figure 5.52: The Long-term Monthly Average Discharges of Kargicak River (DSI) 203
Figure 5.53: Average monthly temperatures of Kargicak River (1991-1993)..... 204
Figure 5.54: The FLOW 3D Output Bathymetric Map for Lake Köyceğiz 205
Figure 5.55: The velocity vectors colored by 2D velocity magnitude for z=0 m after 2 days (November)..... 206
Figure 5.56: The velocity vectors colored by 2D velocity magnitude after 2 days (November)..... 207
Figure 5.57: The velocity vectors colored by 2D velocity magnitude for z=0 m after 7 days (November)..... 208
Figure 5.58: The velocity vectors colored by 2D velocity magnitude after 7 days (November)..... 209
Figure 5.59: The velocity vectors colored by 2D velocity magnitude for z=0 m after 14 days (November)..... 210
Figure 5.60: The velocity vectors colored by 2D velocity magnitude after 14 days (November)..... 211
Figure 5.61: The velocity vectors colored by 2D velocity magnitude for z=0 m after 18 days (November)..... 212
Figure 5.62: The velocity vectors colored by 2D velocity magnitude after 18 days (November)..... 213
Figure 5.63: The temperature contours at surface of Lake Köyceğiz after 2 days (November)..... 214
Figure 5.64: The temperature contours at surface of Lake Köyceğiz after 7 days (November)..... 215
Figure 5.65: The temperature contours at surface of Lake Köyceğiz after 14 days (November)..... 216
Figure 5.66: The temperature contour at surface of Lake Köyceğiz after 18 days (November)..... 217
Figure 5.67: The Salinity color shaded contours of Lake Köyceğiz after 2 days (November)..... 218
Figure 5.68: The Salinity color shaded contours of Lake Köyceğiz after 7 days (November)..... 219
Figure 5.69: The Salinity color shaded contours of Lake Köyceğiz after 14 days (November)..... 220
Figure 5.70: The Salinity color shaded contours of Lake Köyceğiz after 18 days (November)..... 221

Figure 5.71: The velocity vectors colored by 2D velocity magnitude for z=0 m after 2 days (December) 222
Figure 5.72: The velocity vectors colored by 2D velocity magnitude after 2 days (December) 223
Figure 5.73: The velocity vectors colored by 2D velocity magnitude for z=0 m after 7 days (December) 224
Figure 5.74: The velocity vectors colored by 2D velocity magnitude after 7 days (December) 225
Figure 5.75: The velocity vectors colored by 2D velocity magnitude for z=0 m after 14 days (December) 226
Figure 5.76: The velocity vectors colored by 2D velocity magnitude after 14 days (December) 227
Figure 5.77: The velocity vectors colored by 2D velocity magnitude for z=0 m after 18 days (December) 228
Figure 5.78: The velocity vectors colored by 2D velocity magnitude after 18 days (December) 229
Figure 5.79: The temperature contours at surface of Lake Köyceğiz after 2 days (December) 230
Figure 5.80: The temperature contours at surface of Lake Köyceğiz after 7 days (December) 231
Figure 5.81: The temperature contours at surface of Lake Köyceğiz after 14 days (December) 232
Figure 5.82: The temperature contours at surface of Lake Köyceğiz after 18 days (December) 233
Figure 5.83: Y-Z cross-sections of Lake Köyceğiz for thermal stratification changes after 18 days (December) 234
Figure 5.84: X-Z cross-sections of Köyceğiz part for thermal stratification changes after 18 days (December) 234
Figure 5.85: X-Z cross-sections of Sultaniye part for thermal stratification changes after 18 days (December) 234
Figure 5.86: The Salinity color shaded contours of Lake Köyceğiz after 2 days (December) 235
Figure 5.87: The Salinity color shaded contours of Lake Köyceğiz after 7 days (December) 236
Figure 5.88: The Salinity color shaded contours of Lake Köyceğiz after 14 days (December) 237
Figure 5.89: The Salinity color shaded contours of Lake Köyceğiz after 18 days (December) 238
Figure 5.90: Y-Z section of Lake Köyceğiz for salinity (%0) after 18 days (December) 239
Figure 5.91: The velocity vectors colored by 2D velocity magnitude for z=0 m after 2 days (August) 239
Figure 5.92: The velocity vectors colored by 2D velocity magnitude after 2 days (August) 240
Figure 5.93: The velocity vectors colored by 2D velocity magnitude for z=0 m after 7 days (August) 241
Figure 5.94: The velocity vectors colored by 2D velocity magnitude after 7 days (August) 242
Figure 5.95: The velocity vectors colored by 2D velocity magnitude for z=0 m after 14 days (August) 243

Figure 5.96: The velocity vectors colored by 2D velocity magnitude after 14 days (August) 244
Figure 5.97: The velocity vectors colored by 2D velocity magnitude for z=0 m after 18 days (August) 245
Figure 5.98: The velocity vectors colored by 2D velocity magnitude after 18 days (August) 246
Figure 5.99: The temperature contours at surface of Lake Köyceğiz after 2 days (August) 247
Figure 5.100: The temperature contours at surface of Lake Köyceğiz after 7 days (August) 248
Figure 5.101: The temperature contours at surface of Lake Köyceğiz after 14 days (August) 249
Figure 5.102: The temperature contours at surface of Lake Köyceğiz after 18 days (August) 250
Figure 5.103: The temperature contours of Köyceğiz and Sultaniye parts of Lake after 18 days (August) 251
Figure 5.104: The Salinity color shaded contours of Lake Köyceğiz after 2 days (August) 252
Figure 5.105: The Salinity color shaded contours of Lake Köyceğiz after 7 days (August) 253
Figure 5.106: The Salinity color shaded contours of Lake Köyceğiz after 14 days (August) 254
Figure 5.107: The Salinity color shaded contours of Lake Köyceğiz after 18 days (August) 255
Figure 5.108: The suspended sediment distribution at Lake Köyceğiz after an unexpected event (Flood from Namnam) 257
Figure 5.109: The suspended sediment distribution at Lake Köyceğiz after an unexpected event (Flood from Kargicak) 258
Figure 5.110: The suspended sediment distribution at Lake Köyceğiz after an unexpected event (Flood from Kargicak and Namnam)..... 259
Figure 5.111: The segmentation of the CE-qual-W2 model..... 261
Figure 5.112: CE-qual-W2 results compared with observed data (Köyceğiz part) 262
Figure 5.113: CE-qual-W2 results compared with observed data (Sultaniye part) 262
Figure 5.114: The comparition of lake surface modeled and observed temperatures 263
Figure 5.115: Output result of CE-qual-W2 model for thetmal stratification in Lake Köyceğiz..... 264
Figure 5.116: Thermal layers of Lake Köyceğiz 265
Figure A1: Simulation S1: a) time-step size, b) cumulative volume error (%), c) volume of fluid, d) fluid surface area, e) estimated mean kinetic energy, f) average turbulent kinetic energy, g) total fluid mass, h) total fluid energy.....295
Figure A2: Simulation S2: a) time-step size, b) cumulative volume error (%), c) volume of fluid, d) fluid surface area, e) estimated mean kinetic energy, f) average turbulent kinetic energy, g) total fluid mass, h) total fluid energy.....296
Figure A3: Simulation S3: a) time-step size, b) cumulative volume error (%), c) volume of fluid, d) fluid surface area, e) estimated mean kinetic energy, f) average turbulent kinetic energy, g) total fluid mass, h) total fluid energy.....297

Figure A4: Simulation S4: a) time-step size, b) cumulative volume error (%), c) volume of fluid, d) fluid surface area, e) estimated mean kinetic energy, f) average turbulent kinetic energy, g) total fluid mass, h) total fluid energy.....298
Figure A5: Simulation S5: a) time-step size, b) cumulative volume error (%), c) volume of fluid, d) fluid surface area, e) estimated mean kinetic energy, f) average turbulent kinetic energy, g) total fluid mass, h) total fluid energy.....299
Figure A6: Simulation S1: a) time-step size, b) cumulative volume error (%), c) volume of fluid, d) fluid surface area, e) estimated mean kinetic energy, f) average turbulent kinetic energy, g) total fluid mass, h) total fluid energy.....300
Figure A7: Simulation S7: a) time-step size, b) cumulative volume error (%), c) volume of fluid, d) fluid surface area, e) estimated mean kinetic energy, f) average turbulent kinetic energy, g) total fluid mass, h) total fluid energy.....301
Figure A8: Simulation S8: a) time-step size, b) cumulative volume error (%), c) volume of fluid, d) fluid surface area, e) estimated mean kinetic energy, f) average turbulent kinetic energy, g) total fluid mass, h) total fluid energy.....302
Figure A9: Simulation S9: a) time-step size, b) cumulative volume error (%), c) volume of fluid, d) fluid surface area, e) estimated mean kinetic energy, f) average turbulent kinetic energy, g) total fluid mass, h) total fluid energy.....303
Figure A10: Simulation S10: a) time-step size, b) cumulative volume error (%), c) volume of fluid, d) fluid surface area, e) estimated mean kinetic energy, f) average turbulent kinetic energy, g) total fluid mass, h) total fluid energy.....304
Figure A11: Simulation S11: a) time-step size, b) cumulative volume error (%), c) volume of fluid, d) fluid surface area, e) estimated mean kinetic energy, f) average turbulent kinetic energy, g) total fluid mass, h) total fluid energy.....305
Figure A12: Simulation S12: a) time-step size, b) cumulative volume error (%), c) volume of fluid, d) fluid surface area, e) estimated mean kinetic energy, f) average turbulent kinetic energy, g) total fluid mass, h) total fluid energy.....306
Figure A13: Simulation S13: a) time-step size, b) cumulative volume error (%), c) volume of fluid, d) fluid surface area, e) estimated mean kinetic energy, f) average turbulent kinetic energy, g) total fluid mass, h) total fluid energy.....307
Figure A14: Simulation S14: a) time-step size, b) cumulative volume error (%), c) volume of fluid, d) fluid surface area, e) estimated mean kinetic energy, f) average turbulent kinetic energy, g) total fluid mass, h) total fluid energy.....308
Figure A15: Simulation S15: a) time-step size, b) cumulative volume error (%), c) volume of fluid, d) fluid surface area, e) estimated mean kinetic energy, f) average turbulent kinetic energy, g) total fluid mass, h) total fluid energy.....309
Figure A16: Simulation S16: a) time-step size, b) cumulative volume error (%), c) volume of fluid, d) fluid surface area, e) estimated mean kinetic energy,

f) average turbulent kinetic energy, g) total fluid mass, h) total fluid energy.....310
Figure A17: Simulation S17: a) time-step size, b) cumulative volume error (%), c) volume of fluid, d) fluid surface area, e) estimated mean kinetic energy, f) average turbulent kinetic energy, g) total fluid mass, h) total fluid energy.....311
Figure A18: Simulation S18: a) time-step size, b) cumulative volume error (%), c) volume of fluid, d) fluid surface area, e) estimated mean kinetic energy, f) average turbulent kinetic energy, g) total fluid mass, h) total fluid energy.....312
Figure A19: Simulation S19: a) time-step size, b) cumulative volume error (%), c) volume of fluid, d) fluid surface area, e) estimated mean kinetic energy, f) average turbulent kinetic energy, g) total fluid mass, h) total fluid energy.....313
Figure A20: Simulation S20: a) time-step size, b) cumulative volume error (%), c) volume of fluid, d) fluid surface area, e) estimated mean kinetic energy, f) average turbulent kinetic energy, g) total fluid mass, h) total fluid energy.....314
Figure A21: Simulation S21: a) time-step size, b) cumulative volume error (%), c) volume of fluid, d) fluid surface area, e) estimated mean kinetic energy, f) average turbulent kinetic energy, g) total fluid mass, h) total fluid energy.....315
Figure A22: Simulation S22: a) time-step size, b) cumulative volume error (%), c) volume of fluid, d) fluid surface area, e) estimated mean kinetic energy, f) average turbulent kinetic energy, g) total fluid mass, h) total fluid energy.....316
Figure A23: Simulation S23: a) time-step size, b) cumulative volume error (%), c) volume of fluid, d) fluid surface area, e) estimated mean kinetic energy, f) average turbulent kinetic energy, g) total fluid mass, h) total fluid energy.....317
Figure A24: Simulation S24: a) time-step size, b) cumulative volume error (%), c) volume of fluid, d) fluid surface area, e) estimated mean kinetic energy, f) average turbulent kinetic energy, g) total fluid mass, h) total fluid energy.....318
Figure A25: Simulation B1: a) time-step size, b) cumulative volume error (%), c) volume of fluid, d) fluid surface area, e) estimated mean kinetic energy, f) average turbulent kinetic energy, g) total fluid mass, h) total fluid energy.....319
Figure A26: Simulation B2: a) time-step size, b) cumulative volume error (%), c) volume of fluid, d) fluid surface area, e) estimated mean kinetic energy, f) average turbulent kinetic energy, g) total fluid mass, h) total fluid energy.....320
Figure A27: Simulation B3: a) time-step size, b) cumulative volume error (%), c) volume of fluid, d) fluid surface area, e) estimated mean kinetic energy, f) average turbulent kinetic energy, g) total fluid mass, h) total fluid energy.....321
Figure A28: Simulation B4: a) time-step size, b) cumulative volume error (%), c) volume of fluid, d) fluid surface area, e) estimated mean kinetic energy, f) average turbulent kinetic energy, g) total fluid mass, h) total fluid energy.....322

Figure A29: Simulation B5: a) time-step size, b) cumulative volume error (%), c) volume of fluid, d) fluid surface area, e) estimated mean kinetic energy, f) average turbulent kinetic energy, g) total fluid mass, h) total fluid energy.....323
Figure A30: Simulation B6: a) time-step size, b) cumulative volume error (%), c) volume of fluid, d) fluid surface area, e) estimated mean kinetic energy, f) average turbulent kinetic energy, g) total fluid mass, h) total fluid energy.....324
Figure A31: Simulation B7: a) time-step size, b) cumulative volume error (%), c) volume of fluid, d) fluid surface area, e) estimated mean kinetic energy, f) average turbulent kinetic energy, g) total fluid mass, h) total fluid energy.....325
Figure A32: Simulation B8: a) time-step size, b) cumulative volume error (%), c) volume of fluid, d) fluid surface area, e) estimated mean kinetic energy, f) average turbulent kinetic energy, g) total fluid mass, h) total fluid energy.....326
Figure A33: Simulation B9: a) time-step size, b) cumulative volume error (%), c) volume of fluid, d) fluid surface area, e) estimated mean kinetic energy, f) average turbulent kinetic energy, g) total fluid mass, h) total fluid energy.....327
Figure A34: Simulation B10: a) time-step size, b) cumulative volume error (%), c) volume of fluid, d) fluid surface area, e) estimated mean kinetic energy, f) average turbulent kinetic energy, g) total fluid mass, h) total fluid energy.....328
Figure A35: Simulation B11: a) time-step size, b) cumulative volume error (%), c) volume of fluid, d) fluid surface area, e) estimated mean kinetic energy, f) average turbulent kinetic energy, g) total fluid mass, h) total fluid energy.....329
Figure A36: Simulation B12: a) time-step size, b) cumulative volume error (%), c) volume of fluid, d) fluid surface area, e) estimated mean kinetic energy, f) average turbulent kinetic energy, g) total fluid mass, h) total fluid energy.....330
Figure A37: Simulation B13: a) time-step size, b) cumulative volume error (%), c) volume of fluid, d) fluid surface area, e) estimated mean kinetic energy, f) average turbulent kinetic energy, g) total fluid mass, h) total fluid energy.....331
Figure A38: Simulation B14: a) time-step size, b) cumulative volume error (%), c) volume of fluid, d) fluid surface area, e) estimated mean kinetic energy, f) average turbulent kinetic energy, g) total fluid mass, h) total fluid energy.....332
Figure A39: Simulation B15: a) time-step size, b) cumulative volume error (%), c) volume of fluid, d) fluid surface area, e) estimated mean kinetic energy, f) average turbulent kinetic energy, g) total fluid mass, h) total fluid energy.....333
Figure A40: Simulation B16: a) time-step size, b) cumulative volume error (%), c) volume of fluid, d) fluid surface area, e) estimated mean kinetic energy, f) average turbulent kinetic energy, g) total fluid mass, h) total fluid energy.....334
Figure A41: Simulation B17: a) time-step size, b) cumulative volume error (%), c) volume of fluid, d) fluid surface area, e) estimated mean kinetic energy,

f) average turbulent kinetic energy, g) total fluid mass, h) total fluid energy.....335
Figure A42: Simulation B18: a) time-step size, b) cumulative volume error (%), c) volume of fluid, d) fluid surface area, e) estimated mean kinetic energy, f) average turbulent kinetic energy, g) total fluid mass, h) total fluid energy.....336
Figure A43: Simulation B19: a) time-step size, b) cumulative volume error (%), c) volume of fluid, d) fluid surface area, e) estimated mean kinetic energy, f) average turbulent kinetic energy, g) total fluid mass, h) total fluid energy.....337
Figure A44: Simulation B20: a) time-step size, b) cumulative volume error (%), c) volume of fluid, d) fluid surface area, e) estimated mean kinetic energy, f) average turbulent kinetic energy, g) total fluid mass, h) total fluid energy.....338
Figure A45: Simulation B21: a) time-step size, b) cumulative volume error (%), c) volume of fluid, d) fluid surface area, e) estimated mean kinetic energy, f) average turbulent kinetic energy, g) total fluid mass, h) total fluid energy.....339
Figure A46: Simulation B22: a) time-step size, b) cumulative volume error (%), c) volume of fluid, d) fluid surface area, e) estimated mean kinetic energy, f) average turbulent kinetic energy, g) total fluid mass, h) total fluid energy.....340
Figure A47: Simulation B23: a) time-step size, b) cumulative volume error (%), c) volume of fluid, d) fluid surface area, e) estimated mean kinetic energy, f) average turbulent kinetic energy, g) total fluid mass, h) total fluid energy.....341
Figure A48: Simulation B33: a) time-step size, b) cumulative volume error (%), c) volume of fluid, d) fluid surface area, e) estimated mean kinetic energy, f) average turbulent kinetic energy, g) total fluid mass, h) total fluid energy.....342
Figure B1: Wentworth grain size chart from united states geological survey.....343

SYMBOLS

c	Suspended sediment concentration
D	Diffusion term
D( ) / Dt	Material derivate
dV	Selected infinitesimal fixed control volume
E	Turbulence model term
F_b	Body forces
F_i	Component of the body forces per unit volume in the i-direction
G,g	Gravity
K	Turbulent kinetic energy
L	Length dimension
U	Velocity dimension
P	Pressure
P_k	Turbulent production
$-\nabla P$	Pressure gradient term
Pr	Prandtl number
Pr_t	Turbulent Prandtl number
Q	Discharge
Re	Reynolds number
R_t	Turbulent Reynolds number
S	Turbulence model source term
S_c	Sink or source of suspended sediment
S	Surface of control volume V
T	Temperature
t	Time
$\overline{T}$	Temporal average temperature
T'	Fluctuating temperature
u,v,w	Velocity components in x, y and z directions
$\overline{u},\overline{v},\overline{w}$	Temporal average velocity components in

	directions of x, y and z axis
$\mathbf{U_i}$	Velocity
$\mathbf{u.\nabla u}$	Convection acceleration
$\mathbf{u_i'}$	Fluctuating velocity
$\mathbf{\overline{u_i' u_j'}}$	Reynolds stresses
$\mathbf{u_*}$	Shear velocity
$\mathbf{\frac{\partial u}{\partial t}}$	Unsteady acceleration
3D	Three-dimensional
2D	Two-dimensional
1D	One-dimensional
$\boldsymbol{\alpha}$	Turbulence model coefficient, Heat dissipation, Diffusion coefficient
$\boldsymbol{\beta}$	Turbulence model coefficient
$\boldsymbol{\varepsilon}$	Dissipation rate
$\boldsymbol{\upsilon}$	Kinematic viscosity
$\boldsymbol{\mu}$	Dynamic viscosity
$\mathbf{\mu_t}$	Turbulent dynamic eddy viscosity
$\boldsymbol{\rho}$	Density
$\boldsymbol{\sigma}$	Turbulent Schmidt number
$\boldsymbol{\Gamma}$	Molecular diffusivity coefficient
Ax	Horizontal eddy viscosity
Dx	Horizontal eddy diffusivity
EXH2O	Solar radiation extinction of water
WSC	Wind sheltering coefficient

STUDY ON STRATIFIED RESERVOIR OF DAMS AND LAKES WITH NUMERIC MODELING

SUMMARY

Due to drought in most of the countries in recent years, the protection and control of water resources have particular importance. These water resources have two forms included man made water resources structures such as dams, and natural water resources like lakes. The complexity of real fluid flow makes it impossible to solve the governing equations without making some form of simplifying approximation, even with the use of complex models and fast computers.

This dissertation models and studied on the stratification of reservoirs or lakes with different conditions by changing some important parameters that can affect the temperature and suspended sediment distrubution patterns in reservoir/lake, numerically. Several models and simulations were performed for this goal. The commercial software package Flow 3D was selected as the numerical model for simulations of this dissertation. Near this code, the CE-qual-W2 was used to achieving the purpose of this thesis. Therefore, this program is used to analyse the thermal stratification of case study. The Lake Köyceğiz was selected as the case study, because of the importance of this lake as a water resource. Before simulating the Lake Köyceğiz, a series of model scenarios and sensitivity simulations were done to understand and quantify the formation of the stratification and propagation of suspended sediments in reservoirs and lakes with several changes in some important parameters included as discharge, temperature of water, suspended sediment concentrations and outlet type. Comparison of these results of scenarios shows that the changing in selected parameters could affect the position and thickness of the suspended sediment and temperature layers in reservoir. It was found changes in position and location of plunging point in most of the simulation results with a denser inflow current than reservoir. It was also concluded that the bottom outlet could be very effective on water quality of reservoir, when density/turbidity currents occurred.

In the case study simulations, in first step, the hydrodynamic of Lake Köyceğiz was studied. In defined conditions, the approximate velocity vectors and directions were determined in different depths. Then, the salinity and temperature variations during time in defined conditions were investigated. In this part of simulations, the environment temperature was not definable to the FLOW3D program. Therefore, the temperature variations in depths and surface of the lake were under the influence of heat transfer between different layers. There was another parameter affected these temperature. This parameter was temperature of the inflow rivers. After that, three scenarios were done for the aim of evaluating and investigating the suspended sediment distribution pattern in the lake, in an unexpected flood event. According to these simulations, the flood was happened in only Namnam river, only Kargicak river and filnally, in both of Namnam and Kargicak rivers, simultaneously.

In the next part of the simulations of Lake Köyceğiz, the thermal stratification modeling of this lake was considered. In these models, which were done using CE-qual-W2 two-dimensional program, the output results of temperature of model in different depths were compared with observed data. The model results were harmonious with the measurements conducted in Lake Köyceğiz. Modeled values of temperature in epilimnion and thermocline layers had a good concordance with the observed data. In other part of this thesis, effect of a possible dam construction on Namnam river is studied, briefly. Totally, it could conclude that the construction of dam on Namnam river will affect the Lake Köyceğiz. These effects will be in the case of the salinity, temperature, suspended sediment concentration, sediment particles type and diameter, dissolved oxygen and other parameters.

TABAKALI HAZNELİ BARAJLAR VE GÖLLERİN NÜMERİK OLARAK ARAŞTIRILMASI

ÖZET

Dünyadaki tatlı su, toplam mevcut suyun ancak yaklaşık %2.6'sı olmaktadır. Bu tatlı su miktarı buhar şeklinde atmosferdeki sular, kutupta buz şeklindeki sular, yer yüzeyindeki sular ve yeraltı sularından oluşmaktadır. Son yıllarda, kuraklık, birçok ülkenin en önemli konularından biri haline gelmiştir. Bu ülkelerde, araştırmacılar tarafından, bölgesel olarak tatlı su kaynakları hakkında sureklı ve çeşitli araştırmalar yapılmaktadır. Söz konusu araştırmalar ve çalışmalar, mevcut su kaynaklarinin hem kalite açısından, hemde miktar açısından korumak ve kontrolu amacı ile yürütülmektedir. Bu su kaynakları insan yapımı ve doğal olabilmektedir.

Bu çalışmada, haznelerde ve göllerde farklı parametrelerin askıdaki katı madde (sediment) dağılımına olan etkisi araştırıldı. Bunun yanı sıra, seçilmiş parametrelerın değişiklikleriyle, tabakaların kalınlıklarının değişimide araştırıldı. Söz konusu parametreler, hazneye giren suyun sıcaklığı, haznedeki suyun sıcaklığı, hazneye giren suyun askıdaki katı madde (sediment) konsantrasyonu, haznedeki suyun askıdaki katı madde (sediment) konsantrasyonu, hazneye giren suyun debisi ve haznedeki çıkış tipi olarak seçilmiştir. Haznedeki çıkış tipi dolu savak ve dip savak olarak seçilmiştir. Giren suyun debileri için 20 m^3/sn., 50 m^3/sn. ve 100 m^3/sn. olarak üç farklı değer düşünüldü. Hem giren akım ve hem haznedeki su için, askıdaki katı madde konsantrayonlar değerleri, 15 g/l ve 20 g/l olarak seçıldı. Tezin ilk kısmında toplam 48 tane farklı senaryo oluşturuldu. Bunların 24'ü dolu savakli modelleri ve diğer 24 model ise, dip savaklı modelleri oluşturmaktadırlar. Bu senaryolarda belirtilen parametreler değerlerinde değişiklik yapılarak sonuçlar karşılaştırılarak, değerlendirmeler yapılmıştır. Sadece dolu savakla çalıştırılan simulasyonların isimleri S ile belirlendı ve bu harftan sonra gelen sayı, senaryonun numarasını göstermek için kullanıldı. Dip savak ise, B harfı ve senaryo numarasıyla belirlendi.

Senaryoların modellenmesi sonucunda, sıcaklık, askıdaki katı madde ve debilerin değişmesi sonucunda, akım davranışında çok önemli değişiklikler ortaya çıkmıştır. Sonuçlar karşılaştırdığında, giren suyun askıdaki katı madde konsantrasyonun hazneye göre fazla ve su sıcaklığının hazneye göre az olan modellerde, giren suyun dansitesi haznedekine göre daha fazla olup, hazne tabanında yoğun akımlar oluşmuştur. Bu durumda, Hyperpycnal akımı adlandırılan, taban akımı ortaya çıkmaktadır. Bu akımların hız ve yapıları, giren debinin büyüklüğü ile doğrudan ilişkisi olup ve farkli debilerle değişmektedirler. Bu tür akımlar deltaların oluşmasına neden olmaktadır ve sürekli ve sıkça rtaya çıkması halinde haznenin ömrünü azaltmaktadır. Diğer taraftan hazneye giren akımın sıcaklığı ve askıdaki katı madde konsantrasyonu, haznedekine göre daha az olması durumuyla da karşılaşabiliriz. Bu halde, akımın haznenin tabanında değil, belki daha üst seviyelerinde ve hatta hazne suyunun yüzeyinde hareket ettmesi beklenmektedir. Bu durumda, Hypopycnal akımı adlandırdığımız durum ortaya çıkmaktadır.

Yukarıdaki bahsı geçen parametrelerin yanı sıra, haznelerde, çıkış tipi ve yeri önem arz etmektedir. Özellikle yoğun akımlarda, dip savak su kalitesi açısından çok önemli röl aldığını sonuçlar neticesinde anlamak mümkün. Bu hazne çıkışları, tabakalaşmış haznelerde tabakaların kalınlıkları üstünde çok önemli etkileri olduğunu gördük. Ayrıca, savakların gövde yakınında hız vektörlerini çok fazla etkilemektedirler. Tüm senaryolara ait sonuçlar grafik olarak gösterilmiş ve yorumları yapılmıştır.

Bu çalışmanın bir diğer amacı, Köyceğiz gölü'nün hidrodinamik modellenmesi. Köyceğiz gölü Türkiye güney, güney batı bölgesinde yer almakta olup, bölgenin en önemli su kaynaklarından birisi olmaktadır. Gölün deniz yüzeyinden yüksekliği yaklaşık 8 metre kadardır. Bu göl, iki çanaktan oluşmaktadır. Gölün kuzeyinde bulunan çanağa Köyceğiz adı, güney kısımında bulunan çanağa ise Sultaniye adı verilmiştir. Köyceğiz çanağı en fazla 25-26 metre derinliğe sahiptir. Sultaniye çanağında ise en derin yer 33 metre derinliktedir. Göle üç önemli akım girerken, gölden sadece bir çıkış vardır. Göle akımların girişleri kuzeyde olup, çıkış ise güneydedır. Gölün suyu, Dalyan kanalı vasıtası`le gölden çıkıp ve Akdenize dökülmektedır. Köyceğiz gölüne bir çok akım girmektedir. Bu akımların en önemlileri Namnam çay, Yuvarlak çay ve Kargıcak`dır. Namnam çay, Köyceğiz gölüne en fazla su getiren bir akım olup, bu nedenle Köyceğiz gölüne en fazla etkisi olan akımdır. Namnamın yılın bir çok ayında, özellikle kış ve bahar aylarında, dolu olup ve yüksek debilere sahip olmasına rağmen, yaz mevsiminde çok az bir debisi vardır. Hatta yazın çok sıcak aylarında tamamen kuru olduğu görülmüştür. Yaz aylarında, sıcaklık ve buharlaşmanın arttığı ve yağışların azaldığı ve hatta hiç olmaması nedeniyle, Köyceğiz gölünün su seviyesi azalmaktadır. Yılın bu mevsiminde, göle en fazla su getiren akarsu ise, Yuvarlak çay`dır. Bu nedenle, yaz aylarında, Köyceğiz gölünün kuzey kısmına en çok etkisi olan akımın Yuvarlak çay olduğu anlaşılmaktadır. Genel olarak, Yuvarlakçay her zaman yaklaşık sabit bir debiye sahiptir. Bu akarsu Bu akarsuların yanı sıra, göle yeraltı suları, termal suları ve birçok kaplıca suyu girmektedir. Bu tip su girişleri, hem göl suyunun altında, hemde gölün etrafında yer almaktadırlar. Sultaniye çanağı etrafında bulunan kaplıcaların sıcaklığı 39 derece olduğu söylenmektedir. Akdenizle bağlantısı olan Köyceğiz gölünün, suları tuzlu ve acıdır. Ancak giren çayların suları tatlı olup, göl sularıyla karışması sonucunda tuzluluğu azaltmaktadır. Yinede, derinlikle suyun tuzluluğu arttığı görülmektedir.

Bu göl ile ilgili mevcut veriler toplanmış olup, gözlemler sayı açısından az olup ve güncel veriler olmadığından, 1990-1999 senelerine ait veriler kullanıldı. Batimetri haritası çizilerek, Autocad programı kullanılarak, üç boyutlu solid cisim hale getirilmiştir. Ağustos, Kasım ve Aralık aylarının verileri kullanılarak, hızlar ve yönleri belirtildi. Bu aylara göre, Namnam, Yuvarlakçay ve Kargıcak akımlar vasıtasiyle göle giren tuzluluk ve sıcaklık dağılımı araştırılmıştır. FLOW3D programı, çevredeki hava sıcaklığını modelliyemediği için, termal tabakalaşmayı modellemek için, CE-qual-W2 iki boyutlu programı kullanıldı. Modelleme sonucunda, sonuçlar karşılaştırıldı. Modelin doğrulanması için bazi standartlar kullanıldı. Bu standartlar: mutlak ortalama hata (AME), ortalama kare hata (MSE) ve kök ortalama karesel hata (RMSE) olarak seçıldı. Modellenen epilimnion ve thermocline tabakalarının sıcaklıkları ve kalınlıklarını mevcut ölçülmüş değerlerle karşılaştırdığında, modelleme sonuçlarının bu tabakalarda ölçümlerle iyi uyumda oldukları sonucuna varıldı. Ancak modelde hypolimnion adlandırdığımız alt tabakda, ölçülmüş değerlerle karşılaştırdığında, diğer tabakalara göre daha az uyum sağladığı belirlendi.

Barajların çevreye ve özellikle mansaba etkileri birçok tez, makale ve araştırma projeleri adı altında incelenmiştir. Namnam çayının üzerine baraj yapılması imkanı her zaman olmuştur. Bu yüzden, bir mühtemel barajın, bölgeye, Namnama ve özellikle`de Köyceğiz gölüne etkisi çok önemli konulardan biri haline gelmiştir. Bu tezin son bölümünde, bu etkilere değinmiş olup, kısaca incelenmiştir. Bu tezin sonuçlarından yararlanarak, Namnam üzerinde yapılması muhtemel olan barajın yapılması durumunda, Köyceğiz gölünde olası değişimlerin tahmin edilmesi mümkündür. Aynı zamanda, bir göle veya hazneye farklı koşullarla giren bir nehrin, sicaklık ve suspended sediment yayılma şeklinin tahmin edilebilir.

1. INTRODUCTION

Water is the most basic requirement of human. More than 70 percent of surface of the Earth is covered by water, approximately. From this huge amount of water on the Earth, only fresh water is usable for human. It is an insignificant amount of the total water on earth. Fresh water is available in various forms such as surface waters, groundwaters or atmospheric waters. Fresh water is available on the earth's surface in several forms such as ice sheets, ice caps, glaciers, icebergs, bogs, ponds, lakes, rivers and streams, and underground as groundwater in aquifers and underground streams. There is an uneven distribution of fresh water. It means that some countries have an abundant supply of fresh water, but others do not have as much. A reason for the uneven distribution of fresh water supply may be the differences in climate. One of these reasons that led to insufficient water supply is the frequent lack of rain. Figure 1.1 shows the distribution of water on the Earth.

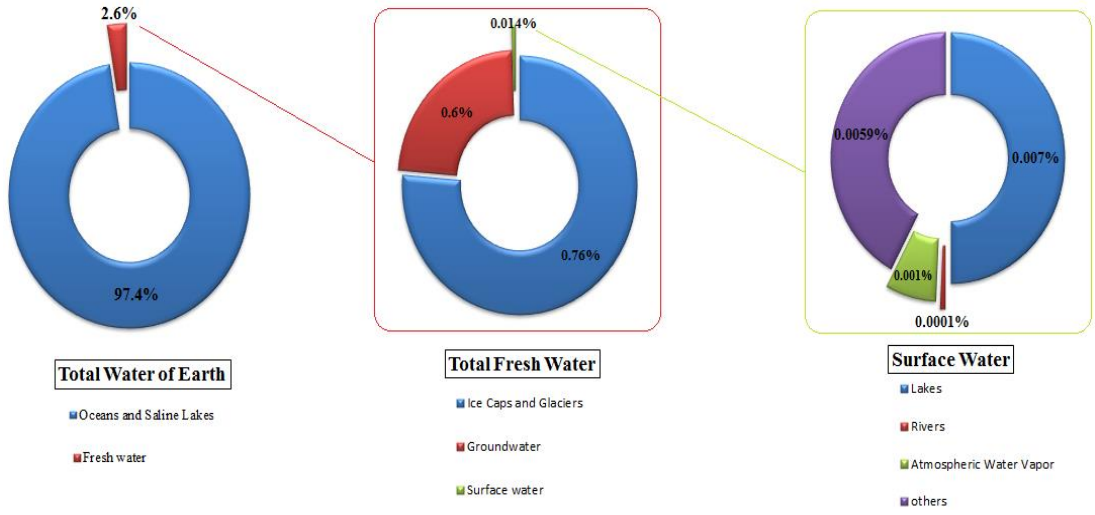

Figure 1.1 : Distribution of Water on the Earth (Brooks/Cole-Thomson, 2005).

Nowadays, aridness is the main problem for the arid and semi-arid regions. On this basis, the preservation of the water resources has high attention and particular importance. For this reason, policies and patterns of water use have major role. One of these policies is construction of dams. The importance of dam construction in these regions has increased in recent years. Therefore, in these regions, dams are

important manmade structures, because they are the only source of water during water shortage seasons. For this reason, at the end of the 20th century, approximately 45,000 large dams with height of more than 15 m, which classified as large dams by ICOLD and a total reservoir surface of more than about 500000 km^2 have been exploited in the world, mainly for irrigation, hydroelectricity and as drinking water reservoirs (Wildi, 2010; Gleick, 1998; WCD, 2000). In arid and semi-arid countries, dams are mostly constructed for supplying the drinking water and irrigation. Here, management of these resources plays a major role than the construction of them. So, water resources need a good management in the present century because of these limitations of water resources, especially. For better management of water resources, investigation of all parameters of the hydrologic cycle and climatic characteristics including precipitation, wind, temperature, runoff, evaporation and etc. is required. These natural and climatic characteristics affect the water quality of the water resources, dam reservoirs and lakes. In this study, dam reservoirs and lakes are considered.

There are several factors and phenomena that affect the quality of water in lakes and reservoirs. One of the most important problems that occurs in dam reservoirs is sedimentation. There are some problems caused by sedimentation in dam reservoirs such as decreasing of storage volume of the reservoirs after operation. Sedimentation is the main phenomena that lead to dam death. This phenomena is endangering the life of dams, insensibly and during the time, gradually. Beyond that sedimentation makes project uneconomical; in arid and semi-arid regions, it is important specially due to water shortage. Evaluation of sedimentation and the distribution of sediments in dam reservoir is necessary to increase the efficiency of hydrofacilities. One of the other phenomenon that affects water quality in reservoirs is named as stratification. Study of stratification phenomena has special significance because of the importance of water quality.

Stratification in lakes and dam reservoirs has two forms as: thermal stratification and the stratification that caused by concentration of suspended particles. Each of these phenomena could effect on the water quality of reservoirs or lakes, extremely. So, study on these phenomena is one of the important subjects that should be done in water resources management in reservoirs and lakes, especially. Stratification has

important implications for fisheries management, phytoplankton (algae) populations, and water supply quality, generally.

1.1 Thermal Stratification

The thermal stratification of lakes and reservoirs refers to a change in the temperature at different depths, and is due to the change in water density with temperature. In deep reservoirs or lakes, this kind of stratification is separated into three layers. However, in shallow reservoirs and lakes, it could be seen that two layers of thermal stratification are available. In deep reservoirs and lakes, the first layer is a well-mixed zone of reservoir or lake and is named as Epilimnion layer. In other words, epilimnion is the upper layer of reservoir or lake. In summer, temperature of the water column decreases from the free water surface to the bottom in thermally stratified reservoirs and lakes. Regardless of the other parameters, it is expected that the density of water is increasing from the surface to the bottom. In winter or cold areas, temperature of water increases from the surface of the water to the bottom. Therefore, the Epilimnion layer has the higher value of water temperature than the other layers, which are located in the deeper (Boehrer and Schultze, 2007).

The second layer in thermally stratified lakes or reservoirs, that temperature changes more rapidly with depth, is called Metalimnion or Thermocline layer. This layer of the lake or reservoir also known as transitional zone (Arnon, et al. 2014). The last layer in thermally stratified reservoirs or lakes named as Hypolimnion layer. This layer is the bottom layer of water. In summer, the Hypolimnion layer is the coldest layer of a lake or reservoir, and it is the warmest layer during winter. A Schematic figure of these layers are shown in Figures 1.2. The values are just to indicate the changes of temperature through the depth in different seasons (Horne and Goldman, 1994).

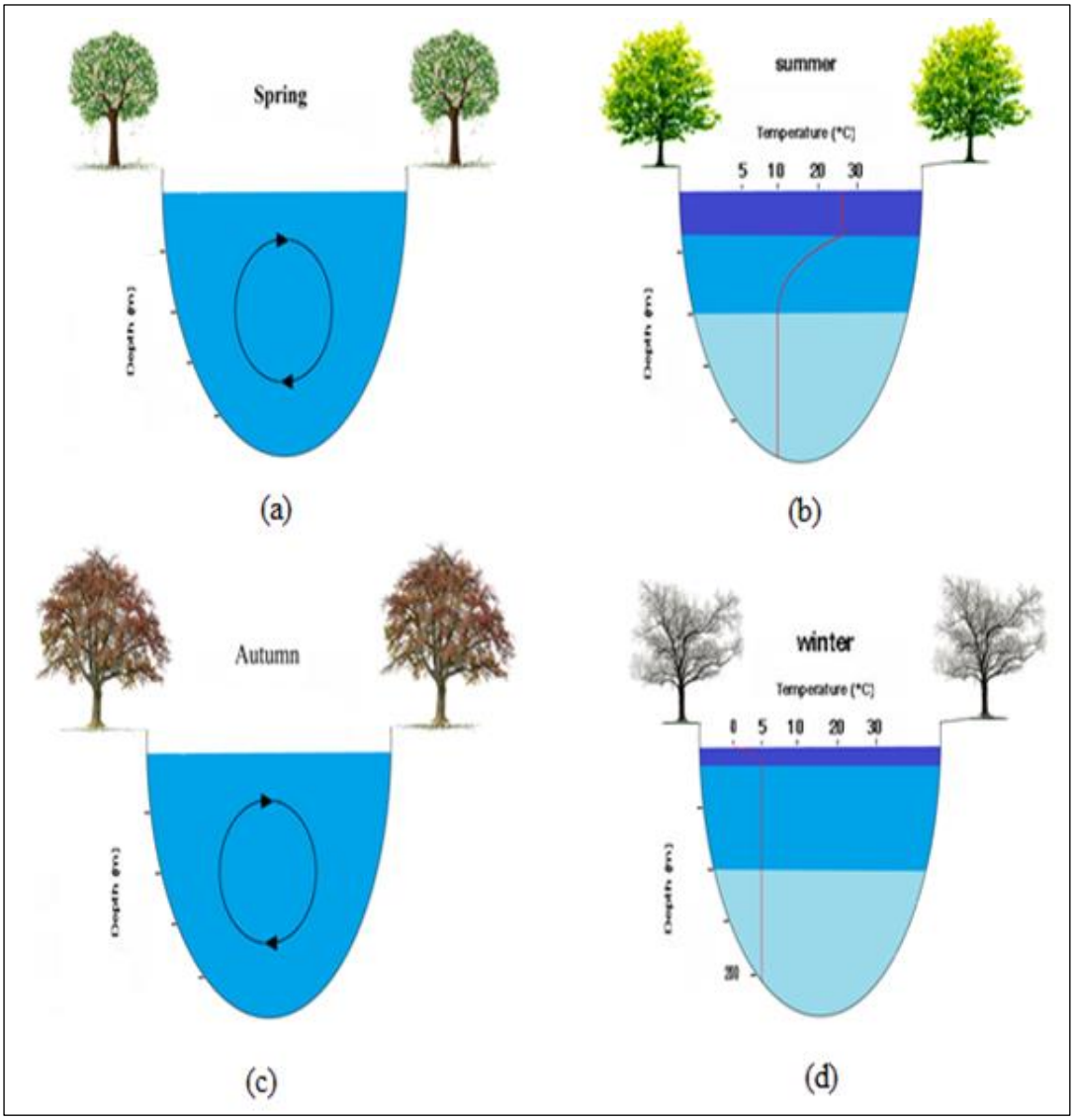

Figure 1.2 : A schematic figure for thermal stratification in reservoirs and lakes a) Spring, b) Summer, c) Autumn and d) Winter.

1.2 Density Stratification (Caused by Concentration of Suspended Sediments)

As it is clear from the title, this kind of stratification occurrs when densities due to sediment concentrations of the layers of water in the reservoir/lake have different values. These differeces in densities caused by concentrations of sediment, result from the sediment transport. Therefore, sediment transport is one of the important subjects that should be given more attention.

1.3 Sediment Transport

Sediment transport occures in all rivers, reservoirs and lakes. It is very useful having some information and knowledge about sedimentation and sediment transport. Sediment transport may occur in four modes (Kipling, n.d.; Hickin, n.d.):

1. The first mode is bed load. Material in this mode is denser particles, coarser-grained earth material (sands and gravels) that remain on the bed and travel along the bottom of the stream. This travel of the sediment particles has several forms. Sediment particles at the bottom of the river move by rolling, dragging, sliding or saltating along the bed and close to it. These forms of bed load transport have been shown in Figure 1.3.

2. Second mode is named as dissolved load. Dissolved load is the material that has gone into solution and is part of the water moving through the river. In other words, solid particles are dissolved and chemically carried and move along with the water. An example of these material is dissolved salts, which leads to salinity of water. This material is typically much smaller than the suspended load that will be described. One difference between this load and others is that the dissolved load is invisible. This is because of dissolving of the ions in water.

3. Suspended load is another mode of sediment transport. This type of sediment transport has particulate sediment that is carried in the body of the flow. It is the fine-grained (clay and silt) sediment that remains in water during transportation.

4. One more form of transport of sediment particles is saltation load or intermittent suspension load. It consists of the coarser part of the suspended load. This form occurs when loose material is removed from a bed and carried by the stream, before being transported back to the surface.

Suspended load also has two forms such as wash load and bed material load. Wash load is the portion of sediment that is carried by a stream, usually in a river, such that it always remains close to the free surface and near the top of the flow in a river. The bed material load is the portion of the sediment load that is transported by current that contains material derived from the bed (Kipling, n.d.; Stevens and Yang, 1989).

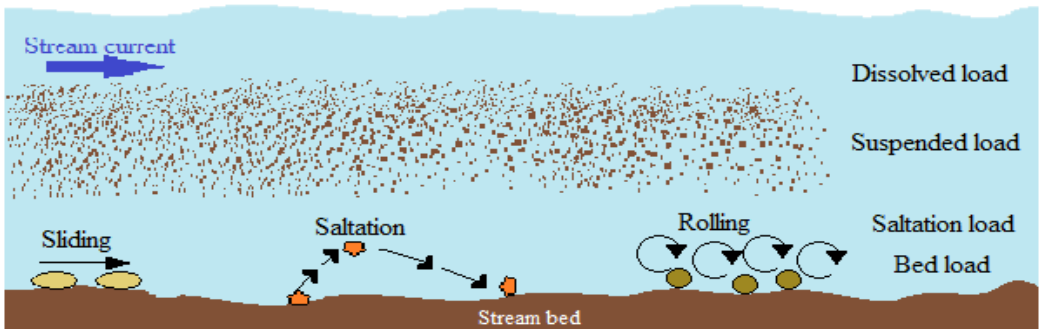

Figure 1.3 : Sediment transport modes (McKnight and Hess, 2000).

Sedimentation is one of the most serious environmental problems that needs lots of attention with an appropriate management. This phenomenon becomes more important in manmade structures like dam projects, especially. Entering sediments by rivers into dam reservoirs caused to be filled and led to decreasing the economic lifetime of these structures. It is also due to some problems and risks such as reduction of volume of the reservoir, risk and insecurity in the face of pressure from the accumulation of silt behind the dam structure, creation of operation failure of valves etc. In adition to these failures and risks, irreparable environmental damages are the most important subject in this case.

With entering the river flow into the reservoir or the lake, the hydraulic conditions of the flow such as flow velocity is greatly reduced. This factor leads to decreasing of the potential of sediment transport. As a result of these changes in hydraulic conditions, sediment particles begin to be deposited, gradually. Bed load and the coarse-grained part of the suspended load deposits in the primary area of the reservoir immediately and delta is formed in this area. While the fine grain suspended sediment go forward to deeper parts of the reservoir near the dam body and then deposited there.

Totally, with facing rivers or shallow streams with a reservoir or lake,which are deepest than these currents, we have different types of propagation and diffusion of fluid depend on sediment type, sediment concentration and water temperature. Graph in 1983 has mentioned one of the following factors are caused to density differences:

1) Temperature differences.

2) Differences between concentration of two fluids resulting from dissolved substances.

3) Differences between concentration of two fluids resulting from suspended materials.

Types of flows according to differences between density of river flow and density of water in reservoir or lake are defined here. When a river flow with the density equal to ρ_{river} comes into the reservoir or lake with density of $\rho_{reservoir/lake}$, it can has one of the following behaviors shown in Figure 1.4, totally (Ford, 1983; Hipsey and Brook, 2013).

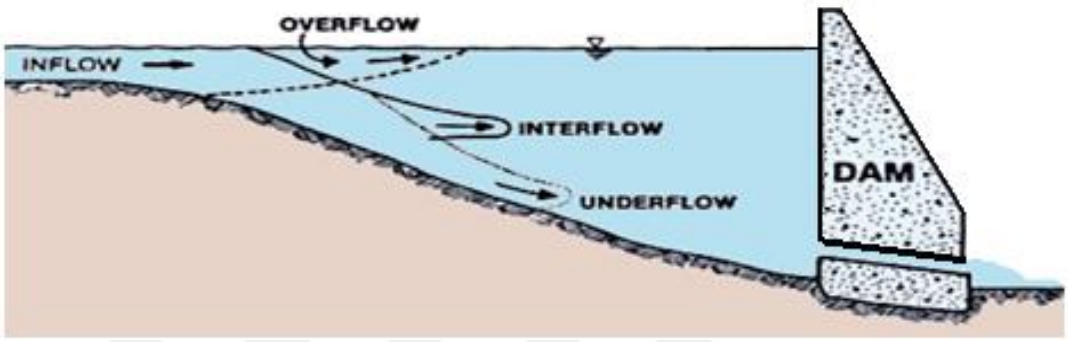

Figure 1.4 : Behavior of river water meets reservoir/lake (Hipsey & Brooks, 2013).

Over flow, inter flow and under flow could be named as Hyperpycnal, Hypopycnal, Homopycnal and Hyperpycnal flow, respectively. In this part of current chapter, these flows are described in detail.

1.3.1 Hyperpycnal Flow

This kind of flow is named as the underflow type. Hyperpycnal flows were first reported in Lake Leman by Forel in 1885 (Mulder et al., 2003). The hyperpycnal flows occured when density of water in river mouth, where entering into the reservoir or lake, is higher than the density of the water in the resrvoir or lake. In other words, with entering water from the river with density of $\rho_0 + d\rho_0$ into water in the reservoir or lake with density of ρ_0, these kind of flows occurs. These flows are commonly referred to as gravity flows, mass flows or density flows too. Hyperpycnal flows are mixtures of sediment and fluid flowing down a slope by the virtue of gravity force. In other words, when the inflow water is denser than the water in reservoir or lake, the inflow will plunge and propagate across the bottom of reservoir or lake (Meiburg, 2009). Hyperpycnal flows have two types. The first type of these flows named as waxing flow. As it is clear from Figure 1.5, in this type of

flow, turbidity travels a further distance at the bottom or near the bottom of the reservoir or lake. In small scale reservoirs and when the distance between the entrance of inflow and body of dam is short, this turbidity flow could reach up near the body of the dam and could be passed from the bottom outlets of the dam to the downstream region of the dam body. The other case about hyperpycnal flows is named as early waning flow. Figure 1.6 shows this type of hyperpycnal flows.

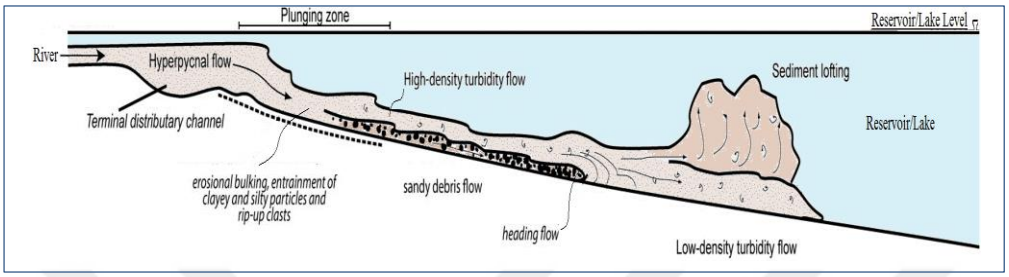

Figure 1.5 : Hyperpycnal flows (waxing flow).

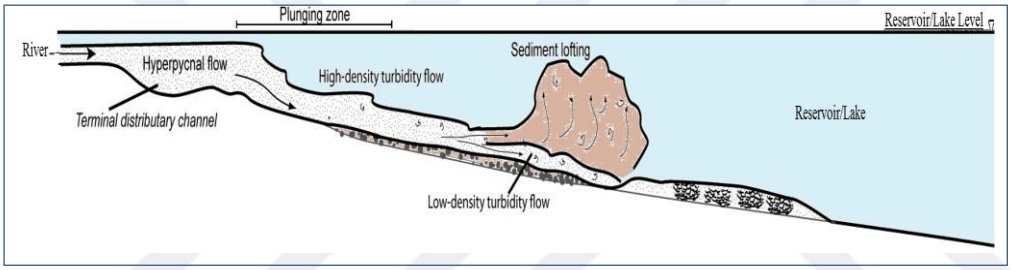

Figure 1.6 : Hyperpycnal flows (early waning flow).

1.3.2 Hypopycnal Flow

These flows are related to buoyant flows and are known as overflow type. These kind of flows are formed when a river water with lower density entering a reservoir or lake with higher water density. So, the river water is buoyant and flows above the reservoir/lake water (Figure 1.7). This is typical of the situation where a river enters the sea, because of the difference in density between fresh and salt water (Bates, 1953).

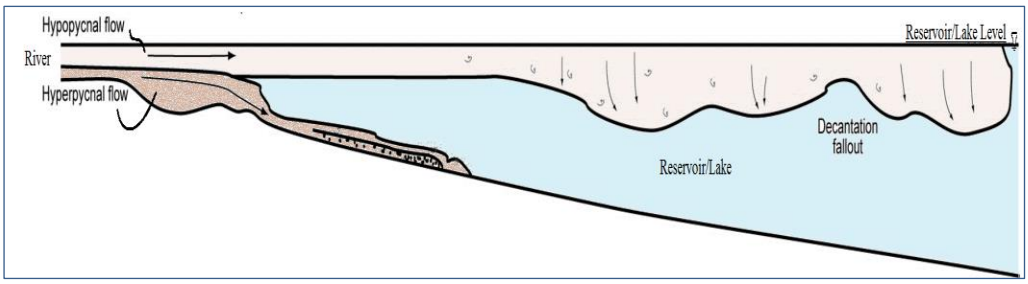

Figure 1.7 : Hypopycnal flow in a reservoir/lake.

1.3.3 Homopycnal Flow

These flows happen if the density of water in river mouth is equal to the density of water of the reservoir/lake, approximately. Homopycnal flow is associated with mixing throughout the general flow, rapidly. The better difinition of homopycnal flow is that a condition in which the outflow water from a river or the coastal inlet and the water in the receiving reservoir or lake have the same density and vertically mixed. Figure 1.8 represented homopycnal flow, schematically.

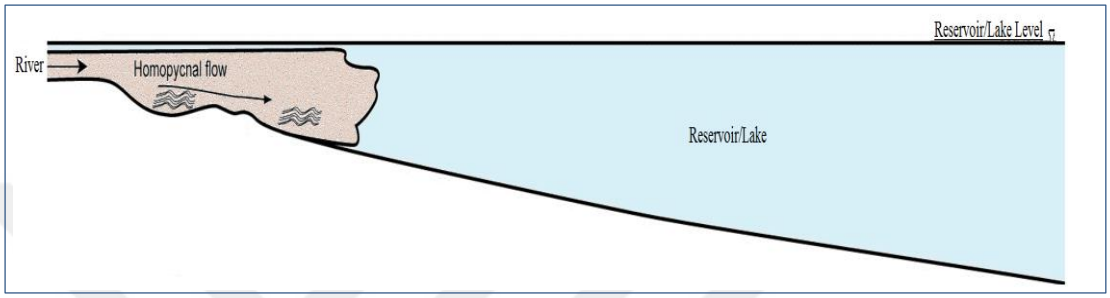

Figure 1.8 : Homopycnal flows in a reservoir/lake.

1.3.4 Mesopycnal

These deposits are partially buoyant flows. The mesopycnal flows are like hypopycnal flows and in this type of flows the oberflow condition occurred. The difference between this condition and hypopycnal flow is that the sediments starts to settling faster than the hypopycnal flows in this condition. Figure 1.9 presents Mesopycnal type (Ducassou et al. 2008).

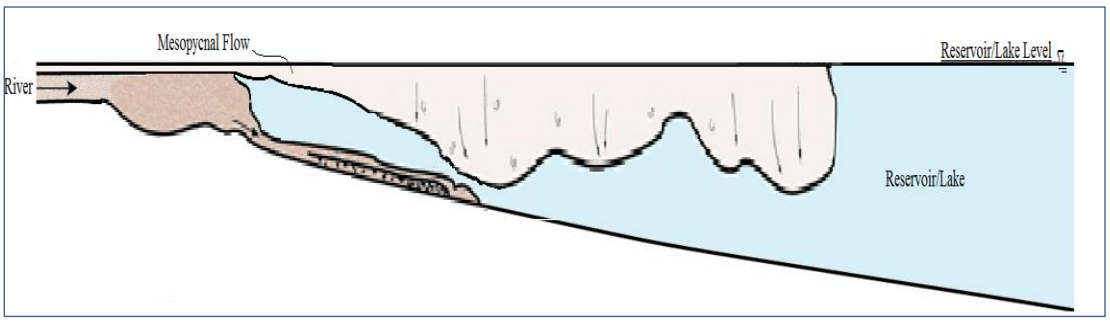

Figure 1.9 : Mesopycnal flow in reservoir/lake.

1.4 Purpose of Thesis

The main purpose of this study was to investigate the hydrodynamics of stratified dam reservoirs and stratified lakes for different flow and reservoir conditions using numerical modeling. The distribution and deposition of sediment could be varying due to the changes of some parameters related to the inflow water and reservoir or lake. Such important cases of these parameters include the discharge of inflow water comes to the reservoir or lake, dimension of reservoir or geometry of lake, temperature of inflow water and reservoir of dam or lake, sediment concentration of inflow and reservoir/lake, sediment diameter, slope of the bed of reservoir or lake, stratification due to seasons etc.

To the present, numerous studies are available in the case of sediments motion and sediment distribution in reservoirs and lake due to changes in conditions of river mouth and reservoir/lake. Despite of these researches, which will be refered them in the following sections, the simultaneous influence of water temperature and concentration, in the propagation of entering sediments into reservoirs and lakes have not been evaluated. The main difference of this thesis with other studies is related to these simultaneous changes of mentioned parameters. In fact, the main objective of this thesis is a numerical study on distribution of suspended sediment and temperature, which resulted from the temperature differences between river and reservoir/lake water, sediment concentration differences between river and reservoir/lake, and some of other parameters such as outlet type and position. In the meantime, the outlet situation of the reservoir could affect the stratification near dam body. All of mentioned parameters affect the thickness of the stratification layers. Therefore, this study could help us to imagine the river current behavior when faces with reservoir or lake and how it leads to stratification.

The main use of results of this study is to improve the dam reservoirs or lakes operation. Because it is necessary to predict effects of sediment distribution and loss of storage capacity and its rate for better operation of the reservoirs. A three-dimensional numerical modeling was used in the present study to model the hydrodynamics in reservoirs or lakes. FLOW-3D computational fluid dynamic code was selected for numerical solutions because of its capabilities and advantages.

The thermal stratification is one of the objectives of this thesis. Lake Köyceğiz was selected as a case study as major water resources of Turkey with complex conditions, unique to this region. For modeling the thermal stratification of this lake, the FLOW 3D computational code was not able to simulate the thermal stratification, because it is not able to define the environment temperature (weather) to this program. Therefore, it was decided to choose another program for this goal. In this way, the CE-qual-W2 program was choosen.

Importance of the subject of this thesis:

1- The conclusion and results of this study could be used in other studies and researches, related to the water quality modeling.

2- Controlling of suspended sediment transport in reservoirs and lakes.

3- Selecting the true water releasing level of the reservoir.

4- Formation of stratification in lakes and reservoirs.

This thesis includes six chapters. Chapter 1 aims to present an introductory background to the research subject, briefly. In addition to this, it is focused on previous relevant studies about modeling of reservoirs and lakes and literature review in this chapter.

Chapter 2 discusses the physics of fluid dynamics including theory and governing equations. These equations will be explained in Cartesian, cylindrical and spherical coordinates, thoroughly.

Chapter 3 aims to define computational fluid dynamics. This chapter introduces the CE-qual-W2 and FLOW 3D computational codes, used in this study. In this chapter, several CFD modeling programs will be introduced, briefly. The reasons for use of FLOW 3D will be described. This part of this thesis also introduces the governing equations used in FLOW 3D and CE-qual-W2 programs. In this section, some related and unrelated studies,which done using by FLOW 3D, will be mentioned.

Chapter 4 will define the numerical models of hydrodynamics and the boundary conditions of the reservoir/lake. Models used in the study and results of these simulations are discussed in this chapter.

In Chapter 5, Lake Köyceğiz, as case study, will be introduced. The results of the modeling of case study will be presented. These results will be shown in graphical

figures, tables etc. and will be compared and discussed with each other. The thermal stratification is modeled using another useful program, which is CE-qual-W2. It is also investigated the effect of the dam construction on the Namnam river to the Lake Köyceğiz. This part of Chapter 5 will be investigated for pre-dam and post-dam situations for Namnam river.

Finally, the conclusions of the study are summarized and discussed in chapter 6.

1.5 Literature Review

Sediment transport phenomenon is such as an important hydrodynamic process that affects many river structures and construction facilities. It is as the one of the greatest problems of utilization of surface water resources as the fresh water resoursces in the world. The scientific investigation history on the suspended sediment transport is more than about one and a half centuries. The Study on suspended sediment transport in rivers dated back to more than hundred years ago (Walling and Webb, 1981). First sampling of suspended sediment of rivers was done at Mississippi river in 1845. It is reported many sedimentation processes in reservoirs and lakes by many authors and researchers. Thermal and density stratification are other cases of research studies that many researchers in the field of hydraulic and water resources management have done in recent years, mostly. In this part, some of these studies are classified and mentioned.

1.5.1 Sediment transport

Milliman (1981) studied on the transfer of river-born particular material to the ocean river inputs to ocean systems. Van Rijn (1982) studied on the suspended sediment transport, and investigated the parameters controlling the suspended load transport. In another research, Van Rijn (1985) evaluated on the suspended sediment transport by currents and waves using two-dimensional vertical mathematical model. Williams (1989) studied on the topic titled as sediment concentration versus water discharge during single hydrological events in rivers and investigated the relation between sediment concentration and water discharge. Kostic and Parker (2003) have developed a moving boundary model of deltaic sedimentation in lakes and reservoirs that captures the co-evolution of the river-delta morphology and the associated

deposit. Salant et al. (2008) concluded the directly relation between suspended sediment concentrations and discharge. Algan et al. (2000) investigated the sediment and freshwater discharges of the Anatolian river into the Black sea. Berkun and Aras (2012) researched on the river sediment transport and coastal erosion in the southeastern black sea rivers. Fang & Wang (2000) worked on a topic entitled three-dimensional mathematical model of suspended-sediment transport. They predicted the deposition of suspended sediment in Yangtze River. Fang & Wang (1996) in another study also used the three-dimensional mathematical model of river bed erosion for water-sediment two phase flow. Hyperconcentrated flow and sediment transport at steep slopes is a research that Rickenmann (1991) studied. Ashley et al. (1994) studied on the fluid sediment in combined sewers and indicated that the granular materials are traveled as a pure bed load. Study of sediment transport processes using Reynolds averaged Navier-Stokes and Large-Eddy simulation was a subject that Patryk Widera (2011) worked on. United States Sociecty of Dams, Committee on Hydraulics of Dams, Subcommittee on Reservoir Sedimentation (USSD) studied and prepared a report under titled the modeling sediment movement in reservoirs (2015). The main aim of USSD's report was to inform reserearchers with the existing mathematical methods available to predict sediment movement in and around reservoirs.

1.5.2 Thermal stratification studies

Morkofsky et al. (1973) studied on prediction of water quality in stratified reservoir. Many researchers found the significance of the effects of thermal stratification on the hydrodynamic mixing, contaminant transport, and water quality of reservoirs and lakes (Hodges et al. 2000; Hall, 2008; Okely et al., 2010; Hogg, 2014; Fischer et al., 1979; Kennedy et al., 1982). Dake and Harleman (1969) investigated the analytical and laboratory studies of thermal stratification in lakes. Modiri-Ghareveran et al. (2013) worked on effects of climate change on the thermal regime of a reservoir. They modeled the thermal stratification of Latian dam, which is located in Iran. Henderson-Sellers (1988) considered about the sensitivity of thermal stratification models to changing boundary conditions. Irtem (1991) works on a topic entitled as determination of water movement in stratified bays and its application to the Izmit Bay. Nandalal (1995) investigated the reservoir management under consideration of

stratification and hydraulic phenomena. Gunduz et al. (1998) investigated the development of water quality management strategies for the proposed Isikli Reservoir. Ottosson and Abrahamsson (1998) presented a numerical approach for simulation of heat transport in epilimnion and hypolimnion of the water column. Jin et al. (2000) applied a three-dimensional hydrodynamic and heat transport model for Lake Okeechobee located in South Florida. Gal et al. (2003) simulated the thermal dynamics of lake Kinneret. Ancon consultants company (2006) studied on the thermal stratification of reservoir of the under construction Yusuflu dam. Elci et al. (2007) described the deposition of cohesive sediments in Hartwell Lake located in Georgia, which was thermally stratified reservoir. Baharim et al. (2011) invetigated the effects of thermal stratification on the concentration of iron and manganese in a tropical water supply reservoir.

In recent years, monitoring of water quality in reservoirs and lakes has become one of the most important issues for the determination and prediction of flow condition and long term pattern for future management of reservoirs and lakes (Swanson and Zurawell, 2006; Sharip and Jusoh, 2010; Hanson-Lee, 2003; Sharip and Zakaria, 2008; Gulati and Donk, 2002; Holmes and Kelly, 2012). Many other researches are available in the case of thermal stratificaion included as: Talling, 1963; Lathrop and Lillie, 1980; Imberger, 1985; Monismith et al. 1999; Martin and McCutcheon, 1999; Huang and Jones, 2003; Yang et al. 2015; Lee et al. 2015. Simulation of thermal stratification in urban man made lakes was the topic that Nouri et al. (2004) studied on. Nazariha et al. (2009, 2010) predicted the thermal stratification in proposed Bakhtyari reservoir. Batick (2011) modeled temperature and dissolve oxygen in the Cheatham reservoir. The relationship between dissolved oxygen and depth has been widely investigated by Koretsky et al. (2011) and Mcleod et al. (2011). The physicochemical and biological characteristics of water in reservoirs are mostly under the influence of seasonal variations of inflow river water, water level fluctuations, and the hydraulic residence time (Gikas, 2009). Koretsky et al. (2014) researched on Redox stratification and salinization of three kettle lakes in Southwest Michigan. Boike et al. (2015) worked on subject entitled as thermal processes of thermokarst lakes in the continuous permafrost zone of northern Siberia; observed and modeled the Lena river delta in Siberia. Santos et al. (2015) investigated the short-term thermal stratification and partial overturning events in a warm polymictic

reservoir: effects on distribution of phytoplankton community. Goncu et al. (2015) made research on the thermal stratification in Borabey lake in Turkey. Simulation of thermal stratification and salinity in dam reservoir using CE-qual-W2 software is one of the examples of studies that was done for a reservoir of Baft dam, which was investigated by Ebrahimi et al. (2015). Nsiri et al. (2016) modeled the thermal stratification and the effect on water quality in four reservoirs in Tunisia.

1.5.3 Density stratification (Caused by Concentration of Sediments and Salinity)

Ford and Johnson (1983) Studied and reported an assessment of reservoir density currents and inflow processes. Von Karman (1940) first derived a formula for the propagation speed of head of a steady density flow. He used Bernoulli's equation, assuming a perfect fluid and irrotational flow to get. Keulegan (1957) studied the motion of saline water from locks into horizontal fresh water channels. He suggested the relation between the velocity of a density current head and the depth of the flow head. Ford et al (1980) studied on density flow in Degray lake. Harleman and Stolzenbach (1972) studied the density flows developed by the heated water disposal from a power generation.

An observation of density flows has been monitored by Alavian and Ostrowski (1992) in reservoirs of the Tennessee valley. Hebbert et al. (1971) investigated about these types of flows that was occured in Wellington dam's reservoir located in Western Australia. Lowe et al. (2002) derived the theoretical head speed of the currents based on the analysis of Holyer and Huppert (1980), and De Rooij et al. (1999) assuming the flow to be energy-conserving and applied Bernoulli's equation along streamlines of the intrusion currents. In addition, Singh and Shah (1971) studied on plunging phenomenon of density currents in reservoirs, Savage and Brimberg (1975) analysed the plunging phenomenon in reservoirs. Akiyama and Stefan (1984) summarized equations proposed by several investigators for determining the plunge depth. Farrell and Stefan (1986) reported about buoyancy induced plunging flow into reservoirs and coastal regions in a project of Minnesota and studied on mathematical modelling of plunging reservoir flows. Cossu et al. (2015) investigated the subject under the title of seasonal variability in turbidity currents in Lake Ohau and their influence on sedimentation.

2. PHYSICS OF FLUID DYNAMICS

Behavior of fluids in motion is studied by Fluid dynamics. In a better definition, the fluid mechanics science is the study of the flow of fluids known as hydrodynamics. In fluid dynamics, fundamental laws can be used to derive governing differential equations. These laws are conservation of mass or continuity, Newton's second law known as conservation of linear momentum, the first law of thermodynamics named as conservation of energy. The governing equations, which used in fluid dynamics, will be discussed in this chapter.

2.1 Governing Equations

The governing equations, used in fluid dynamics, are discussed in this chapter. In fluid dynamics, the term Navier-Stokes is usually used to include both momentum and continuity equations, and even energy equation sometimes. Most of the problems in fluid dynamics can be described mathematically by using continuity and momentum equations.

Laminar and turbulent flow are two conditions that can occur in fluid flow. In laminar flow, a fluid particle flows in parallel layers with no disruption between the layers of flow. Flow condition will change from laminar into turbulent flow, when the fluid viscosity is low and characteristic length and flow velocity have high values (Batchelor, 2000). In other words, in the turbulent flow, fluid particles are moving in irregular paths due to the high kinetic energy and as well as overcoming the viscosity force. Momentum transfer in laminar flow is in the molecular scale and momentum transfer occurs with collision of molecules with each other. A criterion for determination of laminar and turbulent flows is Reynolds number. The dimensionless Reynolds number is an important parameter in the equations that determine whether flow conditions lead to laminar or turbulent. Flows with Reynolds number of larger than 5000 are typically turbulent, while those at low Reynolds numbers usually

remain laminar **(**Tennekes and Lumley, 1972). The governing equations for laminar and turbulent conditions of flow have some differences. In this chapter, both the laminar and turbulent flow governing equations are presented and described in detail.

2.1.1 Continuity Equation

Figure 2.1, for a selected infinitesimal fixed control volume, expressions of conservation of mass are represented as (McDonough, 2009; White, n.d.):

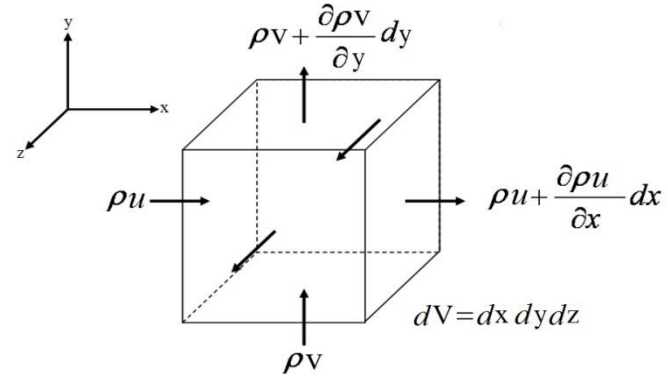

Figure 2.1: Selected infinitesimal fixed control volume (Anderson, 2009).

$$\int_{CV} \frac{\partial \rho}{\partial t} dV = -\int_{CS} \rho n.udS \tag{2.1}$$

or,

$$\int_{CV} \frac{\partial \rho}{\partial t} dV + \int_{CS} \rho n.udS = 0 \tag{2.2}$$

where, S is the surface of control volume V. The term in the left side of equation (2.1) shows the ratio of change of mass, and the term in the right side of this equation presents the net inflow of mass. This term is known as the flux term. This term can be analyzed as follows (White, n.d.; Tryggvason, 2011):

$$\int_{CS} \rho U_i n_i dA = \int_{CS(x)} \rho U_i n_i dA + \int_{CS(y)} \rho U_i n_i dA + \int_{CS(z)} \rho U_i n_i dA \tag{2.3}$$

The flux integrals through surfaces perpendicular to x, y, and z axis are:

$$\int_{CS(x)} \rho U_i n_i dA = -\rho u\, dy\, dz + \left[\rho u + \frac{\partial(\rho u)}{\partial x} dx\right] dy\, dz = \frac{\partial(\rho u)}{\partial x} dx\, dy\, dz = \frac{\partial(\rho u)}{\partial x} dV \tag{2.4}$$

$$\int_{CS(y)} \rho U_i n_i dA = -\rho v\, dx\, dz + \left[\rho v + \frac{\partial(\rho v)}{\partial y} dy\right] dx\, dz = \frac{\partial(\rho v)}{\partial y} dx\, dy\, dz = \frac{\partial(\rho v)}{\partial y} dV \quad (2.5)$$

$$\int_{CS(z)} \rho U_i n_i dA = -\rho w\, dx\, dy + \left[\rho w + \frac{\partial(\rho w)}{\partial z} dz\right] dx\, dy = \frac{\partial(\rho w)}{\partial z} dx\, dy\, dz = \frac{\partial(\rho w)}{\partial z} dV \quad (2.6)$$

In equation (2.2), if the surface integral is converted to the volume integral, then it gives the equation (2.7) (White, n.d.):

$$\int_V \left[\frac{\partial \rho}{\partial t} + \nabla.(\rho u)\right] dV = 0 \quad (2.7)$$

For the selected control volume, equation (2.8) is given. This is known as conservative form of mass conservation equation. Conservation forms of equations can be obtained by applying the underlying physical principle (mass conservation) to a fluid element fixed in space.

$$\left[\frac{\partial \rho}{\partial t} + \nabla.(\rho u)\right] = 0 \quad (2.8)$$

With vector analysis, equation (2.8) is changed to:

$$\frac{D\rho}{Dt} + \rho(\nabla.\vec{u}) = 0 \quad (2.9)$$

or,

$$\frac{\partial \rho}{\partial t} + u.\nabla\rho + \rho\nabla.u = 0 \quad (2.10)$$

Equation (2.9) also is known as non-conservative form of mass conservation equation. Non-conservative forms are obtained by considering fluid elements moving in the flow field.

The $\frac{D\rho}{Dt}$ term in equation (2.9) is known as material derivatives of ρ. This state is described in the following form (White, n.d.; Anderson, 2009; McDonough, 2009).

$$\frac{D\rho}{Dt} = \frac{\partial \rho}{\partial t} + u.\nabla\rho \quad (2.11)$$

First term of the right hand side of equation (2.11) is the partial time derivative or local derivative. Last term of this equation is named as the convective derivative of ρ. The final form of continuity equation in cartesian coordinates (x, y, z) is presented in equation (2.12). (Unes, 2004; Bakker, 2006; Bird et al., 1960; Morrison, 2011).

$$\frac{\partial \rho}{\partial t} + \frac{\partial}{\partial x}(\rho u) + \frac{\partial}{\partial y}(\rho v) + \frac{\partial}{\partial z}(\rho w) = 0 \tag{2.12}$$

For cylindrical coordinates (r, θ, z), equation (2.12) is changed to (Bird et al., 1960):

$$\frac{\partial \rho}{\partial t} + \frac{1}{r}\frac{\partial}{\partial r}(\rho r u) + \frac{1}{r}\frac{\partial}{\partial \theta}(\rho v) + \frac{\partial}{\partial z}(\rho w) = 0 \tag{2.13}$$

and in spherical coordinates (r, θ, ϕ) to (Bird et al.,1960):

$$\frac{\partial \rho}{\partial t} + \frac{1}{r^2}\frac{\partial}{\partial r}(\rho r^2 u) + \frac{1}{r sin\theta}\frac{\partial}{\partial \theta}(\rho v sin\theta) + \frac{1}{r sin\theta}\frac{\partial}{\partial \phi}(\rho w) = 0 \tag{2.14}$$

If the density of a fluid element does not change during its motion, this flow is said to be incompressible. In other words, the density of a fluid element should not change in time as it moves through space. In incompressible flow conditions, the divergence of the velocity field is identically zero. The density field need not be uniform in incompressible flow and the flow is independent of being permanent or not. Therefore, the term $\frac{\partial \rho}{\partial t}$ is equal to zero in equation (2.12) and ρ is constant. For incompressible flow, the continuity equation is given in equation (2.15) (Sumer et al., n.d.).

$$\nabla . V = 0 \tag{2.15}$$

This equation for Cartesian coordinates systems gives (Ilgaz et al., n.d; Anderson, 2009):

$$\frac{\partial u}{\partial x} + \frac{\partial v}{\partial y} + \frac{\partial w}{\partial z} = \mathbf{0} \tag{2.16}$$

2.1.2 Momentum Equation

The general momentum equation is also known as the equation of motion or the Navier-Stokes equation. The equation of continuity is frequently used in conjunction with the momentum equation.

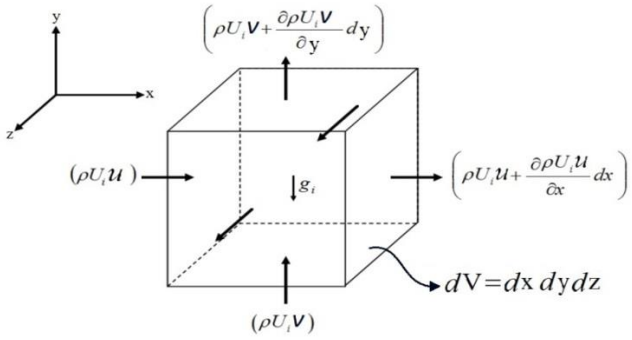

Figure 2.2: Selected infinitesimal fixed control volume (Anderson, 2009).

From Figure 2.2, the momentum conservation integral equation is given as equation (2.17) (Tryggvason, 2011; McDonough, 2009).

$$\sum F_i = \frac{\partial}{\partial t}\int_{CV} \rho U_i dV + \int_{CS} \rho\, U_i U_j n_j dA \tag{2.17}$$

The flux term can be analyzed as follows:

$$\int_{CS} \rho U_i U_j n_j dA = \int_{CS(x)} \rho U_i U_j n_j dA + \int_{CS(y)} \rho U_i U_j n_j dA + \int_{CS(z)} \rho U_i U_j n_j dA \tag{2.18}$$

The momentum flux through the surfaces in x, y and z directions are presented as:

$$\int_{CS(x)} \rho U_i U_j n_j dA = -\rho U_i u\, dy\, dz + \left[\rho U_i u\, dy\, dz + \frac{\partial}{\partial x}(\rho U_i u) dx\right] dy\, dz = \frac{\partial}{\partial x}(\rho U_i u) dx\, dy\, dz = \frac{\partial}{\partial x}(\rho U_i u) dV \tag{2.19}$$

$$\int_{CS(y)} \rho U_i U_j n_j dA = -\rho U_i v\, dx\, dz + \left[\rho U_i v\, dx\, dz + \frac{\partial}{\partial y}(\rho U_i v) dy\right] dx\, dz = \frac{\partial}{\partial y}(\rho U_i v) dx\, dy\, dz = \frac{\partial}{\partial y}(\rho U_i v) dV \tag{2.20}$$

$$\int_{CS(z)} \rho U_i U_j n_j dA = -\rho U_i w\, dx\, dy + \left[\rho U_i w\, dx\, dy + \frac{\partial}{\partial z}(\rho U_i w) dz\right] dx\, dy = \frac{\partial}{\partial z}(\rho U_i w) dx\, dy\, dz = \frac{\partial}{\partial z}(\rho U_i w) dV \tag{2.21}$$

From equation (2.17), $\sum F_i$ could be determined as:

$$\sum F_i = \left[U_i \frac{\partial \rho}{\partial t} + \left(\rho \frac{\partial U_i}{\partial t}\right) + U_i \frac{\partial}{\partial x_j}(\rho U_j) + \rho U_j \frac{\partial U_i}{\partial x_j}\right] dV =$$

$$U_i \underbrace{\left[\frac{\partial \rho}{\partial t} + \frac{\partial}{\partial x_j}(\rho U_j)\right]}_{Continuity\ Equation=0} dV + \rho \underbrace{\left[\frac{\partial U_i}{\partial t} + U_j \frac{\partial U_i}{\partial x_j}\right]}_{\left(\frac{DU_i}{Dt}\right)} dV \qquad (2.22)$$

$Substantial\ Derivative\ of\ U_i$

The result of equation (2.22) is obtained here as equation (2.23):

$$\sum F_i = \rho \frac{DU_i}{Dt} dV \qquad (2.23)$$

In the diffrential control volume two kinds of forces are available as body and surface forces. It can be defined as relation (2.24):

$$\frac{dP_i}{dt} = \sum F_i = dF_{Body_i} + dF_{Surface_i} = \rho \frac{dU_i}{dt} dV \qquad (2.24)$$

For body forces, here only the gravitational force is noted. Therefore:

$$dF_{Body_i} = \rho\ dV\ g_i \qquad (2.25)$$

The surface force includes the stresses acting on the control surfaces. Regarding to the Figure 2.3, the differential surface forces in x, y and z directions are presented as equations (2.26), (2.27) and (2.28):

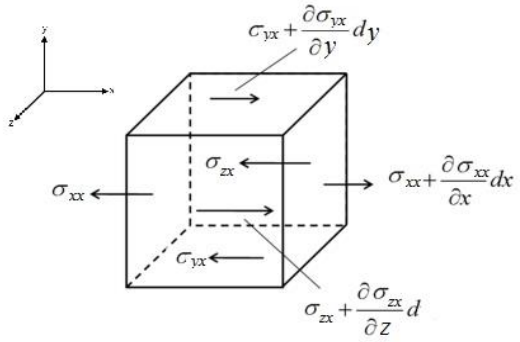

Figure 2.3: Stresses on the surface of the differential control volume in the x direction.

$$dF_{Surface_{(x)}} = \frac{\partial \sigma_{xx}}{\partial x} dx\ dy\ dz + \frac{\partial \sigma_{yx}}{\partial y} dx\ dy\ dz + \frac{\partial \sigma_{zx}}{\partial z} dx\ dy\ dz \qquad (2.26)$$

$$dF_{Surface_{(y)}} = \frac{\partial \sigma_{xy}}{\partial x} dx\, dy\, dz + \frac{\partial \sigma_{yy}}{\partial y} dx\, dy\, dz + \frac{\partial \sigma_{zy}}{\partial z} dx\, dy\, dz \quad (2.27)$$

$$dF_{Surface_{(z)}} = \frac{\partial \sigma_{xz}}{\partial x} dx\, dy\, dz + \frac{\partial \sigma_{yz}}{\partial y} dx\, dy\, dz + \frac{\partial \sigma_{zz}}{\partial z} dx\, dy\, dz \quad (2.28)$$

With knowing that $dV = dx\, dy\, dz$ and $\sigma_{ij} = -p\delta_{ij} + \tau_{ij}$, following results are obtained.

$$dF_{Surface1} = \left(-\frac{\partial P}{\partial x} + \frac{\partial \tau_{xx}}{\partial x} + \frac{\partial \tau_{yx}}{\partial y} + \frac{\partial \tau_{zx}}{\partial z}\right) dV \quad (2.29)$$

$$dF_{Surface_i} = \left(-\frac{\partial P}{\partial x_i} + \frac{\partial \tau_{ji}}{\partial x_j}\right) dV \quad (2.30)$$

Equation (2.30) is the tensor form of the differential surface forces in i direction. Finally, the diffential surface forces are obtained as equation (2.31),

$$dF_{Surface_i} = \left(-\frac{\partial P}{\partial x_i} + \frac{\partial \tau_{ij}}{\partial x_j}\right) dV \quad (2.31)$$

With knowing the τ_{ij} is a symmetric tensor $(\tau_{ji} = \tau_{ij})$ (McDonough, 2009) and inserting the equation (2.31) into equation (2.24):

$$\rho \frac{DU_i}{Dt} = \rho g_i - \frac{\partial P}{\partial x_i} + \frac{\partial \tau_{ij}}{\partial x_j} \quad (2.32)$$

is obtained as the simplified equation. The left term of this equation is the material derivative (Raudkivi, 1976).

$$\underbrace{\rho \frac{\partial U_i}{\partial t} + \rho U_j \frac{\partial U_i}{\partial x_j}}_{\text{Material Derivative}} = \rho g_i - \frac{\partial P}{\partial x_i} + \frac{\partial \tau_{ij}}{\partial x_j} \quad (2.33)$$

Totally, the most common expression of the momentum equation is presented as equation (2.34).

$$\frac{\partial u}{\partial t} + u.\nabla u = f - \frac{1}{\rho}\nabla P + \upsilon \nabla^2 u \quad (2.34)$$

Equation (2.35) is another most general form of the Navier-Stokes equation for incompressible fluids.

$$\rho \frac{Du}{Dt} = \rho f - \nabla P + \mu \nabla^2 u \tag{2.35}$$

In order to be able to use an Eulerian description, material derivative at the left hand side, which is the acceleration vector, can be replaced with the sum of local and convective accelerations to get.

$$\rho \left[\frac{\partial u}{\partial t} + (u.\nabla)u\right] = \rho f - \nabla P + \mu \nabla^2 u \tag{2.36}$$

In this equation, $\frac{\partial u}{\partial t}$ is the unsteady acceleration, $u.\nabla u$ is the convection acceleration, f is other body force per unit mass, $\mu\nabla^2 u$ is the total viscous force, $-\nabla P$ is the pressure gradient terms. The body forces include the gravitational, buoyancy, coriolis and other forces. Here, if the weight of the fluid is the only body force, f can be replaced with the gravitational acceleration vector (g).

$\rho \left[\frac{\partial u}{\partial t} + (u.\nabla)u\right]$ ⟶ Inertia (per volume)

$-\nabla P + \mu \nabla^2 u$ ⟶ Divergence of stress

In Cartesian coordinates, more specifically expressed forms of the momentum equation of x, y and z components are presented as equations (2.37), (2.38), (2.39), respectively, as (Bird et al., 1960; Raudkivi, 1976; McDonough, 2009; Morrison, 2011):

$$\underbrace{\frac{\partial u}{\partial t} + u\frac{\partial u}{\partial x} + v\frac{\partial u}{\partial y} + w\frac{\partial u}{\partial z}}_{Acceleration} = \underbrace{-\frac{1}{\rho}\frac{\partial P}{\partial x}}_{\substack{Pressure \\ force}} + \underbrace{g_x}_{\substack{Gravity \\ force}} + \underbrace{v(\frac{\partial^2 u}{\partial x^2} + \frac{\partial^2 u}{\partial y^2} + \frac{\partial^2 u}{\partial z^2})}_{\substack{Shear\ or\ Friction \\ force}} \tag{2.37}$$

$$\frac{\partial v}{\partial t} + u\frac{\partial v}{\partial x} + v\frac{\partial v}{\partial y} + w\frac{\partial v}{\partial z} = -\frac{1}{\rho}\frac{\partial P}{\partial y} + g_y + v(\frac{\partial^2 v}{\partial x^2} + \frac{\partial^2 v}{\partial y^2} + \frac{\partial^2 v}{\partial z^2}) \tag{2.38}$$

$$\frac{\partial w}{\partial t} + u\frac{\partial w}{\partial x} + v\frac{\partial w}{\partial y} + w\frac{\partial w}{\partial z} = -\frac{1}{\rho}\frac{\partial P}{\partial z} + g_z + v(\frac{\partial^2 w}{\partial x^2} + \frac{\partial^2 w}{\partial y^2} + \frac{\partial^2 w}{\partial z^2}) \tag{2.39}$$

In equations (2.37), (2.38) and (2.39), the values of g_x, g_y, g_z depend on the orientation of gravity with respect to the chosen set of coordinates. In turbulent flows, these equation briefly can be presented as equation (2.40), which will be discussed later.

$$\frac{\partial u_i}{\partial t} + \frac{\partial u_i u_j}{\partial x_j} = \frac{F_i}{\rho} - \frac{1}{\rho}\frac{\partial P}{\partial x_i} + \frac{\partial}{\partial x_j}\left(\upsilon \frac{\partial u_i}{\partial x_j} - \overline{u_i' u_j'}\right) \tag{2.40}$$

where, the i and j indexes are the Cartesian directions, which is equal to 1 for x direction, equal to 2 for y and equal to 3 for z direction. The index j is the Cartesian directions perpendicular to i, u_i is the Cartesian component of the velocity along the x_i direction for i=1,2,3, ρ is the fluid density, P is pressure force, υ is the kinematic molecular viscosity, F_i is component of the body forces per unit volume in the i-direction. The term $-\rho\overline{u_i' u_j'}$ is presented as turbulent stresses.

In cylindrical coordinates (r, θ, z), the momentum equations are changed to the equations given below (Morrison, 2011).

$$\left(\frac{\partial u}{\partial t} + u\frac{\partial u}{\partial r} + \frac{v}{r}\frac{\partial u}{\partial \theta} + w\frac{\partial u}{\partial z} - \frac{v^2}{r}\right) = -\frac{1}{\rho}\frac{\partial P}{\partial r} + \upsilon\left[\frac{1}{r}\frac{\partial}{\partial r}\left(r\frac{\partial u}{\partial r}\right) + \frac{1}{r^2}\frac{\partial^2 u}{\partial \theta^2} + \frac{\partial^2 u}{\partial z^2} - \frac{u}{r^2} - \frac{2}{r^2}\frac{\partial v}{\partial \theta}\right] + g_r \tag{2.41}$$

$$\left(\frac{\partial v}{\partial t} + u\frac{\partial v}{\partial r} + \frac{v}{r}\frac{\partial v}{\partial \theta} + w\frac{\partial v}{\partial z} - \frac{uv}{r}\right) = -\frac{1}{\rho}\frac{1}{r}\frac{\partial P}{\partial \theta} + \upsilon\left[\frac{1}{r}\frac{\partial}{\partial r}\left(r\frac{\partial v}{\partial r}\right) + \frac{1}{r^2}\frac{\partial^2 v}{\partial \theta^2} + \frac{\partial^2 v}{\partial z^2} + \frac{2}{r^2}\frac{\partial u}{\partial \theta} - \frac{v}{r^2}\right] + g_\theta \tag{2.42}$$

$$\left(\frac{\partial w}{\partial t} + u\frac{\partial w}{\partial r} + \frac{v}{r}\frac{\partial w}{\partial \theta} + w\frac{\partial w}{\partial z}\right) = -\frac{1}{\rho}\frac{\partial P}{\partial z} + \upsilon\left[\frac{1}{r}\frac{\partial}{\partial r}\left(r\frac{\partial w}{\partial r}\right) + \frac{1}{r^2}\frac{\partial^2 w}{\partial \theta^2} + \frac{\partial^2 w}{\partial z^2}\right] + g_z \tag{2.43}$$

In spherical coordinates (r, θ, ϕ), momentum equations are converted into Equations (2.44), (2.45) and (2.46) (Morrison, 2011):

$$\left(\frac{\partial u}{\partial t}+u\frac{\partial u}{\partial r}+\frac{v}{r\sin(\theta)}\frac{\partial u}{\partial \theta}+\frac{w}{r}\frac{\partial u}{\partial \emptyset}-\frac{v^2+w^2}{r}\right)=-\frac{1}{\rho}\frac{\partial P}{\partial r}+\upsilon\left[\frac{1}{r^2}\frac{\partial}{\partial r}\left(r^2\frac{\partial u}{\partial r}\right)+\frac{1}{r^2\sin(\theta)^2}\frac{\partial^2 u}{\partial \theta^2}+\right.$$

$$\left.\frac{1}{r^2\sin(\theta)}\frac{\partial}{\partial \emptyset}\left(\sin(\theta)\frac{\partial u}{\partial \emptyset}\right)-2\frac{u+\frac{\partial w}{\partial \emptyset}+w\cot(\theta)}{r^2}-\frac{2}{r^2\sin(\theta)}\frac{\partial w}{\partial \theta}\right]+g_r \qquad (2.44)$$

$$\left(\frac{\partial v}{\partial t}+u\frac{\partial v}{\partial r}+\frac{v}{r\,sin(\theta)}\frac{\partial v}{\partial \theta}+\frac{w}{r}\frac{\partial v}{\partial \emptyset}+\frac{uv+vw\,cot(\theta)}{r}\right)=-\frac{1}{\rho}\frac{1}{r\,sin(\theta)}\frac{\partial P}{\partial \theta}+\upsilon\left[\frac{1}{r^2}\frac{\partial}{\partial r}\left(r^2\frac{\partial v}{\partial r}\right)+\right.$$

$$\left.\frac{1}{r^2\,sin(\theta)^2}\frac{\partial^2 v}{\partial \theta^2}+\frac{1}{r^2\,sin(\theta)}\frac{\partial}{\partial \emptyset}\left(sin(\theta)\frac{\partial v}{\partial \emptyset}\right)+\frac{2\,sin(\theta)\frac{\partial u}{\partial \theta}+2\,cos(\theta)\frac{\partial w}{\partial \theta}-v}{r^2\,sin(\theta)^2}\right]+g_\theta \qquad (2.45)$$

$$\left(\frac{\partial w}{\partial t}+u\frac{\partial w}{\partial r}+\frac{v}{r\sin(\theta)}\frac{\partial w}{\partial \theta}+\frac{w}{r}\frac{\partial w}{\partial \emptyset}+\frac{uw-v^2\cot(\theta)}{r}\right)=-\frac{1}{\rho}\frac{1}{r}\frac{\partial P}{\partial \emptyset}+\upsilon\left[\frac{1}{r^2}\frac{\partial}{\partial r}\left(r^2\frac{\partial w}{\partial r}\right)+\right.$$

$$\left.\frac{1}{r^2\sin(\theta)^2}\frac{\partial^2 w}{\partial \theta^2}+\frac{1}{r^2\sin(\theta)}\frac{\partial}{\partial \emptyset}\left(\sin(\theta)\frac{\partial w}{\partial \emptyset}\right)+\frac{2}{r^2}\frac{\partial u}{\partial \emptyset}-\frac{w+2\cos(\theta)\frac{\partial v}{\partial \theta}}{r^2\sin(\theta)^2}\right]+g_\emptyset \qquad (2.46)$$

u, v and w are the velocity components in x, y, z directions for cartesian coordinate system, in r, θ, z, for cylindrical coordinate systems and for spherical systems in r, θ, ϕ directions.

2.1.3 Energy Equation

A statement of this principle is the first law of thermodynamics, which, when applied to the moving fluid element. The law of conservation of energy states that the total energy of an isolated system is constant; energy can be transformed from one form to another, but cannot be created or destroyed.

The energy equation for temperature (thermal energy equation) in Cartesian coordinate systems and laminar flow condition is given by (Unes, 2008):

$$\frac{\partial T}{\partial t}+u\frac{\partial T}{\partial x}+v\frac{\partial T}{\partial y}=\alpha\left(\frac{\partial^2 T}{\partial x^2}+\frac{\partial^2 T}{\partial y^2}\right) \qquad (2.47)$$

where, α is the heat dissipation also called as diffusion coefficient, T is temperature. α is calculated by the equation (2.48).

$$\alpha=\frac{\upsilon}{P_r} \qquad (2.48)$$

In which, υ is the kinematic viscosity, P_r is the dimensionless Prandtl number. For three-dimensional energy equation and turbulent flows, equation (2.49) is obtained (Unes, 2008).

$$\frac{\partial \overline{T}}{\partial t} + \overline{u}\frac{\partial \overline{T}}{\partial x} + \overline{v}\frac{\partial \overline{T}}{\partial y} + \overline{w}\frac{\partial \overline{T}}{\partial z} + f\overline{u} = \alpha_{eff}\left(\frac{\partial^2 \overline{T}}{\partial x^2} + \frac{\partial^2 \overline{T}}{\partial y^2} + \frac{\partial^2 \overline{T}}{\partial z^2}\right) \quad (2.49)$$

In equation (2.49), $\overline{u}$, $\overline{v}$, and $\overline{w}$ are the temporal average velocity components in direction of x, y, and z axis, respectively. Also, for the temperature change (T) in turbulent flow (Unes, 2004):

$$T = \overline{T} + T' \quad (2.50)$$

In equation (2.50), $\overline{T}$ and $T'$are the temporal average temperature and fluctuating temperature values, respectively. In turbulent flows α_{eff} is calculated by:

$$\alpha_{eff} = \left({}^{\upsilon}/_{P_r}\right) + \left({}^{\upsilon_t}/_{P_{r_t}}\right) \quad (2.51)$$

Here, P_r is the dimensionless Prandtl number and P_{r_t} is the turbulent Prandtl number (Coulson, 1999). Prandtl number is the ratio of momentum diffusivity to thermal diffusivity and calculated using following equation.

$$Pr = \frac{viscous\ diffusion\ rate}{thermal\ diffusion\ rate}\frac{\upsilon}{\alpha} = \frac{{}^{\mu}/_{\rho}}{{}^{\kappa}/_{c_P\rho}} = \frac{c_p\mu}{\kappa} \quad (2.52)$$

where, υ is the momentum diffusivity or kinematic viscosity (m^2/s), α is thermal diffusivity (m^2/s), μ is dynamic viscosity (Ns/M2), κ is thermal conductivity (W/m-k), c_p is the specific heat (J/kg-K) and ρ is density (kg/m^3).

2.1.4 Suspended Sediment Transport Equation

Mass conservation law for suspended sediment transport can be written as follows:

$$Sediment\ accumulation\ =$$
$$Input\ sediments - Output\ sediments \pm Multiplier\ or\ reducer\ resources$$

This relationship is expressed mathematically as Equation 2.53.

$$\underbrace{\frac{\partial c}{\partial t}}_{I} + \underbrace{\frac{\partial uc}{\partial x} + \frac{\partial vc}{\partial y} + \frac{\partial wc}{\partial z}}_{II} + \underbrace{\frac{\partial}{\partial x}\overline{u'c'} + \frac{\partial}{\partial y}\overline{v'c'} + \frac{\partial}{\partial z}\overline{w'c'}}_{III} = \underbrace{S_c}_{IV} \tag{2.53}$$

Term (I) in equation (2.53) is related to the local effect of suspended sediment concentration, (II) is depended on diffusion by motion, (III) is related to turbulent diffusion, (IV) is the source or sink, reduction or increasing of sediment or pollution. S_c is the multiplier or reducer source. The other form of the convection-diffusion suspended sediment equation could be written in general as (Bakker, 2006; Raudkivi, 1976; Raberts and Webster, n.d.):

$$\frac{\partial c}{\partial t} + u_i \frac{\partial c}{\partial x_i} = \frac{\partial}{\partial x_i}\left(\Gamma \frac{\partial c}{\partial x_i} - \overline{u_i' c'}\right) + S_c \tag{2.54}$$

where, c is the suspended sediment concentration, Γ is the molecular diffusivity coefficient, S_c is the sink or source of c. The term $-\overline{u_i' c'}$ is named as the turbulent diffusion of c. This term results from averaging of the original Navier-Stokes equations, when the Reynolds decomposition used in this equations.

2.1.5 Non-dimensional Navier-Stokes Equations

Generally, the dimensionless Navier-Stokes Equations are used in fluid dynamics. When the length dimension is taken as L and velocity dimension is taken as U, we have below ralations (Cengel, n.d.; Tryggvason, 2011):

$$\overline{u}, \overline{v} = \frac{u,v}{U}\,,\ \overline{x}, \overline{y} = \frac{x,y}{L}\,,\ \overline{t} = \frac{U}{L}t\,,\ \overline{\nabla} = L\nabla\,,\ \overline{f} = \frac{L}{U^2}f\,,\ \overline{P} = \frac{P}{\rho U^2} \tag{2.55}$$

If Equations (2.55) are inserted into the Navier-Stokes equation (2.35), and all terms of this equation multiplied by $\overline{f}$ $(\frac{L}{U^2})$ (Cengel, n.d.; Tryggvason, 2011):

$$\frac{U^2}{L}\left(\frac{\partial \overline{u}}{\partial \overline{t}} + \overline{u}\frac{\partial \overline{u}}{\partial \overline{x}} + \overline{v}\frac{\partial \overline{u}}{\partial \overline{y}}\right) = -\frac{1}{L\rho}\frac{\partial P}{\partial \overline{x}} + \frac{U}{L^2}\frac{\mu}{\rho}\left(\frac{\partial^2 \overline{u}}{\partial \overline{x^2}} + \frac{\partial^2 \overline{u}}{\partial \overline{y^2}}\right) \tag{2.56}$$

$$\left(\frac{\partial \overline{u}}{\partial \overline{t}} + \overline{u}\frac{\partial \overline{u}}{\partial \overline{x}} + \overline{v}\frac{\partial \overline{u}}{\partial \overline{y}}\right) = -\frac{L}{U^2}\frac{1}{L\rho}\frac{\partial P}{\partial \overline{x}} + \frac{L}{U^2}\frac{U}{L^2}\frac{\mu}{\rho}\left(\frac{\partial^2 \overline{u}}{\partial \overline{x}^2} + \frac{\partial^2 \overline{u}}{\partial \overline{y}^2}\right) \quad (2.57)$$

are obtained.

By knowing that $\overline{P} = \frac{P}{\rho U^2}$ and $Re = \frac{\rho UL}{\mu}$, momentum equations are obtained as equations (2.58), (2.59) and (2.60) (Faber, 1995).

$$\frac{\partial u}{\partial t} + u.\nabla u = -\nabla P + \frac{1}{Re}\nabla^2 u + f \quad (2.58)$$

$$\frac{\partial \overline{u}}{\partial \overline{t}} + \overline{u}\frac{\partial \overline{u}}{\partial \overline{x}} + \overline{v}\frac{\partial \overline{u}}{\partial \overline{y}} = -\frac{\partial \overline{P}}{\partial \overline{x}} + \frac{1}{Re}\left(\frac{\partial^2 \overline{u}}{\partial \overline{x}^2} + \frac{\partial^2 \overline{u}}{\partial \overline{y}^2}\right) \quad (2.59)$$

$$\frac{\partial \overline{v}}{\partial \overline{t}} + \overline{u}\frac{\partial \overline{v}}{\partial \overline{x}} + \overline{v}\frac{\partial \overline{v}}{\partial \overline{y}} = -\frac{\partial \overline{P}}{\partial \overline{y}} + \frac{1}{Re}\left(\frac{\partial^2 \overline{v}}{\partial \overline{x}^2} + \frac{\partial^2 \overline{v}}{\partial \overline{y}^2}\right) \quad (2.60)$$

Reynolds number is one of basic dimensionless numbers in fluid mechanics. The Reynolds number can be defined for several different situations, where a fluid is in relative motion to a surface. Reynolds number is the ratio of the inertial forces to the viscous forces or also the ratio of the total momentum transfer to the molecular momentum transfer. The continuity equation is unchanged here.

$$\frac{\partial \overline{u}}{\partial \overline{x}} + \frac{\partial \overline{v}}{\partial \overline{y}} = 0 \quad (2.61)$$

2.1.6 Reynolds Average Navier-Stokes Equations

This is also known as the time average Navier-Stokes equations. Experimental studies of characteristics of turbulent flow are very costly and time-consuming and the level of details are also low. On the other hand, due to the random nature of the motion of particles and fluid, and their hard irregularities in turbulent flows, the theoretical study of this type of flows is difficult and even impossible. Available models for solving turbulence have not the ability to investigate the turbulence with unlimited details, but they can produce some valuable information. Basis of governing equations are the same for solving the both laminar and turbulent flows and the continuity and Navier-Stokes equations are used. The Reynolds averaged

Navier-Stokes equations are time-averaged equations of motion for fluid flow and this is the difference between laminar and turbulent equations. Other words, when the flow has the turbulent condition, it is preferable to decompose the instantaneous variables into a mean value and a fluctuating value. Therefore, in Navier-Stokes equations a number of additional terms appear which are interpreted as type of stress. This stresses are known as turbulence stresses or Reynolds stresses. Turbulence models are used for solving these additional terms in Navier-Stokes equations. Turbulent velocity fluctuation and time-averaged values are presented as the Figure 2.4 (Sumer, n.d.; McDonough, 2009).

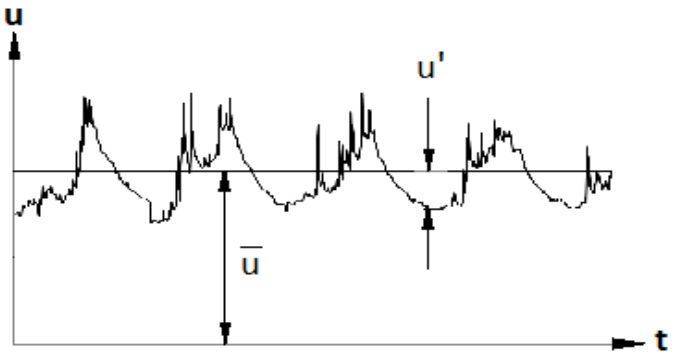

Figure 2.4: Turbulent velocity fluctuation and mean values (Sumer, n.d.; McDonough, 2009).

In order to be able to take a time-average, the momentary value is decomposed into the parts mean value and fluctuating value. The momentary velocity component is u, $\overline{u}$ is the time-averaged value and u' is the fluctuating velocity. From this definition, the decomposition can be written mathematically as (Sumer, M.):

$$u_i = \overline{u}_i + u_i' \quad , \quad v_i = \overline{v}_i + v_i' \quad , \quad w_i = \overline{w}_i + w_i' \tag{2.62}$$

Moreover, for pressure it could be written as (Nguyen, 2005):

$$P = \overline{P} + P' \tag{2.63}$$

Reason of these decompositions is that the Navier-Stokes equations can be used to study about the turbulent flows.

With taking a time-averaged of resulting equations and the time-averaged values of the fluctuating values are defined to be zero as (2.65) (Roberts and Webster, n.d.).

$$\overline{u} = \frac{1}{\Delta t}\int_{t_0}^{t_0+t_1} u\, dt \tag{2.64}$$

$$\overline{u'} = 0,\ \overline{v'} = 0,\ \overline{w'} = 0,\ \overline{P'} = 0 \tag{2.65}$$

If equations (2.64) and (2.65) are substituted in Navier-Stokes and continuity equations, the continuity equation is changed to equation (2.66):

$$\frac{\partial \overline{u}}{\partial x} + \frac{\partial u'}{\partial x} + \frac{\partial \overline{v}}{\partial y} + \frac{\partial v'}{\partial y} + \frac{\partial \overline{w}}{\partial z} + \frac{\partial w'}{\partial z} = 0 \tag{2.66}$$

With applying the time-average for equation (2.66), the converted equation is shown in equation 2.67.

$$\overline{\frac{\partial \overline{u}}{\partial x} + \frac{\partial u'}{\partial x} + \frac{\partial \overline{v}}{\partial y} + \frac{\partial v'}{\partial y} + \frac{\partial \overline{w}}{\partial z} + \frac{\partial w'}{\partial z}} = 0 \tag{2.67}$$

It is useful and necessary to knowing the following relations (Savli, 2012):

$$\overline{\frac{\partial \overline{u}}{\partial x}} = \frac{1}{\Delta t}\int_{t_0}^{t_0+t_1} \frac{\partial u}{\partial x} dt = \frac{1}{\Delta t}\frac{\partial}{\partial x}\int_{t_0}^{t_0+t_1} u\, dt = \frac{\partial \overline{u}}{\partial x} \tag{2.68}$$

$$\overline{\frac{\partial u'}{\partial x}} = \frac{1}{\Delta t}\int_{t_0}^{t_0+t_1} \frac{\partial u'}{\partial x} dt = \frac{1}{\Delta t}\frac{\partial}{\partial x}\int_{t_0}^{t_0+t_1} u'\, dt = 0 \tag{2.69}$$

$$\overline{\overline{f}} = \overline{f},\ \overline{f+g} = \overline{f} + \overline{g},\ \overline{\overline{f}.g} = \overline{f}.\overline{g} \tag{2.70}$$

$$\overline{\frac{\partial f}{\partial s}} = \frac{\partial \overline{f}}{\partial s},\ \overline{\int f\, ds} = \int \overline{f}\ ds \tag{2.71}$$

$$\overline{f.g} \neq \overline{f}.\overline{g} \tag{2.72}$$

Then, the continuity and Navier-Stokes equations for incompressible fluid are converted to the equations (2.73) and (2.74), (2.75), (2.76), respectively.

$$\frac{\partial \overline{u}}{\partial x} + \frac{\partial \overline{v}}{\partial y} + \frac{\partial \overline{w}}{\partial z} = 0 \tag{2.73}$$

$$\rho\left(\frac{\partial \overline{u}}{\partial t} + \overline{u}\frac{\partial \overline{u}}{\partial x} + \overline{v}\frac{\partial \overline{u}}{\partial y} + \overline{w}\frac{\partial \overline{u}}{\partial z}\right) = -\frac{\partial \overline{P}}{\partial x} + F_x + \mu\Delta\overline{u} - \rho(\frac{\partial \overline{u'u'}}{\partial x} + \frac{\partial \overline{u'v'}}{\partial y} + \frac{\partial \overline{u'w'}}{\partial z}) \tag{2.74}$$

$$\rho\left(\frac{\partial \overline{v}}{\partial t} + \overline{u}\frac{\partial \overline{v}}{\partial x} + \overline{v}\frac{\partial \overline{v}}{\partial y} + \overline{w}\frac{\partial \overline{v}}{\partial z}\right) = -\frac{\partial \overline{P}}{\partial y} + F_y + \mu\Delta\overline{v} - \rho(\frac{\partial \overline{u'v'}}{\partial x} + \frac{\partial \overline{v'v'}}{\partial y} + \frac{\partial \overline{v'w'}}{\partial z}) \tag{2.75}$$

$$\rho\left(\frac{\partial \overline{w}}{\partial t} + \overline{u}\frac{\partial \overline{w}}{\partial x} + \overline{v}\frac{\partial \overline{w}}{\partial y} + \overline{w}\frac{\partial \overline{w}}{\partial z}\right) = -\frac{\partial \overline{P}}{\partial z} + F_z + \mu\Delta\overline{w} - \rho(\frac{\partial \overline{u'w'}}{\partial x} + \frac{\partial \overline{v'w'}}{\partial y} + \frac{\partial \overline{w'w'}}{\partial z}) \tag{2.76}$$

The last terms of the Navier-Stokes equation that given above are known as the Reynolds stress or apparent turbulent shear stress (friction). Navier-Stokes equations can be written in the tensor form (Nguyen, 2005).

$$\rho\frac{D\overline{u_i}}{Dt} = F_i - \frac{\partial \overline{P}}{\partial x_i} + \mu\Delta\overline{u_i} - \rho \underbrace{\left(\frac{\partial \overline{u_i' u_j'}}{\partial x_j}\right)}_{\text{Reynolds stress}} \tag{2.77}$$

Turbulence models are trying to find a solution to estimation of the Reynolds stress in equation (2.77).

2.2 Boussinesq Assumption

The Boussinesq assumption, which was proposed in 1877, developing ideas of Saint-Venant is often expressed as turbulent fluctuations are dissipative on the mean flow. Boussinesq assumption is used for solving Reynolds stresses in most of turbulence models. Newton's viscosity law is shown as equation (2.78), for constant viscosity (Woelke, n.d.; Davidson, 2015; McDonough, 2009).

$$\tau = \mu\frac{\partial u}{\partial y} \tag{2.78}$$

This equation is an emperical equation and used for laminar flows with constant viscosity. This principle attributed Reynolds stresses to velocity gradients (or the strain rate) using a coefficient called eddy viscosity (Sert, n.d.).

$$-\overline{u_i' u_j'} = \upsilon_t \left[\frac{\partial u_i}{\partial x_j} + \frac{\partial u_j}{\partial x_i}\right] \tag{2.79}$$

$$\tau_{i,j} = -\rho\overline{u_i' u_j'} = \mu_t \left[\frac{\partial u_i}{\partial x_j} + \frac{\partial u_j}{\partial x_i}\right] \tag{2.80}$$

Where, υ_t is the turbulent kinematic eddy viscosity and μ_t represents the turbulent dynamic eddy viscosity. An important point here must be noted is that the turbulent viscosity is flow properties and it is not properties of the fluid. It vary from one flow to another. With the approach of the eddy viscosity principle after Boussinesq, the general time-averaged Navier-Stokes equations can be written in tensor form as equation (2.81).

$$\rho\left(\frac{Du_i}{Dt}\right) = -\frac{\partial P}{\partial x_i} + F_i + \frac{\partial}{\partial x_j}\tau_{i,j} \tag{2.81}$$

Where, $\tau_{i,j}$ is given in equation (2.81) (Tritton, 1988; Faber 1995).

$$\tau_{i,j} = \mu\frac{\partial u_i}{\partial x_j} + \rho\left(\vartheta_t\left(\frac{\partial u_i}{\partial x_j} + \frac{\partial u_j}{\partial x_i}\right) - \frac{2}{3}k\delta_{i,j}\right) \tag{2.82}$$

Eddy viscosity should be a function of the characteristics of turbulent flow, because it is used to the estimation of turbulence stresses. Dynamic eddy viscosity is determined using:

$$\mu_t = C\rho v_t l \tag{2.83}$$

where, C is a constant coefficient, ρ is the fluid density, v_t is the velocity scale, and l is the length scale. Turbulence models have been developed for estimation of these velocity and length scale parameters. Different types of these turbulence models are described in the next parts of this chapter.

2.3 Fick's First and Second Laws of Diffusion

Adolf Fick was a physiologist and he offered his famous laws in 1855, whitch known as Fick's law, later (Wikipedia, 2015). When diffusion takes place with contacting two miscible flows, the macroscopic concentration follows these Fick's laws. Here, the mathematical definition of the diffusion is important. Diffusion is the movements of molecules of any substance or fluid, depending on the concentration difference, from the intense and dense region to the less dense region individually and randomly. The diffusion of molecules of fluid is a kinetic event and expressed by Fick's laws, mathematically (Green et al., n.d.)

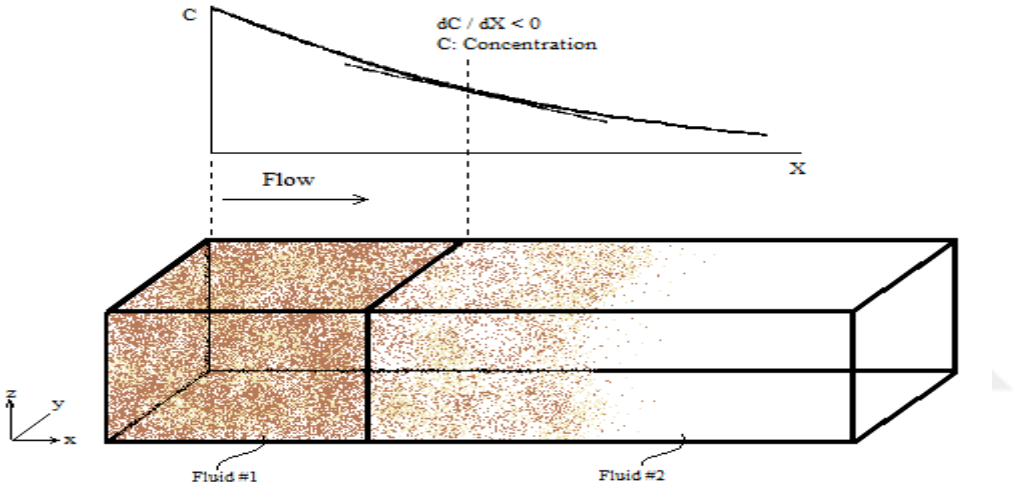

Figure 2.5: Diffusion of fluid's mulecules (Tirnaksiz, n.d.).

The diffusion rate of molecules from one region to another is called flux. Flux value could be determined using the following equation (Tirnaksiz, n.d.).

$$\boldsymbol{J = \frac{1}{A}\frac{dm}{dt}} \tag{2.84}$$

where t is time, m is diffused mass and A is the cross section area (in width). Fick's first law is obtained from equation (2.83). It is sufficient to write this equation based on the concentration difference. According to obtained equation, the molecular movement between two regions will continue until the concentration gradient (dC/dx) becomes zero. At a constant temperature and pressure, the molar diffusion

flux (J) of a substance, is proportional to the molar concentration gradient dC/dx. Equation (2.85) is known as Fick's first law (Zielinski, 2006; Suni, n.d.).

$$\boldsymbol{J = -D\frac{dC}{dx}} \tag{2.85}$$

where, D is the diffusion coefficient of the molecule (area per time) in the unit cm^2/s. Diffusion coefficient Indicates that the mass of the substance diffuses through a unit surface in a unit time at a concentration gradient of unity. The dimension of D in the SI system is a square meter per second. The value of D coefficient of a molecule is not constant and depends on some conditions like as pressure, temperature and the conditions and properties of the environment that molecule diffusion is occurred there. In addition, diffusion coefficient depends on the size and shape of molecules, interaction with solvent and viscosity of solvent. C is concentration (g/cm^3) and x represents the distance traveled by molecule in x direction and horizontally (cm). In following relation, $\frac{dC}{dx}$ is the concentration gradient, which is independent of time. Thus, according to Fick's first law, the diffusion flux along direction x is proportional to the concentration gradient or in other words and in the simplest definition, the first law of Fick assumes a fixed concentration gradient.

Fick's second law describes that the concentration profile and the concentration gradient are changing with time in most real situations. It means that the concentration depends on both the time and distance parameters. Thus, concentration and flux are the function of time and distance. This state can be mathematically defined as C(x,t). Therefore, we have the following relation (2.86) (Zielinski, 2006; Oudenaarden, 2009; Milligen, 2005; Wikipedia, 2016).

$$\boldsymbol{\frac{\partial C}{\partial t} = \frac{\partial}{\partial x}\left(D\frac{\partial C}{\partial x}\right) = D\frac{\partial^2 C}{\partial x^2}} \tag{2.86}$$

Acoording to Fick's second law, an example profile of changes of concentration is similar to the profile represented in Figure 2.6 (Suni, n.d.).

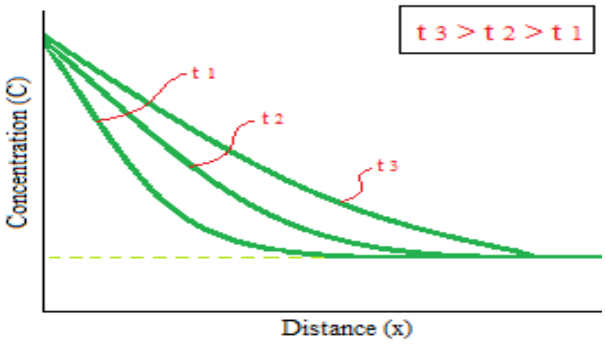

Figure 2.6: Example of changes of concentration through time and x according to fick's second law (Suni, n.d.)

2.4 Types of Turbulence Models

Many Turbulence models have been developed by different researchers to simulate the turbulent flows of their studies. These models are divided into various categories based on technique and the number of differential equations used for Turbulence quantities. Five main categories of turbulence models are given here (Karthik, 2011).

- Algebraic models (zero-equation models)

-One-equation models

-Two-equation models

-Reynolds normalized group models (RNG)

-Large eddy simulation models (LES)

These turbulence models are described below, briefly.

2.5.1 Algebraic Models (Zero-Equation Models)

Algebraic turbulence models or zero-equation turbulence models are models that do not require the solution of any additional equations. Thus, they are calculated directly from the flow variables. These models are relatively simple and are developed based on experimental and empirical data. There are several types of these models available such as (Celik, 1999):

-Prandtl mixing-length model

-Constant eddy viscosity model

-Prandtl's free shear layer model

2.5.2 One-Equation Models

As an alternative to the algebraic or mixing length model, one-equation models have been developed in an attempt to improve turbulent flow predictions by solving one additional transport equation. This equation is usually the turbulent kinetic energy (k). The turbulent kinetic energy is defined as follow (Saad, n.d.; Davidson, 2015; Celik, 1999).

$$k = \frac{1}{2}\left(u'^2 + v'^2 + w'^2\right) \tag{2.87}$$

Velocity scale is defined as equation (2.88).

$$v_t = \sqrt{k} \tag{2.88}$$

Hence, all unknown parameters in turbulence are converted to k and l. k quantity is determined with solving the Navier-Stokes equation for this parameter. From here, this models have two main disadvantages. The disadventages of this model are that the length scale still remains as an algebraic quantity and also, it is computationally more difficult.

2.5.3 Two-Equation Models

Two equation turbulence models are one of the most common type of turbulence models. The length scale in this kind of turbulence models, unlike the one-equation models, is estimated without relying on experimental and empirical relations. Obviously the two-equation models use two equations to describe the eddy-viscosity, while the algebraic or zero-equation models use a geometrical relation to compute the eddy viscosity. In these models, turbulence quantities,which are obtained from solving the differential equations, are used for estimation of the velocity and length scales. Some types of these models are (Davidson, 2015; Saad, n.d.; Celik, 1999):

-Eddy vescosity models

-Algebraic models

-nonlinear Reynolds stresses

In these models, another turbulence quantity is defined. This quantity is estimated, like k parameter, using Navier-Stokes equation. One of the main quantities defined in these models is the turbulence loss quantity. This quantity is shown by ε and have the unit of $\left(m^2/_{s^3}\right)$. This quantity is the representative of length scale.

Two-equation turbulence models are very much still an active area of research and new refined two-equation models are still being developed. Actually, length scale represents the large vortices with kinetic energy that makes the turbulence transfer in the body of fluid.

Totally, these models uses two main assumptions. The first major assumption of most two-equation models is that the turbulent fluctuations, u', v', and w', are locally isotropic or equal. The second major assumption of most two-equation models is that the production and dissipation terms, given in the k-equation, are approximately equal locally. This is known as the local equilibrium assumption.

2.5.4 Renormalizeds Group Models

This approach includes statistical techniques for obtaining averaged equations for the turbulence quantities such as turbulence kinetic energy and its dissipation (loss) rate. The RNG model uses relations such as available relations in $k-\varepsilon$ model. With the exception that the constant coefficients in $k-\varepsilon$ model, which were obtained experimentally, are calculated explicitly (Yakhot et al., 1992).

2.5.5 Large Eddy Simulation Models (LES)

Large eddy simulation model was initially proposed in 1963 by Joseph Smagorinsky to simulate atmospheric air currents (Wikipedia, 2016). The primary idea behind large eddy simulation is to simulate only the larger scales of turbulence that are set by the geometry or specific flow conditions, and to account for the influence of the neglected smaller scales by use of a model. Other words, the basic idea of this model is that all structures of turbulence, that are computable using computational grid, are directly calculated and only the tiny structures that could not be calculated, are approximated. This model operates on the Navier–Stokes equations to reduce the range of length scales of the solution, reducing the computational cost. This model

generates further information than RNG method (Smagorinsky, 1963; Frohlich & Rodi, 2002).

3. COMPUTATIONAL FLUID DYNAMICS (CFD), CE-qual-W2 and FLOW3D

Experimental study of events related to fluid provides accurate and detailed information about the phenomena, which was noted in the past chapters, to researchers and scientists. However, due to limitations in equipments, time, cost and the lack of exact similarity between natural fluid flow and the physical models, this kind of study is not a good solution. Nowadays, in the case of the fluid environment studies, numerical and analytical methods have been developed and these methods are good alternatives in comparison with physical models. In the case of hydrodynamic modeling for a large water body such as lakes or reservoirs, numerical simulation can be more attractive than laboratory experiments due to the complicated geometry and unsteady hydrological and hydraulic data. Numerical methods are applied with the aid of computational power to solution of fluid flow in computational fluid dynamics (CFD). Computational Fluid Dynamics (CFD) is a method of simulating a flow process in which standard flow equations such as the Navier-Stokes and continuity equation are discretized and solved for each computational cell. Computational fluid dynamics is an emerging field that can be applied to a wide class of hydraulics and dam safety problems. The physics of fluid flow is described by the Navier-Stokes equations, which can be solved analytically only for special, mostly academic cases. The environment to be studied is virtualized and simplified into a digital model in CFD projects. In comparison between Mathematical models of fluid flow simulations based on the CFD and the experimental methods, several advantages are seen. Some of these advantages are:

- Substantial reduction in design time.

-Reduction in design cost.

- Increasing of ability to study of complex systems.

- Results with more detail etc.

Several models of computational fluid dynamics are available such as FLUENT, FLOW 3D, FIDAP, TECPLOT, TELEMAC, PHOENICS, CFX, etc.

In this study, Flow 3D software was selected for modeling. The reason of this selection is the advantages of FLOW 3D in comparison of the other programs. For example, simulation that done by FLUENT, are limited to a single-phase model with a rigid lid assumption. Whiles FLOW-3D uses a two-phase model, when it needed. This was due to the powerful volume of fluid (VOF) and fractional area volume obstacle representation (FAVOR) methods, which FLOW-3D utilizes during a two-phase simulation. The important thing must be noticed here is knowing that the using CFD software is in many ways similar to setting up an experiment. If the experiment is not set up correctly to simulate a real-life situation, then the results will not reflect the real-life situation. In the same way, if the numerical model does not accurately represent the real-life situation, then the results will not reflect the real-life situation.

Flow 3D is the CFD software program that was used in this study. FLOW3D employs specially developed numerical techniques to solve the equations of motion for fluids to obtain transient, three-dimensional solutions to multi-scale, multi-physics flow problems. Briefely, the computational fluid dynamics algorithm solves the fluid motion governing equations such as fundamental conservation laws include Continuity Equation, Momentum Equation (Navier-Stokes), and Energy Equation; transport equations; boundary conditions and turbulence. In this thesis, FLOW 3D is chosen for the aim of solving these equations to numerical modeling and simulation of reservoirs or lakes. In the next chapter, FLOW 3D will described compeletely.

Near the usage of FLOW 3D code, Tecplot 360 code will used to achieve better graphical results in this dissertation. Tecplot 360 is a powerful and suitable tool for visualizing a wide range of data. With Tecplot 360 it is possible to offering the results as line plotting, 2D and 3D surface plots in a variety of formats, and 3D volumetric visualization. In addition to using of FLOW3D program, CE-qual-W2 code was used for a part of the case study of this thesis.

3.1 Introduction of CE-qual-W2

CE-qual-W2 program is a two-dimensional code that was used for simulating the thermal stratification part of the case study. This model is based on the finite

difference method. Averaged equations include equation of free water surface, z-momentum equation, z-momentum equation, continuity equation, component transport and equation of state. These equations are represented below, respectively (Cole, 2015; CE-qual-W2 user manual).

$$\frac{\partial B_\eta \eta}{\partial t} = \frac{\partial}{\partial z}\int_\eta^h UBdz - \int_\eta^h qBdz \tag{3.1}$$

$$\frac{\partial P}{\partial z} = \rho g\, cos\alpha \tag{3.2}$$

$$\frac{\partial UB}{\partial t} + \frac{\partial UUB}{\partial x} + \frac{\partial WUB}{\partial z} = gB\, sin\alpha + g\, cos\alpha B\frac{\partial \eta}{\partial x} - \frac{g\, cos\alpha B}{\rho}\int_\eta^z \frac{\partial \rho}{\partial x}dz + \frac{1}{\rho}\frac{\partial B\tau_{xx}}{\partial x} + \frac{1}{\rho}\frac{\partial B\tau_{xz}}{\partial z} + qBU_x \tag{3.3}$$

$$\frac{\partial UB}{\partial x} + \frac{\partial WB}{\partial z} = qB \tag{3.4}$$

$$\frac{\partial B\emptyset}{\partial t} + \frac{\partial UB\emptyset}{\partial x} + \frac{\partial WB\emptyset}{\partial z} - \frac{\partial\left(BD_x\frac{\partial \emptyset}{\partial x}\right)}{\partial x} - \frac{\partial\left(BD_z\frac{\partial \emptyset}{\partial z}\right)}{\partial z} = q_\emptyset B + s_\emptyset B \tag{3.5}$$

$$\rho = f(T_w, \emptyset_{TDS}, \emptyset_{SS}) \tag{3.6}$$

where, the x and z are the horizontal and vertical coordinates; B is the width of the water body; U is the width averaged horizontal velocity; W is width averaged vertical velocity; ρ is water density; t is time; P is pressure; g is gravity acceleration; q is inflow and outflow discharge; α is the slope of the water body bed; ϕ is concentration of averaged width; D_x and D_z are the thermal diffusivity coefficients in x and z directions; τ_{xx} and τ_{xz} are the turbulent shear stresses in x and z directions; q_ϕ is the inflow and outflow concentrations; S_ϕ is a term related to the sources or sinks; β_η is the width of the water surface; which varies with time and place; η is location of the water free surface and h is the depth. In this program, computations along the length of the reservoir or lake are averaged across the reservoir width. Whereas, CE-QUAL-W2 requires the reservoir or lake be discretized into longitudinal segments and vertical layers that may vary in length and height. Many researches are available for usage of this code. All of these available studies with CE-qual-W2 were done for modeling the water quality of lakes, rivers and reservoirs, mostly.

3.2 Introduction of FLOW3D

Study on fluid dynamics is one of the most interesting sciences, despite of its complication. Until a few decades ago, to study on the phenomena in this field, only

the experimental or analytical methods with many assumptions were used. Computational costs decreased with advent of computers. Computational ability of the human was increased and many improvements were done in the field of computational fluid dynamics, consequently. Nowadays, CFD besides the laboratory and analytical methods are used as an useful tool in studies of behavior of fluids. This science has improved, by advancements in the field of computational methods and development of computers with powerful processors in the second half of the twentieth and new century. Computational Fluid Dynamics (CFD) covers a wide range of methods by which computers numerically simulate fluid flow and its behavior. Nowadays, CFD is widely used in the various industrial fields related to fluid, heat transfer and material transport by fluid such as aerospace industries, military industries, automotive industries, hydraulics, oil and gas and energy industries, etc. In spite of the low age of Computational Fluid Dynamics science in the world, developments and improvements in this case been considerable.

One of the scientific branches of computational fluid dynamics that has many remarkable progresses is water engineering science or hydraulics. Microscopic study of water behavior in natural currents indicates the complexities because of their random and accidently nature. But, with advent of computers, CFD science achieved success in simulation and forecasting of water behavior using turbulence models.

Nowadays, there are several models available for simulation of the fluid environment. One of the strongest and the most widely used models, especially in recent years, is Flow 3D model. This model developed by Flow Science Company. Flow Science, Inc. is a developer of software for computational fluid dynamics, also known as CFD, a branch of fluid mechanics that uses numerical methods and algorithms to solve and analyze problems that involve fluid flows. Hirt C.W.T. founded this company in 1980. New versions of this model involve many functional areas. Nowadays, this model is very popular and used in research and industry. This software is able to analyzing a two-dimensional or three-dimensional flow field as a volume. One reason for the popularity of this model is good and acceptable graphical results. The software includes many optional models that add to or modify the basic Navier-Stokes equations. Additional models that are used frequently in hydraulics include options for describing the effects of turbulence, surface tension, heat transfer, fluid solidification, sediment scour, particles, granular flows, moving solids, solid

deformation, air entrainment, cavitation, and porous media. In addition, this model has a high and efficient ability to simulate the water flow, sediment transport and scour and is an appropriate model to hydraulical simulations.

In this study, three-dimensional computational fluid dynamic models were simulated with a CFD code named FLOW-3D. It is general-purpose computational fluid dynamics software. It employs specially developed numerical techniques to solve the equations of motion for fluids to obtain transient, three-dimensional solutions to multi-scale, multi physics flow problems. An array of physical and numerical options allows users to apply FLOW 3D to a wide variety of fluid flow and heat transfer phenomena.

The governing equations used in FLOW 3D model are Navier-Stokes equations and the equation of mass conservation. This model also uses five methods for solving turbulence. FLOW 3D includes several physical patterns such as shallow water, viscosity, cavitation, turbulence, porous environments etc. Meshing in these models consists of rectangular cube cells. This kind of mesh seems as a limitation, initially. But it is an advantage because of the simple generation of this type of mesh, appropriate order and less memory requirement, and also, due to use of two useful tools of Volume of Fluid (VOF) and Fractional Area-Volume Obstacle Representation (FAVOR) in FLOW 3D model.

Using VOF method to predict the fluid level and combination of that with FAVOR method for detection of rigid boundaries, and also using rectangular cubes in solution mesh, are the main features of this code that distinguishes it from similar codes. VOF and FAVOR methods will be discussed in the next sections of this chapter. But it is necessary to mention some examples of the researches and studies carried out by FLOW 3D code, firstly.

3.3 Previous studies using FLOW 3D

FLOW 3D code is used in different branches and fields of science suach as mechanichal engineering, coastal engineering, hydraulic and water resources engineering, civil engineering, aerology, environmental engineering, aerospace engineering, geological and atmospheric sciences, ocean sciences and technologies, etc. Some of these usages of FLOW 3D code are mentiond as an example here.

Jae-Seol Shim et al. (2013) performed 2D and 3D numerical simulations of the storm surge and inundation over Masan Bay in South Korea using FLOW 3D. This study was about the ocean sciences and coastal engineering. A computational study on hydraulic jumps, including air entrainment is the subject that Di Ning choosen for modeling using FLOW 3D (2014). He selected two turbulence models for his simulations of transportation of air as bubbles. This was an environmental engineering research. As an example of an usages of FLOW 3D code in the field of hydraulic engineering, Jorge Abad et al. (2008) investigated on a subject under the title of flow structure at different stages in a meander-bend with bendway weirs.

José F. Rodriguez et al. (2004) studied on the high-resolution numerical simulation of flow through a highly sinuous river reach as an example of water resources management case study.

In other study, Reza Marsooli and Weiming Wu developed a 3D model for dam break flows using FLOW 3D code. Three-dimensional hydrodynamic modeling of density currents in the Chicago river is a topic that studied by Fabián A. Bombardelli and Marcelo H. García (2001) at Illinois. In mentioned study, the FLOW 3D code was used for modeling the density current. W. Daley Clohan was modeled aerial landslide generated wave simulations using FLOW3D.

3.4 Significant features of FLOW 3D (From FLOW 3D Manual Book)

In this part some important features of FLOW 3D code will be explained. This part of this section is prepared using FLOW3D user maual., with selecting the useful parts and equations related to this thesis.

3.4.1 Volume of fluid (VOF)

Several methods such as height functions, line segments, Hirt and Nichols and marker particles have been used to approximate free boundaries in finite-difference numerical simulations, previously. The fractional volume of fluid is a simple and powerful method and is shown to be more flexible and efftcient than other methods for treating complicated free boundary configurations. The volume of fluid (VOF) method has been applied for several decades to problems in computational physics and computational fluid dynamics (Hirt and Nichols, 1981). In FLOW 3D free

surfaces are modeled with the Volume of Fluid (VOF) technique, which was first reported in Nichols and Hirt (1975), and more completely in Hirt and Nichols (1981). The volume of fluid is an example of volume-fraction methods. In computational fluid dynamics, the volume of fluid method is a free-surface modelling technique. In This method, the area to be modeled is divided into a mesh with smaller elements or control volumes. For the elements with fluid, numerical values for each of the flow variables such as pressure, temperature and velocity is kept inside those elements. These values represent the mean volume of values for each element. The VOF method consists of three ingredients as a scheme to locate the surface, an algorithm to track the surface as a sharp interface moving through a computational grid, and a means of applying boundary conditions at the surface. When flow has the free surface condition, all the cells are not occupied with fluid and some of the cells, that are located at the flow surface, are half-full or partly full. Appropriate method to show the status of the cells is defining the quantity that named as F. This F represents the part of the cell that is filled with fluid. This quantity is called as volume of fluid function. By knowing the values of F, it is possible to determine the position and the angle of free surface in the cells of mesh blocks. This is achieved by controlling the amount of fluid at the adjacent cells.

Value of function F is unity at any point occupied by fluid and zero otherwise. The average value of F in a cell would then represent the fractional volume of the cell occupied by fluid. In particular, a unit value of F would correspond to a cell full of fluid, while a zero value would indicate that the cell contained no fluid and in the other words, this value of F corresponds to a void region. Voids are regions without fluid mass that have a uniform pressure appointed to them. Cells with F values between zero and one must then contain a free surface. An example for the F values is presented as Figure 3.1 (FLOW 3D user manual; Abbaspour et al., 2009).

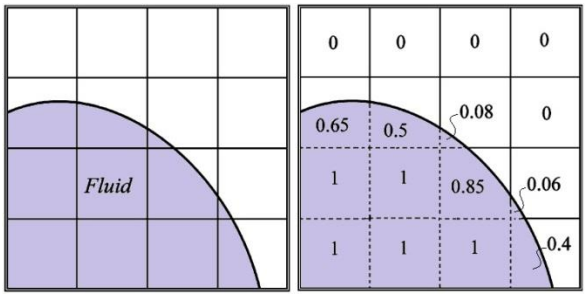

Figure 3.1 : Values of funcion F in volume of fluid method (FLOW3D user manual).

The evolution of the F field is governed by the following transport equation, written in a conservative form (3.7) (FLOW 3D user manual; de Juette et al., n.d.):

$$\frac{\partial F}{\partial t} + \frac{\partial uF}{\partial x} + \frac{\partial vF}{\partial y} + \frac{\partial \omega F}{\partial z} = 0 \qquad (3.7)$$

where, t is the physical time, (x, y, z) are the Cartesian system, (u, v, w) are the Cartesian components of the velocity.

After determination of position and angle of the flow surface, applying the appropriate boundary conditions in flow surface would be possible to calculate the fluid motion. It is important to note the great advantage of volume of fluid method is that the fluid flows in a fixed-grid and there is no deformation and displacement of grids. Also according to the effect of forces the fluids can be mixed together or to be separated.

3.4.2 Fractional area-volume obstacle representation

Modeling fluid flow in complex geometry is easy using FAVOR method in FLOW 3D. In addition to the volume of fluid technique, the structured fractional area-volume obstacle representation method is used to get better geometric representations of complex geometries in the grid system, based on rectangular cell meshes. Fractional area-volume obstacle representation or FAVOR method is another volume-fraction technique that is used to determination of the geometry. The fractional area-Volume obstacle representation method used exclusively in FLOW3D eliminates stairstep effect that might otherwise occur with a simple Cartesian grid system by smoothly blocking out fractional portions of grid cell faces and volumes. FAVOR also consists of a collection of special algorithms for computing interfacial areas, evaluating wall stresses, enhancing numerical stability, and for computing advection along solid boundaries. In this technique, each cell has all variables at its center except velocity, which is recorded at the cell faces.

Briefly, the philosophy behind FAVOR method is that the numerical algorithms are based on information consisting of only one pressure, one velocity, one temperature, etc., for each control volume. So it would be inconsistent to use much more information to define the geometry. Thus, the FAVOR technique retains the simplicity of rectangular elements while representing complex geometric shapes at a

level consistent with the use of averaged flow quantities within each volume element. The FAVOR method could be described, graphically, as Figure 3.2.

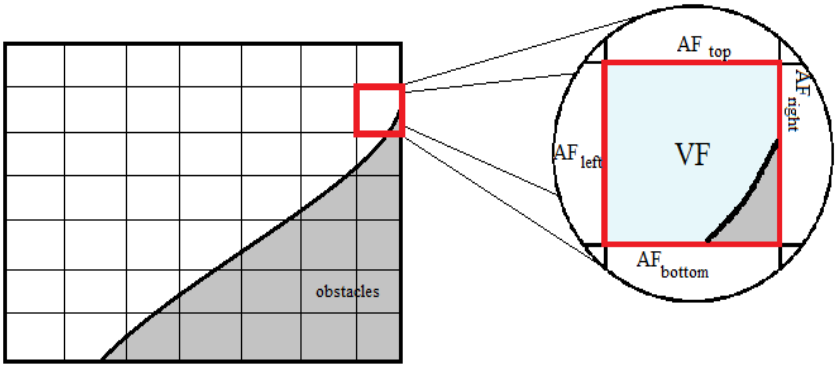

Figure 3.2 : FAVOR Method (FLOW 3D user manual, 2008).

In Figure 3.2, VF and AF values could be calculated using the relations given as Equations (3.8) and (3.9) (FLOW3D user manual).

$$VF = \frac{Open\ Volume}{Volume\ of\ Cell} \tag{3.8}$$

and,

$$AF = \frac{Open\ Area}{Cell\ Edge\ Area} \tag{3.9}$$

3.5 Coordinate systems used in FLOW3D

The differential equations that must be solved in FLOW3D model can be written in the form of Cartesian (x, y, z) and cylindrical (r, θ, z) coordinates. Cylindrical coordinate form has additional terms that these terms have a coefficient named as ξ. Here, if ξ is equal to zero, then the coordinate id related to the Cartesian geometry. On the other hand, if ξ is equal to one, then it is related to the cylindrical geometry.

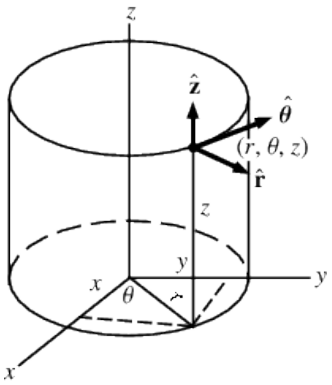

Figure 3.3 : Cartesian and cylindrical coordinates (Cooley, n.d.).

From Figure 3.3, relation between components of Cartesian and Cylindrical coordinates are:

$$r = \sqrt{x^2 + y^2} \tag{3.10}$$

$$\theta = tan^{-1}\left(\frac{y}{x}\right) \tag{3.11}$$

$$z = z \tag{3.12}$$

Where, r in [0,∞), θ in [0,2π), z in (-∞,∞), and the inverse tangent must be suitably defined to take the correct quadrant of (x, y) into account.

Generally, in FLOW 3D, area and volume fractions are time independent. However, these quantities may vary with time when the moving obstacle model is employed.

3.6 Governing equations used in FLOW 3D

In this section, governing equations and their forms, that is used in FLOW 3D, are described. These equations are the simplified equations. This simplification is caused by the usage of a non-compressible fluid.

3.6.1 Continuity Equation

Continuity equation is an equation in physics that describes the transport of a conserved quantity. Continuity equations are a stronger, local form of conservation laws. Totally, the continuity equation is obtained from mass conservation law and the mass balance equation for a fluid element. In general, the mass continuity equation is as follows (3.13) (Flow 3D user manual, 2008; Kaheh et al., n.d.).

$$V_f \frac{\partial \rho}{\partial t} + \frac{\partial}{\partial x}(\rho u A_x) + R\frac{\partial}{\partial y}(\rho v A_y) + \frac{\partial}{\partial z}(\rho w A_z) + \xi \frac{\rho u A_x}{x} = R_{DIF} + R_{SOR} \tag{3.13}$$

In this equation, V_f is the volume fraction of flow, $\boldsymbol{\rho}$ is the fluid density, R_{DIF} is the term of turbulent diffusion, R_{SOR} is the mass source. As mentioned before, the (u, v, w) velocity components are in directions of (x, y, z) for Cartesian or (r, θ, z) for Cylindrical coordinate systems. A_x, A_y and A_z are the area fractions of the flow in x, y and z directions. Coefficient of R is related to type of the coordinate system. When the cylindrical coordinate is used, derivations of y must be

converted to the azimuthal derivations. This conversion can be done by using the following equation (3.14), (3.15) (FLOW 3D user manual):

$$\frac{\partial}{\partial y} = \frac{1}{r}\frac{\partial}{\partial \theta} \tag{3.14}$$

$$\frac{1}{r}\frac{\partial}{\partial \theta} = \frac{r_m}{r}\frac{\partial}{\partial y} \tag{3.15}$$

In equation (3.15), $y = r_m\theta$ and r_m is equal to constant reference radius. In Cartesian coordinates, R is equal to 1 and the ξ is zero. Whereas in the cylindrical coordinates, ξ is equal to 1. The first term in right side of the mass continuity equation is turbulent diffusion term (3.16) (FLOW 3D user manual).

$$R_{DIF} = \frac{\partial}{\partial x}\left(\upsilon_\rho A_x \frac{\partial \rho}{\partial x}\right) + R\frac{\partial}{\partial y}\left(\upsilon_\rho A_y R\frac{\partial \rho}{\partial y}\right) + \frac{\partial}{\partial z}\left(\upsilon_\rho A_z \frac{\partial \rho}{\partial z}\right) + \xi\frac{\rho \upsilon_\rho A_x}{x} \tag{3.16}$$

where,

$$\upsilon_\rho = \frac{C_p \mu}{\rho} \tag{3.17}$$

In equation (3.17), $\boldsymbol{\mu}$ is momentum diffusion coefficient (viscosity), and C_p is an constant coefficient and the inverse of this coefficient related with turbulent Schmidt number. This type of mass diffusion is only used for the turbulent mixing processes in fluids, which has non-uniform density gradient.

The last term of the right side of the mass continuity equation,R_{SOR}, is related to the density that is used for example for modeling the mass injection from a porous wall. $\boldsymbol{\rho}$ is constant in continuity equation for incompressible fluids. Therefore, equation (3.13) is simplified in equation (3.18) (FLOW 3D user manual).

$$\frac{\partial}{\partial x}(uA_x) + R\frac{\partial}{\partial y}(vA_y) + \frac{\partial}{\partial z}(wA_z) + \xi\frac{\rho u A_x}{x} = \frac{R_{SOR}}{\rho} \tag{3.18}$$

3.6.2 Momentum Equation

The momentum equation was described in last chapters. Here, equations, which used in FLOW 3D, with some additional terms are presented. The equations of motion for

the fluid velocity components (*u, v, w*) in the three coordinate directions (x, y, z) (FLOW 3D user manual):

$$\frac{\partial u}{\partial t}+\frac{1}{V_F}\left[uA_x\frac{\partial u}{\partial x}+vA_yR\frac{\partial u}{\partial y}+wA_z\frac{\partial u}{\partial z}\right]+\xi\frac{A_yV^2}{xV_F}=$$

$$-\frac{1}{\rho}\frac{\partial P}{\partial x}+G_x+f_x-b_x-\frac{R_{SOR}}{\rho V_F}(u-u_w-\delta u_s) \quad (3.19)$$

$$\frac{\partial v}{\partial t}+\frac{1}{V_F}\left[uA_x\frac{\partial v}{\partial x}+vA_yR\frac{\partial v}{\partial y}+wA_z\frac{\partial v}{\partial z}\right]+\xi\frac{A_yuv}{xV_F}=$$

$$-\frac{1}{\rho}(R\frac{\partial P}{\partial x})+G_y+f_y-b_y-\frac{R_{SOR}}{\rho V_F}(v-v_w-\delta v_s) \quad (3.20)$$

$$\frac{\partial w}{\partial t}+\frac{1}{V_F}\left[uA_x\frac{\partial w}{\partial x}+vA_yR\frac{\partial w}{\partial y}+wA_z\frac{\partial w}{\partial z}\right]=$$

$$-\frac{1}{\rho}\frac{\partial P}{\partial z}+G_z+f_z-b_z-\frac{R_{SOR}}{\rho V_F}(w-w_w-\delta w_s) \quad (3.21)$$

In equations (3.19), (3.20) and (3.21), G_x, G_y and G_z are the body accelerations, f_x, f_y and f_z are viscous accelerations, b_x, b_y and b_z are flow losses in porous media or across porous baffle plates, and the final terms account for the injection of mass at a source represented by a geometry component.

In these equations, when δ value is equl to zero, then the source is of the stagnation pressure type. On the other hand, if the value of the δ is equal to 1.0, then the source is of the static pressure type. At a stagnation pressure source, fluid is assumed to enter the domain at zero velocity. As a result, pressure must build up at the source to move the fluid away from the source. At a static pressure source the fluid velocity is computed from the mass flow rate and the surface area of the source. In this case, no extra pressure is required to propel the fluid away from the source. The static or stagnation pressure property does not apply to negative mass source like sinks.

For a variable dynamic viscosity (μ), the viscous accelerations are presented in equations (3.22), (3.23) and (3.24) (FLOW 3D user manual).

$$\rho V_F f_X=w_{sx}-\left[\frac{\partial}{\partial x}(A_x\tau_{xx})+R\frac{\partial}{\partial y}\left(A_y\tau_{xy}\right)+\frac{\partial}{\partial z}(A_z\tau_{xz})+\frac{\xi}{x}\left(A_x\tau_{xx}-A_y\tau_{yy}\right)\right] \quad (3.22)$$

$$\rho V_F f_y = w_{sy} - \left[\frac{\partial}{\partial x}\left(A_x \tau_{xy}\right) + R\frac{\partial}{\partial y}\left(A_y \tau_{yy}\right) + \frac{\partial}{\partial z}\left(A_z \tau_{yz}\right) + \frac{\xi}{x}\left(A_x - A_y \tau_{xy}\right)\right] \quad (3.23)$$

$$\rho V_F f_z = w_{sz} - \left[\frac{\partial}{\partial x}\left(A_x \tau_{xz}\right) + R\frac{\partial}{\partial y}\left(A_y \tau_{yz}\right) + \frac{\partial}{\partial z}\left(A_z \tau_{zz}\right) + \frac{\xi}{x}\left(A_x \tau_{xz}\right)\right] \quad (3.24)$$

Where the parametersw_{sz}, w_{sy} and w_{sx} are wall shear stresses. Viscous stress terms in above equations are defined as follows (FLOW 3D user manual):

$$\tau_{xx} = -2\mu\left\{\frac{\partial u}{\partial x} - \frac{1}{3}\left(\frac{\partial u}{\partial x} + R\frac{\partial v}{\partial y} + \frac{\partial w}{\partial z} + \frac{\xi u}{x}\right)\right\} \quad (3.25)$$

$$\tau_{yy} = -2\mu\left\{R\frac{\partial v}{\partial y} + \xi\frac{u}{x} - \frac{1}{3}\left(\frac{\partial u}{\partial x} + R\frac{\partial v}{\partial y} + \frac{\partial w}{\partial z} + \frac{\xi u}{x}\right)\right\} \quad (3.26)$$

$$\tau_{zz} = -2\mu\left\{\frac{\partial w}{\partial z} - \frac{1}{3}\left(\frac{\partial u}{\partial x} + R\frac{\partial v}{\partial y} + \frac{\partial w}{\partial z} + \frac{\xi u}{x}\right)\right\} \quad (3.27)$$

$$\tau_{xy} = -\mu\left\{\frac{\partial v}{\partial x} + R\frac{\partial u}{\partial y} - \frac{\xi v}{x}\right\} \quad (3.28)$$

$$\tau_{xz} = -\mu\left\{\frac{\partial u}{\partial z} + \frac{\partial w}{\partial x}\right\} \quad (3.29)$$

$$\tau_{yz} = -\mu\left\{\frac{\partial v}{\partial z} + R\frac{\partial w}{\partial y}\right\} \quad (3.30)$$

In these equations, μ is the the dynamic viscosity and it can be assigned constant molecular values for each fluid in a one or two fluid problem. In mesh cells with a mixture, the viscosity is evaluated as a volume fraction weighted average of the constant values. In the single-fluid model the fluid can consists of two components, each with its own constant density. If the viscosity (μ) is zero, no viscous stresses are computed. In the above expressions, the terms w_{sx}, w_{sy} and w_{sz} are wall shear stresses. If these terms are omitted, there is no wall shear stress because the remaining terms contain the fractional flow areas A_x, A_y and A_z which vanish at walls. The wall stresses are modeled by assuming a zero tangential velocity on the portion of any area closed to flow.

3.6.3 Fluid Energy Equation

Energy equation, which used in FLOW 3D, for compressible or thermal flow problems is presented in equation (3.31) (FLOW 3D user manual).

$$V_f \frac{\partial}{\partial t}(\rho I) + \frac{\partial}{\partial x}(\rho I u A_x) + R\frac{\partial}{\partial y}(\rho I v A_y) + \frac{\partial}{\partial z}(\rho I w A_z) + \xi \frac{\rho I u A_x}{x} =$$
$$RI_{DIF} + RI_{SOR} + T_{DIF} - \left[P\left(\frac{\partial u A_x}{\partial x} + R\frac{\partial v A_y}{\partial y} + \frac{\partial w A_z}{\partial z} + \xi \frac{u A_x}{x}\right)\right] \quad (3.31)$$

In equation (3.31), I is the macroscopic mixture internal energy. In cylindrical coordinates, ξ is equal to 1 and in Cartesian coordinates its value is zero.

3.6.4 Sediment Transport Equations

In this part of this chapter, the equations used to simulate the erosion, transport and deposition of sediments in FLOW 3D will be explained. Erosion and sediment models in FLOW 3D includes the calculation of suspended sediment transport, calculation of the gravitational sedimentation, calculation of entering of sediments into the flow due to shear stresses and turbulent flow, calculation of bed material handling due to rolling or mutations. In FLOW 3D, two kind of sediments can be available includes the suspended sediment and packed sediment. Suspended sediment transport equation without considering of the volume of fluid (VOF) and Fractional area-volume obstacle representation (FAVOR) functions is presented here.

$$\frac{\partial c_{s,i}}{\partial t} + \nabla.\left(\overline{u} c_{s,i}\right) = 0 \quad (3.32)$$

where $c_{s,i}$the concentration of suspended sediment, in unit of is mass per unit volume, $\overline{u}$ is the average or mean velocity of the sediment and fluid mixtures. Since the density of sediments is greater than the density of fluid around of that, then they will sink, or drift, relative to the surrounding flow. The drift velocity is computed based on the assumption that the drift sediment particles can be considered. Intensity of this deviation depends on the balance between buoyancy and drag forces. The rate of this drift is related to the balance between the buoyancy force and the drag force.

Thus, equation of momentum balances for each sediment particle and for the fluid and sediment mixture without considering of VOF and FAVOR functions could be written as (FLOW 3D user manual)::

$$\frac{\partial u_{s,i}}{\partial t} + \overline{u}.\nabla u_{s,i} = -\frac{1}{\rho_{s,i}}\nabla P + F - \frac{K_i}{f_{s,i}\rho_{s,i}}u_{r,i} \tag{3.33}$$

$$\frac{\partial \overline{u}}{\partial t} + \overline{u}.\nabla \overline{u} = -\frac{1}{\overline{\rho}}\nabla P + F \tag{3.34}$$

Where $u_{s,i}$ is the local sediment velocity (velocity of sediment particles), $\rho_{s,i}$ is the sediment material density, $f_{s,i}$ is the sediment particle volumetric fraction, P is pressure, K is the drag function, F consists of the body and viscosity force, $u_{r,i}$ is the relative velocity. Equation (3.35) is given for calculating the relative velocity in equation (3.34) (FLOW 3D user manual).

$$u_{r,i} = u_{s,i} - u_f \tag{3.35}$$

In equation (3.35), u_f is the local fluid velocity. Average or mean velocity ($\overline{u}$) is also calculated with equation (3.36) (FLOW 3D user manual).

$$\overline{u} = \left(1 - \sum_{i=1}^{n} f_{s,i}\right)u_f + \sum_{i=1}^{n} f_{s,i}u_{s,i} \tag{3.36}$$

where n is the total number of sediment particles. With subtracting Equation (3.33) from equation (3.34), resulting equation (3.37) is obtained(FLOW 3D user manual).

$$\frac{\partial u_{drift,i}}{\partial t} + \overline{u}.\nabla u_{drift,i} = \left(\frac{1}{\overline{\rho}} - \frac{1}{\rho_{s,i}}\right)\nabla P - \frac{K_i}{f_{s,i}\rho_{s,i}}u_{r,i} \tag{3.37}$$

where, the $u_{drift,i}$ is drift velocity, the velocity needed to compute the transport of sediment due to drift and can be calculated with:

$$u_{drift,i} = u_{s,i} - \overline{u} \tag{3.38}$$

The drift velocity is used for calculation of the sediment deviation. This velocity, is calculated by assuming that the motion of each sediment particle is independent of another particles. With assuming that the sediments motion is approximately steady in the computational time scale and the movement term has a negligible value, equation (3.37) changes to equation (3.39).

$$u_{r,i} = \frac{\nabla P}{\overline{\rho} K_i}\left(\rho_{s,i} - \overline{\rho}\right) f_{s,i} \tag{3.39}$$

The average density of fluid and sediment mixture ($\overline{\rho}$) is determined with equation (3.40) (FLOW 3D user manual).

$$\overline{\rho} = \left(1 - \sum_{i=1}^{n} f_{s,i}\right)\rho_f + \sum_{i=1}^{n} f_{s,i}\rho_{s,i} \tag{3.40}$$

The $\overline{\rho}$ is also named as mixture density. Note that in most simulations the pressure gradient, especially nearby the free surface, can be extremely oscillation and noisy. Usually in the most cases, ratio of the pressure gradient to the mixed density is equal to the gravity acceleration (g) (FLOW 3D user manual).

$$u_{r,i} = \frac{g}{K_i}\left(\rho_{s,i} - \overline{\rho}\right) f_{s,i} \tag{3.41}$$

In fluid dynamics, drag refers to forces acting opposite to the relative motion of any object moving with respect to a surrounding fluid. Form drag or pressure drag arises because of the shape of the object. The general size and shape of the body are the most important factors in form drag; bodies with a larger presented cross-section will have a higher drag than thinner bodies. Streamlined objects have lower form drag. Stokes drag is the frictional force and it is acting on the interface between the fluid and the particle. In equation (3.41), the combination of form drag and Stokes drag is the reasonable choice for the drag function of K_i. It could be calculated with by equation (3.42) (FLOW 3D user manual).

$$K_i = \frac{3}{4}\frac{f_{s,i}}{d_{s,i}}\left(C_{D,i}\left\|u_{r,i}\right\| + 24\frac{\mu_f}{\rho_f d_{s,i}}\right) \tag{3.42}$$

where, $d_{s,i}$ is the diameter of the sediment particle is, $C_{D,i}$ is the drag coefficient of sediment particles, and μ_f is the fluid viscosity. Finally, drift velocity (u_{drift}) is calculated using the relative velocity (FLOW 3D user manual).

$$u_{drift} = (1 - f_{s,i})u_{r,i} - \sum_{j=1}^{n(-i)} f_{s,j} u_{r,j} \tag{3.43}$$

Entering sediment particles from bed into flow occurs with sediments withdraw from bottom and suspending of them. Since the the calculation of flow dynamics is impossible for each individual particle, and on the other hand, since the calculation of the boundary layer is difficult on the bed level, therefore using the empirical models can be extremely helpful in this case.So, the model has been used here is based on the model of Mastbergen and Van den Berg. Shields-Rouse equation is applicable as well as for prediction of the Shields critical parameter. The first step in calculation of critical Shields parameter is calculation of the overall Richardson number dimensionless parameterR_i^*. This parameter could be calculated from the equation (3.44) (FLOW 3D user manual, 2008).

$$R_i^* = d_{s,i} \frac{\sqrt{0.1(\rho_{s,i} - \rho_f)\rho_f \| g \| d_{s,i}}}{\mu_f} \tag{3.44}$$

With calculating the R_i^*, the critical Shields number is obtained by equation (3.45).

$$\theta_{cr,i} = \frac{0.1}{R_i^{*\frac{2}{3}}} + 0.054 \left[1 - exp\left(\frac{R_i^{*\,0.52}}{10}\right)\right] \tag{3.45}$$

Armoring effect of the bed is also included in the model. So, larger particles protect to entering the smaller particles into the flow. Here, bed's average particle size must be calculated in the computational cell with equation (3.46) (FLOW3D user manual).

$$d_{50} = \frac{1}{\sum_{i=1,ns} c_{s,i}} \sum_{i=1,ns} c_{s,i} d_{s,i} \tag{3.46}$$

where, the $c_{s,i}$ is the Mass concentration of sediment particles. In order to consider the effect of the bed armoring, critical Shields parameter is re-written using Egiazaroff function. This function is also known as Hiding-Exposure function.

$$\xi_i = \frac{1.666667}{\log_{10}\left(19\frac{d_{s,i}}{d_{50}}\right)^2} \tag{3.47}$$

where ξ_i is the Egiazaroff function. Modified critical Shields parameter is presented below (FLOW 3D user manual, 2008).

$$\theta'_{cr,i} = \theta_{cr,i}\frac{1.666667}{\log_{10}\left(19\frac{d_{s,i}}{d_{50}}\right)^2} \tag{3.48}$$

In equation (3.48), if value of $d_{s,i}$ is much less than value of thed_{50}, then denominator of this equation has a small value. Thus, the value of $\theta'_{cr,i}$ is rises. The reason of this rise in value of the critical Shields parameter is that the small particles are surrounded by the larger particles. On the contrary, the upper equation is decreasing the value of $\theta'_{cr,i}$, if the value of $d_{s,i}$ is much larger than the value of d_{50}. The reason for this reduction in $\theta'_{cr,i}$ is that the the larger particles are surrounded by the smaller particles and will lead to increasing the erosion. For bed with slope conditions, the modified critical Shield number is available (3.49) (FLOW3D; 2008).

$$\theta''_{cr,i} = \theta'_{cr,i}\frac{cos\psi sin\beta + \sqrt{cos^2\beta tan^2\varphi_i - sin^2\psi sin^2\beta}}{tan\varphi_i} \tag{3.49}$$

where β is the angle between bed surface normal vector and the gravity vector, φ_i is the static angle of sediment particles, ψ is the angle between stream and the upward slope. The local shields parameter is calculated based on local shear stress (τ).

$$\theta_i = \frac{\tau}{\|g\|d_{s,i}(\rho_{s,i} - \rho_f)} \tag{3.50}$$

In which, $\|g\|$ is the norm magnitude of gravity vector. Sediment lift velocity is calculated with equation (3.51) (FLOW3D user manual, 2008):

$$u_{lift,i} = \alpha_i n_s d_*^{0.3} \left(\theta_i - \theta_{cr,i}\right)^{0.5} \sqrt{\frac{\|g\| d_{s,i}(\rho_{s,i}-\rho_f)}{\rho_f}} \tag{3.51}$$

Equation (3.51) is known as Mastbergen-Van de Berg equation. In the mentioned equation, d_* presents the dimensionless particle average diameter. It could be obtained by the equation (3.52) (FLOW 3D User manual, 2008).

$$d_* = d_{50} \left[\frac{\rho_f(\rho_{s,i}-\rho_f)\|g\|}{\mu^2}\right]^{\frac{1}{3}} \tag{3.52}$$

The simplified form of the equation (3.52) is:

$$d_* = d_{50} \left[\frac{(s-1)g}{\vartheta^2}\right]^{\frac{1}{3}} \tag{3.53}$$

where, the $\boldsymbol{\vartheta}$ is kinematic viscosity, s is relative density and equal to $\left({}^{\rho_s}/_{\rho}\right)$. ρ_s and ρ are sediment and fluid densities, respectively. In equation (3.52), α_i is the entrainment parameter. The amount suggested by Mastbergen and Van den berg for this parameter is equal to 0.018. So, this equation is became to the following form (3.54) (FLOW 3D user manual, 2008).

$$u_{lift,i} = (0.018) n_s \, (d_{50})^{0.3} \left[\left(\frac{\rho_f(\rho_{s,i}-\rho_f)\|g\|}{\mu^2}\right)^{\frac{1}{3}}\right]^{0.3} \left(\left(\theta_i - \theta_{cr,i}\right)\frac{\|g\| d_{s,i}(\rho_{s,i}-\rho_f)}{\rho_f}\right)^{0.5} \tag{3.54}$$

According to equation (3.54), the n_s is normal vector of the dense bed. $u_{lift,i}$ is used for calculating of amount of dense bed sediments that become suspended. These suspended sediment particles begin to moving and rolling by fluid. In FLOW 3D, Mayer-Peter-Muller model has been used for simulation the bed load transport. This model is presented as equation (3.55) (FLOW 3D user manual, 2008).

$$\Phi_i = \beta_i \left(\theta_i - \theta^{"}_{cr,i}\right)^{3/2} \tag{3.55}$$

According to suggestion of Van Rijn (1984) Value of β_i is equal to 8 in this equation. θ_i and $\theta^{"}_{cr,i}$ are provided in equations (3.52) and (3.51), respectively. The Φ_i is the

dimensionless bed load transport intensity and related to the volumetric rate of the bed load transport per unit width ($q_{b,i}$) (FLOW 3D user manual, 2008).

$$q_{b,i} = \Phi_i \left[\|g\| \left(\frac{\rho_{s,i} - \rho_f}{\rho_f} \right) d_{s,i}^3 \right]^{1/2} \quad (3.56)$$

In FLOW 3D computational code, bed load thickness can be calculated by equation (3.57) (FLOW 3D user manual, 2008).

$$\frac{\delta_i}{d_{50}} = 0.3 d_*^{0.7} \left(\frac{\theta_i}{\theta_{cr,i}^{"}} - 1 \right)^{0.5} \quad (3.57)$$

For calculating the sediment motion in each computational cell, value of volumetric rate of the bed load transport per unit width ($q_{b,i}$) is changed to bed load velocity.

$$u_{bedload,i} = \frac{q_{b,i}}{\delta_i f_{b,i}} \quad (3.58)$$

Where, the $f_{b,i}$ is volumetric component of sediment particles in bed load layer. Van Rijn suggested the following equation to predict the $f_{b,i}$ (FLOW 3D user manual).

$$f_{b,i} = 0.18 \frac{f_{packed}}{d_*} \left(\frac{\theta_i}{\theta_{cr,i}^{"}} - 1 \right) \quad (3.59)$$

The bed motion direction is determined by fluid motion direction nearby the bed. Volumetric flux is presented as(FLOW 3D user manual, 2008):

$$u_{bedload,i} = u_{bedload,i} \frac{\overline{u}}{\|\overline{u}\|} \quad (3.60)$$

In which, the $\frac{\overline{u}}{\|\overline{u}\|}$ indicates the direction of the fluid-sediment mixture nearby the dense bed. Resulting bed load velocity from equation (3.60), $u_{bedload,i}$ is used for calculation of transport of bed dense sediments. Therefore, sediment mass flux is calculated as equation (3.61) (FLOW 3D user manual, 2008).

$$Q_{b,i} = u_{bedload,i}\delta_i f_{b,i}\rho_{s,i} \tag{3.61}$$

In this study, the bed load and equations related to the bed load not be investigated, and the important and major subject, that will be studied and evaluated, is the suspended load.

3.7 Turbulence Solution Models

Turbulence occurs when forces are not sufficient to stabilize the flow. Flows in nature are turbulent, mostly. Turbulent Flows have the following characteristics:

-These type of flows are extremely nonuniform and unstable and always highly irregular.

-It usually has the three-dimensional nature.

- They typically consist of many small vortices with asymmetric form. Variations of these vortexes are proportional to the intensity of the pressure fluctuations.

- Due to flow Turbulence and fluctuations of value of the flow characteristic, intensity of spin currents is high.

In turbulent flows, flows with different amounts of momentum collide and velocity gradients are reduced by effect of viscosity. It reduces the kinetic energy of the fluid. Therefore, turbulence will be a dissipating phenomenon of energy.

3.8 Turbulence models used in FLOW 3D

Turbulence is simulated in FLOW 3D by using one of the five turbulence models used in this software. This software includes the following turbulence models (Karthik, 2011):

-Prandtl mixing-length model

-One-equation turbulent kinetic energy model

-Two-equation $(\boldsymbol{k}-\boldsymbol{\varepsilon})$ model

-Renormalized group model (RNG)

-Large eddy simulation model (LES)

Turbulence modeling in FLOW 3D is partly different from the previous model, because the most of volumetric and area fractions of FAVOR method have been

applied in equations related to turbulence models and generation or degradation of turbulence are generalized by buoyancy forces (FLOW3D user manual). Therefore, turbulence models, that are used in FLOW 3D, will be explained briefly in this section.

3.8.1 Prandtl Mixing-Length Model

The Prandtl mixing length model is the simplest model and this model assumes that the fluid viscosity is enhanced by turbulent mixing processes in regions of high shear, e.g., near solid boundaries. However, this is really only adequate for fully developed, nearly steady flows. More generally, it is necessary to account for some transport processes (i.e., convection and diffusion) to better emulate the space and time distributions of turbulence intensity.

The Prandtl mixing length model assumes that turbulence production and dissipation are in balance everywhere in the flow:

$$P_T + G_T = \varepsilon_T \tag{3.62}$$

where P_T and G_T are the turbulence productions due to shearing and buoyancy effects, respectively, and ε_T is the turbulence dissipation. In other words, advection, diffusion, and the time rate of change of turbulent energy are neglected. The turbulence dissipation also can be written as Equation (3.63) (FLOW3D, 2008).

$$\varepsilon_T = CNU\sqrt{\frac{3}{2}}\frac{k_T^{3/2}}{TLEN} \tag{3.63}$$

where, CNU is a parameter with a default value of 0.09. k_T is the turbulent kinetic energy and TLEN is the turbulent length scale. TLEN is a parameter defined by user. Relationship between ε_T and k_T can be determined by combination of equations (3.62) and (3.63). With this relationship between ε_T with k_T, one can compute k_T in terms of TLEN and the local shear rates and pressure or density gradients. Then k_T and TLEN could be used to computing the turbulent kinematic viscosity ϑ_T by the equation (3.64) (FLOW 3D user manual, 2008).

$$\vartheta_T = TLEN\sqrt{\frac{2k_T}{3}} \tag{3.64}$$

Because of its restrictive assumptions, this model is less useful than the one-equation and two-equation turbulence transport models.

3.8.2 Turbulence Transport Models

The one-equation turbulence transport model consists of a transport equation for the specific kinetic energy associated with turbulent velocity fluctuations in the flow or the turbulent kinetic energy (Celik, 1999; Pitsch, 2014).

$$k_T = \frac{1}{2}\left(\overline{u'^2} + \overline{v'^2} + \overline{w'^2}\right) \tag{3.65}$$

where u', v', w' are the x, y, and z components of the fluid velocity associated with chaotic turbulent fluctuations. The factor of 3/2 comes from the sum of the kinetic energy of the fluctuations in each of the three coordinate directions. This transport equation includes the convection and diffusion of the turbulent kinetic energy. The production of turbulent kinetic energy due to shearing and buoyancy effects, diffusion, and dissipation due to viscous losses within the turbulent eddies are also included in the model. Buoyancy production only occurs if there is a non-uniform density in the flow, and includes the effects of gravity and non-inertial accelerations. The turbulence kinetic energy (k) and its rate of dissipation (ε) are obtained from the following transport equation (3.66) (FLOW 3D user manual, 2008).

$$\frac{\partial k_T}{\partial t} + \frac{1}{V_F}\left\{uA_x\frac{\partial k_T}{\partial x} + vA_y\frac{\partial k_T}{\partial y} + wA_z\frac{\partial k_T}{\partial z}\right\} = P_T + G_T + Diff_T - \varepsilon_T \tag{3.66}$$

where k_T is the turbulent kinetic energy, V_F, A_x, A_y, A_z are the FAVOR functions used by FLOW 3D, P_T presents the turbulent kinetic energy production or the shear production, G_T is the buoyancy production, $Diff_T$ represents diffusion. P_T can be calculated from equation (3.67) (FLOW 3D user manual, 2008).

$$P_T = CSPRO\left(\frac{\mu}{\rho V_F}\right)\begin{Bmatrix} 2A_x\left(\frac{\partial u}{\partial x}\right)^2 + 2A_y\left(R\frac{\partial v}{\partial y} + \xi\frac{u}{x}\right)^2 + 2A_z\left(\frac{\partial w}{\partial z}\right)^2 \\ +\left(\frac{\partial v}{\partial x} + R\frac{\partial u}{\partial y} - \xi\frac{v}{x}\right)\left[A_x\frac{\partial v}{\partial x} + A_y\left(R\frac{\partial u}{\partial y} + \xi\frac{v}{x}\right)\right] \\ +\left(\frac{\partial u}{\partial z} + \frac{\partial w}{\partial x}\right)\left(A_z\frac{\partial u}{\partial z} + A_x\frac{\partial w}{\partial x}\right) \\ +\left(\frac{\partial v}{\partial z} + R\frac{\partial w}{\partial y}\right)\left(A_z\frac{\partial v}{\partial z} + A_y R\frac{\partial w}{\partial y}\right) \end{Bmatrix} \quad (3.67)$$

where CSPRO is a turbulence parameter with a default value of equal to 1. If cylindrical coordinat system is used, R and ξ parameters will appear in equation. ξ is equal to 0 in Cartesian geometry, while its value is equal to 1 in cylindrical geometry. In Cartesian coordinates, R is set to 1. The buoyancy production term (G_T) in equations (3.66) and (3.67) is obtained by equation (3.68) (FLOW 3D, 2008).

$$G_T = -CRHO\left(\frac{\mu}{\rho^3}\right)\left(\frac{\partial\rho}{\partial x}\frac{\partial P}{\partial x} + R^2\frac{\partial\rho}{\partial y}\frac{\partial P}{\partial y} + \frac{\partial\rho}{\partial z}\frac{\partial P}{\partial z}\right) \quad (3.68)$$

where, CRHO is another turbulence parameter. The value of this parameter is equal to zero, defaultly. However, the parameter for thermally buoyant flow problems should be chosen to about 2.5. For turbulence diffusion term in equation (3.66), the equation (3.69) is given.

$$Diff_T = \frac{1}{V_F}\begin{Bmatrix} \frac{\partial}{\partial x}\left(\upsilon_k A_x\frac{\partial k_T}{\partial x}\right) + R\frac{\partial}{\partial y}\left(\upsilon_k A_y R\frac{\partial k_T}{\partial y}\right) \\ +\frac{\partial}{\partial z}\left(\upsilon_k A_z\frac{\partial k_T}{\partial z}\right) + \xi\frac{\upsilon_k A_x k_T}{x} \end{Bmatrix} \quad (3.69)$$

where, υ_k is the diffusion coefficient and is computed based on the local value of the turbulent viscosity. Turbulence models, used in FLOW 3D, are defined here. $k-\varepsilon$ is a more sophisticated and widely used model for he turbulent kinetic energy k_T and its dissipation ε_T. This model consists of two transport equations. Equation (3.70) is an additional transport equation for the turbulent dissipation (FLOW 3D, 2008).

$$\frac{\partial\varepsilon_T}{\partial t} + \frac{1}{V_F}\left[uA_x\frac{\partial\varepsilon_T}{\partial x} + vA_y\frac{\partial\varepsilon_T}{\partial y} + wA_z\frac{\partial\varepsilon_T}{\partial z}\right] =$$

$$\frac{CDIS1.\varepsilon_T}{k_T}(P_T + CDIS3.G_T) + Diff_\varepsilon - CDIS2\frac{\varepsilon_T^2}{k_T} \quad (3.70)$$

Where CDIS1, CDIS2, and CDIS3 parameters are dimensionless parameters and user-adjustable parameters and, for the k-ε model, have default values of 1.44, 1.92 and 0.2, respectively. $Diff_{\varepsilon}$ is the diffusion of dissipation and can be determined with equation (3.71) (FLOW 3D user manual, 2008).

$$Diff_{\varepsilon} = \frac{1}{V_F}\begin{Bmatrix} \frac{\partial}{\partial x}\left(v_{\varepsilon}A_x\frac{\partial \varepsilon_T}{\partial x}\right) + R\frac{\partial}{\partial y}\left(v_{\varepsilon}A_y R\frac{\partial \varepsilon_T}{\partial y}\right) \\ +\frac{\partial}{\partial z}\left(v_{\varepsilon}A_z\frac{\partial \varepsilon_T}{\partial z}\right) + \xi\frac{v_{\varepsilon}A_x\varepsilon_T}{x} \end{Bmatrix} \quad (3.71)$$

4. NUMERICAL MODELING

Before explaining the numerical models, it is important to define the numeric approximation in FLOW 3D in this part.

4.1 Numerical Approximation

In mathematics, finite-difference methods are numerical methods that are used for approximating the solutions to differential equations using finite difference equations to approximate derivatives. Flow 3D is a computational code that uses the finite volume method to solve the Reynolds-averaged Navier-Stokes (RANS) equations (. Totally, cells and their centroids, nodes, grid lines and facets are the elements included meshes. Figure 4.1 shows these elements.

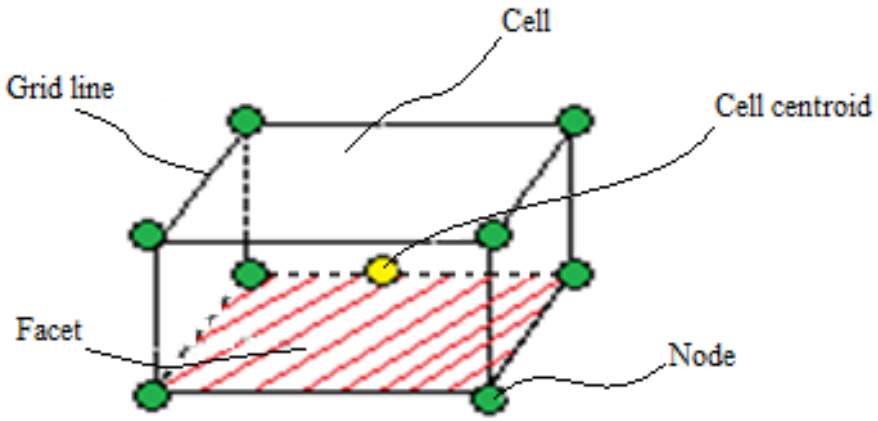

Figure 4.1 : Mesh elements.

The finite-difference mesh used for numerically solving the governing equations consists of only rectangular cells, like as given one in Figure 4.1, with width of δx_i, depth of δy_j and height of δz_k. The active mesh region has IBAR cells in the x-direction labeled with the index i, JBAR cells in the y-direction labeled with the index j, and KBAR cells in the z-direction labeled with the index k. This region is surrounded by the layers of fictitious or boundary cells, used to set mesh boundary

conditions. Totally, there are$(\mathrm{IBAR}+2)\times(\mathrm{JBAR}+2)\times(\mathrm{KBAR}+2)$ cells in a complete mesh block. Figure 4.2 presents the cell labeling nomenclature (FLOW 3D user manual).

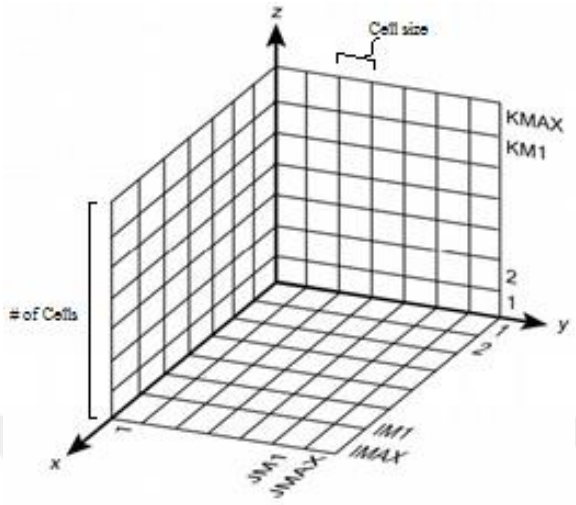

Figure 4.2 : Mesh arrangement and labeling convention (FLOW 3D user manual).

A variable Q at the center of a cell (i, j, k) is denoted as $Q^n_{i,j,k}$, where the superscript n refers to the n-th time step value. Fluid velocities and pressures are located at staggered mesh locations as shown for a typical cell in Figure 4.2. Here, u velocities and fractional areas A_x at the centers of cell faces normal to the x-direction, v velocities and fractional areas A_y at the centers of cell-faces normal to the y-direction, and w-velocities and fractional areas A_z at the centers of cell-faces normal to the z-direction. In addition, pressures (p), fluid fractions (F), fractional volumes (V), densities (ρ), internal energy (I), turbulence quantities for energy (q), dissipation (D), and viscosity (μ) are at the center of the cells (FLOW 3D user manual).

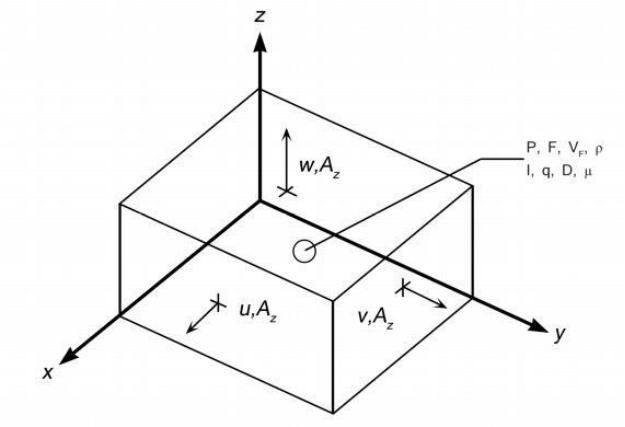

Figure 4.3 : Location of variables in a mesh cell (FLOW 3D user manual).

The finite-difference notation that is used here, depends to that used in the code where fractional index values can not be used. The convention is that all fractional indexes are reduced to the closest whole round number. For example, the *u* velocity at i + ½ which is located on the cell-face between cells(i, j, k) and $(i + 1, j, k)$, is denoted by $u^n_{i,j,k}$. A superscript n refers to the n-th time-step value. Similarly (FLOW 3D user Manual),

$F^n_{i,j,k}$= fluid fraction at center of cell (i, j, k) at time level n.

$P^n_{i,j,k}$= pressure at center of cell (i, j, k) at time level n.

Similarly for ρ , I, q, D, and μ,

$u^n_{i,j,k}$= x-direction velocity at middle of $i + 1/2$ cell-face at time level n.

$v^n_{i,j,k}$= y-direction velocity at middle of $j + 1/2$ cell-face at time level n.

$w^n_{i,j,k}$= z-direction velocity at middle of $k + 1/2$ cell-face at time level n.

Fractional areas and volumes appear with the following notation:

$AFR_{i,j,k}$= fractional area A_x for flow in x-direction at $i + 1/2$ cell-face.

$AFB_{i,j,k}$= fractional area A_y for flow in y-direction at $j + 1/2$ cell-face.

$AFT_{i,j,k}$= fractional area A_z for flow in z-direction at $k + 1/2$ cell-face.

$VF_{i,j,k}$= fractional volume for flow at center of cell (i, j, k).

It is necessary to distinguish those cells that are empty, contain a surface, or are full of one fluid when free surfaces fluid interfaces are present. A surface cell is a cell containing fluid 1 and having at least one adjacent cell (at $\pm 1, j \pm 1, k \pm 1$), that is empty or full of fluid 2 (FLOW 3D user Manual).

A cell with an F value less than unity, but with no empty neighbor, is considered a full cell in one-fluid problems. A flag $NF_{i,j,k}$ is used to label the cells and in the case of surface cells, to indicate which neighboring cell lies in the direction of the inward

normal to the surface. The flag values are given in table (4.1) (FLOW 3D user manual).

Table 4.1 : Flag values ($NF_{i,j,k)}$ (FLOW 3D user manual).

$NF_{i,j,k}$	interpretation
0	full or obstacle cell
1	surface (i-1 inward neighbor)
2	surface (i+1 inward neighbor)
3	surface (j-1 inward neighbor)
4	surface (j+1 inward neighbor)
5	surface (k-1 inward neighbor)
6	surface (k+1 inward neighbor)
7	cell undergoing cavitation
8	empty cell

NF is used to indicate the orientation of the surface between two fluids in an analogous manner.

General form of the finite-difference approximation for momentum equation is represented (FLOW 3D user manual).

$$u_{i,j,k}^{n+1} = u_{i,j,k}^{n} + \delta t^{n+1}\left[-\frac{P_{i+1,j,k}^{n+1}-P_{i,j,k}^{n+1}}{(\rho\delta x)_{i+\frac{1}{2},j,k}^{n}} + G_x - FUX - FUY - FUZ + VISX - BX - WSX\right] \quad (4.1)$$

$$v_{i,j,k}^{n+1} = v_{i,j,k}^{n} + \delta t^{n+1}\left[-\frac{P_{i,j+1,k}^{n+1}-P_{i,j,k}^{n+1}}{(\rho\delta y)_{i,j+\frac{1}{2},k}^{n}}.R_{i+\frac{1}{2}} + G_y - FVX - FVY - FVZ + VISY - BY - WSY\right] \quad (4.2)$$

$$w_{i,j,k}^{n+1} = w_{i,j,k}^{n} + \delta t^{n+1}\left[-\frac{P_{i,j,k+1}^{n+1}-P_{i,j,k}^{n+1}}{(\rho\delta z)_{i,j,k+\frac{1}{2}}^{n}} + G_z - FWX - FWY - FWZ + VISZ - BZ - WSZ\right] \quad (4.3)$$

In equations (4.1), (4.2) and (4.3):

$$(\rho\delta x)_{i+\frac{1}{2},j,k}^{n} = \frac{\left(\rho_{i,j,k}^{n}\delta x_i + \rho_{i+1,j,k}^{n}\delta x_{i+1}\right)}{2} \quad (4.4)$$

$$(\rho\delta y)_{i,j+\frac{1}{2},k}^{n} = \frac{\left(\rho_{i,j,k}^{n}\delta y_i + \rho_{i,j+1,k}^{n}\delta y_{i+1}\right)}{2} \quad (4.5)$$

$$(\rho\delta z)^{n}_{i,j,k+\frac{1}{2}} = \frac{\left(\rho^{n}_{i,j,k}\delta z_i + \rho^{n}_{i,j,k+1}\delta z_{i+1}\right)}{2} \tag{4.6}$$

$$R_{i+\frac{1}{2}} = \begin{cases} 1.0 \text{ in Cartesian coordinates} \\ \frac{x_{max}}{\frac{1}{2}(x_i + x_{i+1})} \text{ in cylindrical coordinates} \end{cases} \tag{4.7}$$

In these equations, FUX indicates the advective flux of u in the x-direction, VISX shows the x-component viscous acceleration, BX show the flow losses for a baffle normal to the x-direction, WSX is the viscous wall acceleration in the x-direction; and G_X includes gravitational, rotational, and general non-inertial accelerations. These are the advective, viscous, and acceleration terms of momentum equation (FLOW 3D user manual).

4.2 Description of Models and Sensivity of Simulations

In this thesis, models have been studied and simulated with changes in some parameters such as inflow discharge (m^3/sec), suspended sediment concentrations or SSC (kg/m^3), inflow water's temperature (ºC) etc. These changes are done for controlling the sensivity of models. Sensivity analysis process involves changing in any of the parameters with a constant percentage of changes and to determine that how the results change. Occurred changes in simulation variables demonstrate the sensitivity of the model to changed parameter. As mentioned in the first chapter, with change in seasons and variations in climatic conditions such as temperature of the environment, some changes at different layers of reservoirs and lakes arise. In this conditions, the thermal stratification in the reservoir occurs and temperature changes with depth. The values and conditions of these parameters, that used in simulations of this study, are described in this section. But for better observation and understanding of the changes caused by changing in the mentioned parameters, in these initial simulations, the stratification caused by seasons will be ignored. This parameter will be applied in the next sections and in the case study part.

4.3 Input Data

The fluid used in the simulation of the reservoir is water. For modeling and simulation, it is important to know and then define the water characteristics to

FLOW 3D computitional code. The unit selected to all parts of simulations is international system of units (SI) and in the metric mode.

In this section of this dissertation, selected fluid and its properties, reservoir dimension, discharges, tempertures, concentrations of suspended sediment and other parameters are described. After these decribtions, simulations and their output results will presented and compared.

4.3.1 Fluid Type

The fluid used for both the inflow current and reservoir/lake in this study is water. Temperature of the water changes in simulations, that will be discussed in this chapter. The characteristics of water vary with changes in temperature. Physics of the water used in FLOW 3D is described here. Fluid flow in this study is an incompressible flow that have free surface. Unlike most other fluids, the density of water is not a monotonic function of its temperature. So, it has a special equation for calculating of water density in diffdrent temperatures, that is given as Equations (4.8) and (4.9) .

$$\rho_0 = \alpha_0 + \alpha_1 T + \alpha_2 T^2 + \alpha_3 T^3 + \alpha_4 T^4 + \alpha_5 T^5 \quad (4.8)$$

or,

$$\rho_0 = \sum_0^5 \alpha_i T^i \quad (4.9)$$

Where, the is density of fresh water (kg/m^3), and the $\boldsymbol{\alpha_0, \alpha_1, \alpha_2, \ldots, \alpha_5}$ are the constant coefficients.

$$\alpha_0 = 999.84259\,, \alpha_1 = 6.793952 \times 10^{-2}, \alpha_2 = -9.09529 \times 10^{-3}$$

$$\alpha_3 = 1.00168 \times 10^{-4}, \alpha_4 = -1.12008 \times 10^{-6}, \alpha_5 = 6.53633 \times 10^{-9}$$

The following Figure gives the variations of water density in kilograms per cubic meter (kg/m^3) at various temperatures in degrees Celsius (℃).

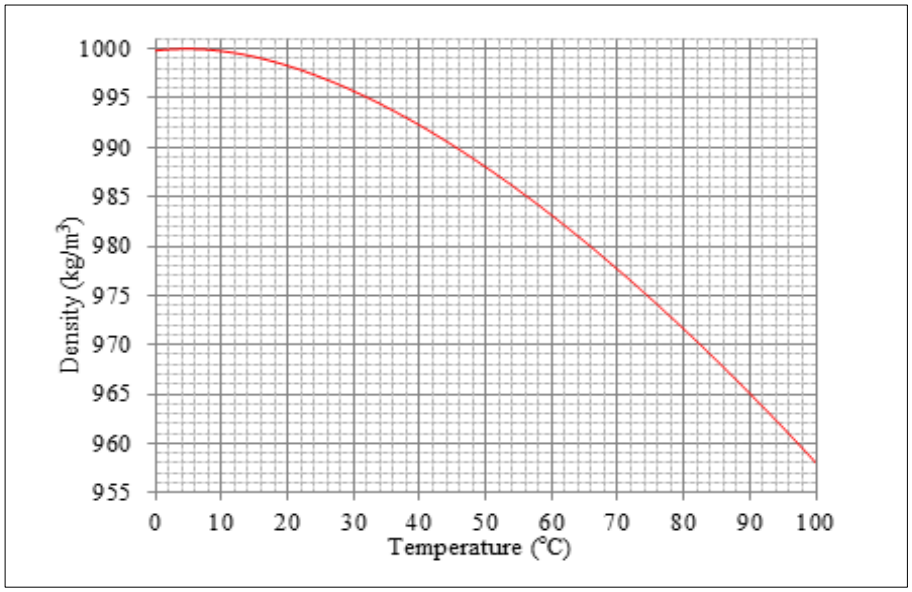

Figure 4.4 : Density-Temperature relation of water.

From Figure 4.4, pure water reaches its maximum density of 999.97 kg/m3 (approximately 1000 kg/m3) at approximately 4 °C. Water near the boiling point (100°C) is about 96 percent as dense as water at 4 °C. Temperature variations also affect the viscosity of fluids such as water. Figure 4.5 shows the dynamic and kinematic viscosity variations caused from temperature changes.

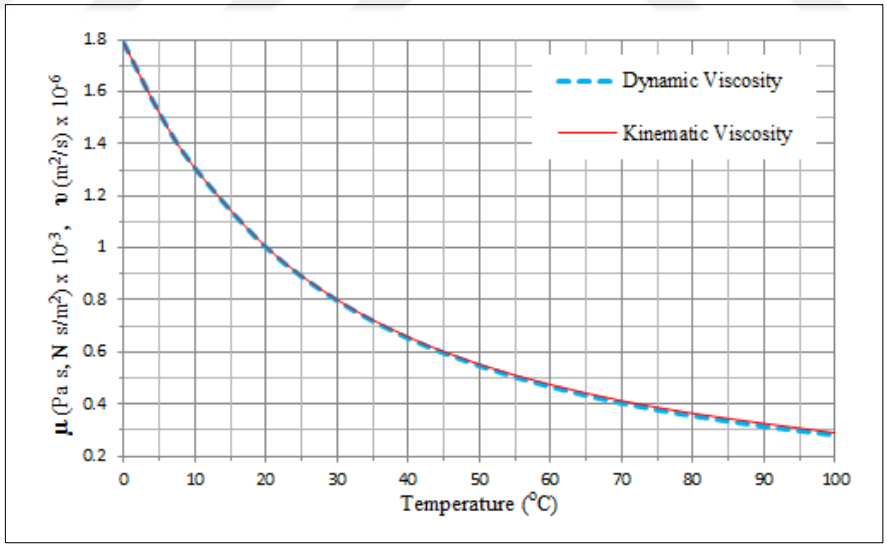

Figure 4.5 : Dynamic (μ) /Kinematik (υ) viscosity of water with temperature changes.

Water in different temperatures also have different thermal conductivities. Thermal conductivity of water, is an intensive property that indicates its ability to conduct heat. Figure 4.6 represents relation between thermal conductivity in unit of watts per

meter celsius (W/(m·C)) and temperture (^{o}c) of water at the constant pressure of 1 bar.

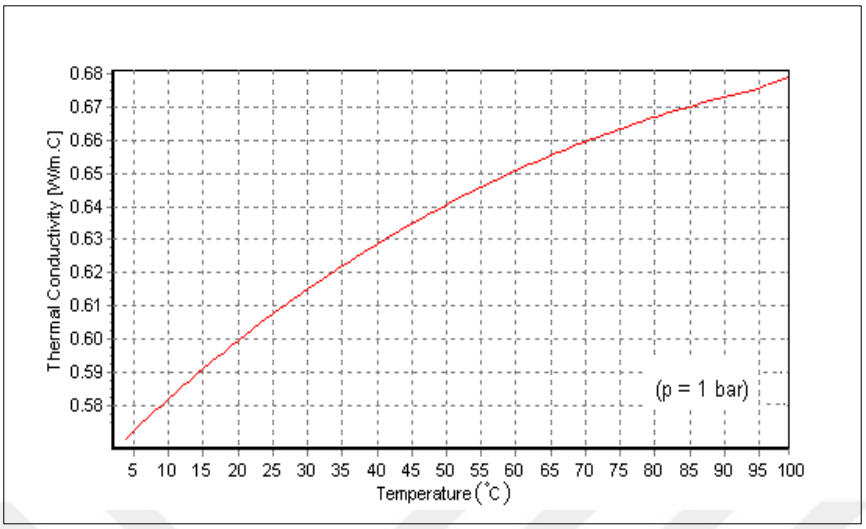

Figure 4.6 : Thermal conductivity-Temperature relation of water.

In this study, water with these characteristics were used. Other properties of water, that were needed for simulation analysis, were applied automatically by FLOW 3D program.

4.3.2 Reservoir Dimensions

Topography of the region of the reservoir or lake is one of the important subjects. In numerical and experimental studies and researches dimensions of choosen models have a significant impact in results. Depth of the reservoir or lake, slope of the bottom of the reservoir or sea floor, length of the reservoir or lake etc. Selected dimension for geometery of simulations of this study will be described in the section of geometery of models of this chapter.

4.3.3 Seasons

Layers of thermal stratification change due to season and environmental climatic changes. These changes in layers of reservoir/lake have some important effects on reservoir's behavior on incoming river flows, which contains different types and concentrations of sediment. As mentioned before, there is no stratification in the initial simulations (sensitivity control simulations). But in the case study models, the stratification will be applied to the simulations.

4.3.4 Discharges

The discharge of inflow river water, which comes into the reservoir/lake, plays an important role in the mixing of river and resrvoir waters, which have different densities, concentrations and also differences in other properties.

Discharge also has an important impact on the determination of rate of the fluid volume propagation in reservoir. Hence, effects of low, medium and high magnitute of discharges are not same and similar in the hydrodynamic of reservoirs/lakes. For this purpose, three values were selected as inflow discharges for sensivity simulations. These selected discharges for initial simulations (sensitivity control) were 20 m^3/s , 50 m^3/s and 100 m^3/s.

4.3.5 Temperature

As mentioned in first chapter and in section 4.3.3, due to the season and climatic changes, stratified layers have variations in their thicknesses and temperatures. In addition to the significance of defining of the differences in these temperatures of layers, the temperature of inflow water (river into reservoir) has an particular importance. But it is assumed that there is no variations of temperature of the water in the reservoir. It means that the reservoir has the constant value of water temperature during the depth in the initial simulations. The temperature of the reservoir's water is selected as 24 ^{o}C for all of the simulations.

For the more useful, practical and clear results of this thesis, four amounts of temperatures for inflow water were considered and then defined to FLOW 3D. These values of temperatures were 4 ^{o}C, 12 ^{o}C, 24 ^{o}C and 40 ^{o}C. Although, the amount of 40 ^{o}C for temperature of water may not available in nature, but it is possible to encountere with this situation in the industry conditions such as factories. Anyway, with considering this high value of water temperature, it is possible for us to understanding the changes which occurred with temperature differences.

4.3.6 Suspended Sediment Types and Concentrations

Sediment has a standard classification. Sediment sizes are divided into clays (less than 0.004 mm), silts (0.004-0.062 mm), sands (0.062-2 mm), gravels (2-64 mm), cobbles (64-256 mm), and boulders (greater than 256 mm), generally. Types of

sediments and diameter of the sediment particles are described in greater detail in table 4.2.

Table 4.2 : Sediment classification.

No.	Type	Diameter of each class (mm)	Average size (mm)
1	Clay	< 0.004	-
2	Very Fine Silt	0.004-0.008	0.005
3	Fine Silt	0.008-0.016	0.011
4	Medium Silt	0.016-0.031	0.022
5	Coarse Silt	0.031-0.062	0.044
6	Very Fine Sand	0.062-0.125	0.088
7	Fine Sand	0.125-0.250	0.177
8	Medium Sand	0.250-0.50	0.354
9	Coarse Sand	0.5-1	0.707
10	Very Coarse Sand	1-2	1.414
11	Very Fine Gravel	2-4	2.828
12	Fine Gravel	4-8	5.657
13	Medium Gravel	8-16	11.31
14	Coarse Gravel	16-32	22.63
15	Very Coarse Gravel	32-64	45.26

For this dissertation, suspended sediment (suspended load) is considered. So, selected class of sediment was the clay type. Diameters of Clay sediment particles were defined to the FLOW 3D as mud1 with value of 0.0035 mm. The concentrations of the suspended load of inflow (river) and reservoir's water for these initial simulations were considered as 15 g/l and 20 g/l for different simulations. These changes were to obtain the sensitivity of the models and for the aim of comparison of results. The selected scenarios will be represented as tables after discription of the geometry of models.

4.4 Geometry of Models

In FLOW-3D, geometry of simulations are constructed by assembling solid objects and combine to define the flow regions for the simulation. In this study the geometry of reservoir is created using its own modeler (using the Flow 3D GUI and solids modeler). For drawing the geometries, components should be created first. Each model, which created in this study, has a component and 3 subcomponents. FLOW

3D creates subcomponents as solid objects defaultly, and this is the only option when the subcomponent belongs to a new component. Subcomponents indicate solid objects, holes and supplements within a defined component.

The Global branch displays the minimum, maximum and extent of all geometry in each direction of the entire domain. The selected dimension for the geometry is shown here. It has about 390 meters lenght, 120 meters width and 60 meters depth, when reservoir is completely full of water.

Table 4.3 : The selected dimensions for the models.

Length (x) (m)	Width (y) (m)	Depth (z) (m)	Slope (θ) (degree)	Longitudinal section	Cross section
390	120	60	~ 9°	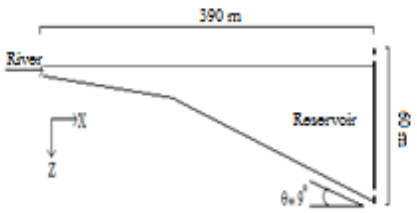	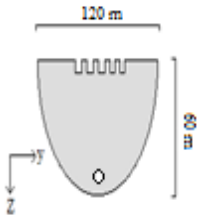

The component type was selected as standard for all models in Flow 3D. As seen in the table (4.3), two outlets were considered to the models. The first outlet has been selected as spillway in the upper part of body of dam, for maximum water level conditions of the reservoir before overtapping. This state could also define for the lakes. The second selected outlet has been considered as lower sluice near the bottom of the reservoir. İt is necessary because the situation and position of the outlet could have effect on the flow pattern in the reservoir.

4.5 Meshes and Grids of Models

The domain can be contained within a single grid or several grids types, which called as multi blocks. In this thesis, mesh structure of models consists of four mesh blocks in all initial simulations (Figure 4.11) of sensitivity. Each grid in these models contained within a larger grid or adjacented to another grid, completely.

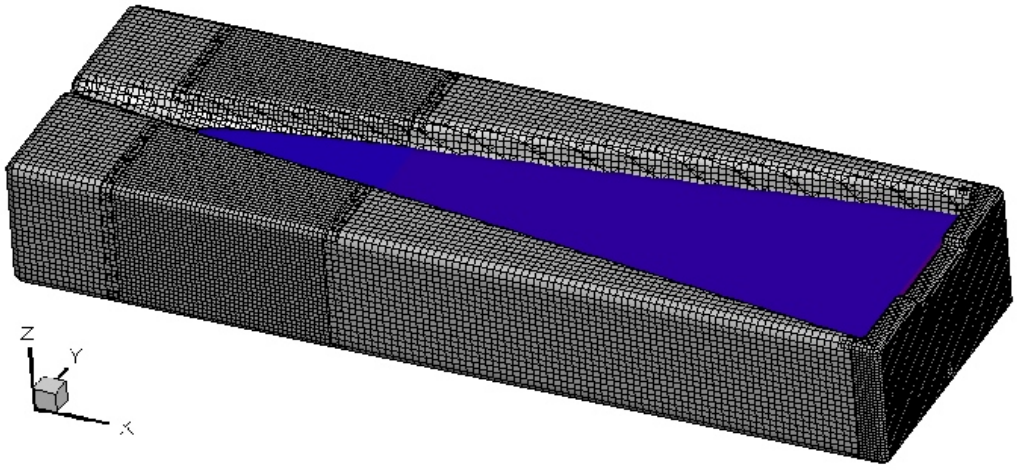

Figure 4.7 : Mesh structure of models.

Number of cells varies in different models, because of the differences in dimentions and conditions of the geometry of models. These differences in blocks are because of the importance of the situation of parts of geometry.

General form, the number and position of the blocks are represented as Figure 4.8.

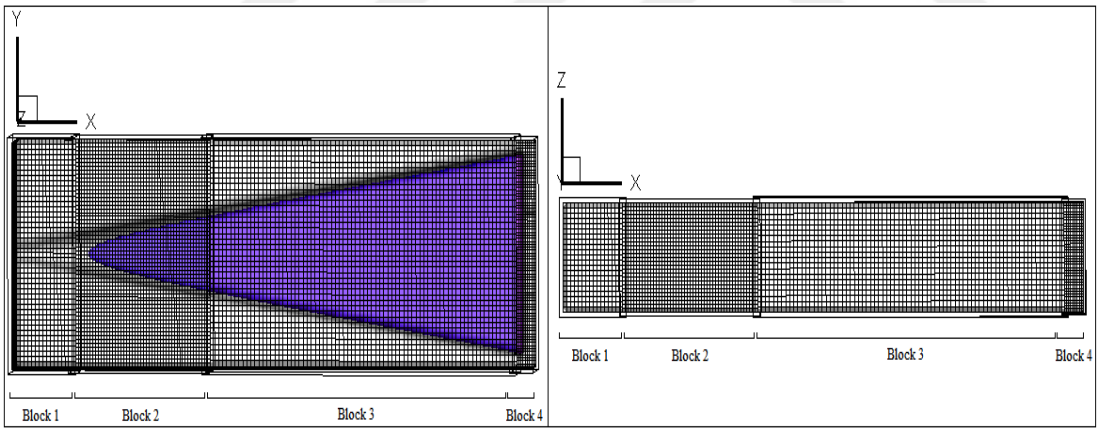

Figure 4.8 : Number and position of blocks in all models.

As seen in Figure 4.8, the geometry consists of four separate blocks. Block and grid information of the models for each block are presented in Table 4.4. The cells in block number 2 and 4 are smaller than the other block. In block 2, it is similar to shallow water condition. So, the details are very important in this region. On the other hand, in block 4, the spillway and bottom outlet are available. Then, the smaller cells are needed to creation of a good shape structure of these outlets.

Table 4.4 : Grid information of each mesh block

Mesh Block No.	Direction	Total number of real cells	Minimum cell size	Maximum cell size	Total number of real cells of each block	Total number of real cells in model
I	x	16	2.50	2.50	14784	181708
	y	44	2.50	2.50		
	z	21	2.52	2.52		
II	x	48	1.87	1.87	79296	
	y	59	1.86	1.86		
	z	28	1.89	1.89		
III	x	76	2.69	2.69	62320	
	y	41	2.68	2.68		
	z	20	2.65	2.65		
IV	x	9	1.44	1.44	25308	
	y	76	1.44	1.44		
	z	37	1.43	1.43		

4.6 Boundary Conditions of Models

Each boundary of the computational domain has an associated boundary condition. x_{min} was selected as the inflow boundary. The defined boundary condition for this point of model was volume flow rate, which defines the inflow dischrges to the FLOW3D (V_{fr} or Q). For this boundary condition, inflow discharge, sediment concentration of inflow water and the thermal informations of inflow water were adjusted, depends on the selected models. Here, the values and parameters were set as time-dependent conditions.

The boundary condition at x_{max} , in block number 4 in models, was selected as outflow boundary (O), where the body of the dam is located. The outflows were considered as a spillway at the dam crest and the lower outlet near the bottom of the body of dam, which were discribed in the section of 4.3 of this chapter. There are two types of models defined here such as S and B. S models represent models that only spillways work. Although, in the other types of simulations of initial models (for sensitivity), only the bottom outlet of the model works.

The bottom (z_{min}), right (y_{min}) and left (y_{max}) boundary conditions of reservoir were selected as wall type (W). In this type of boundaries, fluid could not be entered to the boundary. Zmax boundary of models was defined as the symmetry condition (S). Figure (4.9) represents these boundary conditions (BCs).

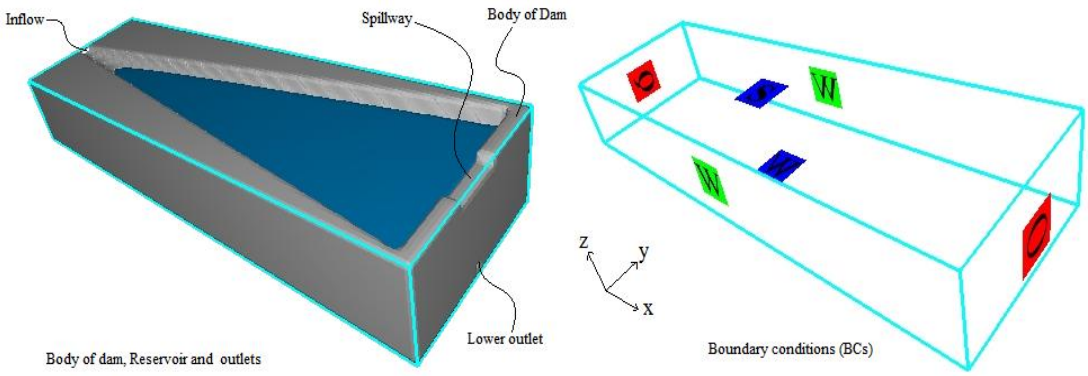

Figure 4.9 : Body of dam, reservoir, outlets and boundary conditions.

Volume flow rate or inflow discharges could be defined as a fixed quantity over the time or as a hydrograph. This is also applied for the sediment concentration of inflow fluid (water and sediment mixture). In these simulations it is assumed the discharges have constant value.

4.7 Selected Turbulence Models

In last chapter, the major turbulence models were discussed and described in detail. Those typically robust turbulence models have been well tested and documented in the relevant technical literatures. Based upon prior experience with Flow 3D and the selected size of the domain, two types of those models were appropriate to use in this study for all simulations.

From these two turbulenc models, the renormalized group turbulence model was selected for all the simulations of this study. This turbulence model is also known as RNG, briefly.

As mentioned before and in last chapters, FLOW 3D code has five types of turbulence models.. In this category of simulations, turbulence was modeled with renormalized group model (RNG) with dynamically computation of maximum turbulent mixing length. This selected turbulence model was two-equation model. The maximum turbulent mixing length is used to describe the characteristic size of the turbulent eddies exist in the fluid flow and is used to define the maximum allowed value of the turbulent viscosity coefficient. Other words, this value is used by turbulence models to limit the turbulent dissipation ε, so that the turbulent viscosity does not become excessively large. It is defined 10% of the depth of the water in many researches. But, in this study, this value was computed dynamically.

A remarkable point about the k-ε standart turbulence model, that must be noted here, is that the RNG model uses equations similar to the equations for the k-ε model.

4.8 Computational Modeling Scenarios

48 separate simulations (scenarios) were performed under the scope of this dissertation, without the simulations of case study, which wll be described in the next Chapter (Chapter 5) of this study. These simulations were included the changes in obtained and mentioned parameters in last parts of this chapter. A briefly matrix of simulations performed during this dissertation is represented in table 4.5 and 4.6. The first category of these scenarios, which has been shown as table 4.5, is related to reservoir operated with the spillway. These simulations were named with S and a number that shows the simulation number.

Table 4.5 : Matrix of Simulations (Scenarios) of Reservoir Operating with Spillway.

	River			Reservoir			
No.	Q (m^3/s)	C (g/l)	T (°C)	T (°C)	C (g/l)	Outlet Type	Turbulence Model
S1	20	20	4	24	15	Spillway	RNG
S2	50	20	4	24	15	Spillway	RNG
S3	100	20	4	24	15	Spillway	RNG
S4	20	20	12	24	15	Spillway	RNG
S5	50	20	12	24	15	Spillway	RNG
S6	100	20	12	24	15	Spillway	RNG
S7	20	20	24	24	15	Spillway	RNG
S8	50	20	24	24	15	Spillway	RNG
S9	100	20	24	24	15	Spillway	RNG
S10	20	20	40	24	15	Spillway	RNG
S11	50	20	40	24	15	Spillway	RNG
S12	100	20	40	24	15	Spillway	RNG
S13	20	15	4	24	20	Spillway	RNG
S14	50	15	4	24	20	Spillway	RNG
S15	100	15	4	24	20	Spillway	RNG
S16	20	15	12	24	20	Spillway	RNG
S17	50	15	12	24	20	Spillway	RNG
S18	100	15	12	24	20	Spillway	RNG
S19	20	15	24	24	20	Spillway	RNG
S20	50	15	24	24	20	Spillway	RNG
S21	100	15	24	24	20	Spillway	RNG
S22	20	15	40	24	20	Spillway	RNG
S23	50	15	40	24	20	Spillway	RNG
S24	100	15	40	24	20	Spillway	RNG

The second category of scenarios, are named with B and a number besied it. These simulations are related to the reservoir with a outlet in bottom.

Table 4.6 : Matrix of Simulations (Scenarios) of Reservoir Operating with Bottom Outlet.

	River			Reservoir			
No.	Q (m^3/s)	C (g/l)	T (°C)	T (°C)	C (g/l)	Outlet Type	Turbulence Model
B1	20	20	4	24	15	bottom	RNG
B2	50	20	4	24	15	bottom	RNG
B3	100	20	4	24	15	bottom	RNG
B4	20	20	12	24	15	bottom	RNG
B5	50	20	12	24	15	bottom	RNG
B6	100	20	12	24	15	bottom	RNG
B7	20	20	24	24	15	bottom	RNG
B8	50	20	24	24	15	bottom	RNG
B9	100	20	24	24	15	bottom	RNG
B10	20	20	40	24	15	bottom	RNG
B11	50	20	40	24	15	bottom	RNG
B12	100	20	40	24	15	bottom	RNG
B13	20	15	4	24	20	bottom	RNG
B14	50	15	4	24	20	bottom	RNG
B15	100	15	4	24	20	bottom	RNG
B16	20	15	12	24	20	bottom	RNG
B17	50	15	12	24	20	bottom	RNG
B18	100	15	12	24	20	bottom	RNG
B19	20	15	24	24	20	bottom	RNG
B20	50	15	24	24	20	bottom	RNG
B21	100	15	24	24	20	bottom	RNG
B22	20	15	40	24	20	bottom	RNG
B23	50	15	40	24	20	bottom	RNG
B24	100	15	40	24	20	bottom	RNG

4.9 Results of Simulations

The graphical results shown here, are the variations of the temperature and the concentrations by changing in depths. The results are compared in different times included: 100 s, 150 s, 200 s, 250 s, 500 s, 750 s, 1000 s, 1500s, 2000 s, 2500 s and 3000 s. These times are the times passed from beginning of the simulations. When time is equal to zero, it expresses the time that the inflow water (river) received to the reservoir. The results are compared at the middle of the width of the reservoir, where

the y is equal to 60 meters. The selected distances from the beginning of the reservoir are 100 m, 150 m, 200 m, 250 m and 300 m.

The main aim of these simulations are for determining the effect of changes in some parameters of inflow water and the reservoir's water. So, these simulations will be compared and described three by three. In conclusion chapter of this thesis, the result of all of these simulations will be described. In all the following figures, as could seen, the reservoir starts from -35 m in lenght and -5 m in depth. These values are relating to the coordinates of the geometry of the reservoir, which is defined to the FLOW3D program. -35 meters indicates the starting point of the reservoir and -5 m in depth indicates the deepest point of the geometry.

4.10 Results for Reservoir with Spillway outlet (S Type Simulations)

When spillway is operated, the following results are given by FLOW3D for mentioned scenarios.

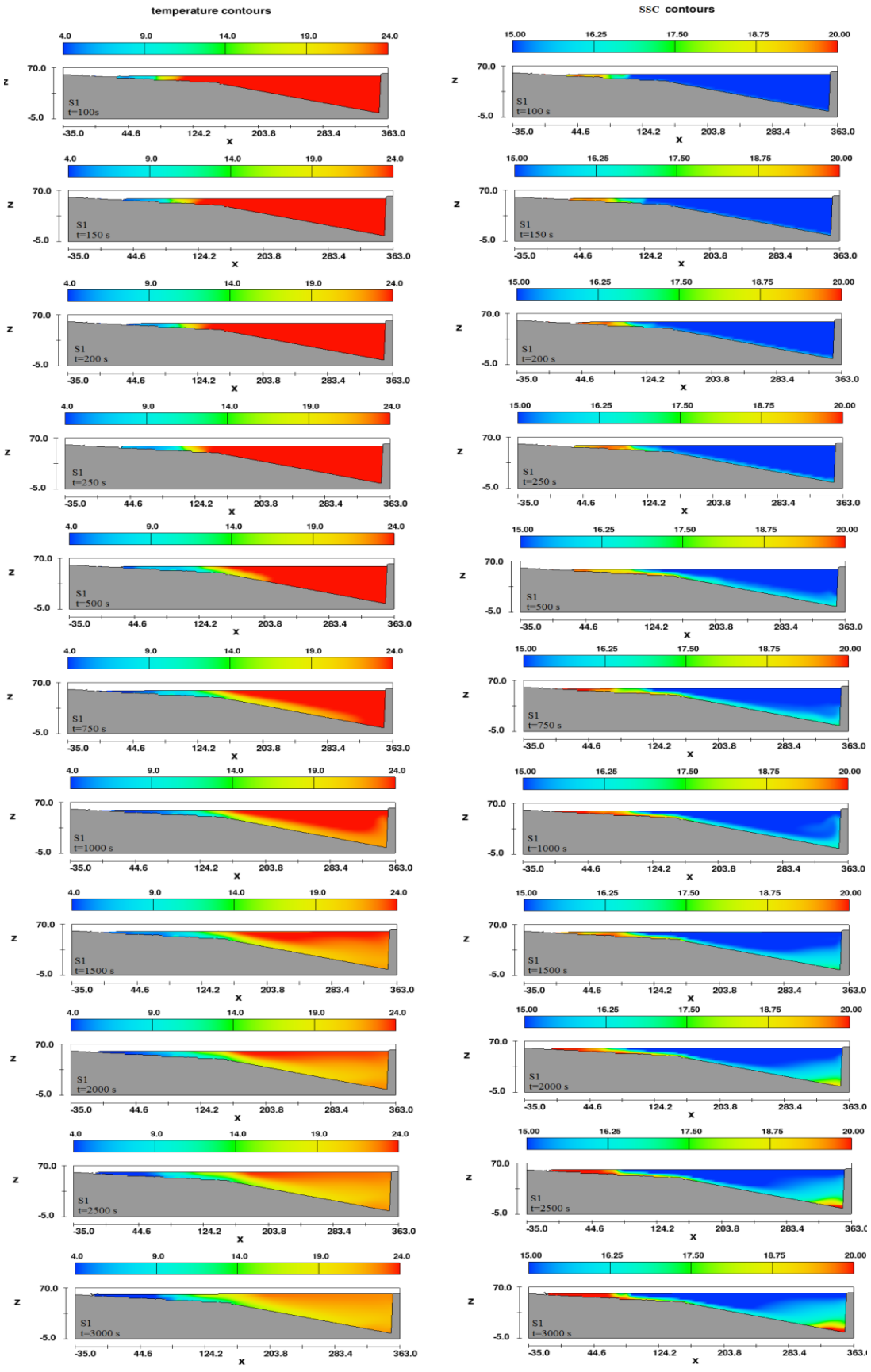

Figure 4.10 : Temperature and SSC Contours of Simulation S1.

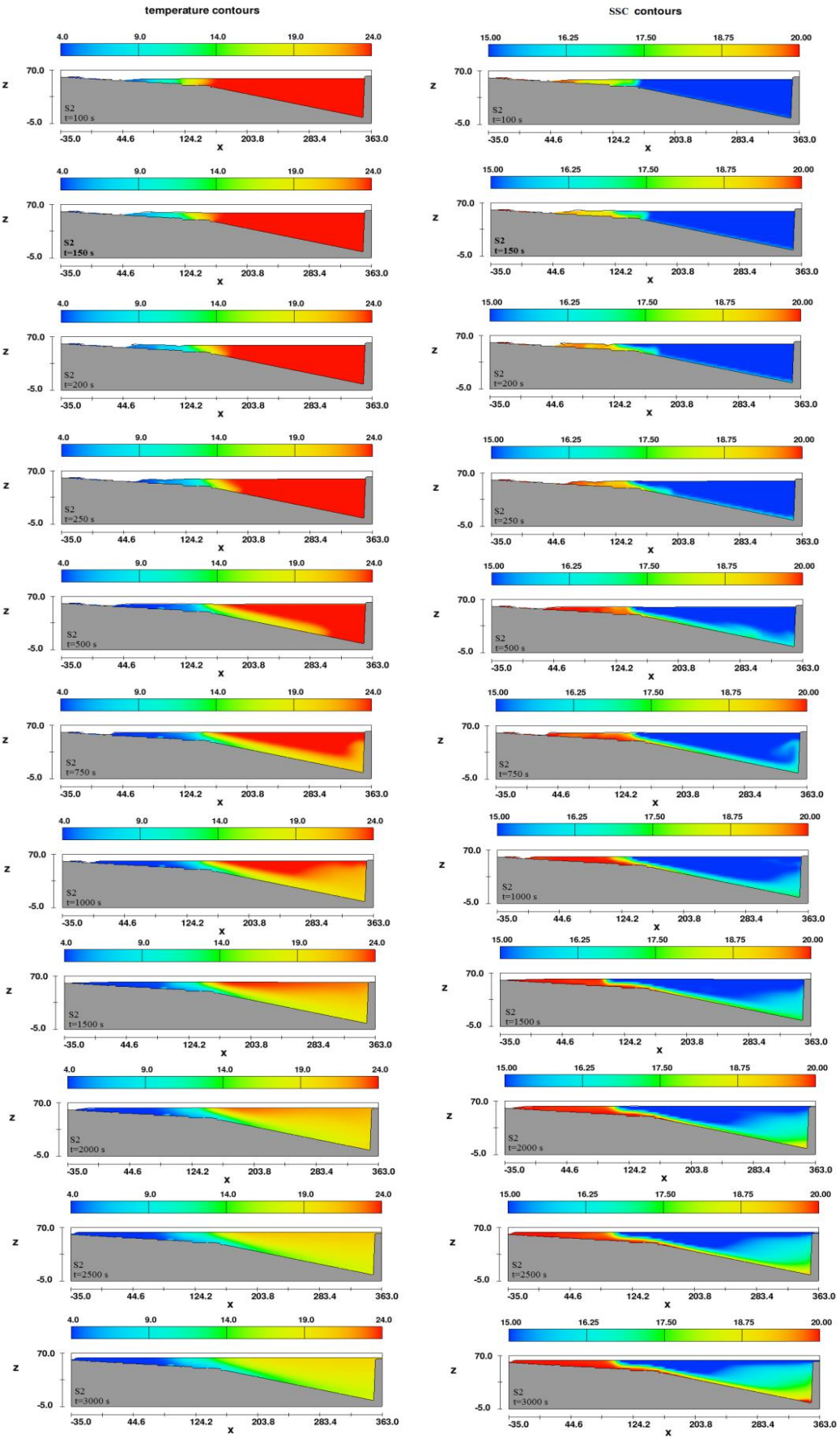

Figure 4.11 : Temperature and SSC Contours of Simulation S2.

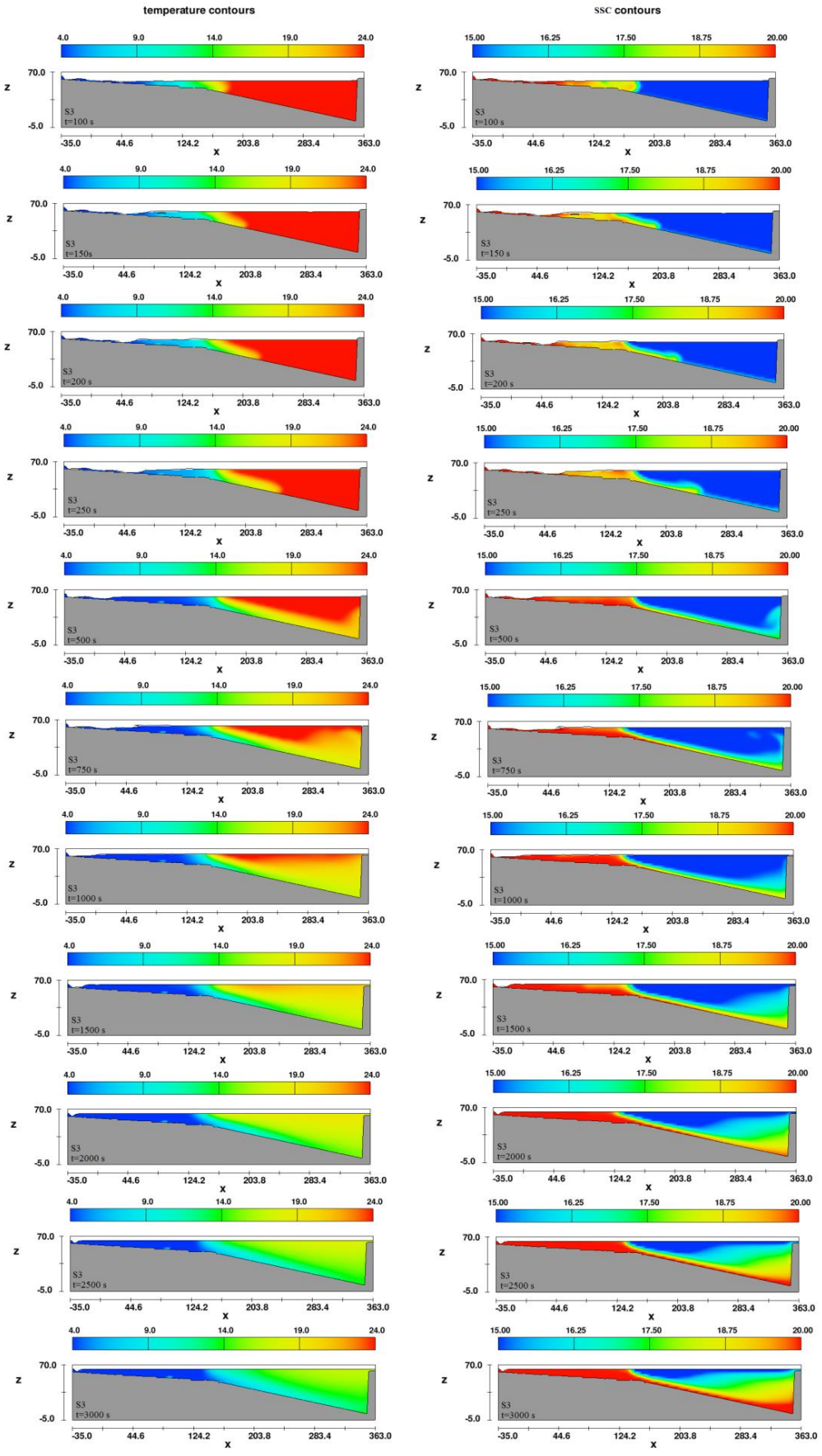

Figure 4.12 : Temperature and SSC Contours of Simulation S3.

As mentioned in the table (4.5), S1, S2 and S3 simulations have same inflow and reservoir water temperatures and concentrations. In each of these simulations, only discharge is changed. As the inflow water's concentration is higher than the reservoir's water, the inflow water is denser than the reservoir one. As a result, it is expected that the under flow condition occurred. On the other hand, since the cold water is denser than warm and hot water, the inflow water is denser than the reservoir's one. Then it is expected that the inflow water sinks to the reservoir water and the thermal under flow condition occurs.

From the results of theses three simulations, it is seen that increasing of discharge affects the thickness of turbidity current. It is also seen the impacts of increasing of discharge on the turbidity current's propagation. It means that if discharge increases, then the rate of the propagation of the turbidity current will increased and the current with higher values of concentrations and temperatures will arrive earlier to the body of dam. In S3 simulation and in the time between 150 s to 250 s, the structure of the turbidity current appears, obviously.

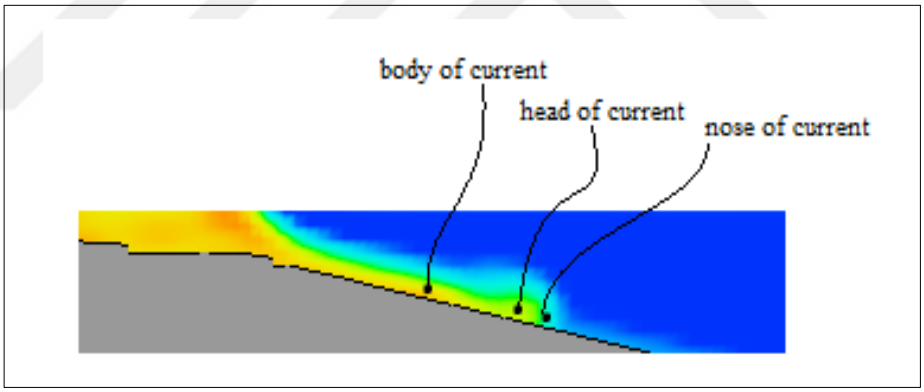

Figure 4.13 : Structure of Turbidity Current Formed in Simulations.

In Figure 4.13, the nose, head and the body of the turbidity current are displayed, clearly. While the existence of part of this current is not visible in the simulations with the lower amount or magnitude of discharge, obviously. Therefore, the discharge magnitude is a major parameter for formation of the structure of the turbidity current.

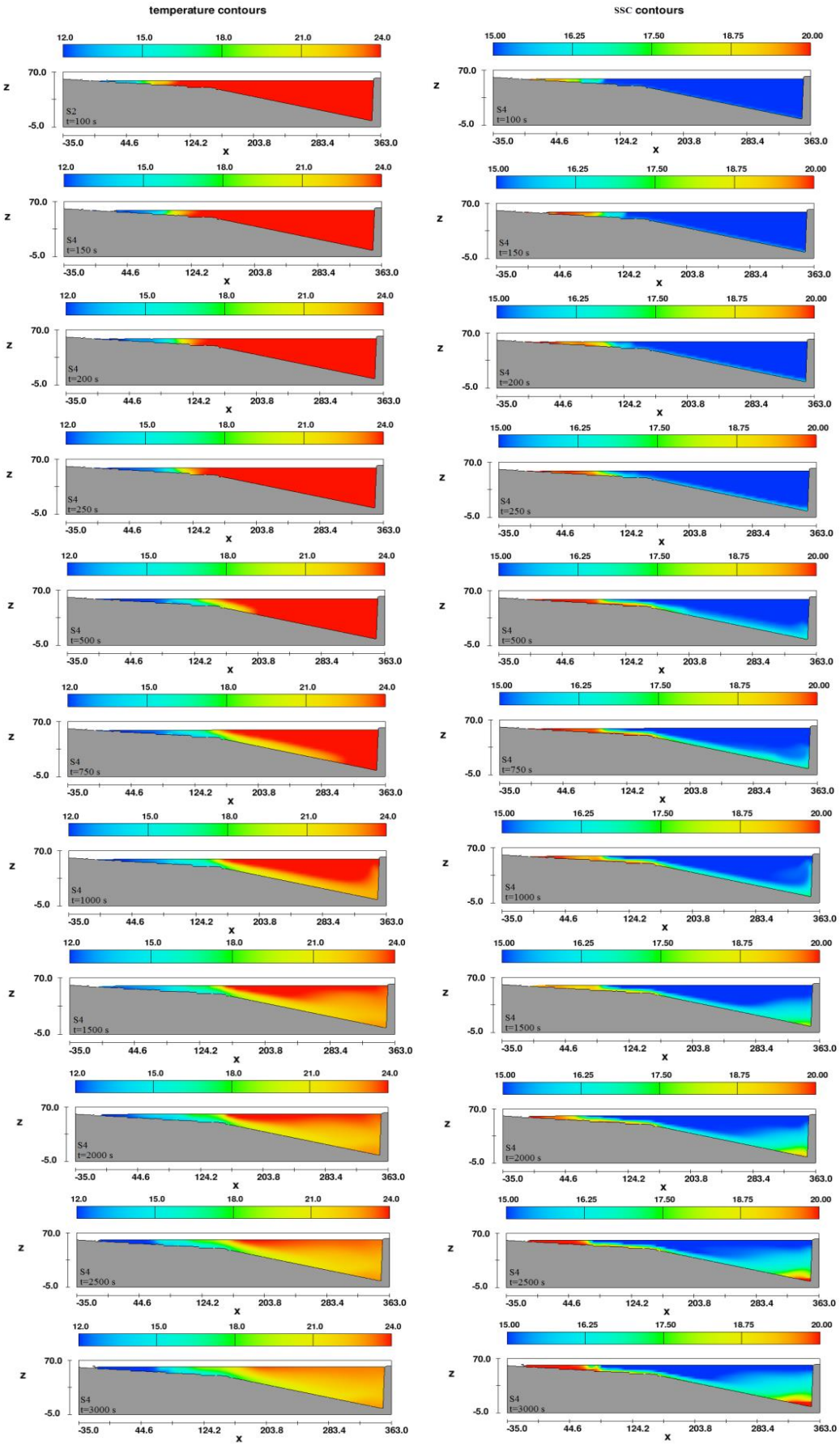

Figure 4.14 : Temperature and SSC Contours of Simulation S4.

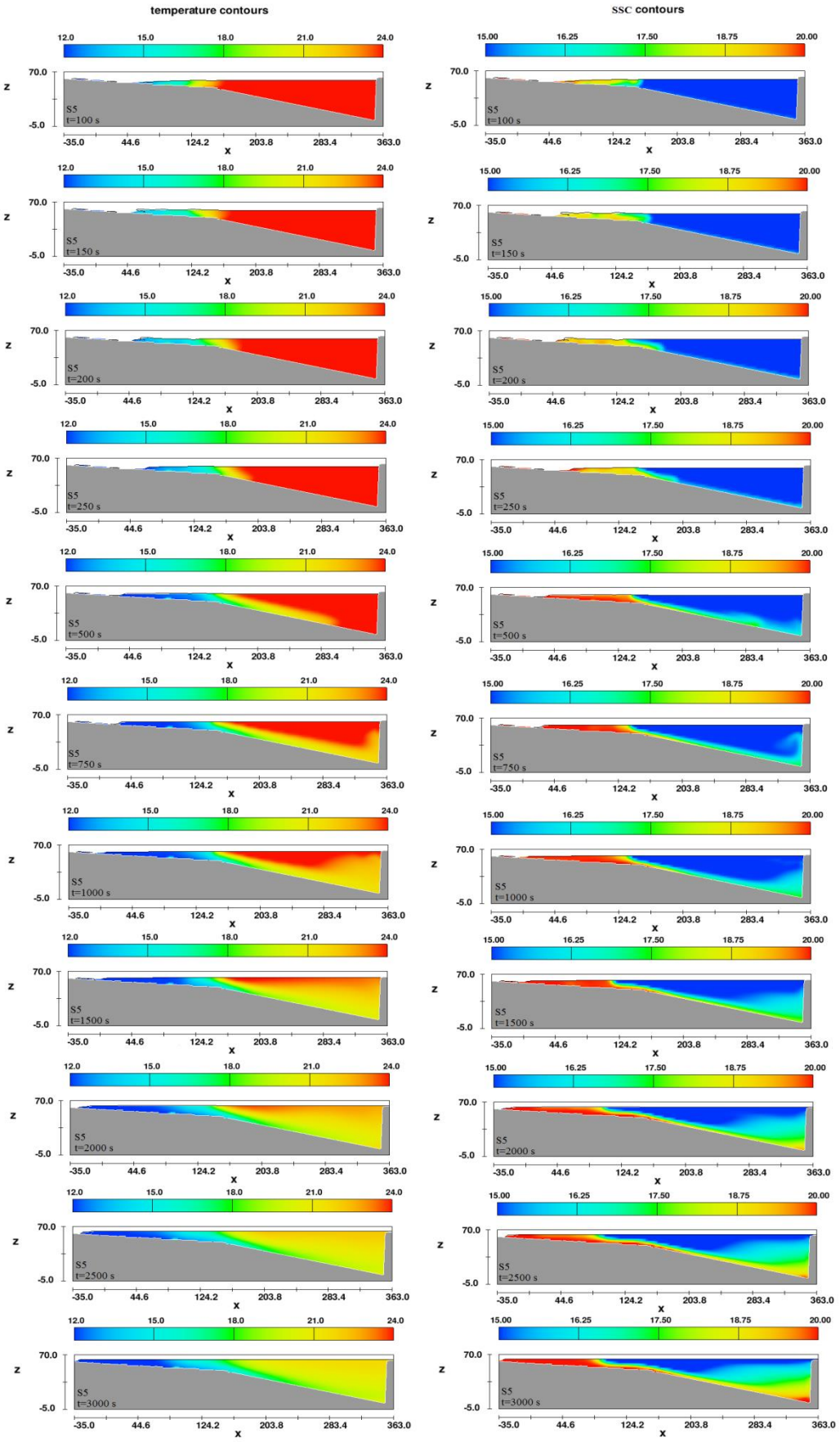

Figure 4.15 : Temperature and SSC Contours of Simulation S5.

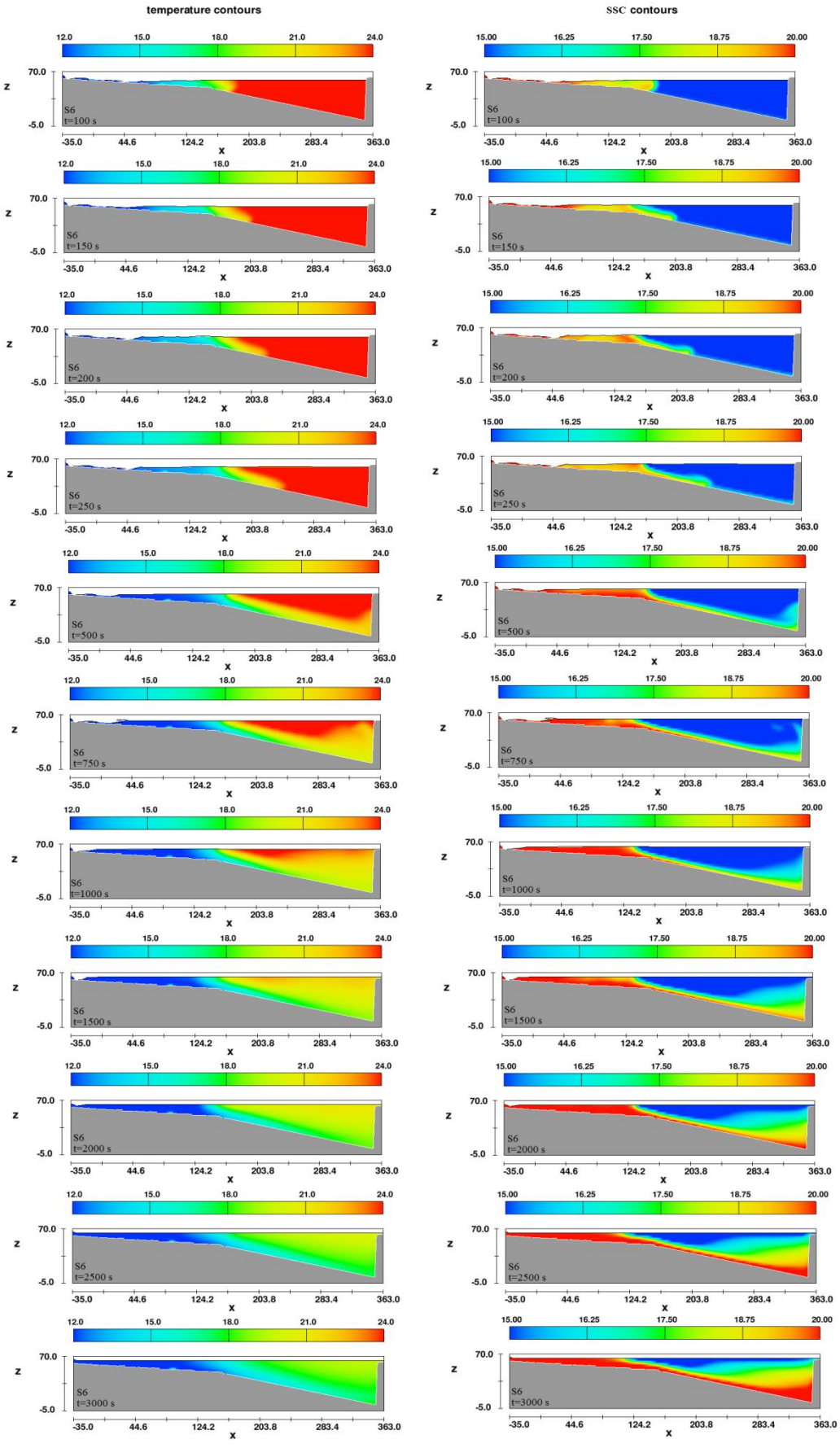

Figure 4.16 : Temperature and SSC Contours of Simulation S6.

In the next three simulations, which included as S4, S5 and S6 simulations, the all parameters are unchanged in comparison with previous models, except for the temperature of inflow water. This parameter is changed to 12^{o}C. With this change in inflow water temperature, the spread of temperature and concentration are changed.

In simulations S7, S8 and S9, the temperature of inflow and reservoir water are same and equal to 24^{o}C. Therefore, there is no change in water's temperature. These three simulations are affected only by discharge magnitude. The discharges for S7, S8 and S9 simulations are equal to 20 m^3/s, 50 m^3/s and 100 m^3/s, respectively. As mentioned before, the nose and head of the turbidity current are clearly formed when the discharge has the higher values. This state is abviously observed in the simulation S9. As another important result for all of these simulations, it is seen that the thermal and concentration stratifications are formed.

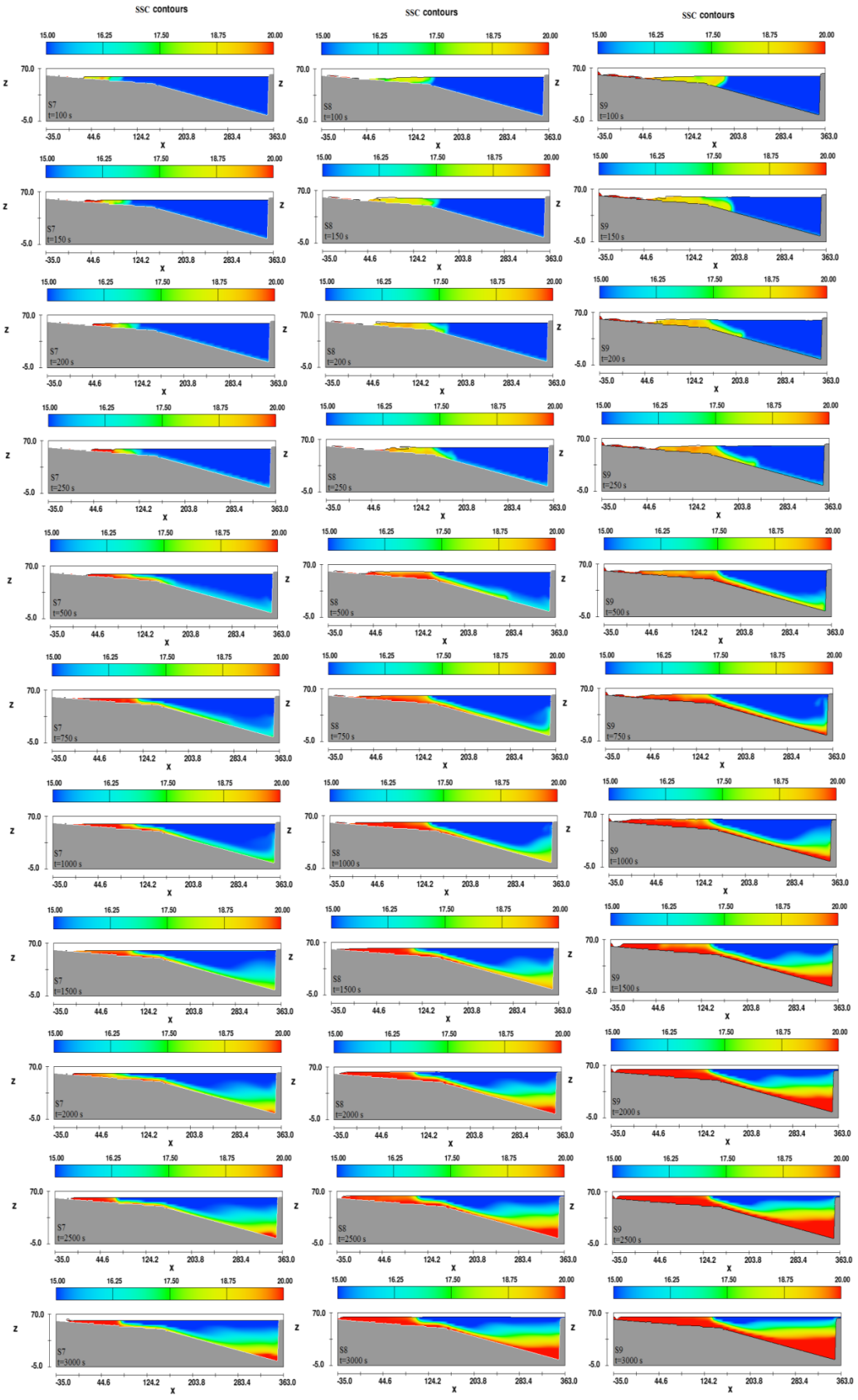

Figure 4.17 : SSC Contours of Simulations S7, S8 and S9.

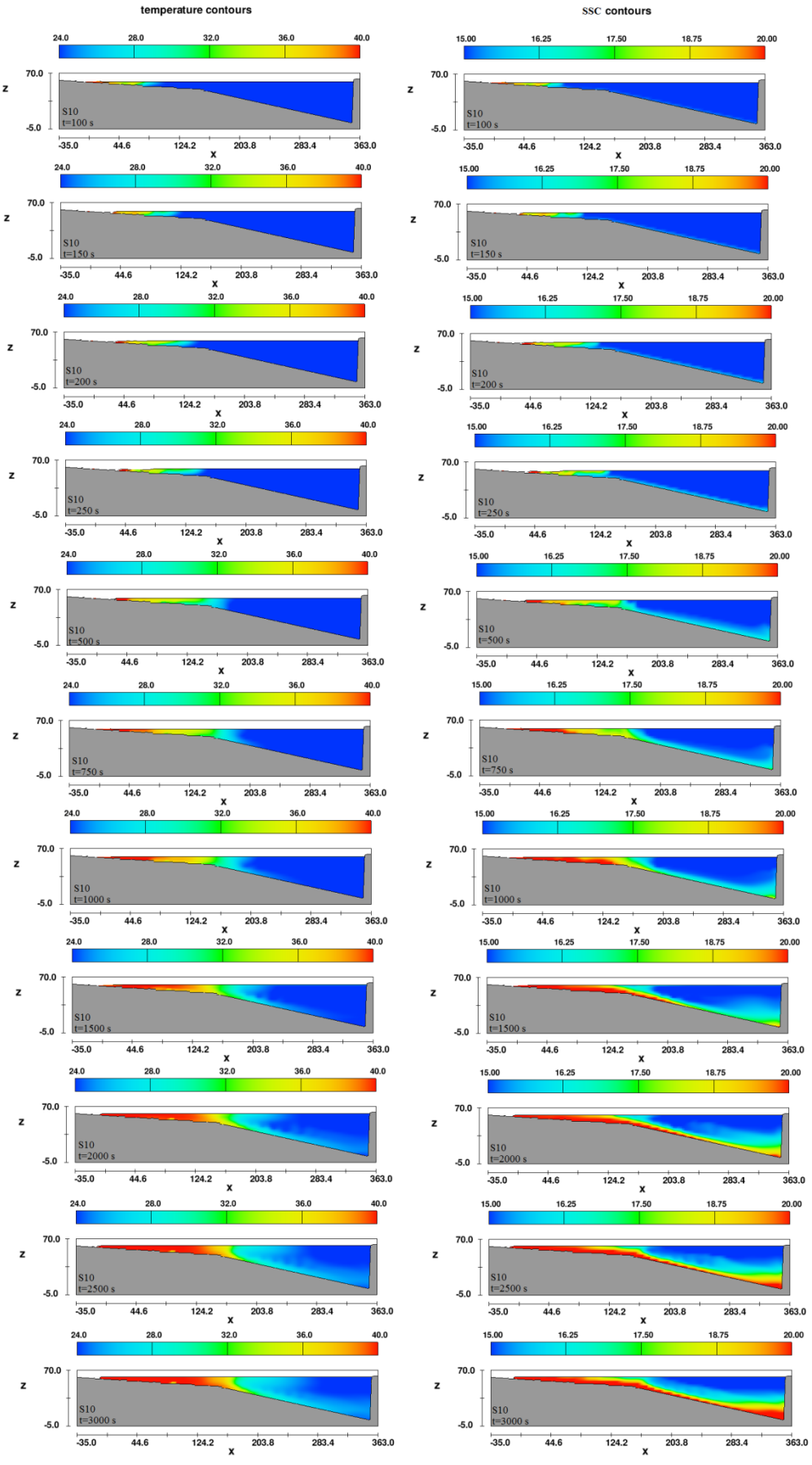

Figure 4.18 : Temperature and SSC Contours of Simulation S10.

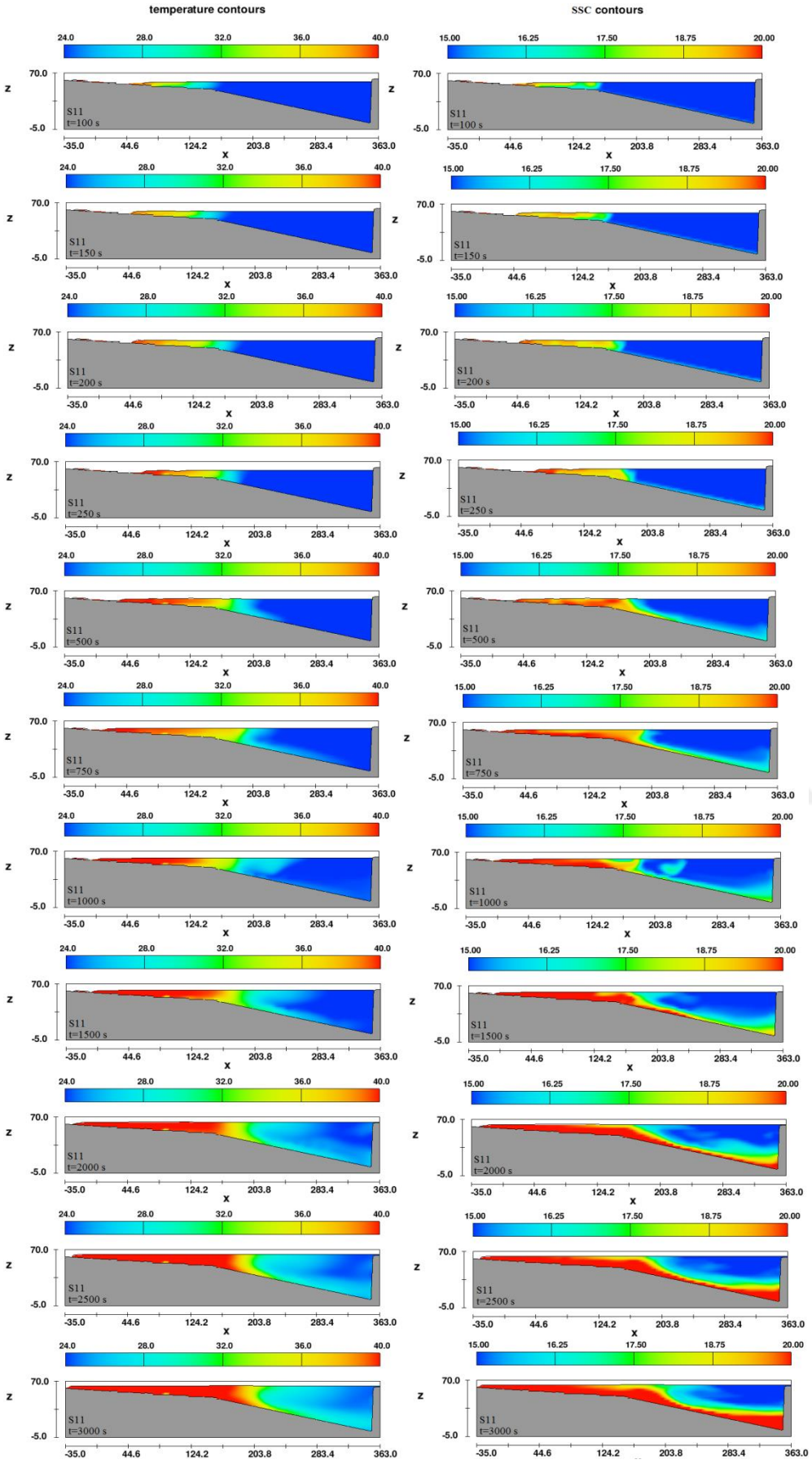

Figure 4.19 : Temperature and SSC Contours of Simulation S11.

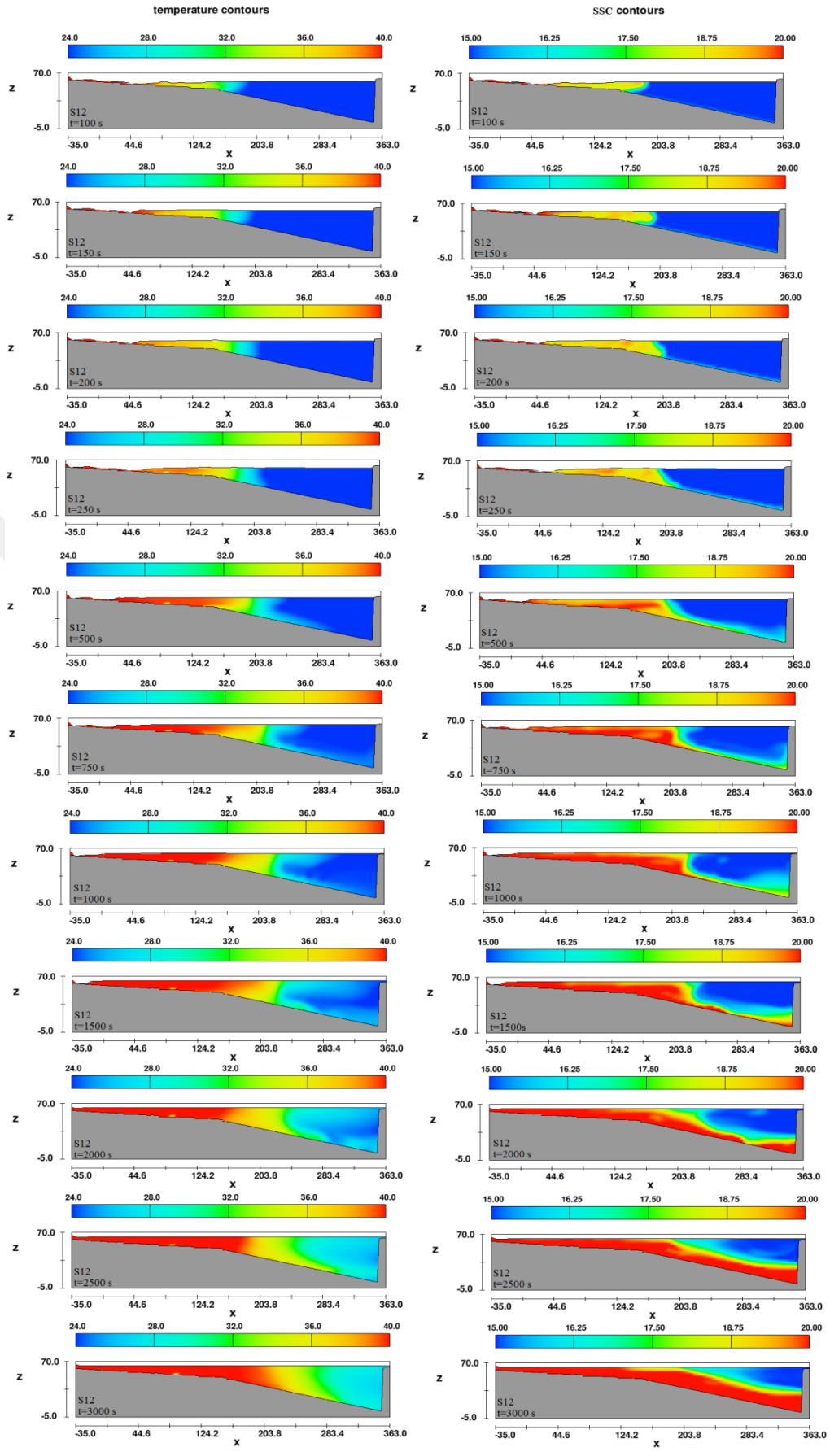

Figure 4.20 : Temperature and SSC Contours of Simulation S12.

The turbidity flow and its structure is shown in Figure 4.21.

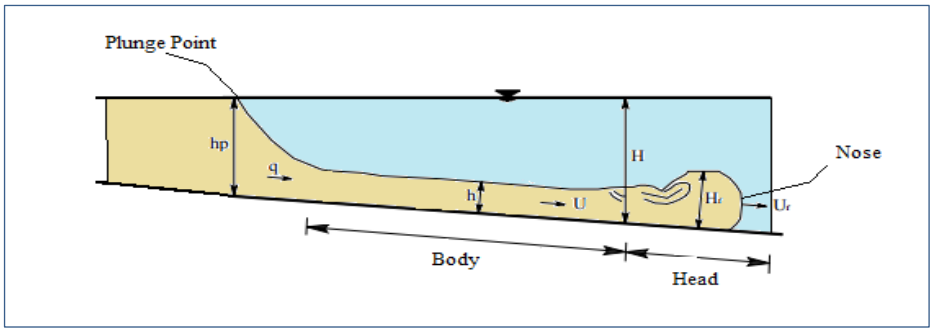

Figure 4.21 : Structure of Turbidty Flow (Graph, 1998).

According to Figure 4.21 and with evaluation of the results figures of first 12 simulations, it is seen that with increasing the inflow water temperature, the plunge point comes to the downstream side of the reservoir and the distance rises from the beginning of the reservoir (river mouth). As an important result, it is clear that the body of turbidity current is formed strongly due to increasing in the inflow water temperature in these simulations. These mentioned states are presented in Figure 4.22.

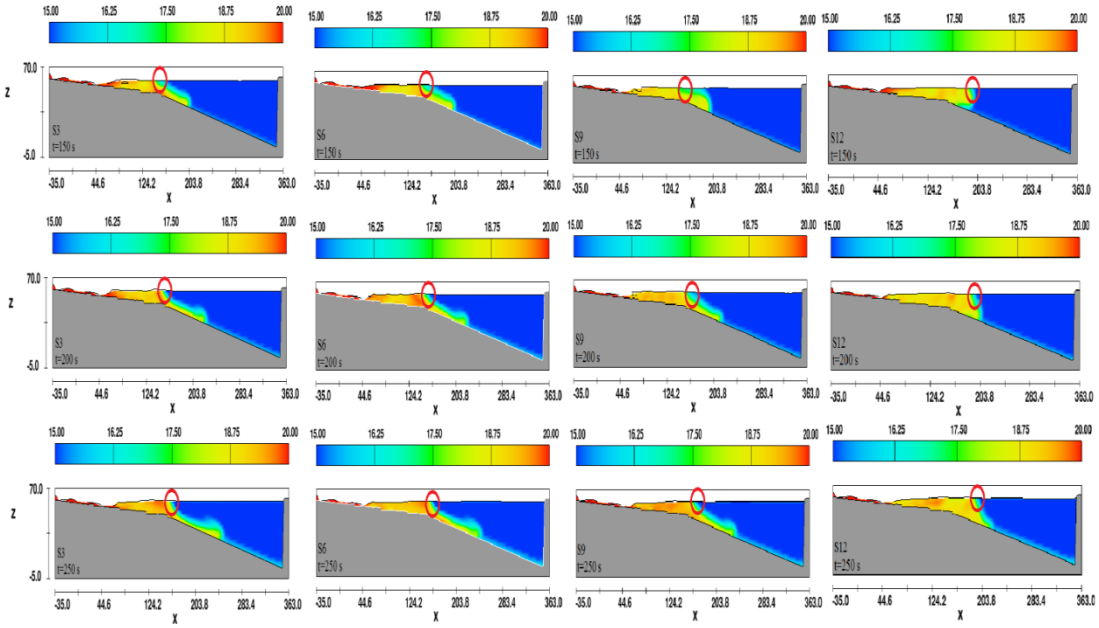

Figure 4.22 : Plunge points of Simulations S3, S6, S9 and S12.

Totally, in all the first 12 simulations, the hyperpycnal flow is occurred. In some simulations such as S11 and S12, in the first 250 seconds, flow gives homopycnal flow form.

It is seen that the turbidity flow in each of these simulations arrive to the dam body in different times. So, the time of arriving the turbidity flow to the body of dam (td) and the location of the plunging point at these times could be compared each other. For these first 12 simulations, S3, S6, S9 and the S12 simulations were selected because of the strongly formation of the structure of turbidity flow in these simulations. In these selected simulations, as previously noted, the head and the nose of these flows are clearly visible. These results are given in the table below. In this table, Δx is the distance from the beginning point of the reservoir to the plunging point (x_p).

Table 4.7 : Comparing Results for S3, S6, S9 and S12.

Simulation ID	t_d	Coordinate of Plunging point (x_p)	Δx
S3	429 s	160 m	195 m
S6	455 s	161 m	196 m
S9	500 s	164 m	199 m
S12	605 s	203 m	238 m

In the last 12 simulations, there is a circulation flow zone formed. The location of this zone is presented in the figure below. This state will be shown in the next figures.

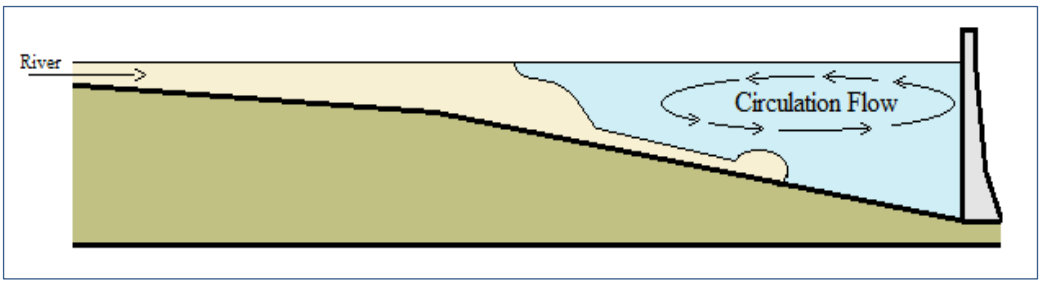

Figure 4.23 : Location of the Circulation Flow.

The plain velocity vectors and the colored 2D velocity magnitude vectors are presented for S3, S6, S9 and S12 simulations for time (t) equal to 500, 1000, 1500 and 2500 seconds, at y-z, x-y and x-z section near dam body. In the figures given here, the circulation phenomena zones are clearly visible for this section.

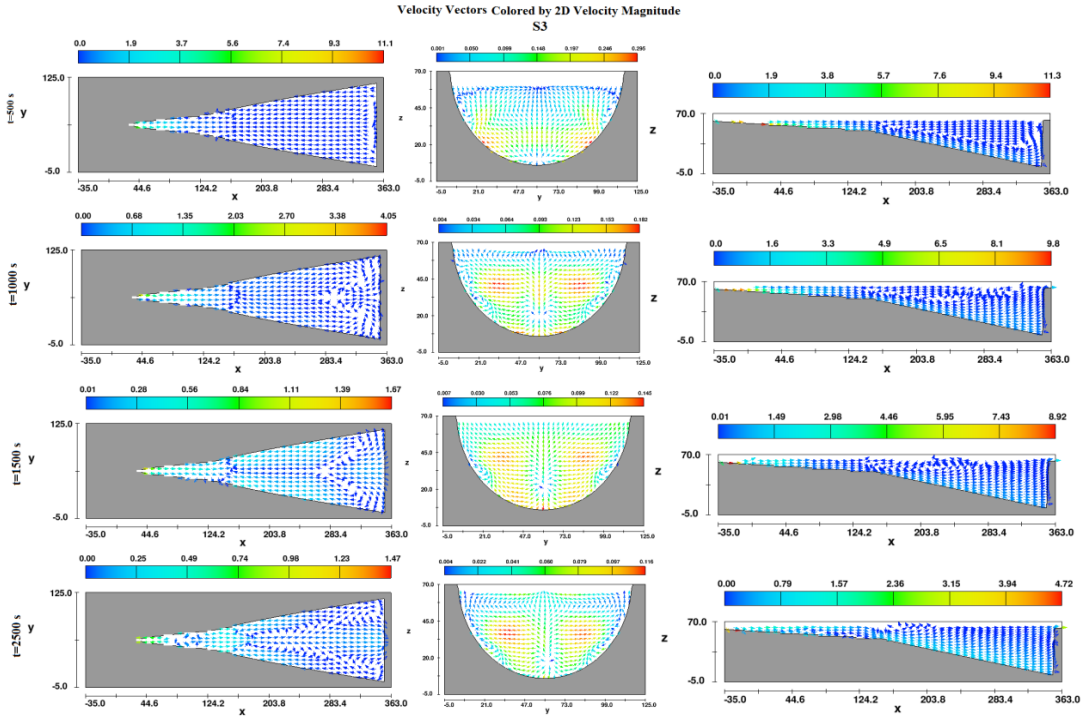

Figure 4.24 : Velocity Vectors Colored by 2D Velocity Magnitude for S3.

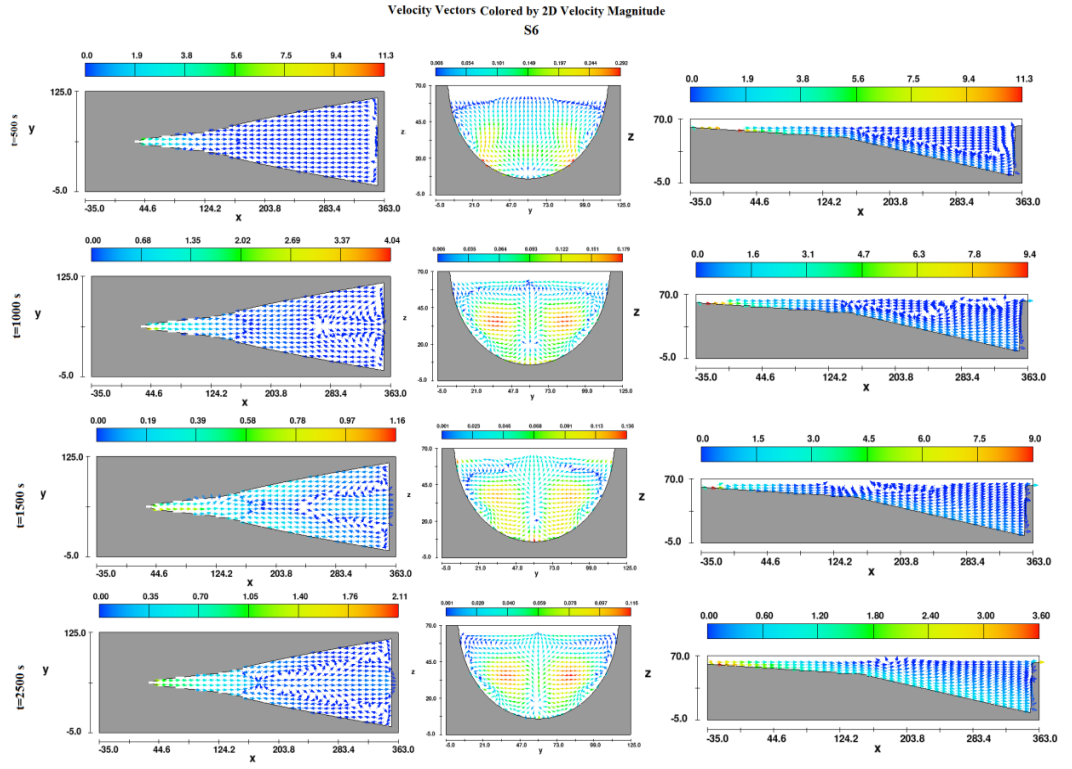

Figure 4.25 : Velocity Vectors Colored by 2D Velocity Magnitude for S6.

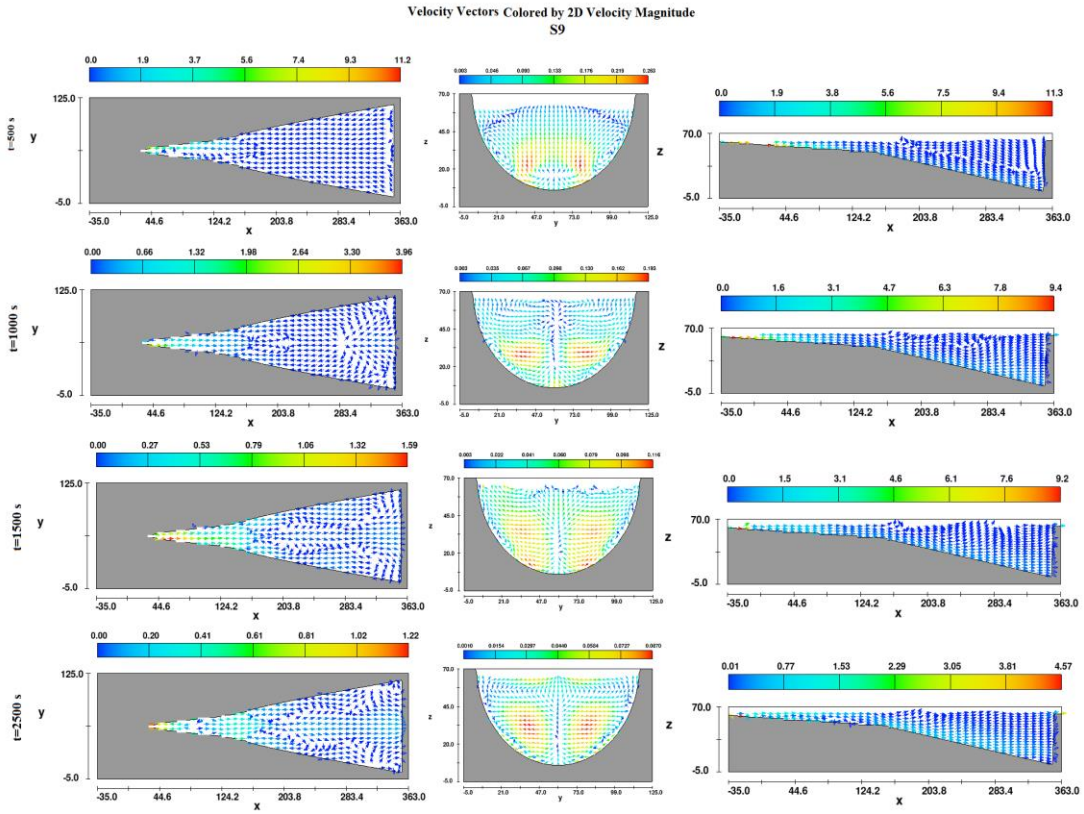

Figure 4.26 : Velocity Vectors Colored by 2D Velocity Magnitude for S9.

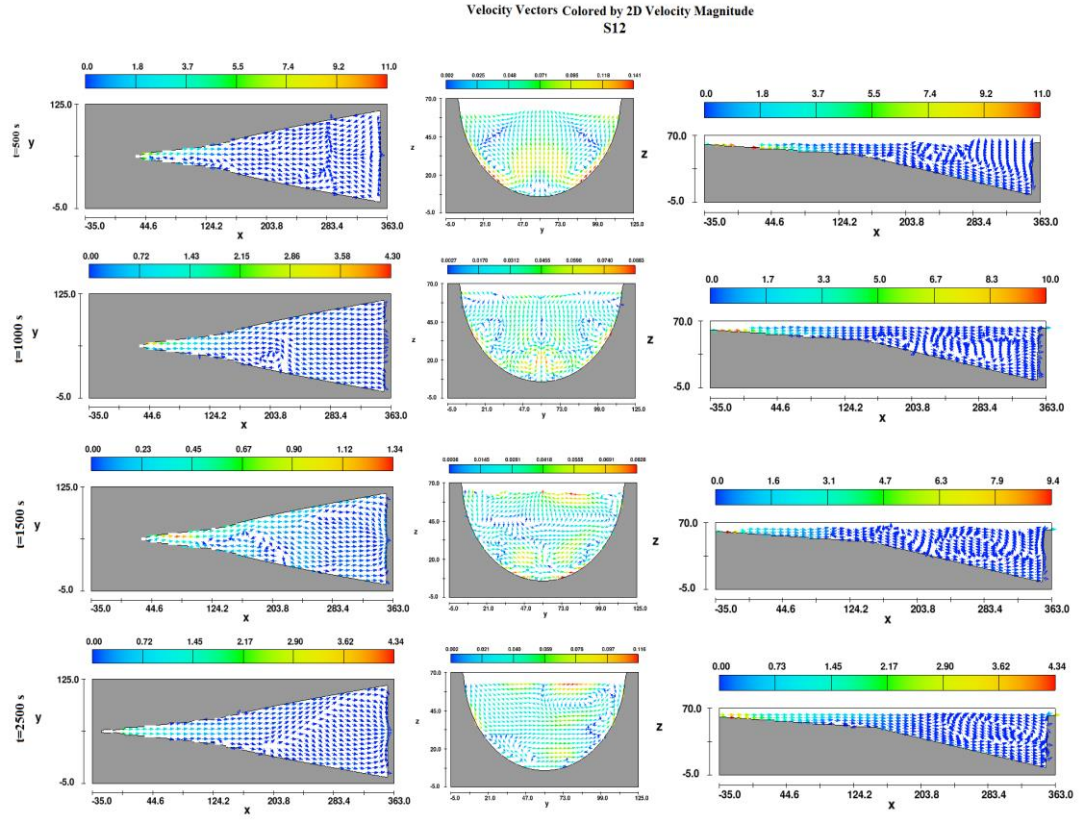

Figure 4.27 : Velocity Vectors Colored by 2D Velocity Magnitude for S12.

With investigating the results figure of velocity vectors, it is observed that the circulation occurs at both the water surface and at depths in different times. The spillway affects on the circulation and the vectors directions, when it operates. The spillway, as mentioned in the last parts of this chapter, operates when the water level arrives to the spillway elevation. Reverse current that appears in most of the last given figures is a normal occurrence that was expected. As an example of one of the results of simulations, the reverse and circulate currents are shown in Figure 4.28.

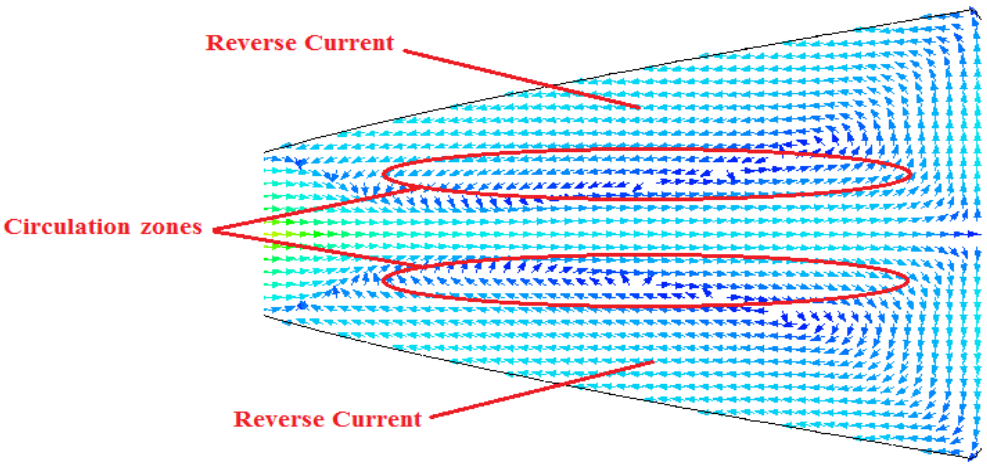

Figure 4.28 : Circulation and the Reverse Current of the simulations S1 to S12.

By study on the given results that were shown in the last figures, the flow direction and pattern is briefly represented for simulations with 100 m^3/s in the following figures.

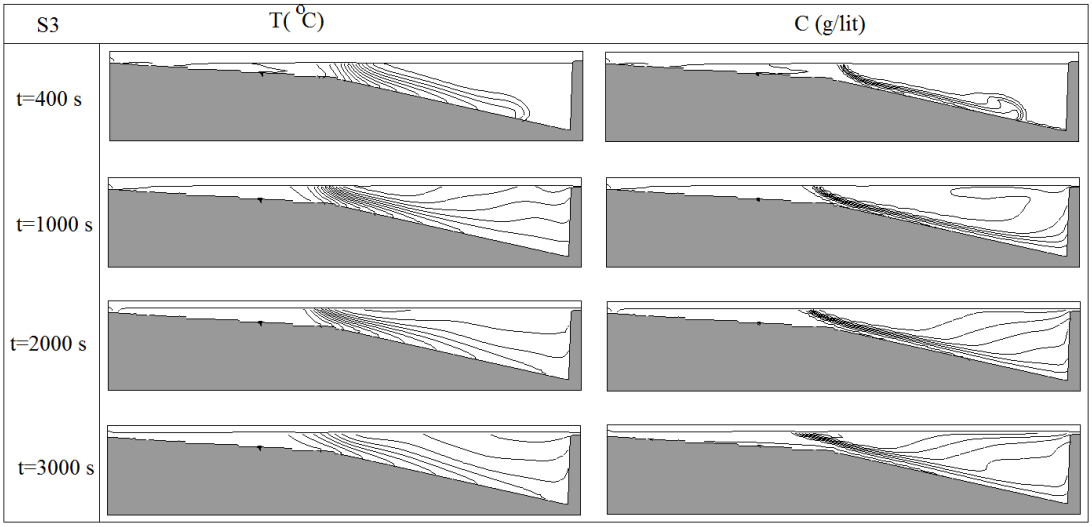

Figure 4.29 : B/W contours of temperature and concentration (S3).

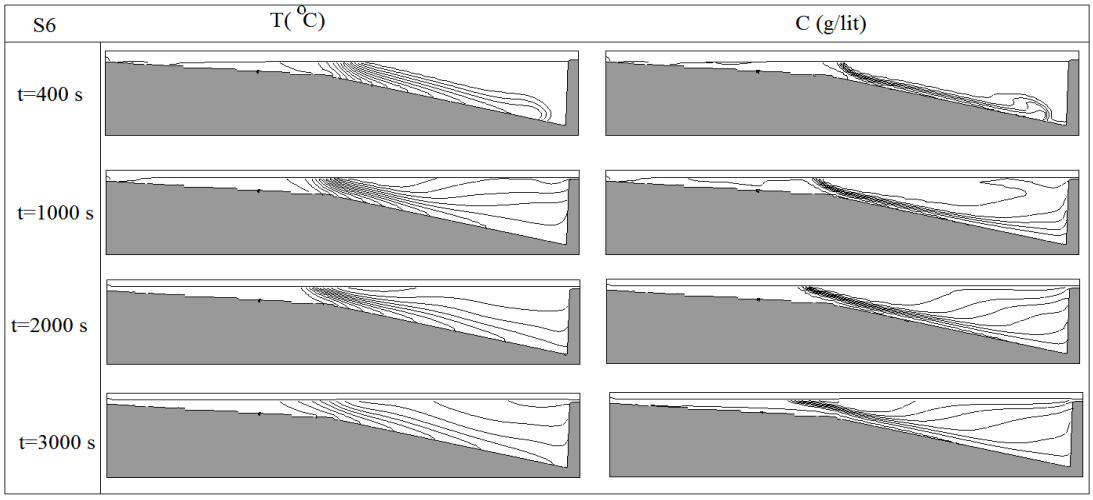

Figure 4.30 : B/W contours of temperature and concentration (S6).

In simulation S9, water temperature of reservoir is as same as the inflow's one as mentioned before. So, the temperature is constant in this simulation during time.

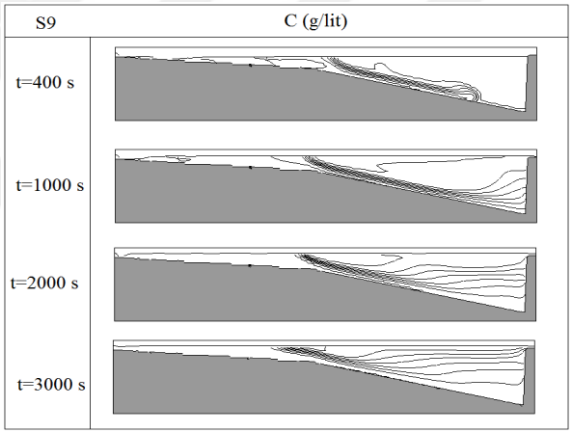

Figure 4.31 : B/W contours of temperature and concentration (S9).

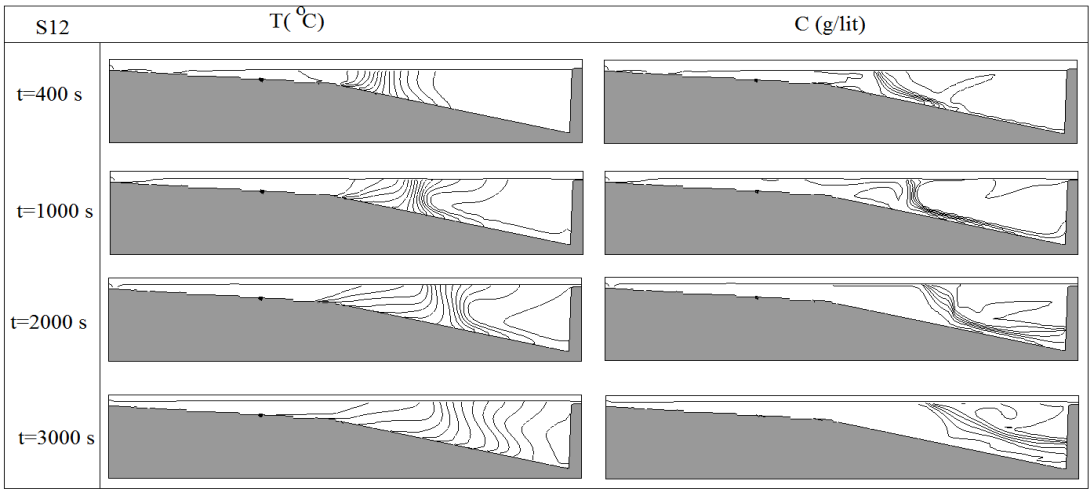

Figure 4.32 : B/W contours of temperature and concentration (S12).

In these 12 simulations, it is seen that the inter flow and mostly under flow conditions occurred. The vector figures of these simulations demonstrate this subject.

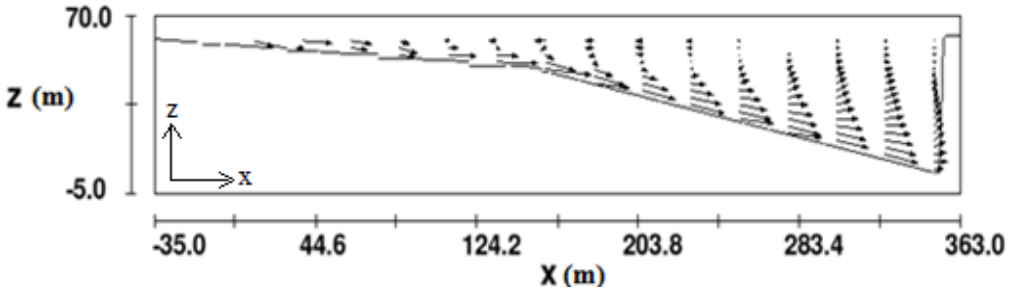

Figure 4.33 : Inter and under flow condition (Velocity vectors).

In these simulations, when the spillway starts to operate, in simulations 11 and 12 specially, the velocity vectors give the following form in Figure 4.34.

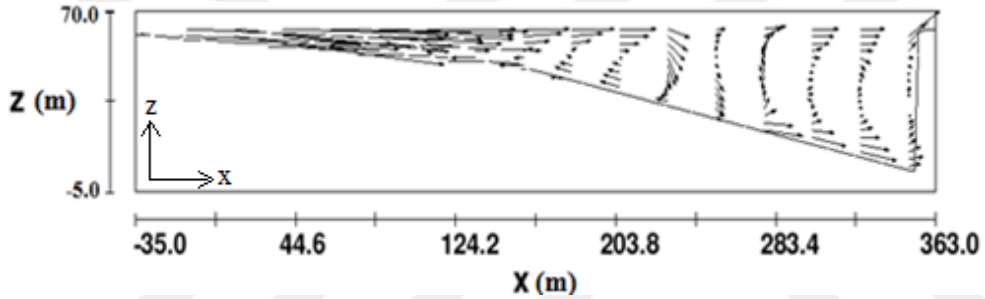

Figure 4.34 : Velocity vectors and flow direction when spillway starts to operate.

In Figure 4.34, incresing of velocity at the upper layer of the reservoir is obvious. This increasing in velocity at the upper layer of reservoir, rises more near the dam body than the othr places farther away from the dam body. It is because of the operation of spillway. The last results are compared each other in two section of the reservoir, which are shown in the figure below. One of these sections was selected next to the dam body and the other one was in the middle of the reservoir, which had the distance from the entrance of reservoir equal to 250 m and 375 m.

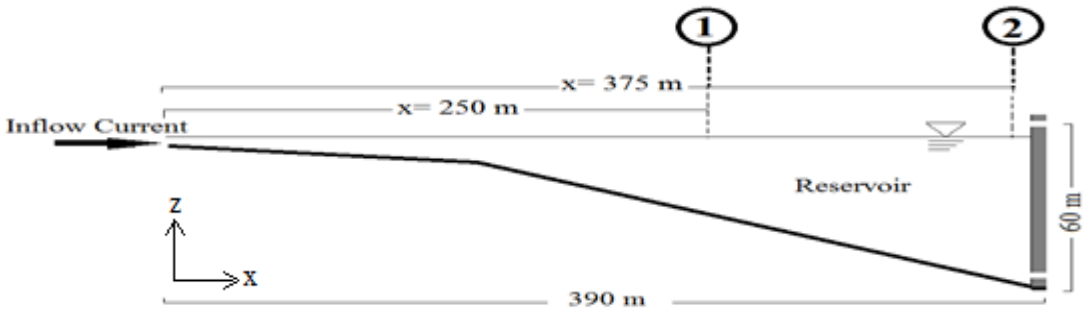

Figure 4.35 : Selected sections for comparing results.

The results are drawn for different selected times included 1000 s, 2000 s and 3000 seconds after running the simulation.

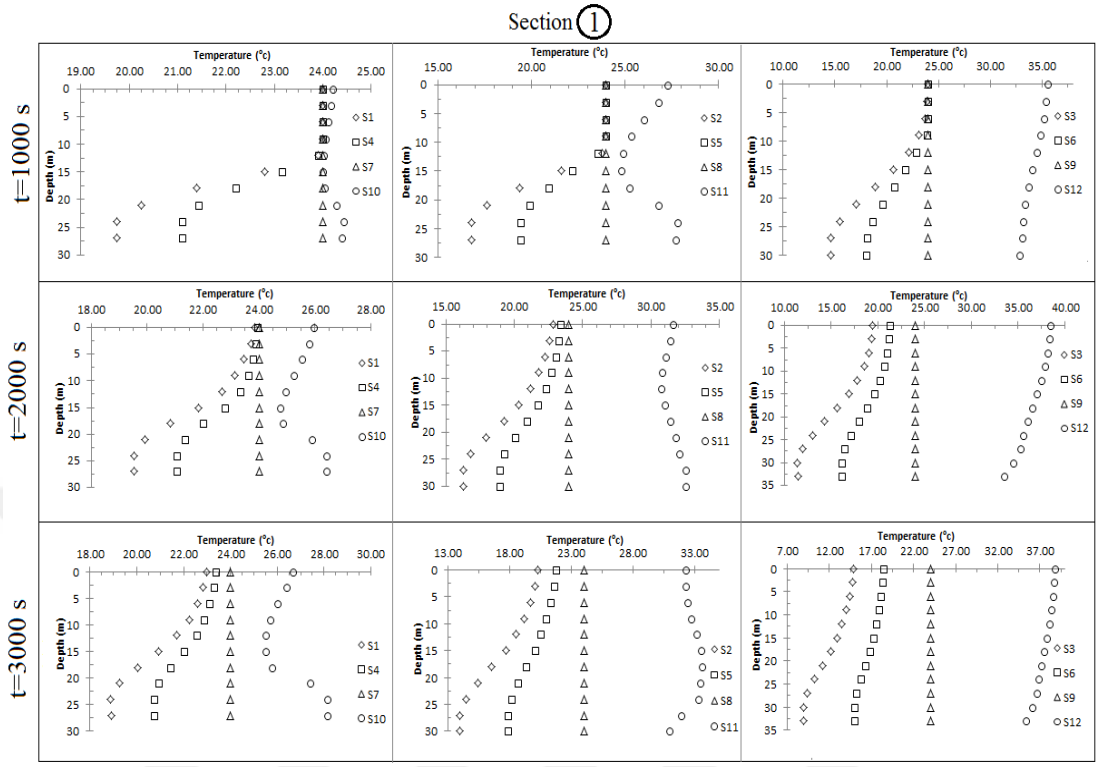

Figure 4.36 : Temperature variations during time in section 1 (S1-S12).

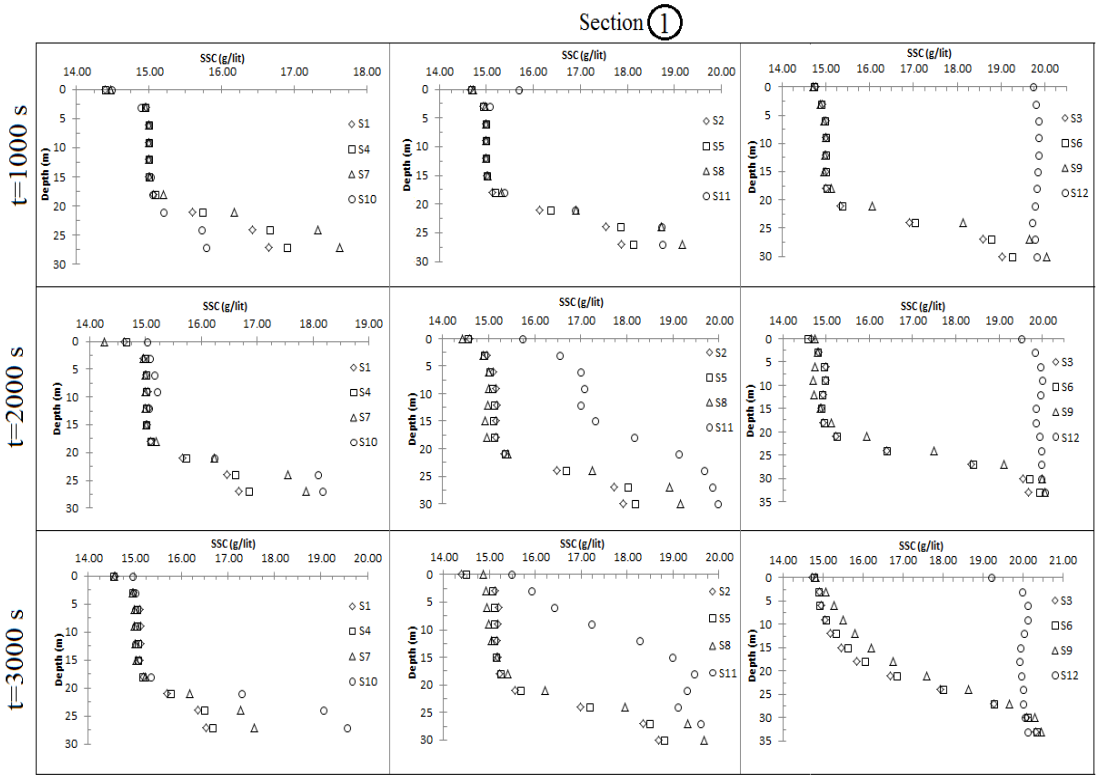

Figure 4.37 : SSC variations during time in section 1 (S1-S12).

At section 2, the following results were obtained for times 1000 s, 2000 s and 3000 seconds after run the simulation.

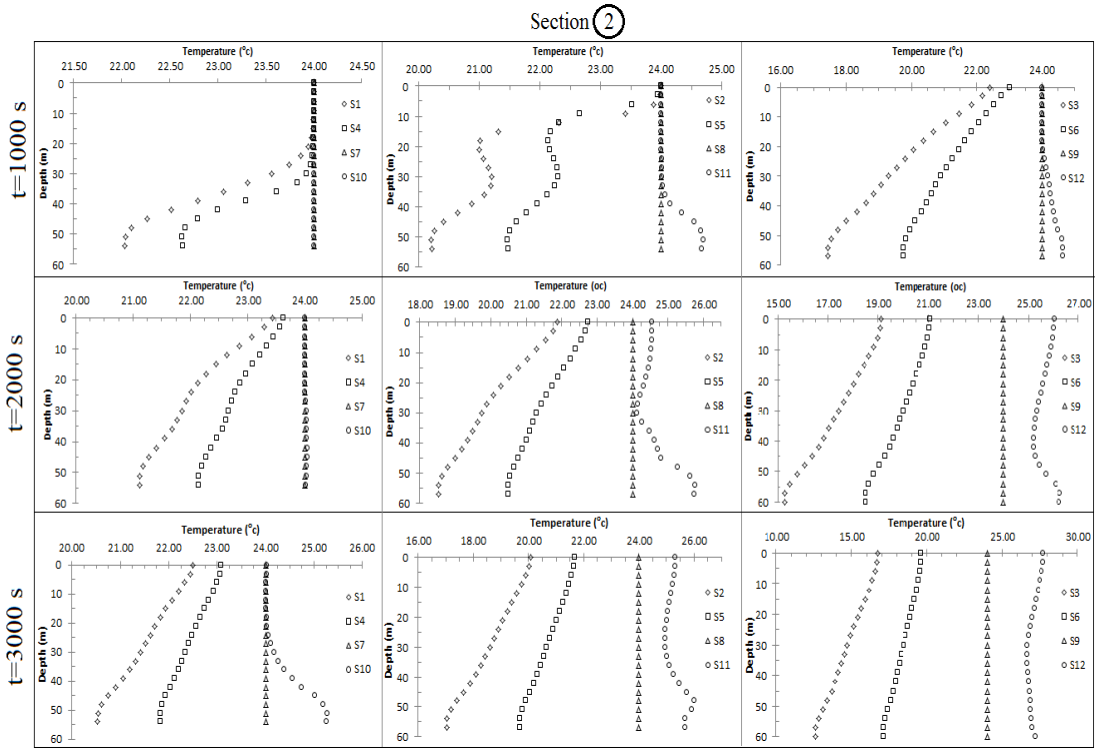

Figure 4.38 : Temperature variations during time in section 2 (S1-S12).

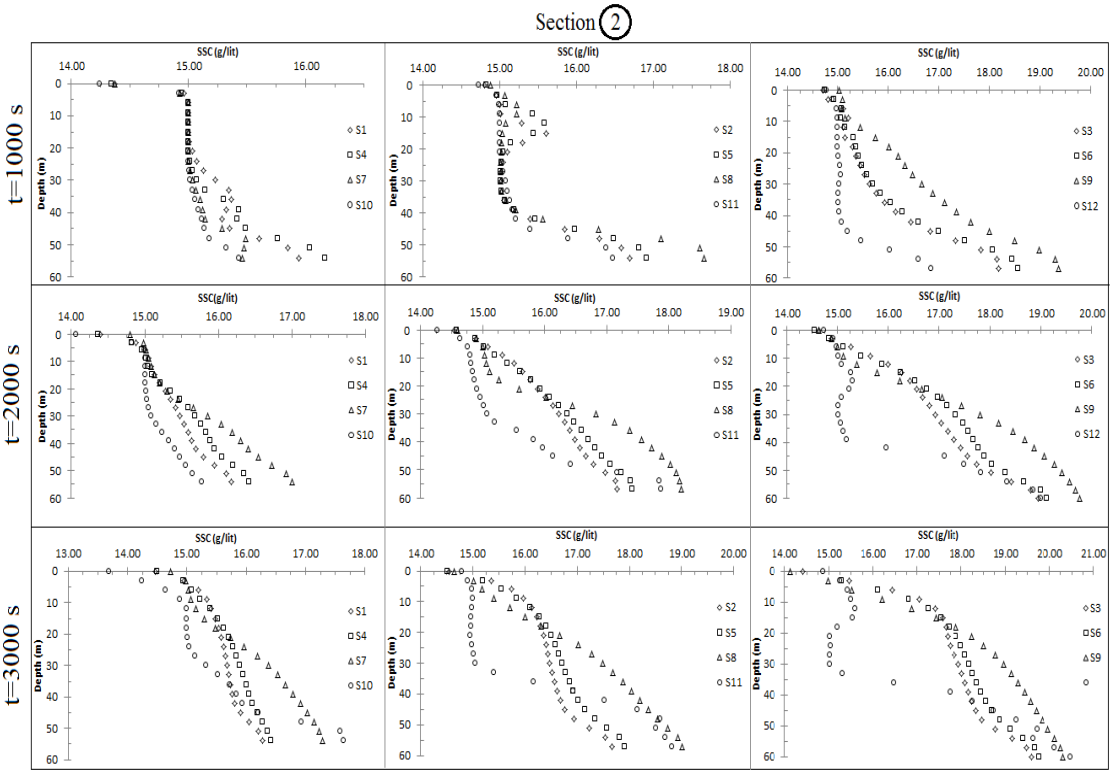

Figure 4.39 : SSC variations during time in section 2 (S1-S12).

According to the figures, the heat transfer occures at the upper layer of the reservoir, when the temperature of inflow water is lower that the reservoir's one. But, in simulation 12, the under flow condition is occurred because of the high suspended sediment concentration of the inflow current than the reservoir. Therefore, the inflow mixture is denser than the reservoir. By effecting of this under flow condition, the heat be transfered at the bottom of the reservoir, near the surface heat transfer of reservoir. It is clearly evident after the time 500 seconds of simulation S12. The spillway starts to operate after the time 700 seconds, approximately. After this time, the velocity at the upper layer of the reservoir and at the surface increases and direction of these velocity vectors are toward the dam body or downstream. So, the distribution of suspended sediment in this layer increase as the given figure shows. It could concluded that the spillway increases the thickness of layers and helps to decreasing of the stratification. At the upper layers of some simulations which have low discharges, the sediment particles start to depositing. This depositing of particles with this particle diameter is normal and obvious. On the other hand, as mentioned in the last pages, the situation of the plunge point could be changed with changing in mentioned parameters in different scenarios, according to Figure 4.22.

In the other category of the simulations that were shown in last table and included the simulations S13 to S24, the concentration of inflow water is less that the concentration of the reservoir water. The inflow and reservoir concentrations were equal to 15 and 20 mg/lit, respectively. The water temperature and discharge were changed according to the models listed in the scenarios table. So, the reservoir water is denser than the inflow water. It is expected that the over flow condition happenend in most of these simulations.

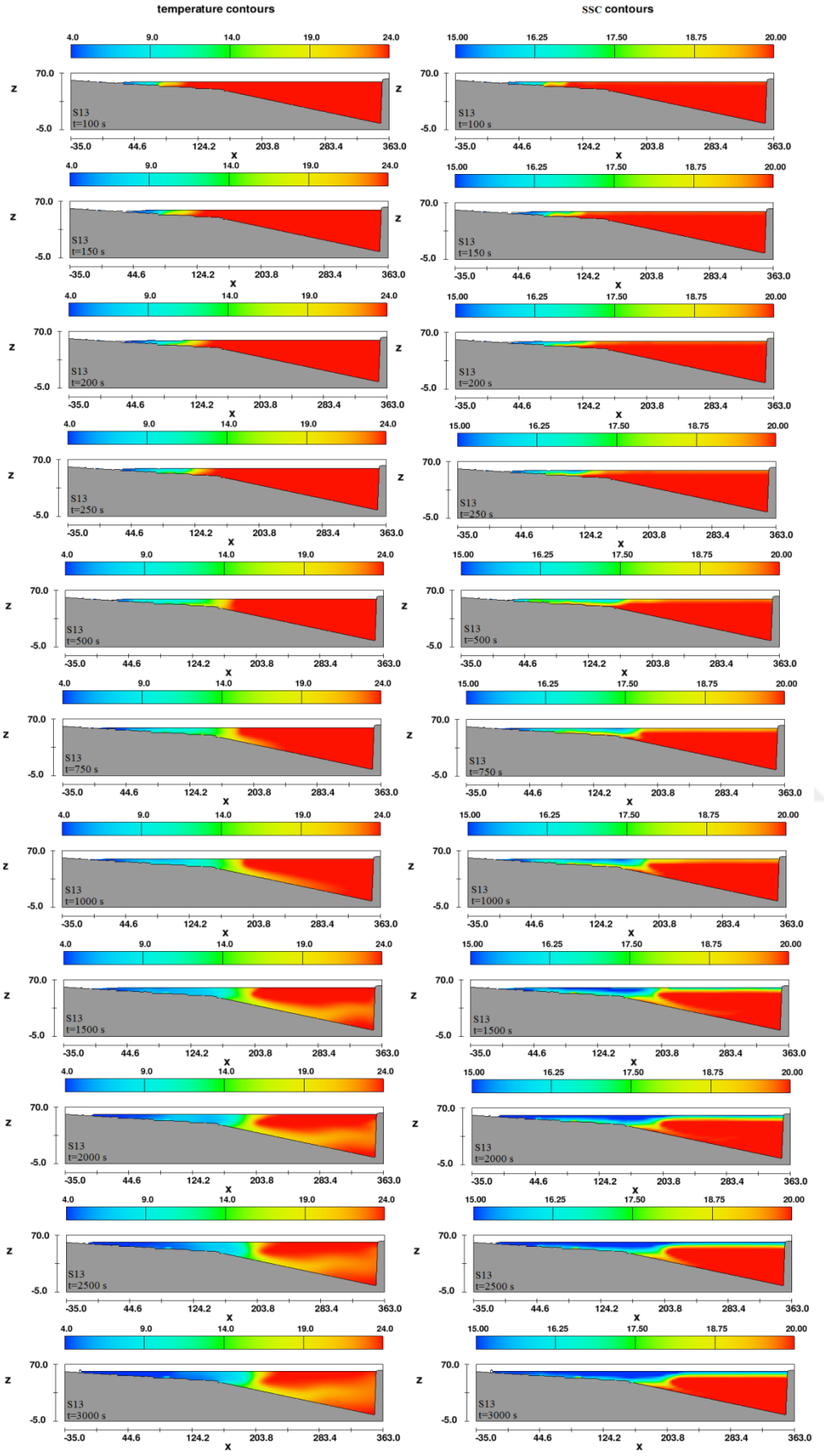

Figure 4.40 : Temperature and SSC Contours of Simulation S13.

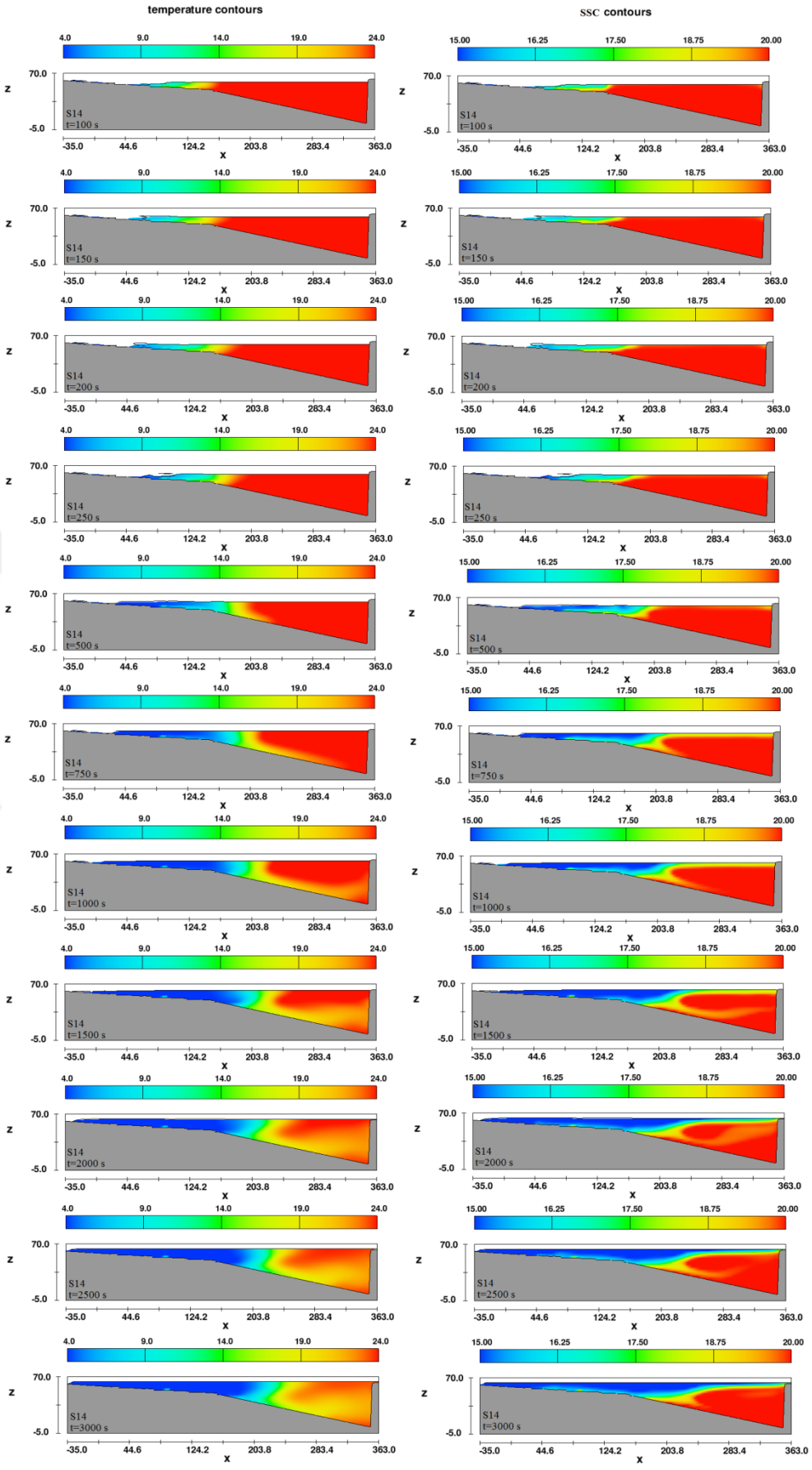

Figure 4.41 : Temperature and SSC Contours of Simulation S14.

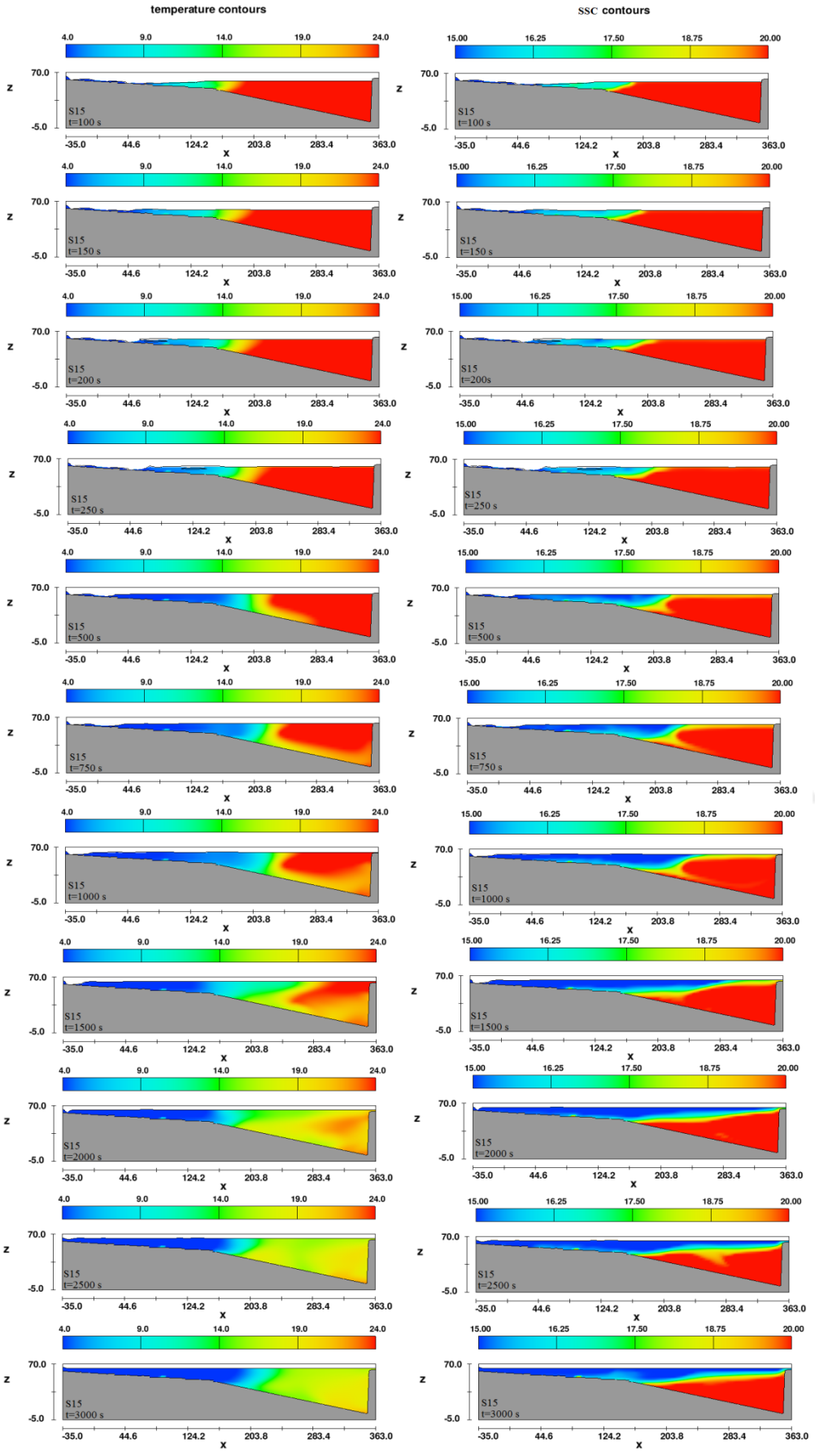

Figure 4.42 : Temperature and SSC Contours of Simulation S15.

With increasing the suspended sediment concentration of reservoir and decreasing the suspended sediment of inflow current, it is expected that the over flow condition happened. It is also known as hypopycnal flow, as mentioned in the first chapter. In the given figures of results for the simulations S13, S14 and S15, this state is visible. As seen in these figures, the hypopycnal and some times, mesopycnal flow conditions occurred and with the effect of changes in discharge magnitude of inflow water, the thicknesses of the stratification layers are varies. It means that the discharge affects the thickness of the layers of the concentration stratification. In the thermal changes case, it is clear that the temperature increasing is acted like the inter flow or under flow in these simulations. The discharge magnitude and the suspended sediments have effects on the pattern of transfer of temperature. As seen in the S15 after the time equal to 1200 seconds, the temperature starts to propagate on the upper layer of reservoir, mostly.

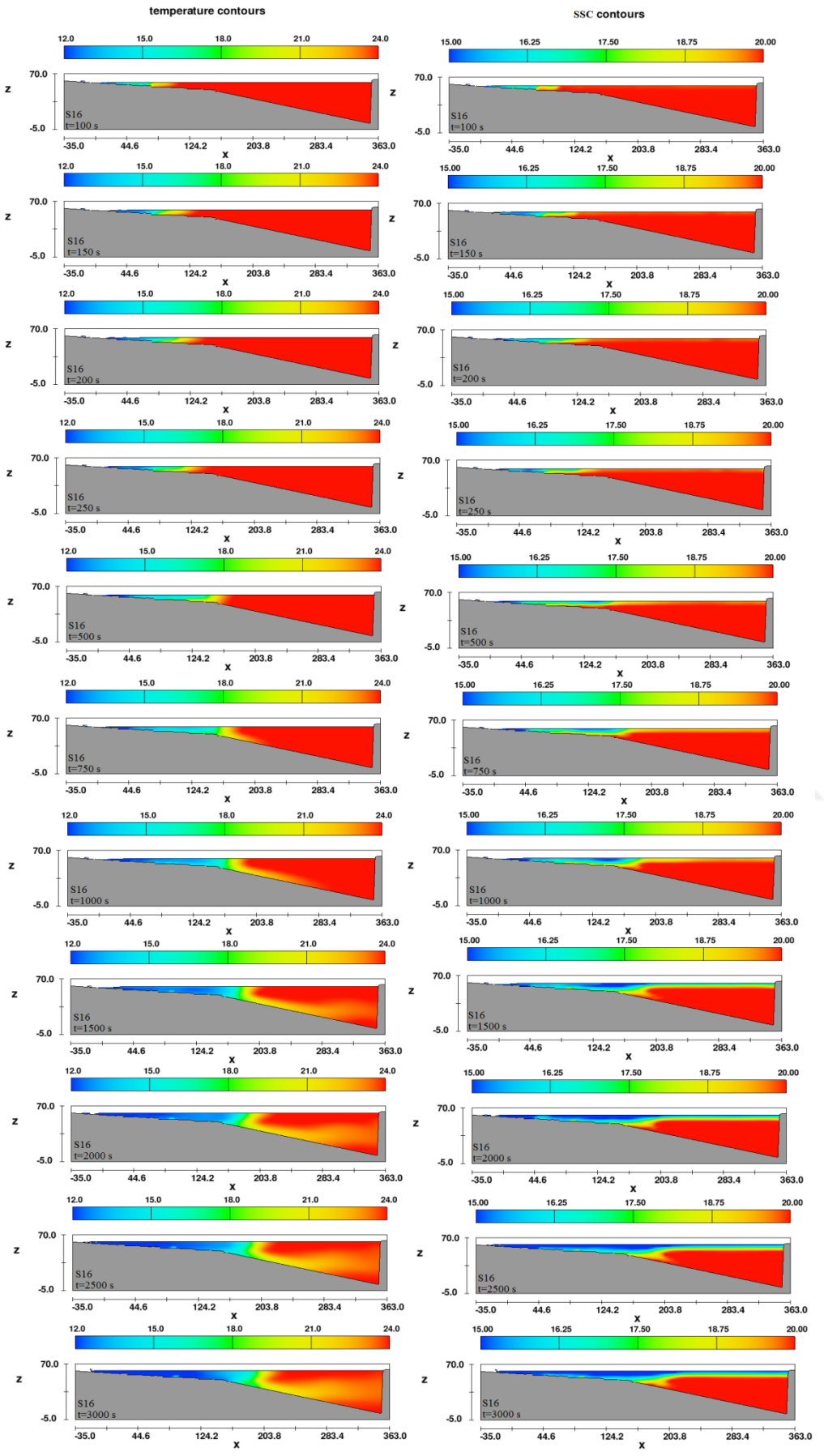

Figure 4.43 : Temperature and SSC Contours of Simulation S16.

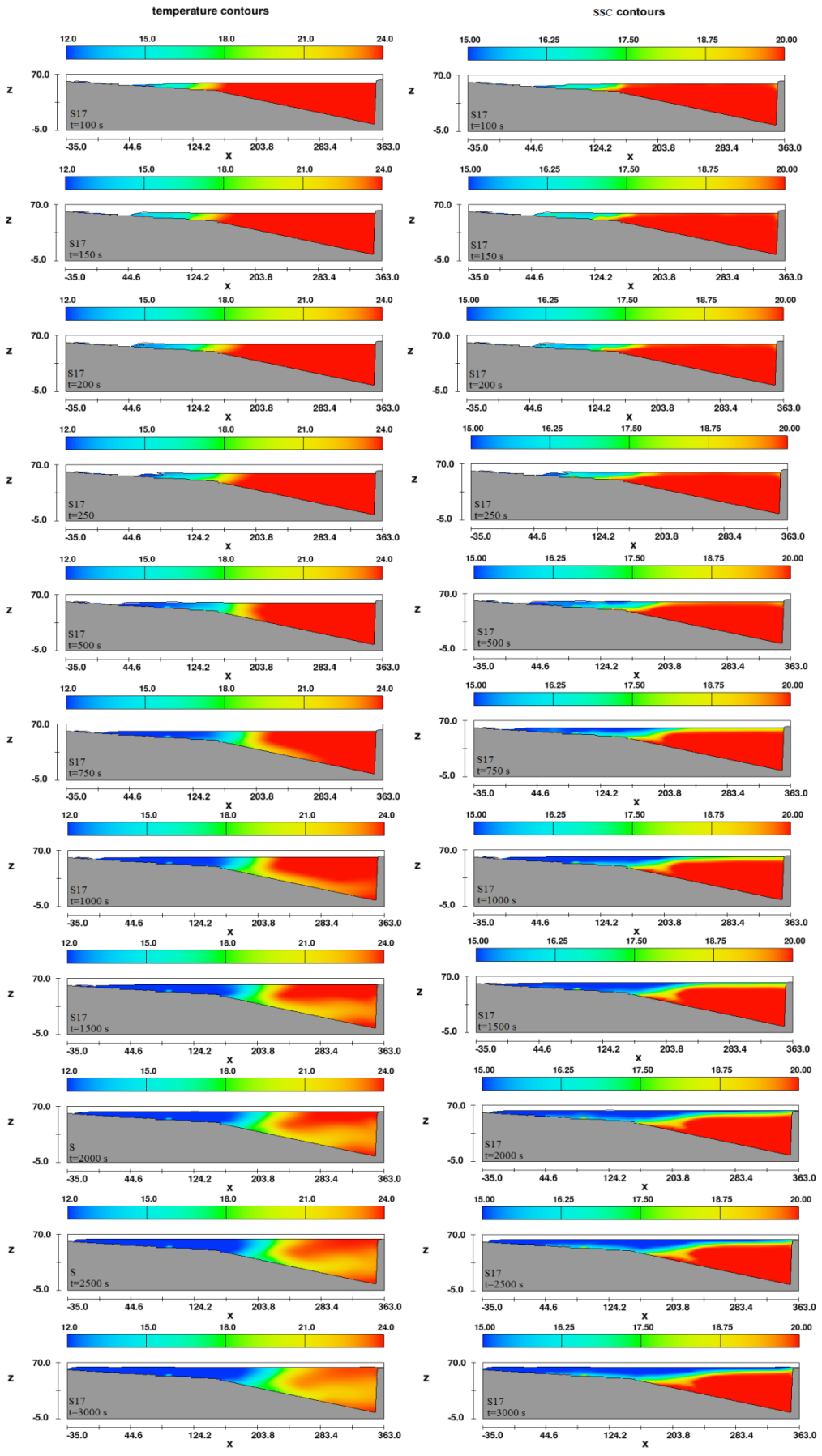

Figure 4.44 : Temperature and SSC Contours of Simulation S17.

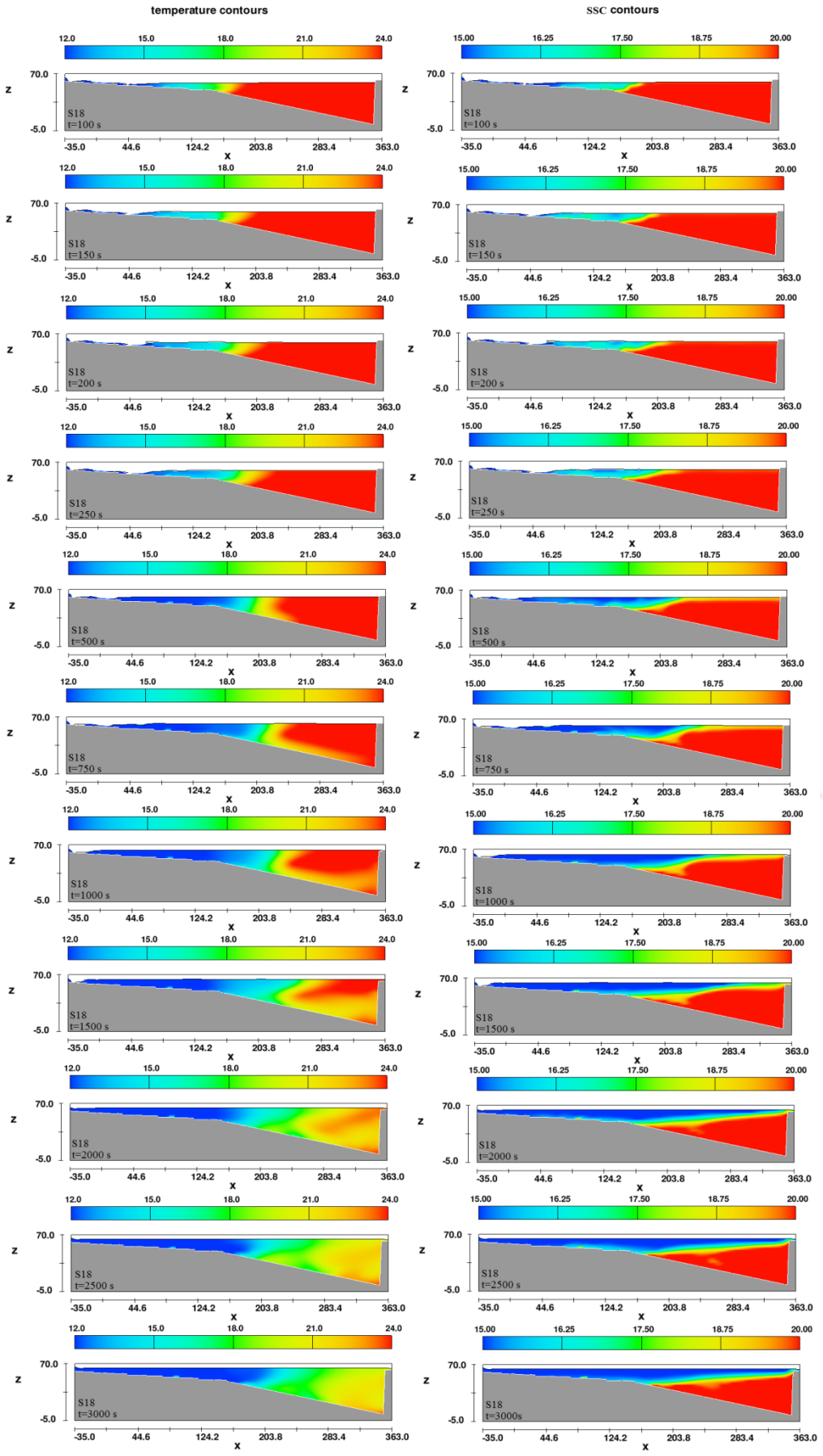

Figure 4.45 : Temperature and SSC Contours of Simulation S18.

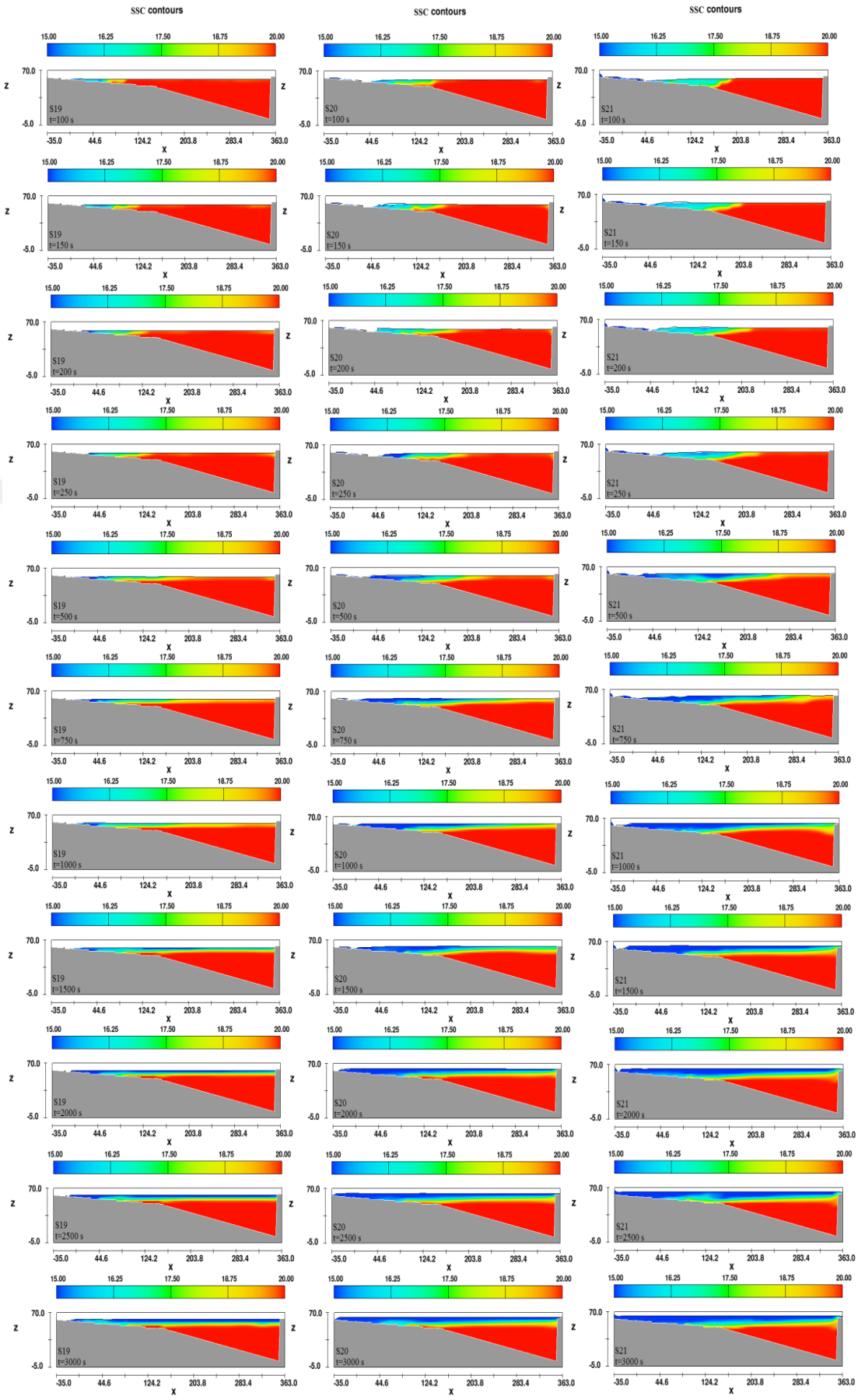

Figure 4.46 : SSC Contours of Simulation S19, S20 and S21.

In simulations S16, S17 and S18, temperature of inflow river water is still less than the reservoir water temperature, as like as the S13, S14 and S15 simulations. It is a little warmer than the water temperature in simulations S13, S14 and S15, and equal to 12 ^{o}C. The reservoir water temperature is as same as the S13, S14 and S15, which was equal to 24 ^{o}C. Outlet type is selected as spillway, again. About the suspended sediment concentration, as mentioned in table 4.5, the inflow river suspended sediment concentration is less than the reservoir's one. The magnitude of the inflow discharge affects the heat transfer, mainly. From the figures, it is obvious that the higher values of discharge leads to increasing in the heat transfer rate.

In simulations S19, S20 and S21, the water temperature of the river and reservoir is equal to 24 ^{o}C. In these simulations, it is clear that the inflow river discharge magnitude has important effects on thickness of the upper layer.

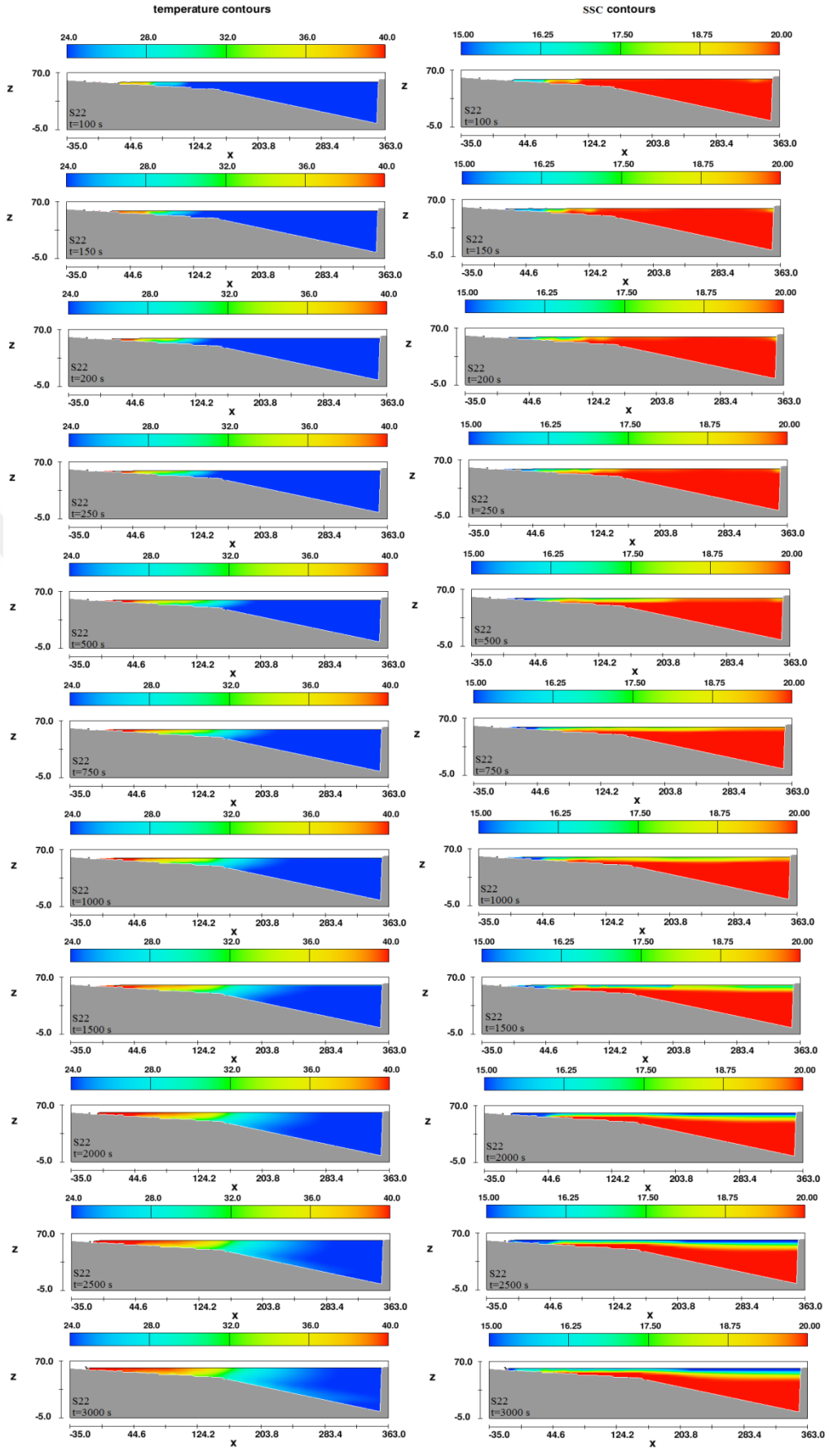

Figure 4.47 : Temperature and SSC Contours of Simulation S22.

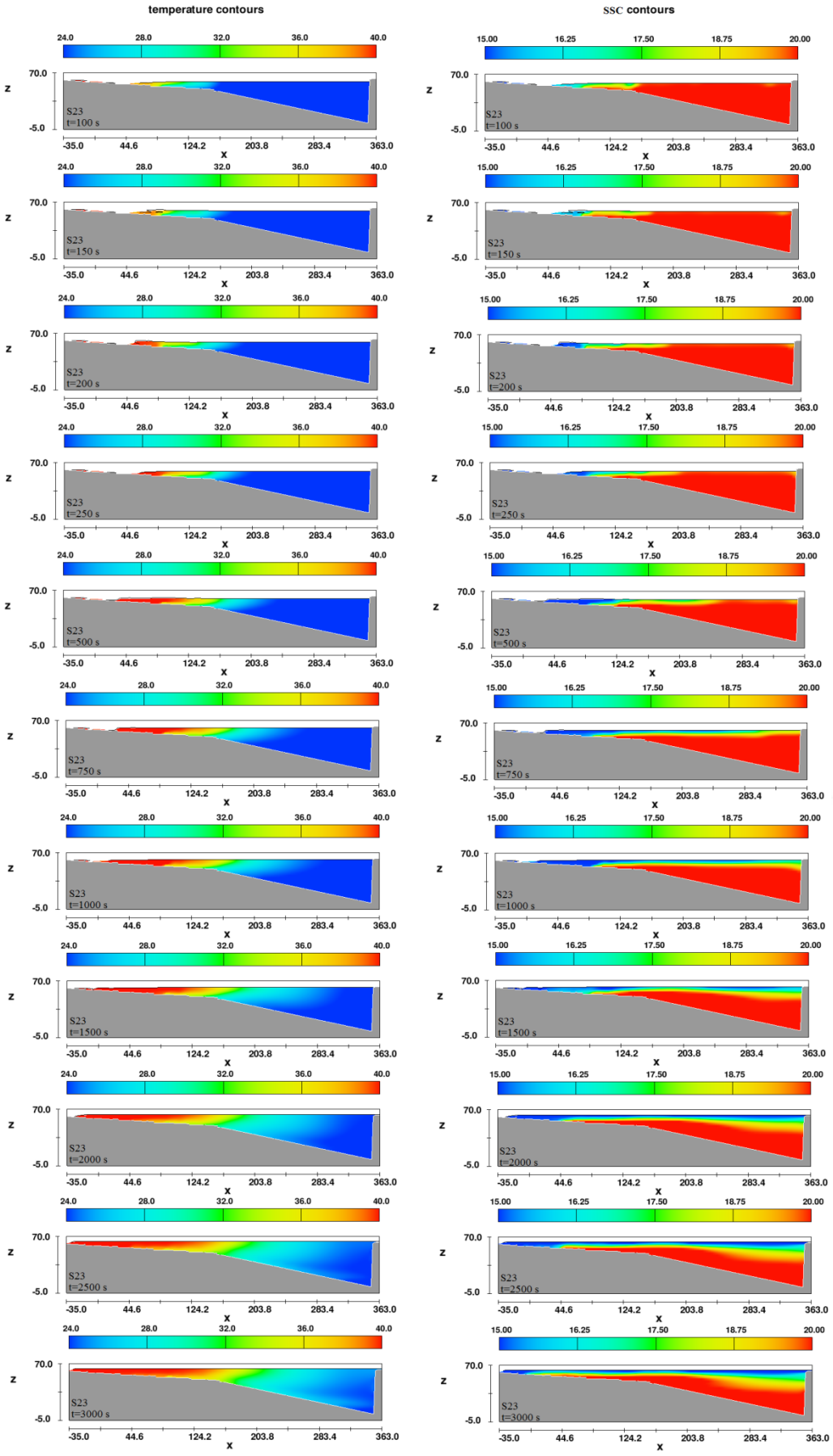

Figure 4.48 : Temperature and SSC Contours of Simulation S23.

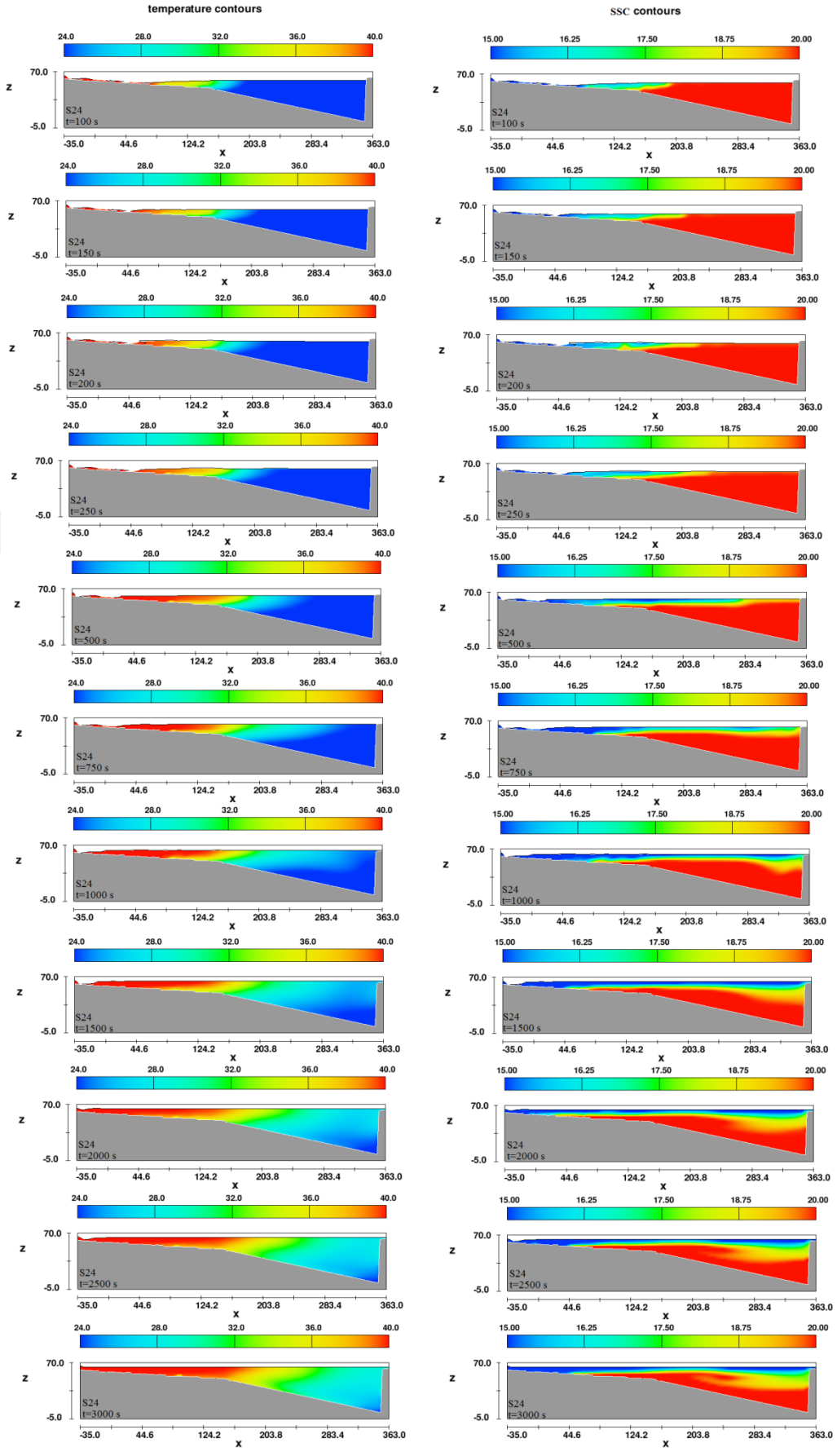

Figure 4.49 : Temperature and SSC Contours of Simulation S24.

As a result, from the last figures, in simulations S15, S18 and S21, it is seen that if the temperature of inflow current's water and the reservoir's one have values close to each other, the thickness of the suspended sediment concentration layers is reduced at the first points of the slope change of reservoir bed in these cases. The existence of the spillway outlet also affects these results. This kind of outlet increases the velocity of the surface of the reservoir. While, in simulation S24, a thin layer of upper suspended sediment concentration can be seen. It is because of that the inflow current is completely underdense campared with the reservoir's mixture.

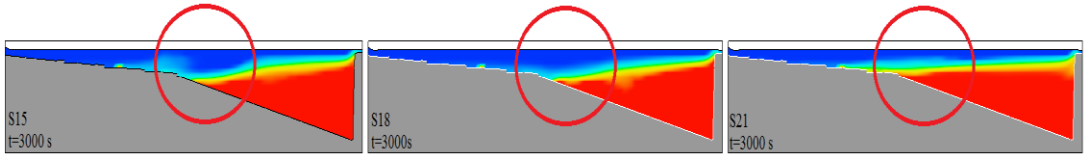

Figure 4.50 : Thickness of the upper layer of SSC at bed slope change area.

In simulations S13 to S24, the over flow conditions were occurred, mostly. However in simulations S13 to S18, inter flow condition was occurred near the over flow condition. These states are represented as the velocity vectors in the following figures.

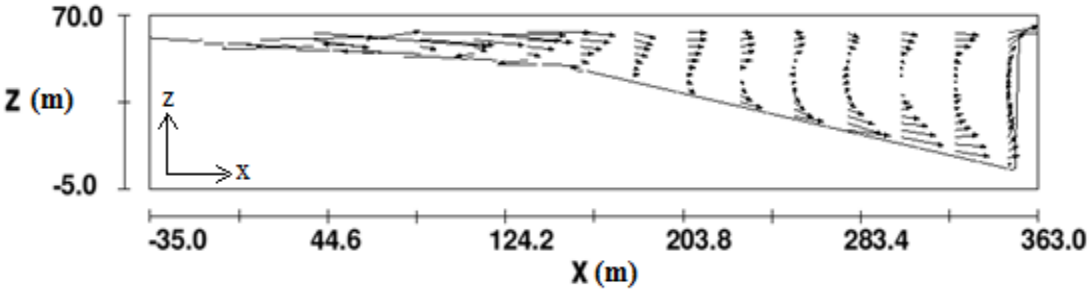

Figure 4.51 : Velocity Vectors and flow directions of simulations S13 to S18.

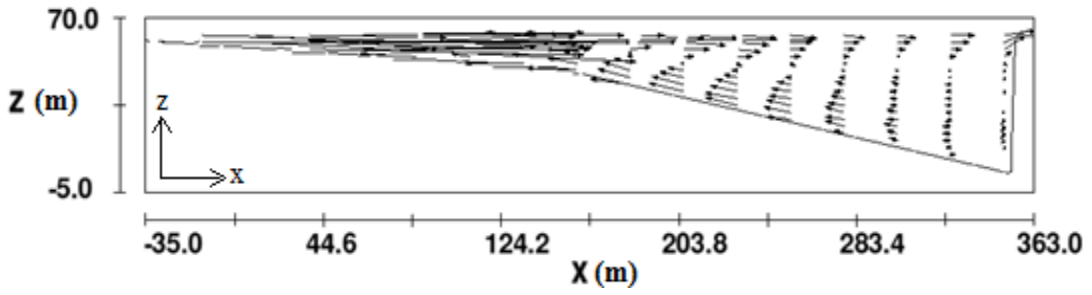

Figure 4.52 : Velocity Vectors and flow directions of simulations S19 to S24.

In these simulations, the reservoir at time t=0 has the total surface (initial free water surface area) of equal to 19,000 square meter, approximately. The value for surface of reservoir varies when reservoir has the maximum water level for different inflow discharges. For simulations with discharge equal to 20 cubic meter per second the approximate value for free surface area is 21,200 square meter. While this value is reached to 21,500 and 22,100 square meter approximately for simulations with discharge of 50 and 100 cubic meter per second, respectively. The total surface of reservoirs for any time of simulations are presented as figures in appendix A. From these figures, which shown in appendix A, the volume of the reservoir and its changes during time could be obtained. Totally, the flow pattern in simulations S15, S18, S21 and S24 are shown in the following figures.

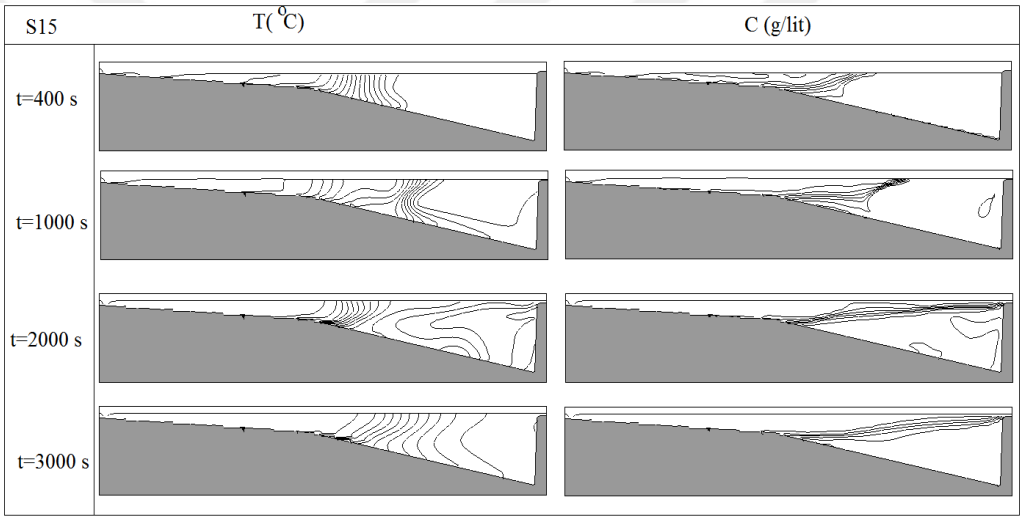

Figure 4.53 : B/W contours of temperature and concentration (S15).

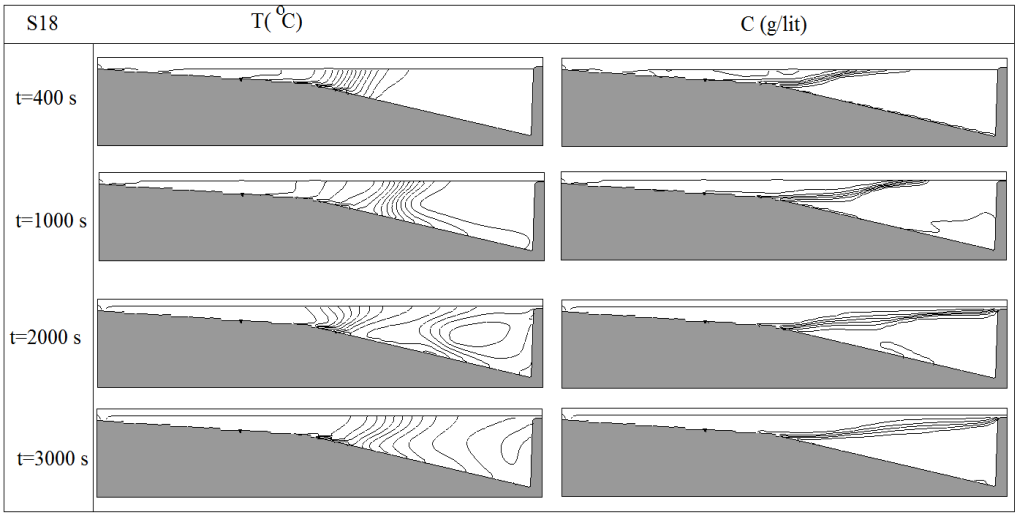

Figure 4.54 : B/W contours of temperature and concentration (S18).

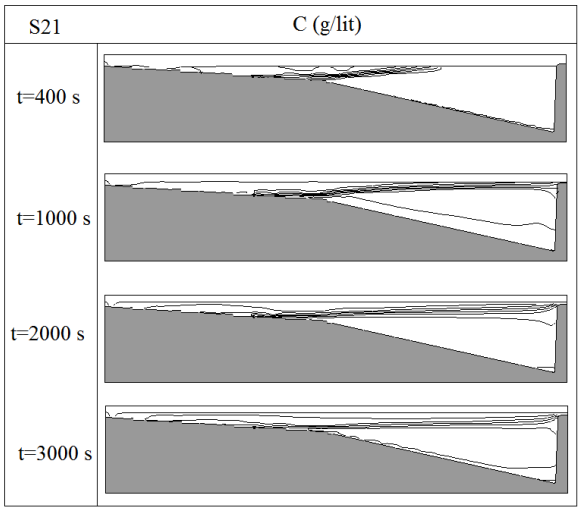

Figure 4.55 : B/W contours of temperature and concentration (S21).

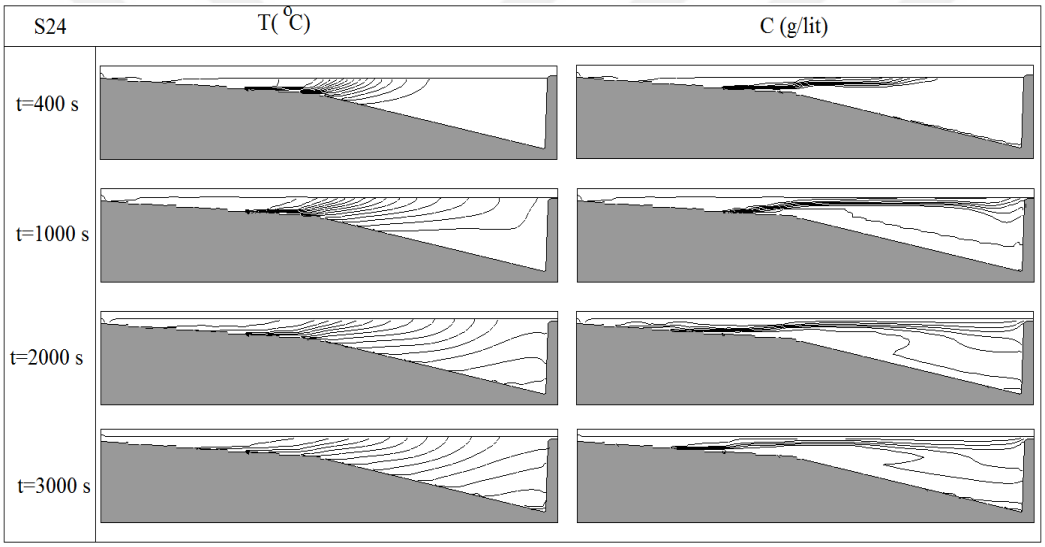

Figure 4.56 : B/W contours of temperature and concentration (S24).

According to figure 4.35 and the selected sections that represented in this figure, the following result could be drawn for simulations S13 to S24 in different times included: 1000 s, 2000 s and 3000 seconds. The distribution of the suspended sediment and temperature could be evaluated using Figures 4.57, 4.58, 4.59 and 4.60.

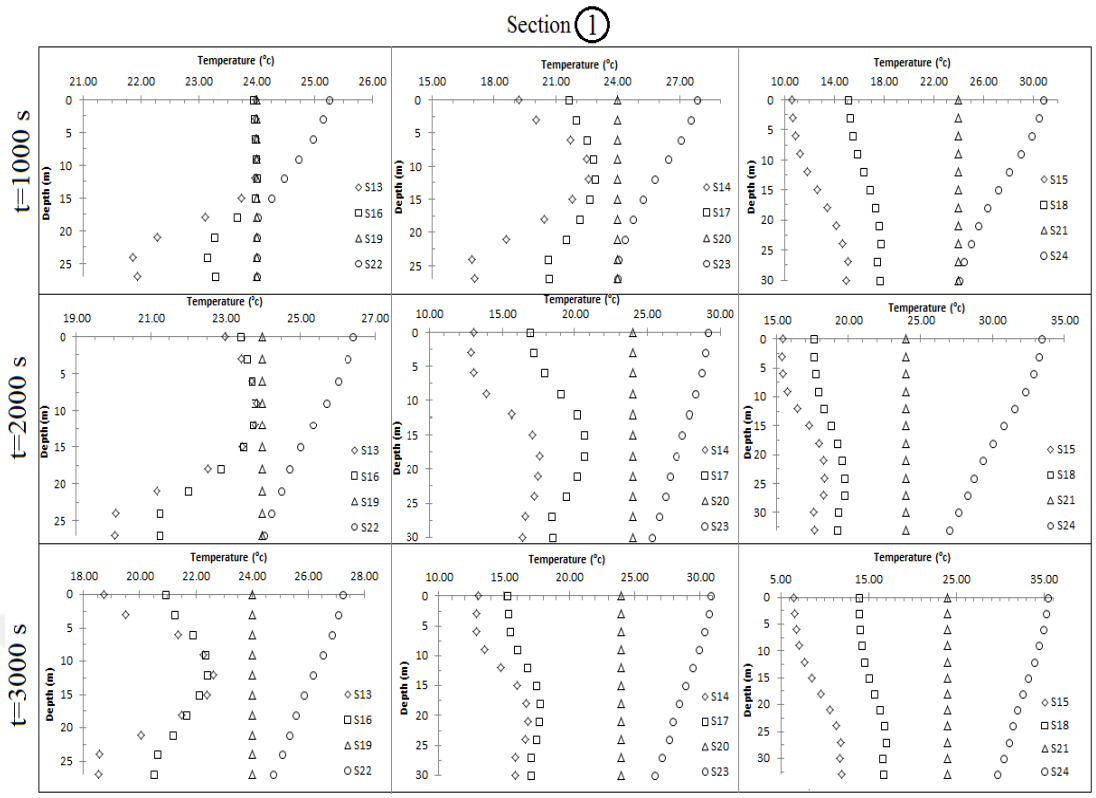

Figure 4.57 : Temperature variations during time in section 1 (S13, S14, ..., S24).

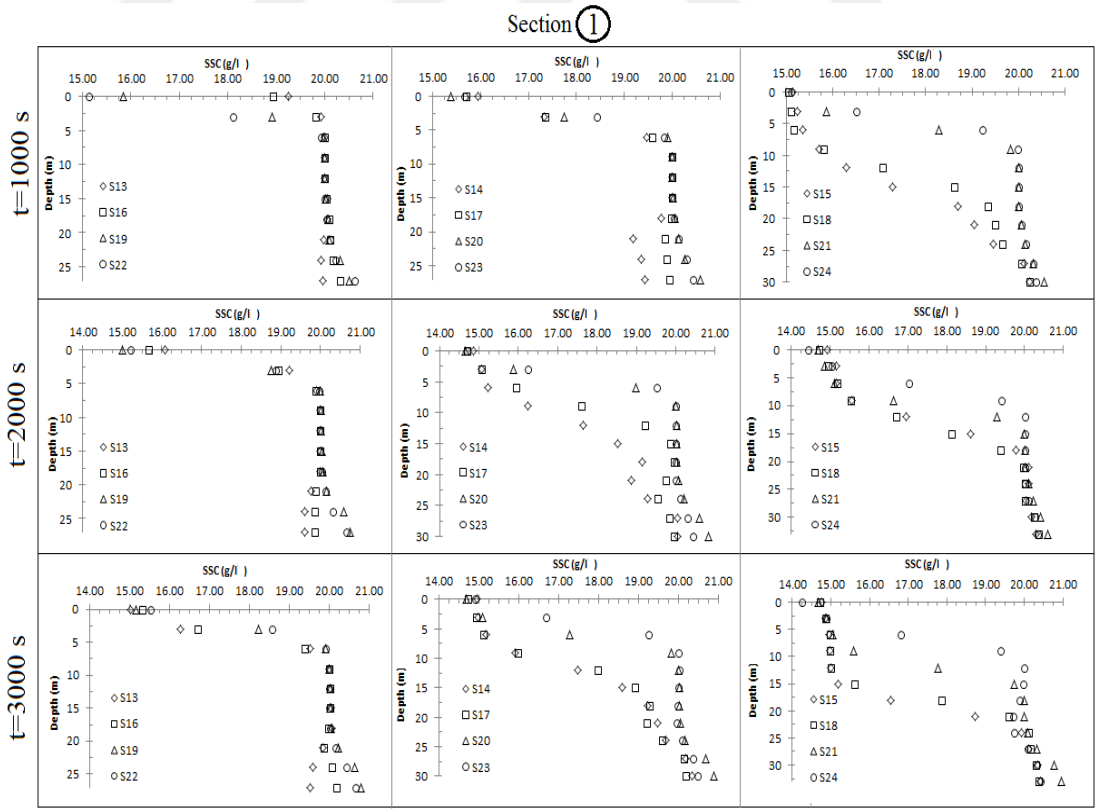

Figure 4.58 : SSC variations during time in section 1 (S13, S14, ..., S24).

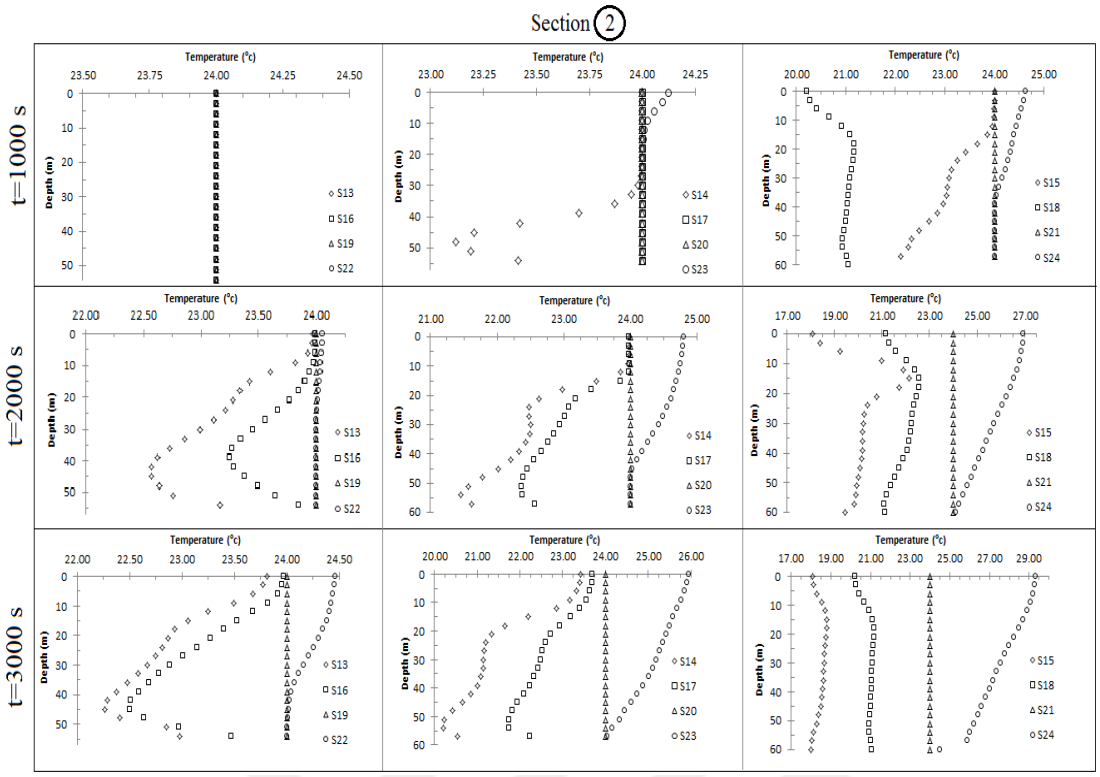

Figure 4.59 : Temperature variations during time in section 2 (S13, S14, ..., S24).

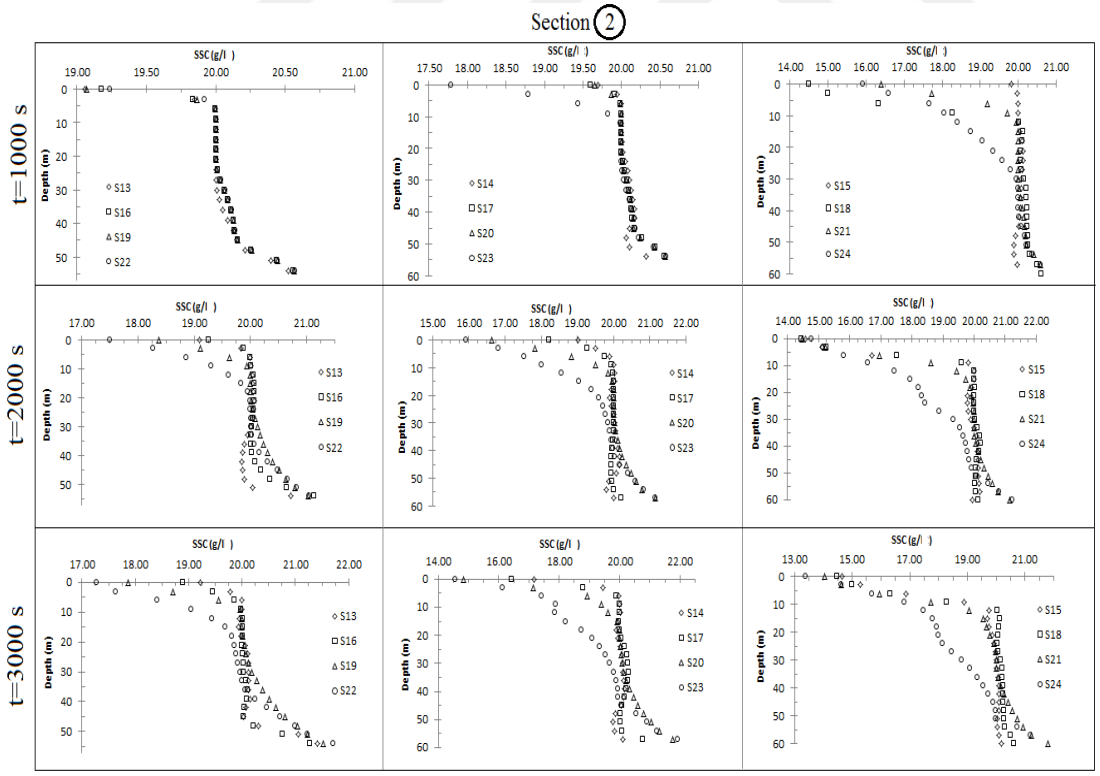

Figure 4.60 : SSC variations during time in section 2 (S13, S14, ..., S24).

The following figures show the colored velocity vector and 2D magnitude of that for x-y, y-z and x-z directions. The selected simulations are S15, S18, S21 and S24 for different times included: t=500 s, t=1000 s, t=1500 s and t=2500 seconds.

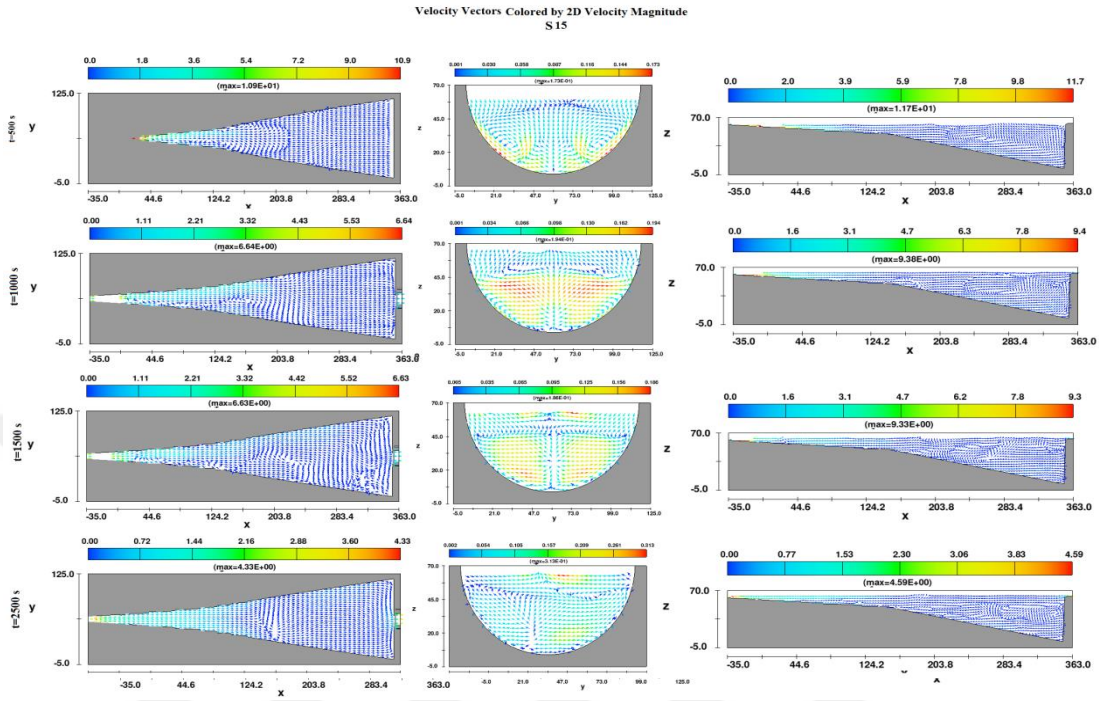

Figure 4.61 : Velocity Vectors Colored by 2D Velocity Magnitude for S15.

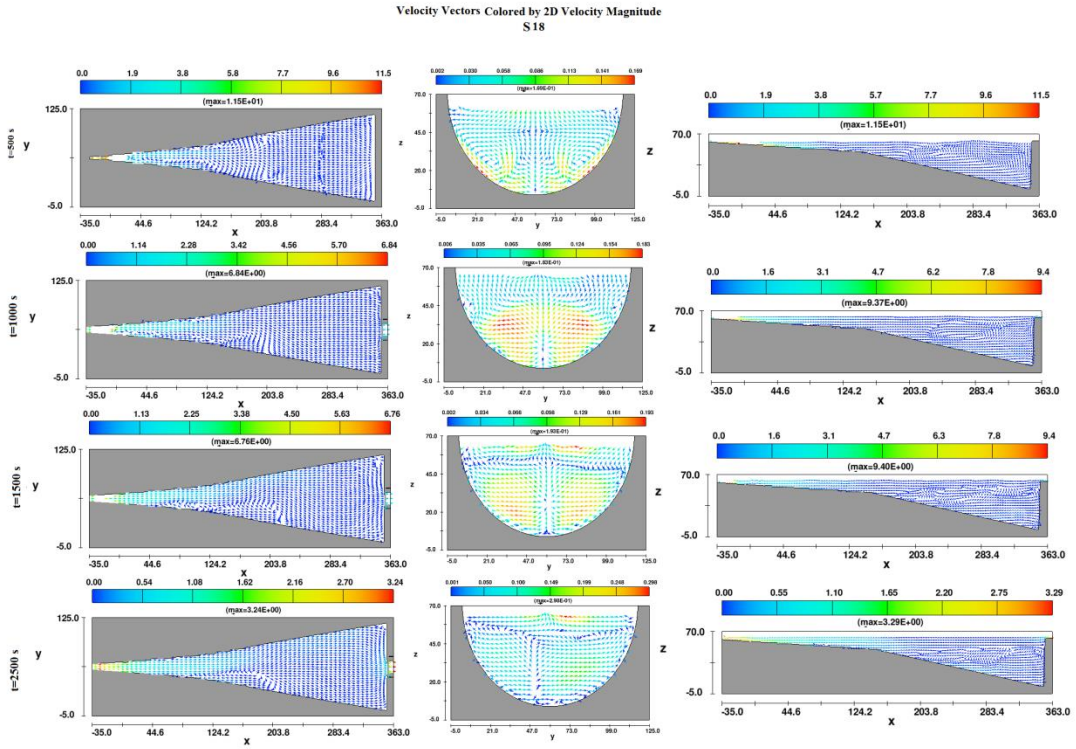

Figure 4.62 : Velocity Vectors Colored by 2D Velocity Magnitude for S18.

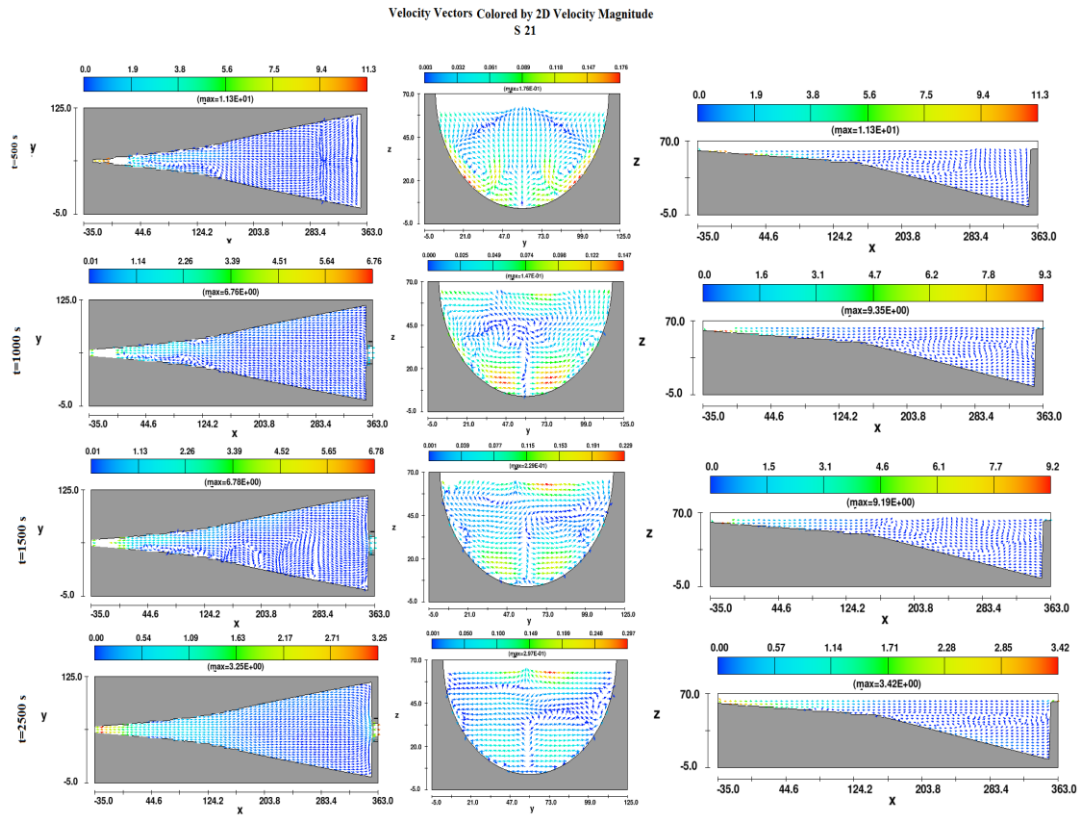

Figure 4.63 : Velocity Vectors Colored by 2D Velocity Magnitude for S21.

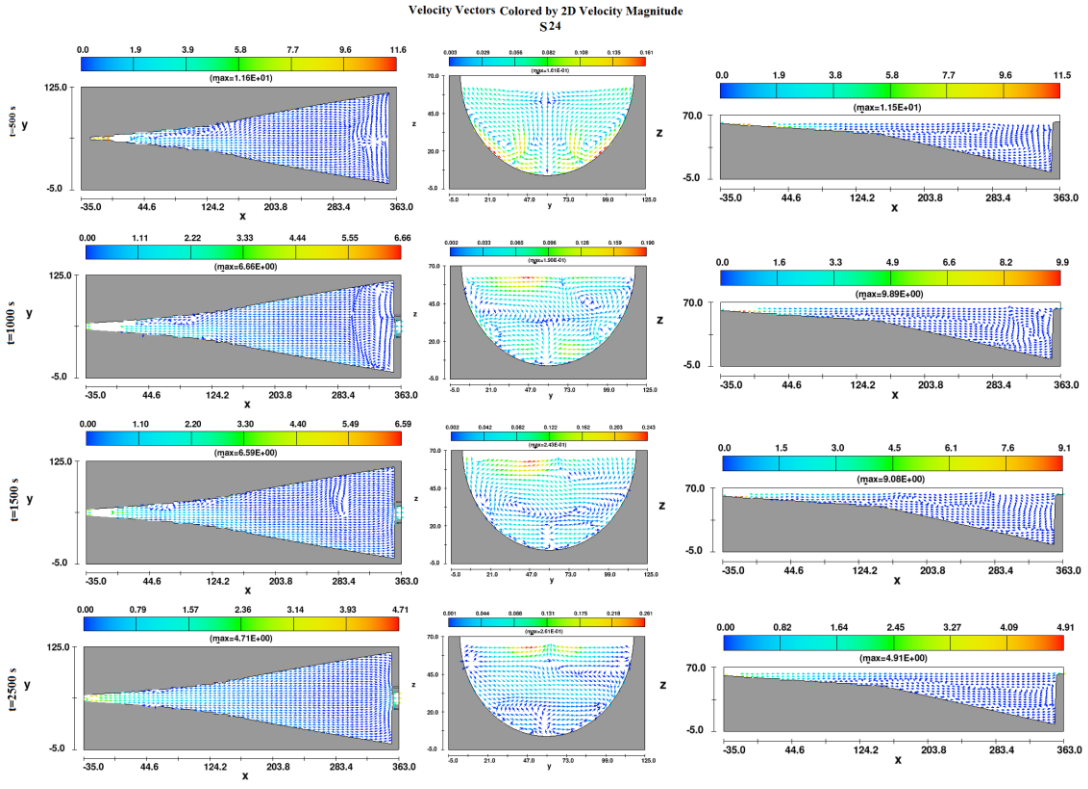

Figure 4.64 : Velocity Vectors Colored by 2D Velocity Magnitude for S24.

From Figures 4.61, 4.62, 4.63 and 4.64, velocities and the vectors, that show the direction of the current in the reservoir, are clearly seen. In the initial times of simulation, with entering the inflow water to the reservoir, the direction of the current towards the dam body. With encountering the volume of water at the surface of reservoir, which caused by inflow water with a high value of discharge, with body of dam the reverse currents (inverse flows) are happened in the upper layers near the free surface of reservoir and body of dam. This reverse current continues up where it faced with inflow current. After this time, regions are appeared at the water surface that have circulation currents. It could be seen that these kind of current are appeared in the lower depths of the reservoir. After the approximatly time 700 seconds, in simulations with 100 cubic meter per second discharge, the surface level of the water in reservoir reached the elevation of the bottom of the spillway. After this time the velocities and the direction of the currents in reservoir are under the influence of the spillway. The velocity vectors in z-y directions show that the jet wall current occured in some simulations. These currents lead to sinking the flow from one side or both sides of the reservoir. Creation of a thermal mid layer is a result of these currents, which appears in some of the simulations of this study.

It could be demonstrated that in the simulated models done in this part of this thesis, the incoming flow into the reservoir is plunge at the beginning of the reservoir into the deeper layers of that and the turbidity current is formed. The discharge magnitude of the inflow current affect the location of the plunging point and the velocity of the turbidity current. As a result of this phenomenon the time that the turbidity currentarrives to the body of dam will change. The obvious point that could be mentioned here is that the spillway has an important role in distrubution of sediment and temperature during the turbidity current phenomenon. Many parameters related to the spillway could be affected these phenomenon included position and location of the spillway gates, dimensions of the spillway and its gates, shape of the spillway entrance etc. A important point that is the main aim of this study, is that the effect of the differences between the inflow's water temperature and suspended sediment concentration and reservoir's water on distrubution of the temperature and suspended sediment in the reservoir. These parameters also have some important effects on the formation of the turbidity current and plunging point.

4.11 Results for Reservoir with Bottom outlet (B Type Simulations)

According to the table 4.6, the results for these category of simulations are summarized as the following figures. Like to the las category of simulations (table 4.7), these result are related to the middle of the width of the reservoir, where the (y) is equal to 60 m. The results are compared in different times included: 100 s, 150 s, 200 s, 250 s, 500 s, 750 s, 1000 s, 1500s, 2000 s, 2500 s and 3000 seconds after the simulations run.

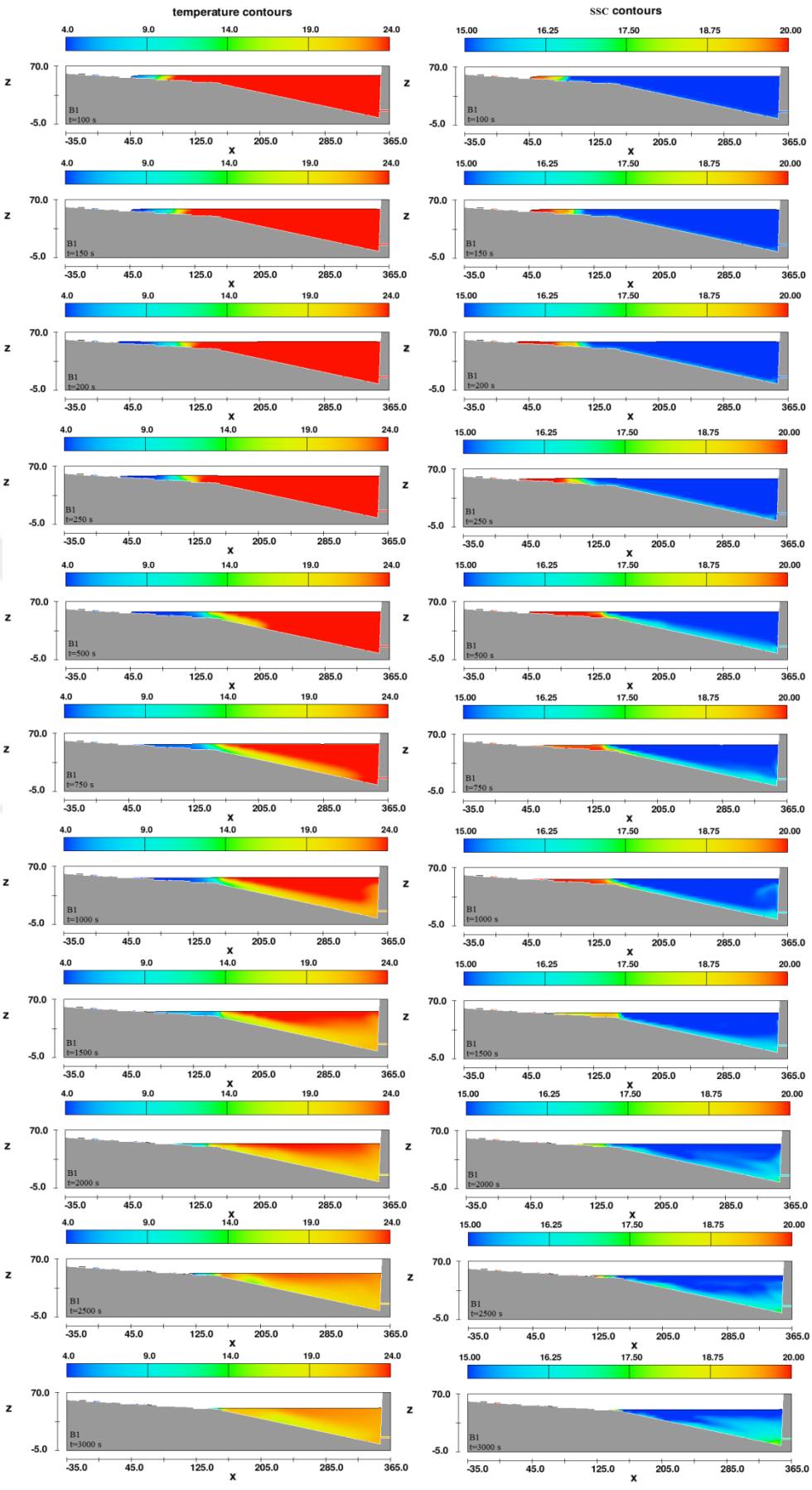

Figure 4.65 : Temperature and SSC Contours of Simulation B1

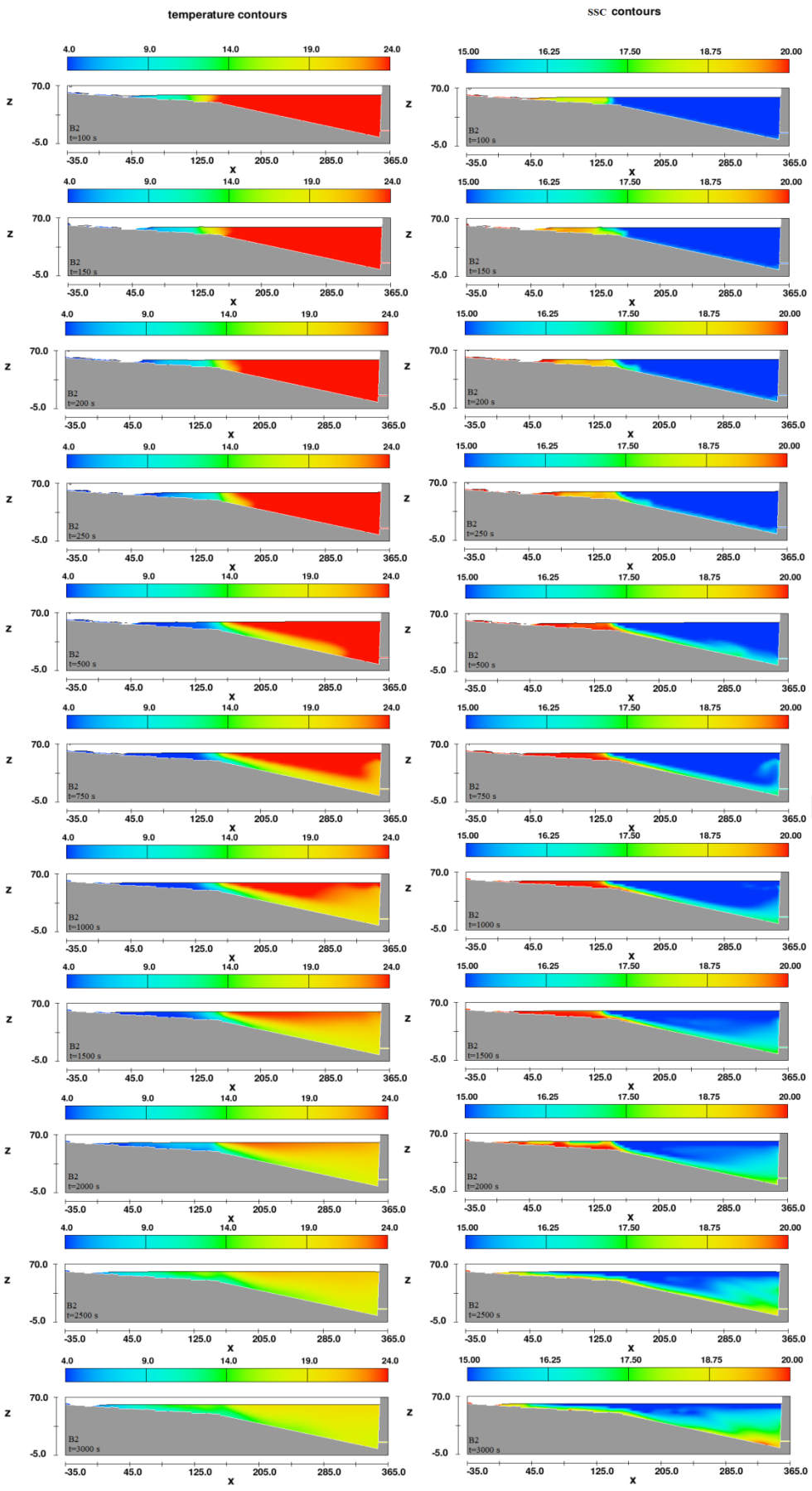

Figure 4.66 : Temperature and SSC Contours of Simulation B2

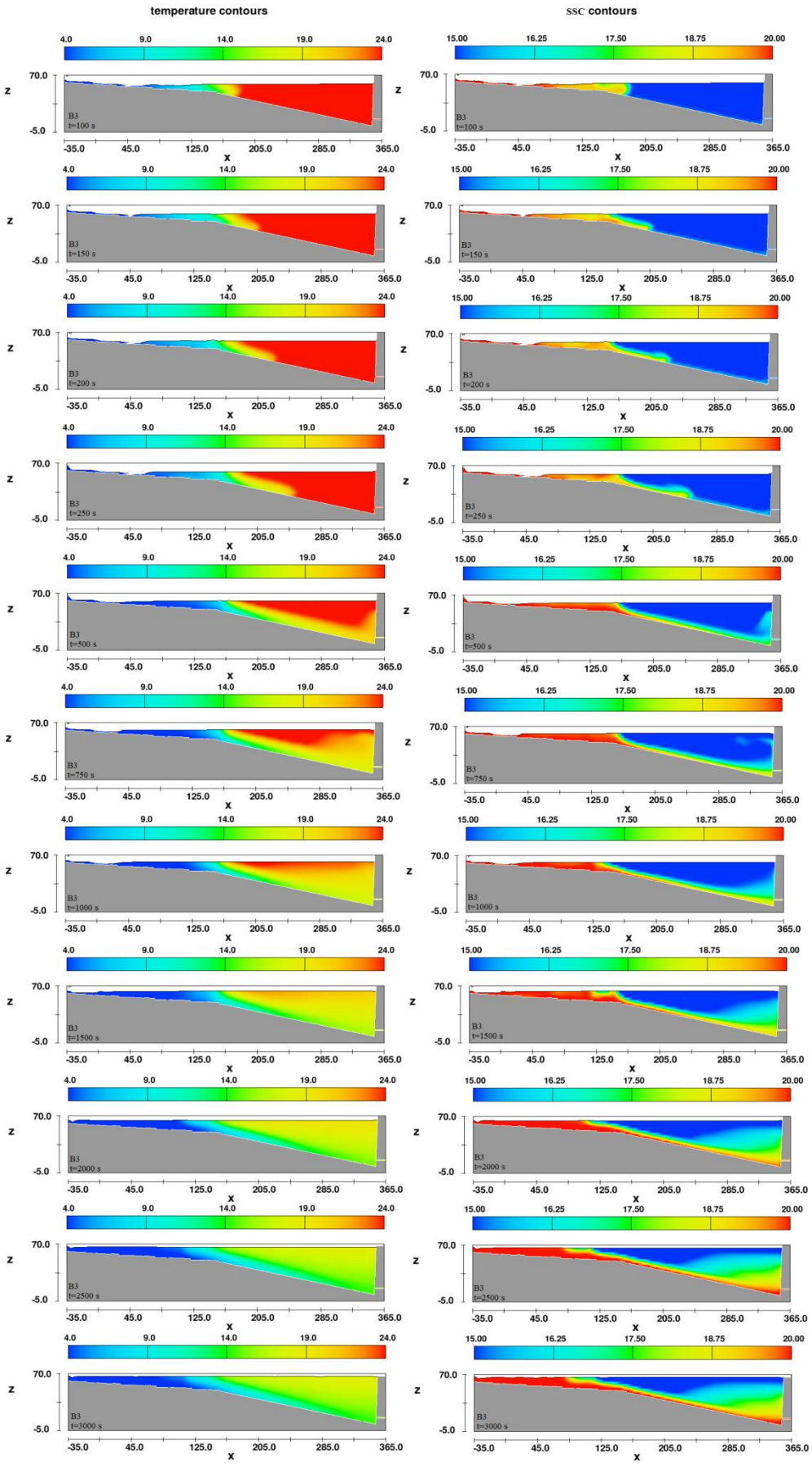

Figure 4.67 : Temperature and SSC Contours of Simulation B3

In this category of simulations, the outlet type was changed from spillway to bottom outlet. The inflow river and reservoir water temperature values were selected as 4 ^{o}C and 24 ^{o}C in simulations B1, B2 and B3, respectively. The suspended sediment concentration of river is more than the reservoir's one. As mentioned in table 4.6, selected values for river and reservoir suspended sediment concentration were 20 g/l and 15 g/l, respectively.

As expected, the underflow condition was occurred near the bed of the reservoir. The bottom outlet helps to reducing the distribution of suspended sediment to upper layers in these simulations in comparison with the simulations with spillway. Therefore, the concentration of suspended sediment in upper layers of reservoirs is less than the suspended sediment concentration in reservoir with conditions as same as B1, B2 and B3 simulations, but with only spillway outlet.

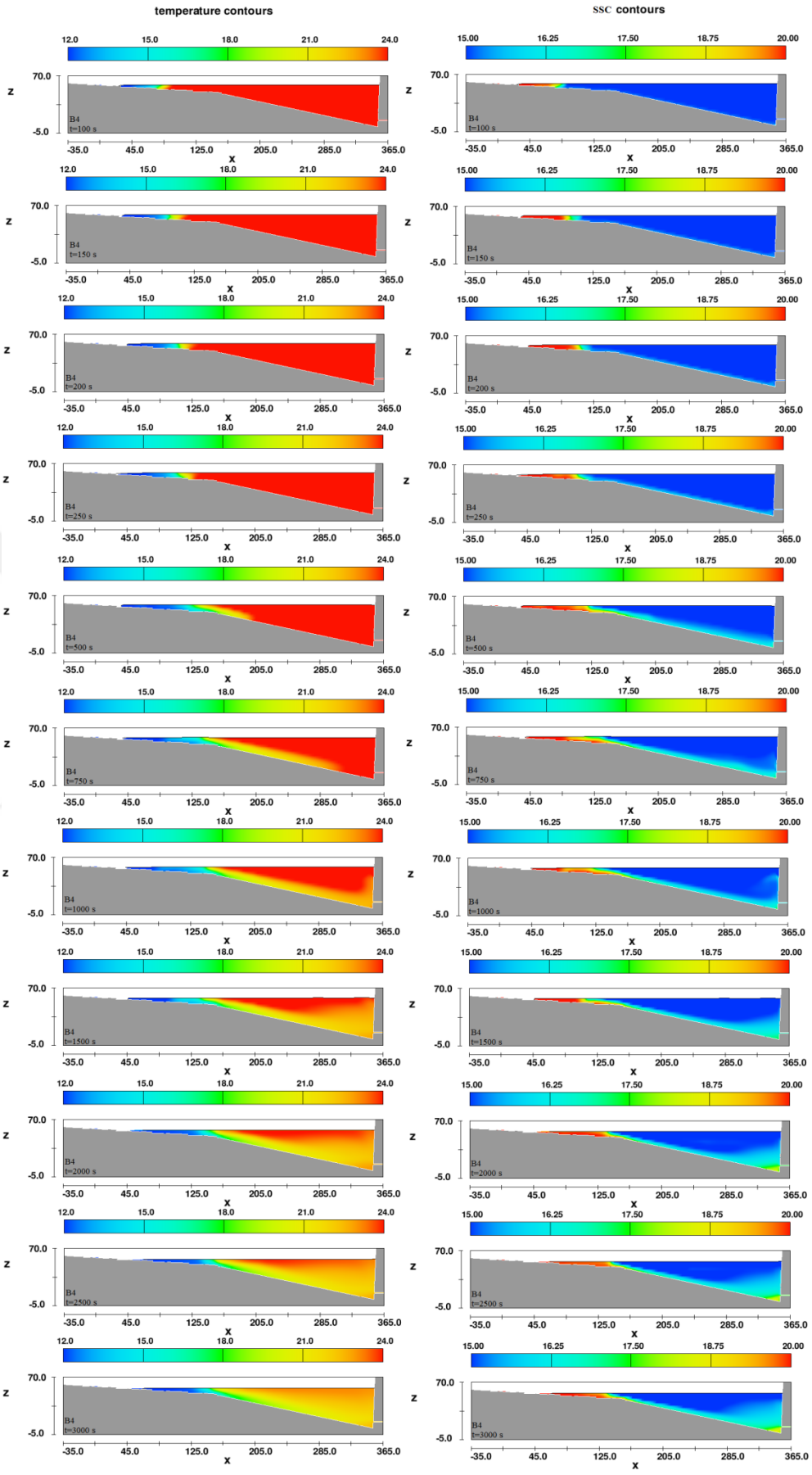

Figure 4.68 : Temperature and SSC Contours of Simulation B4.

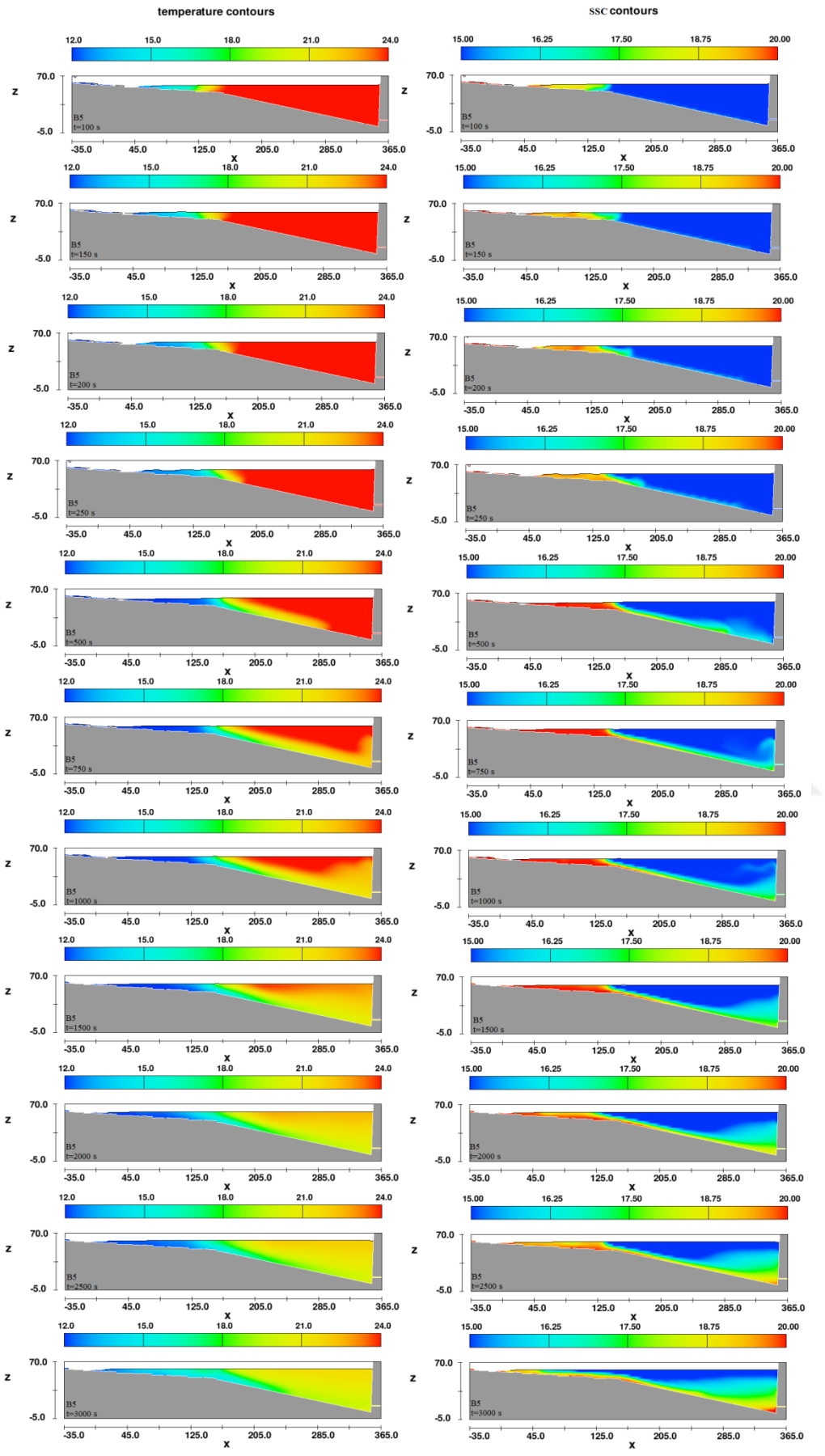

Figure 4.69 : Temperature and SSC Contours of Simulation B5.

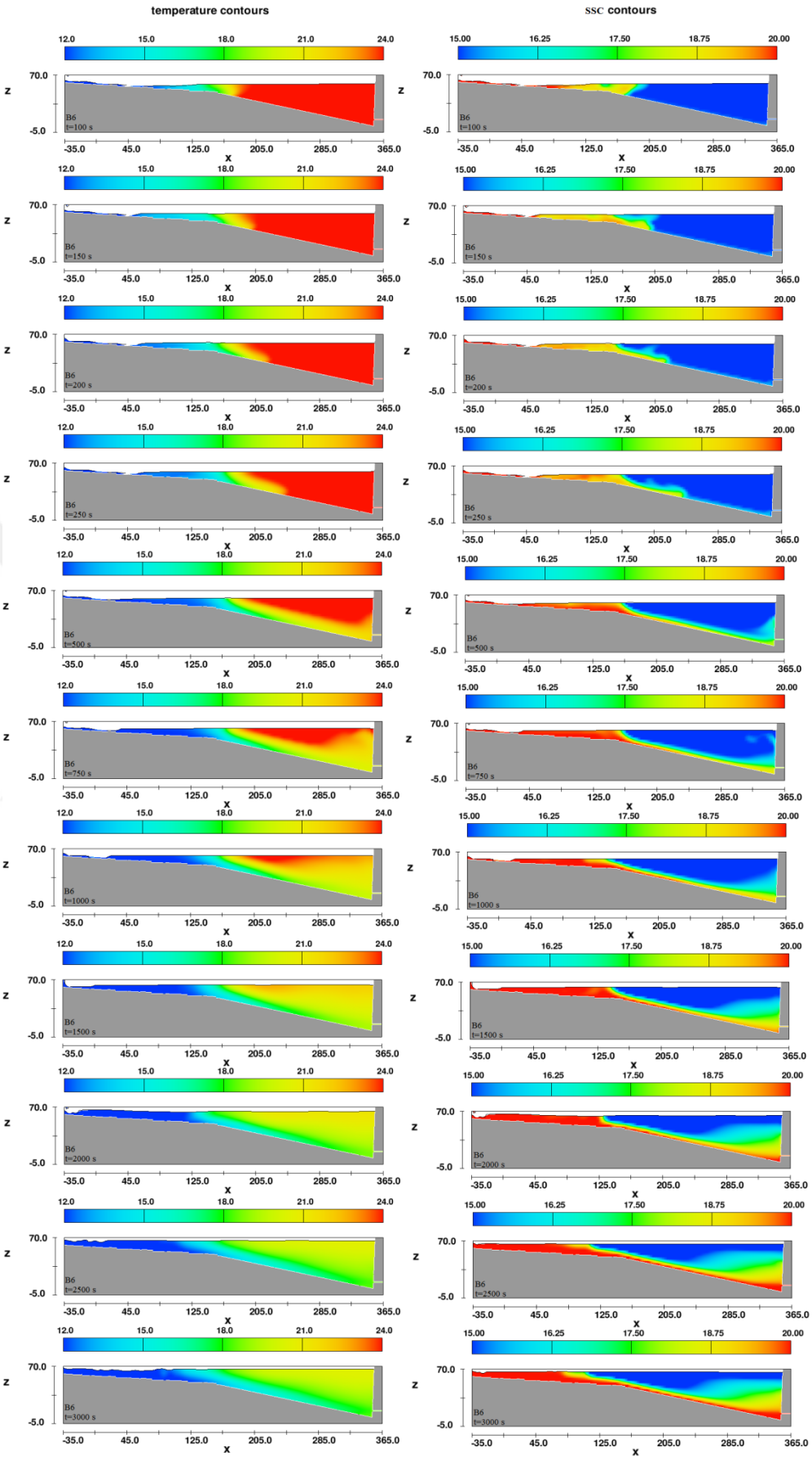

Figure 4.70 : Temperature and SSC Contours of Simulation B6.

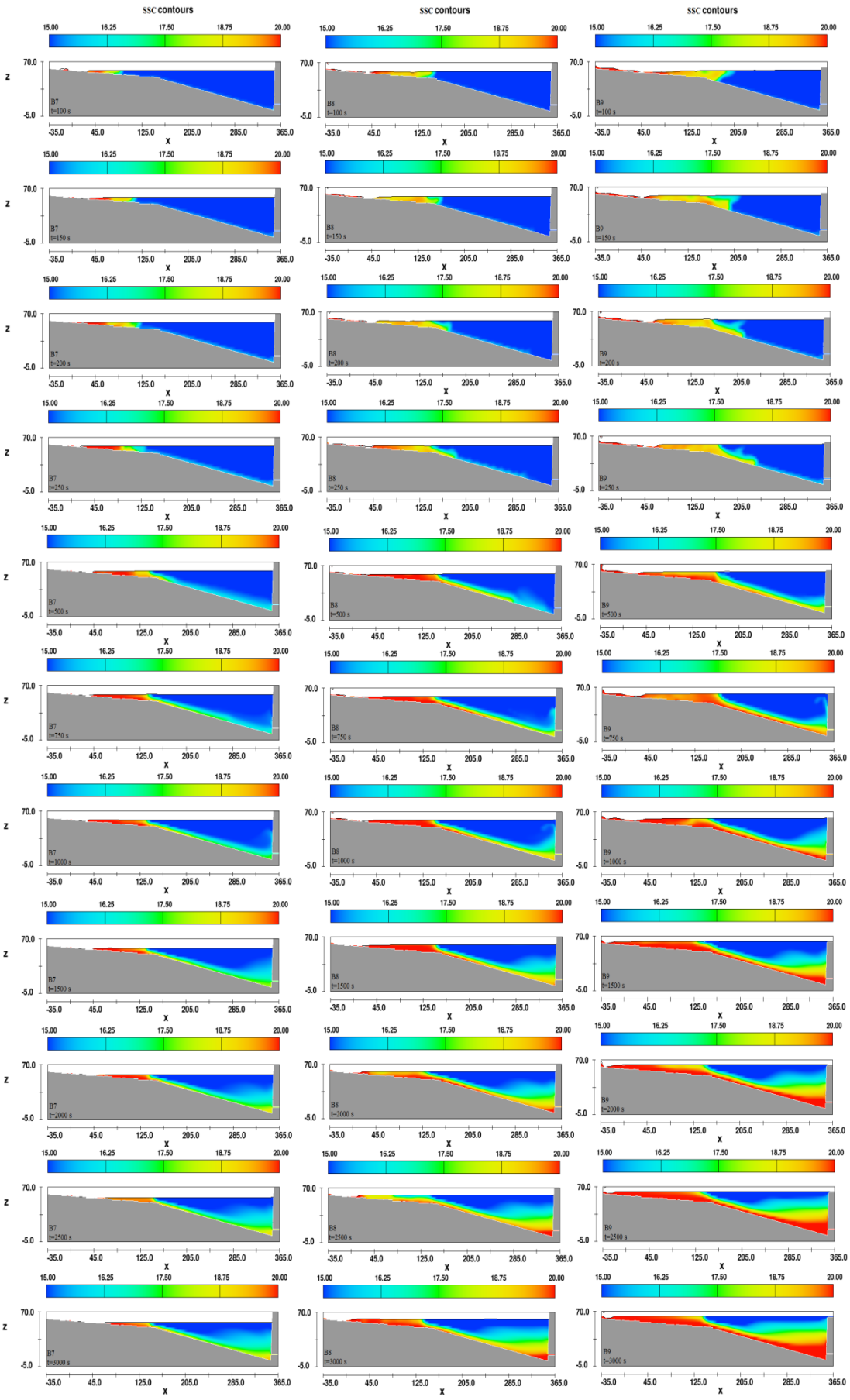

Figure 4.71 : SSC Contours of Simulation B7, B8 and B9

Inflow river water temperature and suspended sediment concentration values are equal to 12 ^{o}C and 20 g/l for simulations B4, B5 and B6, respectively. While, the inflow river and reservoir water temperatures have same values in simulations B7, B8 and B9, which are equal to 24 ^{o}C. The bottom outlet is very effective in these simulations in decreasing and preventing suspended sediments propagated to the upper layers of reservoir, with releasing the under flow currents into downstream of the dam body. The effective role of the inflow discharge magnitude on the structure formation of turbidity currents is also seen in these simulations. According to the results figures, it is clear that the high magnitude of inflow discharge, caused to strong formation of all parts of the turbidity /density current in these simulations. The bottom outlet is also caused to increasing in velocity of the turbidity/density currents.

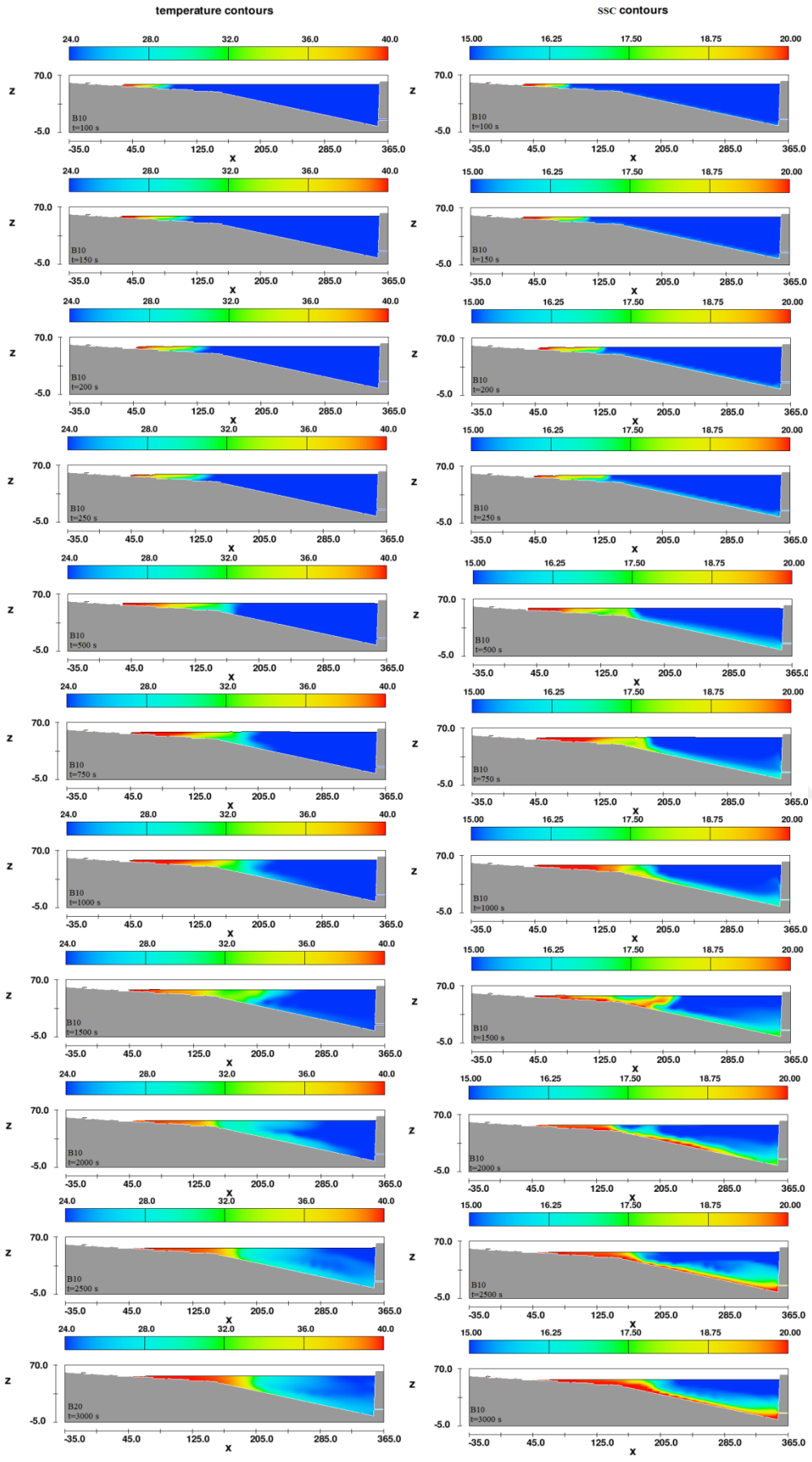

Figure 4.72 : Temperature and SSC Contours of Simulation B10.

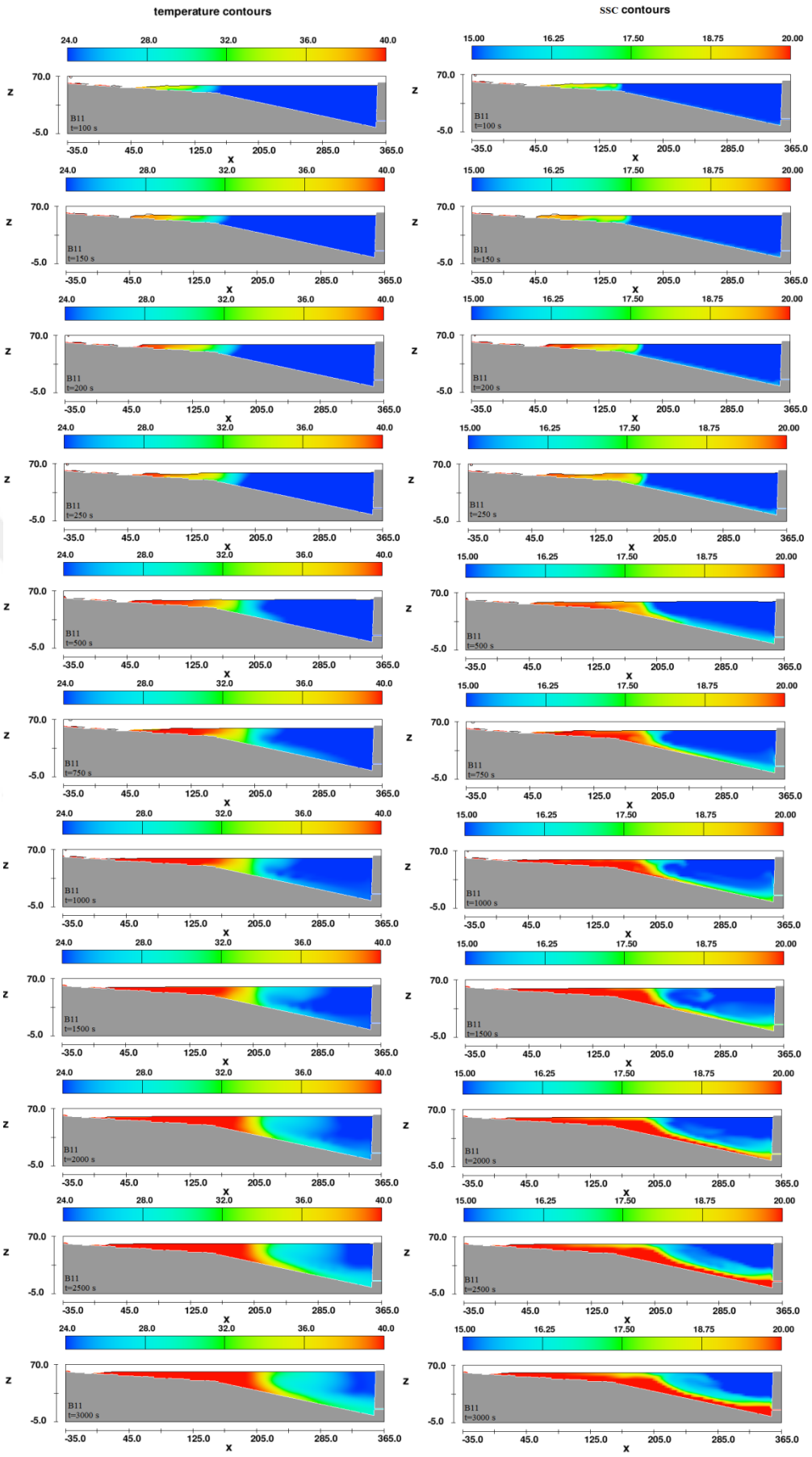

Figure 4.73 : Temperature and SSC Contours of Simulation B11.

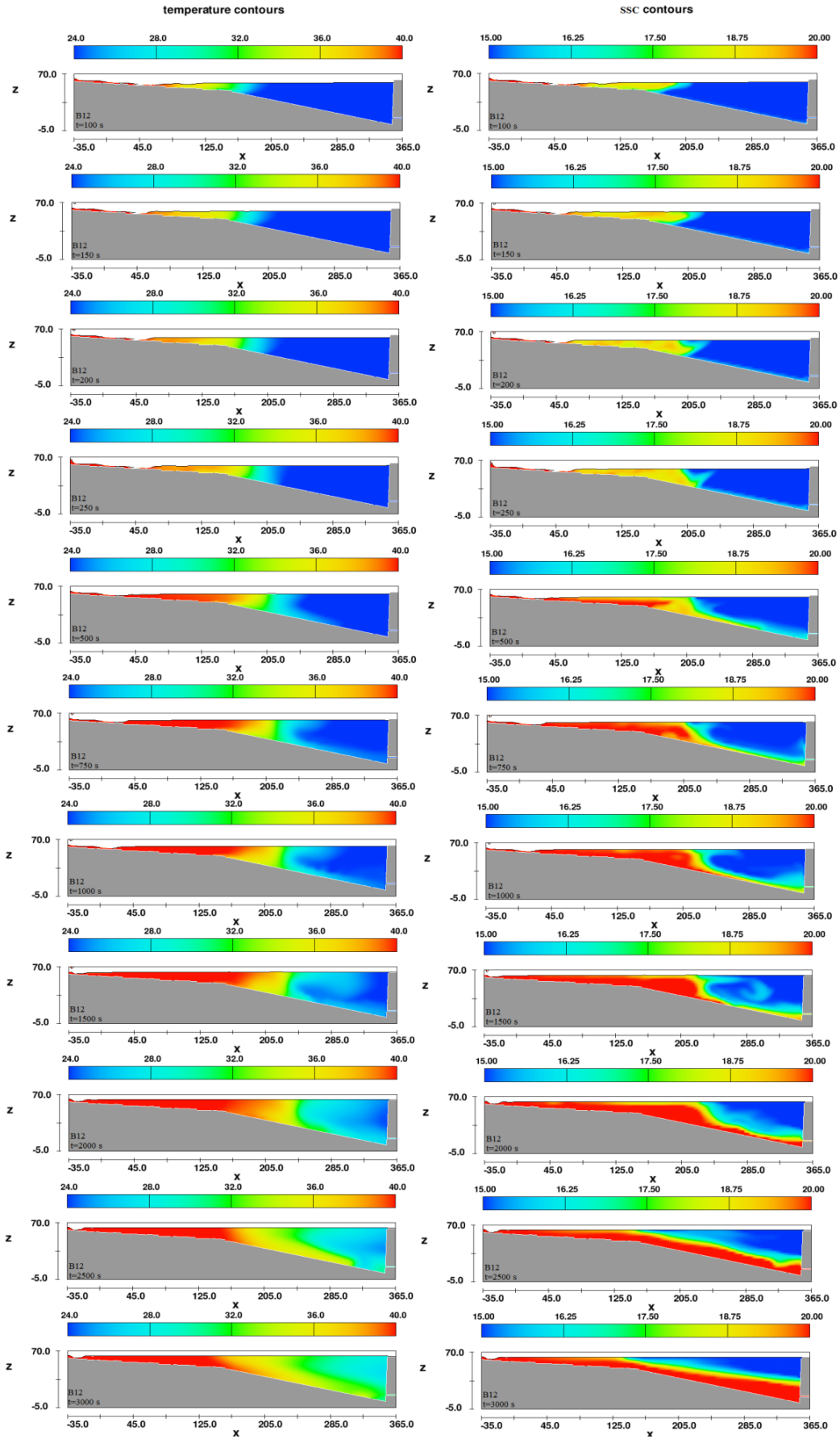

Figure 4.74 : Temperature and SSC Contours of Simulation B12.

By analyzing and comparing the results of the models without bottom outlet and with bottom outlet, it is observed that existing of the bottom outlet affects the speed of arriving the temperature to the dam body. It is seen that with bottom outlet, the area near the dam body is quickly under the influence of temperature variations resulting from the water with a different temperature value that entering into the reservoir. The existence of this outlet is also affecting the thickness of the turbidity current and layers of stratification. The thickness of the turbidity cuurrents decreases with existence of these outlets. However, the position, situation, shape and the diameter of these outlets have a very important role on the velocity and the motion pattern of the turbidity currents, but study on these parameters and their effects is not a subject relevant to this thesis and could be investigated in future studies, separately.

B/W contours of temperature and suspended sediment concentration for high magnitude of discharge included B3, B6, B9 and B12, were prepared and shown in Figures 4.75, 4.76, 4.77 and 4.78.

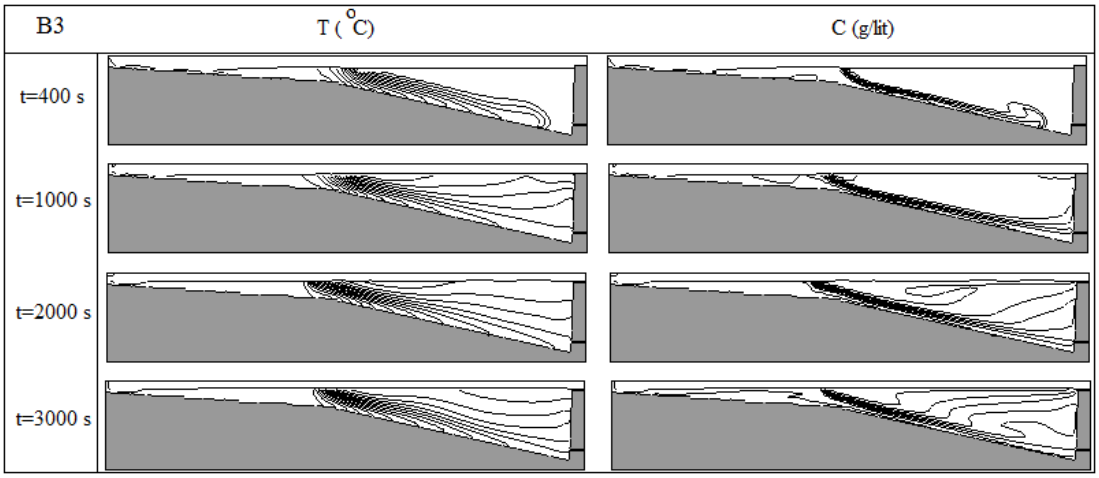

Figure 4.75 : B/W contours of temperature and concentration (B3).

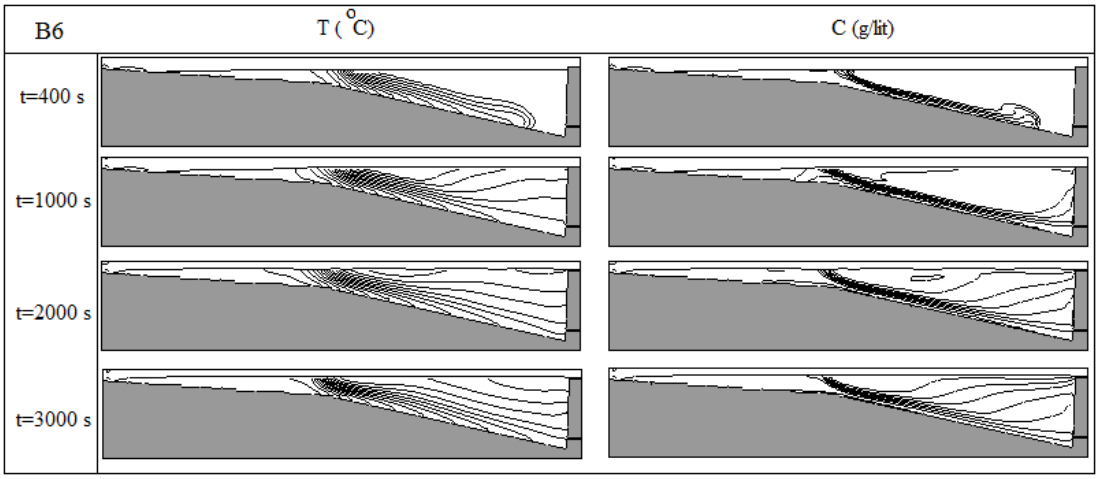

Figure 4.76 : B/W contours of temperature and concentration (B6).

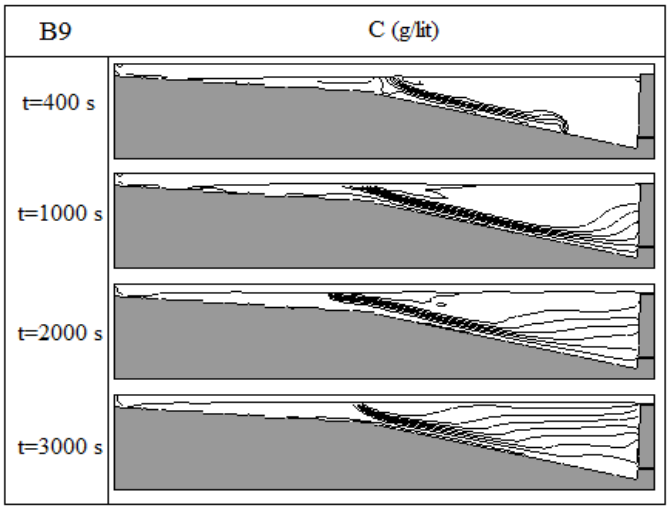

Figure 4.77 : B/W contours of temperature and concentration (B9).

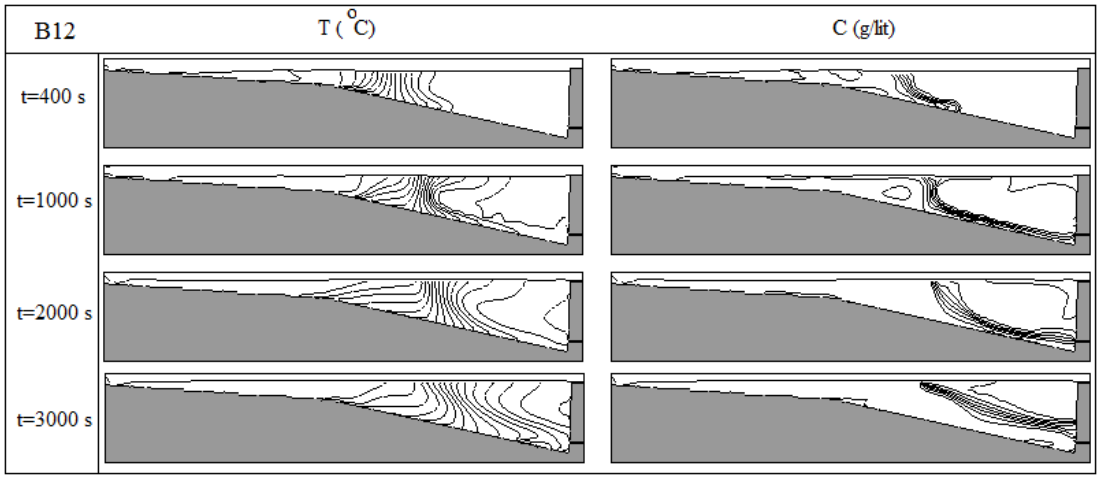

Figure 4.78 : B/W contours of temperature and concentration (B12).

Totally, based on numerical models with different outlets, when a dense inflow current conditions occurred, it is indicated that releasing water from bottom outlet would lead to water quality enhancement, mostly.

As mentiond before and according to figure 4.35, the Figures 4.79, 4.80, 4.81 and 4.82 could be drawn for simulations B1 to B12 in different selected times included: 1000 s, 2000 s and 3000 seconds for section 1 and 2. Velocity vectors that colored by 2D velocity magnitude are given as Figures 4.83, 4.84, 4.85 and 4.86 for simulations B3, B6, B9 and B12 and for t=500 s, t=1000 s, t=1500 s and t=2500 s.

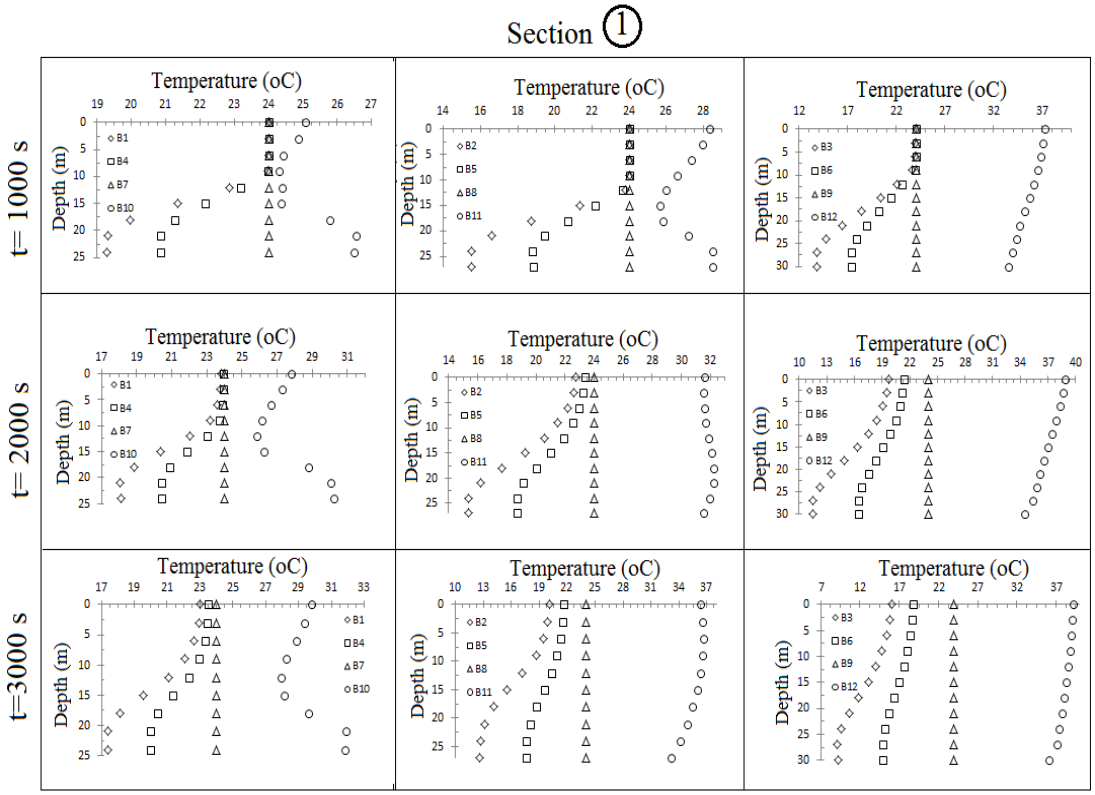

Figure 4.79 : Temperature variations during time in section 1 (B1, B2, ..., B12).

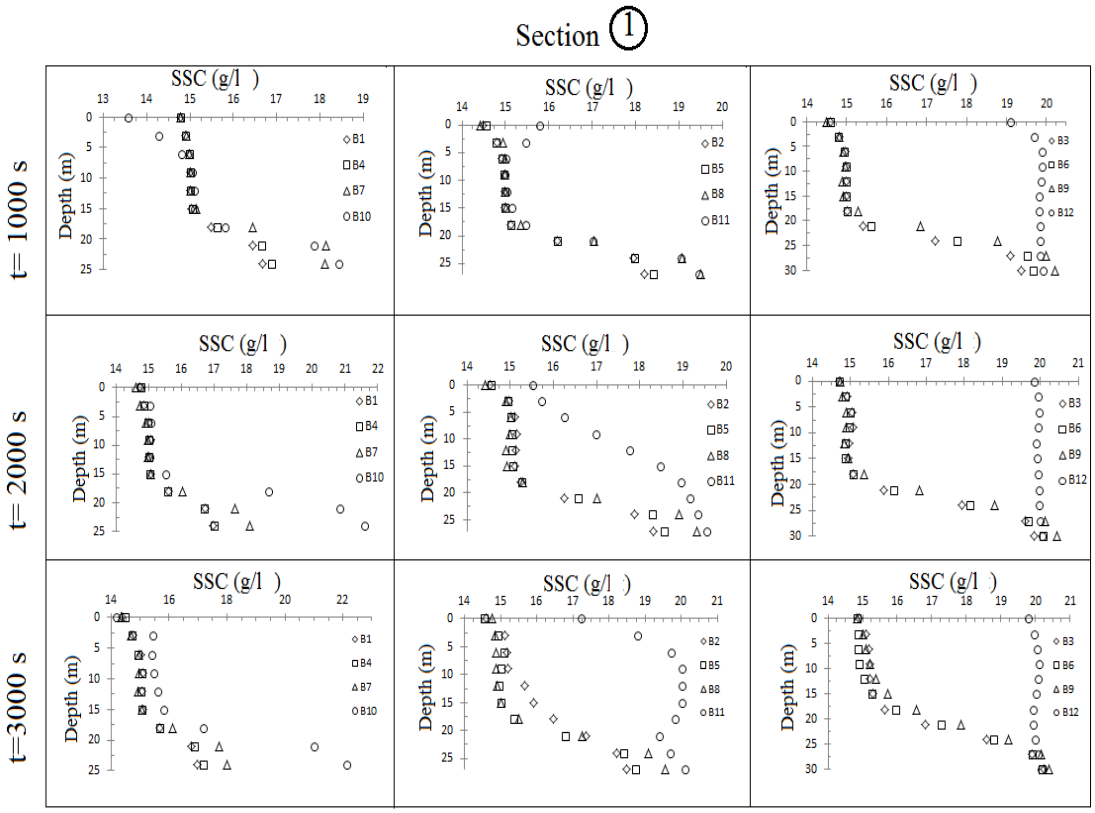

Figure 4.80 : SSC variations during time in section 1 (B1, B2, ..., B12).

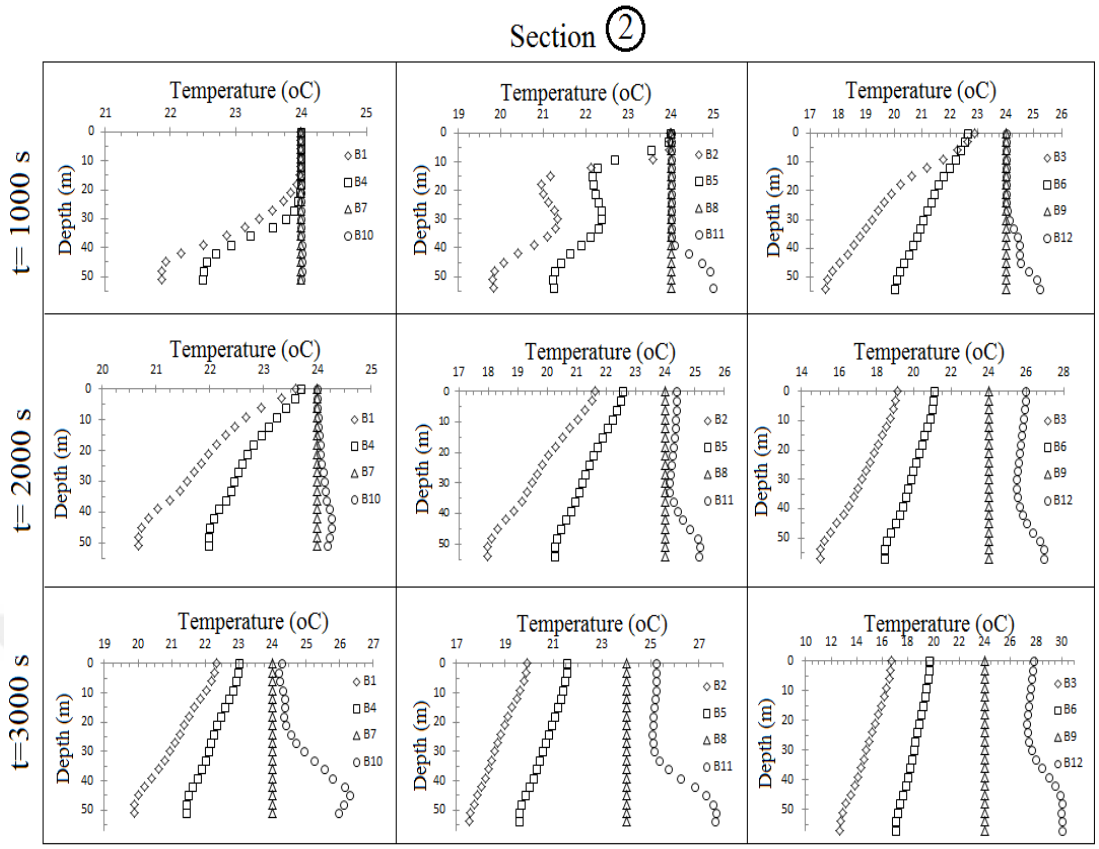

Figure 4.81 : Temperature variations during time in section 2 (B1, B2, ..., B12).

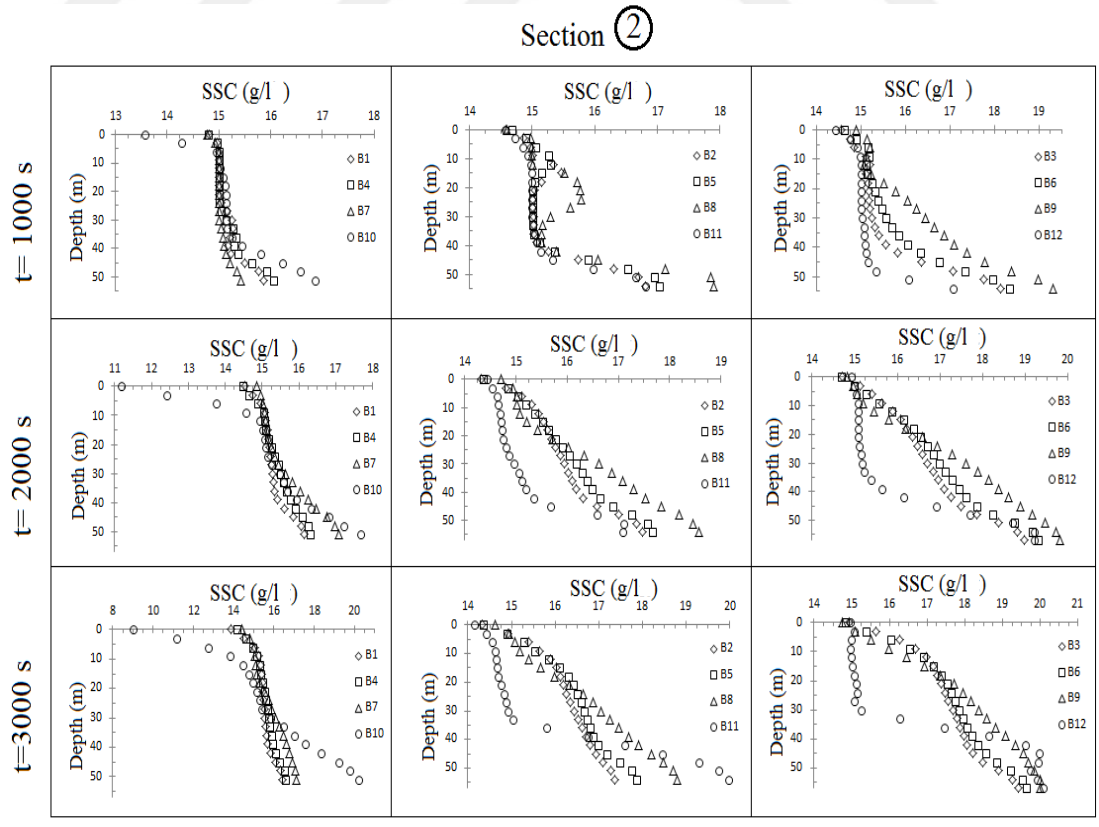

Figure 4.82 : SSC variations during time in section 2 (B1, B2, ..., B12).

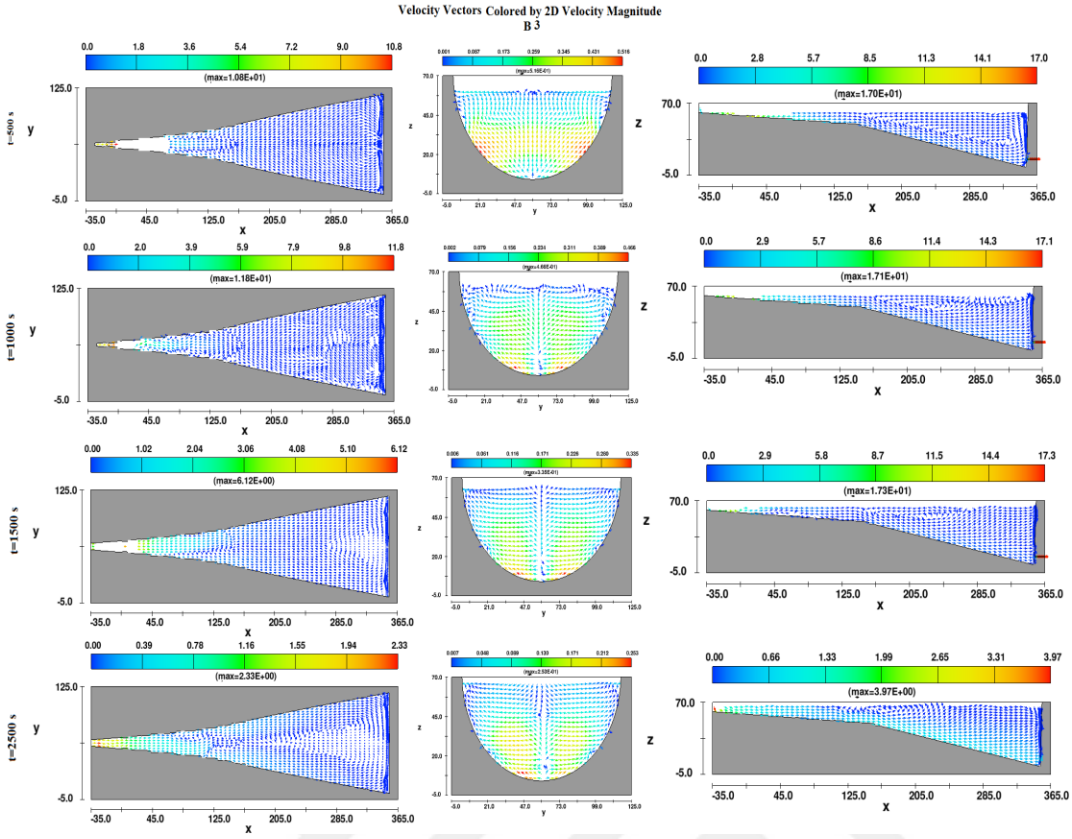

Figure 4.83 : Velocity Vectors Colored by 2D Velocity Magnitude for B3.

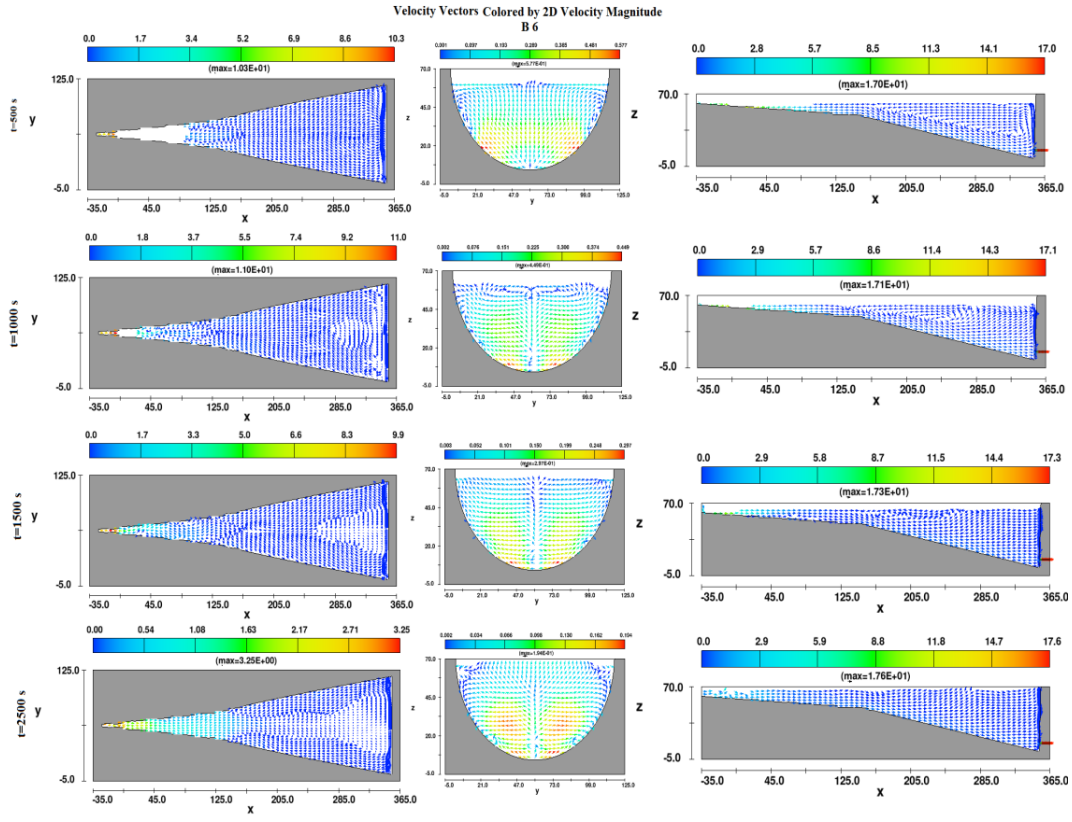

Figure 4.84 : Velocity Vectors Colored by 2D Velocity Magnitude for B6.

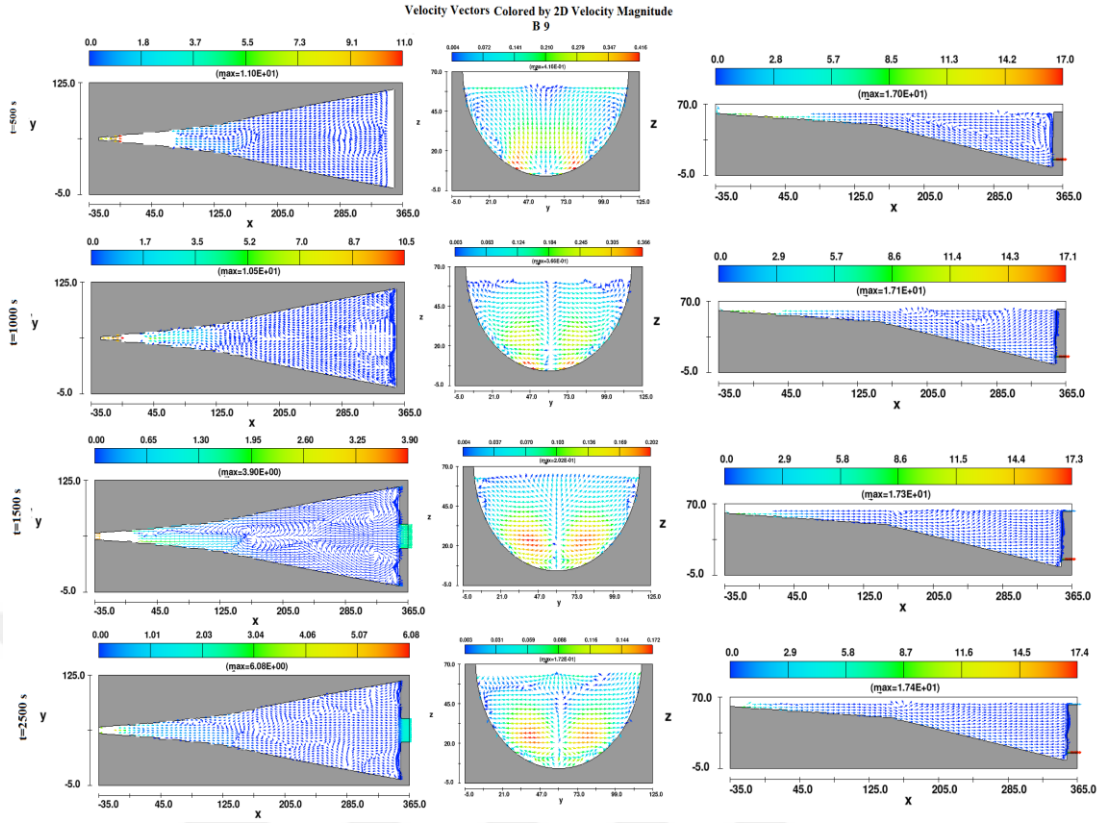

Figure 4.85 : Velocity Vectors Colored by 2D Velocity Magnitude for B9.

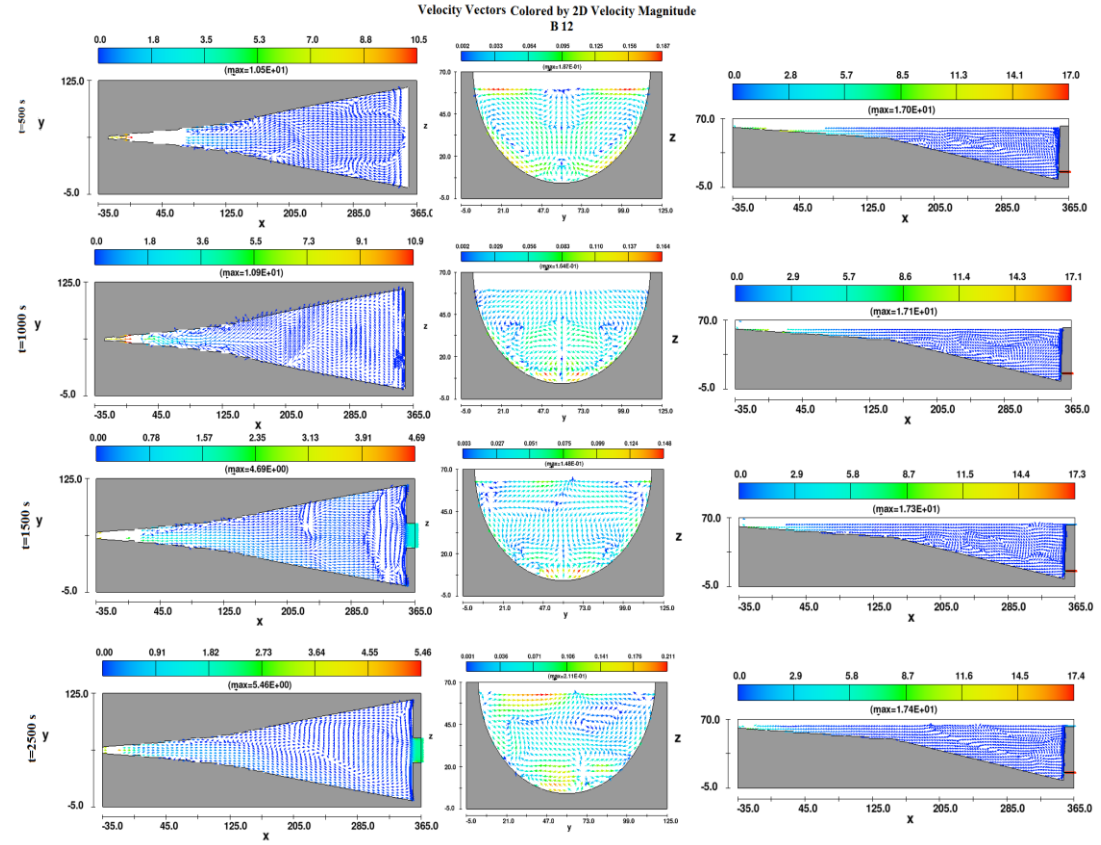

Figure 4.86 : Velocity Vectors Colored by 2D Velocity Magnitude for B12.

For simulations B1 to B12, the flow vectors and directions are represented in the following figure, briefly. In this figure, there is no flow enter to the spillway and the inflow water to the reservoir only exits from the outlet which located at the bottom of the reservoir.

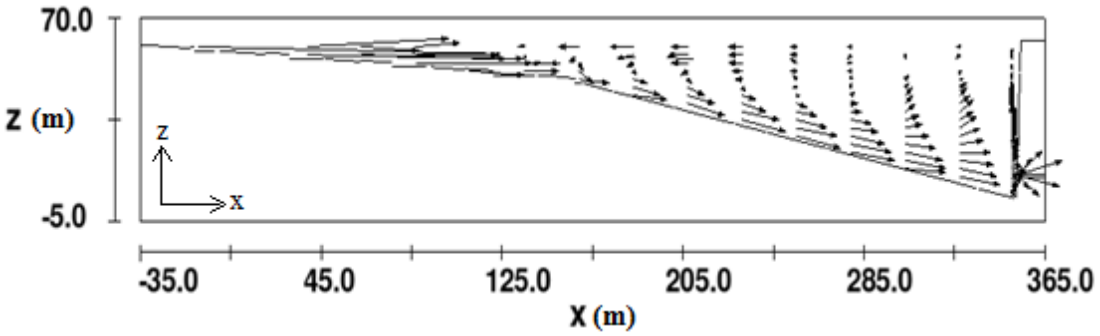

Figure 4.87 : Velocity Vectors and direction of the flow (B1 to B12).

In some of these simulations (B1 to B12), when the discharge is high, the spillway outlet is starting to operate, after some time. In this time, the velocity vectors become more obvious in the upper layer of the reservoir, specially at the surface of the water next to the body of dam and spillway.

In any of last simulations, the reverse and circulation current occurred at different times and depths, and mainly at the surface of reservoir. An example of these cases is shown in Figure 4.88.

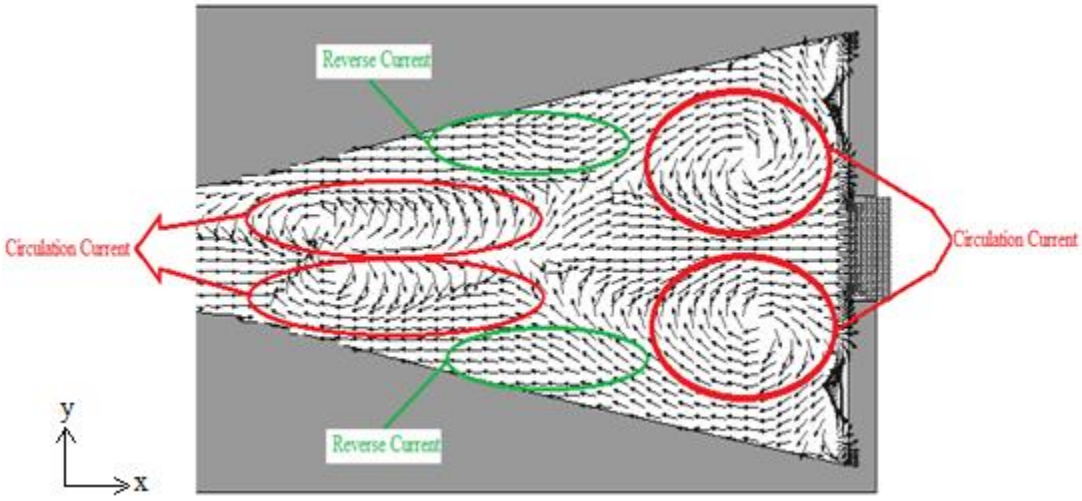

Figure 4.88 : Reverse and circulation current, which occurred in first 12 simulations of reservoir with bottom outlet (B models).

In addition to these currents, it is seen that at the beginning of the reservoir, where the flow comes into the reservoir, and in the binary times of the simulations, the wall jet flow is occurred in one side of the reservoir in simulations, mostly. An example of this state is shown in Figure 4.89.

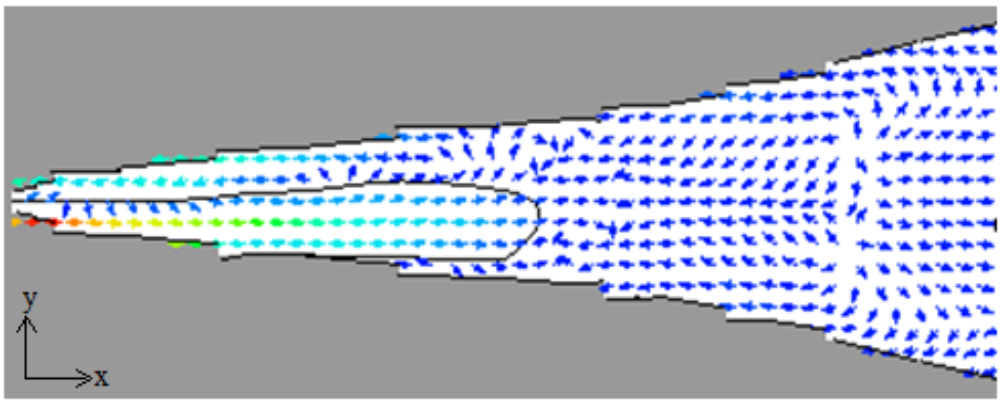

Figure 4.89 : Wall jet current.

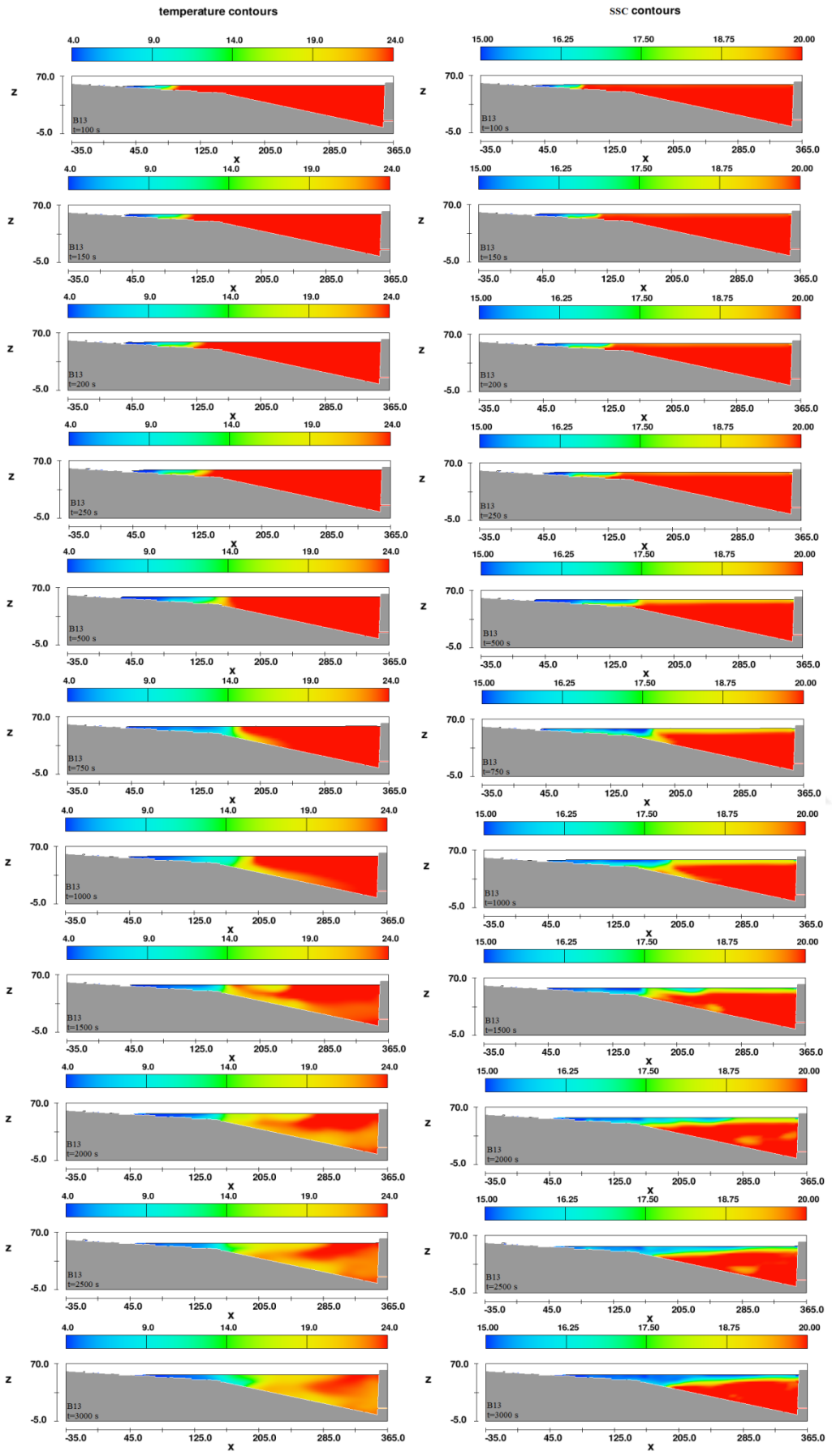

Figure 4.90 : Temperature and SSC Contours of Simulation B13.

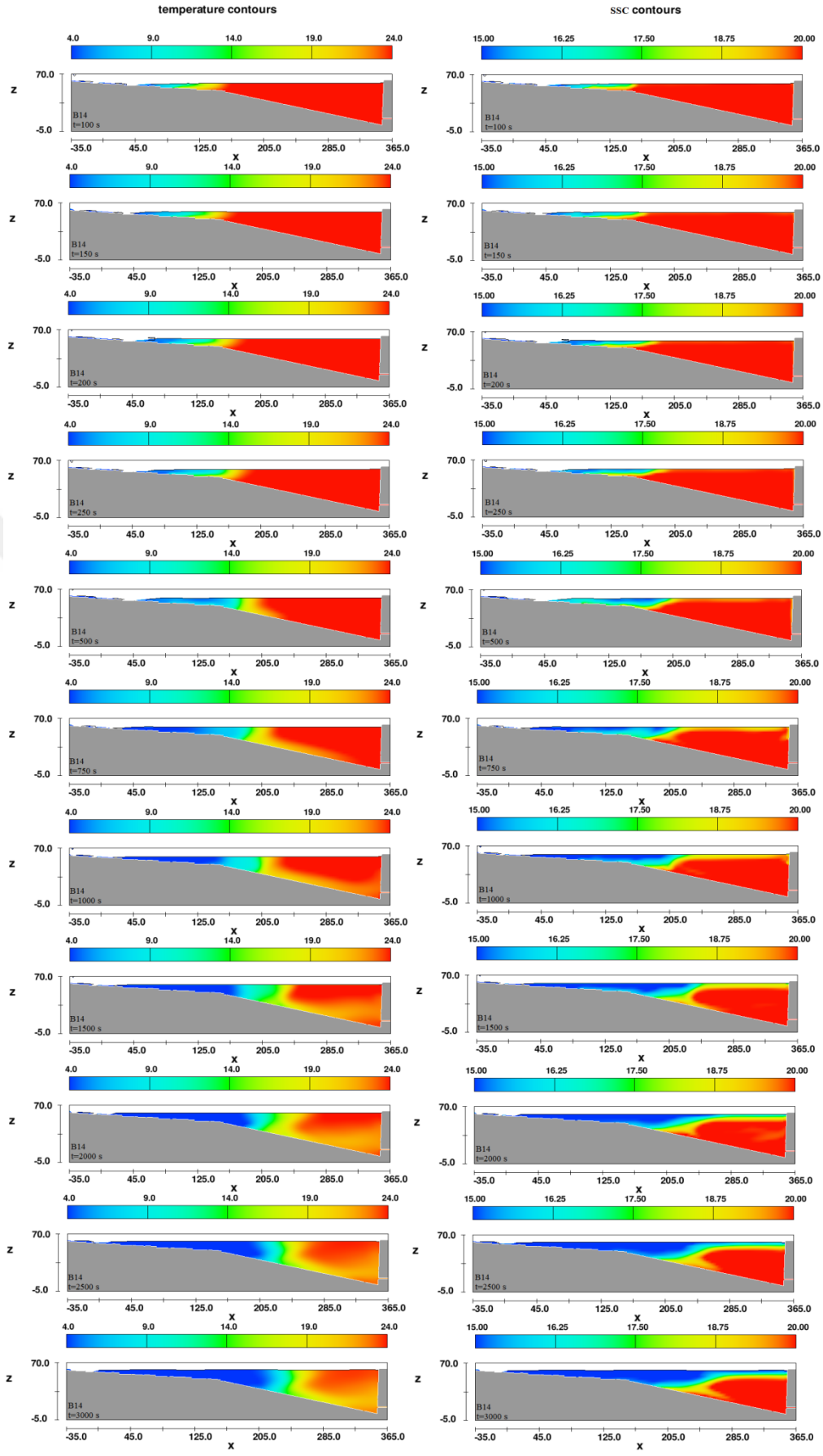

Figure 4.91 : Temperature and SSC Contours of Simulation B14.

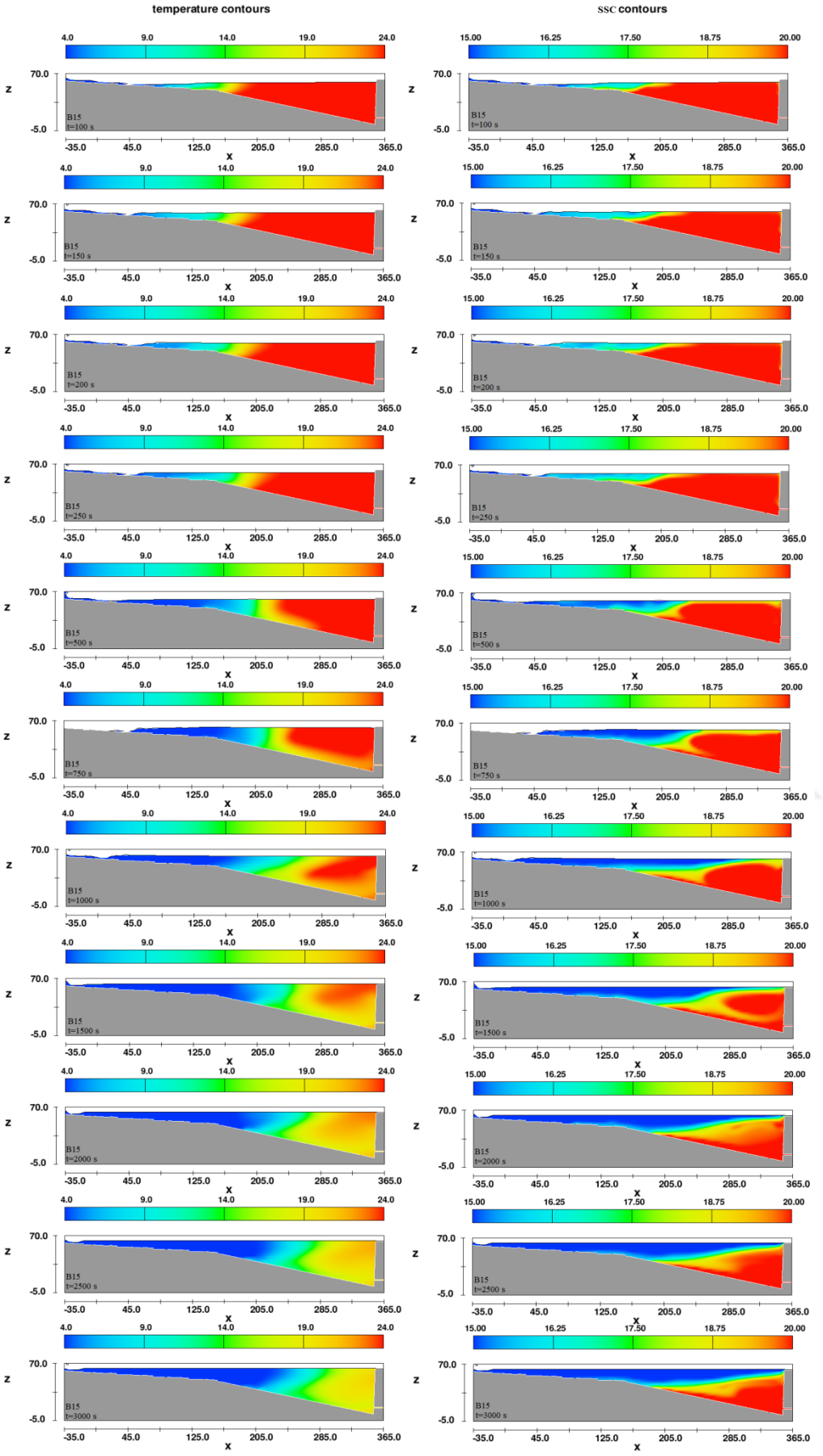

Figure 4.92 : Temperature and SSC Contours of Simulation B15.

In simulations B13, B14 and B15, the over flow condition occures. It is because of the low suspended sediment concentration value of inflow river in comparison with the reservoir suspended sediment concentration. When discharge increases, the heat and temperature start to transfer and distribute in reservoir at the upper layers and at surface of the reservoir, mainly. This state is clear in simulation B15, which has discharge equal to 100 m^3/s. The bottom outlet leads to increasing of velocity in depth and near the outlet, specially. When the water level reaches to its maximum value, in this moment, the spillway starts to operated. In this time, the velocity at the surface of the reservoir increases. It leads to increasing in suspended sediment and temperature distribution rate.

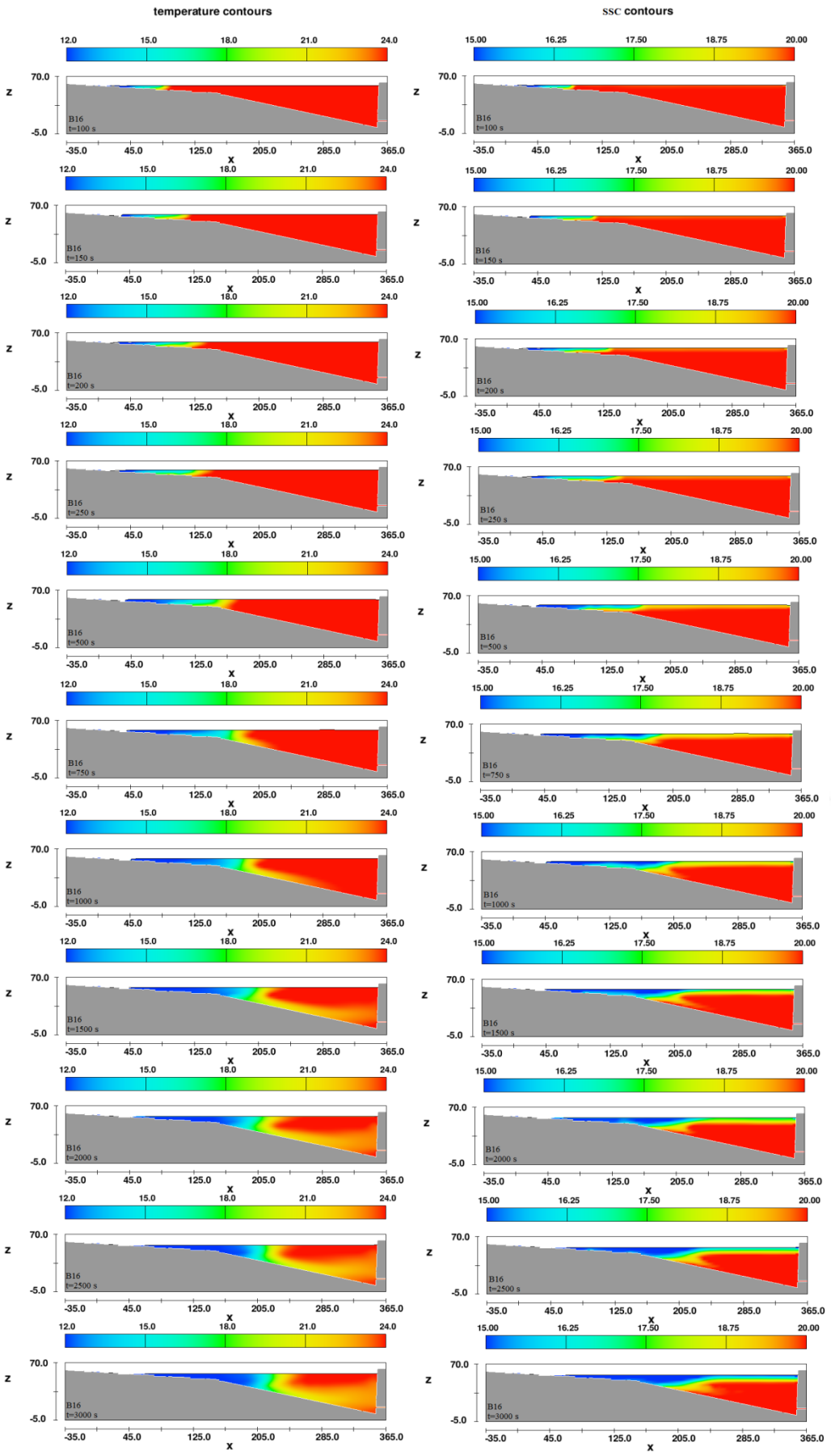

Figure 4.93 : Temperature and SSC Contours of Simulation B16.

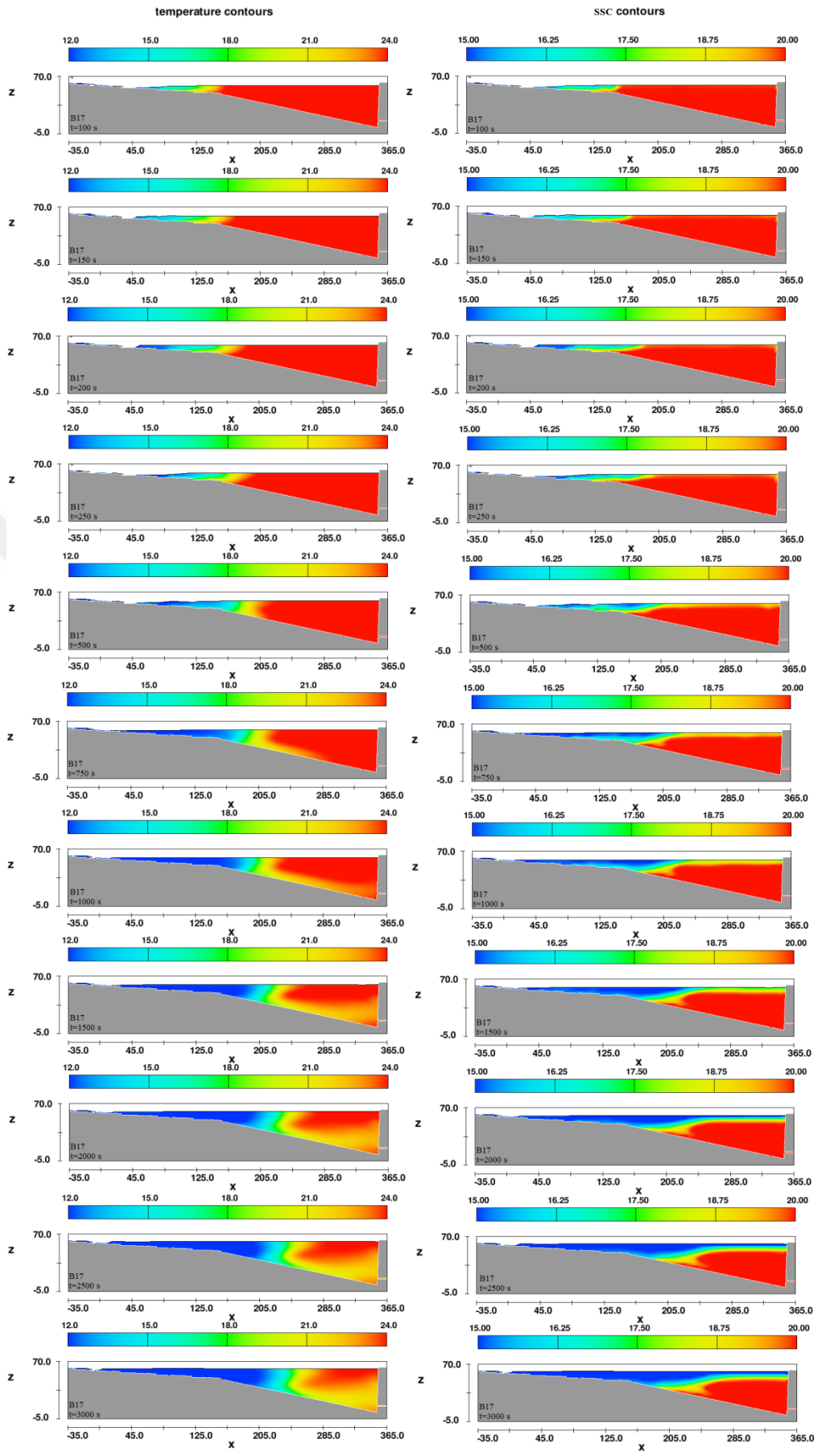

Figure 4.94 : Temperature and SSC Contours of Simulation B17.

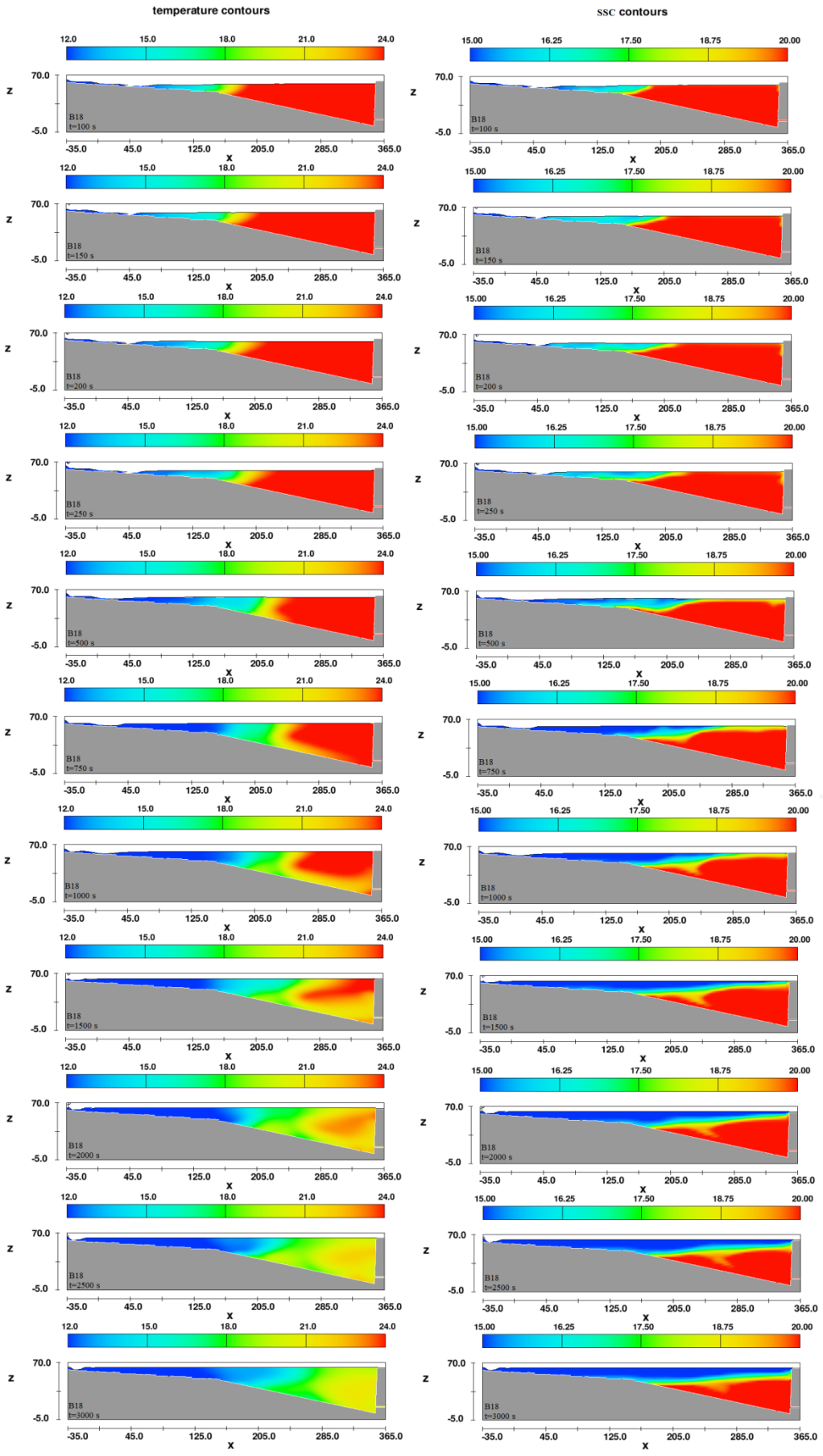

Figure 4.95 : Temperature and SSC Contours of Simulation B18.

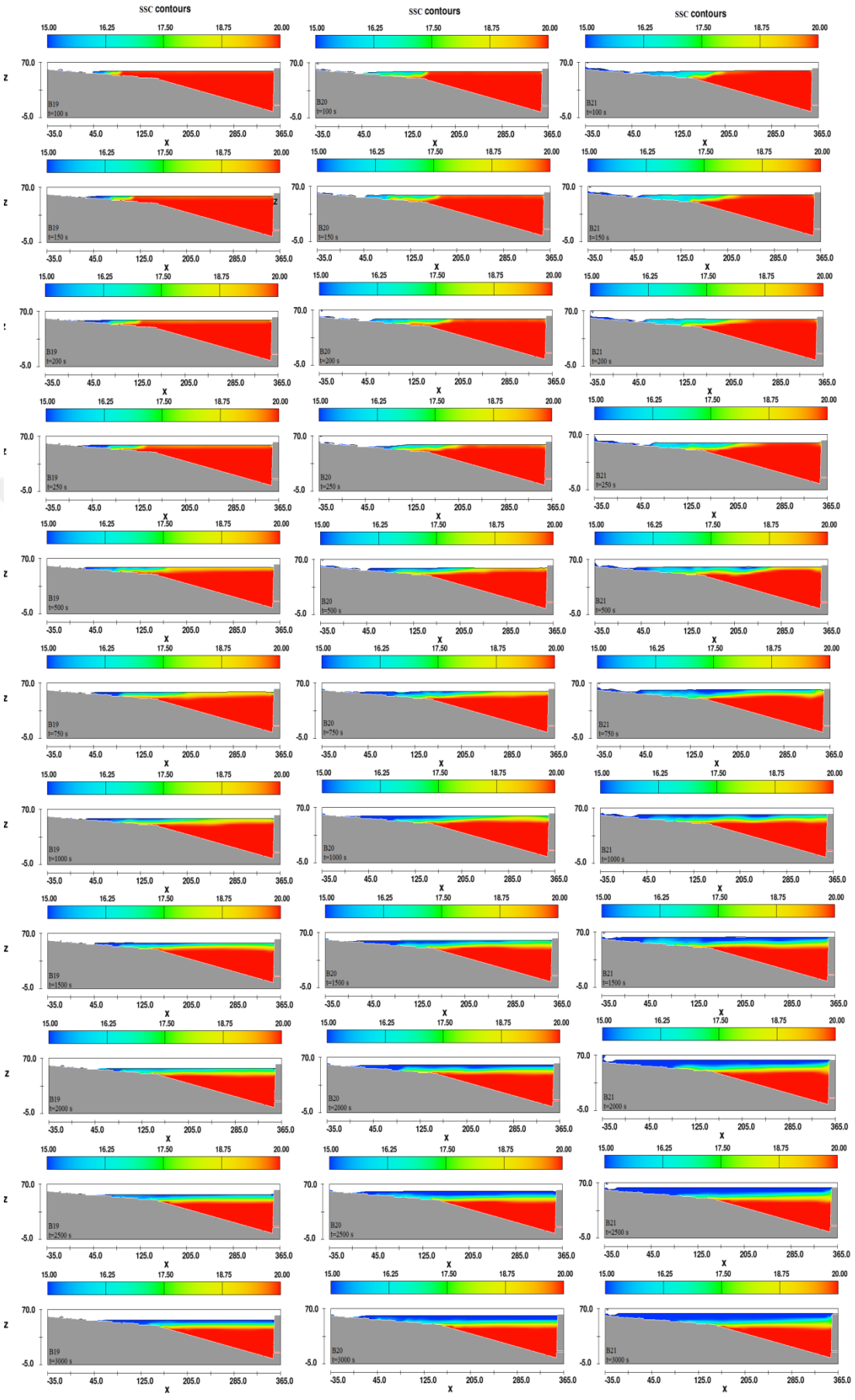

Figure 4.96 : SSC Contours of Simulation B19, B20 and B21.

As it is seen in Figures 4.93, 4.94, 4.95 and 4.96, after 3000 s, with evaluating in the thicknesses of the upper layer, it is obvious that the temperature of the inflow water affects the thickness. The colder inflow water, with temperature equal to 12 ^{o}C, has important effects on the layer thickness and caused to intering the inflow cold water into the deeper layer of the reservoir. With comparing the simulation B21 with simulations B15 and B18, this state is understandable. It is mportant to noticed and mentioned that the inflow temperature for B15, B18 and B21 is equal to 4 ^{o}C, 12 ^{o}C and 24 ^{o}C. Discharge is 100 m^{3}/s for these simulations.Figure 4.97 shows this state.

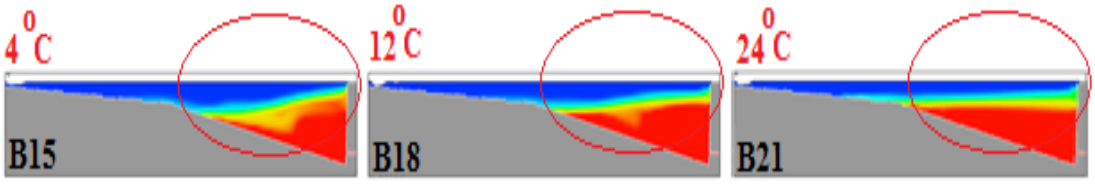

Figure 4.97 : Changes in thickness of SSC layers with temperature after 3000 s for simulations B15, B18 and B21.

With comparing the Figure 4.97 (B15, B18 and B21 simulations) with Figure 4.50 (S15, S18 and S21 simulations), it is concluded that the bottom outlet leads to increasing the thickness of the SSC of the upper layer with lower suspended sediment concentration value. It is because of that this bottom outlet facts like a suction with increasing the velocity in depth.

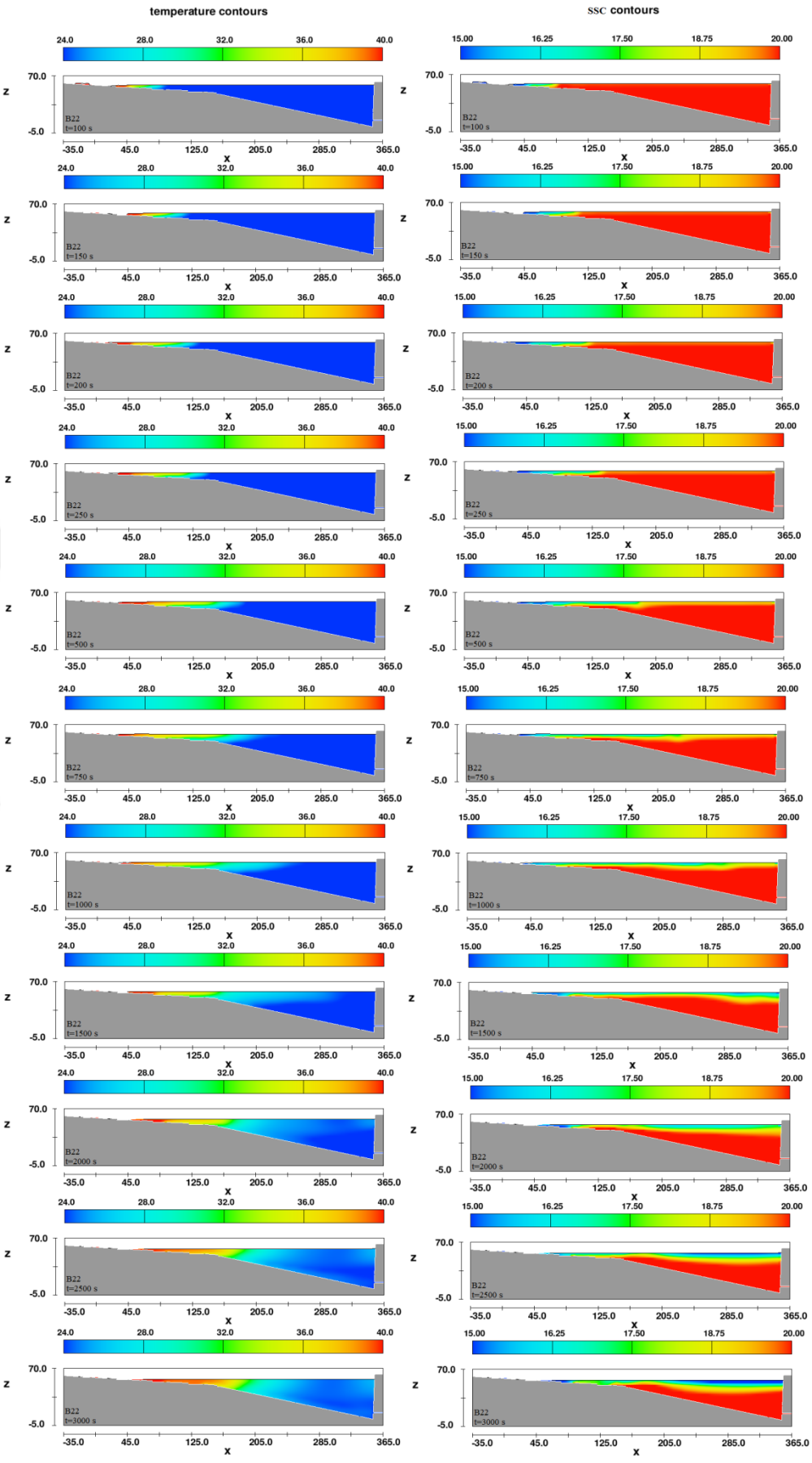

Figure 4.98 : Temperature and SSC Contours of Simulation B22.

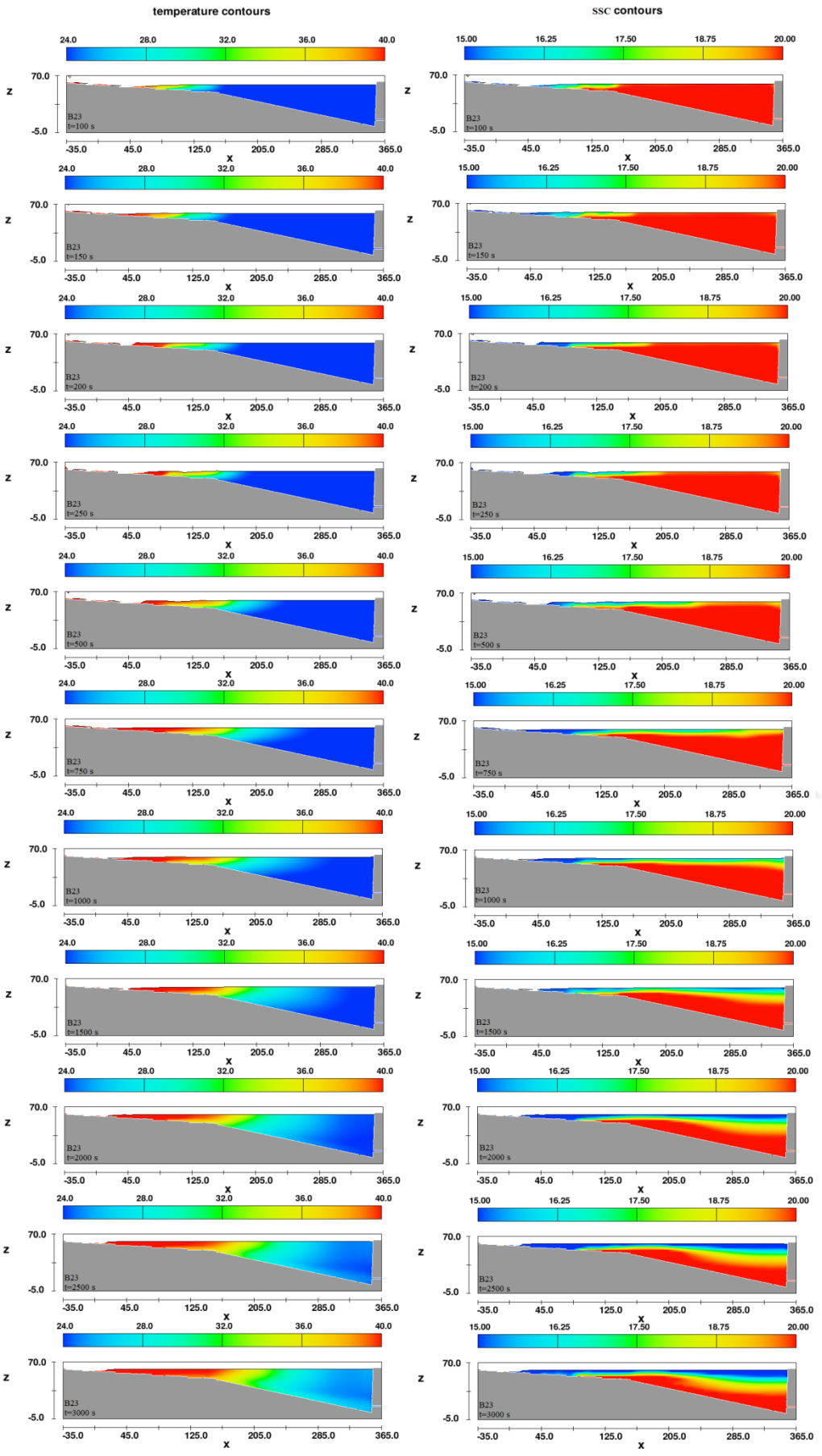

Figure 4.99 : Temperature and SSC Contours of Simulation B23.

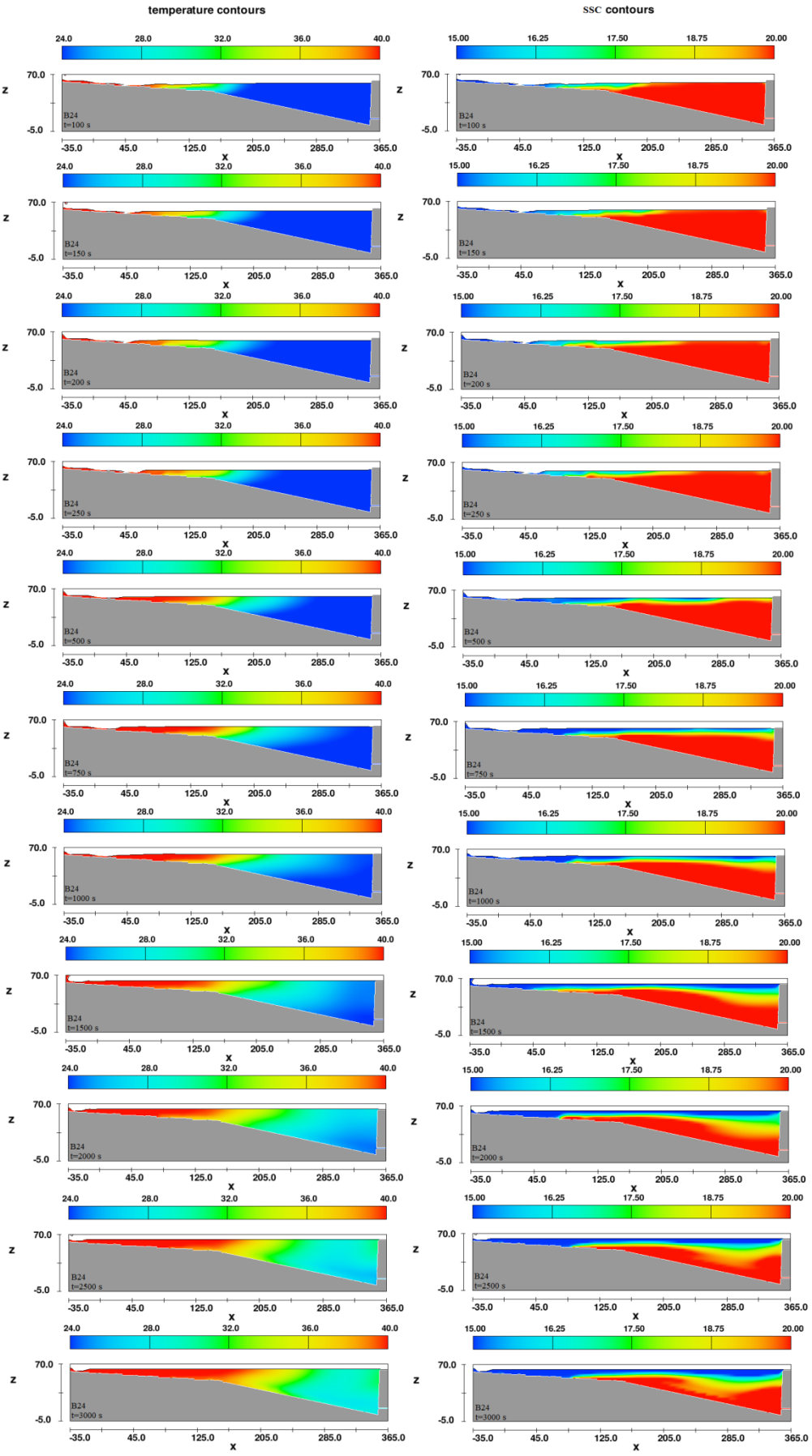

Figure 4.100 : Temperature and SSC Contours of Simulation B24.

It is seen that the bottom outlet is help to reducing the suspended sediment concentration. Existence of these types of outlets helps to guide the turbidity currents to the downstream region of the reservoir. So, the traveling time of the turbidity current are decreasing. Because of this decreasing time of traveling of turbidity current, the deposition of the sediment reduces. Another important result ,that could be seen in the figures of these simulations, is that the thickness of the stratified layers increases. B/W contours of temperature and suspended sediment concentration were drawn for simulations B15, B18, B21 and B24.

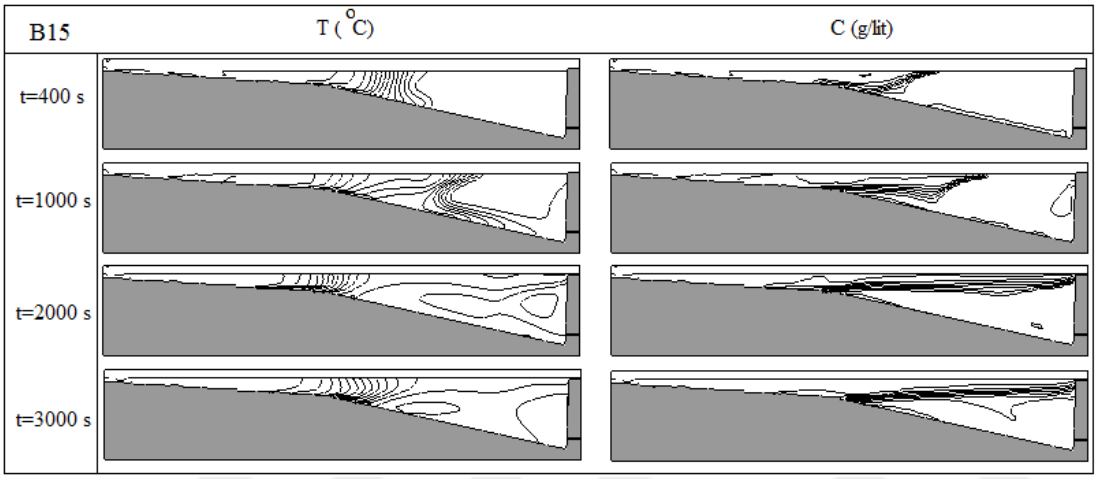

Figure 4.101 : B/W contours of temperature and concentration (B15).

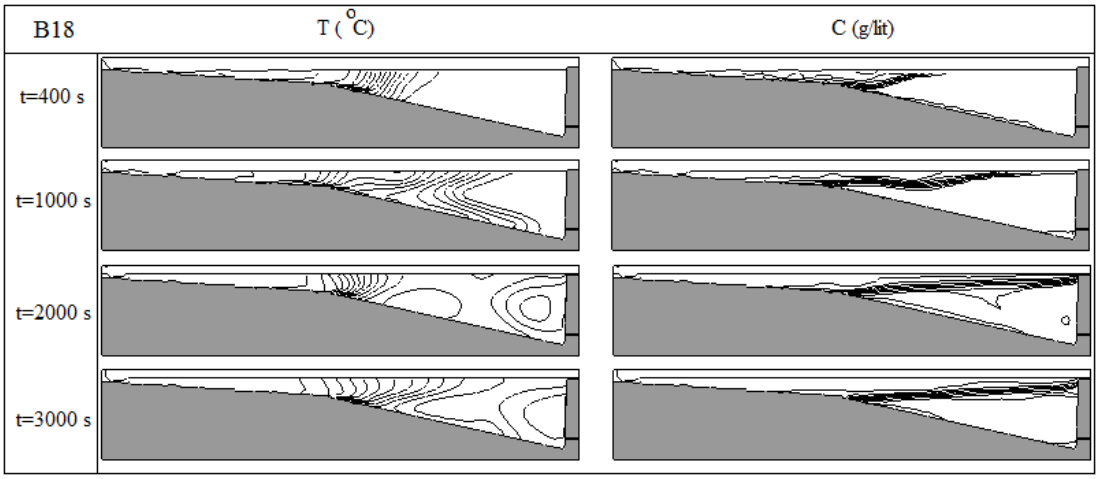

Figure 4.102 : B/W contours of temperature and concentration (B18).

In simulations B19,B20 and B21, the water temperature of the inflow current and reservoir is same and equal to 24 oC, as mentioned in the scenarios table. Therefore, only the suspended sediment concentration B/W contours are drawn for simulation number B21.

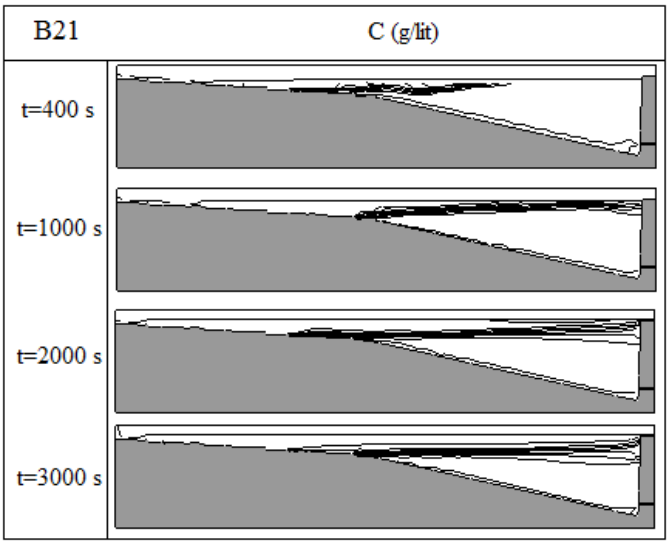

Figure 4.103 : B/W contours of temperature and concentration (B21).

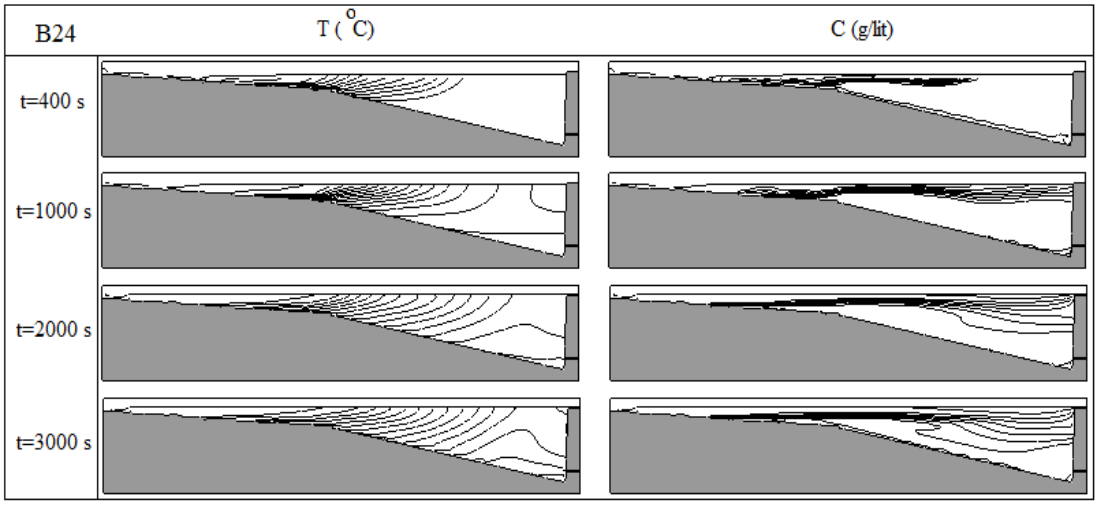

Figure 4.104 : B/W contours of temperature and concentration (B24).

In the above figures and mostly in figure B24, it is obvious that the bottom outlet helps to move about the density/turbidity current to the downstream of the dam.

The variations of temperature and suspended sediment concentration of the last simulation (B13-B24) are represented for the selected sections for times 1000 seconds, 2000 seconds and 3000 seconds as the following figures. In simulation B24, it is clear that over time the suspended sediment concentration is propagated in depth and the suspended sediment stratification is going to be decreased in reservoir. Comparing with S24, it is obvious that the bottom outlet helps to decreasing the suspended sediment stratification.

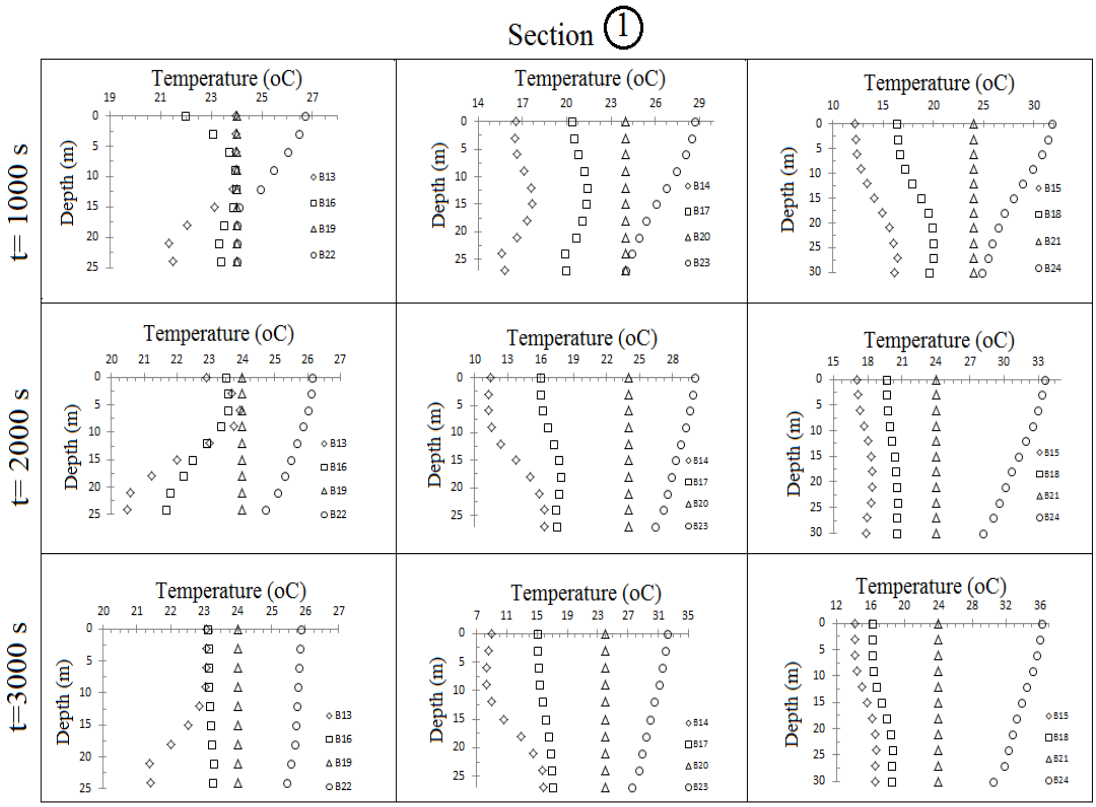

Figure 4.105 : Temperature variations during time in section 1 (B13, B14, ..., B24).

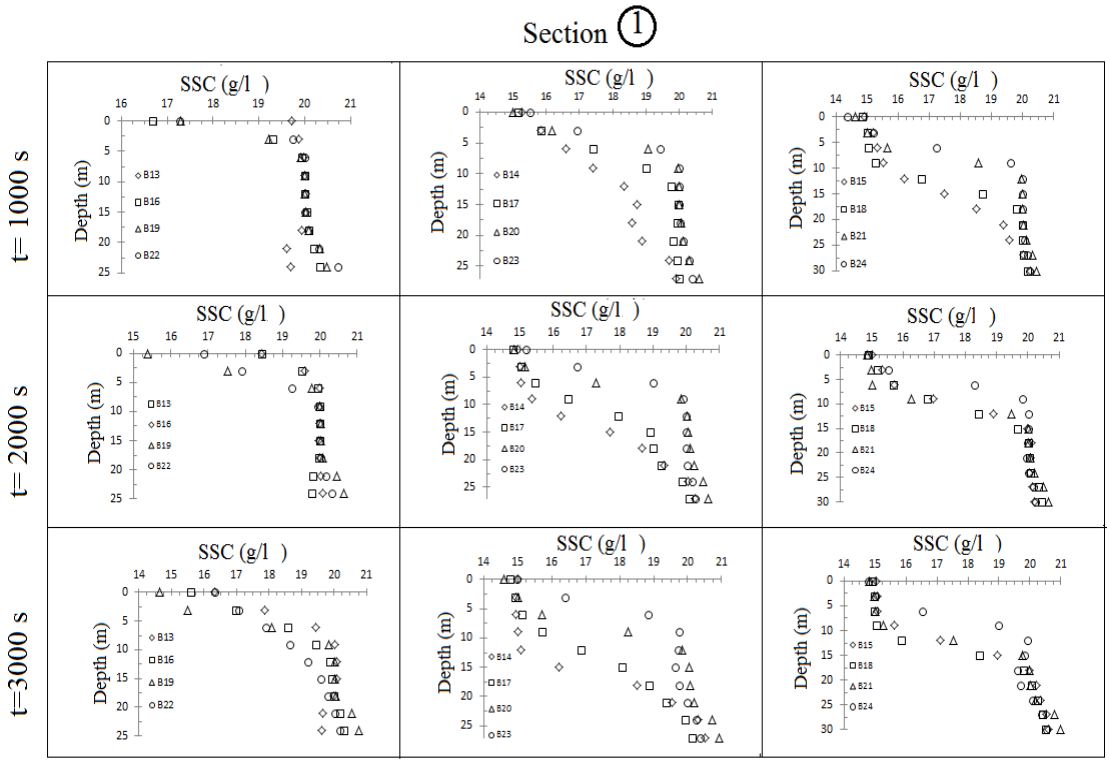

Figure 4.106 : SSC variations during time in section 1 (B13, B14, ..., B24).

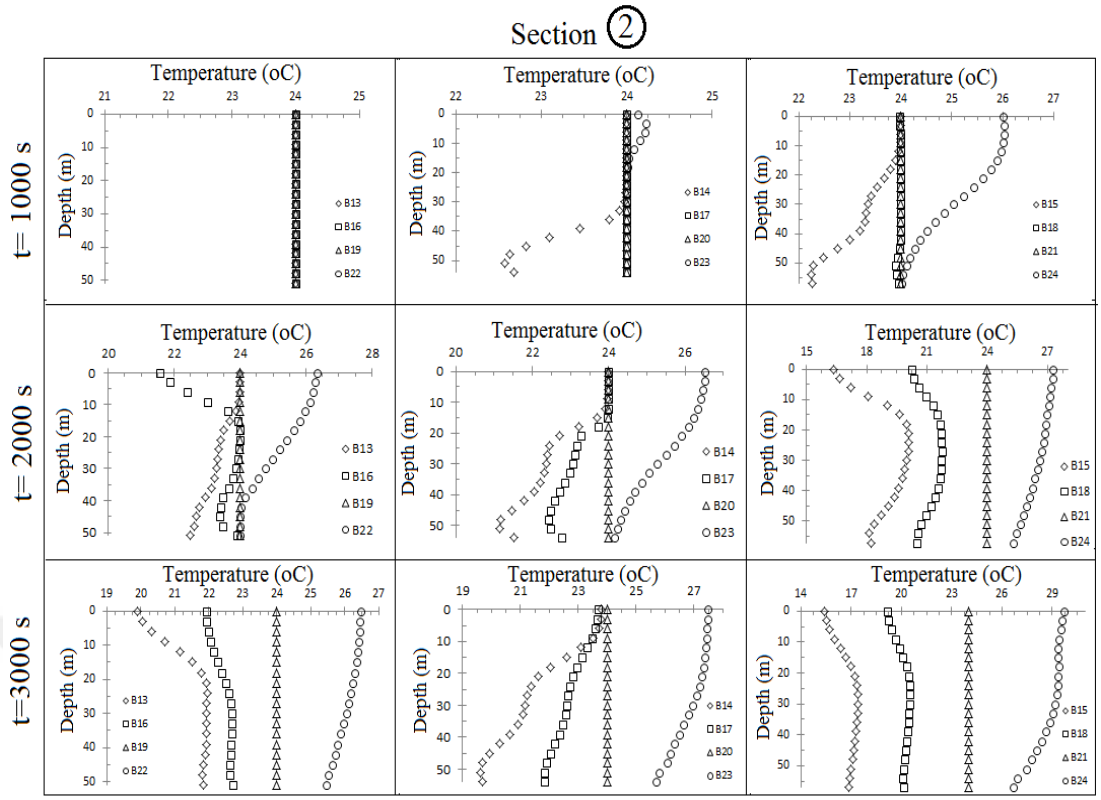

Figure 4.107 : Temperature variations during time in section 2 (B13, B14, ..., B24).

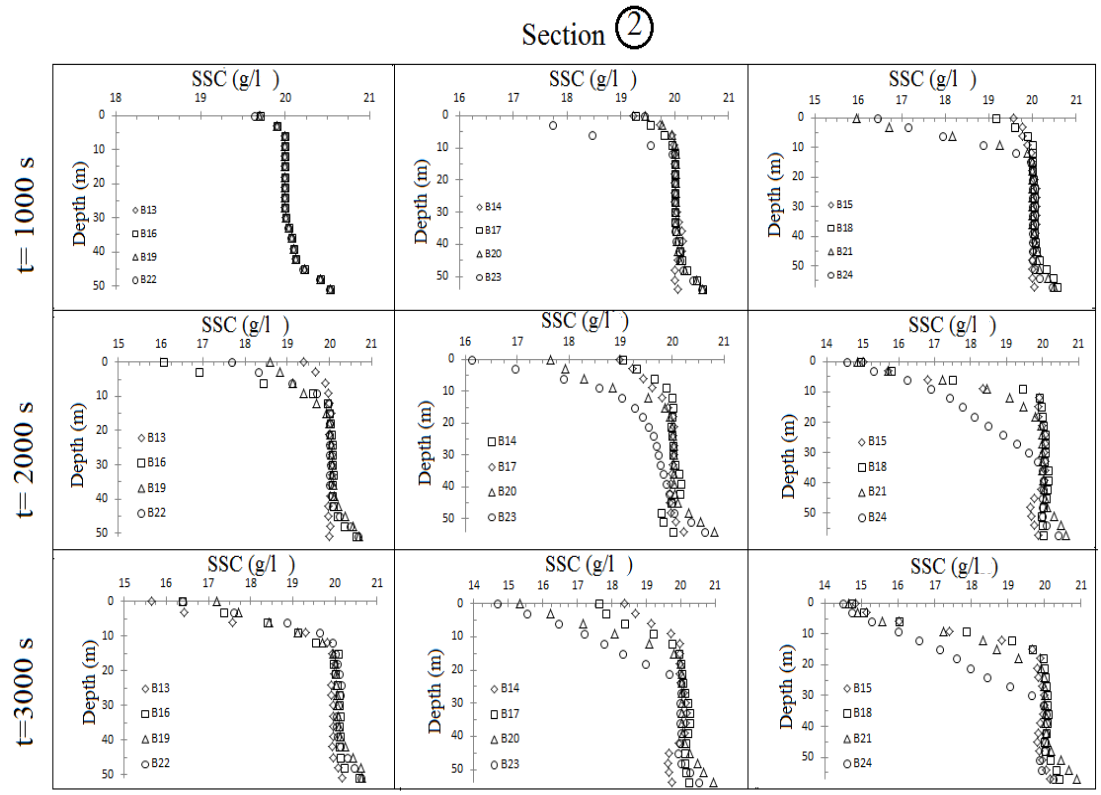

Figure 4.108 : SSC variations during time in section 2 (B13, B14, ..., B24).

From the Figures 4.105, 4.106, 4.107 and 4.108, in B13, B16, B19 and B24 simulations and at section 2, in t=1000 seconds, because of the low magnitude of discharge, there is no variations occurred. In B17 and B23 in this time, the thermal transfer is done like under and over flow conditions, respectively. At time 3000 seconds, the reservoir is going to have a thermal stability. The water temperature of the reservoir in this condition is going to be uniform. The suspended sediment concentration at the upper layer of the reservoir is reduced. This is because of the occurence of the over flow condition. In addition, the existence of an outlet at the bottom of the dam body caused to mixing the upper layer of the reservoir with the middle layer over time. If this situation continues, the mixing of the large part of the reservoir is not unexpected. There fore, the stratification will disapeare, gradually. In simulations B19, B20 and B2, which have a same value for water temperature of inflow current and reservoir, the effective factor (parameter) that affect the thickness of upper layer and stratification is discharge. As seen in figure 4.96, the thickness of the upper layer with lower value of suspended sediment concentration increases with comparing to the B19 and B20 simulations.

About the initial surface area of the reservoir, as mentioned before, the reservoir has the 19,000 m^2 surface area at time zero. The value for surface of the reservoir increases to 20,000-21,000 m^2 in simulations with discharge equal to 50 m^3/s, approximately. The surface for simulations with discharge value of 100 m^3/s is approximately 22,000-24,000 m^2. For the simulations with discharge of 20 m^3/s, the surface area of fluid decreases. This value for these simulations reduces to 16,000-18,000 m^2. Changes of the surface of fluid and volume of the fluid in all of these 48 simulations are represented in Appendix A.

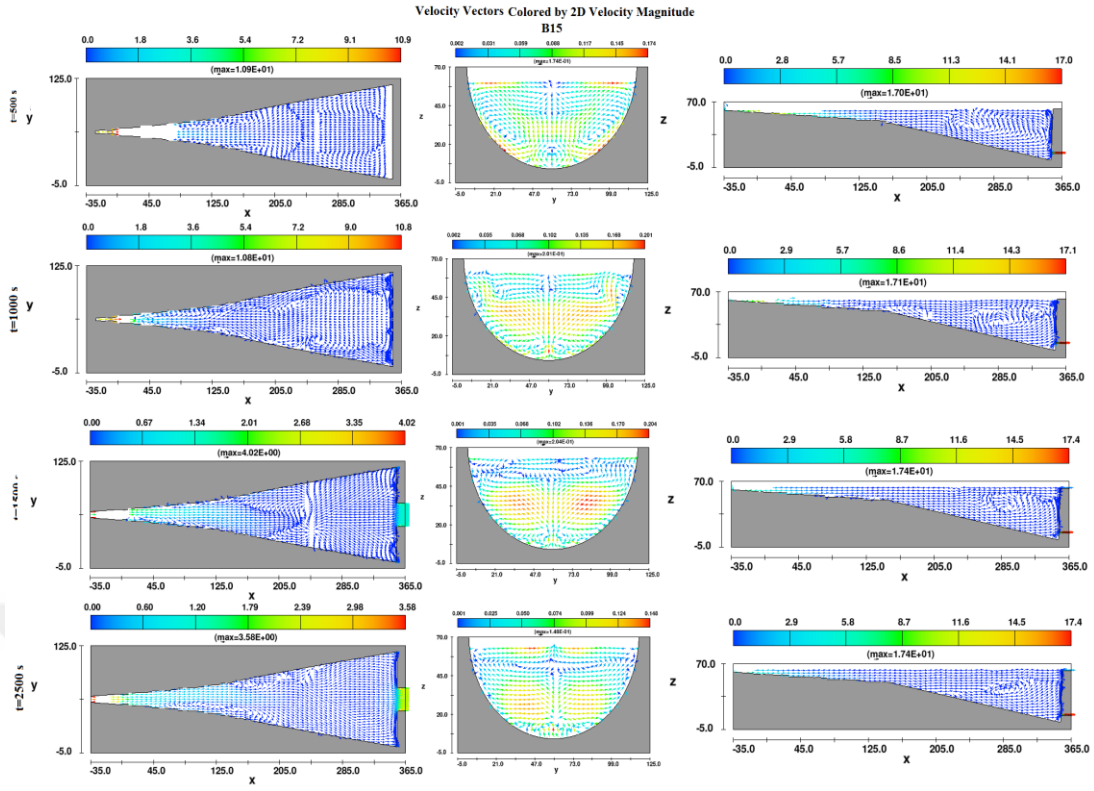

Figure 4.109 : Velocity Vectors Colored by 2D Velocity Magnitude for B15.

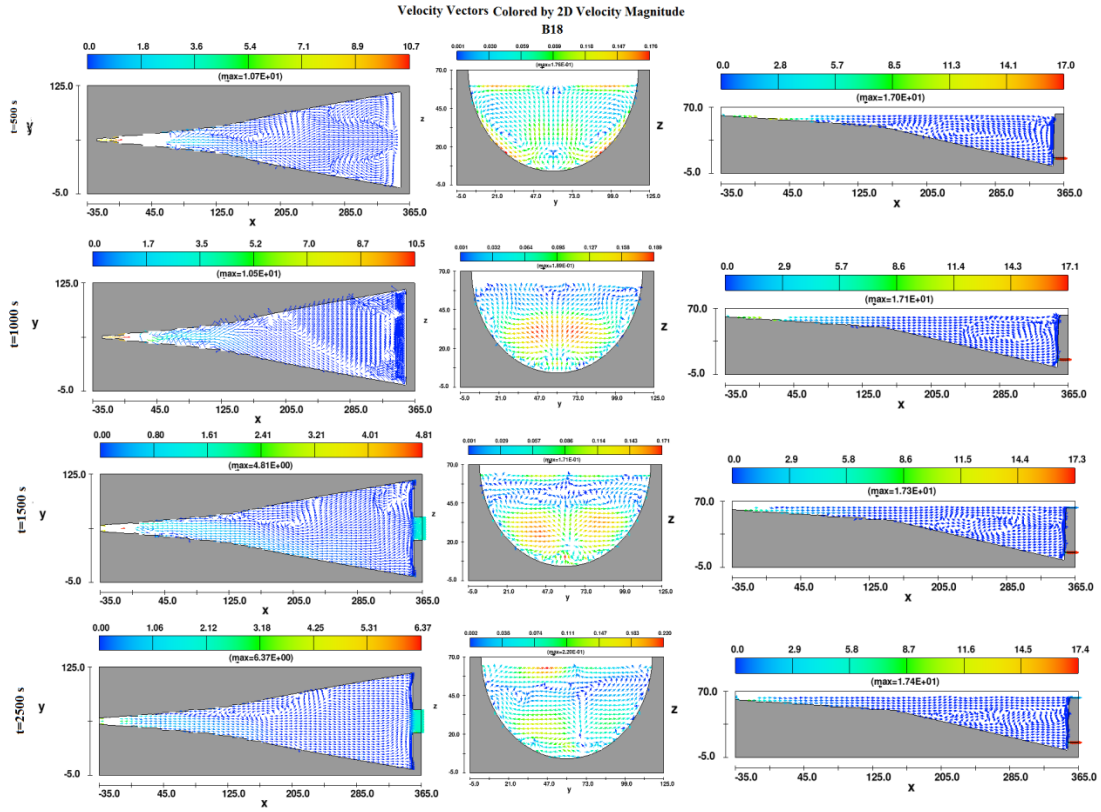

Figure 4.110 : Velocity Vectors Colored by 2D Velocity Magnitude for B18.

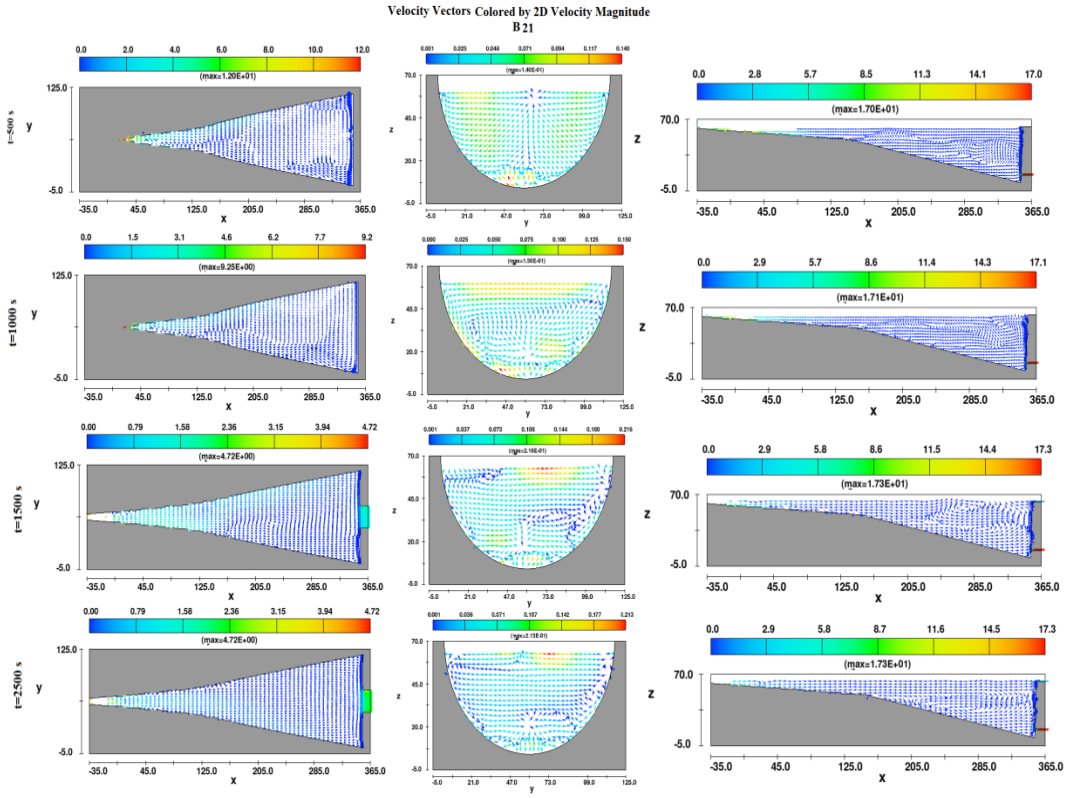

Figure 4.111 : Velocity Vectors Colored by 2D Velocity Magnitude for B21.

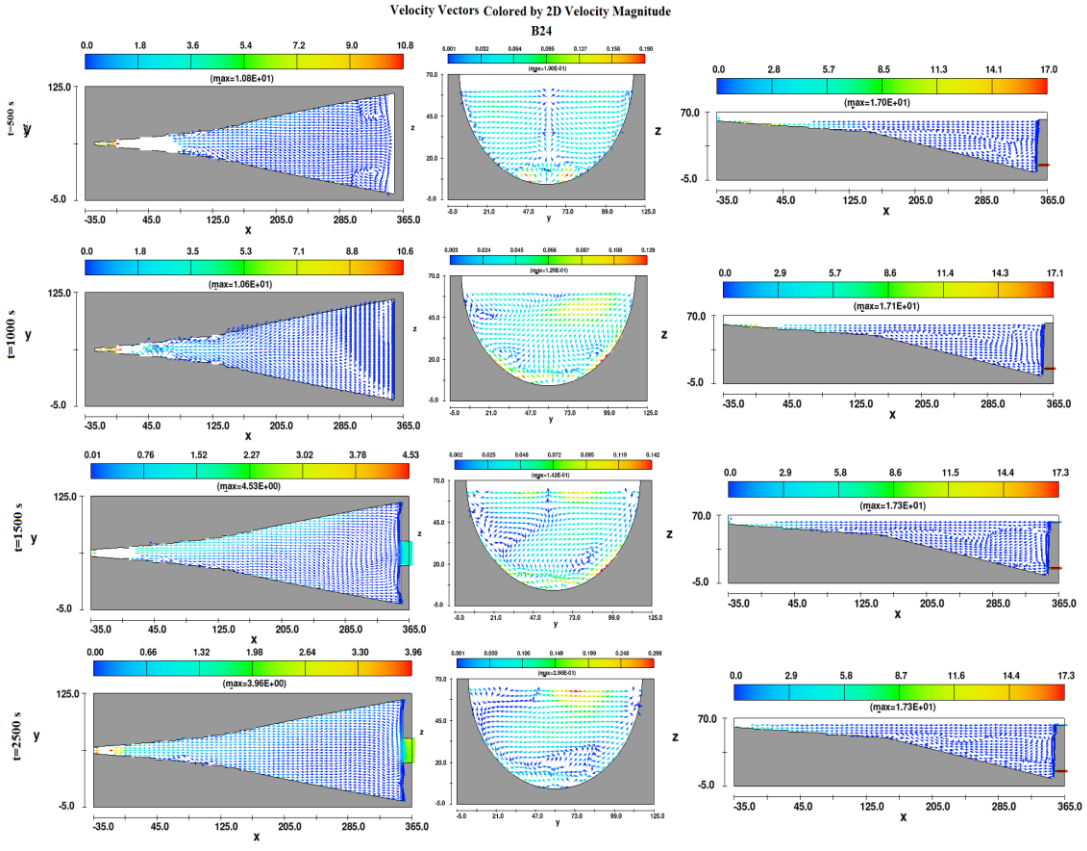

Figure 4.112 : Velocity Vectors Colored by 2D Velocity Magnitude for B24.

Totally, from these 48 simulations, it is concluded that these prepared scenarios of FLOW3D computational code is sensitive for changes in mentioned parameters. Thickness of layers of stratification for suspended sediment concentration are varies during time by changing in these parameters included discharge, water temperature and outlet location and type. Comparing the given result figures, shows this state. The following figures show the changes of thickness of stratified layers for suspended sediment concentration at time 3000 s.

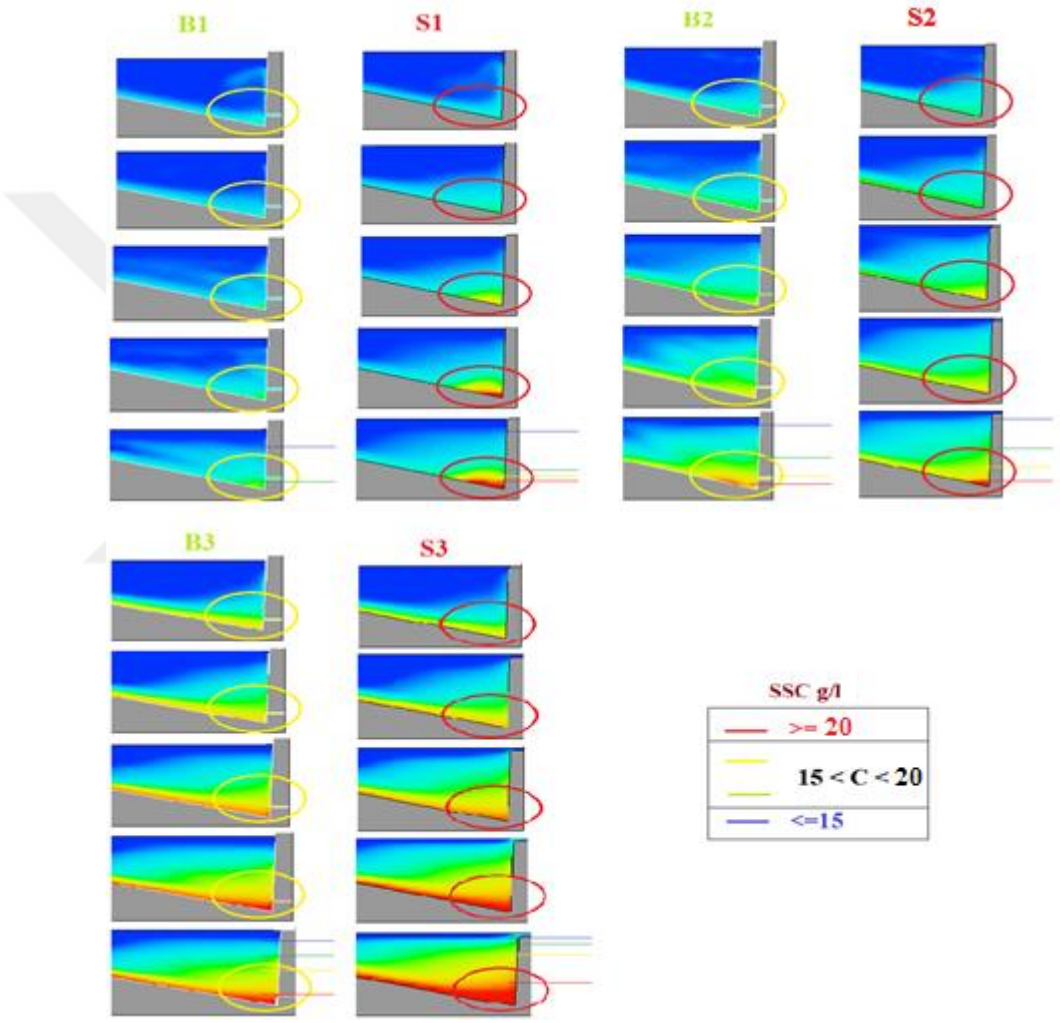

Figure 4.113 : Changes in thickness of stratification layers for suspended sediment concentration (B1 and S1, B2 and S2, B3 and S3).

The differences in thickness of layers are obvious. Near that, the role of the bottom outlet in guidance of the turbidity currentsat bed of the reservoir to downstream is clear in figures. It helps to decreasing the deposition of sediment in reservoir and mainly nearby the dam body and its hydraulic structures. The effects of the turbidity

current on quality of reservoir's water also decreases. Then it is an important point for operating dams.

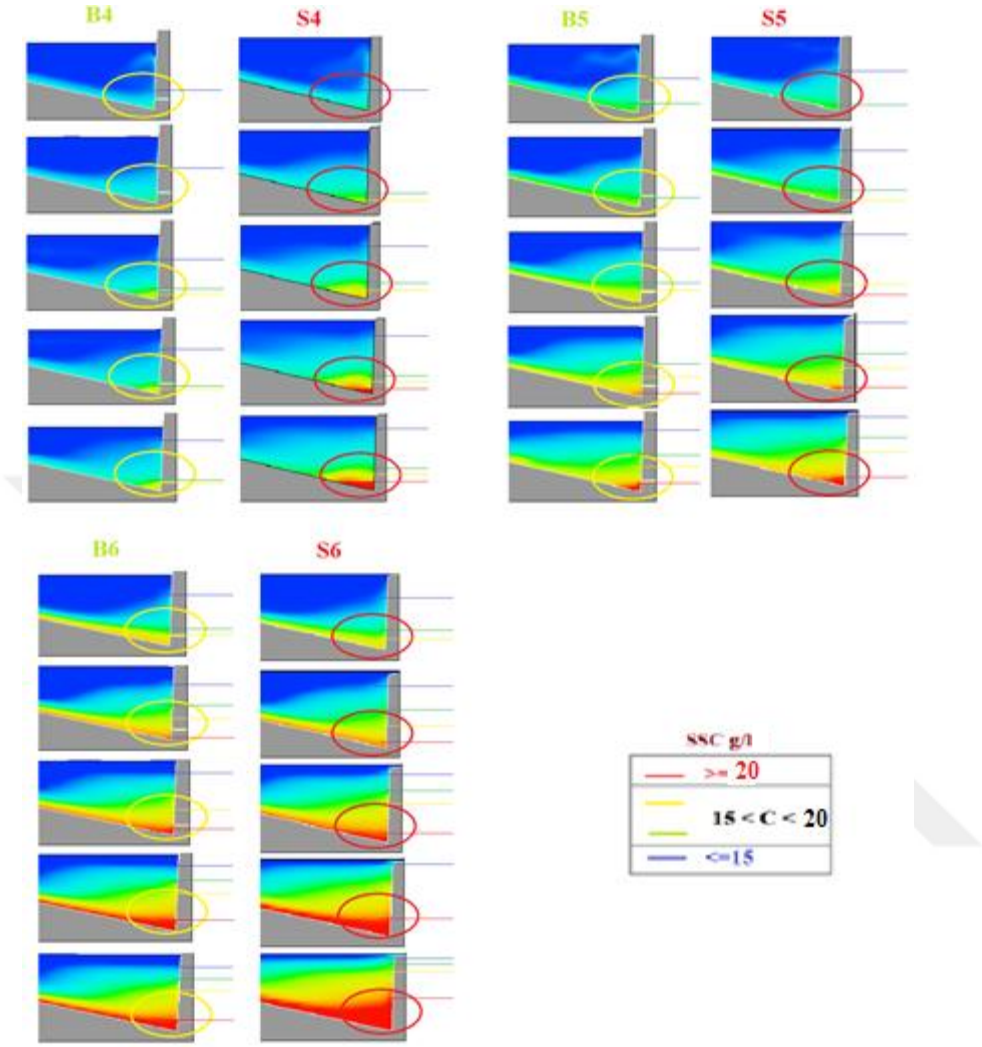

Figure 4.114 : Changes in thickness of stratification layers for suspended sediment concentration (B4 and S4, B5 and S5, B6 and S6).

With comparing the following figures and the thicknesses of the layers, it could be understood that the bottom outlet helps to releasing the turbidity current to the down stream of the dam body and reduces the depositing of the sediments at the bottom of the reservoir near the body. It leads to increasing the dam life.

5. CASE STUDY: Lake Köyceğiz

Turkey is divided to 25 basins, totally. The basin map of Turkey is shown as Figure 5.1.

Figure 5.1: Basin Map of Turkey (State Water Affairs of Turkey).

The selected area as the case study is a part of the western Mediterranean basin (Figure5.2). The western Mediterranean basin has the catchment (area) of approximately 20,953 km^2.

Figure 5.2: Selected Area (Western Mediterranean basin).

Köyceğiz lake was selected as a case study for this thesis, which is located at Köyceğiz sub-basin. Geographic coordinates of Köyceğiz sub-basin is between

36º45' and 37º 15’ North latitude and 28º 22' 30" and 28 º 52’ 30” east longitudes. The total area of the Köyceğiz watershed is equal to 830 square kilometers and the lagoon is 130 square kilometers, approximately.

Figure 5.3: Köyceğiz -Dalyan Sub-Basin.

Elevation map of this region is shown in Figure 5.3 (from Google Map).

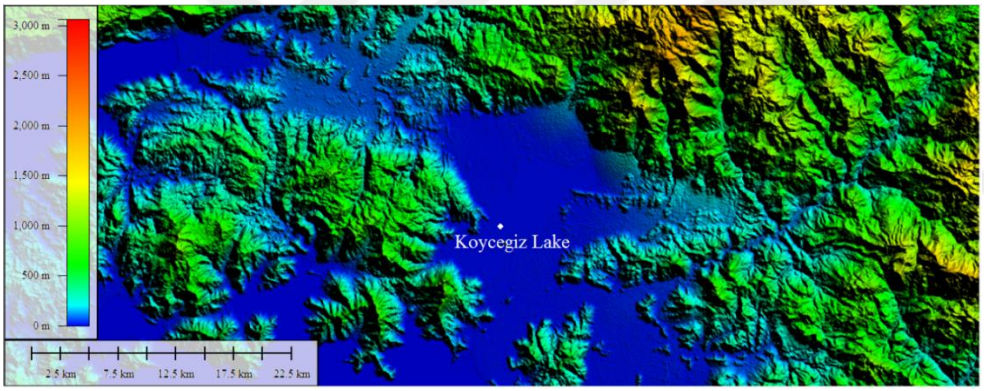

Figure 5.4: Elevation of Köyceğiz Watershed Region (Google map).

In this basin, there are five meteorology stations as Mugla, Marmaris, Fethiye, Dalaman and Köyceğiz stations. Elevations of these stations in meter are +646, +19, +3, +13 and +24, respectively.

In this part of this thesis, Mugla province, Lake Köyceğiz, Namnam river, Yuvarlak river and Kargicak river will be described. The hydrological and meteorological data of these rivers and Köyceğiz lake will explained.

5.1 Mugla Province

Mugla is a province with total area of 13,338 km^2 and an approximate population equal to 817,503. There are some hydrologic information for the years between 1950

to 2014 for the Mugla Province, which were provided from T.C. forestry and water affairs minister, given as Figures 5.5 and 5.6.

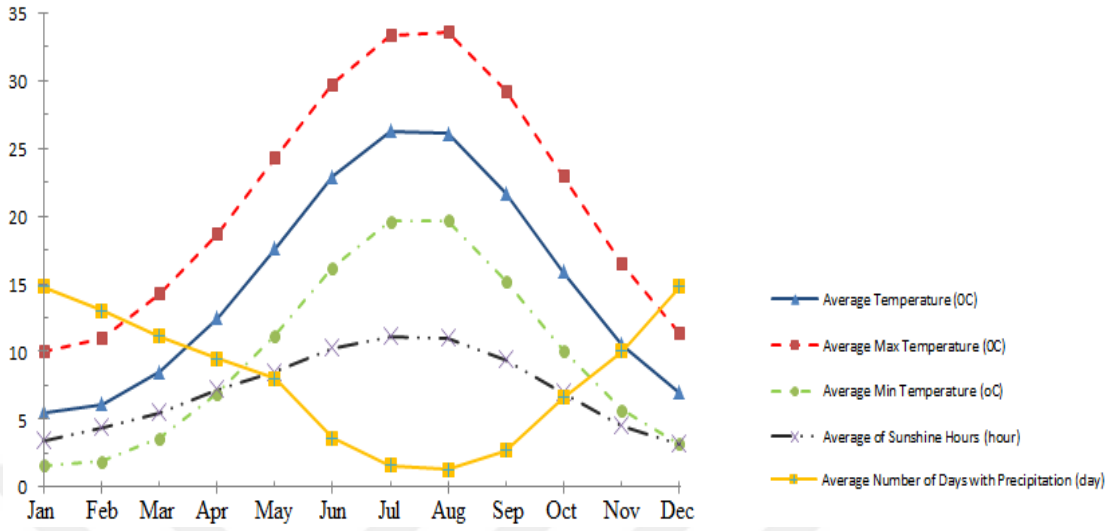

Figure 5.5: Average Values of Temperature, Max temperature, Min Temperature, Sunshine hours and Number of Days with Precipitation (Ministry of Forestry and Water Affairs of Republic of Turkey).

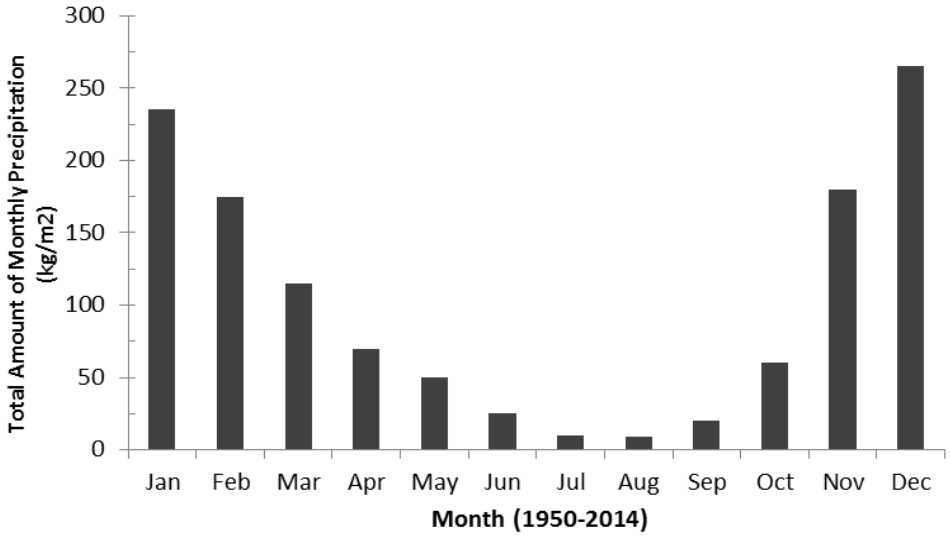

Figure 5.6: Total Amount of Monthly Precipitation for Years 1950 to 2014 (Köyceğiz Basin) (Turkish State Meteorological Service).

In the mentioned time period, as seen in the last figure, the highest value for the long term average monthly total precipitation recorded for December. Whereas the lowest amount of this value is measured for the month August. From the records between

years 1950 to 2014, the recorded total daily maximum precipitation was 168.6 kg/m^2 which occurred in 10th October 2011.

Total yearly precipitation (mm) that measured in the related stations of this province is given as Figure 5.7. The normal annual precipitation which shown with red line has a value equal to 811.3 mm.

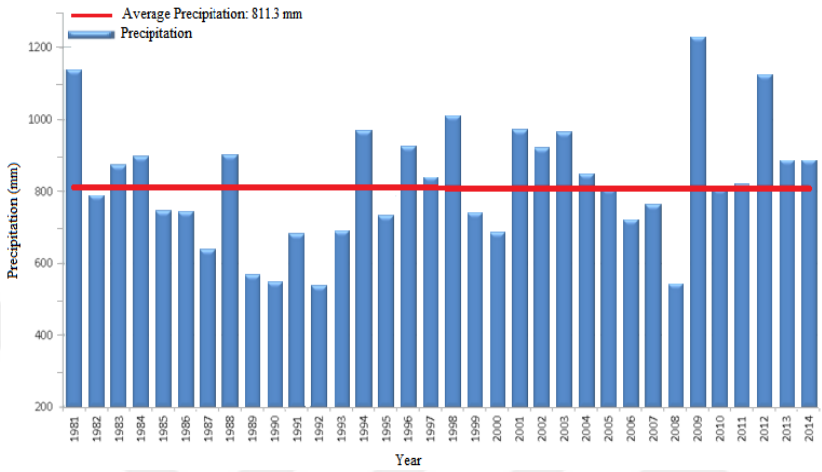

Figure 5.7: The Annual Precipitation in Mugla (mm) (Ministry of Forestry and Water Affairs of Republic of Turkey).

From Figure 5.8 (Turkish State Meteorological Service, 2016), the highest weather temperature that happened in the period between years 1950 to 2014 is equal to 42.1 ^oC, which was occurred in 27th July in 2007. Whereas the lowest value of temperature that recorded in this period is equal to -11 ^oC, 13th January in the year 1954.

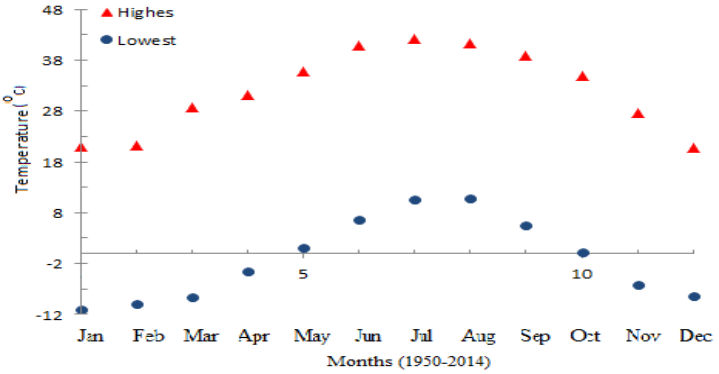

Figure 5.8: Highest and the Lowest Values of Temperature for the Months of the Years Beetween 1950 and 2014 in Mugla province (Turkish State Meteorological Service, 2016).

5.2 Lake Köyceğiz

Köyceğiz lake is located in the province of Muğla in the southwest of Turkey near the Mediterranean sea coast. This region is known as western Mediterranean basin.

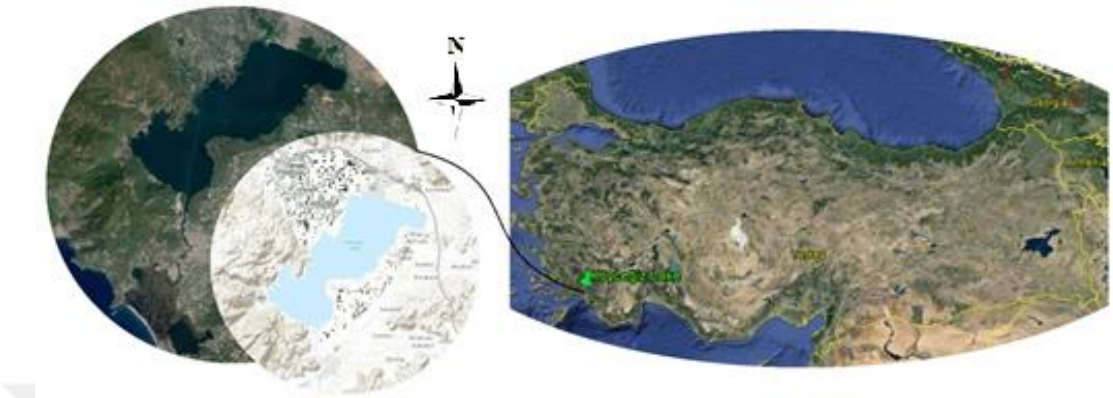

Figure 5.9: Location of the Köyceğiz Lake (Google Earth).

The lake has about 63 square kilometers area. An approximate lake length is about 12 kilometers and the lake width is approximately 6 kilometers. The Köyceğiz lake and its around area have characteristics of Mediterranean climate. In summers weather is hot and dry and in winters is often a little warm and rainy. It means that, this region usually experiences abundant precipitation in cold winters and is drought occurs in hot summers.

Lake Köyceğiz is consists of two parts. First is named as the Sultaniye part at the South of the lake, and the other one is Köyceğiz part that is located at the North part of the lake and connected by a shallow 8m deep strait. At the end point of the south of the lake, there is a naturally formed canal that connects this lake to the Mediterranean sea. This canal has 14 kilometers long and about 1.53 meters depth. This canal is known as Dalyan canal and helps to discharges the excess water, which is arising from the episodic winter rainfalls, surface waters and other streams into the lake, into the Mediterranean sea.

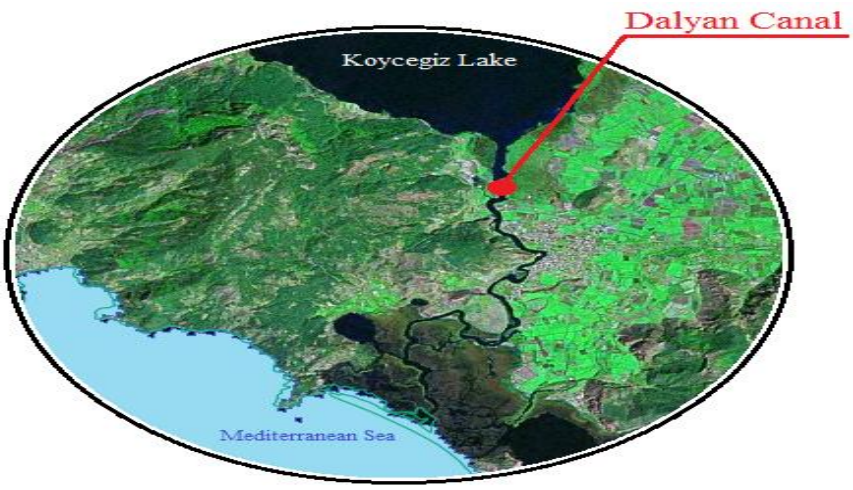

Figure 5.10: Position of Dalyan Canal (Google Earth).

Before explanation of the hydrological and meteorological information of this lake and major rivers flow into that, it is necessary to representing some statistical information of Köyceğiz sub-basin.

For Köyceğiz sub-basin, the monthly stream flows (runoff) are represented in Table 5.1. (Gunenc et al., 2002)

Table 5.1 : Monthly Stream flows for Köyceğiz Sub-basin (Mm^3/month) (Gunenc et al., 2002).

Months	Yuvarlak	Kargicak & Yangi	NamNam	Sarigoz	Hamitkoy	Cakmak	Degirmendere	Camliduzu	Other
Jan	12.10	8.40	64.41	4.68	1.14	1.43	1.15	1.86	8.88
Feb	8.86	6.15	47.17	3.43	0.83	1.05	0.84	1.36	6.51
Mar	6.10	4.24	32.48	2.36	0.57	0.72	0.58	0.94	4.48
Apr	3.30	2.29	17.57	1.28	0.31	0.39	0.31	0.51	2.42
May	1.94	1.35	10.32	0.75	0.18	0.23	0.18	0.30	1.42
Jun	1.04	0.72	5.55	0.40	0.10	0.12	0.10	0.16	0.77
Jul	0.44	0.31	2.36	0.17	0.04	0.05	0.04	0.07	0.33
Aug	0.75	0.52	4.00	0.29	0.07	0.09	0.07	0.12	0.55
Sep	1.17	0.81	6.24	0.45	0.11	0.14	0.11	0.18	0.86
Oct	4.70	3.27	25.03	1.82	0.44	0.56	0.45	0.72	3.45
Nov	8.82	6.12	46.93	3.41	0.83	1.04	0.84	1.35	6.47
Dec	14.07	9.78	74.93	5.45	1.32	1.67	1.34	2.16	10.33
Total	63.29	43.97	336.98	24.49	5.95	7.49	6.02	9.73	46.48

Table 5.1 shows that the Namnam river is an important river with the highest total value of monthly runoff. After Namnam river, the Yuvarlak river has the main water volume that flows into the lake Köyceğiz. The highest values of flows are mostly happened in the last months of the fall season and the initial months of winter, in

December and January, respectively. The following figure (5.11) represents the graphical form of last table with respect to the importance of the streams using their monthly discharges.

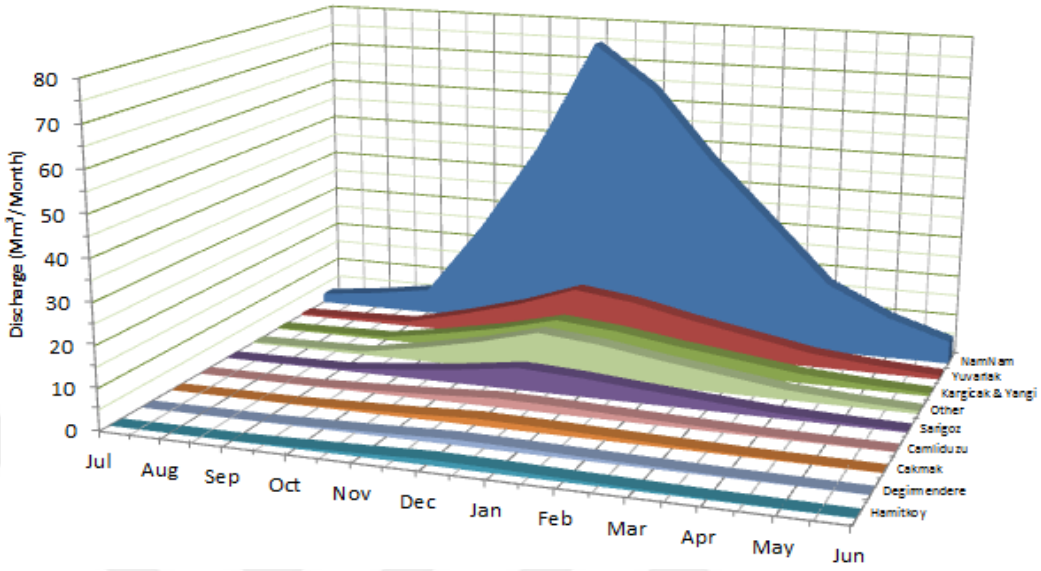

Figure 5.11: Monthly Stream flows for Köyceğiz Sub-basin (Mm^3/month).

The approximate total yearly stream flows of the Köyceğiz sub-basin are obtained by summing the monthly values of streams for this sub-basin with respect to their values, which were given in Table 5.1.

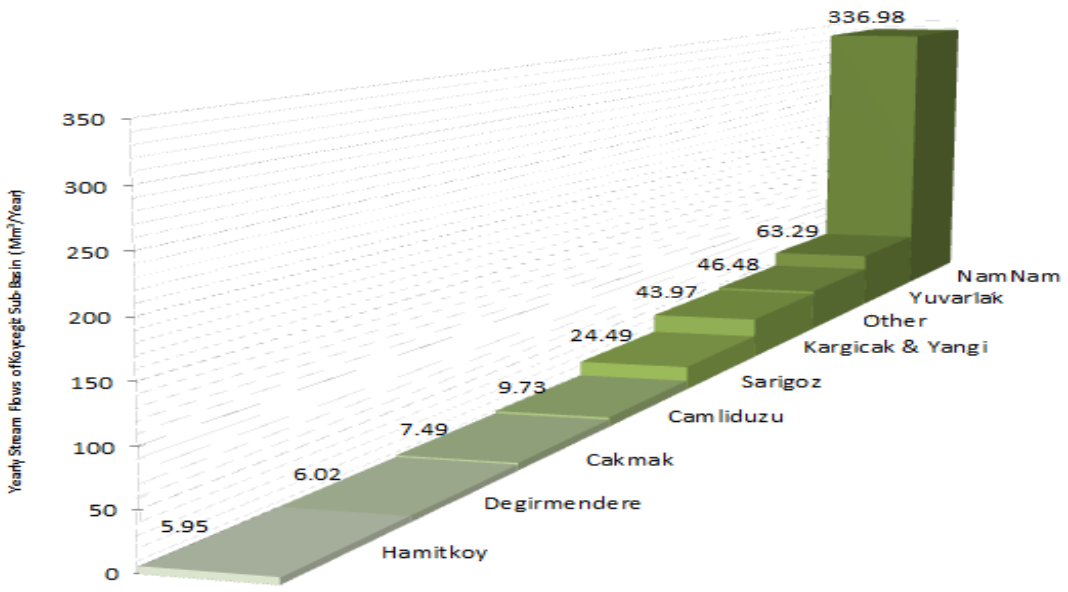

Figure 5.12: Total Yearly Stream Flows of the Köyceğiz Sub-basin

The following figure shows the importance of Namnam River in Köyceğiz watershed and Köyceğiz lake, clearly. With using these data the following figure can obtained, which represents the percentage of distribution of average monthly stream flows (runoffs) in the Köyceğiz watershed.

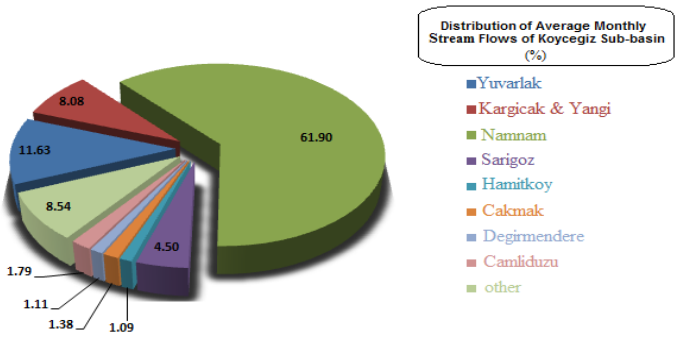

Figure 5.13: Percentage of Distribution of Average Monthly Stream Flows in Köyceğiz Watershed.

Figure (5.13), Namnam, Yuvarlak and Kargicak & Yangi rivers with percentage of average monthly stream flows values of 61.90, 11.63 and 8.08 are the important and major rivers of this watershed, respectively. More detailed explanation will be given in the relevant section about these rivers. Here, hydrological, meteorological, topographic and bathymetric maps and other information about Köyceğiz lake will be explained. The Köyceğiz meteorological station with 17924 station ID is the closest station to the study site. The recorded meteorological data were obtained from this station. A briefly information about the weather temperature is given in the figure (5.14) (Turkish State Meteorological Service, 2016; Sasmaz, 2005).

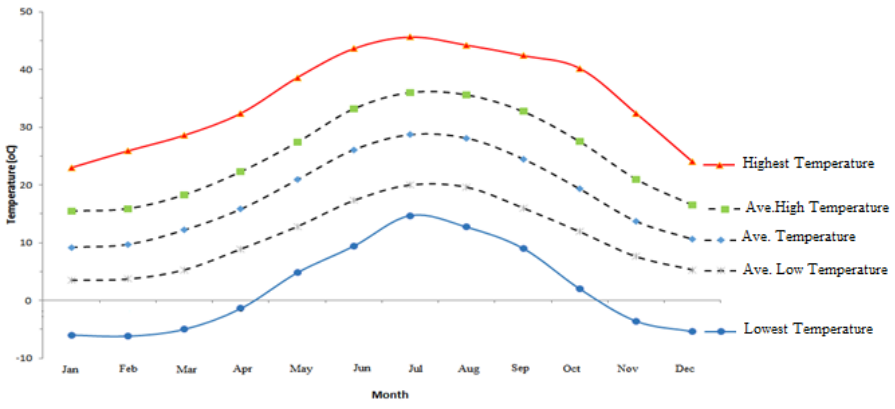

Figure 5.14: Weather Temperature of Köyceğiz Meteorological Station (Turkish State Meteorological Service, 2016; Sasmaz, 2005).

Recorded values show that the precipitation of Köyceğiz region in winter and also in the last month of the fall season has 56 percent of the total annual precipitation. These precipitation is in the rain form mostly and rarely in the snow form. In contrast to the winter, in summer months precipitation has the lower percentage proportion of the total annual precipitation. This is approximately 1.9% of total annual precipitation. The number of days in a month that have snowfall in Köyceğiz region is presents in the figure. As Seen in Figure 5.15, the average numbers of days with precipitation are given.

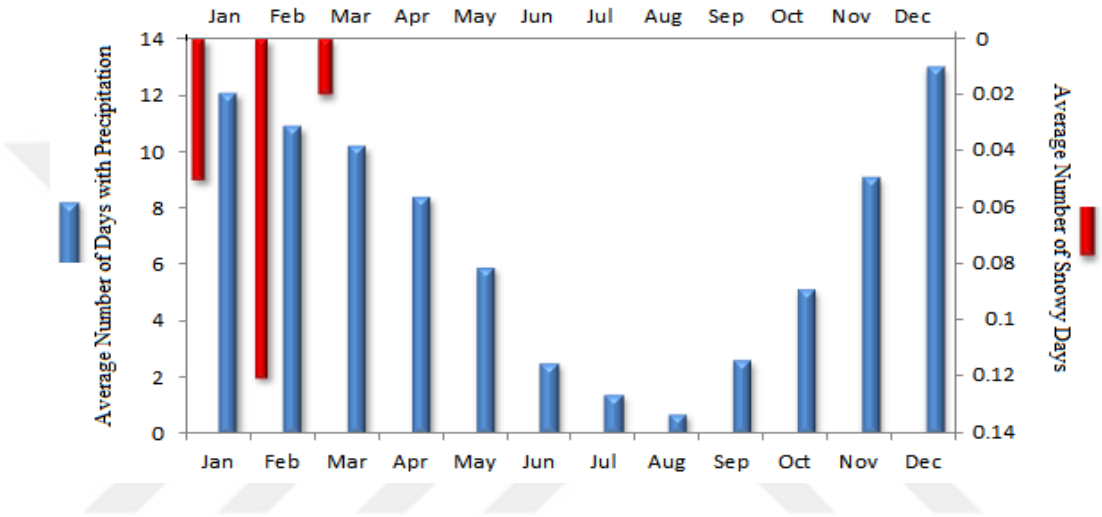

Figure 5.15: The Average Number of Days With Precipitation and Snow.

Figure (5.16) represents the monthly and the annual average precipitations, which were measured in the Köyceğiz station nearby the north boundary of the Köyceğiz lake. These measurments are ralated to the years between 1975 to 2013.

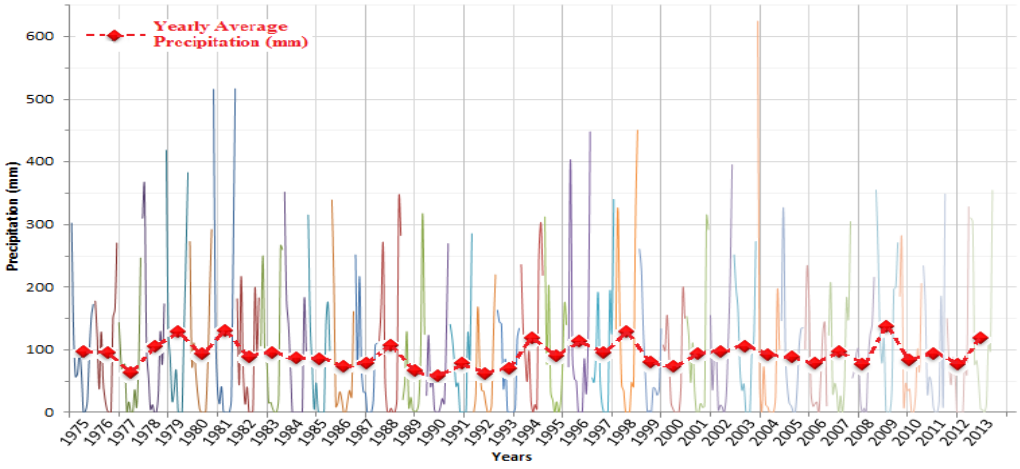

Figure 5.16: The Monthly and the Annual Average Precipitations.

The annualy total precipitation is depicted as following figure using measurments from Köyceğiz station. (Figure 5.17)

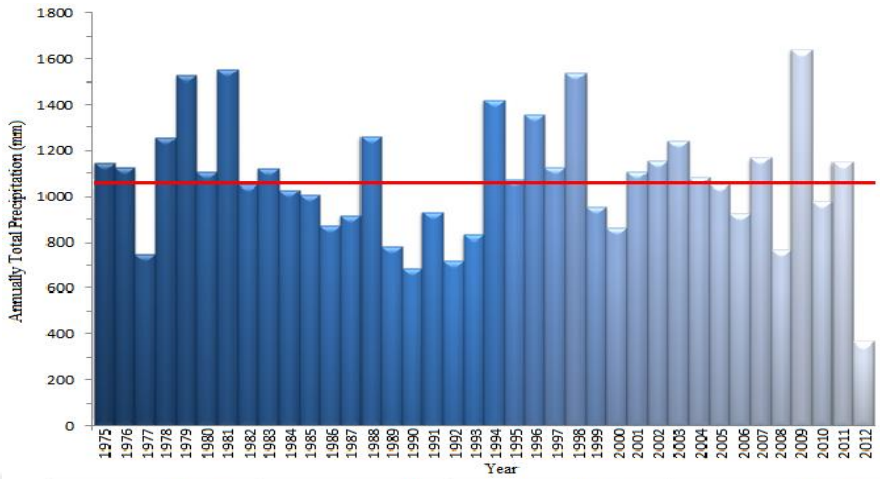

Year	Annually Precipitation (mm)	Year	Annually Precipitation (mm)	Year	Annually Precipitation (mm)	Year	Annually Precipitation (mm)
1975	1145	**1985**	1007.4	**1995**	1069.5	**2005**	1050
1976	1125.2	**1986**	868.7	**1996**	1356.8	**2006**	922.5
1977	746.3	**1987**	916.9	**1997**	1123.7	**2007**	1168.2
1978	1259.6	**1988**	1264	**1998**	1534.3	**2008**	770.3
1979	1526.3	**1989**	783.3	**1999**	954.3	**2009**	1640.6
1980	1104.3	**1990**	685.4	**2000**	862.3	**2010**	980.1
1981	1550.7	**1991**	931.4	**2001**	1107.1	**2011**	1147.4
1982	1052.5	**1992**	720.2	**2002**	1155	**2012**	365
1983	1119.6	**1993**	832.7	**2003**	1244		
1984	1027	**1994**	1421.2	**2004**	1083.2		

Figure 5.17: Annual Total Precipitation.

The long term monthly precipitation averages (mm) were obtained from the mentiond measurments on the Köyceğiz Meteorological station using values of monthly precipitation of 1975 to 2013 years.

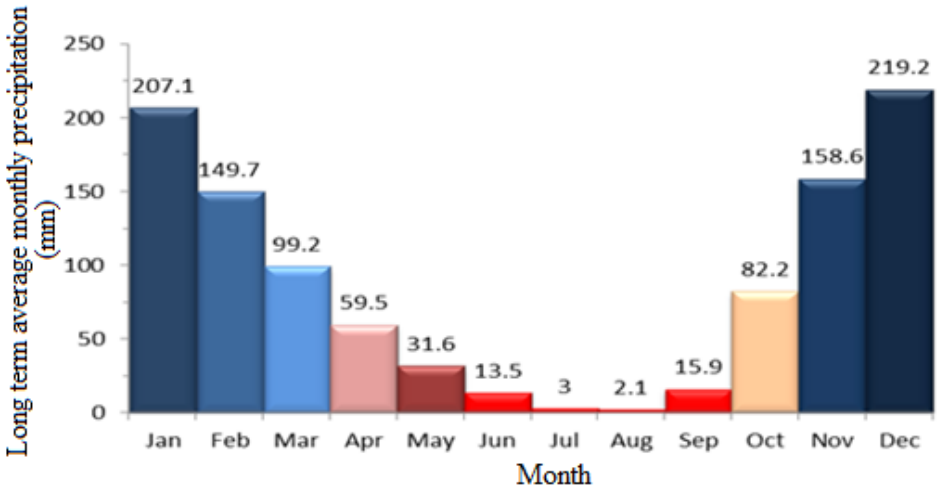

Figure 5.18: Long Term Average Monthly Precipitation (mm) of Köyceğiz Meteorological Station (1975- 2013).

The Ministry of Forestry and Water Affairs of Republic of Turkey gives the following data for Köyceğiz for seasonally and monthly approximate long term precipitation (mm). The annually precipitation is equal to 1000-1250 mm.

Table 5.2 : Seasonally and Monthly Long-Term Precipitation for Köyceğiz.

Season	Spring		Summer		Fall		Winter	
Precipitation (mm)	150-200		0-50		200-300		500-700	
	Month	P (mm)	Month	P (mm)	Month	P (mm)	Month	P (mm)
	Apr	50-75	*		*		*	
	May	25-50	*		*		*	
	Jun	0-25	*		*		*	
	*		July	0-25	*		*	
	*		Aug	0-25	*		*	
	*		Sep	0-25	*		*	
	*		*		Oct	75-125	*	
	*		*		Nov	150-200	*	
	*		*		Dec	200-250	*	
	*		*		*		Jan	175-250
	*		*		*		Feb	125-175
	*		*		*		Mar	100-125

The meteorological recorded data were available in the time period of 1975 to 2013, at Köyceğiz meteorological station, which is located at the north west of the lake.

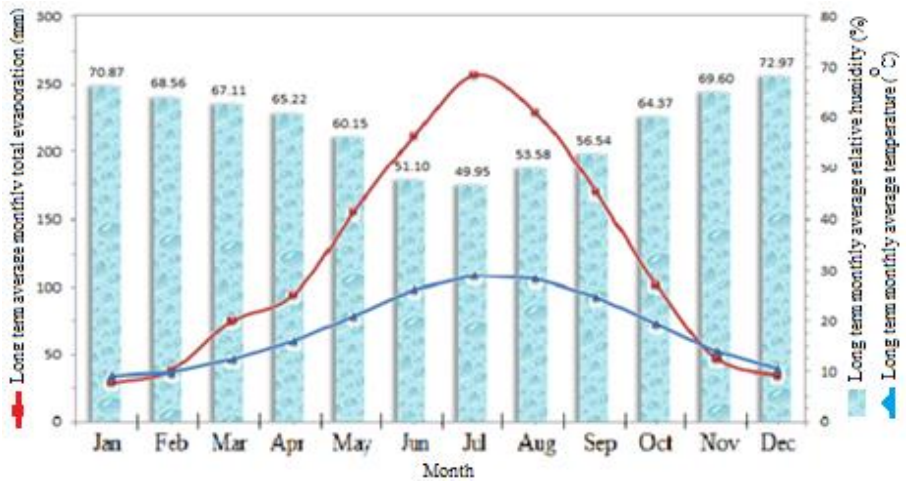

Figure 5.19: Long Term Amount of Average Monthly Total Evaporation (mm), Average Temperature (^{o}C) and Average Relative Humidity (%).

The last figure (fig. 5.19) shows the long term amount of monthly total evaporation (mm), average temperature (^{o}C) and average relative humidity (%). From the figure it is seen that the maximum value for the long term monthly average temperature was approximately 31 ^{o}C, which was occurred in July. The long term average monthly total evaporation has also the highest value in this month. Totally, the forestry and water works ministry of Turkey offers the long term monthly evaporation in Köyceğiz area, for the period of 1981-2010. This measurments were available for months between May and October for these period of years. Table 5.3 shows these values of evaporation.

Table 5.3 : Long-Term Evaporation for Köyceğiz (1981-2010) (Ministry of Forestry and Water Affairs of Republic of Turkey).

May	June	July	August	September	October
126-150	201-240	241-280	241-280	176-200	101-125
Annual Evaporation:	1001-1250 mm				

About the reference total evapotranspiration (ETo), the forestry and water works ministry of Turkey offers ETo maps (1981-2010). These maps show that the value for this parameter in Lake Köyceğiz region is higher than most of the regions of Turkey. These maps show that the reference total evapotranspiration in Köyceğiz area has a highest value in July in comparison of the other months. In this month the ETo's value is equal to 180-190 millimeters per month (mm/month). This parameter for Jun and August is 151-170 and 141-160 mm/month, respectively. This values show that the evatranspiration is very high in summer. Unlike summer, in fall and winter this region experienced a low evatranspiration. For example, in December and January, the measured ETo values are equal to 26-30 and 26-34 mm/month, respectively. The evatranspiration has its minimum value in these months of the year. The annual total evapotraspiration for this region is about 1001-1198 millimeters (mm/year). Figure 5.20 represented this state, which was prepared by the Ministry of Forestry and Water Affairs of Republic of Turkey and meteorological administration.

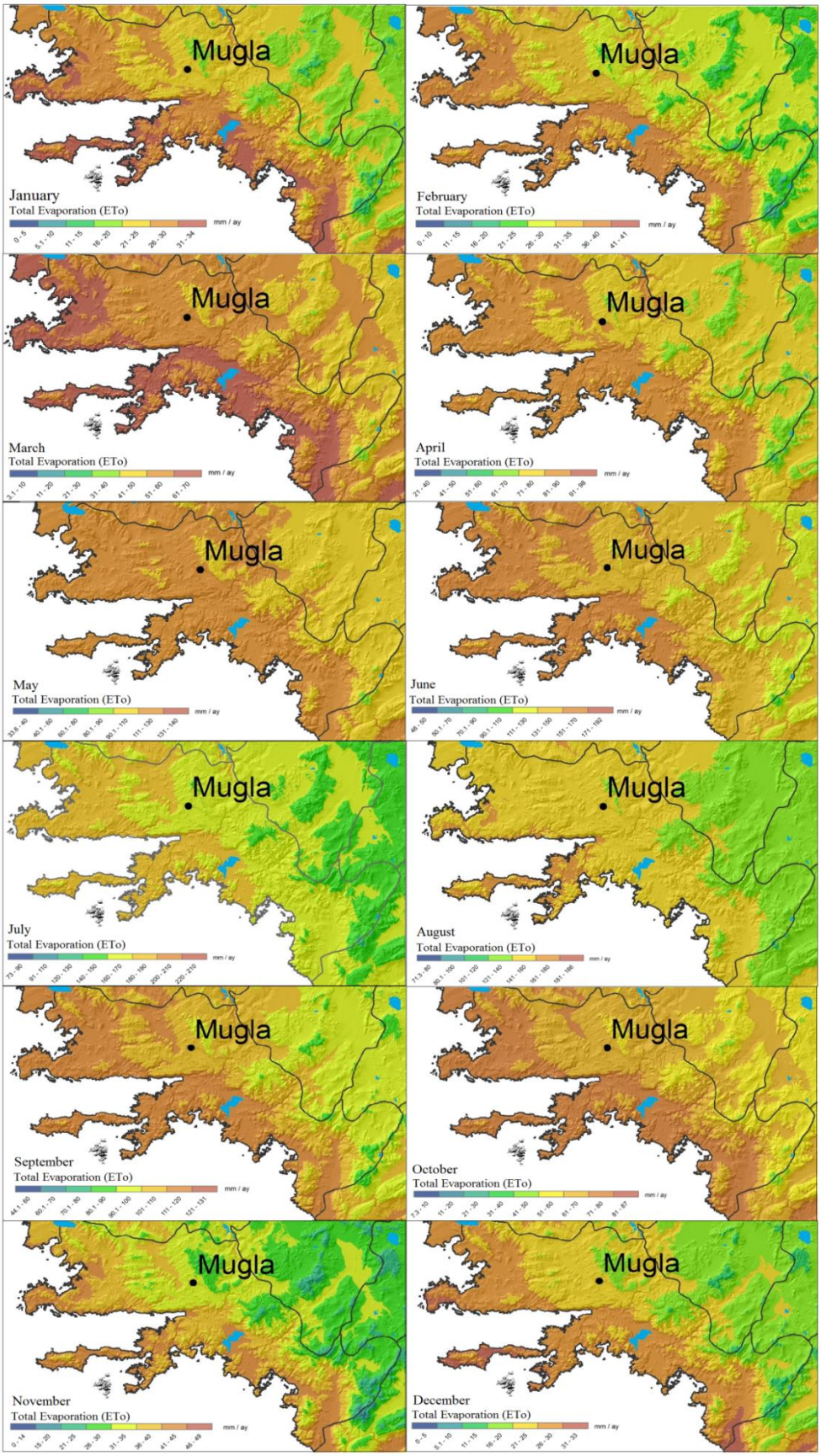

Figure 5.20: Monthly ETo Maps for Köyceğiz Area (Ministry of Forestry and Water Affairs of Republic of Turkey, Meteorological Administration).

Monthly average wind velocities (m/s) related to study site for 1975-2013 are displayed in the Figure 5.21.

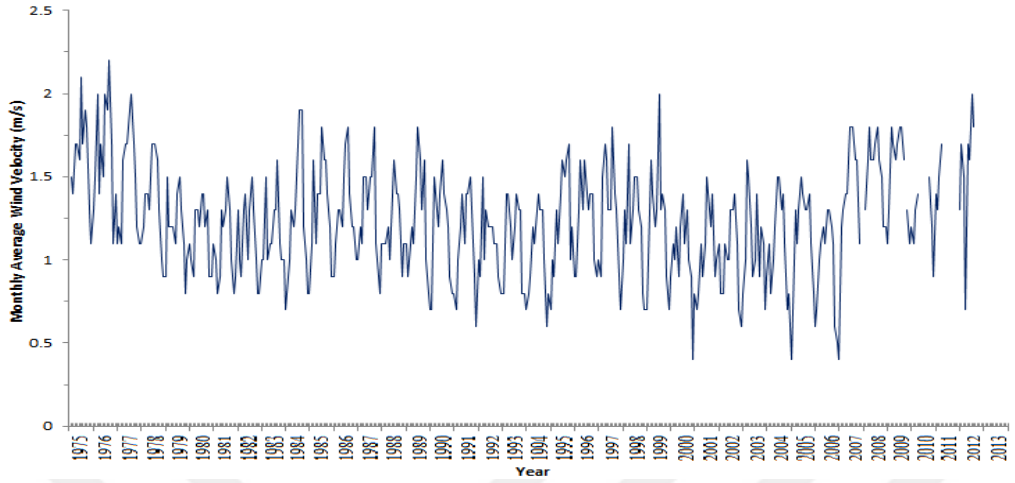

Figure 5.21: Monthly Average Wind Velocities.

The given Figure (5.21) shows that the average wind velocity (m/s) for a month does not exceed the value 2.5 m/s. These winds are blowing from different directions. The monthly number of winds, that were occurred from different directions, are shown as radar chart in Figure 5.22.

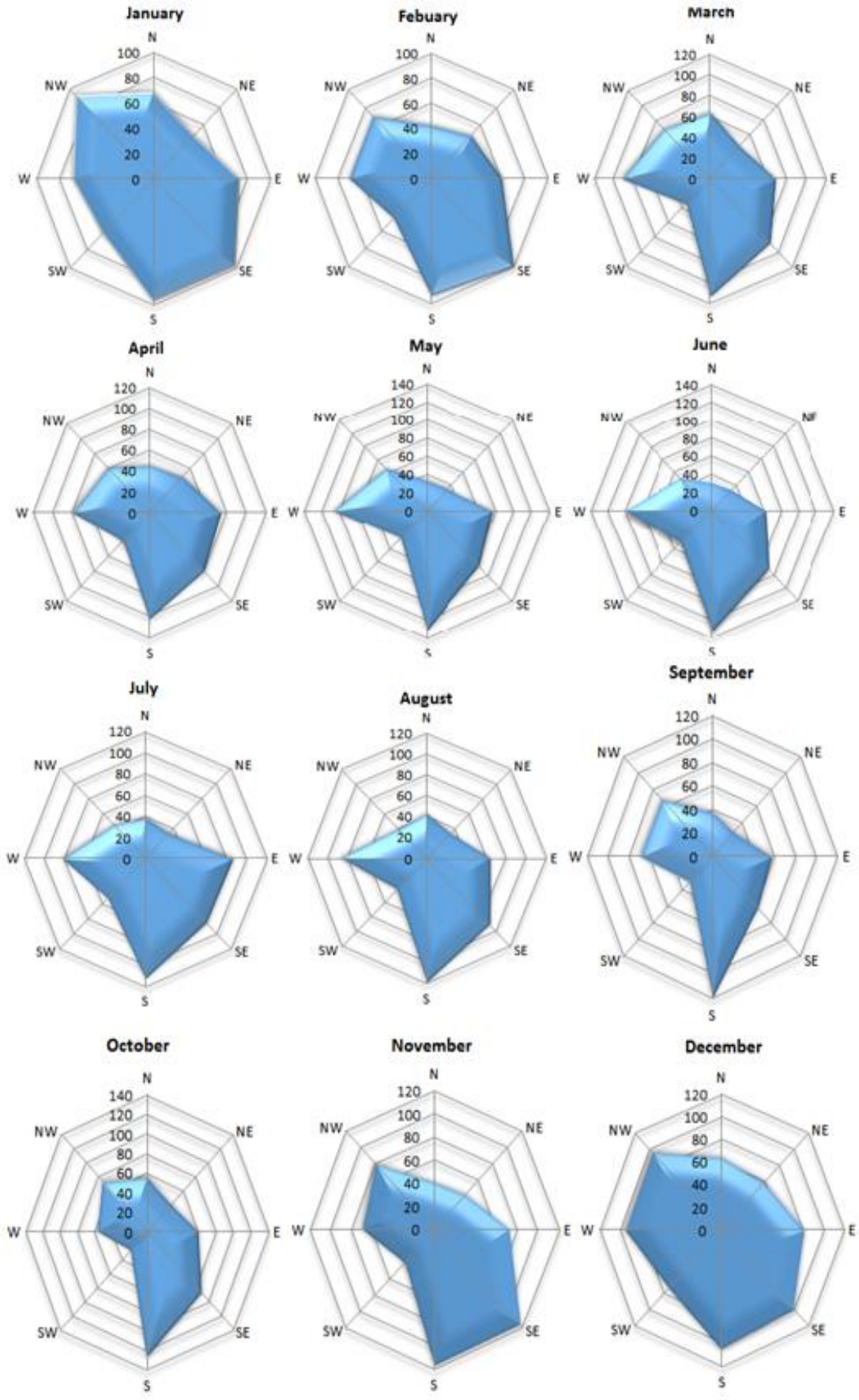

Figure 5.22: Monthly Number of Winds from Different Directions.

From Figure 5.22, it is appear that the region is under the influence of the south winds in all months of the year, approximately. Figure 5.23 shows an approximate number and directions of the winds in a year (Sasmaz, 2005).

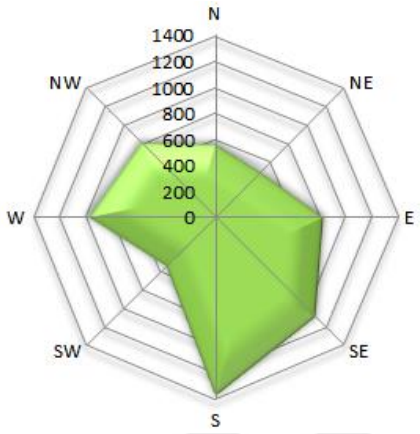

Figure 5.23: An Approximate Number and Directions of the Winds in a Year (Sasmaz, 2005).

In the last presented figure, it is clear that the winds predominantly blow from the south of the region and from the Mediterranean sea in a year. It is possible to presenting the number and direction of winds, seasonally.

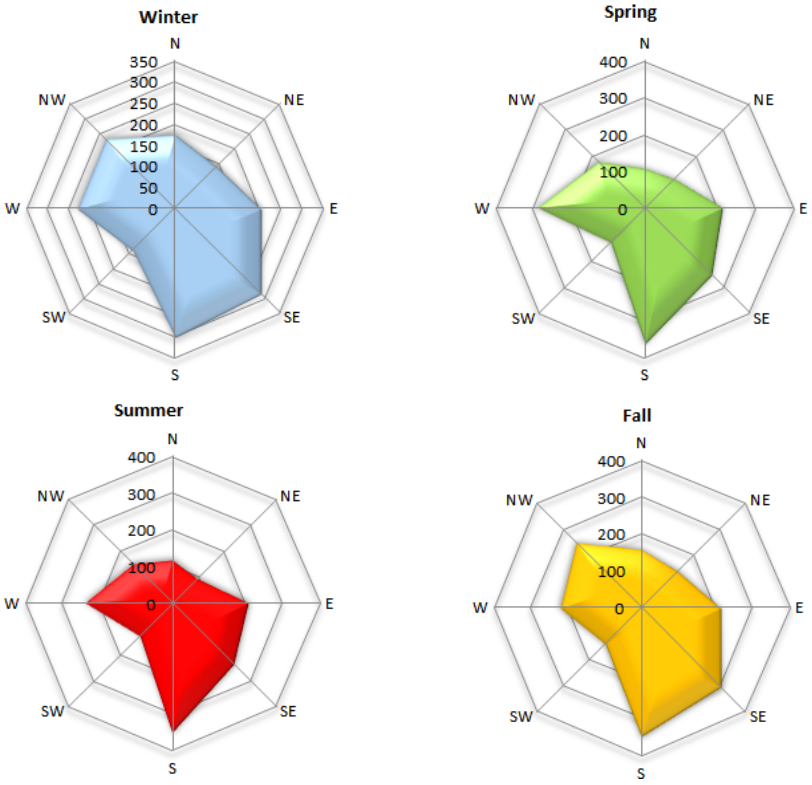

Figure 5.24: The Number and Direction of Winds by Season.

The Majority number of the winds is occurred from the south in all of the seasons. While the small number of winds blow from the north (N) and north-east (NE) directions in all seasons, approximately.

The average monthly velocity of wind (m/s) is obtained for study site using available recorded data from Köyceğiz meteorological station. (Figure 5.25)

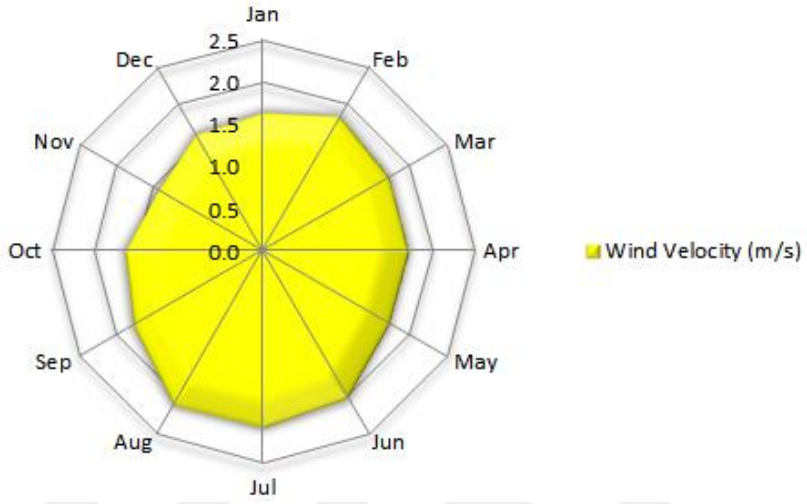

Figure 5.25: Average Monthly Velocity of Wind (m/s)

Available data show that the maximum and minimum average wind velocities have the values of 3.8 m/s and 1.1 m/s, respectively.

Heretofore and in the last pages, some maps about the Köyceğiz lake and situation of that were shown. A schematic map for the study area is given in the following figure. It is prepared for the better understanding of how the system works. In Figure 5.26, the situation and position of the inputs (rivers) and the output (Dalyan channel) are represented.

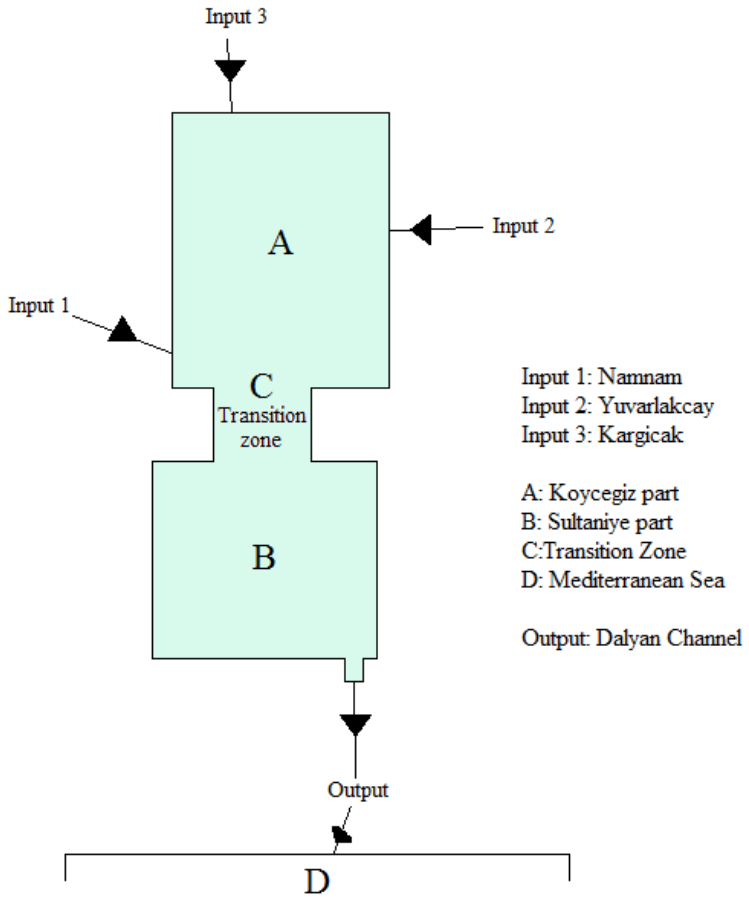

Figure 5.26: A schematic map for the study area (Lake Köyceğiz).

This lake consists of two bowl-shape parts. These parts have different depths and connected to each other with a shallower strait which located between them and has a maximum depth of approximately 8 meters. The north part is known as Köyceğiz part and the south one is named as Sultaniye. These naming are because of the existence of cities with the same name close to each part. The Sultaniye part of the Lake Köyceğiz is deeper than the Köyceğiz part. The maximum depth of Sultaniye part in the south of the lake is 32 to 34 meters, approximately. While the deepest part of the north area of Lake Köyceğiz is equal to 25 meters. The schematic longitudinal section view of the lake is shown in Figure 5.27.

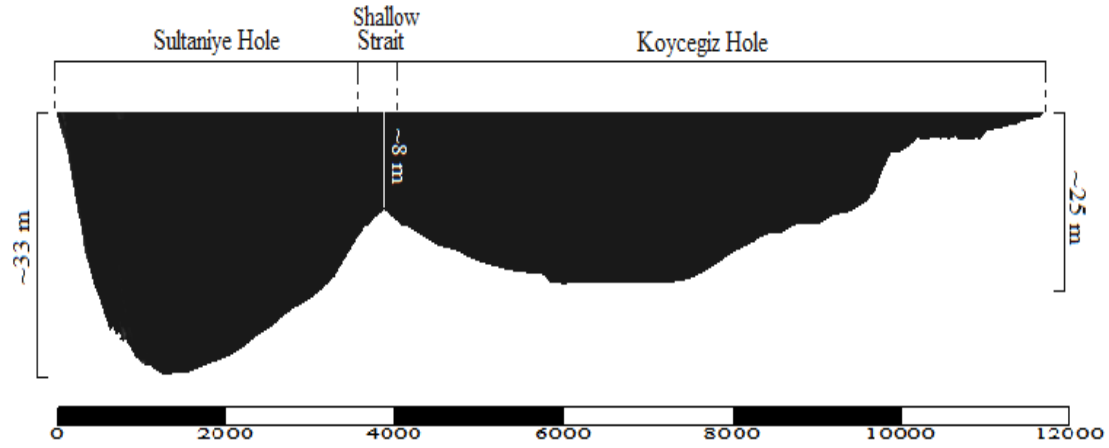

Figure 5.27: The Schematic Longitudinal Section View of the Lake Köyceğiz.

Cross-sections of Köyceğiz and Sultaniye holes of the lake are presented in Figure 5.28. These views of Lake Köyceğiz are from the north of the Köyceğiz part and from the south of the Sultaniye Part of this lake.

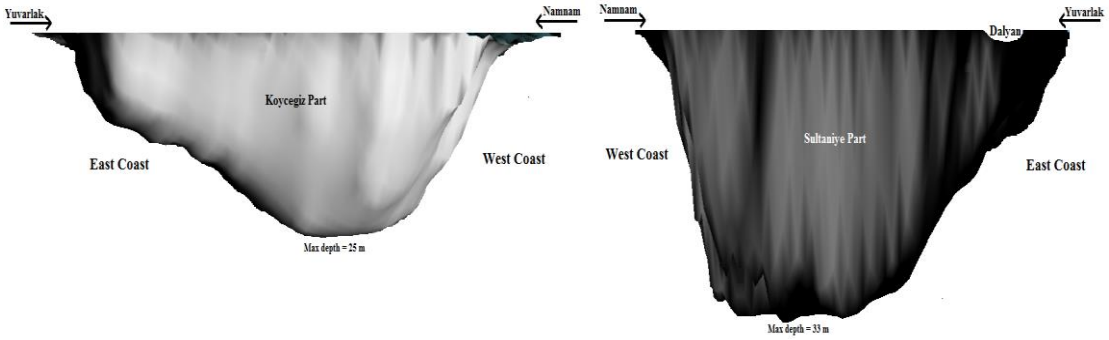

Figure 5.28: Cross-sections of Köyceğiz and Sultaniye Parts of the Lake.

The geometry of Lake Lake Köyceğiz was very important for simulations of this thesis, which was caused to achieving the best results. So, the bathymetric map, which was prepared as a project by Derya Maktav and his colleagues from the remote sensing division of Istanbul technical university, was scanned. First of all, a bathymetric map was drawn using Autocad 2015. Then the elevation of each layer was given to the AutoCAD bathymetric map. According to the bathymetric map, the elevations were set as 2 m by 2 m layers. From the following figure, which is the bathymetric map showing depth contours of Lake Köyceğiz, each of the red contours represents the 10m elevations and each of the green ones have an elevation of 2 m.

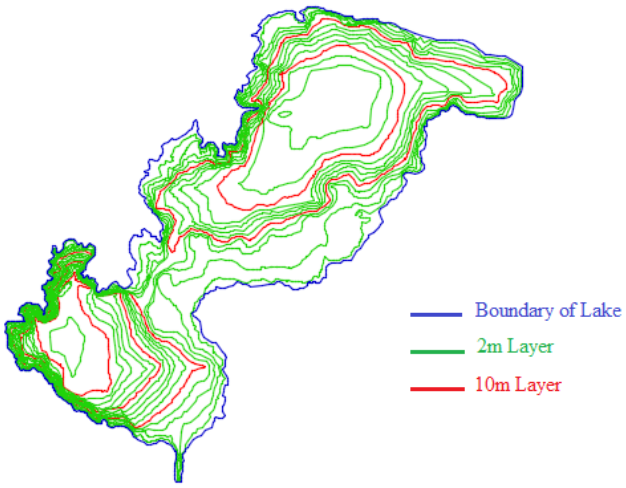

Figure 5.29: The Bathymetric Map of Lake Köyceğiz.

Then, the Surfer program was used to change the AutoCAD map to a three dimensional surface map and prepare the map for the reason of converting to the stereo lithography format (.stl) in SketchUp 2015 program, which was needed to Flow3D CFD code. Before using Surfer program, some points were drawn on the layers of bathymetric map in the AutoCAD program to export a text format data, which was needed to the Surfer (Figure 5.30).

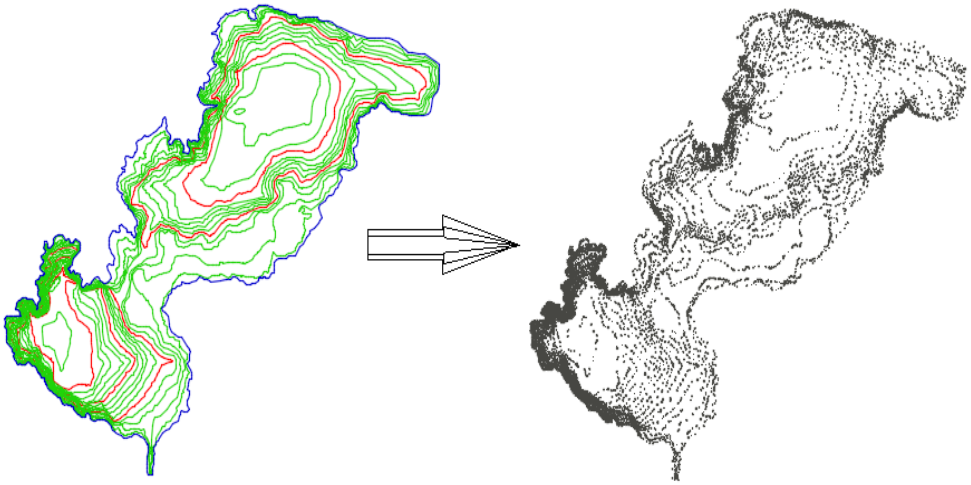

Figure 5.30: The Drawn Point Map of Lake Köyceğiz.

After this step, the prepared text grid data were applied to the Surfer8. The figure that given below is bathymetric map of Lake Köyceğiz, which was an output of the Surfer.

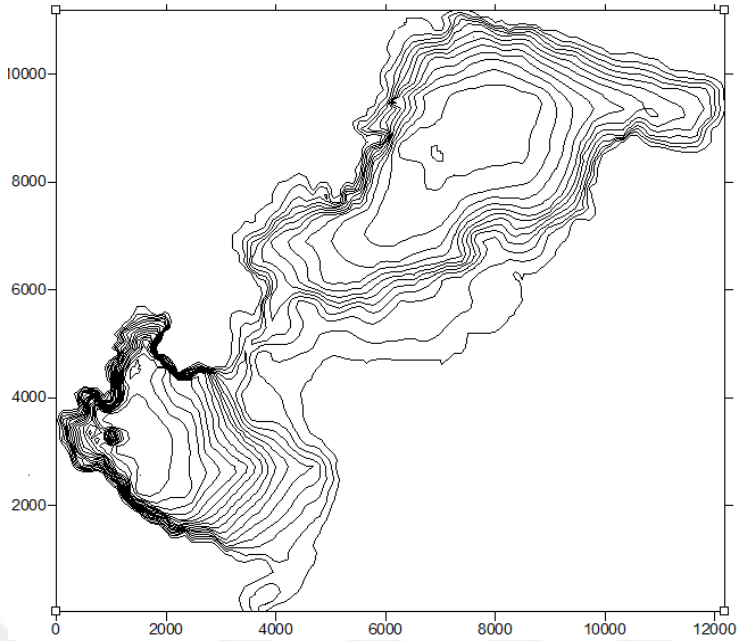

Figure 5.31: Bathymetric Map of Lake Köyceğiz.

This program also gives the wireframe and vector map of Köyceğiz lake. These maps are presented in the following figures for the better understanding of the geometry of the lake.

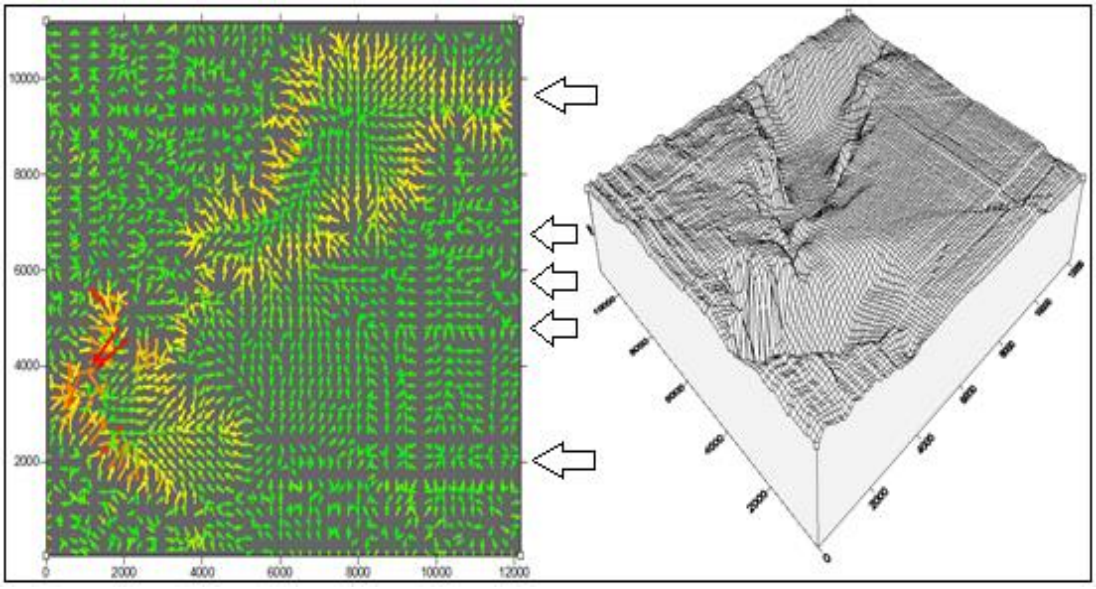

Figure 5.32: Wireframe and Vector Map of Lake Köyceğiz.

After these steps, the approximate bathymetry of the lake was concluded and the figure of the empty lake or its bathymetric map was achieved.

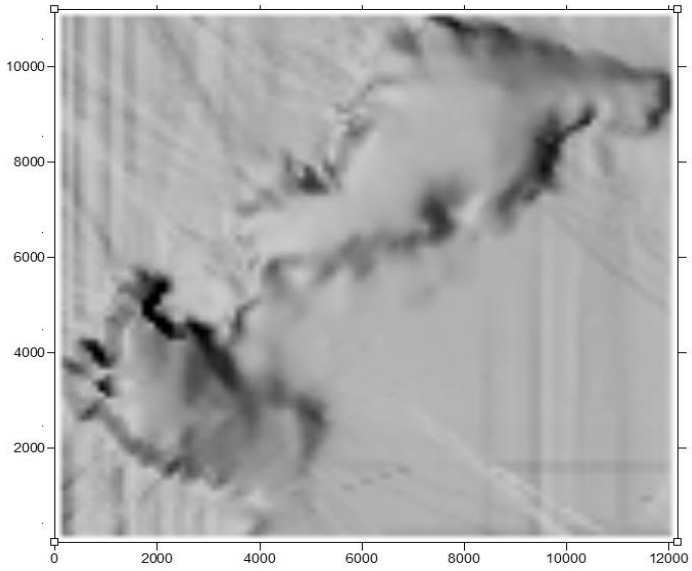

Figure 5.33: Bathymetric Map of Lake Köyceğiz (When Completely Empty).

The three dimensional surface of bathymetry of the Lake Köyceğiz was ready to imported to the SketchUp 2015 program after these steps and this program was able to convert this 3D surface to the lithography format that was could be used in the FLOW 3D program.

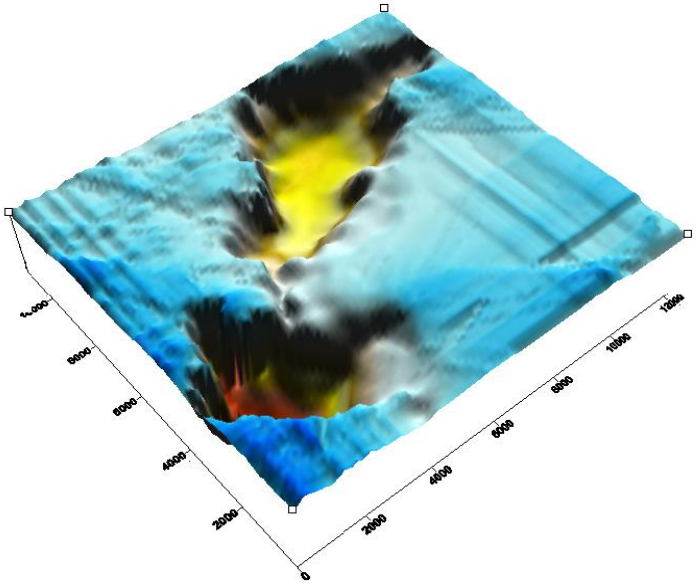

Figure 5.34: The Three Dimensional Surface of Bathymetry of the Lake Köyceğiz.

The relations between area-volume-depth in Lake Köyceğiz and its parts has been provided by Maktav et al. in 1998. These relations are presented as Table 5.4.

Table 5.4 : Area-Volume-Depth Relation in Lake Köyceğiz (Maktav et al., 1998).

Depth (m)	Koycegiz Part (North of lake)		Sultaniye Part (South of lake)		Lake Koycegiz (Total)	
	Area (m^2)	Volume (m^3)	Area (m^2)	Volume (m^3)	Area (m^2)	Volume (m^3)
0	38223492		16776508		55000000	
2	34792851	73016343	15270780	32047288	50063631	105063631
4	30476237	65269088	14222599	29493379	44698836	94762467
6	26085913	56562150	12450160	26672759	38536073	83234909
8	23734925	49820838	11349740	23799900	35084665	73620738
10	21389750	45124675	10308956	21658696	31698706	66783371
12	18806528	40196278	9370908	19679864	28177436	59876142
14	16603598	35410126	8613712	17984620	25217310	53394746
16	14742439	31346037	7953730	16567442	22696169	47913479
18	12379322	27121761	7394840	15348570	19774162	42470331
20	9804769	22184091	6824352	14219192	16629121	36403283
22	7011820	16816589	5943547	12767899	12955367	29584488
24	3289976	10301796	5187475	11131022	8477451	21432818
26	31111	3321087	4447951	9635426	4479062	12956513
28			3863454	8311405	3863454	8311405
30			2970228	6833682	2970228	6833682
32			734187	3704415	734187	3704415

The area and volume variations by depth in Lake Köyceğiz and its parts are represented as separate figures (Figures 5.35 and 5.36).

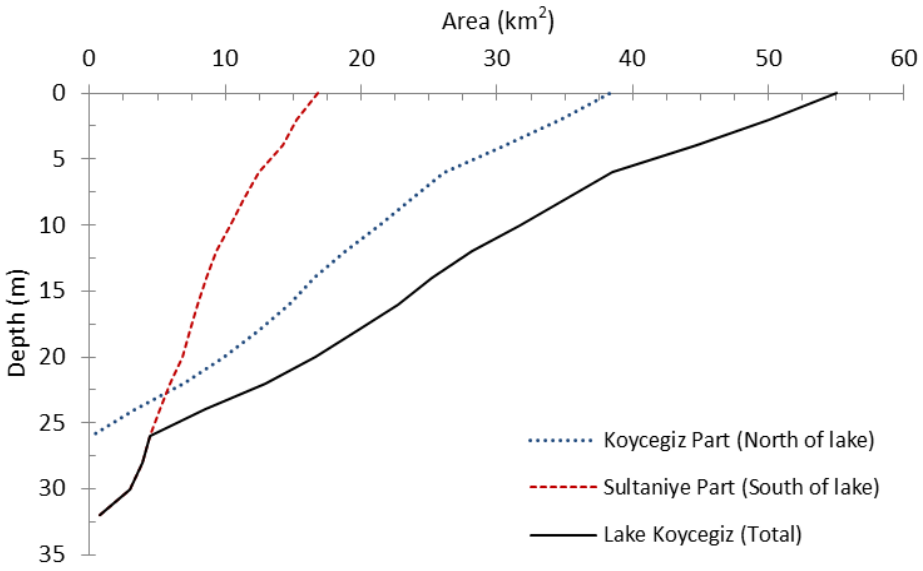

Figure 5.35: The Area-Depth Relation of the Lake Köyceğiz (Maktav-1998).

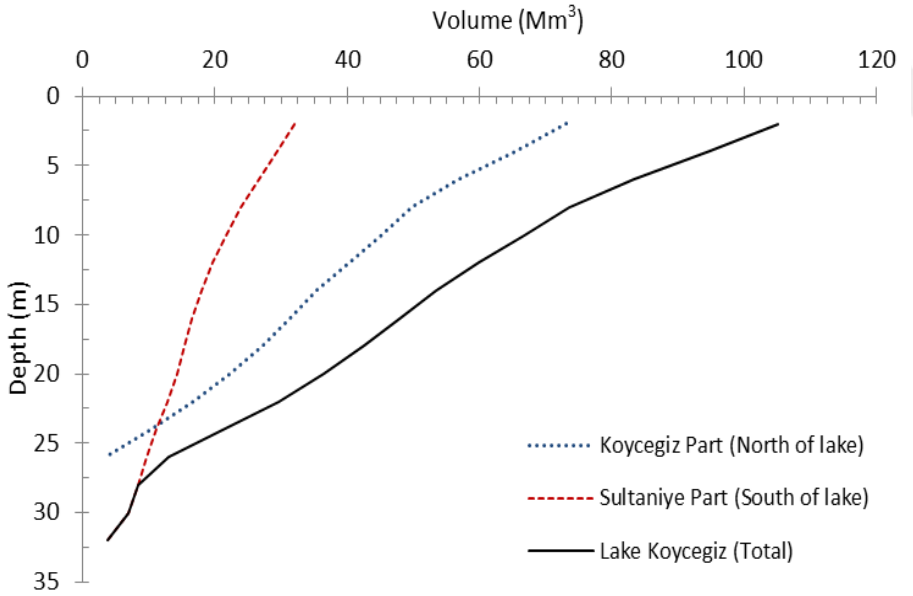

Figure 5.36: The Volume-Depth Relation of the Lake Köyceğiz (Maktav-1998).

The Lake Köyceğiz experienced stratification because of its specific condition. The measurements of temperature due to the different depths of the lake show that the lake is thermally stratified during summer and winter. These stratifications have some differences in temperatures through depth at the north of the lake (Köyceğiz part) and the south of that (Sultaniye part).

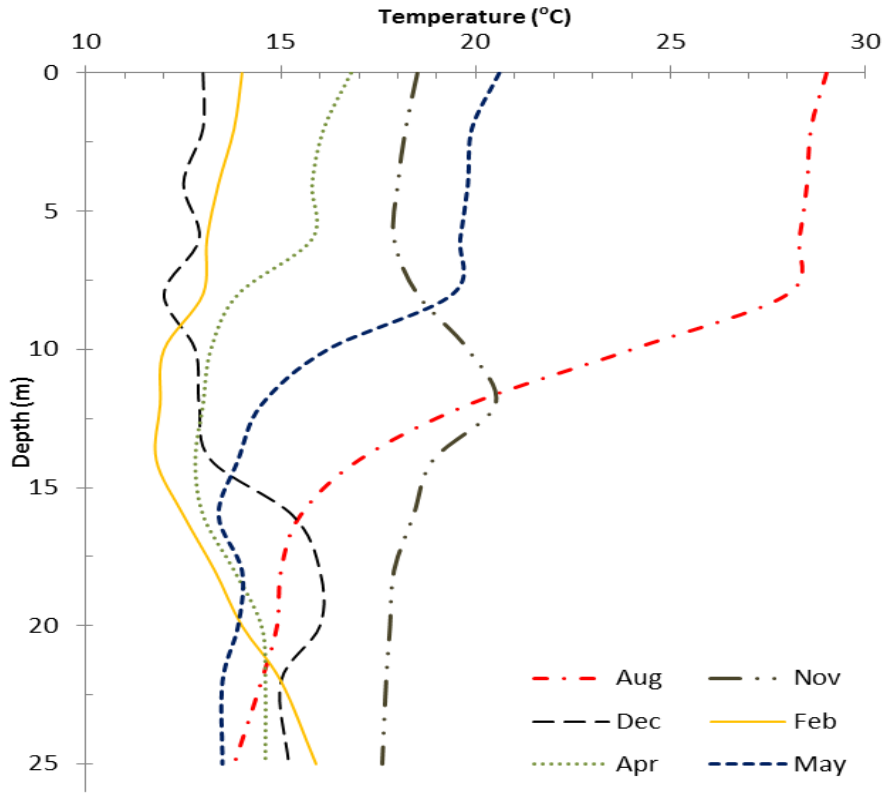

a) Köyceğiz hole (North of the lake).

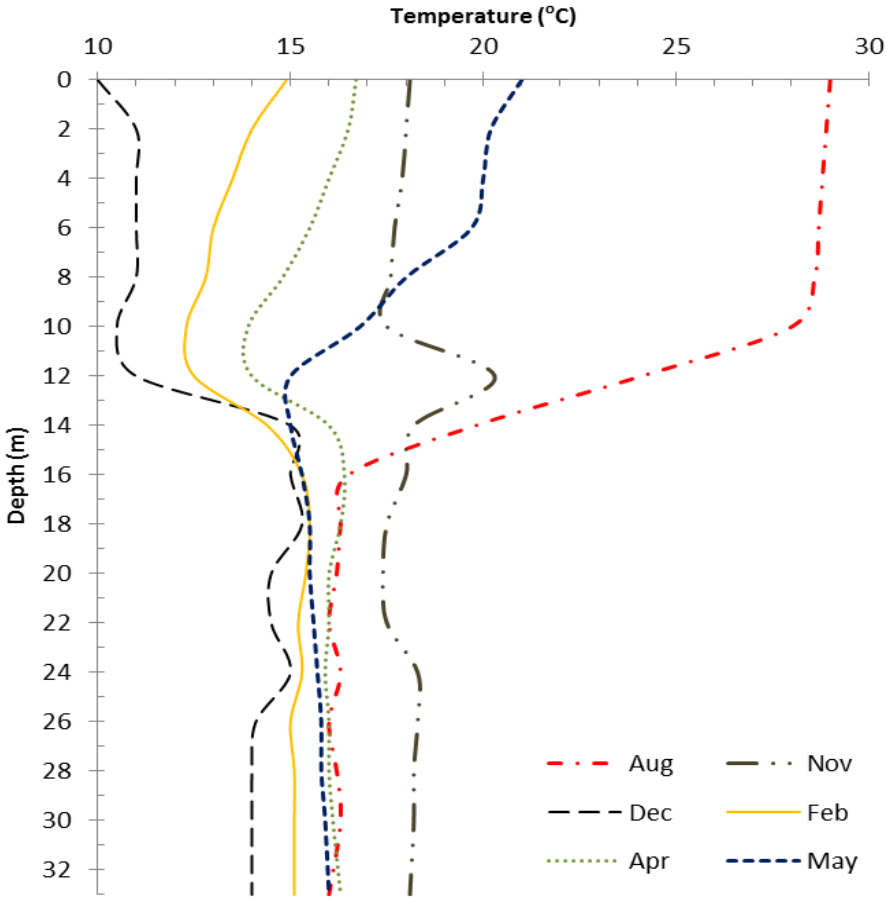

b) Sultaniye hole (South of the lake).

Figure 5.37: Thermal Stratification of Lake Köyceğiz (Kazanci, 1992).

Salinity and density in Köyceğiz lake are varied with depth. Density of lake is depends on temperature of water, salinity, suspended sediment concentration and pressure during depth. Measured salinity (part per thousand) and calculated density (kg/m^3) using these data are presented in Figure 5.38.

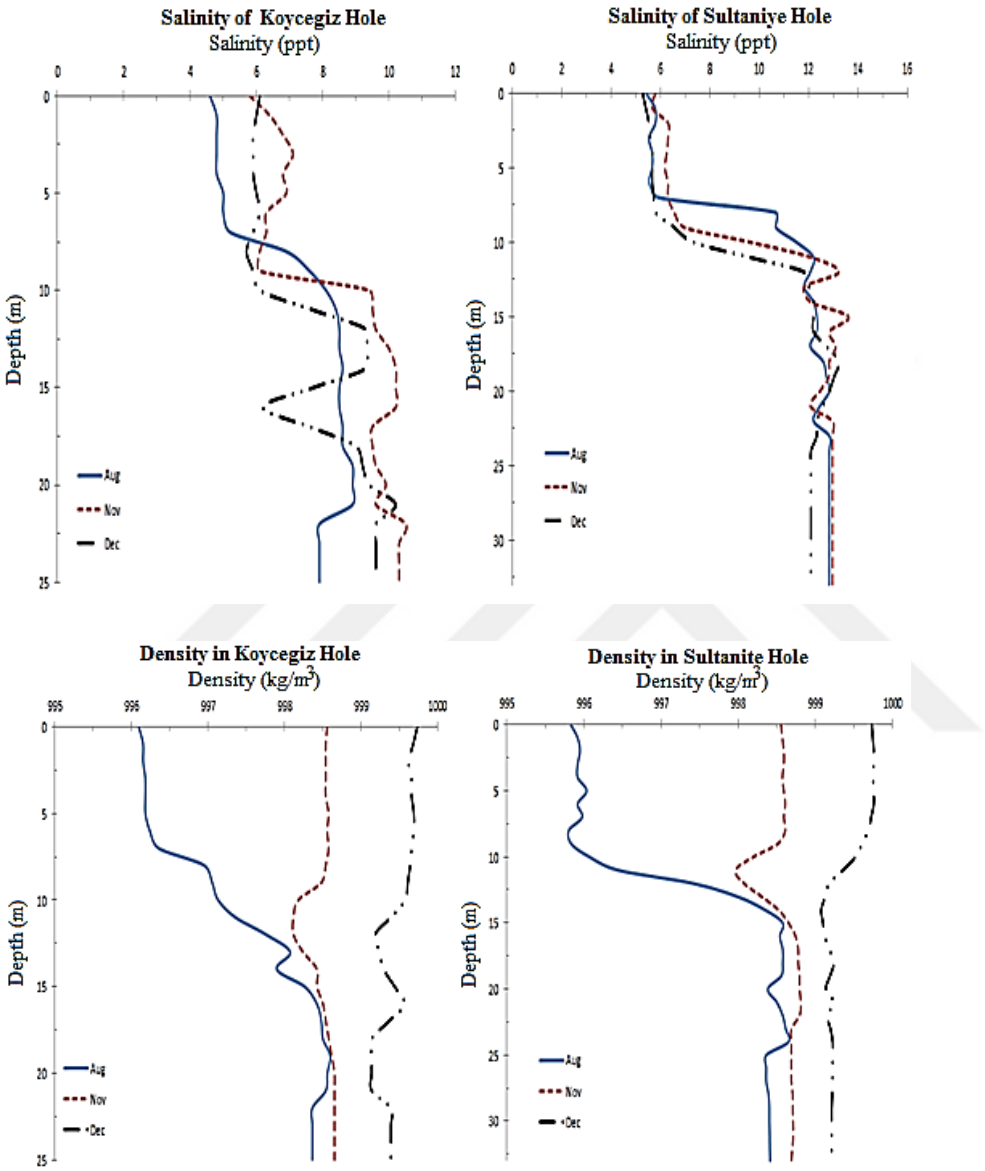

Figure 5.38: Measured Salinity and Calculated Densities of Each Part of the Lake Köyceğiz.

From Figure 5.34 and 5.35, at Köyceğiz hole and its deepest area (approximately depth equal to 25 m), it is seen from the surface of the lake to the depth of approximately 7.5-8 m the epilimnion layer is created in April and Augest. From this depth to approximate depth of 18-18.5 m, the temperature of water varies in defferent

depths, in these months of year. This area could be named as thermocline or metalimnion layer. These variations are because of the exictence of the grounwater springs and also the differences of densities, which appeared from the salinity variations. After this layer the hypolimnion layer is exist, which has temperature value between 15.5 to 16.5 ^{o}C in April and 19 to 21 ^{o}C in Augest. The weather starts to be cold from October. In this month, the temperature of water at the surface of the lake starts to reducing. This reduction of weather and temperature of water affects the epilimnion layer very fast in comparison of other layers. The water temperature value decreases to 18-18.5 ^{o}C from the surface of the water to depth of 10 meters in November. From here to the depth of 14-14.5 meters, an increasing is seen in temperature, which reached to 21 ^{o}C. After this depth, the temperature of water is approximately same to the first layer. As seen, the changes in temperature are negligible after depth 18.5 m, in different months and seasons. The salinity of Lake Köyceğiz is extreamly increased after the depth 7.5 m in all months.

From represented figures about the Lake Köyceğiz, that were shown, and the information and figures about the inflow streams, that will be represented, some conclusions could be determined. With evaluation of the stream's data, it is clearly obvious that in the summer months the discharge of these streams are decreased. This is caused to the reduction in the water level of Lake Köyceğiz. In September and October, the level of the lake is in its lowest value, mostly. By starting the November and December, the precipitation starts to increase. It leads to increasing in inflow river's discharges. By analysing the salinity of the Namnam river, it is seen that in these months, the salinity is decreased. While the salinity of the lake is extreamly increaed in Augest, September and October. The densities of the rivers have a value lower than density of the first layer of the lake. So, it is considered that the over flow occured in the lake. The entering of these flows, reduces the lake's salinity, mostly in the first layer. Totally, salinity in the southern part of the lake (Sultaniye hole) is more than the salinity in north part of the lake (Köyceğiz hole). In most of literatures, the main reason for higher salinity in southern part of the lake is listed as the entering the water of the Mediterranean Sea, which is more saline than the lake's water. The entrering of sea water into the lake is because of the dropping of lake level in summer season. It is also related to the wind velocity and direction in this season.

5.3 Namnam River

Namnam river is the main stream that flows into the Köyceğiz lake. The source of this river is from the west of the Sandras mountains, which has an elevation equal to about 2294 m. The length of Namnam river is 33 km, approximately. The width of Namnam river varies between 25 to 30 m. Position of this river is shown in the figure 5.39.

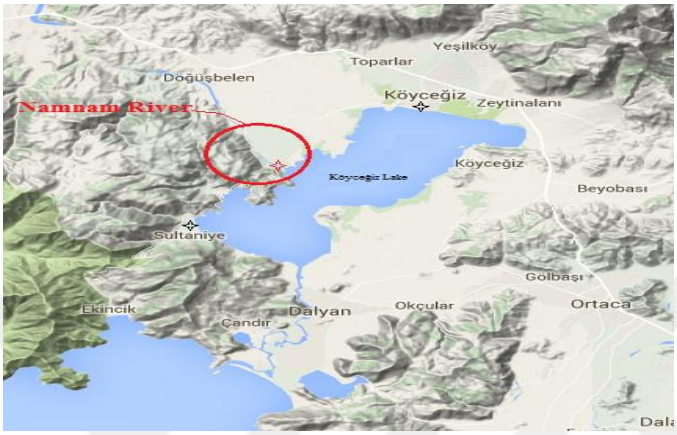

Figure 5.39: Position of Namnam River (Google map).

In winter and spring seasons, the river is full of water, while, in the summer it has a least amount of water because of the drought and intense evaporation. Measured values of minimum, maximum and the average discharges in the Namnam river from 1990 to 1999 are about 0.014 m^3/s, 189 m^3/s and 9.65 m^3/s. Until today, the highest value of discharge that this river has experienced is 556 m^3/s. The daily discharges are given in Figure 5.40 for the time period of 1990 to 1999.

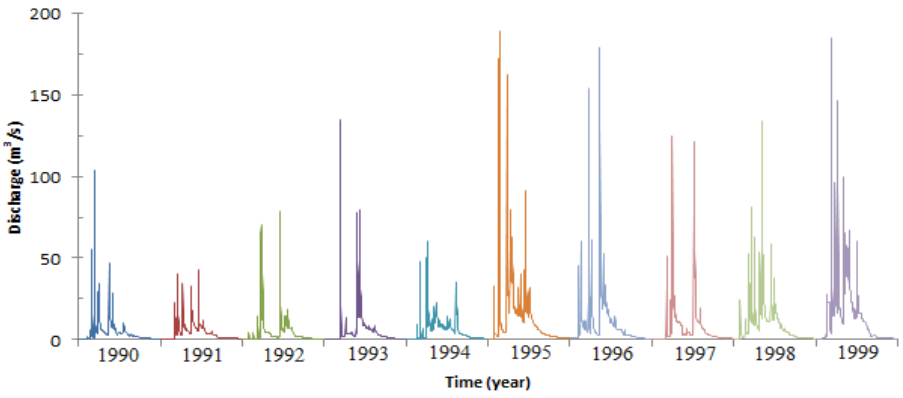

Figure 5.40: The Measured Daily Discharges in Namnam River for the Time Period of 1990 to 1999.

The area chart with table of average monthly discharges are presented in Figure 5.41 for the 1990-1999 years, separately.

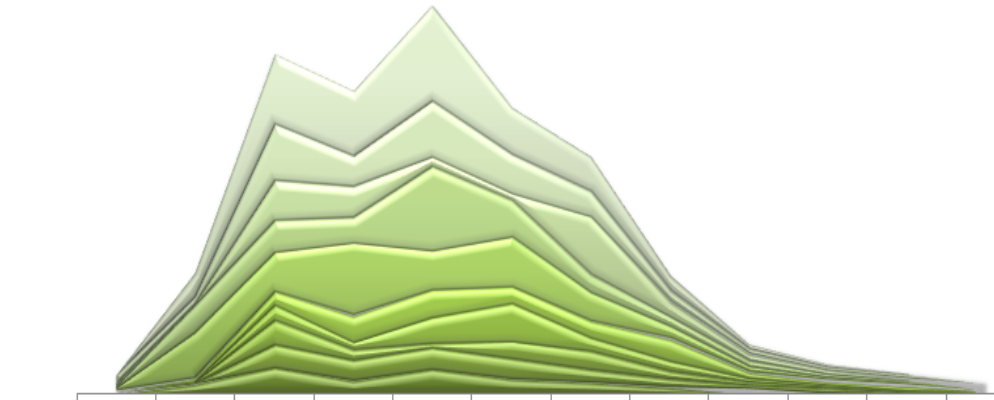

Year	Oct	Nov	Dec	Jan	Feb	Mar	Apr	May	Jun	Jul	Aug	Sep
1999	0.44	11.70	34.00	31.20	45.90	22.40	16.80	7.50	2.30	1.53	1.31	0.82
1998	3.09	3.34	26.80	14.70	26.60	19.00	12.20	5.39	2.63	1.44	1.17	0.83
1997	0.62	0.76	19.40	15.20	5.17	3.69	27.50	7.04	2.91	1.74	1.12	0.79
1996	1.32	12.70	15.00	11.80	40.30	17.50	8.91	5.05	2.92	1.74	0.98	0.73
1995	2.24	21.90	19.00	34.70	18.70	23.70	13.40	5.73	2.88	1.82	1.38	1.12
1994	0.23	1.54	6.81	12.40	12.70	8.09	7.70	10.70	2.81	1.54	1.20	0.37
1993	0.21	0.36	7.18	4.20	12.60	17.90	7.13	4.93	2.27	1.31	0.77	0.33
1992	0.85	0.92	11.70	5.37	2.27	8.48	8.37	4.14	1.72	1.05	0.73	0.30
1991	0.08	0.05	10.70	8.97	10.40	9.65	6.08	3.35	1.83	1.22	1.00	0.72
1990	0.53	4.79	12.10	6.30	11.10	6.65	5.37	3.16	2.04	1.40	0.72	0.13

Figure 5.41: The Area Chart with Table for Average Monthly Discharges for years between 1990 and 1999.

Total annual water volume of this river (Mm^3) are presented as figure 5.42.

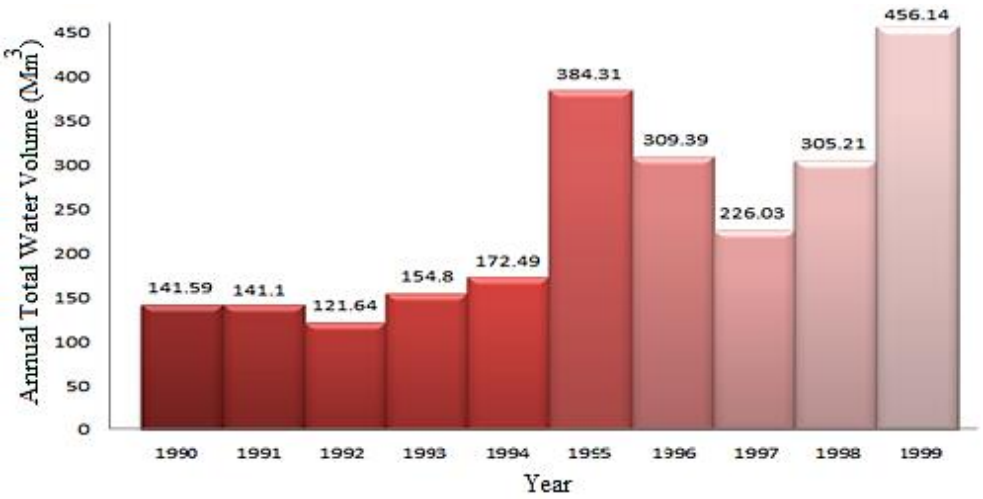

Figure 5.42: Total Annual Water Volume of Namnam River (Mm^3).

The long term average monthly discharges and the monthly precipitation of Namnam river are available from the measurements at Dogusbelen station for years between 1990 to1999. (Figure 5.43).

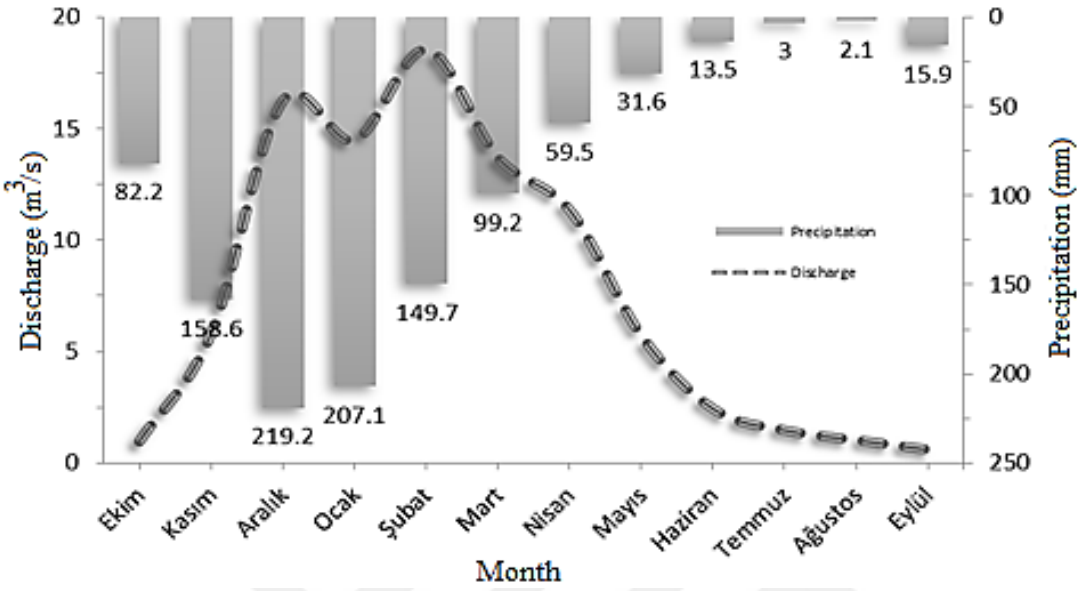

Figure 5.43: The Long Term Average Monthly Discharges (m^3/s) and the Monthly Precipitation (mm) of Namnam River (1990-1999).

General Directorate of State Hydraulic Works of Turkey (DSI) is offered the values that shown in Figure 5.44, for the long term average monthly discharges for this river by adding the years 1981 to 1986.

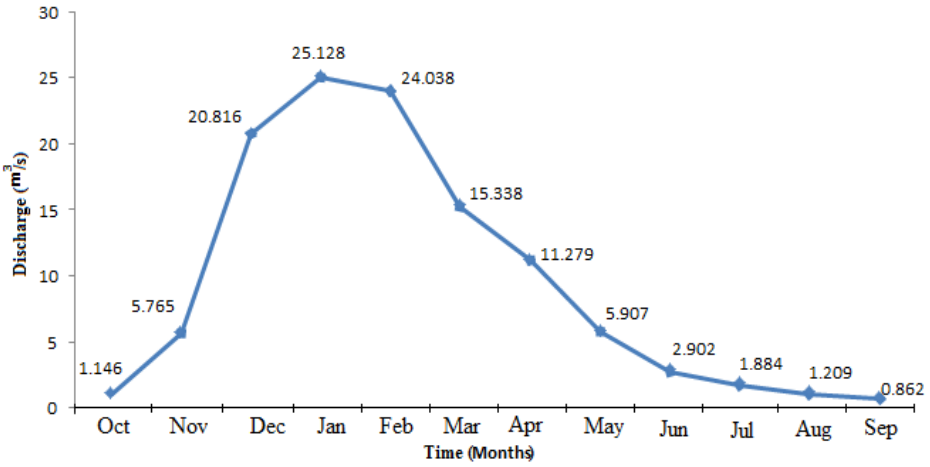

Figure 5.44: The Long Term Average Monthly Discharges for Namnam River By Adding the Years 1981 To 1986 (DSI).

In a research entitled as study on water quality of Namnam river in 2010 some parameters were measured for Namnam river, in the station which was located at the Namnam river before connecting to the lake. The geographic coordinates of the station that these parameters measured, is at 37°01'25" latitude 28°33'45" longitude. In that study, other Physico-chemical characteristics of Namnam river were measured, but here, parameters that will be used in this study are represented. These parameters are maximum, minimum and average values for temperature, total suspended solids, salinity and dissolved oxygen. (Table 5.5)

Table 5.5 : Measured Parameters of Namnam River at Connection point to the Lake.

	Temperature (°C)	TSS (mg/l)	DO (mg/l)	Salinity (‰)
Maximum	25.25	16.25	6.89	0.34
Minimum	15.08	5.05	4.78	0.19
Average	18.34	8.6	5.97	0.26

According to mentioned study, the average monthly temperatures of water are shown in Figure 5.45. These measurements are for 12 months between 2010 and 2011 years.

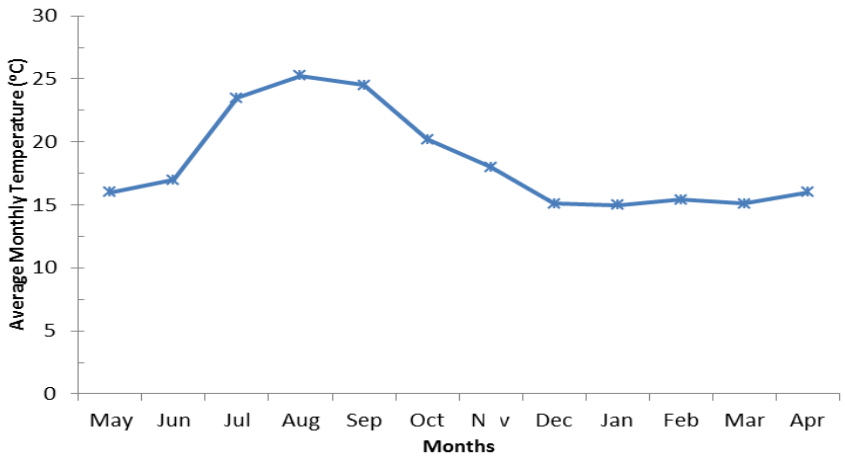

Figure 5.45: The Measured Average Monthly Temperatures of Water in Namnam River.

According to Table 5.6, it shows that the maximum average temperature of water in Namnam river was occurred in August and had a value equal to 25.25 ^{o}C, approximately. Whereas, the lowest amount of this parameter was about 15 ^{o}C, which was measured in January.

The other parameter is salinity. From the Figure 5.46, it is obvious that the salinity had the high values in summer months, clearly. The highest amount for the salinity of this river was happened in September, specially.

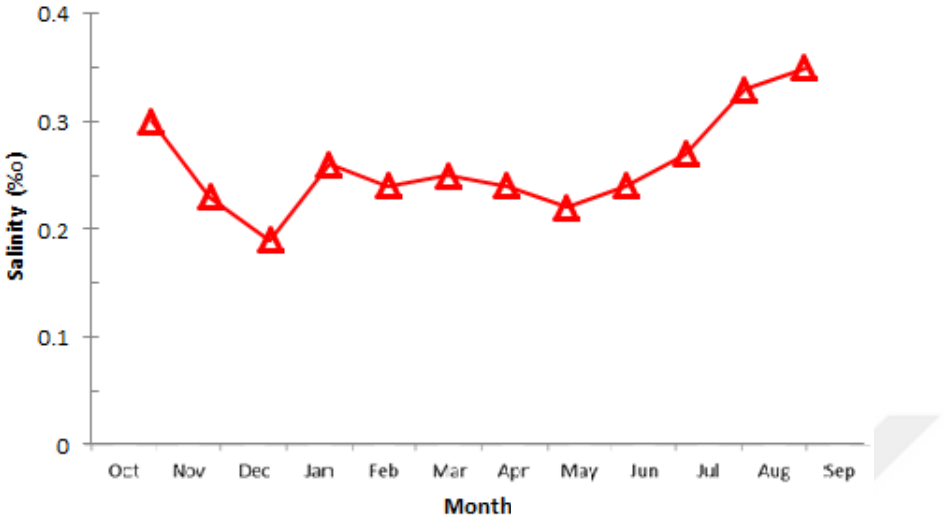

Figure 5.46: The Measured Salinity of Namnam River.

One of the important parameters that is required for modeling of this study is TSS (mg/l). The information and the data for this parameter are just limited for mentioned study. The measurements about TSS are shown as a figure for the months of 2010.

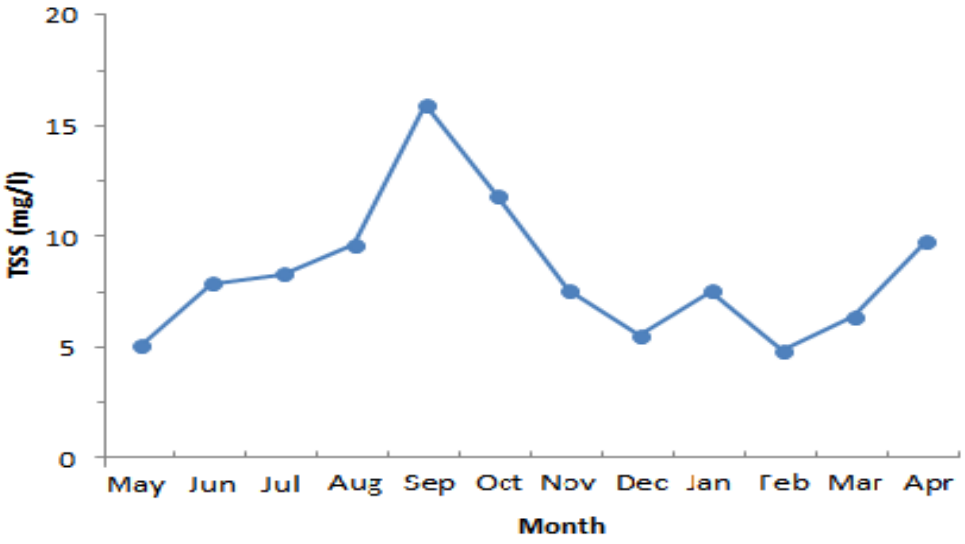

Figure 5.47: The Measured TSS in Namnam River.

Suspended sediments have a special importance in lake and reservoir studies. So, this subject has an important role in hydrodynamic of lakes and reservoirs. Erosion is the main factor and the major source in the sediment transport. Figure 5.48 shows the erosion situation of the

region. From the figure it is understood that the areas next to the Namnam River has no Erosion, mostly. Therefore, it is not expected that the plentiful amount of sediments that come from river into the lake.

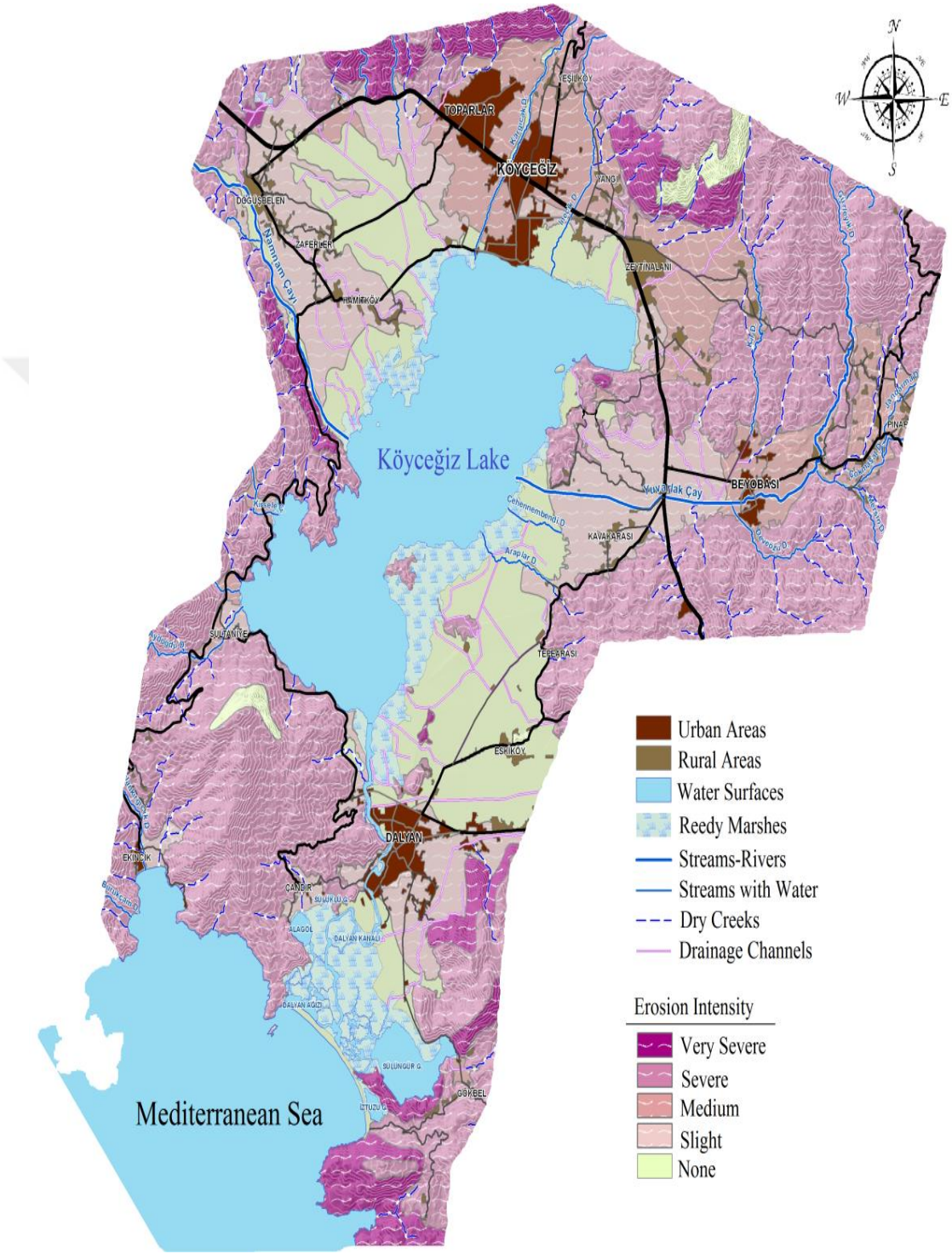

Figure 5.48: Erosion in the Study Area (Anonymous, 2007).

5.4 Yuvarlak River

Yuvarlak river is the second main river, which inflows to the Lake Köyceğiz. It is located at the east side of the Lake Köyceğiz. The length of this river is approximately 21 km. Width of this river varies between 6 and 14 m.

Figure 5.49: Location of Yuvarlak River (Google Earth).

Yuvarlak river long term average discharges are represented in the Figure 5.50. These values were measured at the Yuvarlak kopru station.

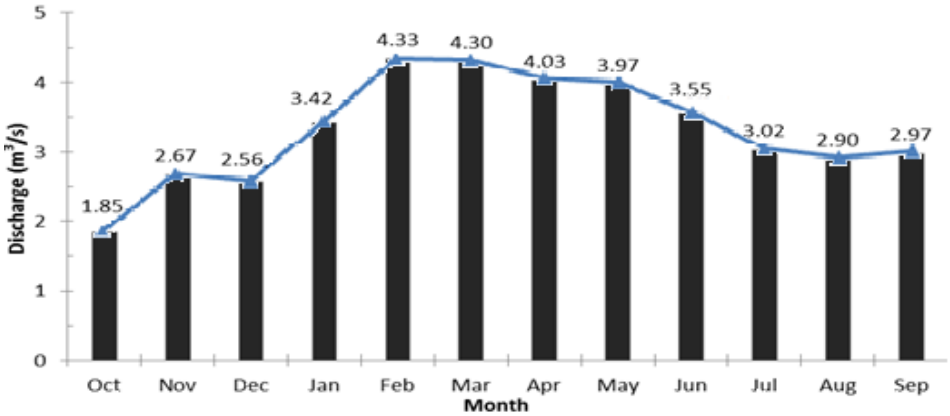

Figure 5.50: The Long-term Average Discharges of Yuvarlak River (General Directorate of State Water Works of Turkey).

The maximum monthly average discharges are happened in the Winter and Spring included the Febuary, March, April and May months. In comparison with Namnam river, this river has low and insignificant discharges. The water's temperature in Yuvarlak river is increased from the source to the mouth, where connected to the

Lake Köyceğiz. The minimum, maximum and average water temperatures at this point of river are 13.5, 35 and 20.3 ^{o}C. The monthly average of measurments for years 1991-1993 are represented as Figure 5.51. (Kazanci, 1993)

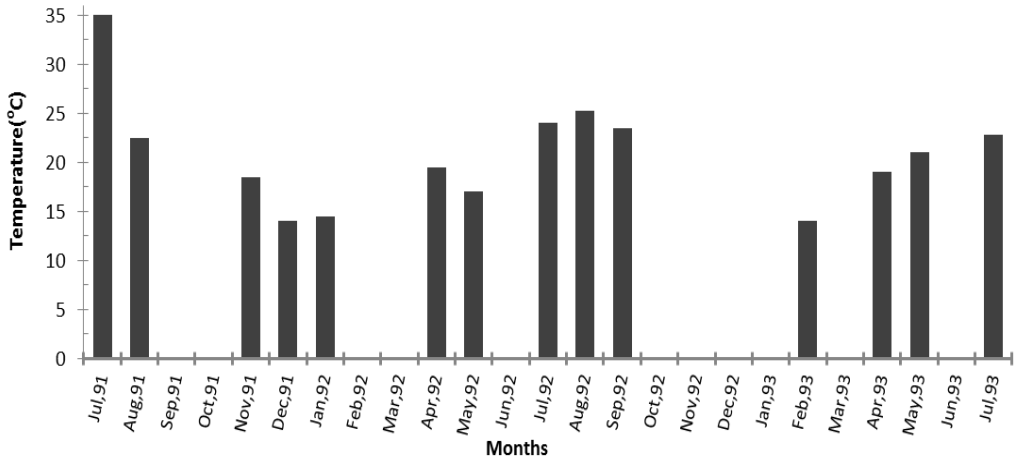

Figure 5.51: Average monthly temperatures of Yuvarlak River (1991-1993). (Kazanci, 1993)

5.5 Kargıcak and Yangi River

This river has a drainage area equal to 46 km^2 with a maximum discharge of 3.650 m^3/s. The minimum and the average values for this stream are 0.350 and 0.950 m^3/s, respectively. In this study, this stream colud be neglected because of the low values of discharge. General Directorate of State Hydraulic Works of Turkey (DSI) is offered the following values for long term Monthly averages of discharge for this river.

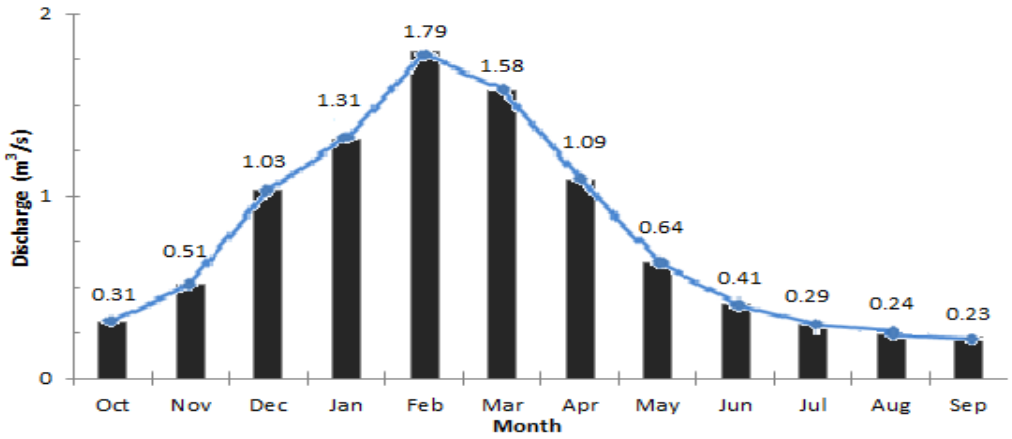

Figure 5.52: The Long-term Monthly Average Discharges of Kargicak River (DSI).

By examining in the discharges of the Namnam, Yuvarlak and Kargicak Rivers, it is obviously visible that they have the highest value of discharges between January and April. Measured temperature of water for some months of 1991-1993 is represented as Figure 5.53. (Kazanci, 1993)

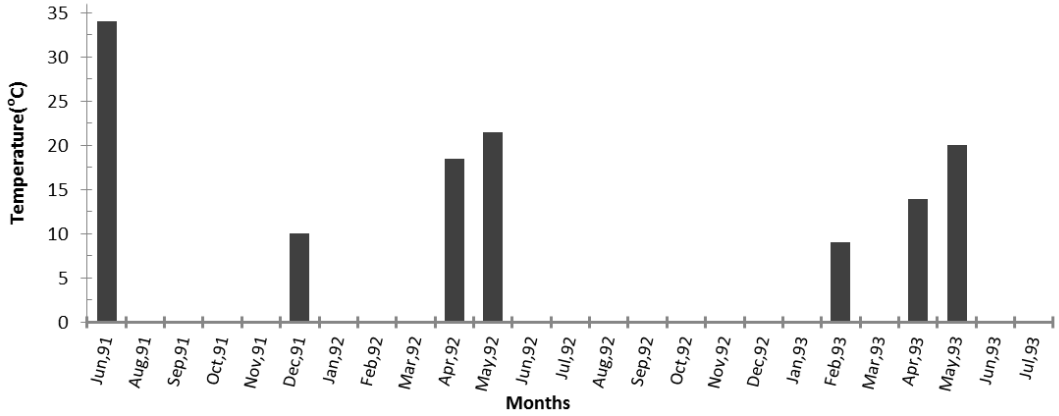

Figure 5.53: Average monthly temperatures of Kargicak River (1991-1993) (Kazanci, 1993).

Although the measured data for the river is not enough, but these are the only data that were measured for this river. On the other hand, because of the discharge of this river has low amount, it is considered that the effect of this river is negligible on the river in most months of the year.

In additional to flowing these rivers into the lake and the precipitation occurences on the lake, the graound waters, which are located under the lake, have an important role in hydrodynamic of this lake. But there is not enough available data for these springs. It is known that there are some exits of these ground and thermal waters under the lake. Tansug & Oztunali (1976) and Gonenc (2002) offered an approximate value for these springs equal to 1.69 Mm^3 for a month (20.3 Mm^3/year). There is no information about the number, locations and situations of the exits of these springs. From this offered value for the ground waters exits under the lake, it is understandable that the discharge of these springs are approximately equal to 0.65 m^3/s.

5.6 Result of Simulations of Lake Köyceğiz

Because the collected data for Lake Köyceğiz and the rivers flow into this lake is not enough, and the measured data were not available as daily values, so the simulations were prepared seasonaly. It is clear if the daily data were available, the results were be realiable. On the other hand, the simulation of the lake for the daily data needs a powerful computer, that this type of computer was not available for these aim.

The depth that defined to FLOW3D is shown in the figure below. In all of the following figures, the units for length and velocity are in meters and m/s, respectively.

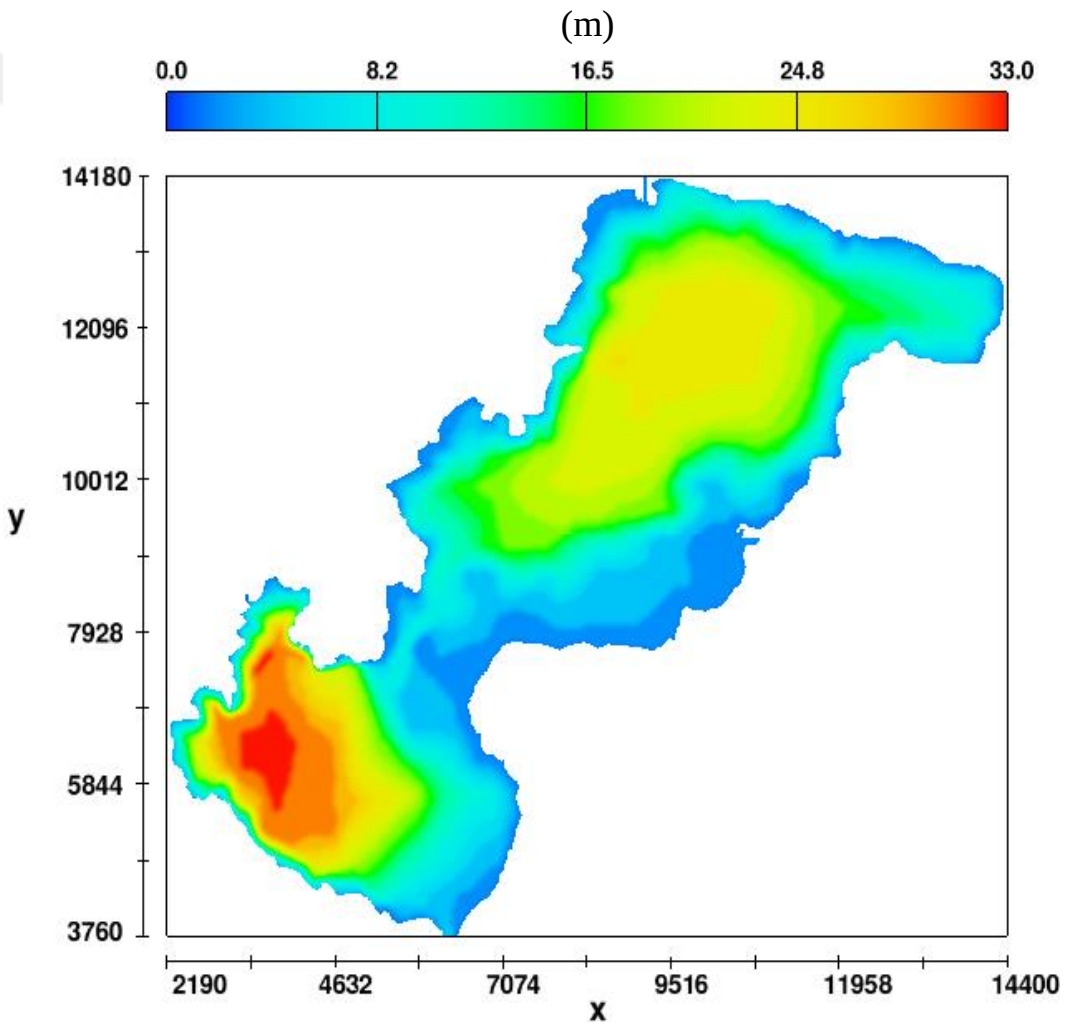

Figure 5.54: The FLOW 3D Output Bathymetric Map for Lake Köyceğiz.

The velocity vectors are presented at the following figures for water free surface level (z=0 m) and depths of -5 m, -10 m and -15 meters for November and for 2, 7, 14 and 18 days after the running simulation, which are colored by 2D velocity

magnitudes. As mentioned before, the thermal stratification for summer was defined for this model.

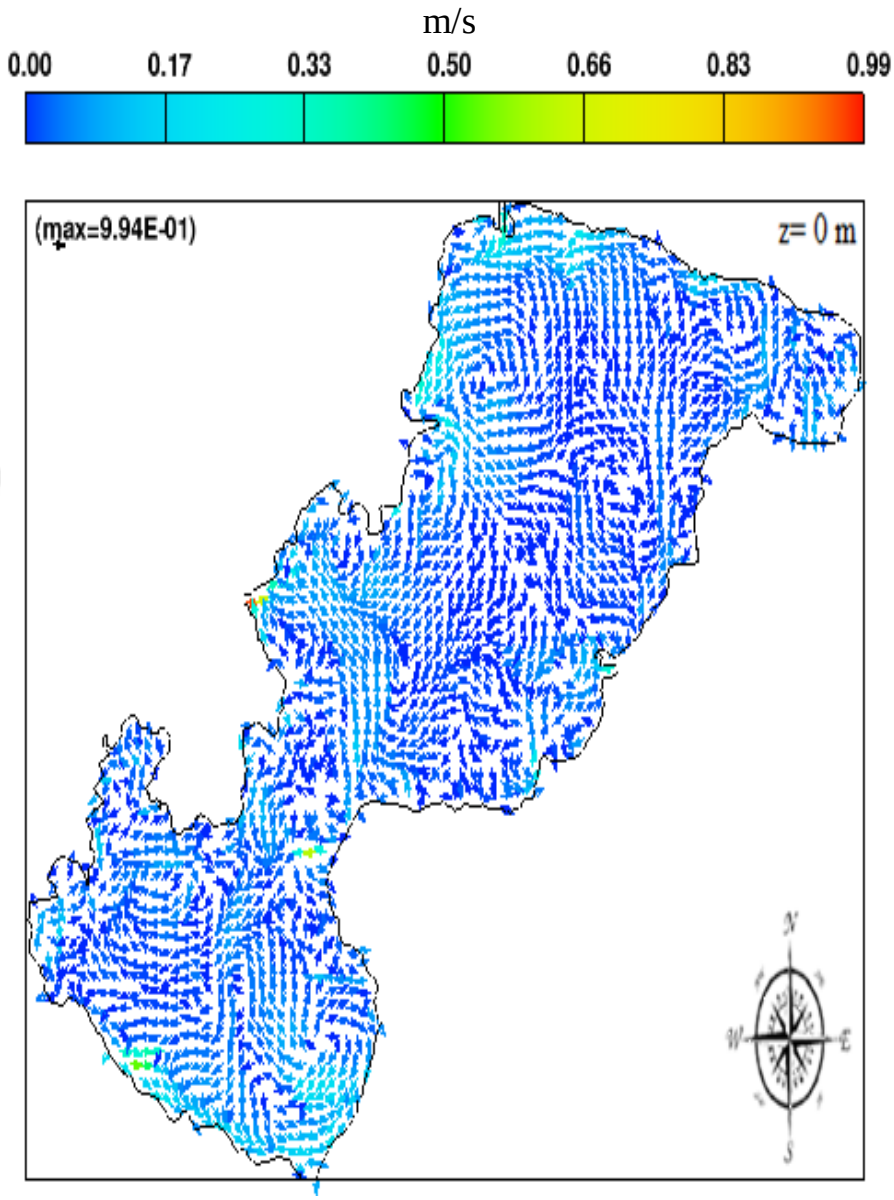

Figure 5.55: The velocity vectors colored by 2D velocity magnitude for z=0 m after 2 days (November).

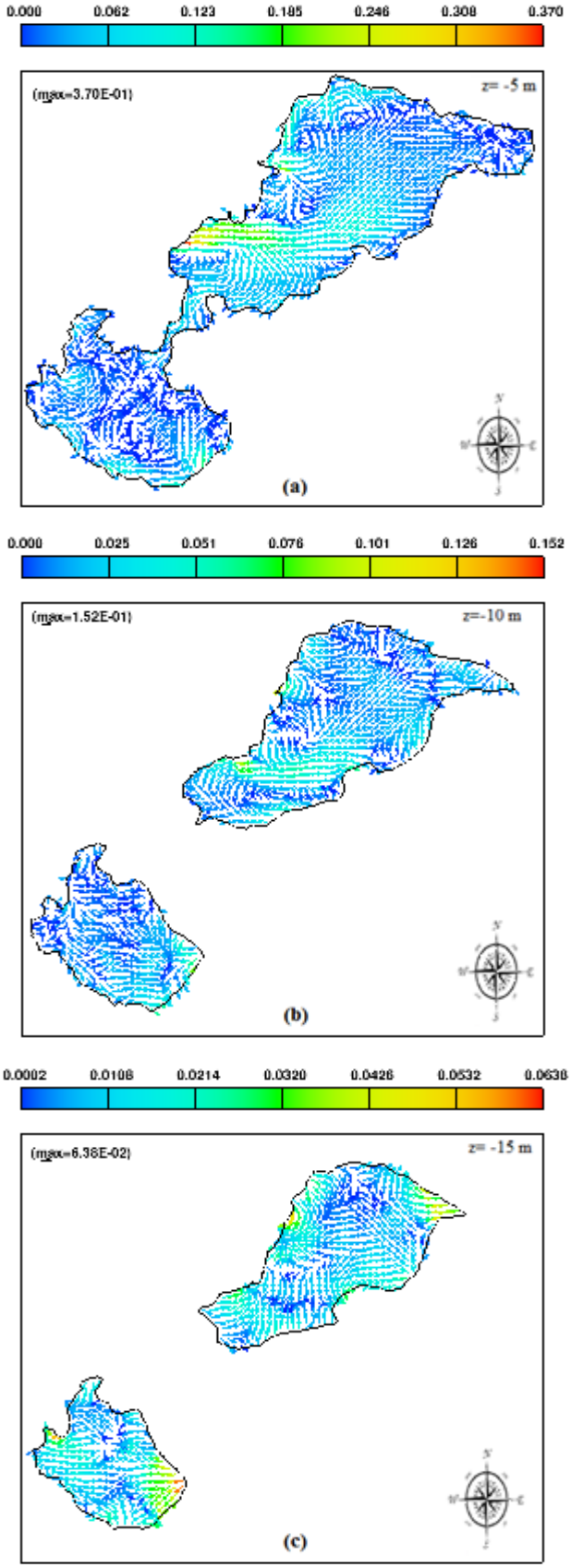

Figure 5.56: The velocity vectors colored by 2D velocity magnitude after 2 days (November): a) -5 m, b) -10 m, c) -15 m.

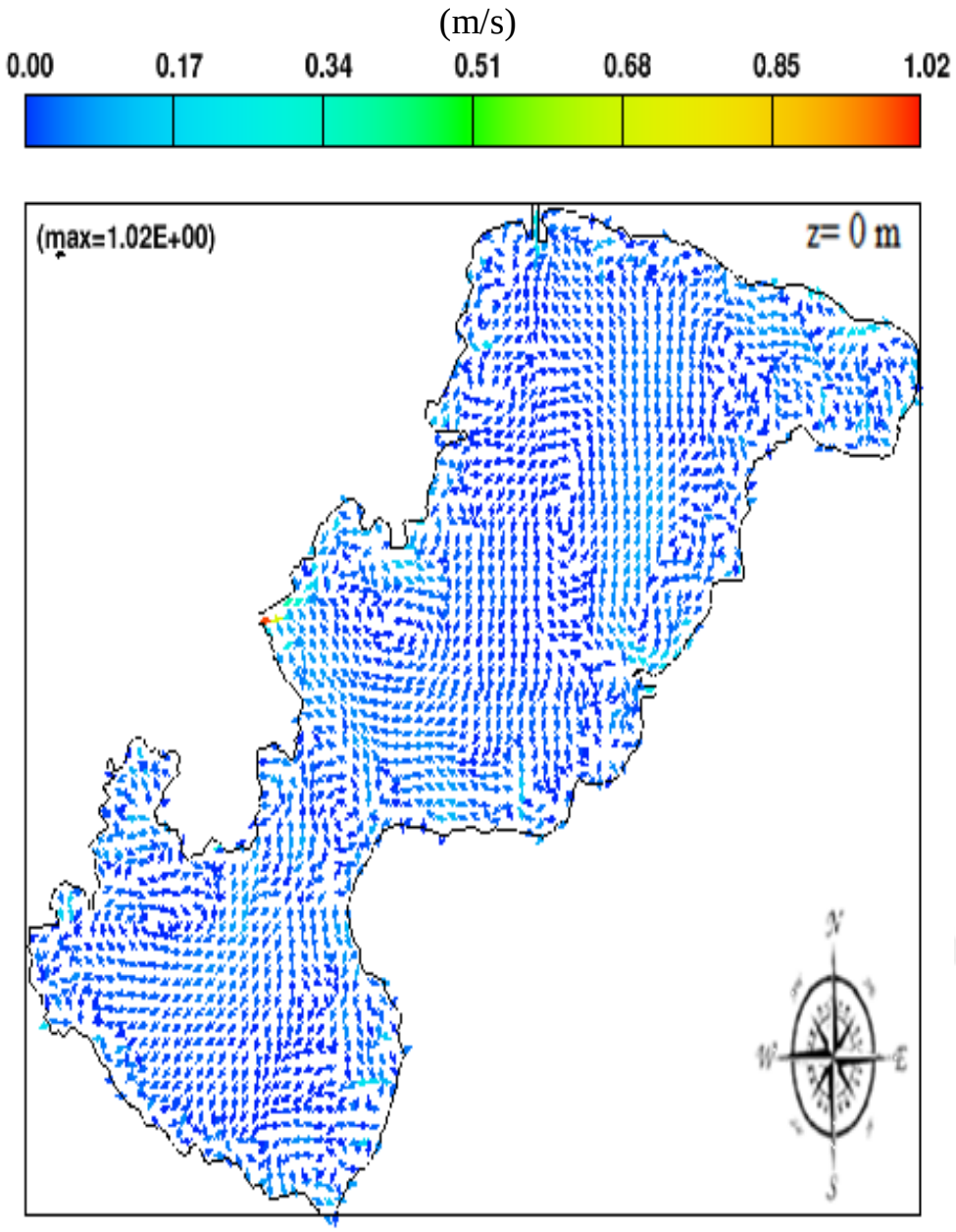

Figure 5.57: The velocity vectors colored by 2D velocity magnitude for z=0 m after 7 days (November).

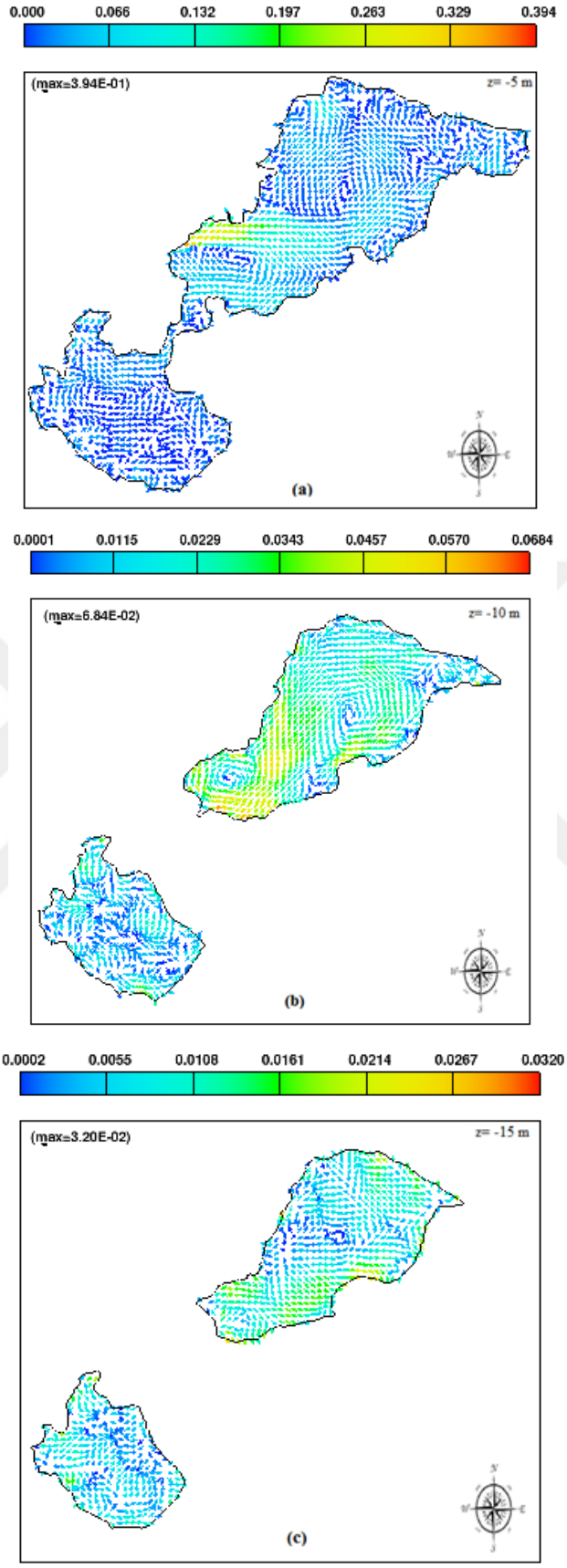

Figure 5.58: The velocity vectors colored by 2D velocity magnitude after 7 days (November): a) -5 m, b) -10 m, c) -15 m.

The direction of flow and the magnitude of velocity are represented as Figure 5.59 and 5.60 in -5 m, -10 m, -15 m depths and at surface)z=0 m) of the Lake Köyceğiz, for November.

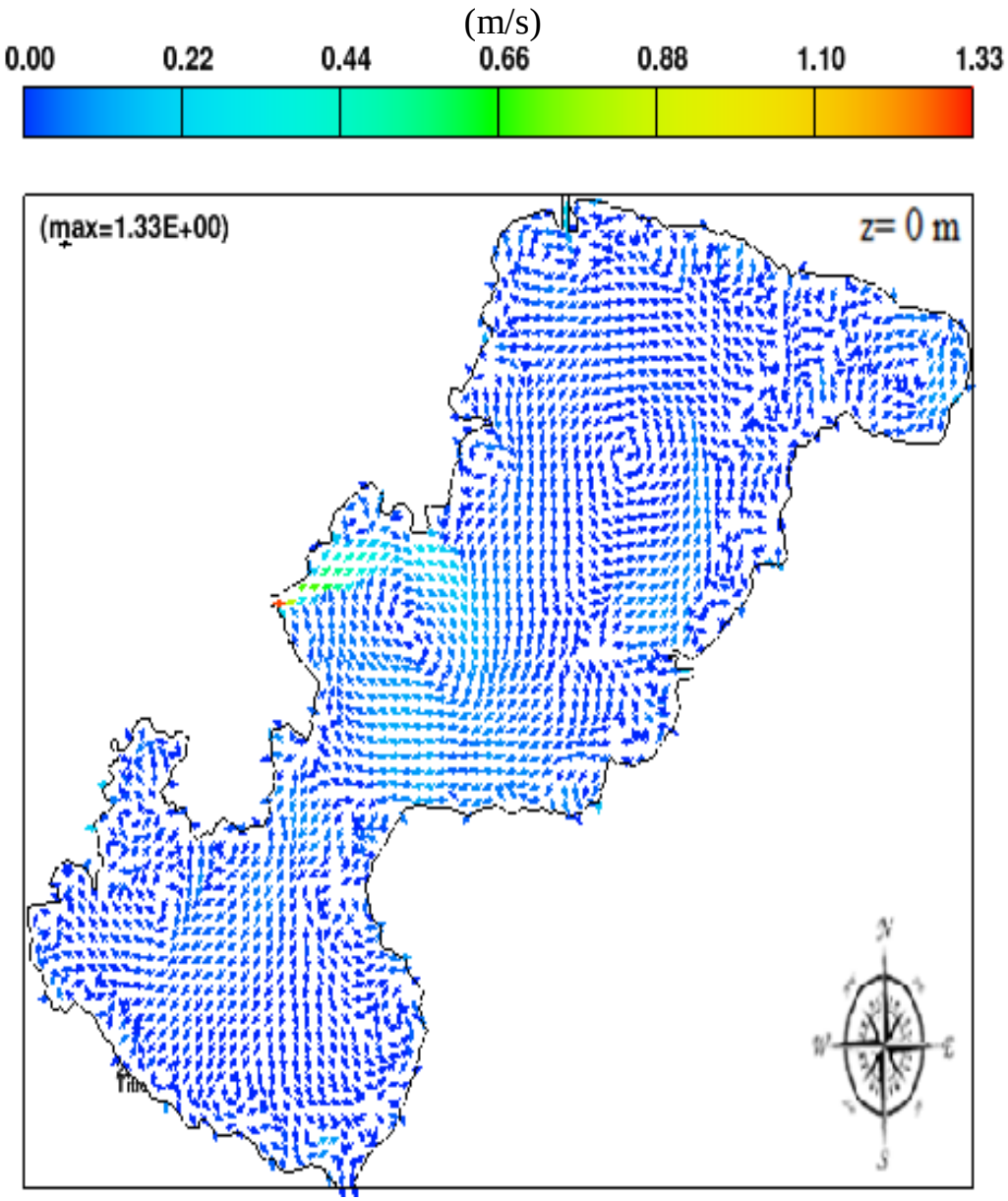

Figure 5.59: The velocity vectors colored by 2D velocity magnitude for z=0 m after 14 days (November).

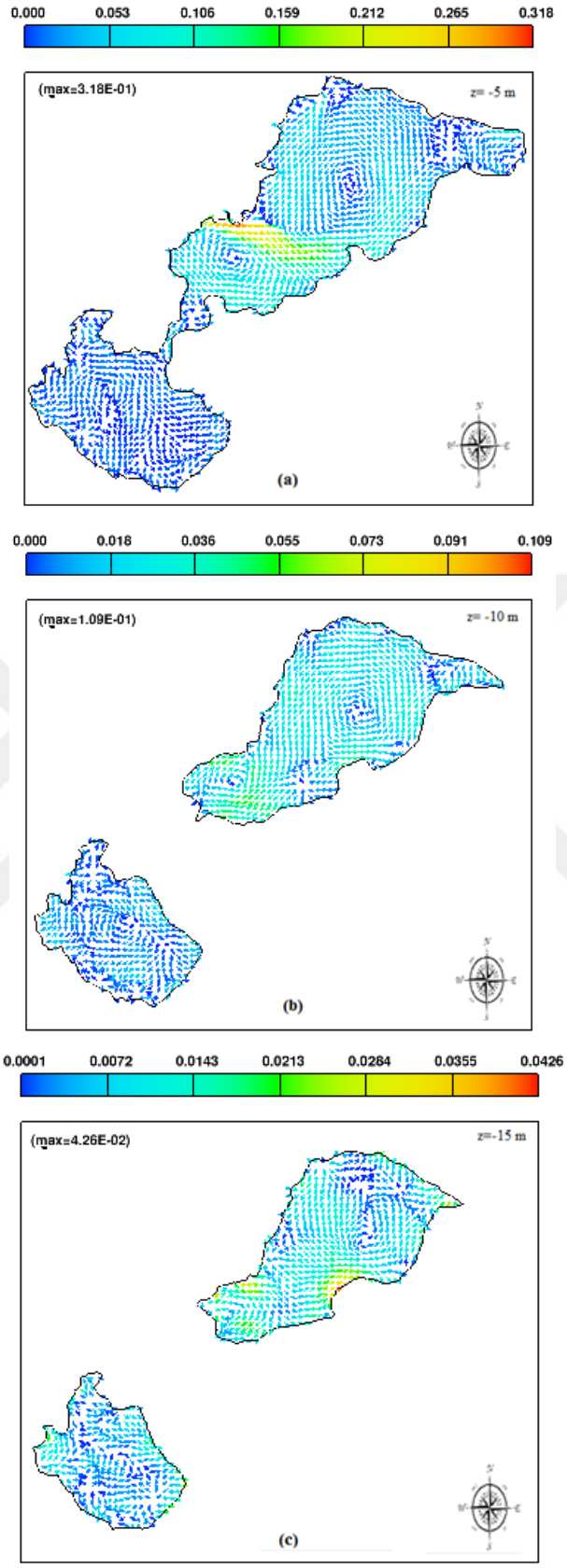

Figure 5.60: The velocity vectors colored by 2D velocity magnitude after 14 days (November): a) -5 m, b) -10 m, c) -15 m.

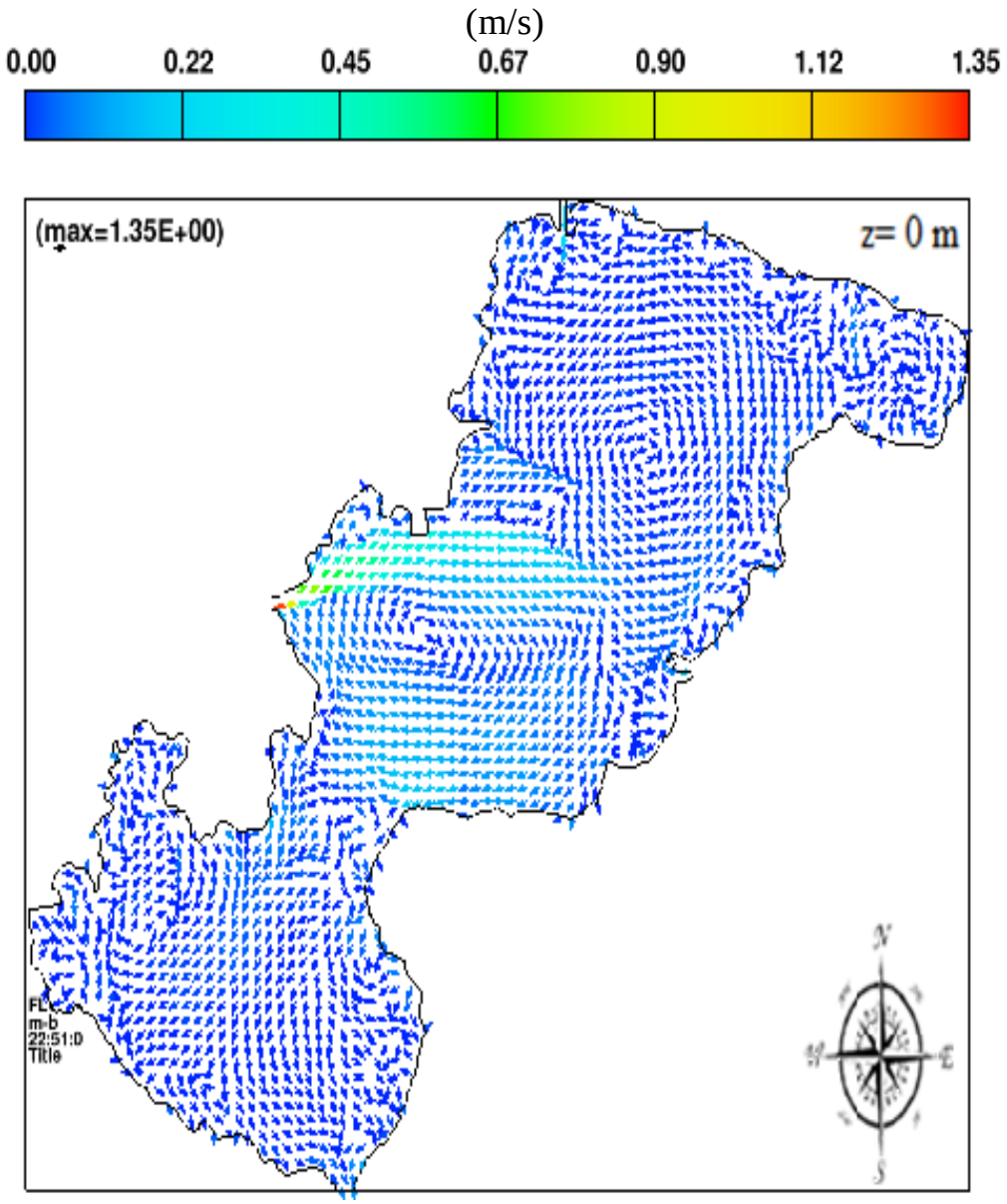

Figure 5.61: The velocity vectors colored by 2D velocity magnitude for z=0 m after 18 days (November).

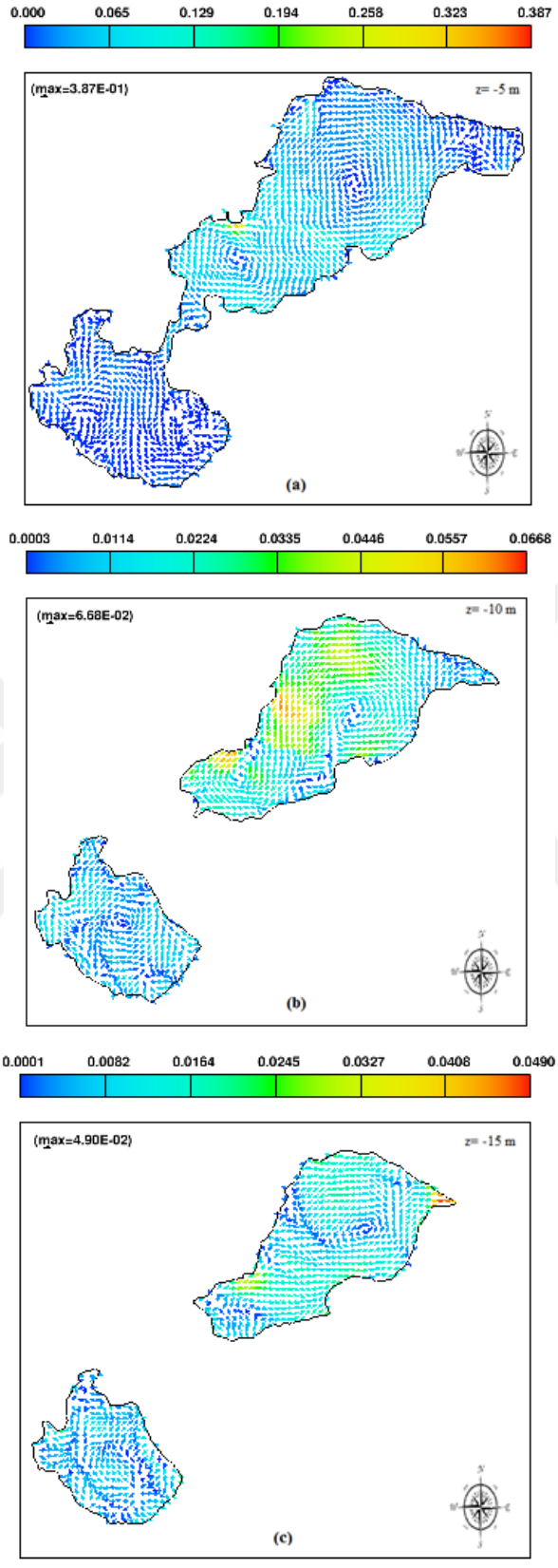

Figure 5.62: The velocity vectors colored by 2D velocity magnitude after 18 days (November): a) -5 m, b) -10 m, c) -15 m.

Available temperature data for different depths for Augest is defined and applied for FLOW 3D. The temperature changes at surface of water in 2, 7, 14 and 18 days will be shown in the lake after October for November.

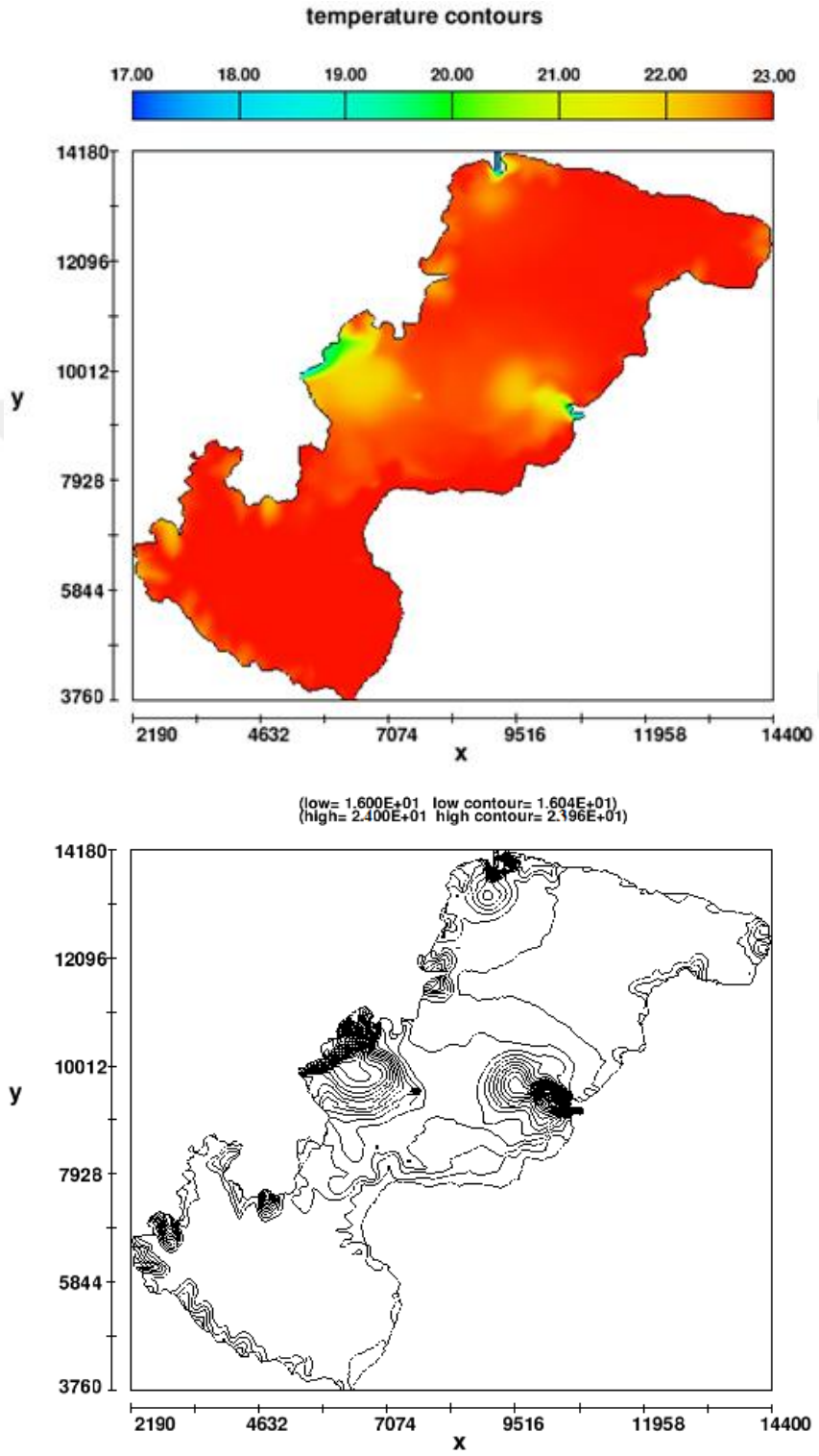

Figure 5.63: The temperature contours at surface of Lake Köyceğiz after 2 days (November).

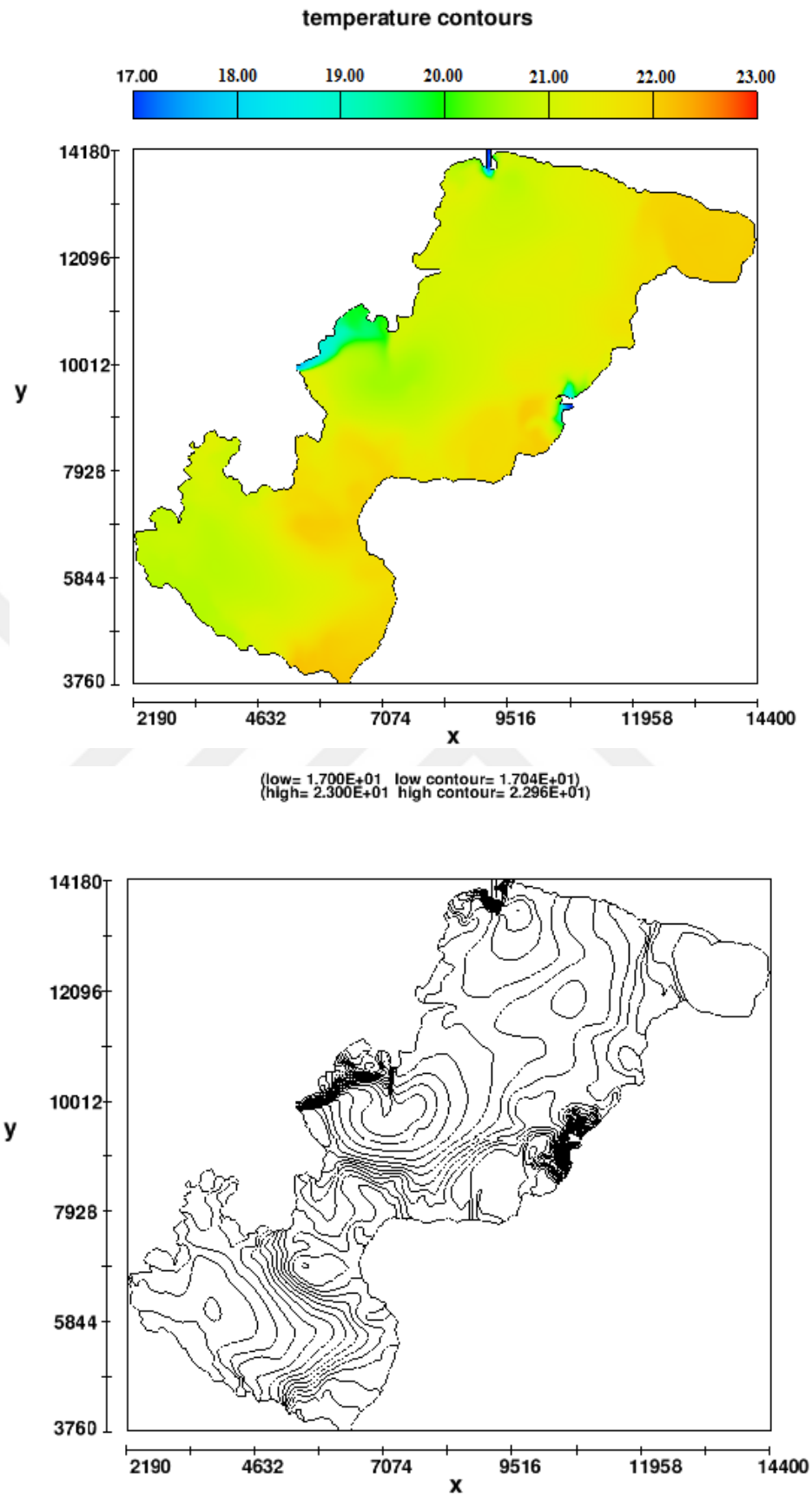

Figure 5.64: The temperature contours at surface of Lake Köyceğiz after 7 days (November).

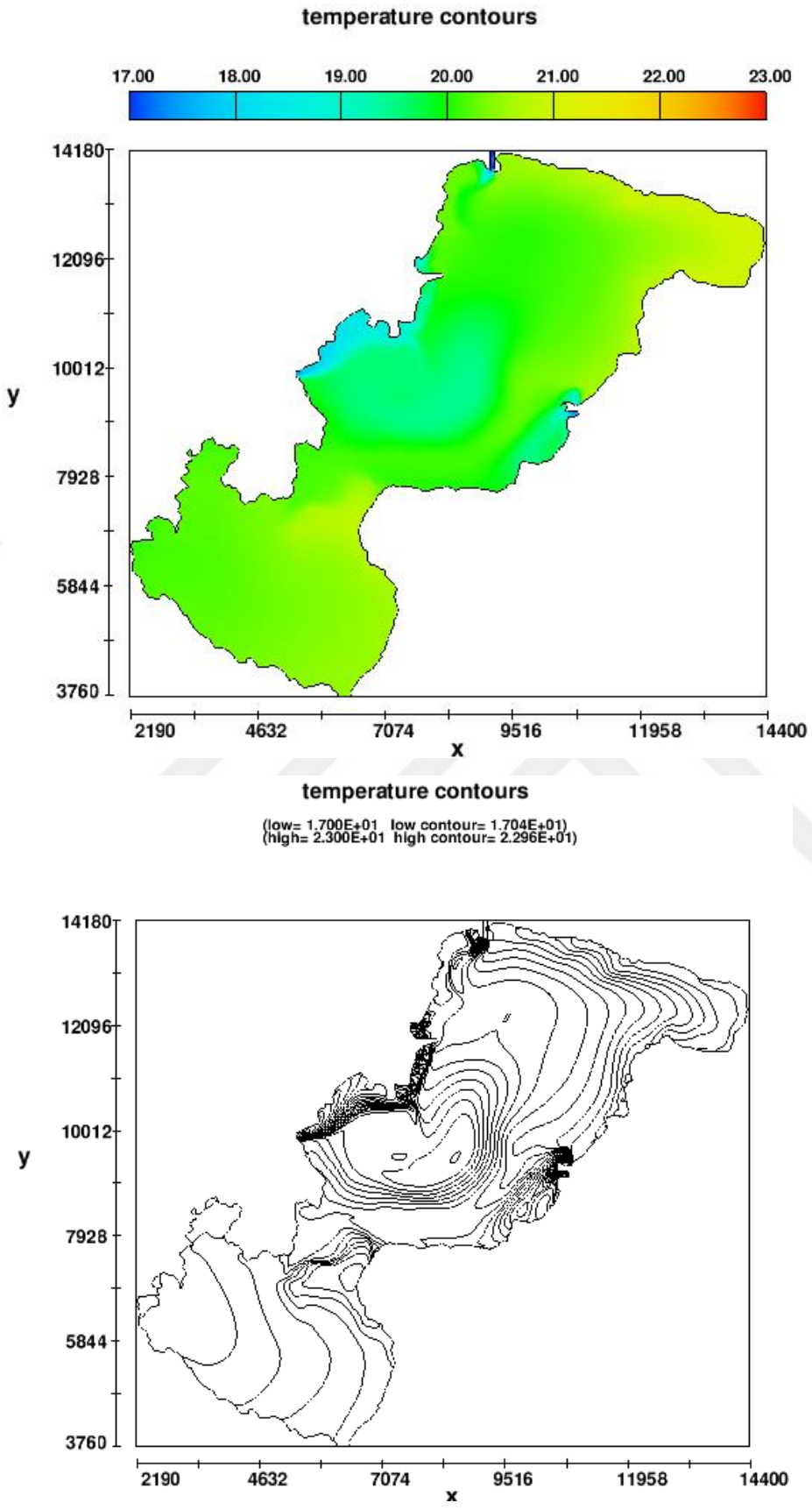

Figure 5.65: The temperature contours at surface of Lake Köyceğiz after 14 days (November).

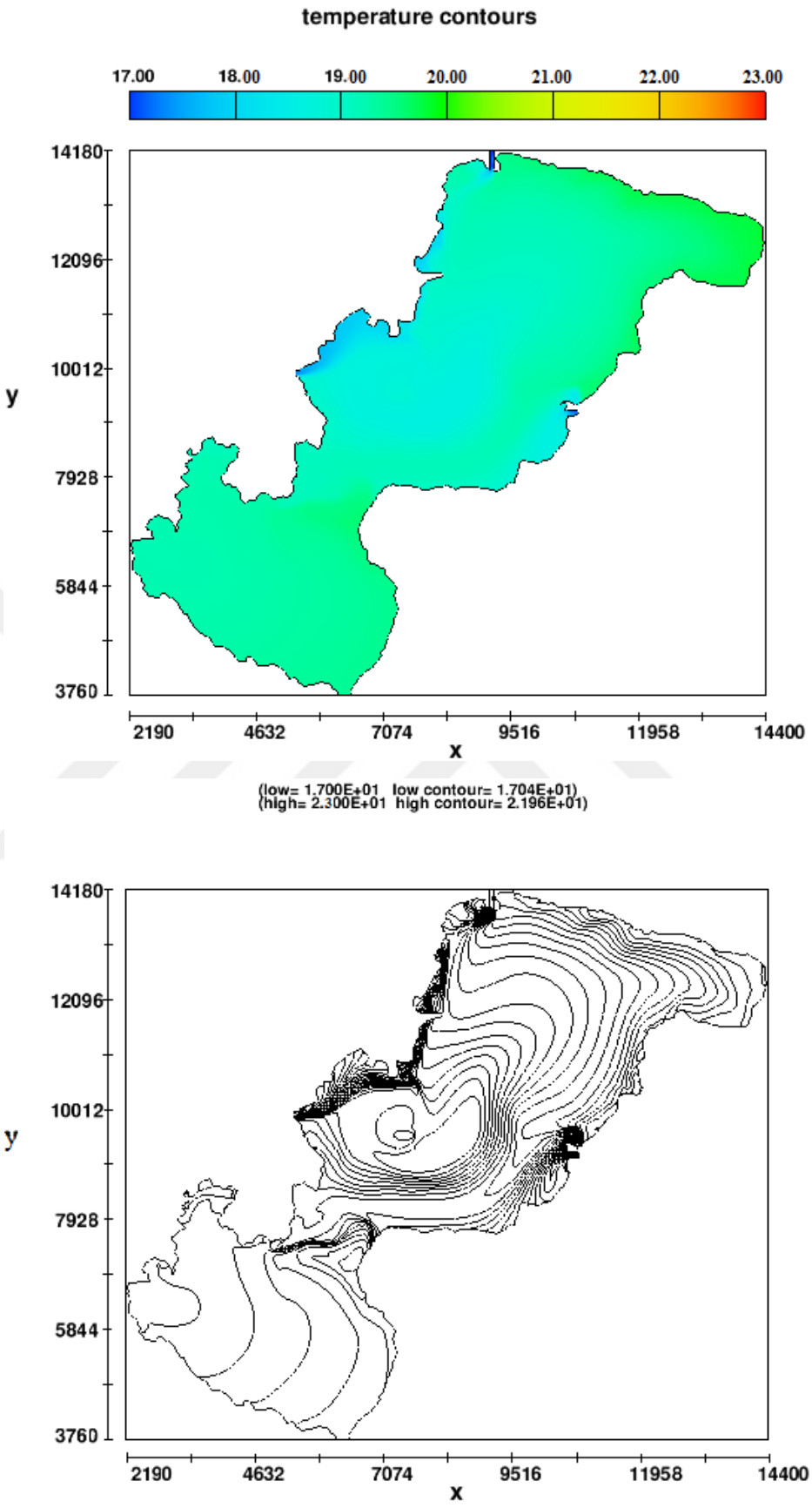

Figure 5.66: The temperature contour at surface of Lake Köyceğiz after 18 days (November).

The salinity changes for November is represented as the following figures.the cross-sections for each of Köyceğiz and sultaniye parts are displayed for the deepest area of these parts.

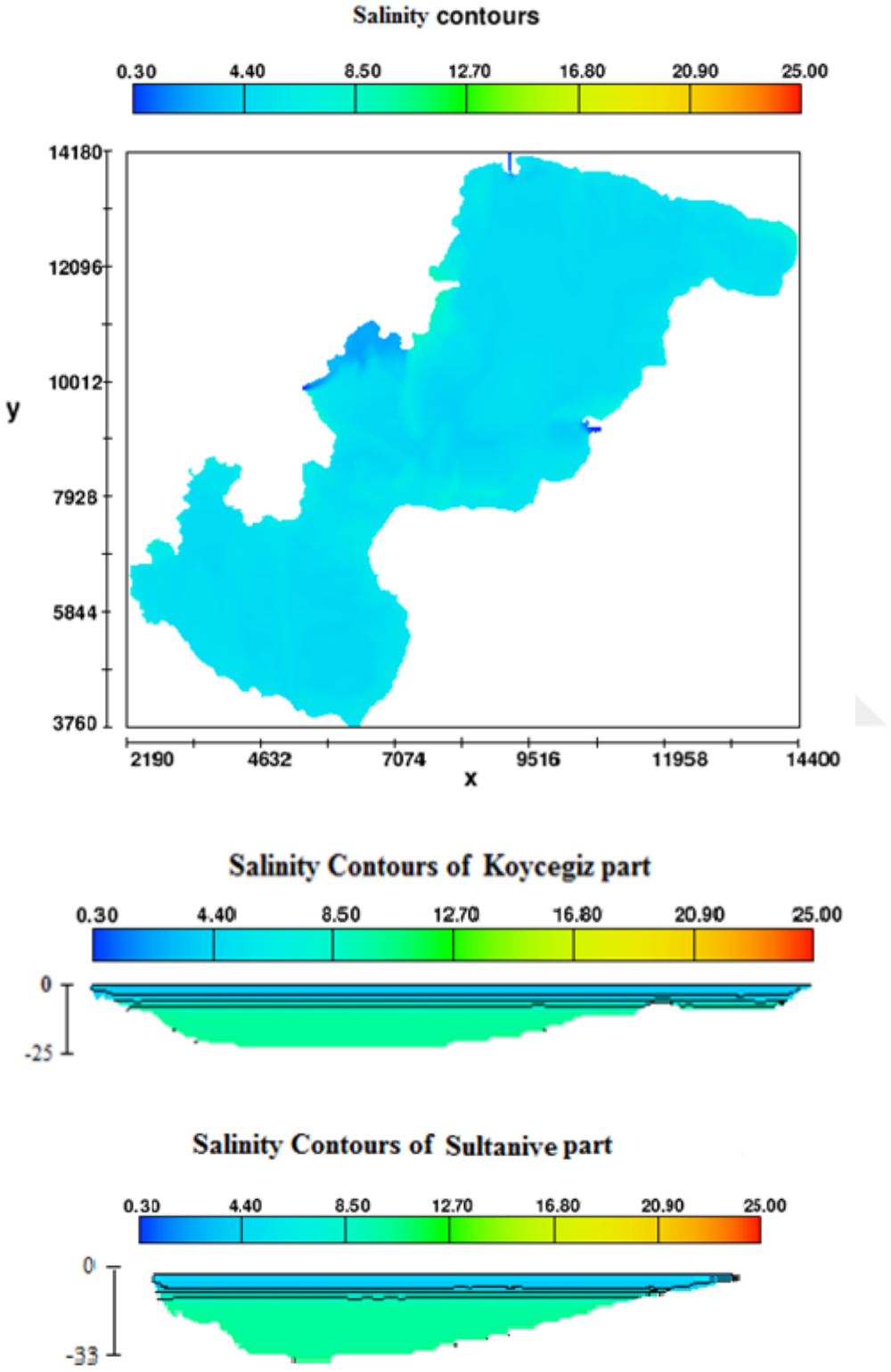

Figure 5.67: The Salinity color shaded contours of Lake Köyceğiz after 2 days (November).

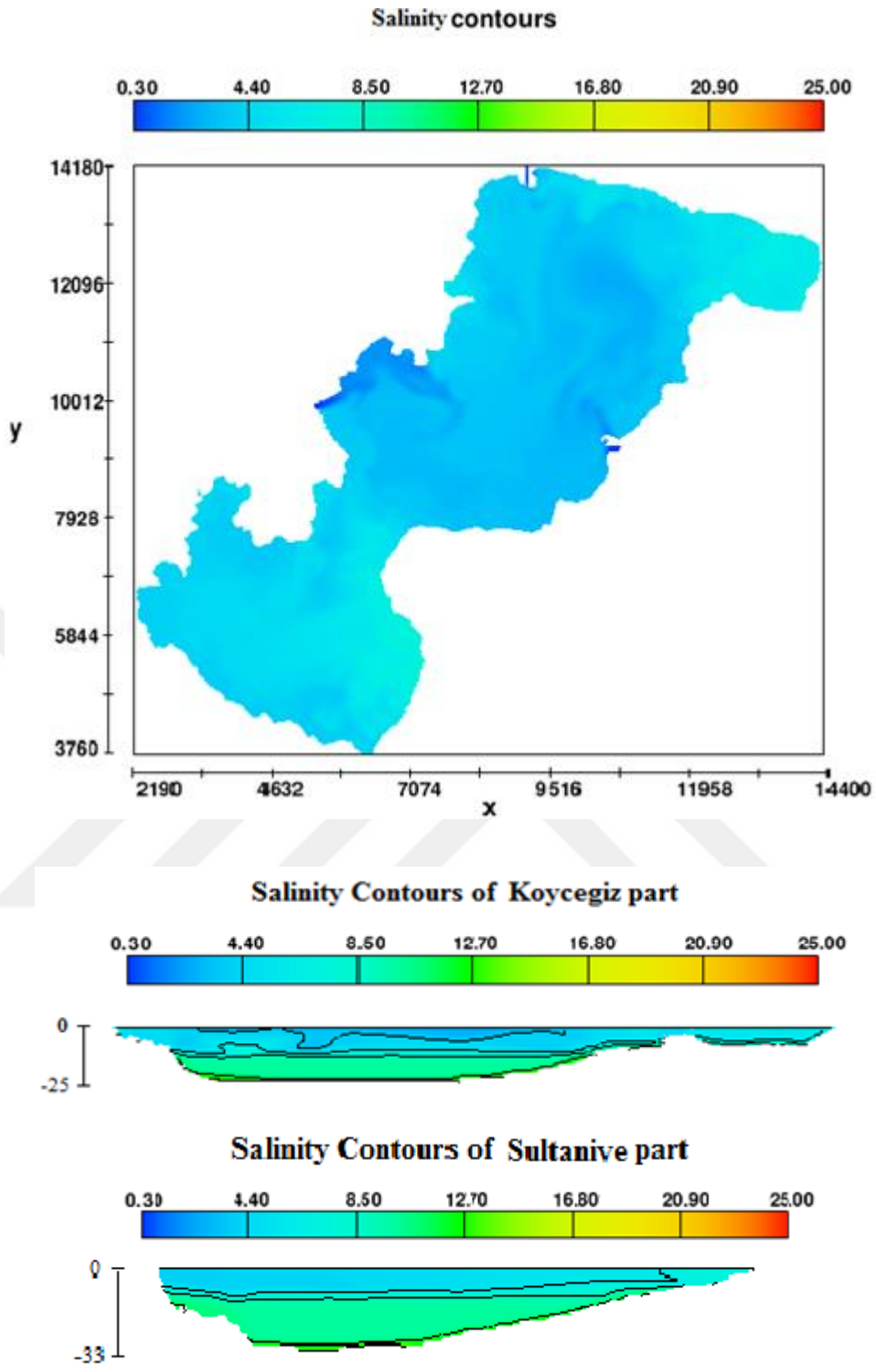

Figure 5.68: The Salinity color shaded contours of Lake Köyceğiz after 7 days (November).

After 7 days, the reduction of salinity under the effect of the low salanity of Namnam river is visible. This reduction of salinity in Köyceğiz part is more than the Sultaniye part.

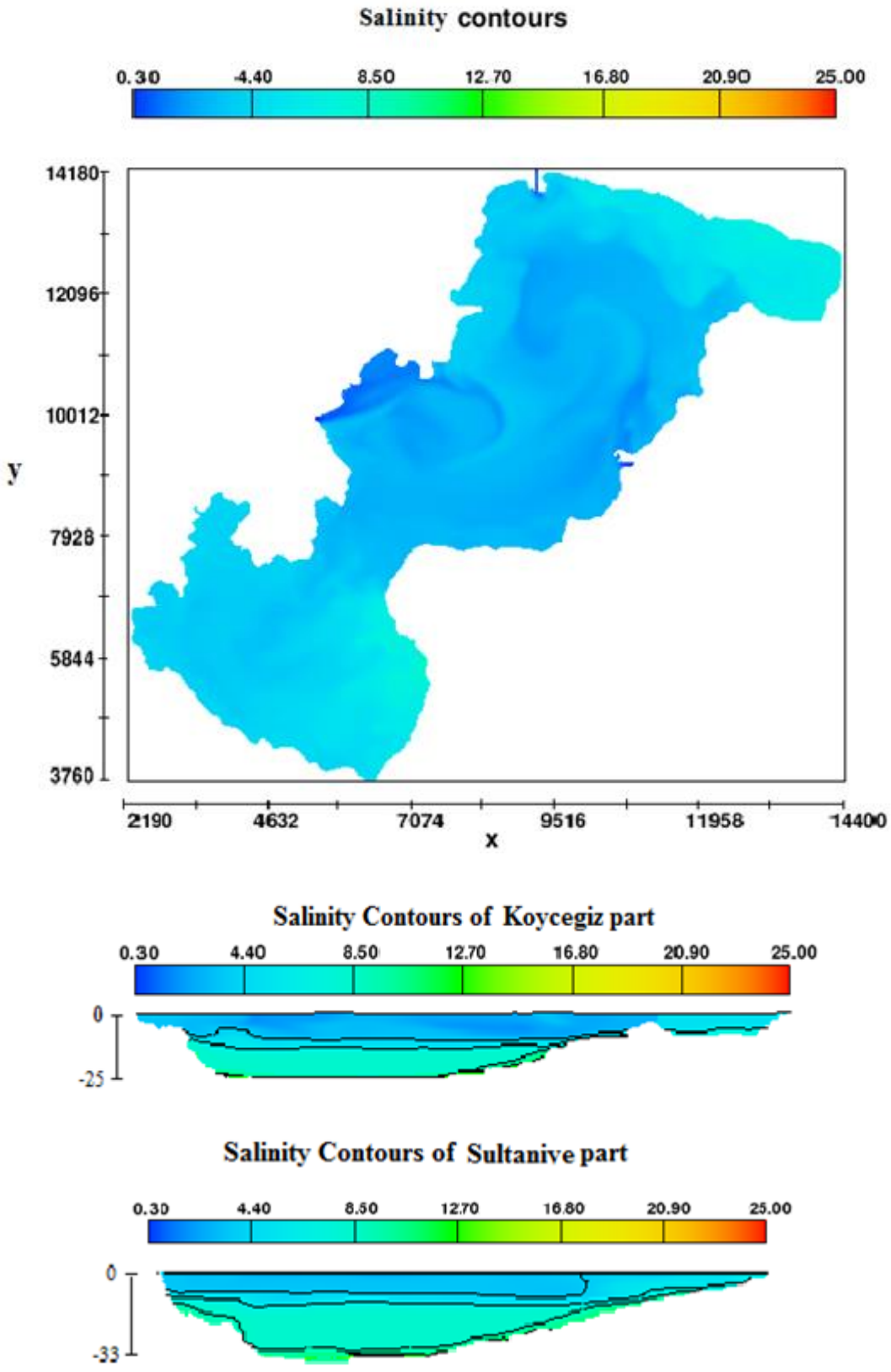

Figure 5.69: The Salinity color shaded contours of Lake Köyceğiz after 14 days (November).

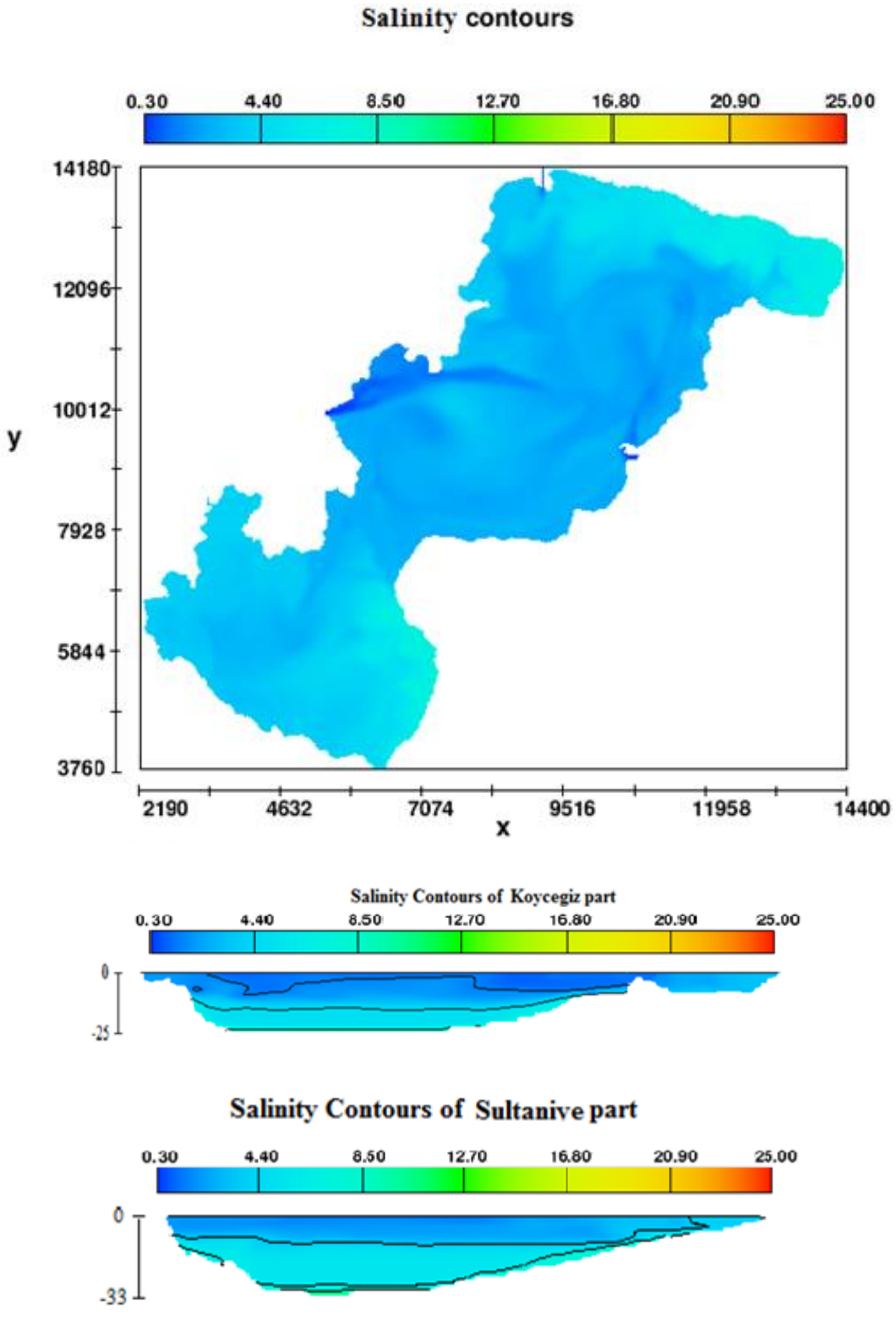

Figure 5.70: The Salinity color shaded contours of Lake Köyceğiz after 18 days (November).

Available data for Lake Köyceğiz and its streams were applied for the simulation for November and the results for December were obtained, approximately. These results are represented in the following figures for December.

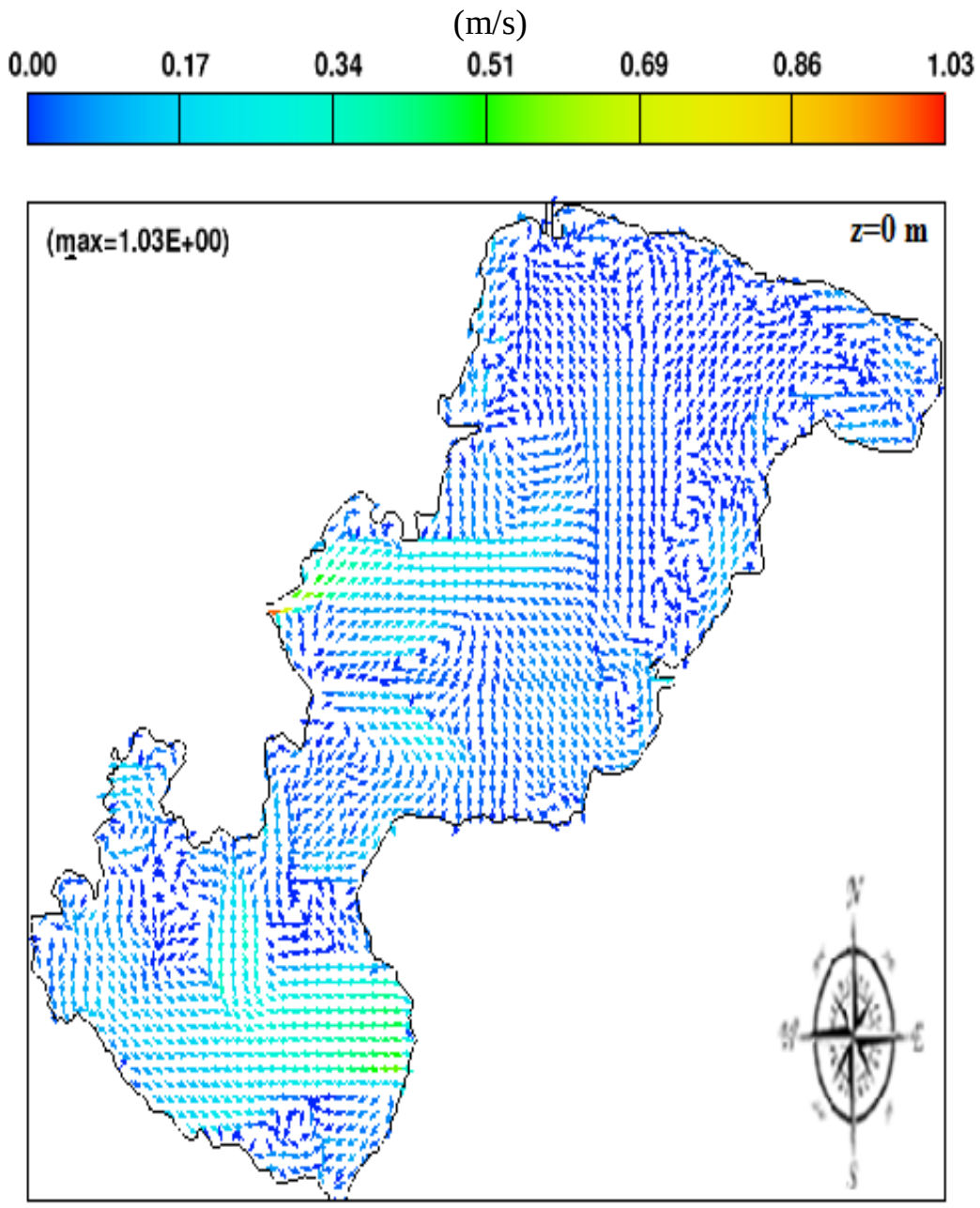

Figure 5.71: The velocity vectors colored by 2D velocity magnitude for z=0 m after 2 days (December).

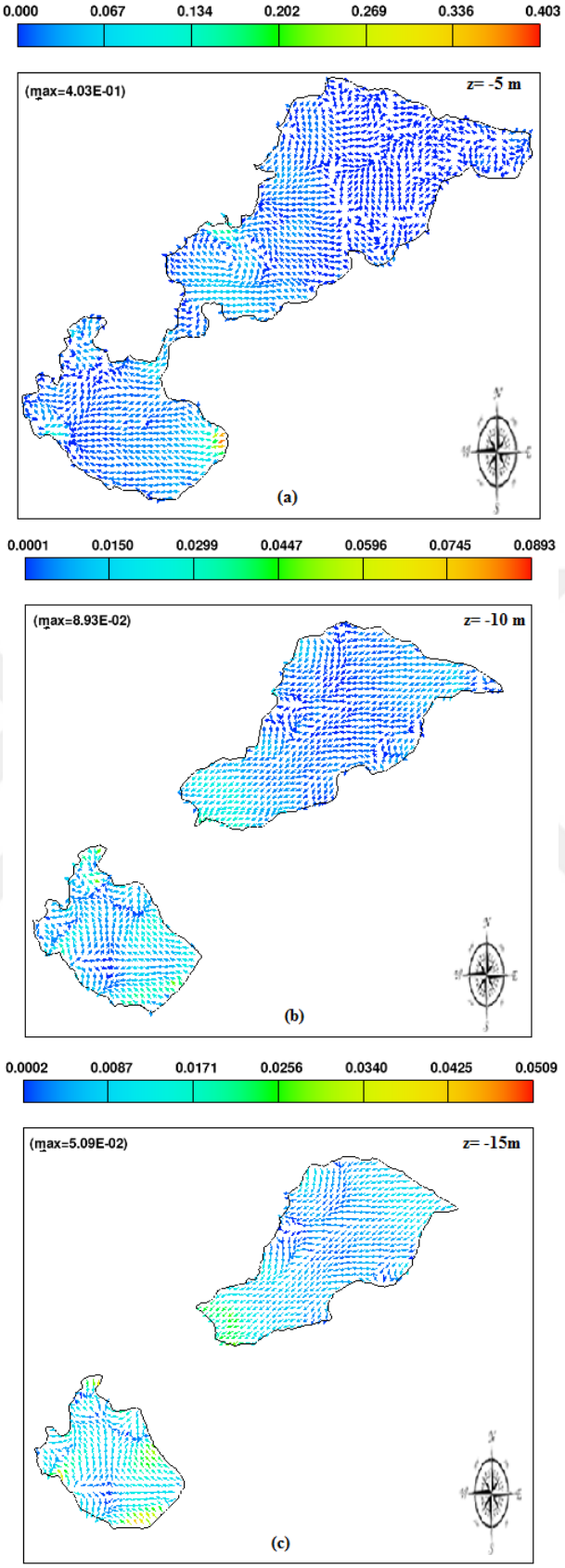

Figure 5.72: The velocity vectors colored by 2D velocity magnitude after 2 days (December): a) -5 m, b) -10 m, c) -15 m.

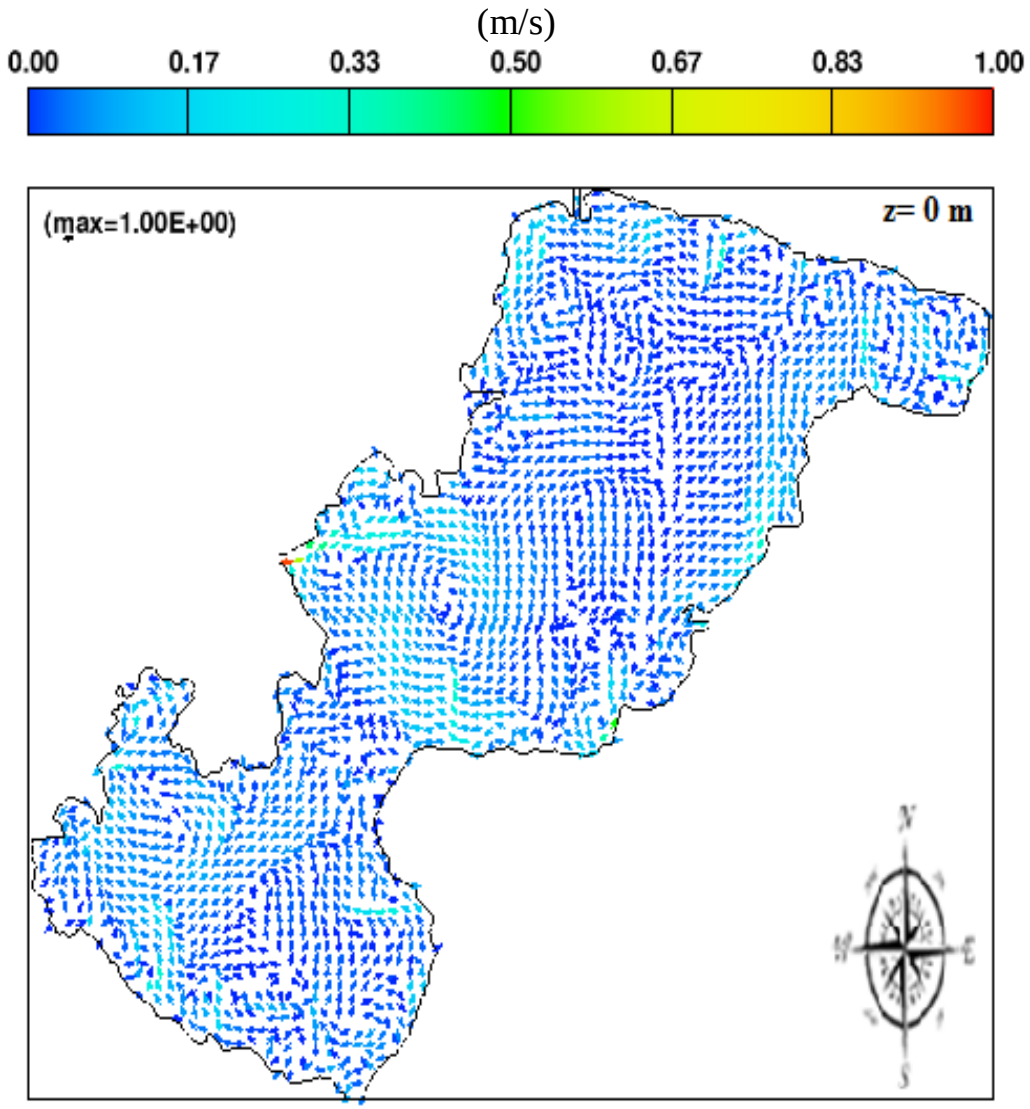

Figure 5.73: The velocity vectors colored by 2D velocity magnitude for z=0 m after 7 days (December).

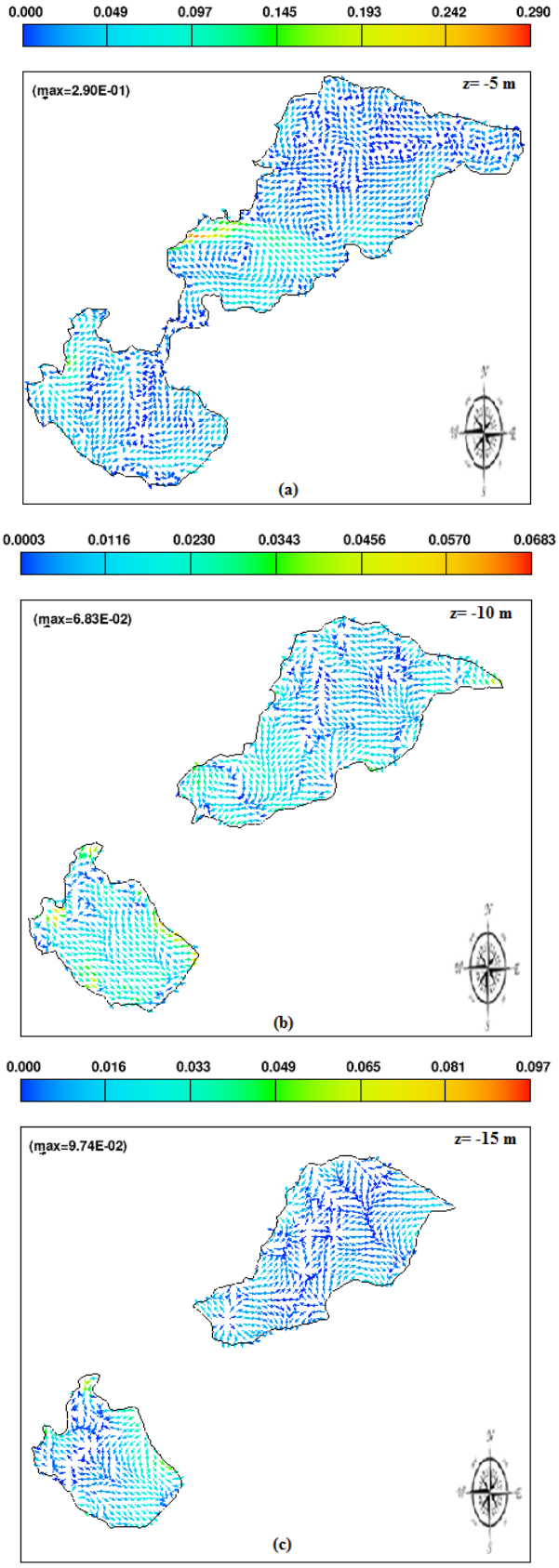

Figure 5.74: The velocity vectors colored by 2D velocity magnitude after 7 days (December): a) -5 m, b) -10 m, c) -15 m.

In December , the discharge of Namnam river increases. Therefore, this high amount of discharge from Namnam river strongly affects the velocity rate and its direction. In Figure 5.75, this state is obvious.

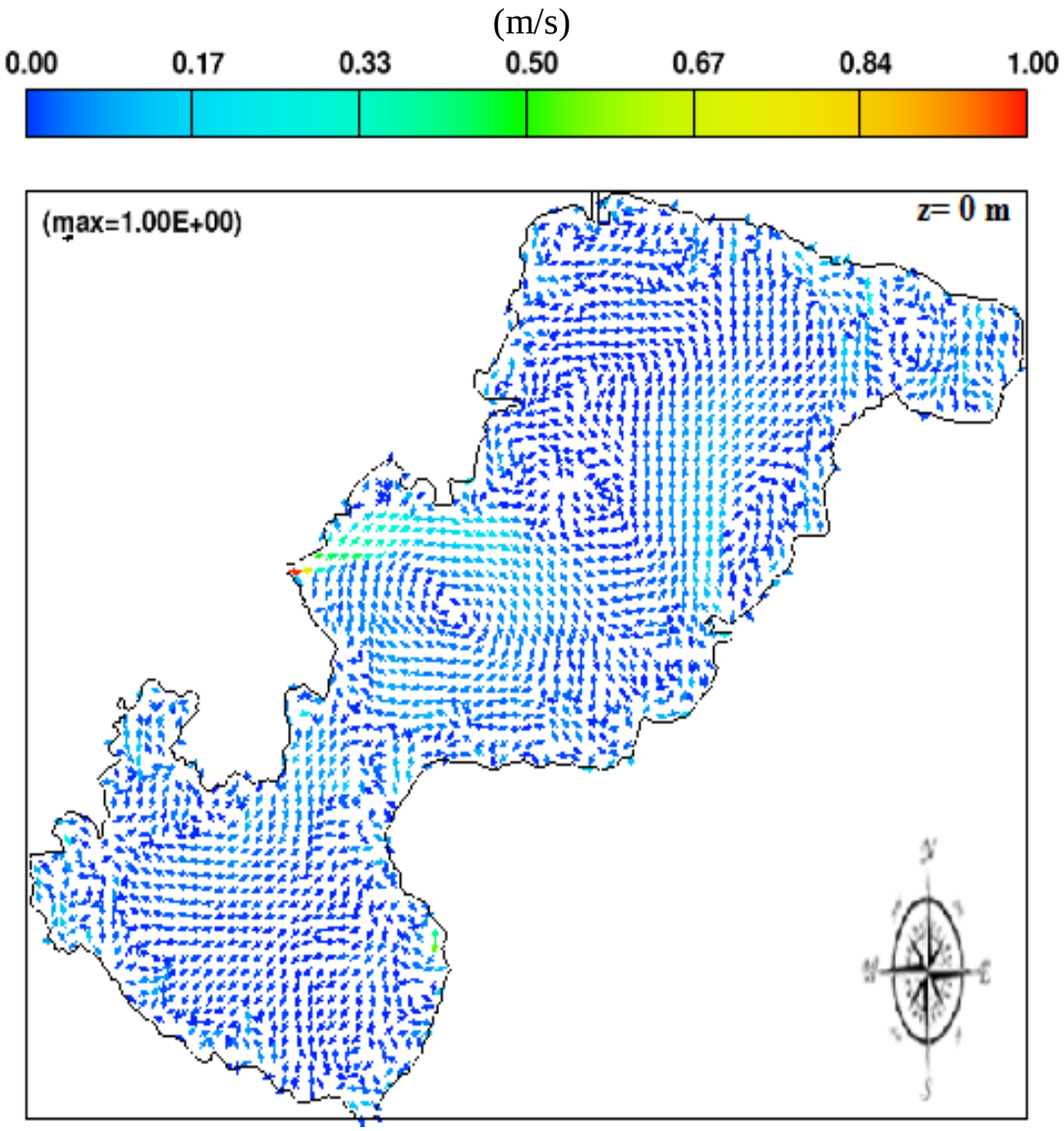

Figure 5.75: The velocity vectors colored by 2D velocity magnitude for z=0 m after 14 days (December).

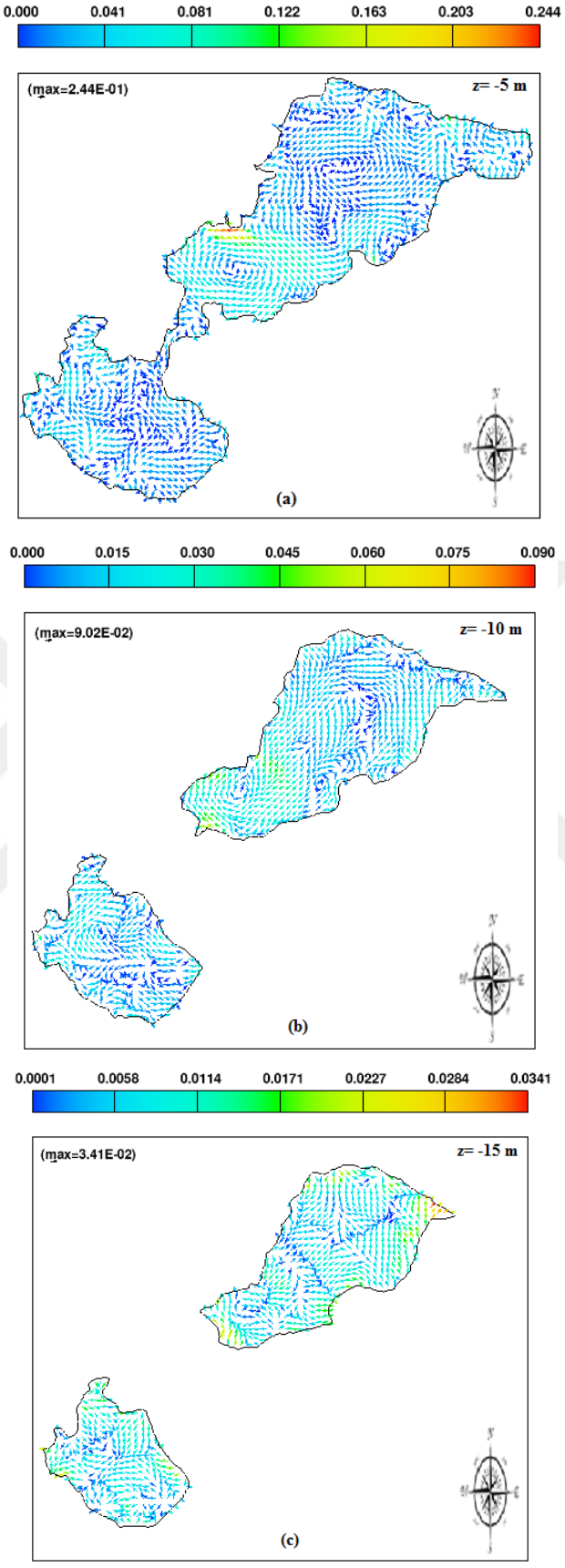

Figure 5.76: The velocity vectors colored by 2D velocity magnitude after 14 days (December): a) -5 m, b) -10 m, c) -15 m.

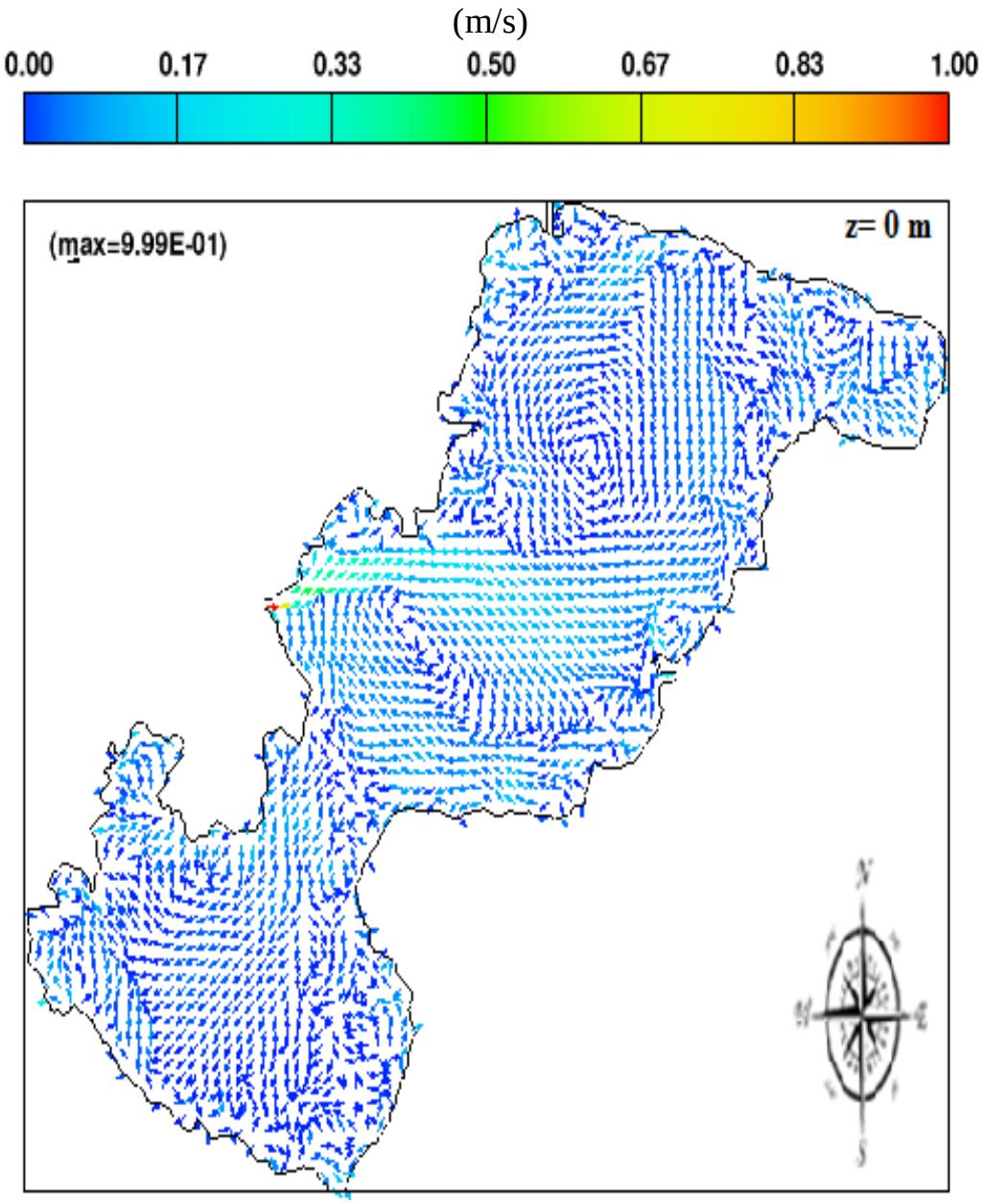

Figure 5.77: The velocity vectors colored by 2D velocity magnitude for z=0 m after 18 days (December).

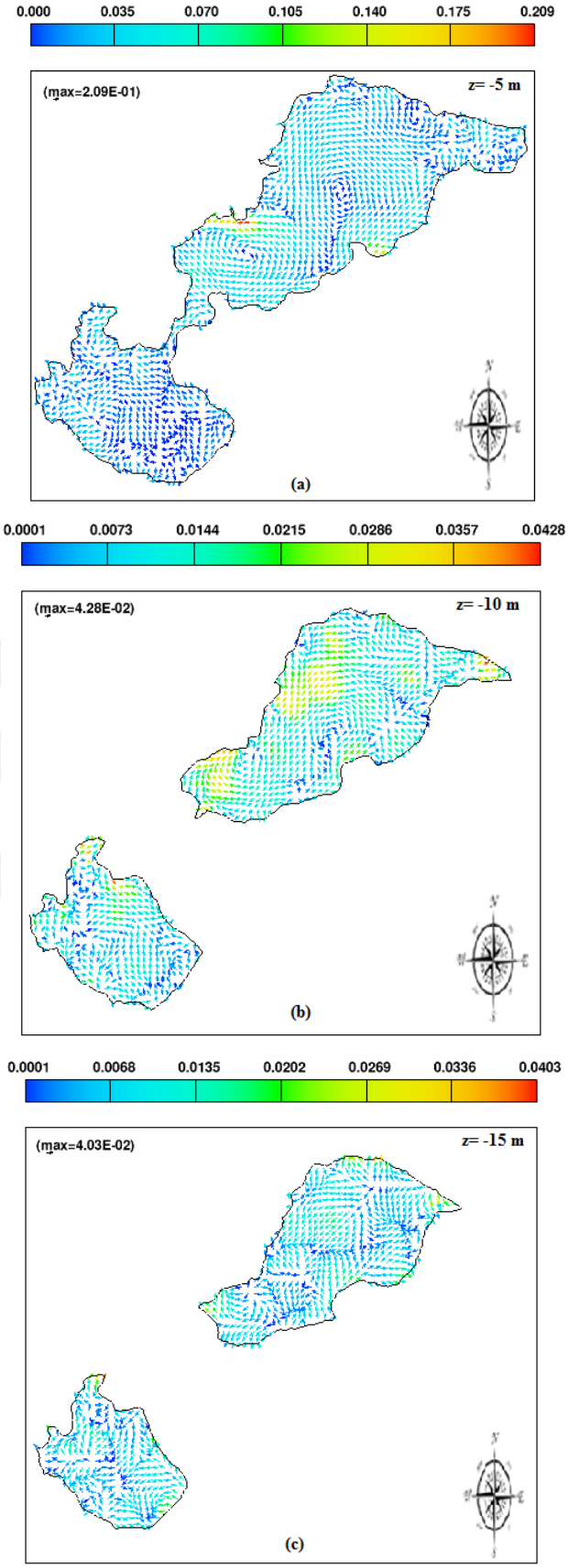

Figure 5.78: The velocity vectors colored by 2D velocity magnitude after 18 days (December): a) -5 m, b) -10 m, c) -15 m.

Temperature color shaded contours related to December, are shown as Figures 5.79, 5.80, 5.81 and 5.82 for Lake Köyceğiz and in t=7 days, t=14 days, t=14 days and t=18 days after running the simulation.

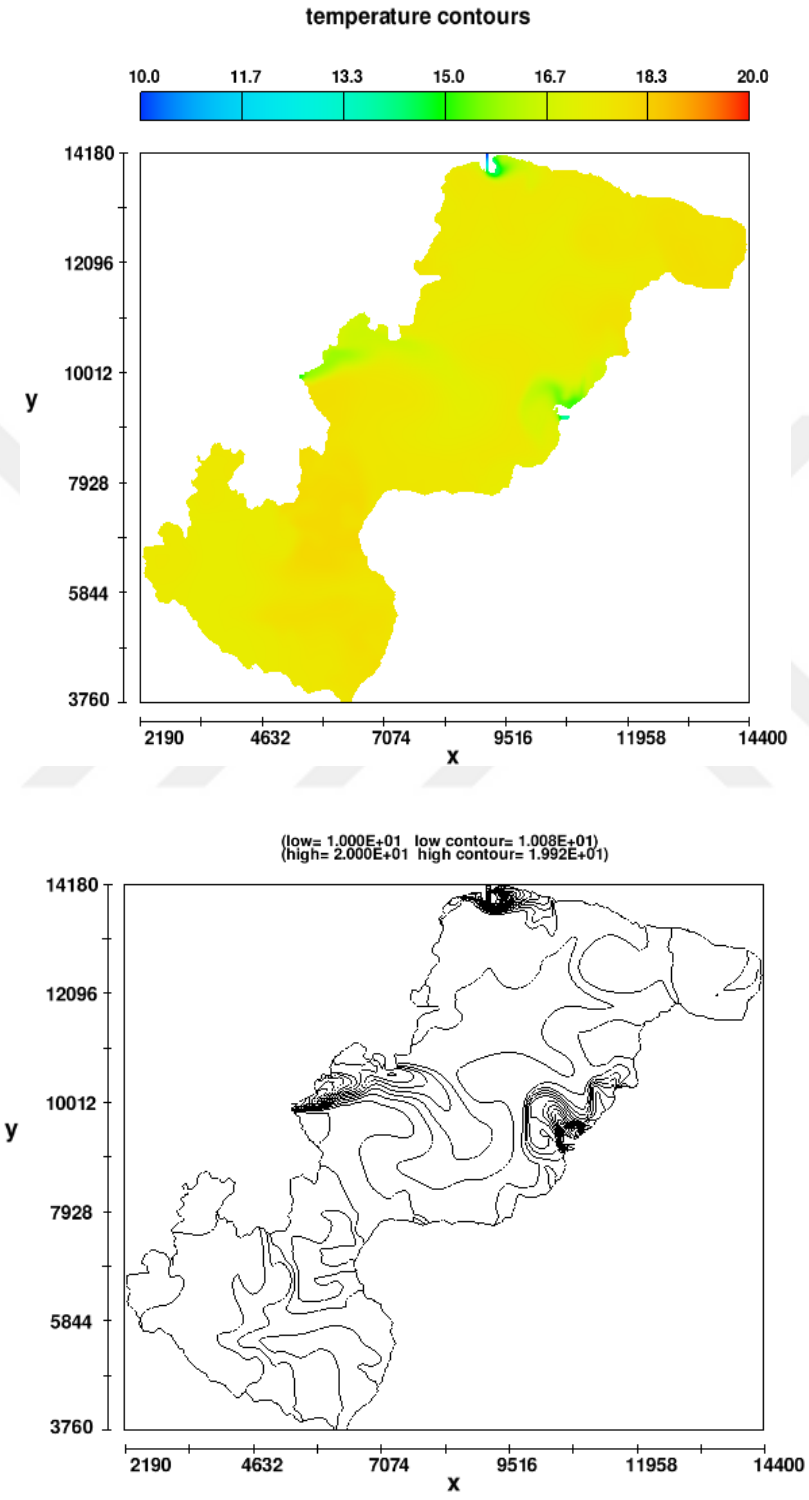

Figure 5.79: The temperature contours at surface of Lake Köyceğiz after 2 days (December).

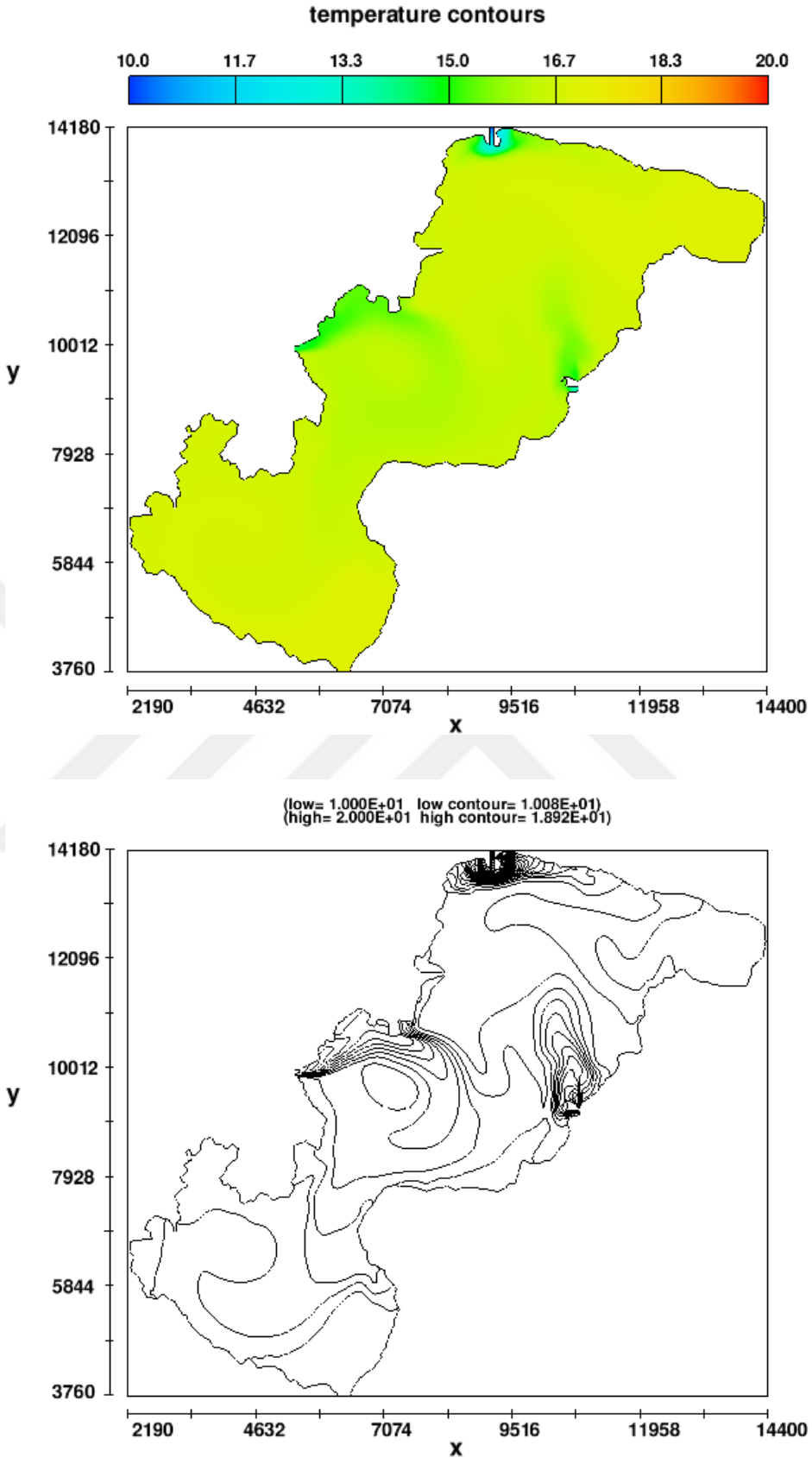

Figure 5.80: The temperature contours at surface of Lake Köyceğiz after 7 days (December).

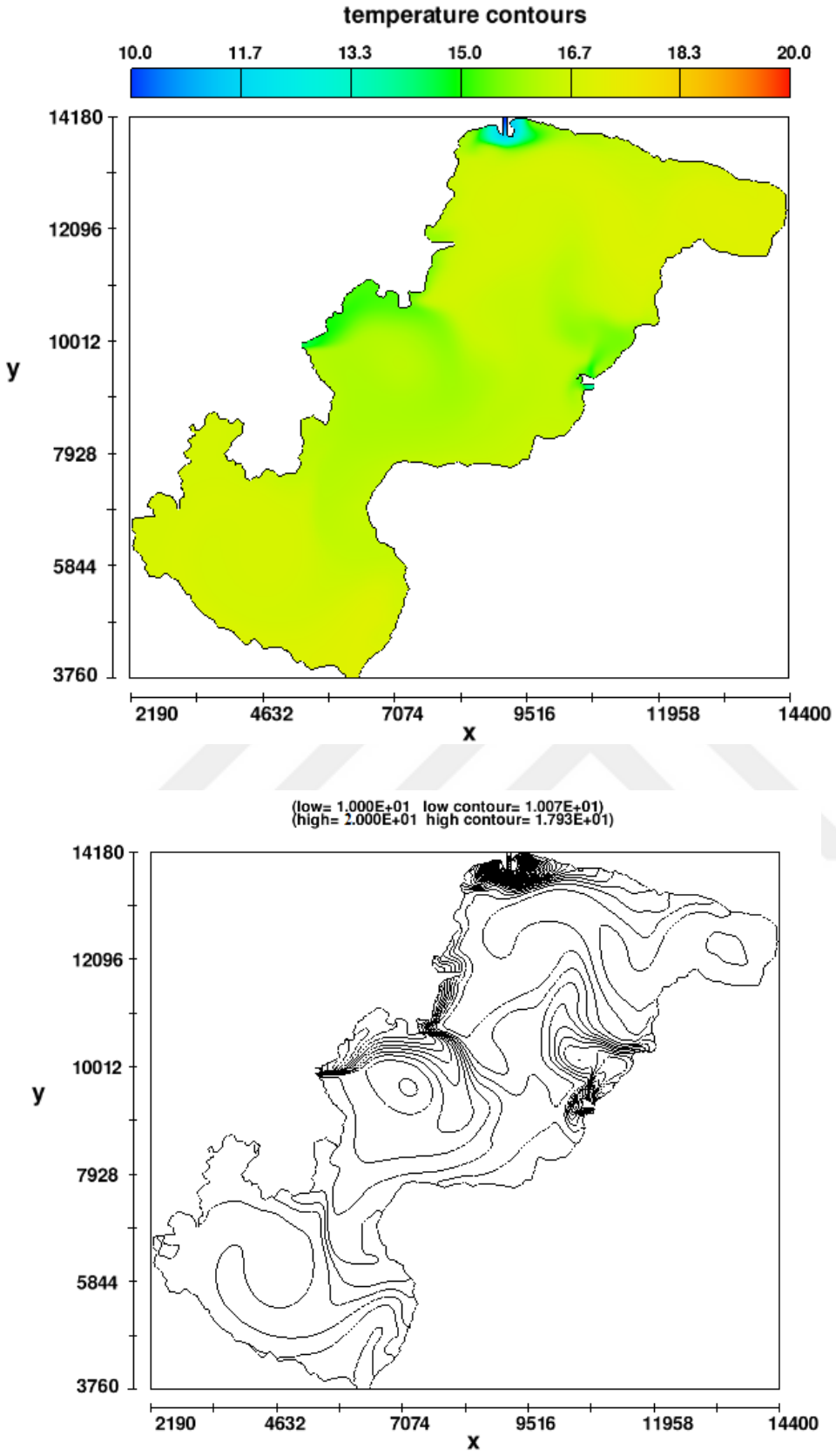

Figure 5.81: The temperature contours at surface of Lake Köyceğiz after 14 days (December).

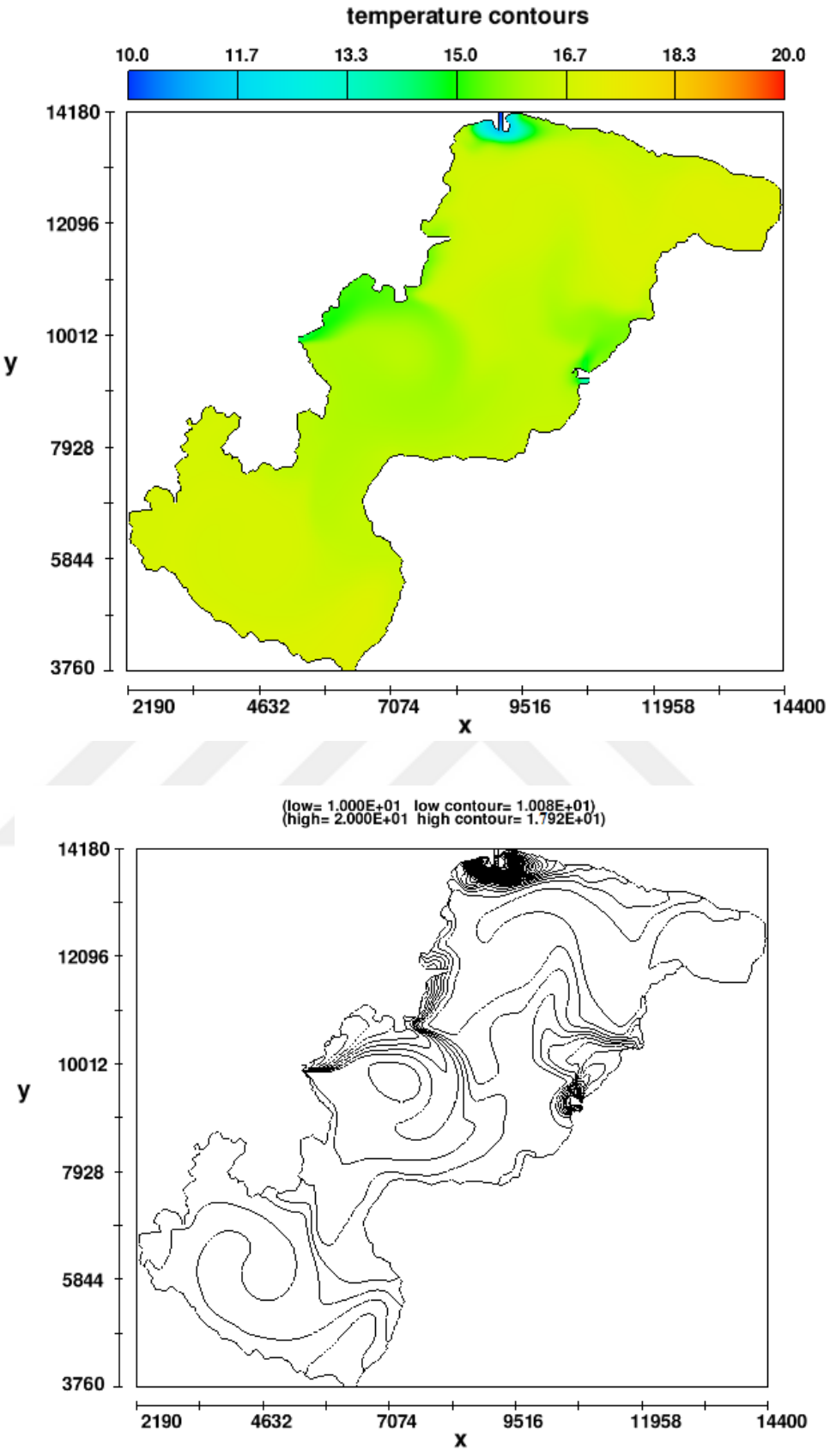

Figure 5.82: The temperature contours at surface of Lake Köyceğiz after 18 days (December).

After 18 days of simulation, Y-Z and X-Z cross-section of each Köyceğiz and Sultaniye parts are represented for showing the thermal stratification of the lake. The figures show that the inflow water has the overflow condition, which is caused by the lower density of the inflow water in comparison of the lake's water. The salinity differences between rivers and lake is one of the main parameters that caused to appearance of this condition.

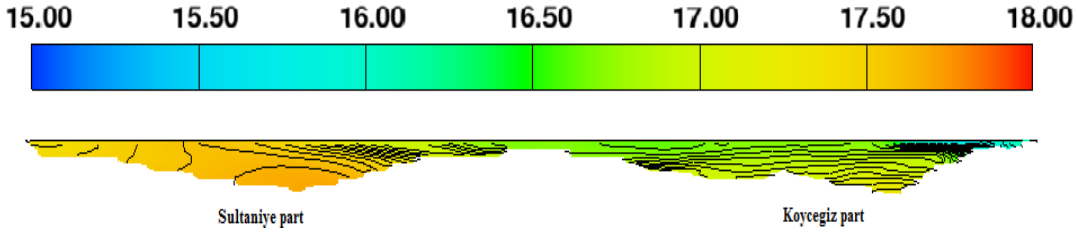

Figure 5.83: Y-Z cross-sections of Lake Köyceğiz for thermal stratification changes after 18 days (December).

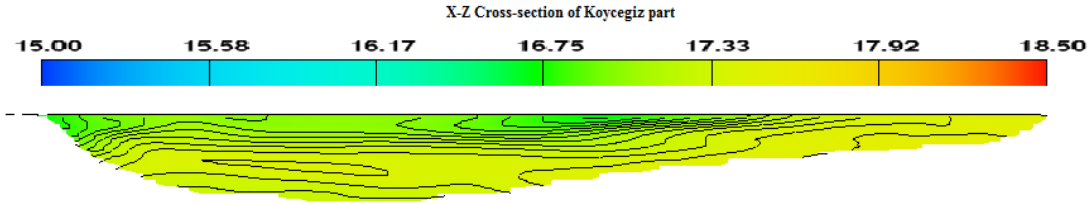

Figure 5.84: X-Z cross-sections of Köyceğiz part for thermal stratification changes after 18 days (December).

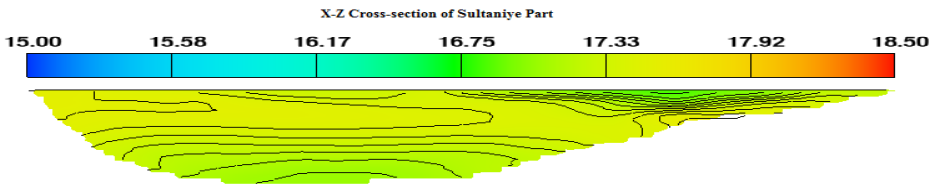

Figure 5.85: X-Z cross-sections of Sultaniye part for thermal stratification changes after 18 days (December).

Figures 5.86, 5.87, 5.88 and 5.89 represents the salinity changes after entering the water from the rivers in to Lake Köyceğiz in December. In these Figures, the salinity variations are shown in both Köyceğiz and Sultaniye parts of Lake Köyceğiz.

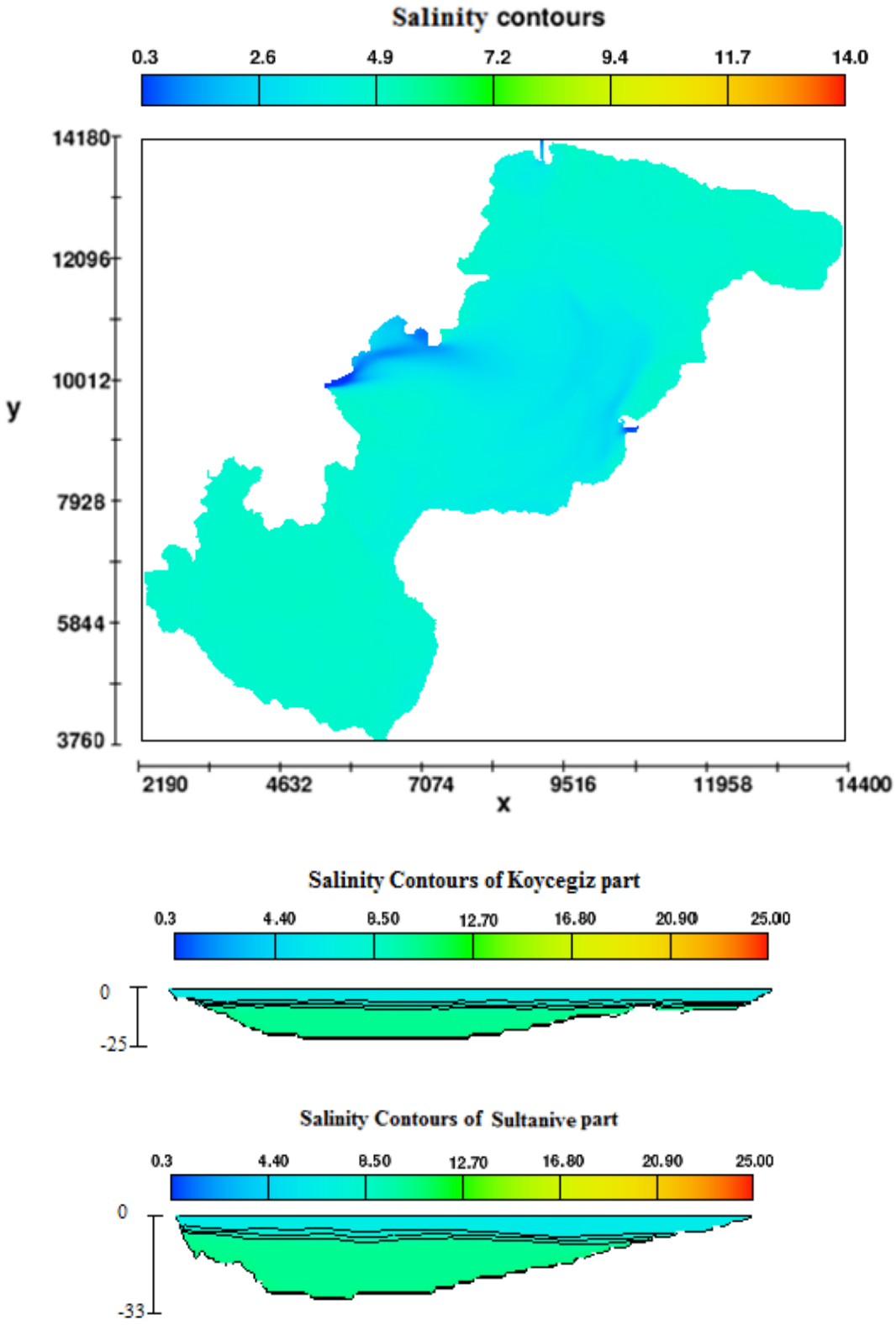

Figure 5.86: The Salinity color shaded contours of Lake Köyceğiz after 2 days (December).

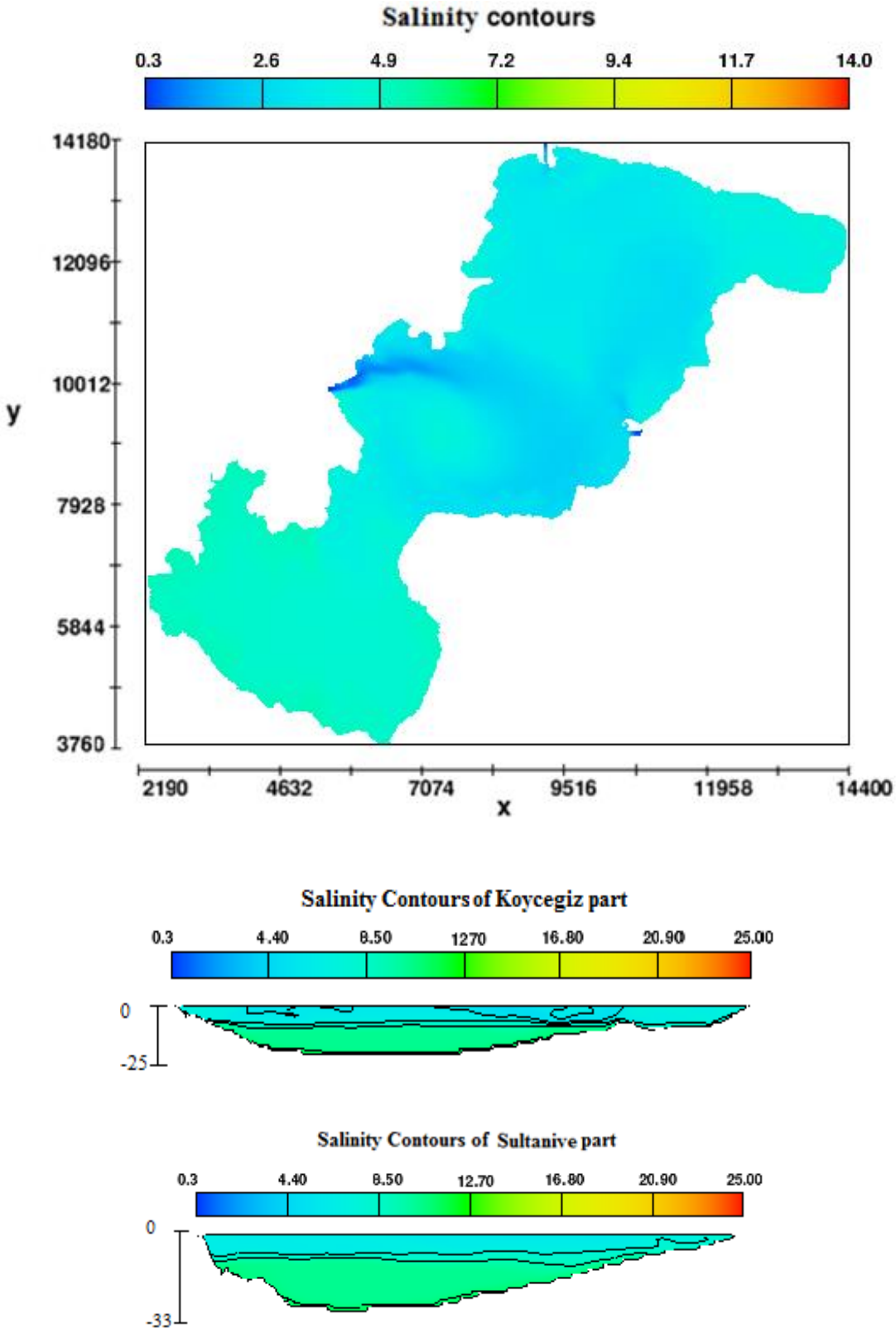

Figure 5.87: The Salinity color shaded contours of Lake Köyceğiz after 7 days (December).

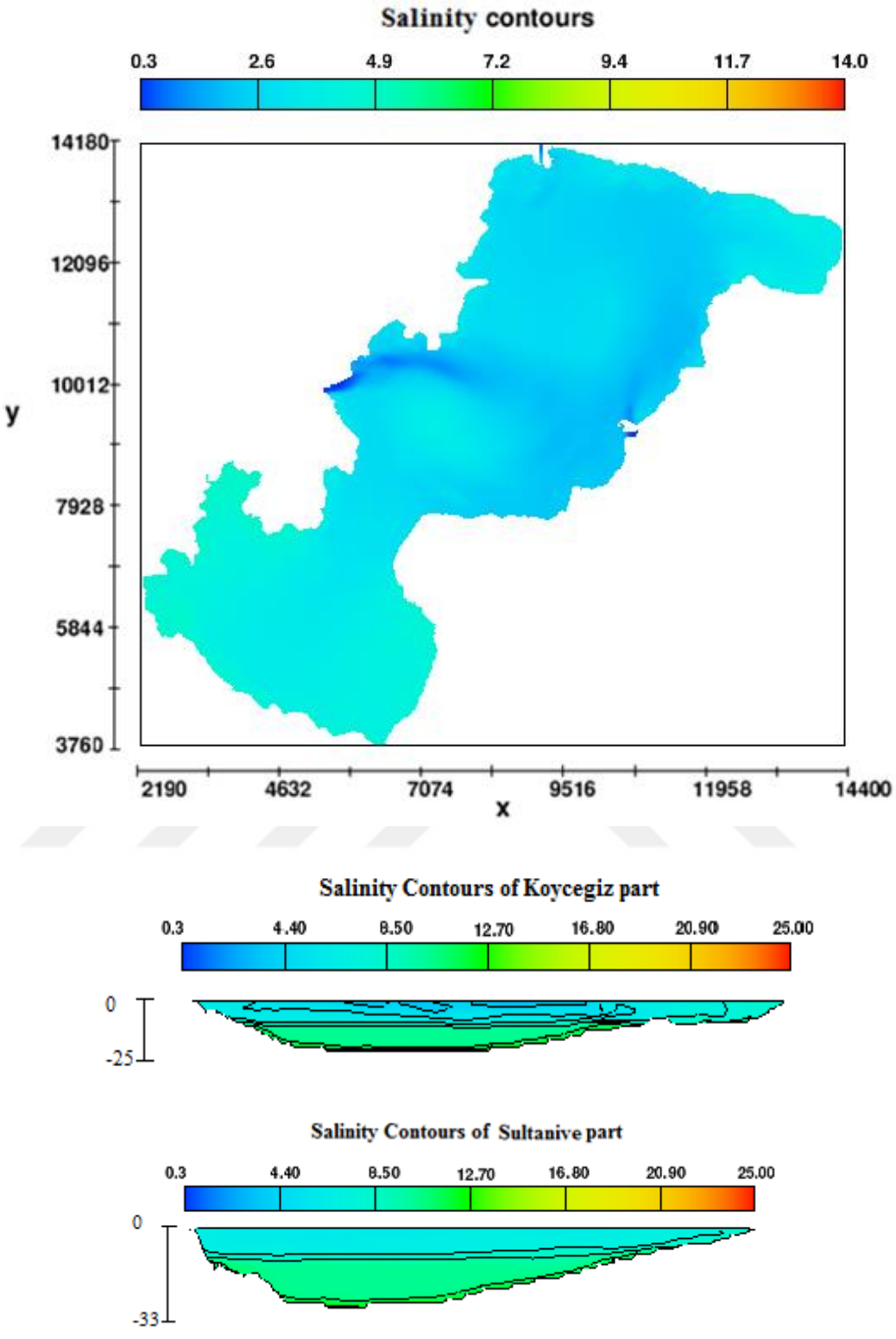

Figure 5.88: The Salinity color shaded contours of Lake Köyceğiz after 14 days (December).

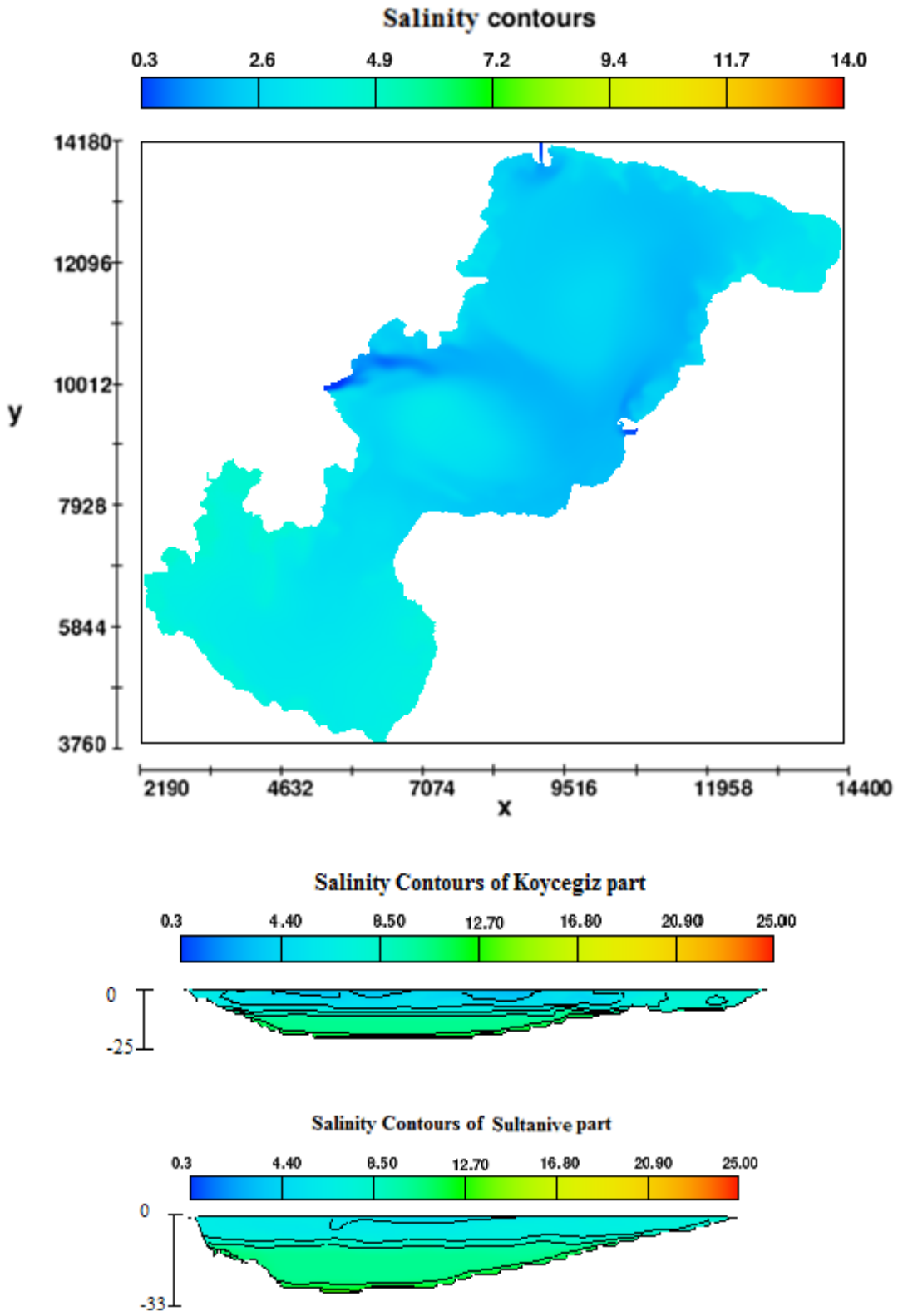

Figure 5.89: The Salinity color shaded contours of Lake Köyceğiz after 18 days (December).

A longitudinal profile (Y-Z section) of lake for salinity is represented in figure 5.87. Both the Köyceğiz and Sultaniye parts could be seen in this figure.

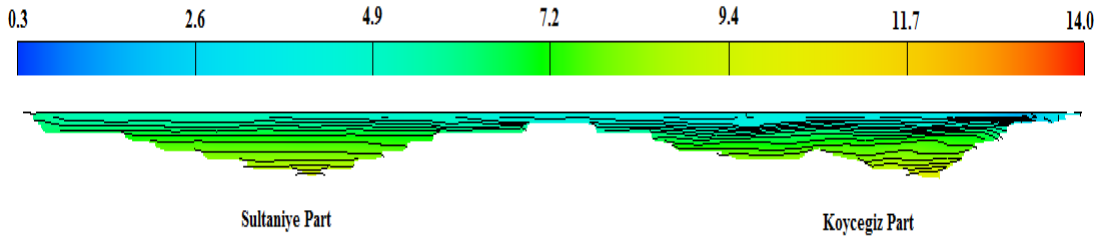

Figure 5.90: Y-Z section of Lake Köyceğiz for salinity (‰) after 18 days (December).

The salinity is decrease with entering the water with a higher value of discharge, when its salinity is lower than the lake's one. The over flow is happened in this time and the inflow water is spread and propagated in the first layers of the lake.

Results for simulation of August in Lake Köyceğiz were prepared and given as the figures that represented below.

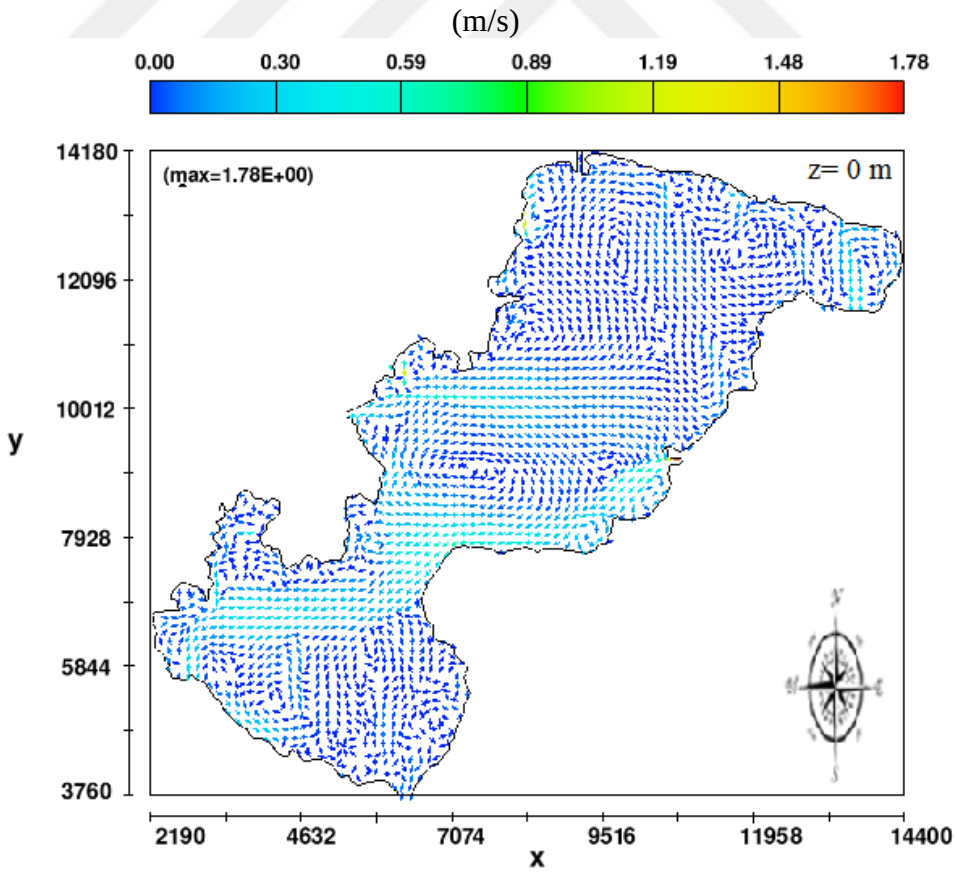

Figure 5.91: The velocity vectors colored by 2D velocity magnitude for z=0 m after 2 days (August).

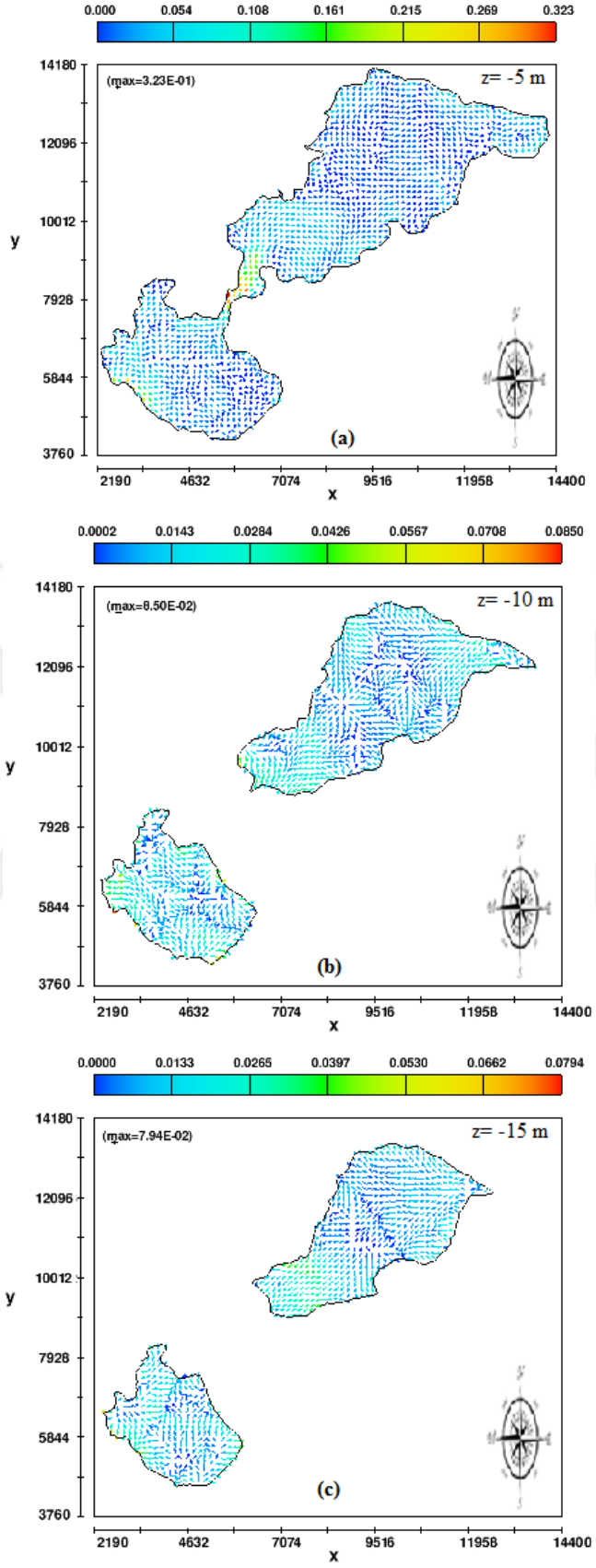

Figure 5.92: The velocity vectors colored by 2D velocity magnitude after 2 days (August): a) -5 m, b) -10 m, c) -15 m.

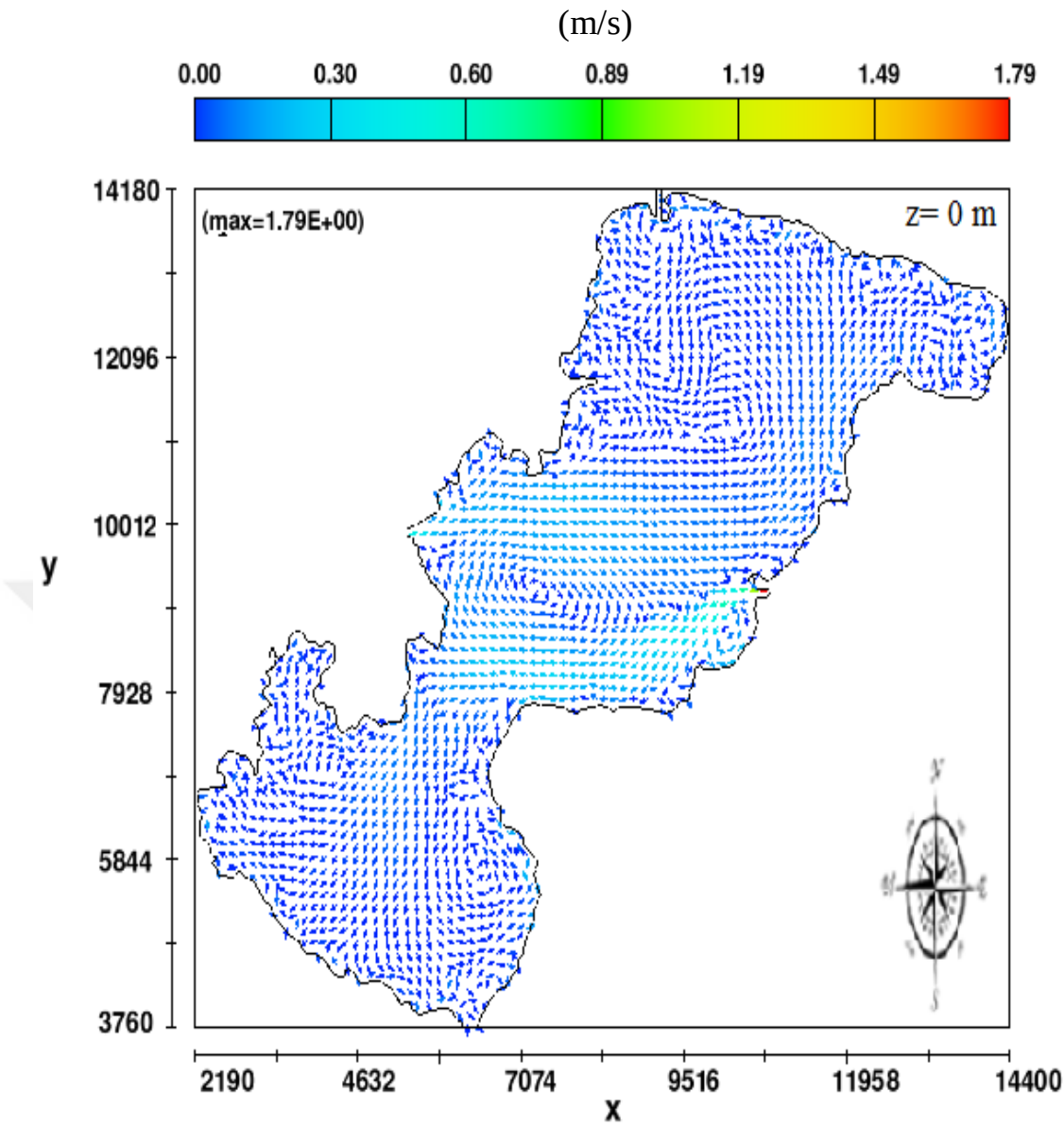

Figure 5.93: The velocity vectors colored by 2D velocity magnitude for z=0 m after 7 days (August).

As seen in Figure, 5.94, the velocity is inconsiderable in depth, and specially, after depth 15 m. This state was expected in accordance with the researches and studies that conducted previously on the Lake Köyceğiz. All researchers, which worked on this lake, believed that there is no transfer between lower layers of Lake Köyceğiz and it makes to formation of seperate layers in this lake.

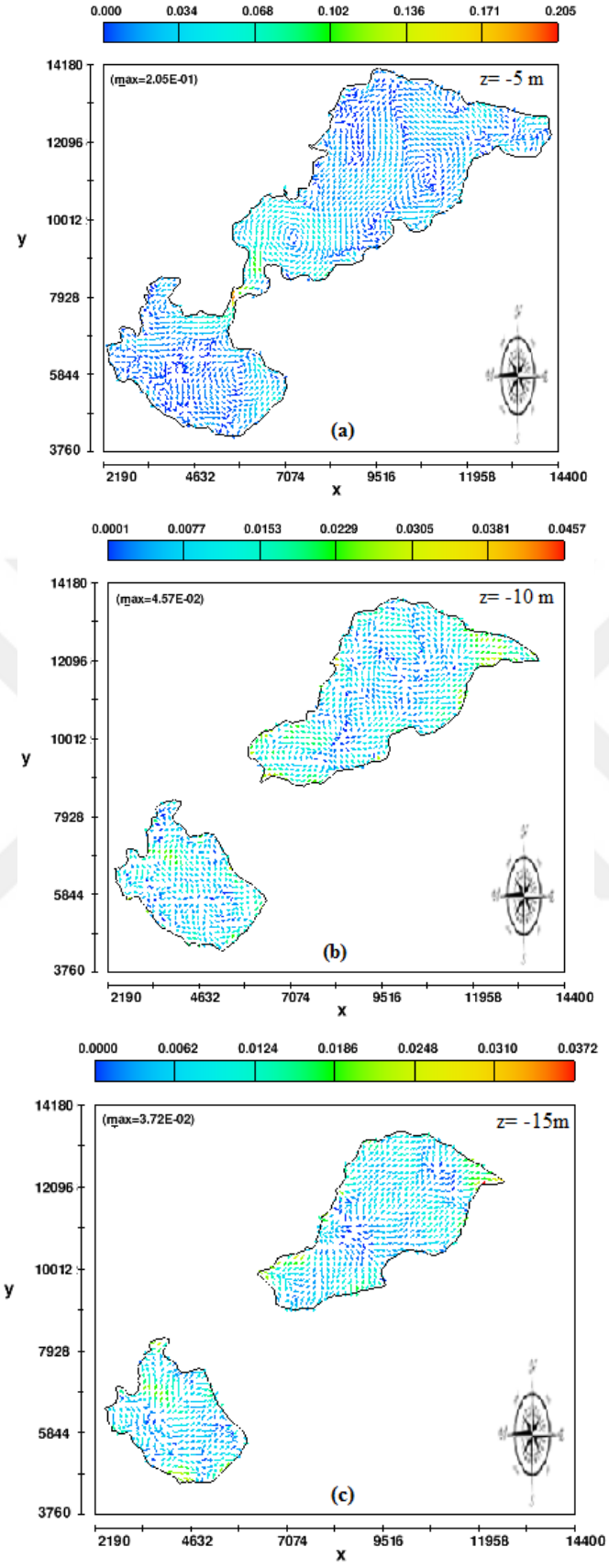

Figure 5.94: The velocity vectors colored by 2D velocity magnitude after 7 days (August): a) -5 m, b) -10 m, c) -15 m.

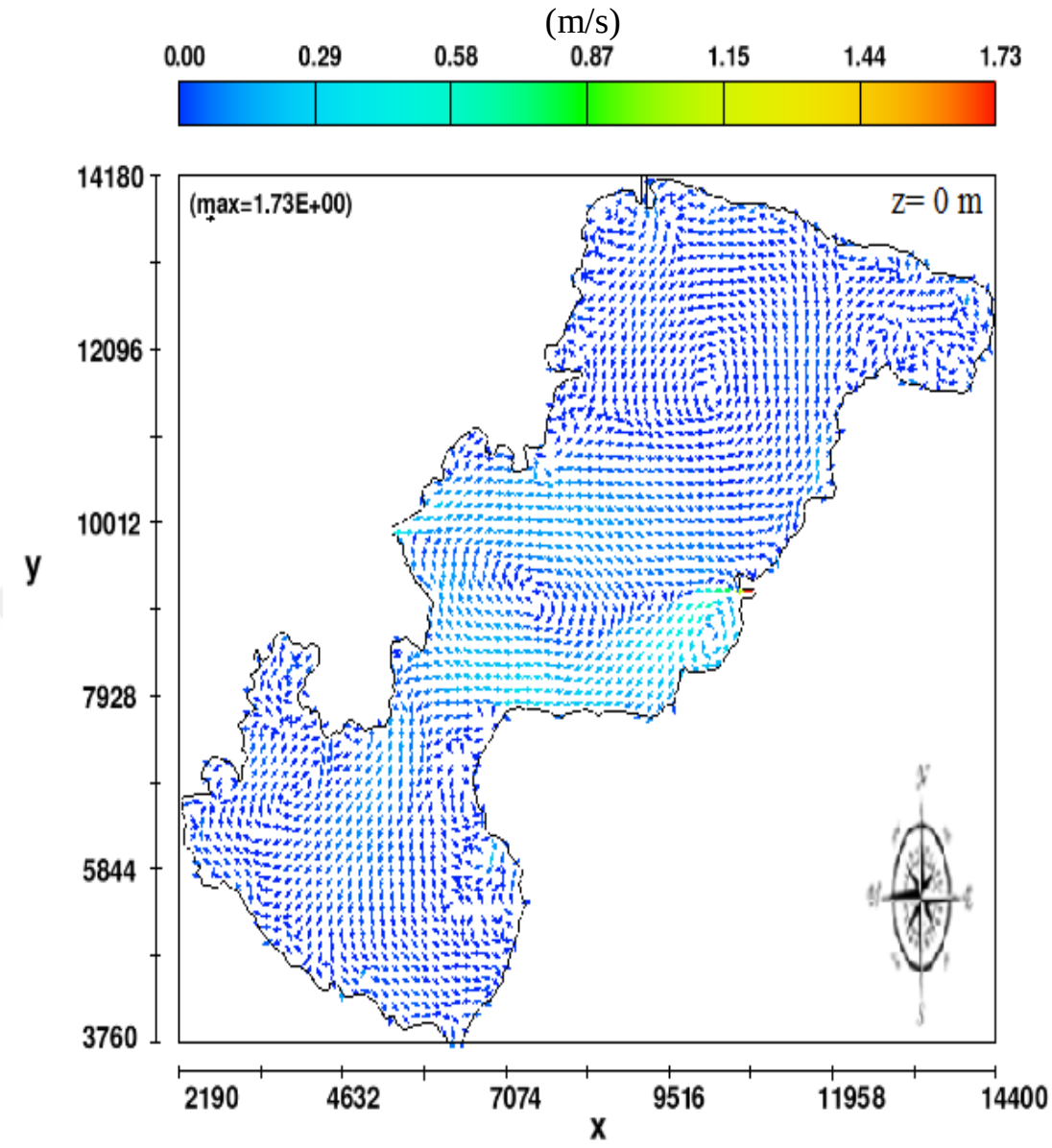

Figure 5.95: The velocity vectors colored by 2D velocity magnitude for z=0 m after 14 days (August).

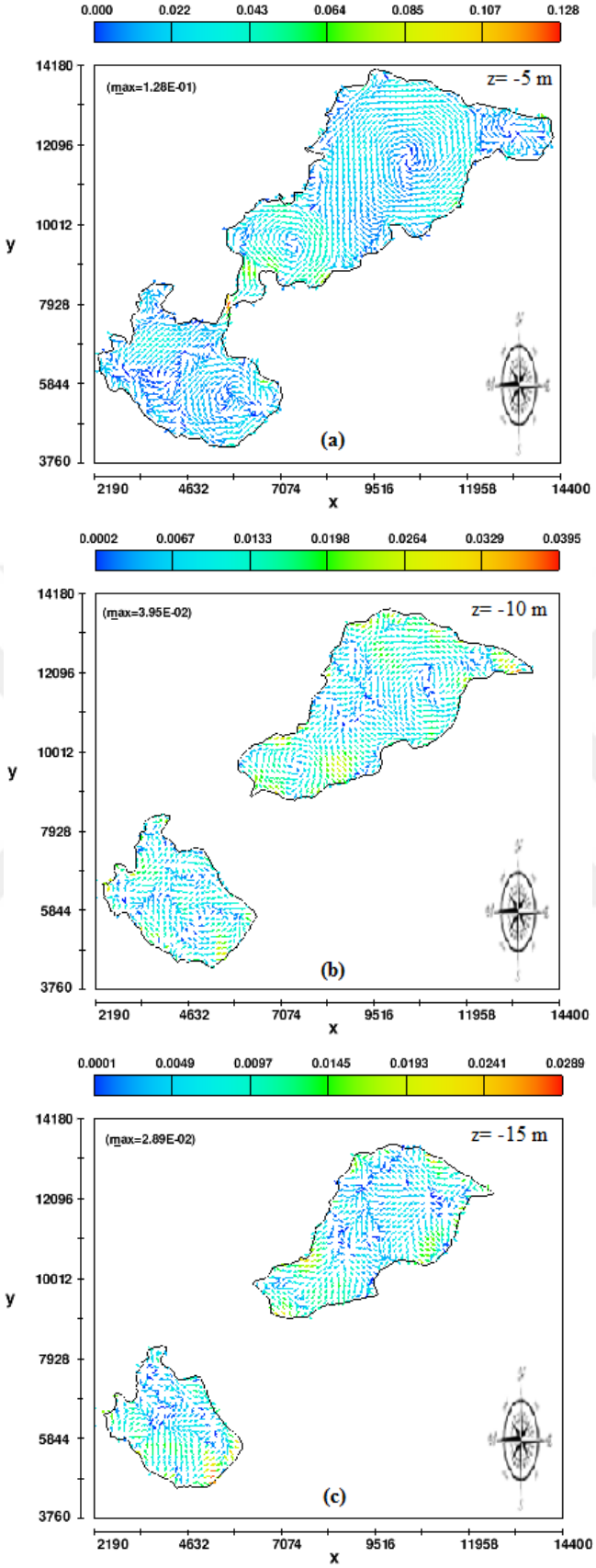

Figure 5.96: The velocity vectors colored by 2D velocity magnitude after 14 days (August): a) -5 m, b) -10 m, c) -15 m.

As it is clear from Figure 5.97, the direction of the current at Lake Köyceğiz is toward the Sultaniye hole, also Dalyan channel after 18 days. the inflow discharge from Yuvarlak river mainly affects the surface and upper layer direction of current in Lake Köyceğiz in August.

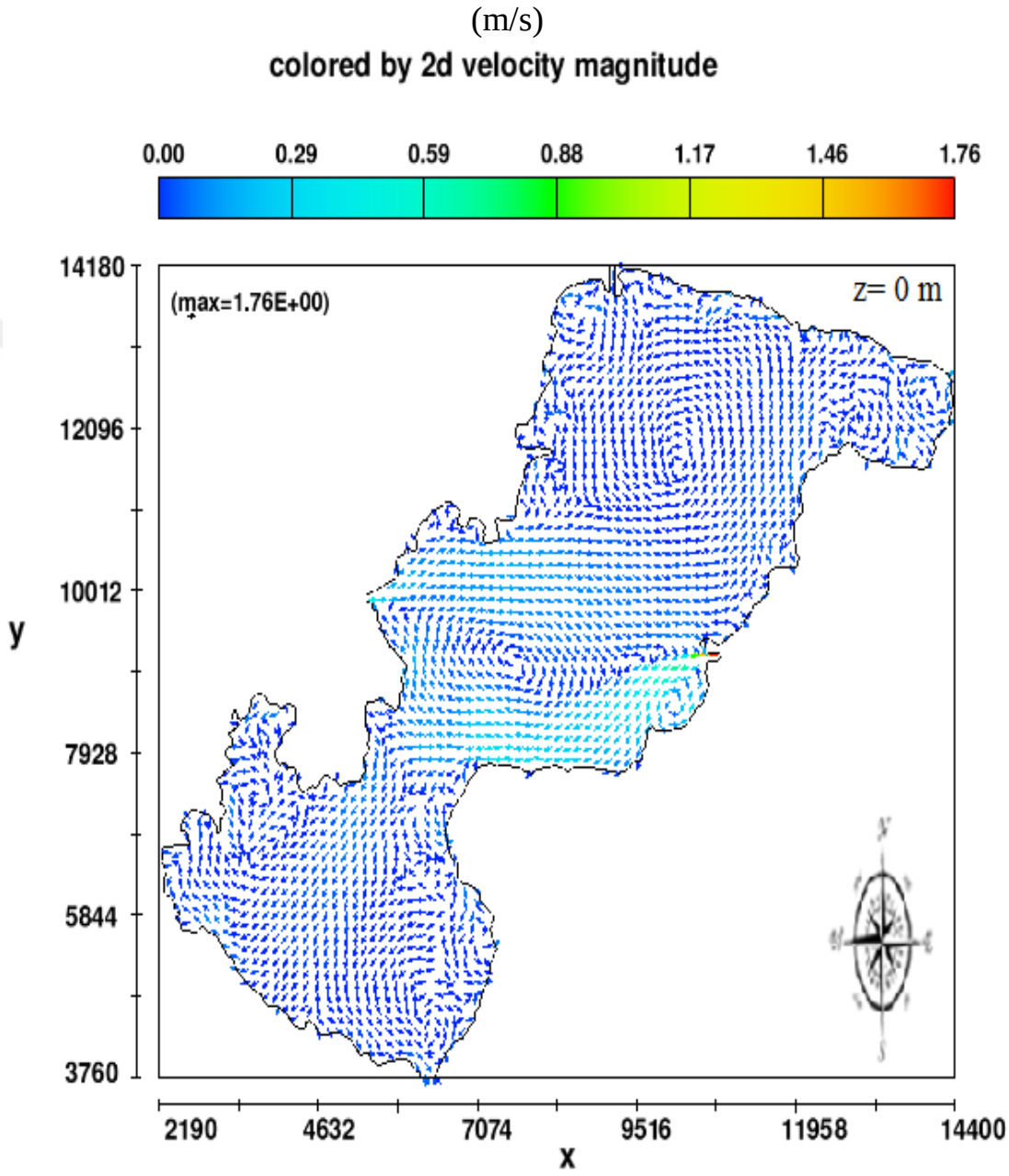

Figure 5.97: The velocity vectors colored by 2D velocity magnitude for z=0 m after 18 days (August).

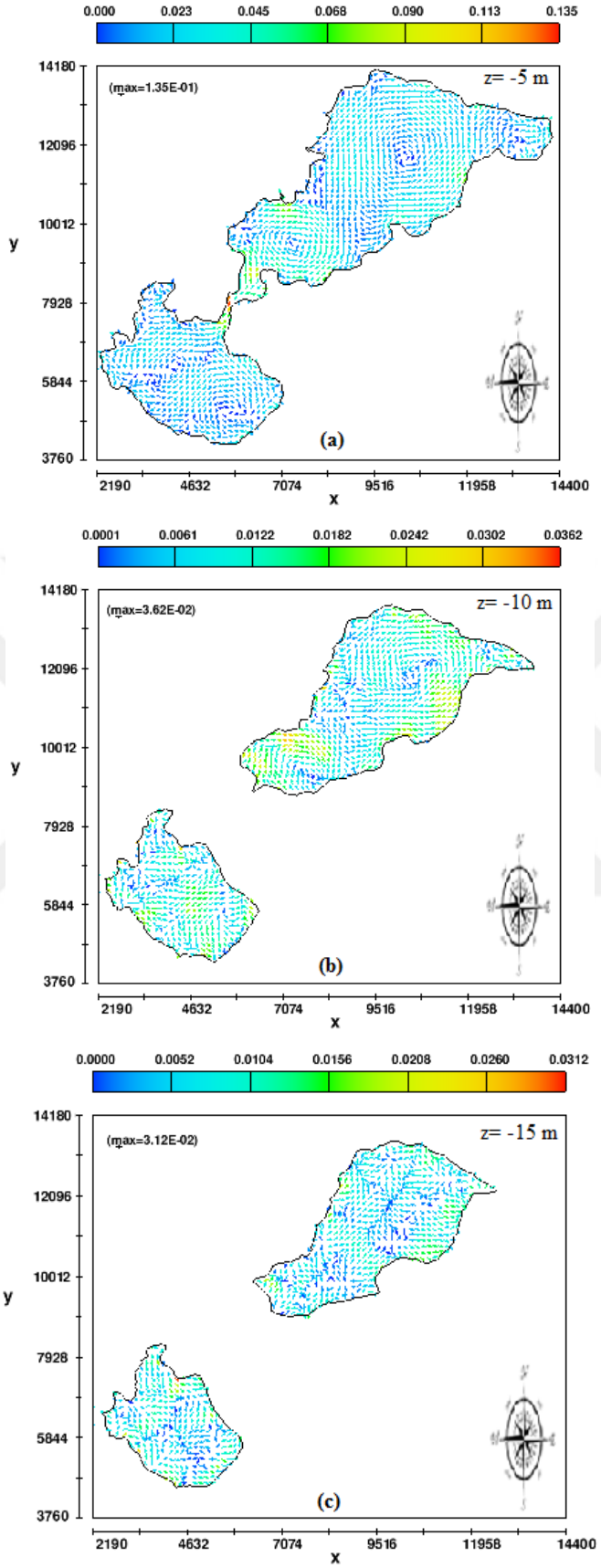

Figure 5.98: The velocity vectors colored by 2D velocity magnitude after 18 days (August): a) -5 m, b) -10 m, c) -15 m.

Temperature contours of August, which represents the temperature changes at surface of the Lake Köyceğiz, for 2 days, 7days, 14 days and 18 days after running the simulation have been shown in Figures 5.99, 5.100, 5.101 and 5.102.

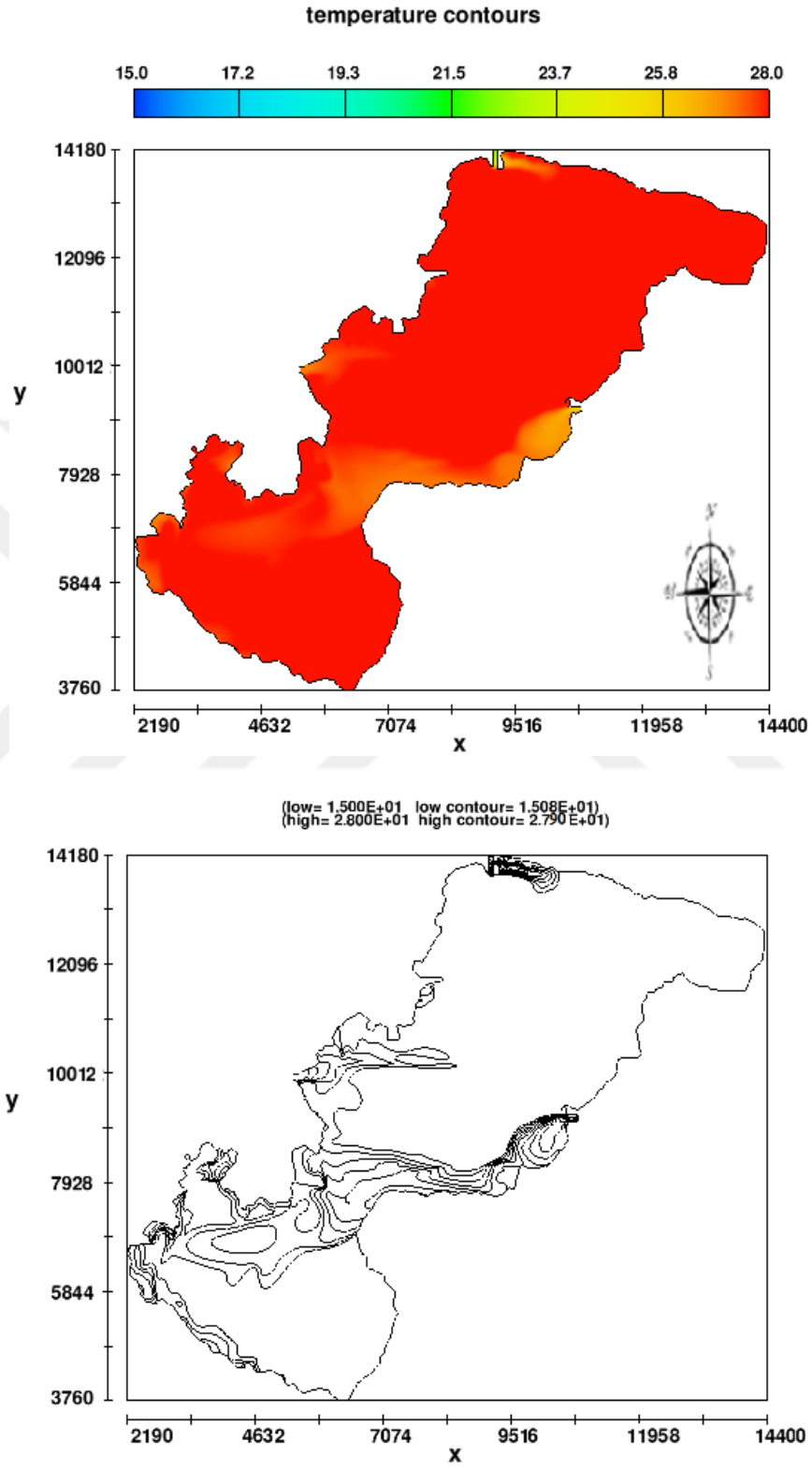

Figure 5.99: The temperature contours at surface of Lake Köyceğiz after 2 days (August).

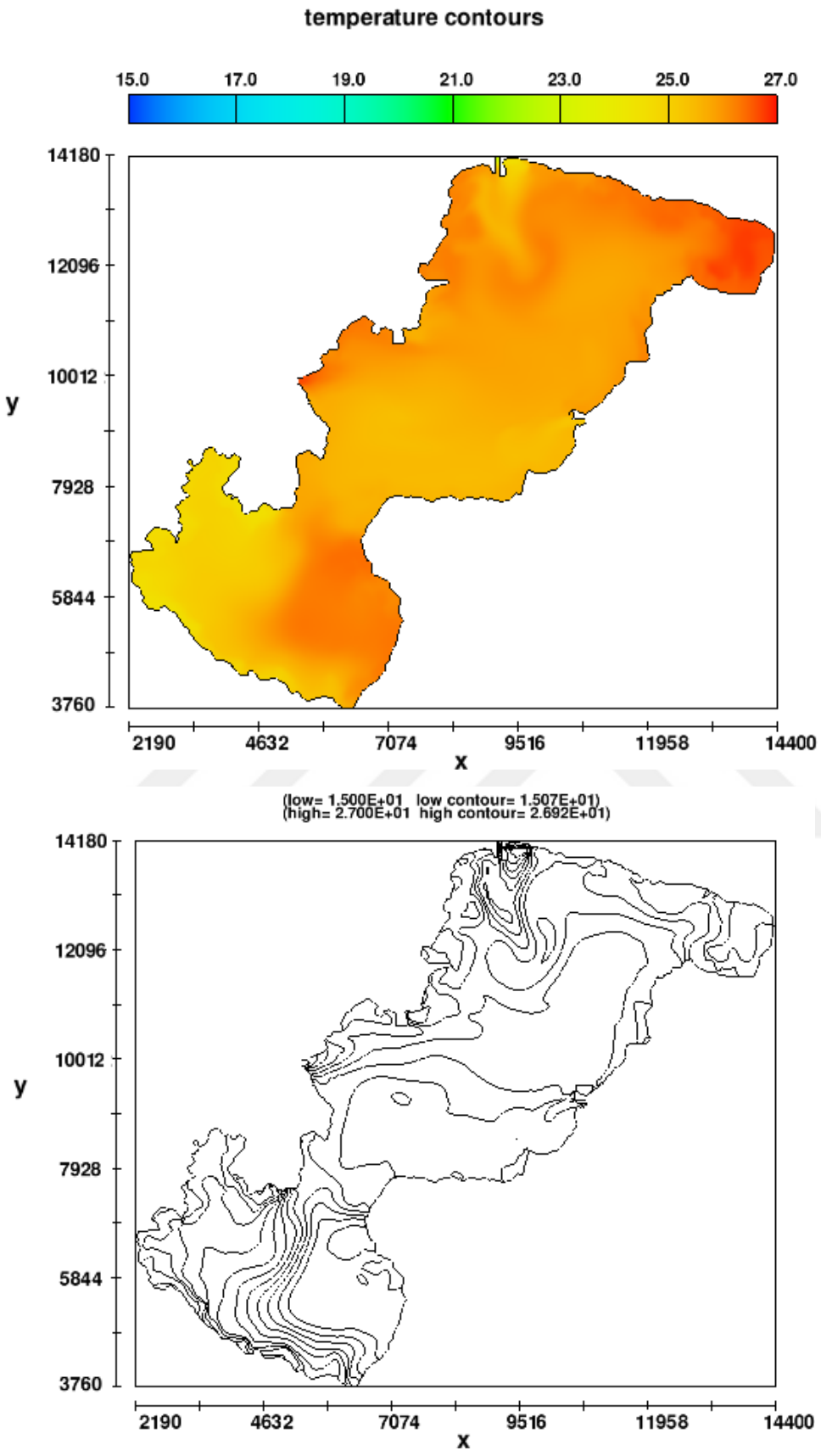

Figure 5.100: The temperature contours at surface of Lake Köyceğiz after 7 days (August).

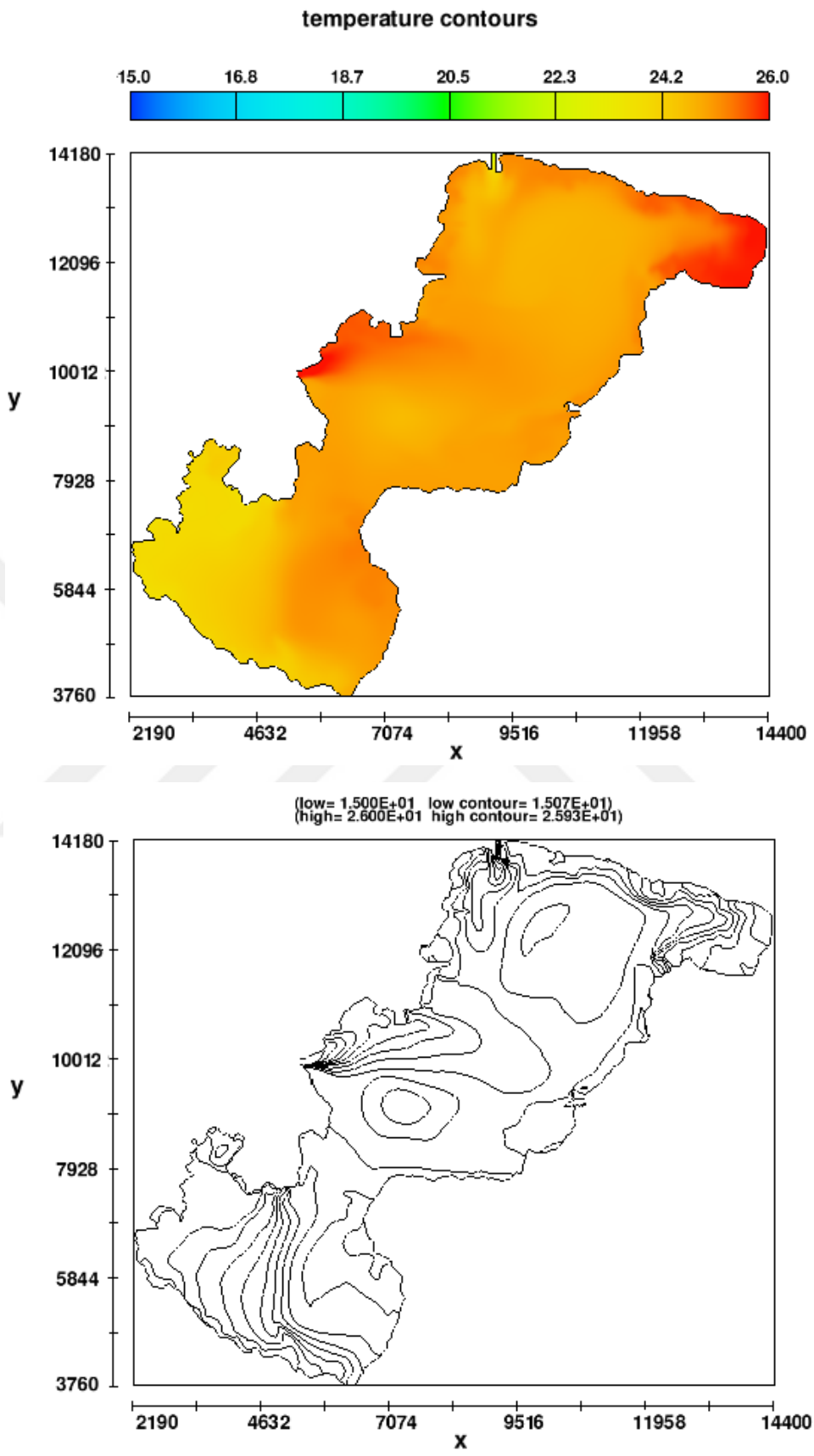

Figure 5.101: The temperature contours at surface of Lake Köyceğiz after 14 days (August).

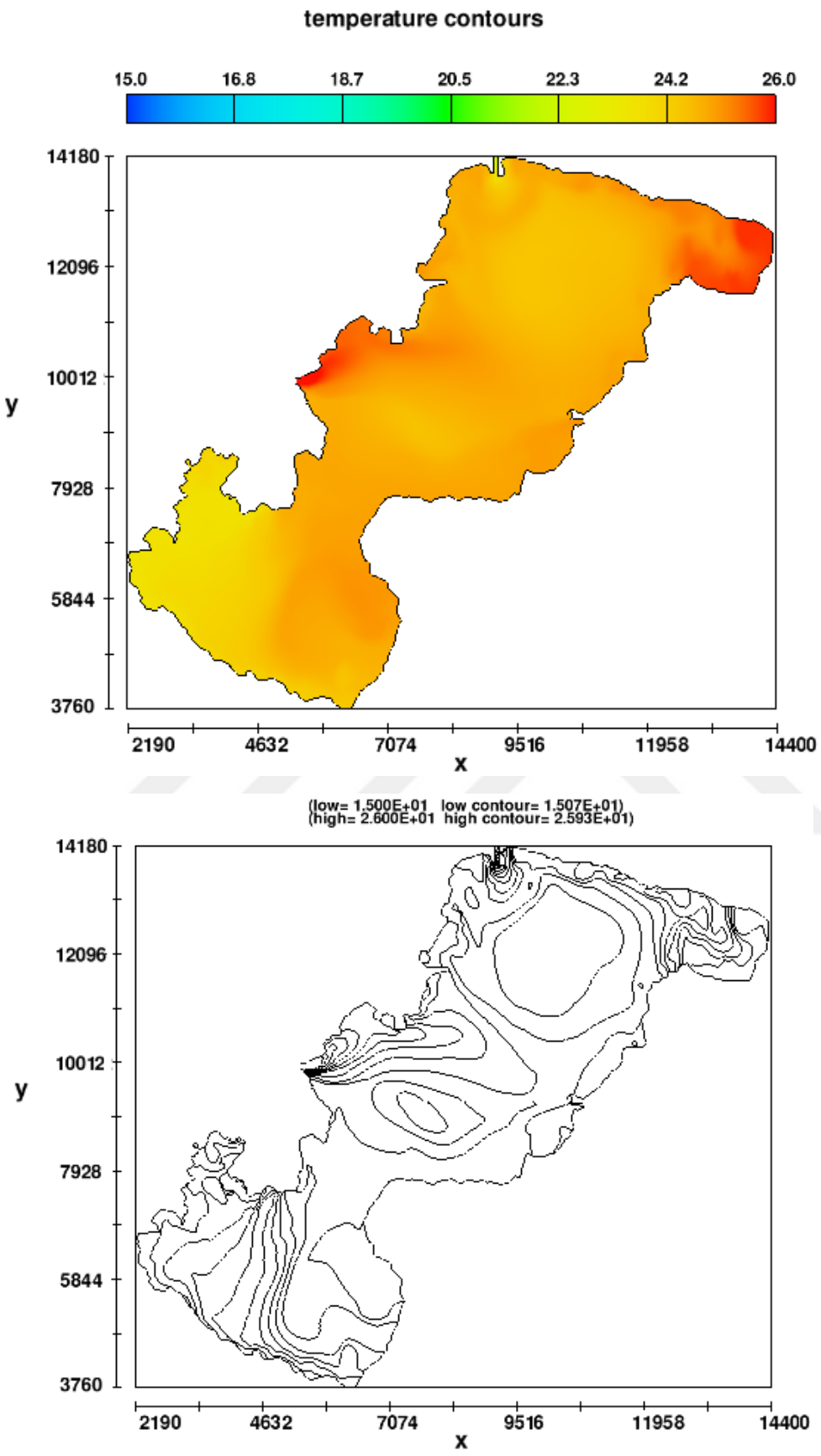

Figure 5.102: The temperature contours at surface of Lake Köyceğiz after 18 days (August).

After 18 days of simulation running, the cross-section of Köyceğiz and Sultaniye parts arerepresented as Figure 5.103 for temperature changes in different layers.

As mentioned before the environment temperature is not applied for simulations, because the FLOW 3D program is not able to modeling the environment (weather) temperature. Unit is degrees Celsius for all the figures related to temperature and heat.

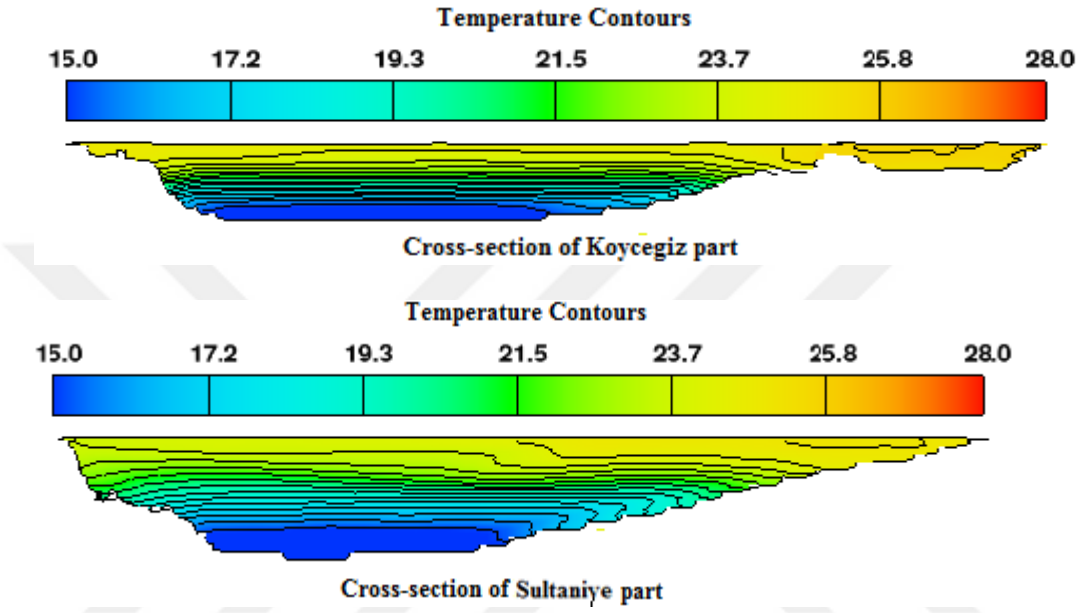

Figure 5.103: The temperature contours of Köyceğiz and Sultaniye parts of Lake after 18 days (August).

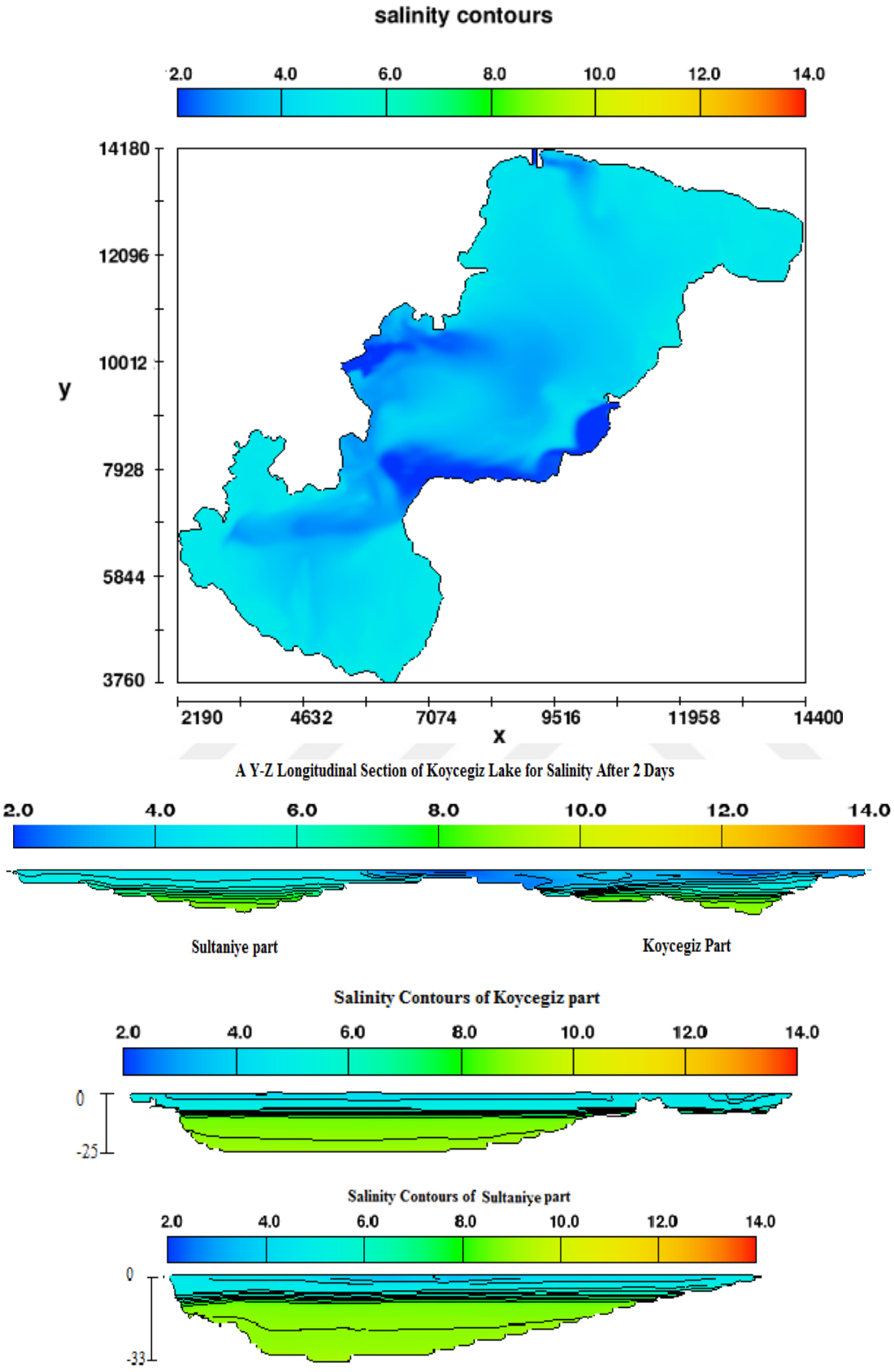

Figure 5.104: The Salinity color shaded contours of Lake Köyceğiz after 2 days (August).

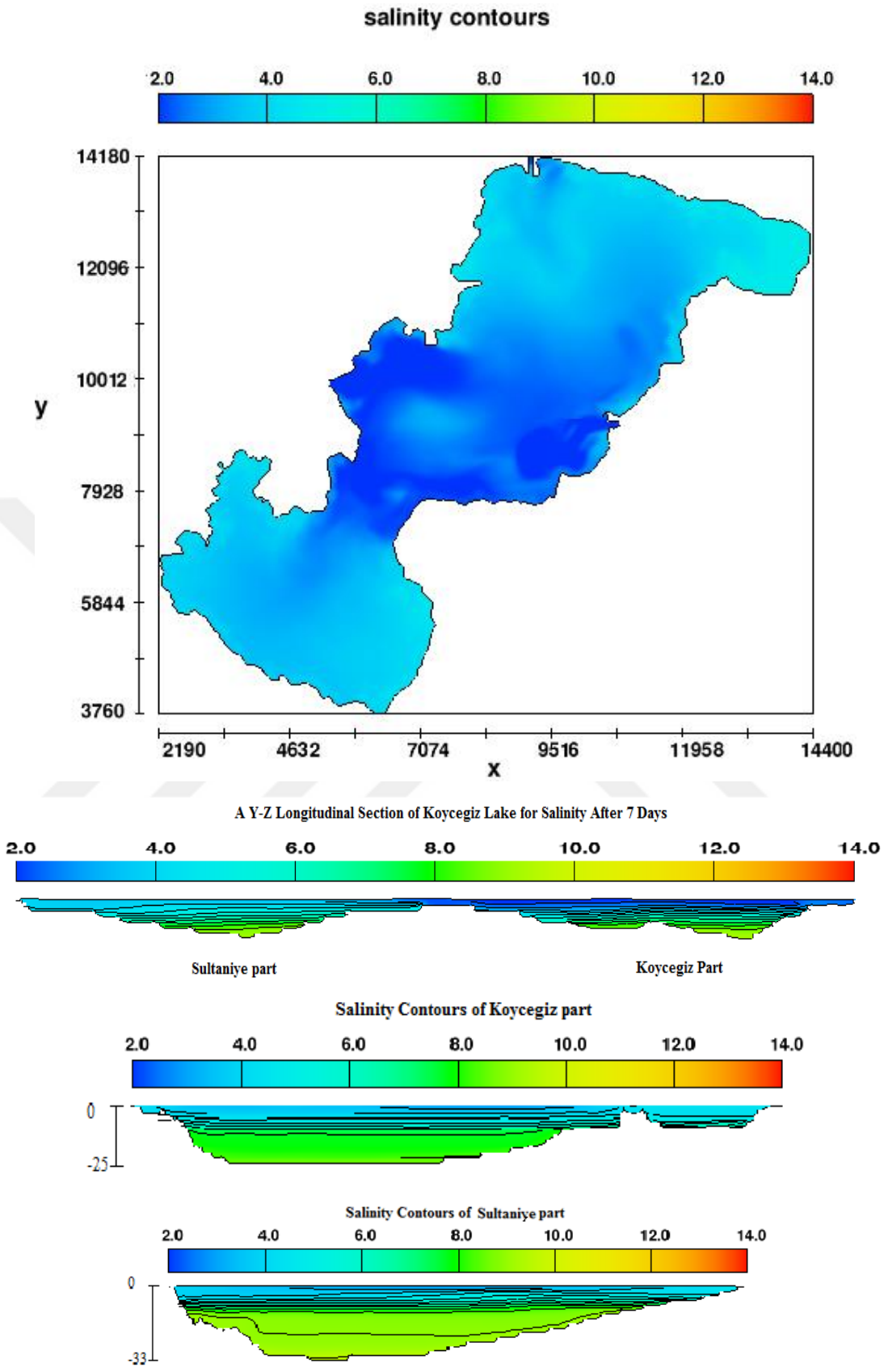

Figure 5.105: The Salinity color shaded contours of Lake Köyceğiz after 7 days (August).

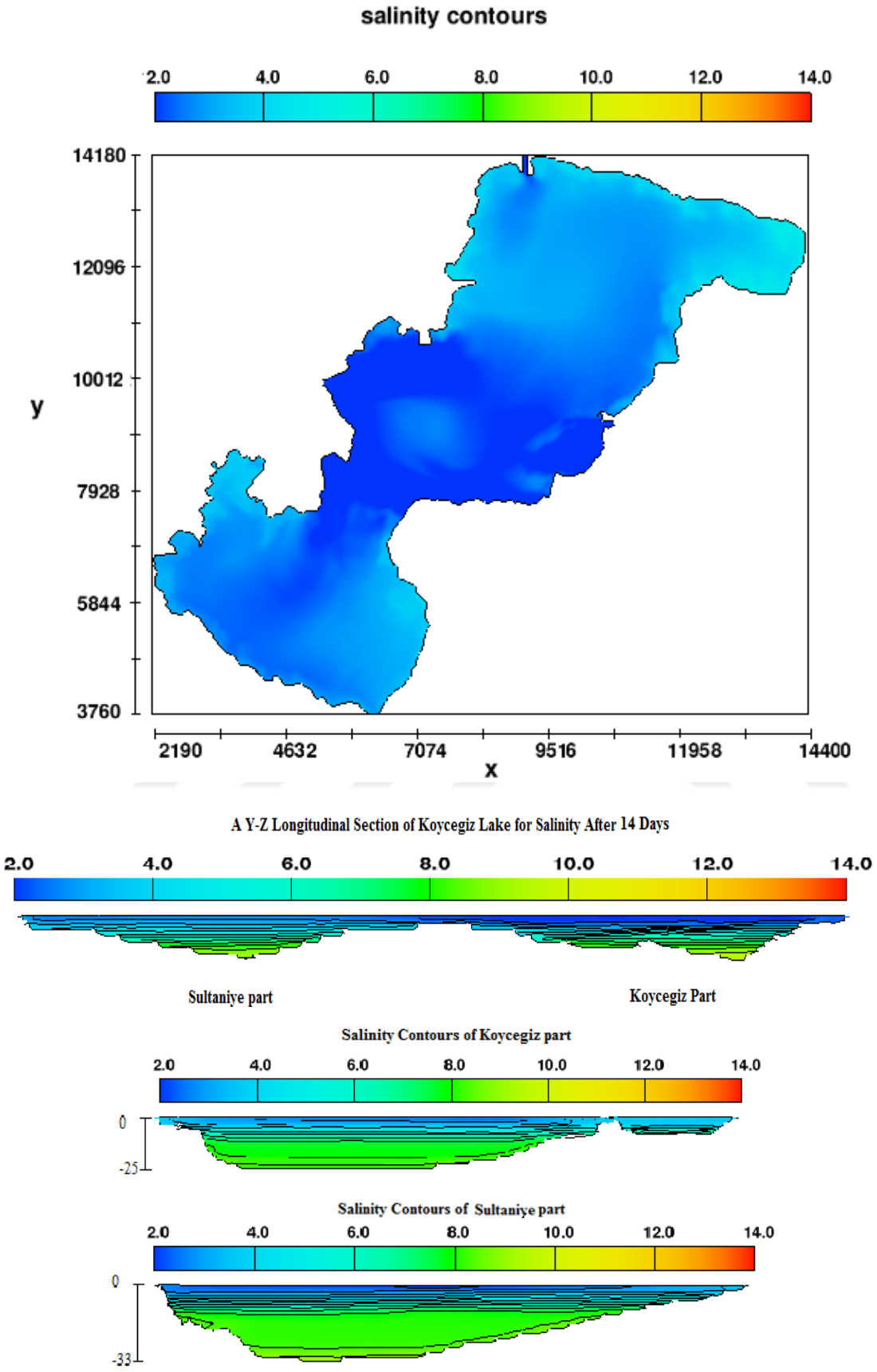

Figure 5.106: The Salinity color shaded contours of Lake Köyceğiz after 14 days (August).

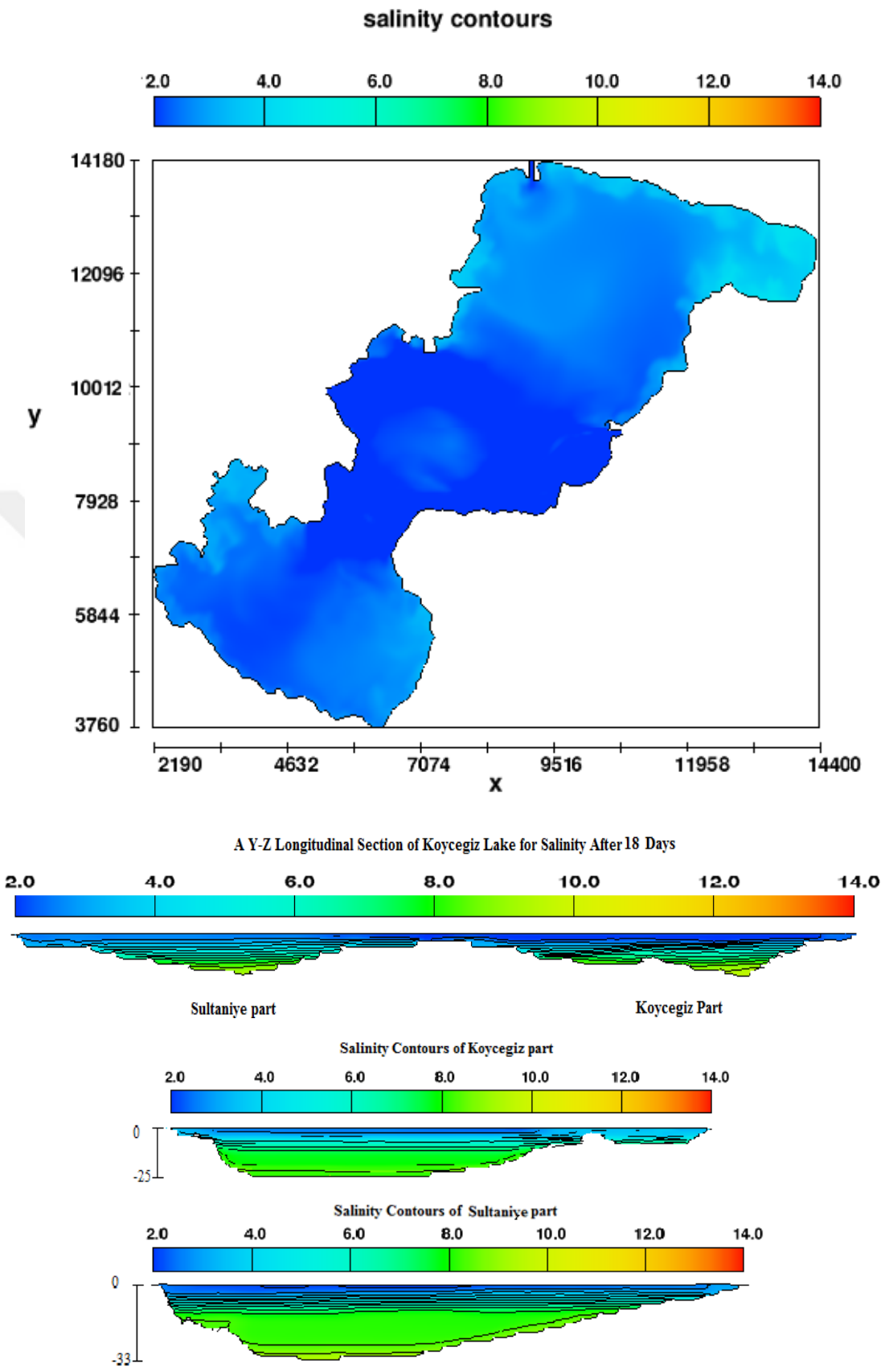

Figure 5.107: The Salinity color shaded contours of Lake Köyceğiz after 18 days (August).

The suspended sediment distribution at Lake Köyceğiz, when an unexpected event after a heavy raining happened and a high magnitude of discharge with high suspended sediment values is came from Namnam river into the lake, is given in the following figures. There are some assumptions in concentration of suspended sediment of namnam river, because of the lack of the measurments and data about this parameter. The distribution of suspended sediment particles are under the effect of the wind velocity and direction, situation and condition of layers due to seasons, density of inflow current and density of water in different layers and etc. The suspended sediment distribution in an unexpected event, simulated using FLOW3D, is represented as following figures for different hours incluede 3 hrs, 5 hrs, 6 hrs, 7 hrs, 8 hrs and 9 hours after starting flood. The possibility of a flood event was considered for Namnam and Kargicak rivers. In first step, the flood was considered only for Namnam. After that and in the other simulation, it was assumed that the flood happened only in Kargicak river. Finally, the suspended sediment distribution was simulated for flood event in both the Namnam and Kargicak rivers at the same time and simultaneously. Unit for simulations related to suspended sediment concentration, in Figures (5.108), (5.109) and (5.110), is kg/m^3 or g/l.

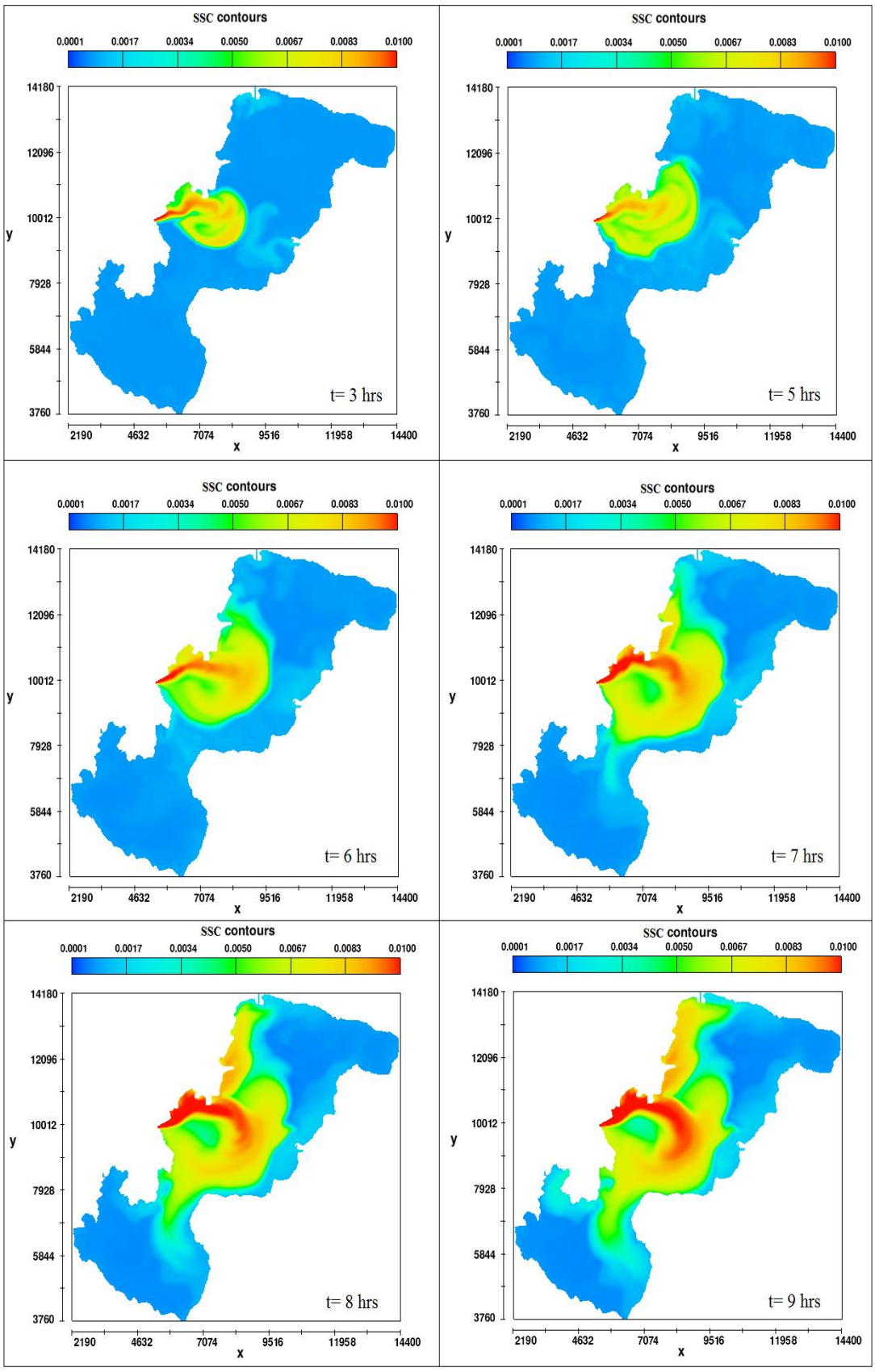

Figure 5.108: The suspended sediment distribution at Lake Köyceğiz after an unexpected event (Flood from Namnam).

If an unexpected flood happened in the Kargicak river and a discharge with a high magnitude came to the Lake Köyceğiz, it is expected that the following distribution patternof suspended sediment, in Figure 5.109, occurred in Lake Köyceğiz.

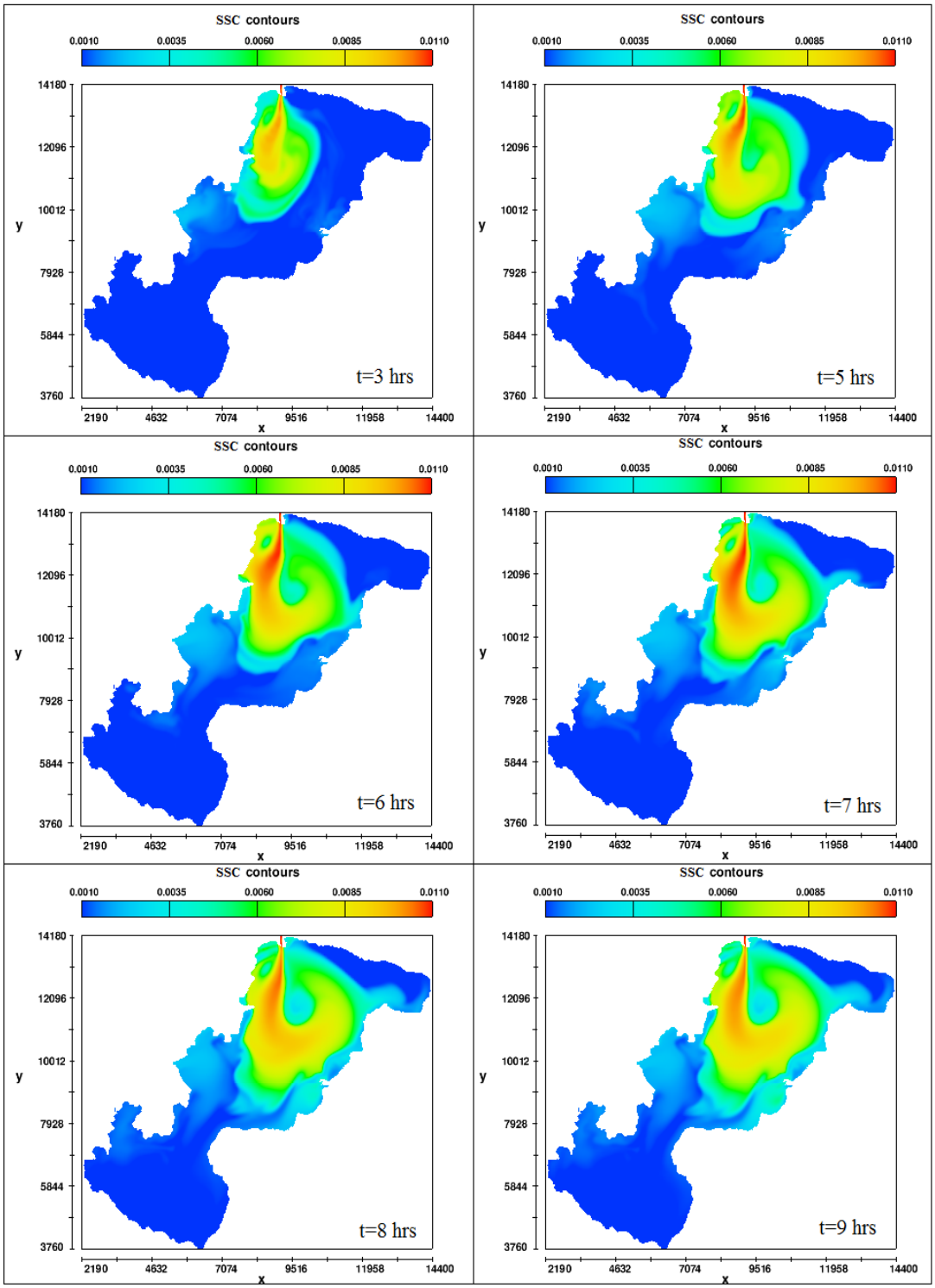

Figure 5.109: The suspended sediment distribution at Lake Köyceğiz after an unexpected event (Flood from Kargicak).

Another possible unexpected event is that the flood came from both the Namnam and Kargicak rivers in a same moment with a higher suspended sediment concentration than the reservoir's suspended sediment concentration into the Lake Köyceğiz. This simulation is represented in Figure 5.110 for different times of the flood.

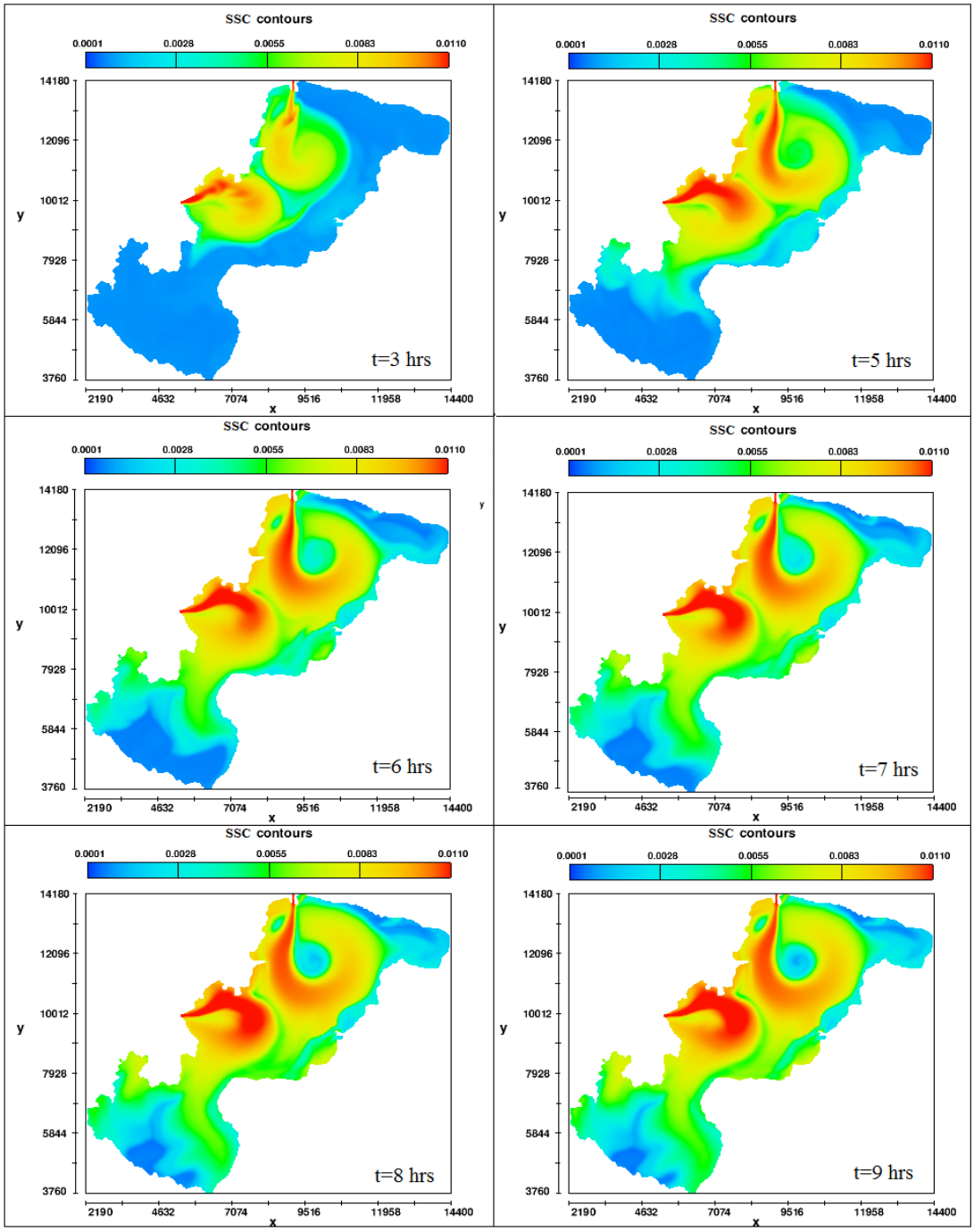

Figure 5.110: The suspended sediment distribution at Lake Köyceğiz after an unexpected event (Flood from Kargicak and Namnam).

5.7 Thermal Stratification Modeling in Lake Köyceğiz using CE-qual-W2

CE-qual-W2 program is a two-dimensional program that is used for modeling the water quality and hydrodynamics of lakes, rivers and mostly reservoirs (Cole and Wells 2000). CE-qual-W2 is developed by the US army corps of engineers. This model is very useful to modeling the longitudinal-vertical hydrodynamics and water quality in stratified and non-stratified systems. CE-QUAL-W2 requires reservoir bathymetry, initial conditions, inflow quantity and quality, outflow quantity, and outlet description (Cole & Tillman, 1999). The model also needs meteorological data and Elevations of water surface. Bathymetric and geometric data of the Lake Köyceğiz are defined to the program. Boundary conditions were set up in three data groups included meteorological variables, inflows and outflows of the system and inflow water's temperature. Main required meteorological data were wind velocity, wind direction, weather temperature and number of cloudy days. The first step for this modeling was defining the geometry of the lake. Therefore, the bathymetry file was prepared. In this regard, the depth-area-volume curve of the lake was difined and calibrated for model, which represented in figures 5.35 and 5.36. These curves were used for water surface level calibration. The bathymetry file were calibrated using trial and error method until generating the defined depth-area-volume curve . After this step, the meteorological data file were applied to CE-qual-W2 program. The initial conditions of the model were temperature profiles for the first month of the simulation. Whereas, the boundary conditions were the inflow discharge, outflow discharge and temperature of inflow water.

Lake Köyceğiz was devided to 31 segments longitudinally and 33 layers in depth (vertical direction) for thermal modeling using CE-qual-W2. About the segmentation of the model, segment layer heights and lengths for Lake Köyceğiz were selected constant. Segments have 400 meters in length, approximately, and thickness of 1 meter in depth, whereas the width of segments varies, which are averaged. The segmentation of the model was chosen so that the averaged width of each segments crossing from the deepest region of Köyceğiz and Sultaniye parts. The Lake Köyceğiz works like a reservoir with three inflow rivers and a spillway. Therefore, we can also simulate this lake as a reservoir.

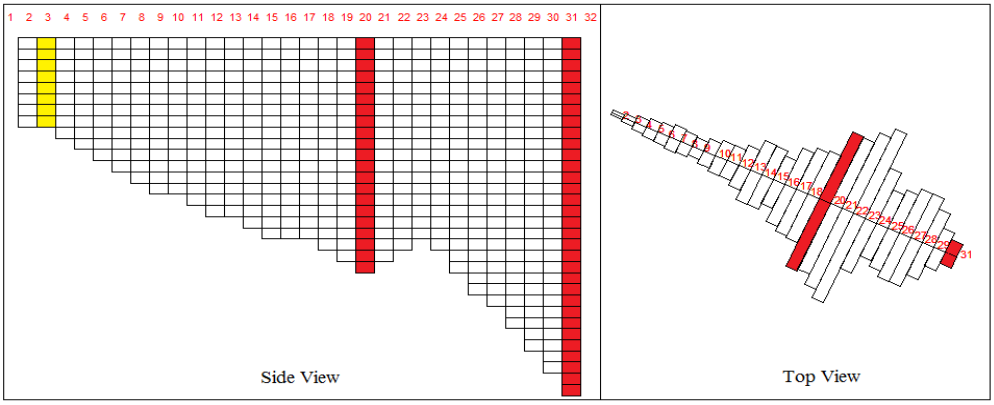

Figure 5.111: The segmentation of the CE-qual-W2 model.

The red columns are the segments that the modeled temperatures will compared with observed temperature data. These columns indicates the deepest areas of Köyceğiz and Sultaniye parts with segment numbers of 20 and 31, respectively. Temperature was calibrated using some coefficients of program. Horizontal eddy viscosity (Ax), horizontal eddy diffusivity (Dx), solar radiation extinction of water (EXH2O) and wind-sheltering coefficient (WSC) were 1 m^2/s, 1 m^2/s, 0.7 1/m and 0.5, respectively. The calibrating coefficients are represented in the following figure, briefly.

Table 5.6 : Temperature calibration coefficients values.

Values for Temperature Calibration Coefficients		
Coefficient	Symbol	Value
Horizontal eddy viscosity	Ax	1
Horizontal eddy diffusivity	Dx	1
Wind-sheltring coefficient	WSC	0.7
Solar radiation fraction absorbed at the water surface	BETA	0.45
Solar radiation extinction-water	EXH2O	0.3

For thermal stratification of this lake, the following results were obtained for model and compared with available observed data. The results shows that the CE-qual-W2 program was modeled the thermal stratification with good results for each month, despite the lack of data. On the other hand, the available data were not up to date measurments.

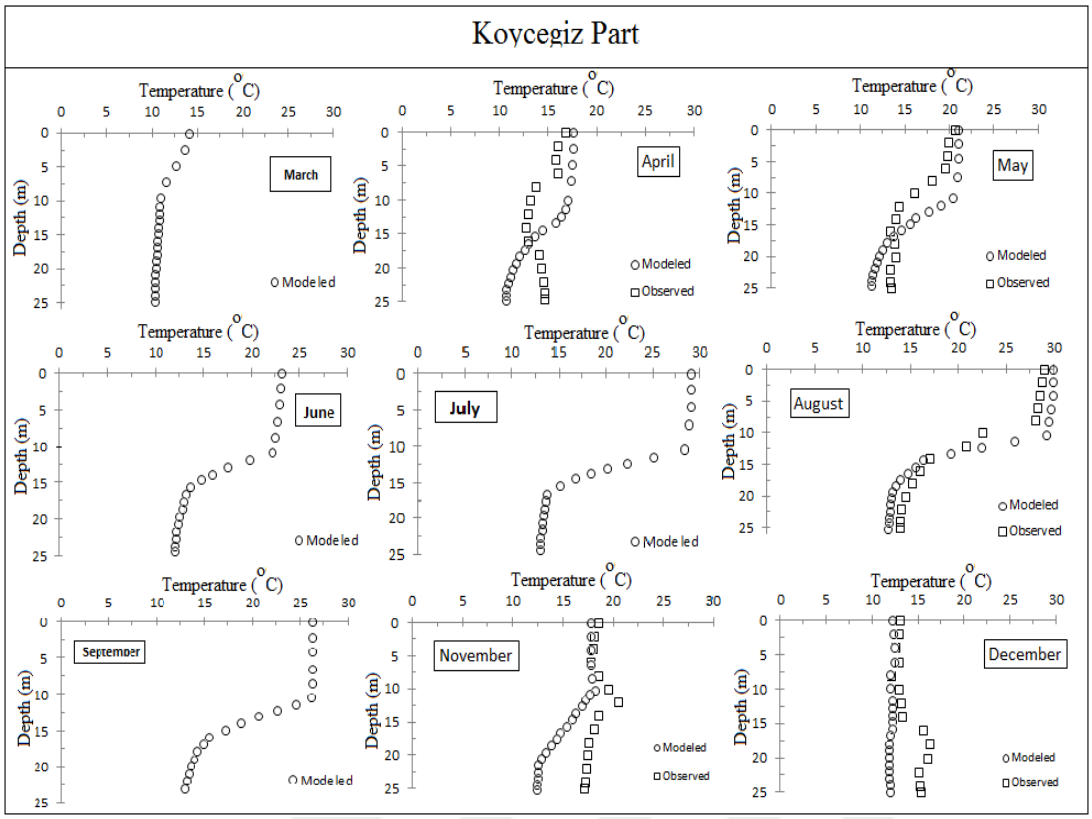

Figure 5.112: CE-qual-W2 results compared with observed data (Köyceğiz part).

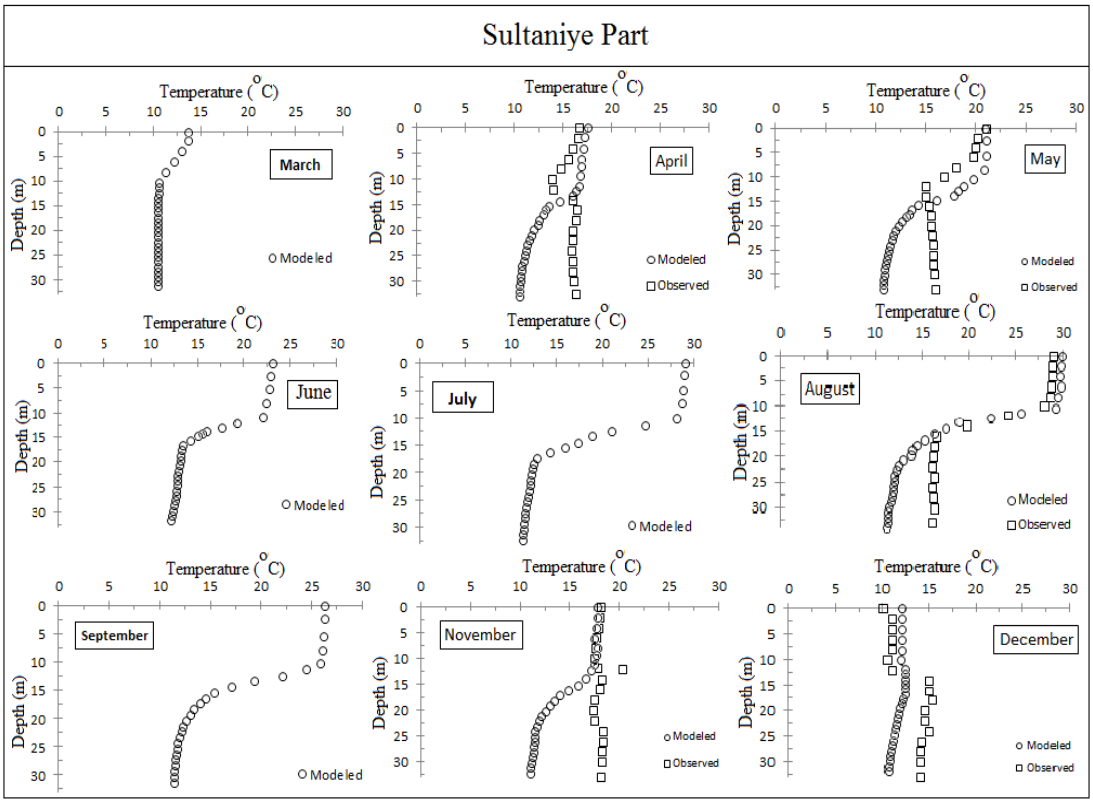

Figure 5.113: CE-qual-W2 results compared with observed data (Sultaniye part).

The last results show that the temperature at the surface of the lake and in the epilimnon layer of the modeled and observed data have a good corresponding. Thermocline layer was also modeled with good results. But in the hypolimnion layer data differences between modeled and observed data are higher than the other layers. It can be related to lack of the daily data. Other parameter, that can affect this difference in observed and modeled data, is existance of the thermal springs and ground waters exits under the lake. The temperature of these thermal springs is about 39^{o}C , approximately. This temperature of water could affects the temperature of the layers, which located at depth. The modeled water temperatures, observedwater temperatures and weather temperatures are represented in Figure 5.114.

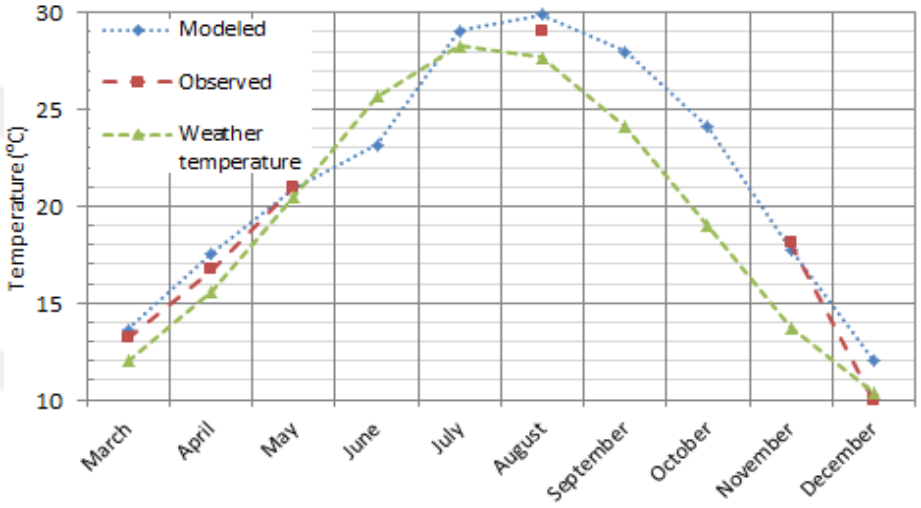

Figure 5.114: The comparition of lake surface modeled and observed temperatures.

The output results of CE-qual-W2 model for Lake Köyceğiz are represented as following graphical figures.

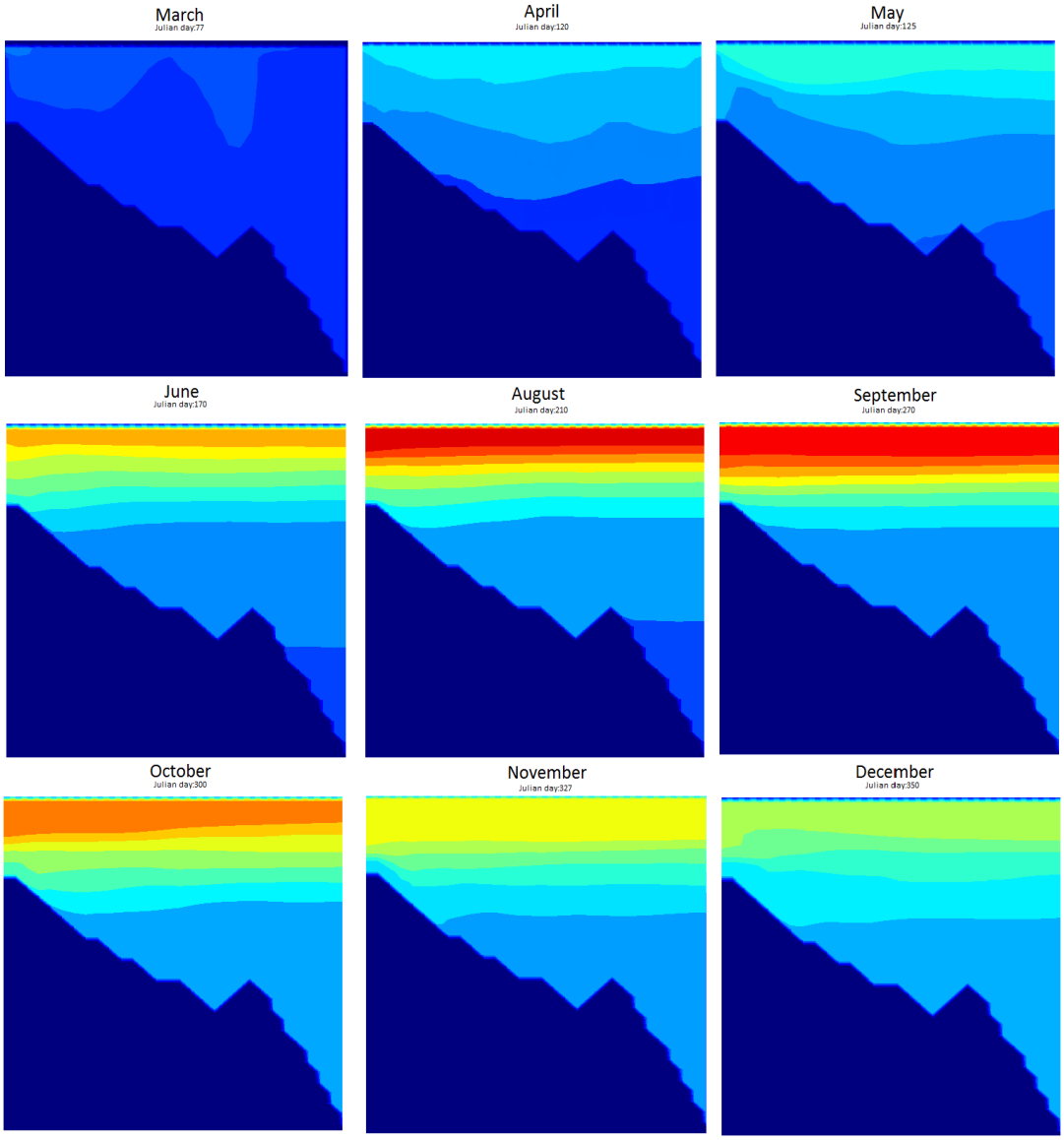

Figure 5.115: Output result of CE-qual-W2 model for thetmal stratification in Lake Köyceğiz.

In most months of the year the thermal stratification is occurred in Lake Köyceğiz. This stat could be concluded from the results of the CE-qual-W2 model for this lake. Analysing the results figures of CE-qual-W2 models of Lake Köyceğiz shows that in most of the months the lake consists of three thermal layers as same as it was measured in 1990-1999. The following figure shows these three layers.

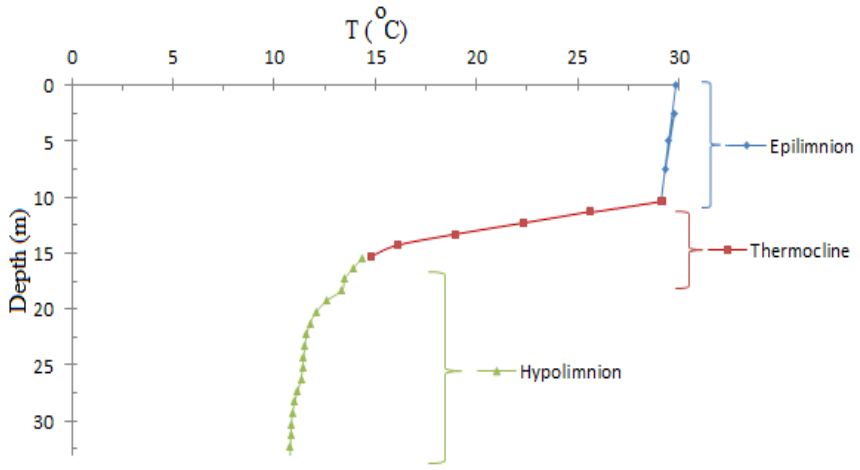

Figure 5.116: Thermal layers of Lake Köyceğiz.

Therefore, the modeled outputs are discussed and compared with observed data in these three layers seperately. Approximate thickness of the layers are briefly represented in the following table for available observed and modeled thermal variations by depth in both Köyceğiz and Sultaniye parts.

Table 5.7 : Approximate thickness of thermal layers in Lake Köyceğiz.

Thickness of Layers (m)							
Month	Part	Observed			Modeled		
		Epilimnion	Thermocline	Hypolimnion	Epilimnion	Thermocline	Hypolimnion
April	Koycegiz part	7	2.5	15.5	12	6	7
	Sultaniye part	10	2.5	20.5	11	5.5	17
May	Koycegiz part	6.5	6	12.5	11.5	7	6.5
	Sultaniye part	8	5.5	19.5	11	6	16
August	Koycegiz part	8	4	13	10	4	11
	Sultaniye part	10	5	18	10.5	5	17.5
November	Koycegiz part	6.5	8	10.5	11	3.5	10.5
	Sultaniye part	11	3	19	14.5	5.5	13
December	Koycegiz part	14.5	7.5	3	25	-	-
	Sultaniye part	12	3	18	17.5	9.5	6

The results of modeled thermal stratification for these 5 months were compared with observed values. These comparisions were conducted using research assessment exercise (RAE), relative error of the mean (REM), mean squared error (MSE), root

mean square error (RMSE) and absolute mean error (AME) criterias. These criterias were obtained from the following equations.

$$AME = \frac{\sum|T_{modeled} - T_{observed}|}{n} \quad (5.1)$$

$$RMSE = \sqrt{\frac{1}{n}\sum(T_{modeled} - T_{observed})^2} \quad (5.2)$$

$$MSE = \frac{\sum(T_{modeled} - T_{observed})^2}{n} \quad (5.3)$$

$$RAE = \sum(|T_{modeled} - T_{observed}|)/\sum T_{observed} \quad (5.4)$$

$$REM = \frac{1}{n}\sum\left|\frac{T_{observed} - T_{modeled}}{T_{observed}}\right| \quad (5.5)$$

where; $T_{modeled}$ is the modeled temperature; $T_{observed}$ is the observed (measured) temperature, n is the number of observations (measurments).

It is important to note that the temperature predictions for lake are averaged over the length, depth, and width of a segment cell, while, the observed and measured data represent observations and measurments at a specific point within the lake (Cole & Tillman, 1999). The values of these criterias are represented as the table for April, May, August, November and December.

Table 5.8 : REM and RAE values for temperature modeled and observed data.

	April	May	August	November	December
REM	0.18	0.18	0.13	0.18	0.16
RAE	0.18	0.17	0.10	0.18	0.17

Table 5.9 : MSE, RMSE and AME criterias for modeled and observed values of thermal stratification in Lake Köyceğiz.

April	MSE	RMSE	AME
Epilimnion	2.76	1.66	1.51
Thermocline	3.70	1.92	1.73
Hypolimnion	19.55	4.42	4.35
Totally	10.83	3.29	2.89

May	MSE	RMSE	AME
Epilimnion	0.63	0.80	0.68
Thermocline	12.21	3.49	3.36
Hypolimnion	16.09	4.01	3.71
Totally	11.54	3.40	2.92

August	MSE	RMSE	AME
Epilimnion	0.81	0.90	0.89
Thermocline	3.10	1.76	0.54
Hypolimnion	17.15	4.14	4.09
Totally	8.08	2.84	2.31

November	MSE	RMSE	AME
Epilimnion	0.06	0.24	0.21
Thermocline	14.02	3.74	3.54
Hypolimnion	44.69	6.68	6.67
Totally	18.11	4.26	3.29

December	MSE	RMSE	AME
Epilimnion	1.83	1.35	1.30
Thermocline	4.24	2.06	2.00
Hypolimnion	8.47	2.91	2.89
Totally	5.63	2.37	2.22

As it is clear from the table and in accordance to that mentioned previously, the modeled temperatures in the upper layer of lake (epilimnion) has good results. These values are very close to the observed data. The calculated criterias in the last table prove this state. In thermocline layer, this state is also ture. Differences in temperatures between modeled and observed data are mainly occurred in hypolimnion layer.

5.8 Formation of Stratification in Lake Köyceğiz Pre- and Post dam Construction on Namnam River

The construction of a large dam on Namnam river is a subject that always has been. Therefore, having some knowledges about the construction of dam and effect of that on downstream of dam has special importance. Thereupon, dam construction on Namnam river could has some important effects on the Lake Köyceğiz. Introducing these effects are the main aim of this part of the thesis. Therefore, some possible effects of dam will be mentioned here for before and after construction. These states will be named as pre and post dam situations.

5.8.1 Effect of Namnam Stream on Lake Stratification in Pre-dam Conditions

As the data is limited and there isn't enough measurments in this area, the seasonal data (average) were used. In Lake Köyceğiz, as mentioned before using figures from measurements and simulations, it is obviously seen that the stratification occurred. The creation of these stratifications are because of the variations between temperature, salinity and specially in densities of inflow water and lake's one. The existence of epilimnion, metalimnion (thermocline) and hypolimnion layers are clearly seen in most seasons. The existence of groundwater exits are affected on the thermal stratification. The epilimnion layer is directly under the effect of the wind velocities and directions. About the thermal stratification, the temperature of weather plays an important role. It is clear that the temperature of the inflow waters are very important, too.

5.8.2 Effect of Namnam Stream on Lake Stratification in Post-dam Conditions

Before study on the possibe post-dam condition of Lake Köyceğiz, the possible changes on the Namnam river after dam construction must be defined. Some important changes that will be occurred after dam construction are described below.

It is should be considered that the construction of the dam will caused to the formation of big lake behind the dam body. This formation of lake leads to creation of fog and then results to increasing in the relative humidity in the region surrounding the dam and its reservoir. The experiences show that construction of these structures has significant impact on climate parameters. It means that the construction of dam will lead to climate change at the micro scale. By increasing the water surface area behind the dam (in the reservoir), the evaporation losses will rise, consequently (Tahmiscioğlu et al.). It is also affects the weather temperature. Although these changes may not have a direct influence on human health, but it could have some indirect effects on human and human life (Tahmicioglu et. al 2007). For example, the weather temperature and the percentage of the humidity variations could effect on some plant species and some animals and sometimes harmful, which could due to loss of these plant species and migration of animals. As a result, it could influence the human life, indirectly.

As one of the other main results of construction of dam, from the studies of other researchers on different dams, is that the temperature of water decreases in downstream (Agiralioglu, 2007). The reason for this phenomenon is that the stored water in reservoir of dam releases to the downstream from the lower depths (lower level) of the reservoir and mostly from the Hypolimnion layer, which has the cold water. It is clear that this decreasing in water temperature could affect the Köyceğiz lake. From the last studies on the effect of dam construction on temperature of water in downstream, in many cases, it was found that the water temperature differences between its values at upstream of dam and before reaching to the reservoir, and after dam at downstream, can be about 6℃ to 7℃. This decreasing in water temperature could affect Köyceğiz lake directly. This decreasing in temperature of Namnam stream's water will changed the thermal stratification of Köyceğiz and the thickness of layers.

Construction of dam is also affects the salinity of downstream. Salination of downstream water is a proven scientific subject in the case of dam construction

effects. With changing in some parameters of water such as temperature of water, concentration of suspended sediment, pH and dissolved oxygen, the solubility of water is changed. These changes of water parameters affect on the factors which that due to the salinity balance and it could be caused to destroying of these factors. This change in solubility of water causes to increasing the salinity at downstream of the dam. In the wake of this phenomenon, the salinity stratification will have change in Lake Köyceğiz.

From the first sections of this thesis, it is known that the dams are experienced the stratification. Since the oxygen could not reach to the lower layers of the reservoir, oxygen is reduced in these layers. So, released water from the reservoir will be harmful and hazardous for the life in downstream. Accordingly, it will affect the Lake Köyceğiz water quality. Construction of dam could effect on the ground water quality. In some cases it is seen that the ground water was salinized after dam construction. Therefore, it is possible that the ground water around this region, which is related to the Lake Köyceğiz, be salted. So, it could affect the Köyceğiz lake water quality and causes to increasing salinity of this lake.

Flow regimen will change after construction of dam or hydropower plant at the downstream. It is because of the magnitude, duration and the frequency of the releasing water from the dam. As an important result of changing in the flow regimen after dam construction, is the effects on the sediment traps at downstream. It affects the erosion and then, affects the bed material sizes during time. Therefore, It will expected that the profile changings occurred in down stream of the dam (Williams, 1984).

6. CONCLUSIONS

Main aim of this study was to investigate and study on the distribution of the suspended sediment and temperature in lakes and reservoirs. The important point that distinguishes this study from other researches is inclusion of effect of several parameters on distribution pattern of temperature and suspended sediment in lakes and reservoirs. Several simulations according to selected scenarios were done. The results of simulations show that the distribution of temperature and suspended sediment is under the effect of changes in parameters. In addition to these binary simulations, the Lake Köyceğiz was simulated as a case study. In this section of thesis the concluded points of the simulations results are summarized.

It is concluded that in the same conditions included the inflow water's suspended sediment concentration, discharge, slope of bed, reservoir's suspended sediment concentration, reservoir's water temperature and situation of outlets, with changing in inflow water temperature, there is some changes occurred in the situation of plunging point. Magnitude of discharge could affect the plunge point and the formation of the density/turbidity currents. If density of inflow water is greater than the reservoir's one, in high discharges, the density/turbidity currents will be formed, obviously and completely. All parts of the structure of these currents were formed in the S type simulations of this thesis. Discharge magnitude also affects on the rate of propagation of these currents. The position and type of the outlet also could affect the layers thickness and velocities in different depths. Wall jet and reverse currents could affect the stratification of some of the simulations in reservoir. In some of simulations the side currents from the side walls of the reservoir lead to creation of a mid layer during simulation time.

In simulations, when turbidity/density currents reached to the dam body, in simulations with spillway (S type) and with a greater inflow density than the reservoir density (S1 to S12), the current was moving upward with collision with body of dam and propagated and distributed in the upper depths of the reservoir near

dam body. Whileas, in simulations with bottom outlet (B type) and with a greater inflow density than the reservoir density (B1 to B12), a large portion of density/turbidity current was releasing to the downstream of the dam body. This shows that the bottom outlet has an major role in reducing the suspended sediment concentration, which reached to the dam body with density/turbidity currents, by releasing these currents to the downstream of dam. Therefore, choosing the situation, position and type of the outlets is very important in dams life. With comparing the results of S and B simulations, which only spillway operates or only bottom outlet exists, it was seen that the bottom outlet decreases the speed of the propagation of the suspended sediment to the upper layers of reservoir by releasing the current to downstream of dam. Therefore, the thickness of layers with higher amount of suspended sediment concentration in simulations with bottom outlet are less than the layers in simulations with only spillway outlet. The bottom outlet leads to incresing the velocity of density/turbidity current and the water volume at bottom of the reservoir. Whereas, the existence of the spillway type outlet causes to increasing the velocity in layers near dam body and also at the surface of the reservoir. This rising in velocity leads to upward motion of suspended sediment in different layers close to dam body. Totally, based on the results of numerical models with different outlets, when a dense inflow current conditions occurred, it is indicated that releasing water from bottom outlet would lead to water quality enhancement in reservoirs, mostly.

The high amount of discharge is caused to non-settling or low settling of suspended sediment particles. The rising of water temperature leads to settling the suspended sediments faster. Therefore, the temperatures of inflow and reservoir water affect the depositing and settling of suspended sediments. Other words, water temperature could mainly affects the distribution of suspended sediment and the thickness of stratification layers in lakes and reservoirs, directly.

The effect of suspended sediment or salinity on temperature distribution is great. In simulations, it is obvious that the over-flow, inter-flow and under-flow mainly depends on the suspended sediment concentration of inflow and reservoir water. The type of current affects the temperature distribution and the characteristics of the stratification layers, directly. Totally, in all simulations, it was seen that the epilimnion, thermocline and hypolimnion layers appear over time. After approximately 3000 seconds, the reservoir was stable, thermally.

About the Lake Köyceğiz simulations, the following conclusions were obtained:

It is seen that in the Kogcegiz Lake, the velocity and direction of the wind affects the direction and magnitude of velocity vectors at the surface of the lake, extremely. It leads to mixing at surface and upper layer of the lake.

Since the total dissolved solids (TDS) or salinity, affects water density, thereby have main effects on water movements in the lake. Therefore, the Salinity or TDS has an important role in hydrodynamics of this lake. In summer months and especially in Auguest, September and October, the precipitation in this region is reduced. Because of the reduction in precipitation events, and due to that, increasing in evaporation from the surface of the lake and rivers, the water level in Lake Köyceğiz, is came down and decreases. Therefore, the salinity in these months has its highest value in comparison with the other months. On the other hand, in November and December, the precipitation starts to increase. Therefore, the discharge of inflow currents from Namnam and Yuvarlak rivers rises. It is concluded that the overflow condition occurred in November, because the inflow salinities from the Namnam and Yuvarlak rivers are less than the salinity of the layers of the lake. The salinity of mentioned rivers are even less than the upper layer of lake. This layer is located above the depth of the 7.5 meters, approximately. By this reason, the density of the inflow current is less that the density of the layer below 7.5 meters. In December, the salinity of Namnam river is reduced slightly. Therefore, this parameter of the lake is a bit reduced at the depth upper than 7.5 meters in December, approximately. It is considered that the existence of the graund water springs under the lake, caused to the appearance of the currents at the lower layer. It leads to partial reduction of salinity in this layer in these months.

Thus, as a main conclusion about the salinity, it could be said that three factors affect the salinity and caused to increasing of that, included:

1- High evaporation from the surface of the lake in summer.

2- Low inflow discharges from the rivers in summer, which caused to reduction in water level of Lake Köyceğiz.

3- The inflow current from Dalyan channel into the lake in summer, which has the high value of salinity. This is because of the reduction of the water level in Lake Köyceğiz, the wind velocity and direction.

There are some studies done about Lake Köyceğiz in the past, that show these mentioned points about salinity. Totally, it could say that the lake is extremely stratified. Thus, the transfer of water, salinity and other ingredients is poorly done between the lower layers of lake in depth.

From the flood scenarios for Namnam and Kargicak rivers, when a flood event occurred in both of these rivers, the current came from Kargicak affects the flow direction and velocity in north part of the lake. In this time, the current from Namnam was not able to flow toward the north of the Köyceğiz part. The Kargicak current guides the Namnam inflow current to the south of the lake and Sultaniye part. When flood only happens in Kargicak river, the inflow suspended sediment enter to the Köyceğiz part and moving in this part. A circulation current zone was observed in this condition, whish was circulated around the deepest part of the Köyceğiz part. Whereas, when flood event happens only in Namnam river, the suspended sediment particles were distributed toward the north of the Köyceğiz part by effect of the wind direction and velocity, in the first moments. After that, the suspended sediment particles were started to move and distribute toward the Sultaniye part and Dalyan channel. About the reason of the deep places of the lake, which are 25 meters at Köyceğiz part and 33 meters at Sultaniye part, from the flood scenarios for Namnam and Kargicak, it could concluded that there is no main deposition and settling of sediments in these areas of the lake. The inflow currents of Lake Köyceğiz are flowing toward the Sultaniye part and then Dalyan channel. One reason for this state is that the elevation of the inflow currents and Dalyan channel as an outlet is approximately same. In this situation, the wind speed and direction has an important role in guidance of the flow in Lake Köyceğiz.

The effect of the Yuvarlak river is more than Namnam river in summer or dry seasons. Because the discharge of Namnam is very low and sometimes, it is facing to the complete dryness condition in summers. In this season, the Yuvarlak is directly affects the Sultaniye part. Because of the discharge controlling on the Yuvarlak river by dam, in all months of year, the water flows in this river. About the FLOW3D, this program is not able to simulate the effect of the environment temperature (weather) on the lake and thermal stratification. Therefore, CE-qual-W2 program was choosen for this aim. The thermal stratification is simulated using this program. In simulations using CE-qual-W2 program, it is seen that the weather (environment

temperature) directly affects the stratification, mainly in upper layers. The numerical thermal stratification model was verified with the field observations. Comparing the output results of the CE-qual-W2 program with observed values, shows that the model has given compatible results of thermal stratification of lake for epilimnion and thermocline layers. Main differences were seen in values of modeled and observed temperature of the Hypolimnion layer. A parameter that can affect the stratification and direction of the flow, specially, at lower layers and Hypolimnion layer in Lake Köyceğiz is ground water and thermal springs under and near the lake. This case is understandable from the results of thermal stratification model using CE-qual-W2 program. It is said that the thermal waters in this region have temperature more than 20^{o}C. In Sultaniye part of the lake, the temperature of the thermal waters reaches up to 39°C. It could be concluded that these waters are thermomineral waters, presumably. In addition to effect of thermal and ground waters on temperature of the Hypolimnion layer, the difference between observed and modeled temperatures in different depths could be caused by the lack of the data. Totally, results of this simulation show that the lake is stratified thermally in most months of year. After December to February, the lake is unstratified, approximately.

The possibility of construction of a large dam on Namnam river, as the most important river of Köyceğiz, always has been. Temprature of water, salinity and dissolved oxygen distribution may change vertically (through depth) because of construction of dam and creation of reservoir on Namnam river. Therefore and based on the items that was noted, it is expected that the construction of dam on Namnam river can change the situation of stratified layers of Lake Köyceğiz and the water quality of that. However, it depends on the depth of water behind dam body, position and type of the intake structure of dam, frequency, discharge and duration of releasing water from dam.

REFERENCES

Abad, J. D., Rhoads, B. L., Güneralp, I., García, M. H., (2008). Flow Structure at Different Stages in a Meander-Bend with Bendway Weirs, *Journal of Hydraulic Engineering,* Vol. 134, No. 8.

Abbaspour, A., Farsadizadeh, D., Hosseinadehdalir, A., Sadraddini, A.A., (2009). Numerical Study of Hydraulic Jumps on Corrugated Beds Using Turbulence Models. *Turkish Journal of Engineering and Enviromental Sciences. VOL.33, P.61 – 72.*

Ağiralioğlu, N. (2007). Baraj Planlama ve Tasarımı. Vol.1, Second Edition, .Istanbul

Akbari, E., Kashefipour, S. M., (n.d.). Three-dimensional Modelling of Developing of Wave Head Caused by Dam Damage, *National Conference on Flood Management, Iran.*

Akiyama, J., Stefan, H. G., (1981). Theory of Plunging Flow into a Reservoir. *Internal Memo IM-97, St. Anthony Falls Hydraulic Laboratory, University of Minnesota, Minneapolis, Minn.*

Alavian, V., Ostrowski, J. P., (1992). Modification of the Thermal Structure in TVA Reservoirs Using a Calculated Density Current Release. *ASCE Journal of Hydraulic Engineering.*

Algan, O., Gazioglu, C., Yucel, Z., Cagatay, N., Gonencgil, B., (2000). Sediment and Freshwater Discharges of the Anatolian River into the Black Sea. *IOC-BSRC Workshop Report, No.145,Paris,UNESCO,P.38–50.*

An, S., (2014). Three-Dimensional Numerical Simulation of Intrusive Density Currents, *Journal of Environmental Science International, 23(7); 1223-1232.*

Anderson, J. D., (2009). Governing Equations of Fluid Dynamics, *Computational Fluid Dynamics, 3rd ed., Springer-Verlag Berlin Heidelberg.*

Ashley, R. M., Arthur, S., Coghlan, B. P., McGregor, I., (1994). Fluid Sediment in Combined Sewers. *Water Science and Technology, 29(1-2), P.113-123.*

Aydin, R., (2009). Estimation of Suspendent Sediment Concentration Using Acoustic Methods, *M.S, Thesis, Izmir Institute of Technology.*

Aytek, A., (2006). Mathematical modeling for river delta formation. *Istanbul Technical University, Ph.D. Thesis.*

Arnon, A., Lensky, N. G., Selker, J. S., (2014). High-resolution Temperature Sensing in the Dead Sea Using Fiber Optics, *Water Resources Research, Vol.50, P.1756–1772.*

Baharim, N. H., Ismail. R., Omar, M. H., *(2011).* Effects of Thermal Stratification on the Concentration of Iron and Manganese in a Tropical Water Supply Reservoir. *Sains Malaysiana, 40(8)(2011), P.821–825.*

Bakker, A., (2006). Fluid Dynamics: Free Surface Flows Applied Computational. *Lecture16. Bakker.org.*

Bakker, A., (2006). Conservation Equations Applied Computational Fluid Dynamics. *Lecture3. Bakker.org.*

Bardina, J., Ferziger, J.H., Reynolds, W.C., (1983). Improved Turbulence Models Based on Large-Eddy Simulation of Homogeneous, Incompressible, Turbulent Flow. *Thermosciences Division Department of Mechanical Engineering, Stanford University.*

Batchelor, G., (2000). Introduction to Fluid Mechanics Book, *Cambridge, University Press.*

Bates, C. C., (1953). Rational Theory of Delta Formation. *Bulletin of American Association of Petroleum Geology, 37(9), 2119–2162.*

Batick, B. M., *(2011).* Modeling Temperature and Dissolved Oxygen in the Cheatham Reservoir with CE-QUAL-W2. *M.Sc. Thesis, Vanderbilt University*

Berkun, M., Aras, E., (2012). River Sediment Transport and Coastal Erosion in the Southeastern Black Sea Rivers. *Journal Hydrology and Hydromechanic, 60, 4, P.299–308.*

Bernard, P. S., Wallace, J. M., (2002). Turbulent Flow: Analysis, Measurement and Prediction. *Wiley.*

Bhattacharya, J. P., MacEachern, J. A., (2009). Restricted access Hyperpycnal Rivers and Prodeltaic Shelves in the Cretaceous Seaway of North America. *Journal of Sedimentary Research.*

Bird, R. B., Stewart, W. E., Lightfoot, E. N., (1960). Transport Phenomena. *Wiley, P.83-91.*

Boehrer, B., Schultze, M., (2008). Stratification of lakes, *American Geophysical Union.*

Bombardelli, F.A., García, M.H., (2001). Three-dimensional hydrodynamic modeling of density currents in the Chicago river, Illinois, *Civil Engineering Series, Hydraulic Engineering Series No.68.*

Boike, J., Georgi, C., Kirilin, G., Muster, S., Abramova, K., Fedorova, I., … Grigoriev, M., (2015). Thermal processes of thermokarst lakes in the continuous permafrost zone of northern Siberia: observations and modeling (Lena River Delta, Siberia), *Biogeosciences, VOL.12, P.5941–5965.*

Boehrer1, B., Schultze1, M., (2007). Stratification of Lakes. *Reviews of Geophysics, 46, P.1-27.*

Brennen, C. E., (2005). Fundamentals of Multiphase Flows. *Cambridge University Press 2005, ISBN 0521 848040.*

Caliskan, A., (2008). Modeling of Hydrodynamics and Sedimentation in a Stratified Reservoir: Tahtali Reservoir, Izmir. *Izmir Institute of Technology, Master Thesis.*

Castillo1, L. G., Álvarez, M. A., Carrillo, J. M., (2014). Numerical Modeling of Sedimentation and Flushing at the Paute-Cardenillo Reservoir, *ASCE-EWRI International Perspective on Water Resources and Environment.*

Celik, I.B., (1999). Introductory Turbulence Modeling. Lectures Notes, *West Virginia University Mechanical & Aerospace Engineering Department.*

Chaturvedi, M.C., (1987).Water resources planning and management. *Tata, McGraw Hill, New Delhi.*

Coulson, J.M., Richardson, J.F., (1999). Chemical engineering. *VOL.1. Sixth Edition, Elsevier.*

Cook, C. B., Richmond, M. C., (2004). Simulating the Flow Field Upstream of the Dworshak Dam Regulating Outlets, *Idaho Fish and Game, Ahsahka, Idaho Dworshak Dam Assessment and Fisheries Investigations Bonneville Power Administration Project 1987-099-00.*

Cole, T.M., Wells, S.A., (2015). CE-QUAL-W2: A Two-Dimensional, Laterally Averaged, Hydrodynamic and Water Quality Model, Version 3.72. UserManual. *Department of Civil and Environmental Engineering Portland State Univeristy.*

Cole, T.M., Wells, S.A., (2000). CE-QUAL-W2: A twodimensional, laterally averaged, hydrodynamic and water quality model, Version 3.0. *Instruction Rep. No. EL-2000, U.S. Army Engineering and Research Development Center.*

Cossu, R., Forrest, A.L., Roop, H.A., Dunbar, G.B., Vandergoes, M.J., Levy, R.H., …, Schladow, S.G., (2015). Seasonal Variability in Turbidity Currents in Lake Ohau, New Zealand, and Their İnfluence on Sedimentation, *Marine and Freshwater Research, CSIRO Publishing.*

Cyberski, J., Cyberska, B., (n.d.). Water Mixing in Different Types of Storage Reservoirs.

Crowe, S.A., O'Neill, A.H., Katsev, S., Hehanussa, P., Haffner, G.D., …… Sundby, B., Mucci, A., Fowle, D.A., (2008). The biogeochemistry of tropical lakes: A case study from Lake Matano, Indonesia, *American Society of Limnology and Oceanography, Limnol. Oceanogr. 53(1), 2008, 319–331.*

Dake, J. M., Harleman, D. R. F., (1969). Thermal Stratification in Lakes: Analytical and Laboratory Studies. *Water Resources Research, Vol.5, No.2.*

Davidson, D., (2015). An introduction to turbulence models. *Department of Thermo and Fluid Dynamics, Chalmers University of Technology, Publication 97/2.*

Davies, A. G., Ribberink, J. S., Temperville, A., Zyserman, J. A., (1996). Comparisons between sediment transport models and observations made in wave and current flows above plane beds, *Coastal Engineering, VOL.31 P.163-198.*

De Rooij, F., Linden, P. F., Dalziel, S. B., (1999). Saline and Particle-driven Interfacial Intrusions. *J. Fluid Mech. 389, P.303-334.*

De juette, C., Le Gouez, J. M., Put, O., Rigaud, S., (n.d.). Volume of fluid method (VOF) applied to non-linear wave problems on body-fitted grids. *International Workshop on Water Waves and Floating Bodies, IWWWFB.*

Deardorff, J., (1970). A numerical study of three-dimensional turbulent channel flow at large Reynolds numbers. *Journal of Fluid Mechanics 41 (2), P. 453–480.*

Delghandil, M., Saghi, H., Broomandnasab, S., (2013). Performance Computational Fluid Dynamics Software Tools in Determination Emitters Outflow, *Iranian Journal of lrrigation and Drainage, No.4, Vol.6, p.245-253.*

Demirci, M., Kocaman, S., Varli, B., (2012). Numerical investigation of velocity distribution around bridge abutment with different geometries, *Erciyes University Journal, 28(3):161-174.*

Dobek, S., (2012). Fluid Dynamics and the Navier-Stokes Equation. *Lecture Notes.*

Durst, F., (2008). Fluid Mechanics: An Introduction to the Theory of Fluid Flows, *Springer, 2008*

Ducassou, E., Mulder, T., Migeon, S., Zaragosi, S., (2008). Nile floods recorded in deep Mediterranean sediments, *Quaternary Research, P.382–391.*

Ebrahimi, M., Jabbari, E., Abbasi, H., (2015). Simulation of Thermal Stratification and Salinity in Dam ReservoirUsing CE-QUAL W2 Software (Case study: Baft Dam), *Journal of Civil Engineering and Urbanism, VOL.5, Issue 1, P.07-11.*

Elçi, S., Work, P. A., Hayter, E. J., (2007). Influence of Stratification and Shoreline Erosion on Reservoir Sedimentation Patterns. *Journal of Hydraulic Engineering, 133(3), P.255-266.*

Emami, S., (n.d.). Evaluation of Hydraulic Operation of Spillways Using Three-dimensional Mathematical Model, *Technical Report.*

Erkek, C., Agiralioglu, N., (2010). Su Kaynaklari Muhendisligi. *Vol.6, Beta.*

Fang, H.W., (1996). Three-dimensional Mathematical Model of River Bed Erosion for Water-sediment Two Phase Flow. *ACTA Mechanic Sinica, 12(1): 85.*

Fang, H. W., Wang, G. Q., (2000). Three-dimensional Mathematical Model of Suspended Sediment Transport. *Journal of Hydraulic Engineering, Vol. 126, No. 8, ASCE.*

Farrell, G. J., Stefan, H., (1986). Mathematical Modeling of Plunging Reservoir Flows. *Journal of Hydraulic Research, 26(5), P.525-537.*

Fischer, H. B., List, E. J., Koh, R. C. Y., Imberger, J., Brooks, N. H., (1979). Mixing in Inland and Coastal Waters. *Academic Press, New York. P.484.*

FLOW 3D User Manual, (2008). *Flow Science Inc.*

Ford, D. E., Johnson, M. C., Monismith, S. G., (1980). Density Inflows to DeGray Lake, Arkansas. *IAHR 2nd International Symposium on Stratified Flows, Trondheim, Norway.*

Ford, D. E., Johnson, M. C., (1983). An Assessment of Reservoir Density Currents and Inflow Processes. *Technical Report, E-83-7, Prepared by Ford, Thornton, Nortonand Associates, Ltd, and the Environmental Laboratory, Waterways Experiment Station, for the U. S. Army Engineer Waterway Experiment Station, Vicksburg, Miss.*

Francisco, J. M., Yang, C. T., (n.d.). Sedimentation Modeling for Rivers and Reservoirs, *Erosion and Sedimentation Manual.*

Frohlich, J., Rodi. W., (2002). Introduction to Large-Eddy Simulation of Turbulent Flows. *Institude for Hydromechanics, University of Karlsruhe, Germany.*

Gal, G., Imberger, J., Zohary, T., Antenucci, J., Anis, A., Rosenberg, T., (2003). Simulating the Thermal Dynamics of Lake Kinneret. *Ecological Modelling, 162, P.69–86.*

Gikas G.D., Tsihrintzis V.A., Akratos C.S. and Haralambidis G. (2009). Water quality trends in Polyphytos reservoir, Aliakmon river, Greece. *Environmental Monitoring and Asseessment, 149, P.163-181.*

Gleick, P., (1998). The World's Water 1998–1999. *Island Press, Washington DC.*

Green, A., Humphreys, J., Mackenzie, R., Jones, I.G. (n.d.). Atomic Diffusion in Metals and Alloys, *Materials Science on CD-ROM User Guide, Ver.2.1.*

Goncu, S., Hasanoglu, E., Avdan, U., Yigit Avdan, Z., Albek, E.A., (2015). Investigation of Thermal Stratification in Borabey Lake, Turkey, *Anadolu University Journal of Science and Technology, Applied Sciences and Engineering, VOL.16, No.3, P.351-366.*

Gulati, R. D., Donk, E. V., (2002). Lakes in the Netherlands, Their Origin, Eutrophication and Restoration: State-of-the-art Review. *Hydrobiologia 478(1), P.73-106.*

Gunduz, O., Soyupak, S., Yurteri, C., (1998). Development of Water Quality Management Strategies for the Proposed Isikli Reservoir. *Water Science and Technology, Vol.37, No.2, P.369-376.*

Haitham, A. H., Rozi, A., Sobri, H., Mohammed, A., (2013). Numerical Model of Baffle Location Effect on Flow Pattern in Oil and Water Gravity Separator Tanks, *World Applied Sciences Journal 26 (10), P.1351-1356.*

Hall, E., (2008). Hydrodynamic Modelling of Lake Ontario. *Master Thesis, Department of Civil Engineering, Quaeen's University.*

Hanson-Lee, M., (2003). The Water Quality of Lake Utopia. *Community, Lake, Education, Monitoring.*

Harelman, D. R. F., Stolzenbach K. D., (1972). Fluid mechanics of heat disposal from power generation. *Annual Review of Fluid Mechanics, 4, P.7-32.*

Hebbert, B., Imberger, J., Loh, I., Paterson, J., (1979). Collie River Underflow into the Wellington Reservoir. *Journal of Hydraulics Div., ASCE, 105, HY5, P.533-545.*

Heimsund, S., (2007). Numerical Simulation of Turbidity Currents, A New Perspective for Small- and Large Scale Sedimentological Experiments, *Thesis of Department of Earth Science, University of Bergen.*

Henderson-Sellers, B., (1988). Sensitivity of Thermal Stratification Models to Changing Boundary Conditions. *Applied Mathematical Modelling 12, P.31–43.*

Hickin, E.J., (n.d.). River Geomorphology. *Chapter 4.*

Hickin, E.J., (n.d.). Sediment Transport. Simon Fraser University, *Chapter 4.*

Hipsey, M. R., Brookes, J. D., (2013). Pathogen Management in Surface Waters: Practical Considerations for Reducing Public Health Risk. *Current Topics in Public Health, Chapter 21.*

Hodges, B. R., Imberger, J., Laval, B., Appt, J., (2000). Modeling the Hydrodynamics of Stratified Lakes. *Hydroinformatics Conference, Iowa Institute of Hydraulic Research.*

Hogg, C. A. R., (2014). The Flow of Rivers into Lakes: Experiments and Models. *Ph.D. Thesis, Robinson College, University of Cambridge.*

Holmes, R., Kelly, D., (2012). Options for Improving Water Quality in the Maitai Reservoir and River. *Cawthron Institute, Report No.2234.*

Holyer, J. Y., Huppert, H. E., (1980). Gravity Currents Entering a Two-layer Fluid. *J. Fluid Mech. 100, P.739-767.*

Horne, A. J., Goldman, C. R., (1994). Lake Ecology Overview, *Limnology. Edition.2, Chapter 1, McGraw-Hill Company. New York, USA.*

Hoseini, S. A., Abdipour, A., (2008). Numercal Modelling of Velocity Profile in Turbidity Currents and Study on the Effect of the Slope, Concentration and Discharge on it, *IAU Civil Engineering Journal, VOL.3, No.3, P.60-69.*

Huang, W., Jones, W. K., (2003). Field Experiment and Hydrodynamic Modeling of an Stratified Estuary in Florida, USA. *International Conference on Estuaries and Coasts, China.*

Ilgaz, C., Karahan, M. E., Bulu, A., (2000). Akışkanlar Mekaniği ve Hidrolik Problemleri Kitabı, *Çağlayan Kitabevi, İkinci baskı.*

Imberger, J., (1985). The Diurnal Mixed Layer. *Limnology and Oceanography, 30, P.737-770.*

Irtem, E., (1991). Determination of Water Movement in Stratified Bays and its Application to the Izmit Bay. *Istanbul Technical University, Ph.D. Thesis.*

Jin, K. R., Hamrick, J. H., Tisdale, T. (2000). Application of Three-dimensional Hydrodynamic Model for Lake Okeechobee. *Journal of Hydraulic Engineering 126(10), P:758-771.*

Kabdaşli, S., Mercan, D. E., Adingakko, A., (2002). Observation of Lake Köyceğiz Water Levels Project. *Istanbul Technical University. Hydraulic and Water Resources Lab.*

Kaheh, M., Kashefipour, S.M., Dehghani, A., (n.d.). Comparison of k-ε and RNG k-ε Turbulent Models for Estimation of Velocity Profiles Along the Hydraulic Jump on Corrugated Beds. *Flowscience Web Page, FLOW3D.*

Kahya, E., (n.d.). Sediment Transport. *Lecture notes, Water resources, ITU.*

Karthik, T. S. D., (2011). Turbulence Models and Their Applications, *10th Indo German Winter Academy.*

Kaykisizli, H., (2006). Formulation of Icompressible Steady Two Dimensional Compact Forth Order Navier-Stokes Equations in General Curvilinear Coordinates. *Gebze Energy Institude, Master of Science Thesis.*

Kennedy, R. H., Thornton, K. W., Gunkel Jr., R. C., (1982). The establishment of water quality gradients in reservoirs. *Journal of Canadian Water Resources, 7, P.71-87.*

Keshtkar, Sh., Ayyoubzadeh, S. A., Firoozabadi, B., (2010). Experimental Studies on Thickness and Vertical Velocity Distribution of Turbidity Current. *Journal of Water and Soil, VOL.24, No.6, P.1073-1082.*

Keulegan, G. H., (1957). An Experimental Study of the Motion of Saline Water from Locks into Fresh Water Channels. *NBS Report No:5168.*

Khayammi, M., Danesh, S., Khodashenas, S., Davari, K., (2009). Simulation of Water Quality in Dam's Basins (Case Study – Torogh Dam Basin). *Journal of Water and Soil, Vol. 23, No. 1, P:17-29*

Kipling, R., (n.d.). Principles and Processes of Sediment Transport, *Chapter 4, Dyke, P.96-124.*

Kocaman, S., (2007). Experimental and Theoretical Investigation of Dam Break Problem, *Ph.D. Thesis, Department of Civil Engineering Institute of Natural and Applied Sciences University of Cukurova.*

Komar, P. D., (1980). Modes of Sediment Transportin Channelized Water Flows with Ramifications to the Erosion of the Martian Outflow Channels, *Academic press, ICARUS, VOL.42, P.317-329.*

Koretsky, C. M., MacLeod, A., Sibert, R. J., Snyder, C., (2011). Redox Stratification and Salinization of Three Kettle Lakes in Southwest Michigan, USA. *Water, Air, & Soil Pollution, Vol.223, Issue.3, P.1415–1427.*

Kostic, S., Parker, G., (2003). Physical and Numerical Modeling of Deltaic Sedimentation in Lakes and Reservoirs. *Proceedings, XXX International Association of Hydraulic Research Congress.*

Lathrop, R.C., Lillie, R.A., (1980). Thermal Stratification of Wisconsin Lakes, *Wisconsin Academy of Sciences, Arts and Letters, Vol.68, P.90-96.*

Langland, M., Cronin, T., (2003). A Summary Report of Sediment Processes in Chesapeake Bay and Watershed, *U.S. Department of the Interior, U.S. Geological Survey.*

Lee, x., Huang, T., Ma, W., Sun, X., Zhang, H., (2015). Effects of Rainfall Patterns on Water Quality in a Stratified Reservoir Subject to Eutrophication: Implications for Management. *Sci. Total Environ. P.521, 27–36.*

Lowe, R. J., Linden, P. F., Rottman, J. W., (2002). A laboratory Study of the Velocity Structure in an Intrusive Gravity Current. *J. Fluid Mech, Vol. 456, P. 33-48.*

Marsooli, R., Wu, W., (n.d.). A Three-dimensional Finite-Difference Dam-Break Wave Model Based on Volume-of-Fluid Surface Tracking Method, *AcademyPublish.org, Wave Propagation.*

Maronga, B., Gryschka, M., Heinze, R., Hoffmann, F., Kanani-Sühring, F., Keck, M., …, Letzel, M.O., (2015). The parallelized large-Eddy simulation model (PALM) version 4.0 for atmospheric and oceanic flows: model formulation, recent developments, and future perspectives, *Geoscience, Model Development, VOl. 8, P.2515–2551.*

Martin, J. L., McCutcheon, S., (1999). Hydrodynamics and transport for water quality modeling. *CRC Press, Inc.*

Mirbagheri, S. A., Boudagpour, S., Monfared, S. A. H., (2007). Using Sediment Transport Simulating Model for Determining of Ekbatan Dam Reservoir Life, *Technology and Education Journal, Vol.2, No.2.*

Milligen, B. Ph., Bones, P. D., Carreras, B. A., Sanchez, R., (2005). On the Applicability of Fick's Law to Diffusion in Inhomogeneous Systems. *European Journal of Physics, No.26, P.913-925.*

Milliman, J. D., (1981). Transfer of River-born Particular Material to the Ocean River Inputs to Ocean Systems. *UNEP UNESCO, Switserland, P.5-12.*

Mefford, B., Higgs, J., (2006). Link River Falls Fish Passage Investigation, Flow Velocity Simulation, *Water Resources Research Laboratory Technical Paper.954.*

Meiburg, E., Kneller, B., (2009). Turbidity Currents and Their Deposits. *Annual Review of Fluid Mechanics.*

Modiri-Ghareveran, M., Jabbari, E., Etemad-Shahidi, A., (2013). Effects of Climate Change on the Thermal Regime of a Reservoir. *Water Management, Institution of Civil Engineers.*

Monismith, S. G., Imberger, J., Morison, M. L., (1990). Convective Motions in the Sidearm of a Small Reservoir. *Limnology and Oceanography Journal, 35(8), P. 1676-1702.*

Morkofsky, M., Harleman, D. R. F., (1973). Prediction of Water Quality in Stratified Reservoir. *Journal of the Hydraulic Division, ASCE, Vol.99.*

Morrison, A., (2011). The Equation of Continuity and the Equation of Motion in Cartesian, Cylindrical, and Spherical Coordinates. *Course Notes.*

Mulder, T., Syvitski, J. P. M., Migeon, S., Faugeres, J., Savoye, B., (2003). Marine Hyperpycnal Flows, Initiation, Behavior and Related Deposits, A Review, *Marine and Petroleum Geology 20, P.861–882.*

Mulder, T., Chapron, E., (2011). Flood Deposits in Continental and Marine Environments: Character and Significance, *AAPG Studies in Geology 61, P.1–30.*

Nandalal, K. D. W., (1995). Reservoir Management under Consideration of stratification and hydraulic phenomena. *Doctoral Dissertation, Wageningen Agricultural University, Netherlands.*

Nazariha, M., Danayi, E., Hashemi, S. H., Izaddustdar, A. H., (2010). Camparison of the Thermal Stratification of Under Construction Bakhtiyari Dam at Reservoir and trasitional Area Using CE-QUAL-W2 Model, *Enviromental Sciences and Technologies, VOL 13, No.3.*

Nazariha, M., Danayi, E., Hashemi, S. H., Izaddustdar, A. H., (2009). Prediction of Thermal Stratification in Proposed Bakhtyari Reservoir with CE-QUAL-W2. *World Environmental and Water Resources Congress 2009.*

Ning, D., (2014). A Computational Study on Hydraulic Jumps, including Air Entrainment, *Dissertations Work. University Of California, Davis.*

Nguyen, C., (2005). Turbulence Modeling. *Course Notes.*

Nouri, J., Rahimipour, H., Nezakati, R., (2004). Simulation of Thermal Stratification in Urban Man made Lakes, *American Journal of Applied Sciences.*

Nsiri, I., Tarhouni, J., Irie, M., (2016). Modeling of Thermal Stratification and the Effect on Water Quality in Four Reservoirs in Tunisia. *Journal of Hydrogeology and Hydrology Engineering, 5:1.*

Okely, P., Imberger, J., Antenucci, J. P., (2010). Processes Affecting Horizontal Mixing and Dispersion in Winam Gulf, Lake Victoria. *Limnology and Oceanography., 55(5), P.1865–188.*

Ongley, E., (1996). Sediment Measurements. *Water Quality Monitoring*-A Practical Guide to the Design and Implementation of Freshwater Quality Studies and Monitoring Programmes, *Published on behalf of United Nations Environment Programme and the World Health Organization, UNEP/WHO.*

Ottosson, F., Abrahamsson, O., (1998). Presentation and analysis of a model simulating epilimnetic and hypolimnetic temperatures in lakes. *Ecol. Model. 110, P.233–253.*

Oudenaarden, A. (2009). Systems Biology. *MIT, P.67-70.*

Parsons, J. D., Bush, J. W. M., Syvıtskı, J. P. M., (2001). Hyperpycnal Plume Formation from Riverine OutfOws with Small Sediment Concentrations. *International Association of Sedimentologists,* No.*48, P.465-478.*

Razmi, A. M., Bakhtyar, R., Firoozabadi, B., Barry, A., (2013). Experimental and Numerical Modeling of Baffle Configuration Effects on the Performance of Sedimentation Tanks, *Canadian Journal of Civil Engineering.*

Raudkivi, A. J., *(1976).* Loose Boundary Condition. *Pergamon International Library of Science, Technology, Engineering and Social Studies.*

Rickenmann, D., (1991). Hyperconcentrated Flow and Sediment Transport at Steep Slopes. *Journal of Hydraulic Engineering, Vol. 117, No, 11, P.1419-1439.*

Richey, J. E., Meade, R. H., Salati, E., Devol, A. H., Nordin, C. F., (1986). Water Discharge and Suspended Sediment Concentrations in the Amazon River, *Water Resources research, VOL.22, No. 5, p 756-764.*

Rijn, L. V., (n.d.). Sedimentation of Sand and Mud in Reservoirs and Rivers.

Rijn, L. V., (1982). Sediment transport: Part II, Suspended load transport. *Journal of Hydraulic Engineering, ASCE, VOL.110, N0.11, P.1613.*

Rijn, L. V., (1985). Two-dimensional Vertical Mathematical model for Suspended Sediment Transport by Currents and Waves. *Research Report S488-IV, Delft Hydraulics Laboratory.*

Roberts, P. J. W., Webster, D. R. (n.d.). Turbulent Diffusion. *School of Civil and Environmental Engineering, Georgia Institute of Technology, Atlanta, Georgia.*

Rodriguez, J. F., Bombardelli, F. A., García, M. H., Frothingham, K. M., Rhoads, B. L., Abad, J. D., (2004). High-resolution Numerical Simulation of Flow Through a Highly Sinuous River Reach. *Water Resources Management 18*: 177–199.

Saghi, H., Delghandi, M., Boroumandnasab, S., (2011). Comparison of Efficiency of FLUENT and FLOW3D Softwares, *Agricultural Scientific Journal, VOL.35, No.2.*

Salant, N. L., Hassan, M. A., Alonso, C. V., (2008). Suspended Sediment Dynamics at High and Low Storm Flows in Two Small Watersheds. *Hydrological Processes, Hydrol. Process. 22, P.1573–1587.*

Santos, R., Saggio, A., Silva, T., Negreiros, N., Rocha, O., (2015). Short-term Thermal Stratification and Partial Overturning Events in a Warm Polymictic Reservoir: Effects on Distribution of Phytoplankton Community. *Braz. J. Biol., Vol75, No.1, P.19-29.*

Sasmaz, A., (2005). Dalyan ve Çevresinin Fiziki Coğrafyasi. *Yüzüncü Yil University, Master thesis.*

Savage, S. B., Brimberg, J., (1975). Analysis of Plunging Phenomena in Water Resources. *Journal of Hydraulic Research, IAHR, Vol.13, No.2, P.187-204.*

Savli, M., (2012). Turbulence Kinetic Energy. *Seminar, University of Ljubljana, Faculty of Mathematics and Physics, Department of Meteorolgy.*

Sonmez, M. E., (2012). The Negative Impacts of Dams on Envıronment and Their Samples in Turkey, *Gaziantep University Social Sciences Journal, 11(1):213-231.*

Saad, T. (n.d.). Turbulence Modeling for Beginners. *University of Tennessee Space Institute.*

Serra, T., Vidal, J., Casamitjana, X., Soler, M., Colomer, J., (2007). The Role of Surface Vertical Mixing in Phytoplankton Distribution in a Stratified Reservoir, *Limnol. Oceanogr, 52(2), 620–634.*

Sert, C., (n.d.). Finite Element Analysis in Thermofluids. *Chapter 1, Course Notes.*

Sharip, Z., Jusoh, J., (2010). Integrated Lake Basin Management and its Importance for Lake Chini and Other Lakes in Malaysia. *Lakes & Reservoirs Research & Management 15(1), P.41 - 51·*

Sharip, Z., Zakaria, S., (2008). Lakes and Reservoir in Malaysia, Management and Researche Challenges. *Proceedings of Taal 2007, The 12th World Lake Conference, P.1349-1355.*

Shim, J. S., Jinah Kim, J., Kim, D. C., Heo, K., Do, K., Park, S. J., (2013). Storm Surge Inundation Simulations Comparing Three-Dimensional With Two-Dimensional Models Based On Typhoon Maemi Over Masan Bay of South Korea, *Journal of Coastal Research. Special Issue No. 65*.

Singh, B., Shah, C. R., (1971). Plunging Phenomenon of Density Currents in Reservoirs. *La Houille Blanche, 26(1), P.59–64.*

Soyinka, O.A., Slatt, R., (2008). Identification and Micro-stratigraphy of Hyperpycnites and Turbidites in Cretaceous Lewis Shale, Wyoming, *Sedimentology, VOL.55 (5):1117-1133.*

Sagaut, P., (2006). Large Eddy Simulation of Incompressible Flow. *Springer, 3rd edition.*

Slotta, L. S., (n.d.). Stratified Reservoir Density Flows Influenced by Entering Streamflows, *Geophisical Monograph Series, Man-made Lakes: Their Problems and Environmental Effects, VOL.17.*

Smagorinsky, J., (1963). General Circulation Experiments With the Primitive Equations. *Monthly Weather Review 91 (3), P.99–164.*

Sousa, V., Bombardelli, F. A., Chanson, H., (2009). Numerical Simulation of Rectangular Dropshafts Using a Volume-of-fluid (VOF) Technique, *33rd IAHR Congress: Water Engineering for a Sustainable Environment, by International Association of Hydraulic Engineering & Research (IAHR).*

Stevens, H. H., Yang, C. T., (1989). Summary and Use of Selected Fluvial Sediment Discharge Formulas. *U.S. Geological Survey, Water Resources Investigations Report 89-4026.*

Sumer, B.M., Unsal, I., Bayazit, M., (2007). Hydraulics, *Birsen Yayinevi.*

Suni, I. I., (n.d.). *Course Notes, Chapter 6, Dept. of Chemical and Biomolecular Engineering, Clarkson University.*

Swanson, H., Zurawell, R., (2006). Lake Newell Reservoir: Water Quality Monitoring Report. *Environmental Monitoring and Evaluation Branch, Alberta Environment, Edmonton.*

Tahmiscioğlu, M.S., Anul, N., Ekmekçi, F., Durmuş, N., (n.d.). Positive and Negative Impacts of Dams on the Environment, *International Congress on River Basin Management, Basin Water Management.*

Taheri, H., hasanialiguodarzi, A. A., Ganjidoost, H., (2013). Simulation of Water Level and Temperature of Sepidrood Dam Reservoir, *Water and Waste Water Journal, No.2, P 129-134.*

Talling, J. F., (1963). Origin of Stratification in an African Rift Lake. *Association for the Sciences of Limnology and Oceanography, Vol.8, Issue:1, P.68-78.*

Tirnaksiz, F., (n.d.). Diffusion, *Modern Pharmaceutical Technology.*

Tafarrojnorouz, A., Bejestan, M. S., Izadjoo, F., (2007). Investigation and Study on the Biological Prameters of Kandak Dam Reservoir, *4th National Congress of Civil Engineering, Tehran University.*

Tryggvason, G., (2011). Computational Fluid Dynamics: The Equations Governing Fluid Motion. *Lecture Notes.*

Unes, F., Varcin, H., (2009). Investigation of Plunging Depth and Density Currents in Eğrekkaya Dam Reservoir, *IMO Technical Journal.*

Unes, F., (2003). Investigation of Temporary Variation of Plunging Point Caused by Density Plunging Reservoir Flow Using Mathematical Modeling, *IMO Technical Journal.*

Unes, F., (2008). Analysis of Plunging Phenomenon in Dam Reservoirs Using Three-Dimensional Density Flow Simulations. *Canadian Journal of Civil Engineering, 35(10), P.1138-1151.*

USSD, (2015). Modeling Sediment Movement in Reservoirs. *Report, Prepared by the United States Society of Dams, Committee on Hydraulics of Dams, Subcommittee on Reservoir Sedimentation.*

Von Karman, T., (1940). The engineer grapples with nonlinear problems. *B. Am. Math. Soc., 46, P.615–683.*

Walling, D. E., Webb, B. W., (1981). The Reliability of Suspended Sediment Load Data, in: Erosion and Sediment Transport Measurements. *IAHS Publications, No.133, P.177-194.*

Warrick, J.A., Milliman, J.D., (2003). Hyperpycnal Sediment Discharge from Semiarid Southern California Rivers: Implications for Coastal Sediment Budgets. *Geological Society of America, VOL.31, NO.9, P.781–784.*

White, F.M., (n.d.). Fluid Mechanics Book, *7th edition, The McGraw-Hill Companies.*

White, F. M. (2006). Viscous Fluid Flow. *Third Edition, McGraw-Hill.*

Widera, P., (2011). Study of sediment transport processes using Reynolds Averaged Navier-Stokes and Large Eddy Simulation. *Ph.D. Thesis, Faculty of Engineering, Vrije Universiteit Brussel.*

Wildi, W., (2010). Environmental Hazards of Dams and Reservoirs. *NEAR Curriculum in Natural Environmental Science, 2010, Terre et Environnement, Vol. 88, P.187–197, ISBN 2–940153–87–6.*

Williams, G.P., *(1989).* Sediment Concentration Versus Water Discharge During Single Hydrological Events in Rivers. *Journal of Hydrology, No.111, P.89-106.*

Williams, G.P., Wolman, M.G., *(1984).* Downstream Effects of Dams on Alluvial Rivers. *Geological Survey Professional Paper 1286.*

Williams, J., Arsenault, M. A., Buczkowski, B. J., Reid, J., Flocks, J., Kulp, M. A., …, Jenkins, C. J., (2006). Surficial Sediment Character Of The Louisiana Offshore Continental Shelf Region, A GIS Compilation, *United States Geological Survey Open-File Report 2006-1195.*

Woelke, M., (n.d.). Eddy Viscosity Turbulence Models Employed by Computational Fluid Dynamic. *Transactions of The Institute of Aviation, No. 191, P.92-113.*

Wu, J., Zou, R., Yu, S.L., *(2006).* Uncertainty Analysis for Coupled Watershed and Water Quality Modeling Systems. *Journal of Water Resources Planning and Management, ASCE.*

Yakhot, V., Orszag, S.A., Thangam, S., Gatski, T.B., Speziale, C.G. (1992). Development of Turbulence Models for Shear Flows by a Double Expansion Technique. *Physics of Fluids, Vol. 4, No. 7, P.1510-1520.*

Yang, X., Huang, T., Zhang, H., (2015). Effects of Seasonal Thermal Stratification on the Functional Diversity and Composition of the Microbial Community in a Drinking Water Reservoir. *Water 7, P.5525-5546.*

Zahiri, A.R., Shafai Bejestan, M., Dehghani, A.A., (2011). Estimation of Sediment Volume Due to Turbidity Currents in Dez Reservoir Dam. *Journal of Water and Soil Conservation, VOL.18, No.1.*

Zhang, D., (2014). Optimize Sedimentation Tank and Lab Flocculation Unit by Cfd, *Master Thesis. Norwegian University of Life Sciences.*

Zielinski, T.J., (2006). Diffusion: A Brief Review. *Monmouth University Department of Chemistry, Medical Technology, and Physics.*

APPENDICES

Appendix A: Additional Plots for Reservoir Simulations.

Appendix B: Wentworth Grain Size Chart from United States Geological Survey.

APPENDIX A: Additional Plots for Reservoir Simulations.

S1

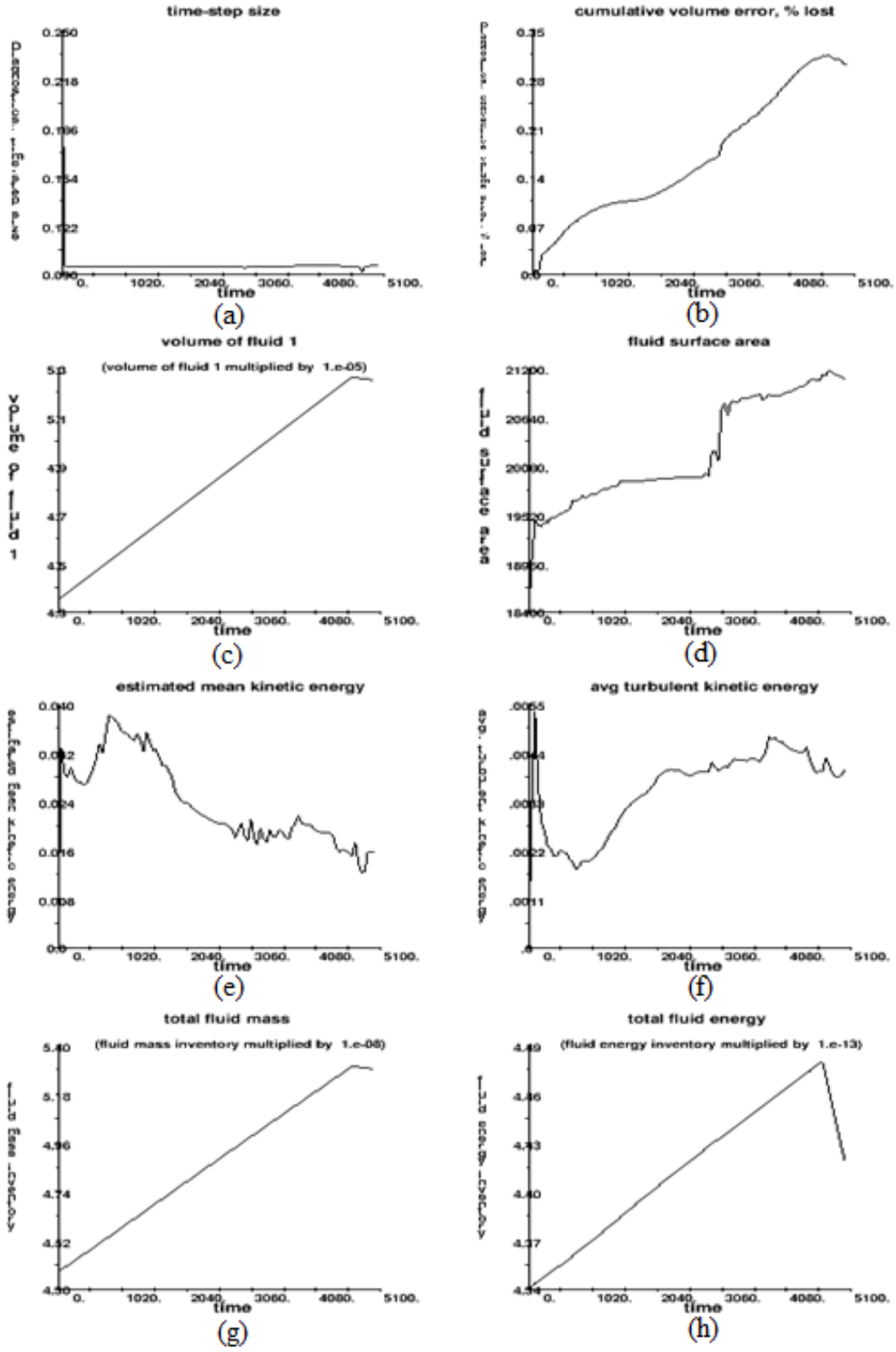

Figure A1: Simulation S1: a) time-step size, b) cumulative volume error (%), c) volume of fluid, d) fluid surface area, e) estimated mean kinetic energy, f) average turbulent kinetic energy, g) total fluid mass, h) total fluid energy.

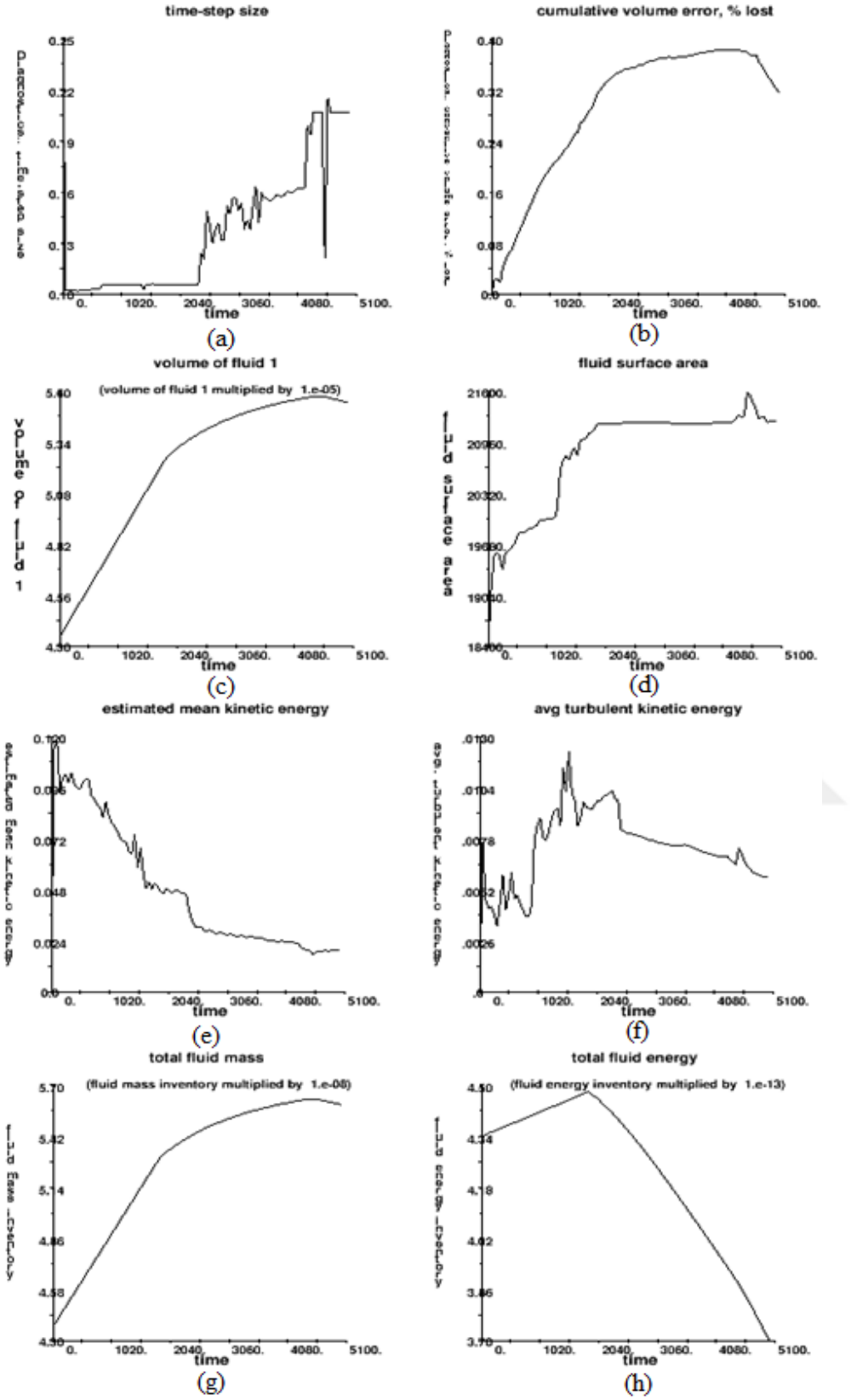

Figure A2: Simulation S2: a) time-step size, b) cumulative volume error (%), c) volume of fluid, d) fluid surface area, e) estimated mean kinetic energy, f) average turbulent kinetic energy, g) total fluid mass, h) total fluid energy.

S3

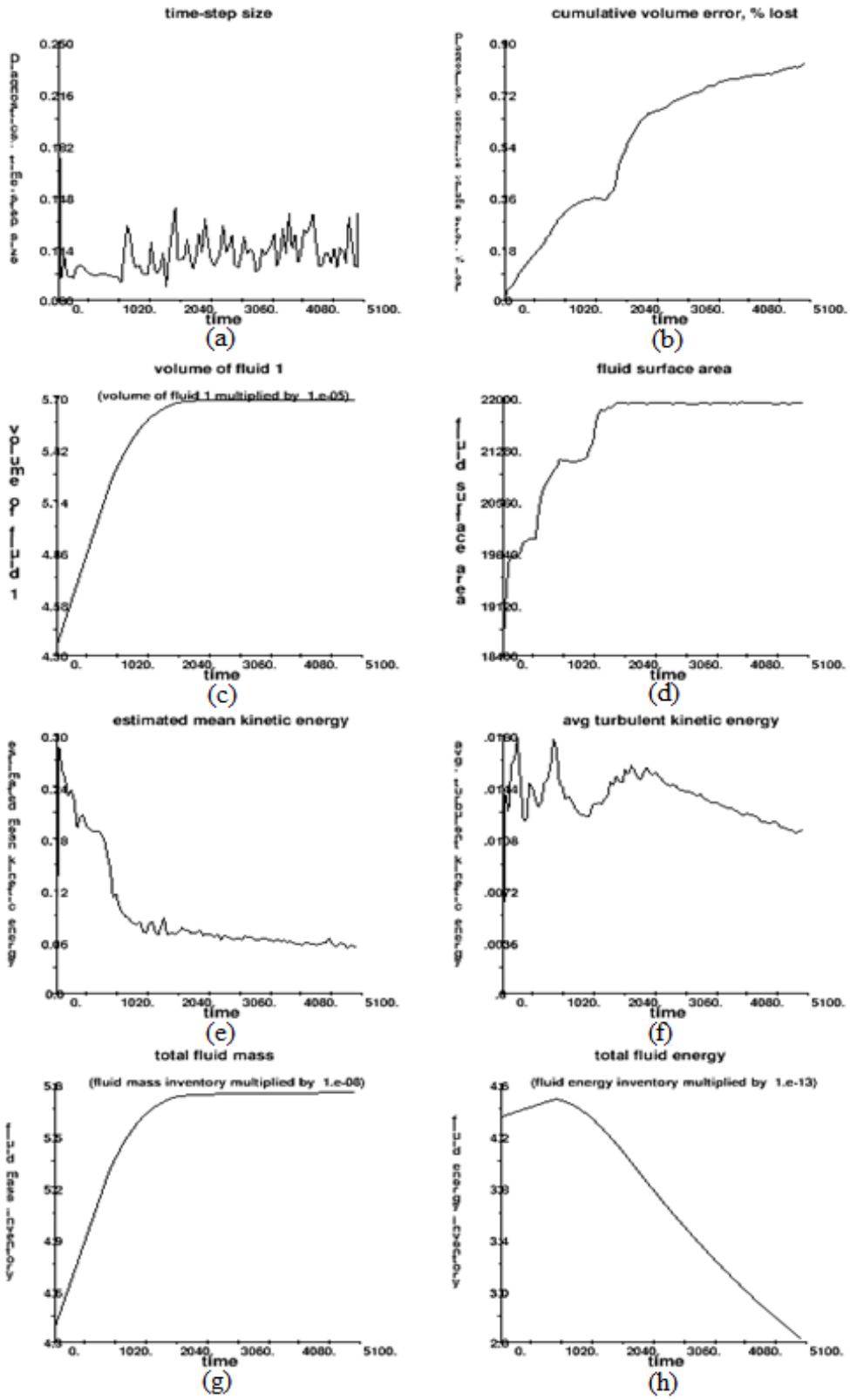

Figure A3: Simulation S3: a) time-step size, b) cumulative volume error (%), c) volume of fluid, d) fluid surface area, e) estimated mean kinetic energy, f) average turbulent kinetic energy, g) total fluid mass, h) total fluid energy.

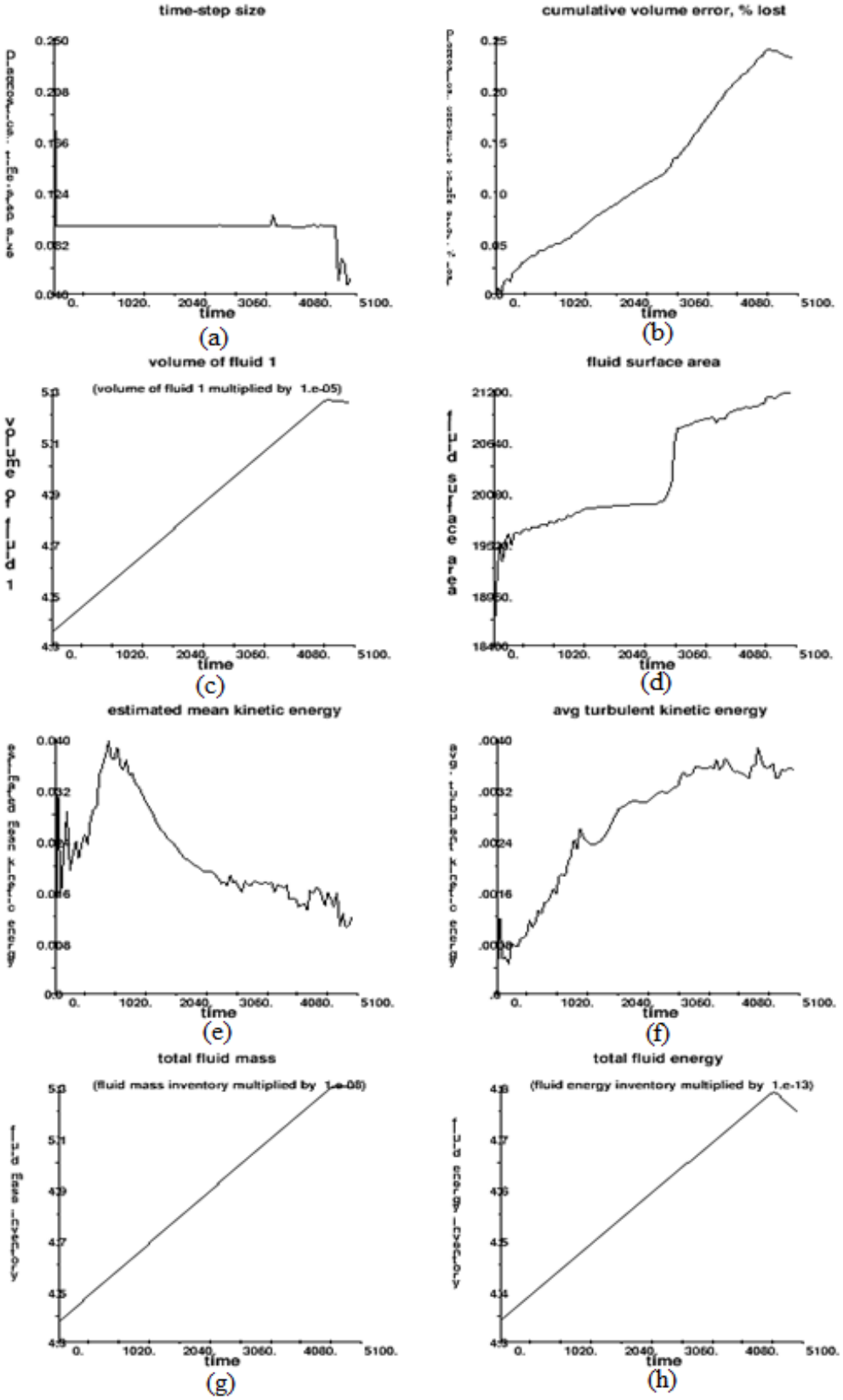

Figure A4: Simulation S4: a) time-step size, b) cumulative volume error (%), c) volume of fluid, d) fluid surface area, e) estimated mean kinetic energy, f) average turbulent kinetic energy, g) total fluid mass, h) total fluid energy.

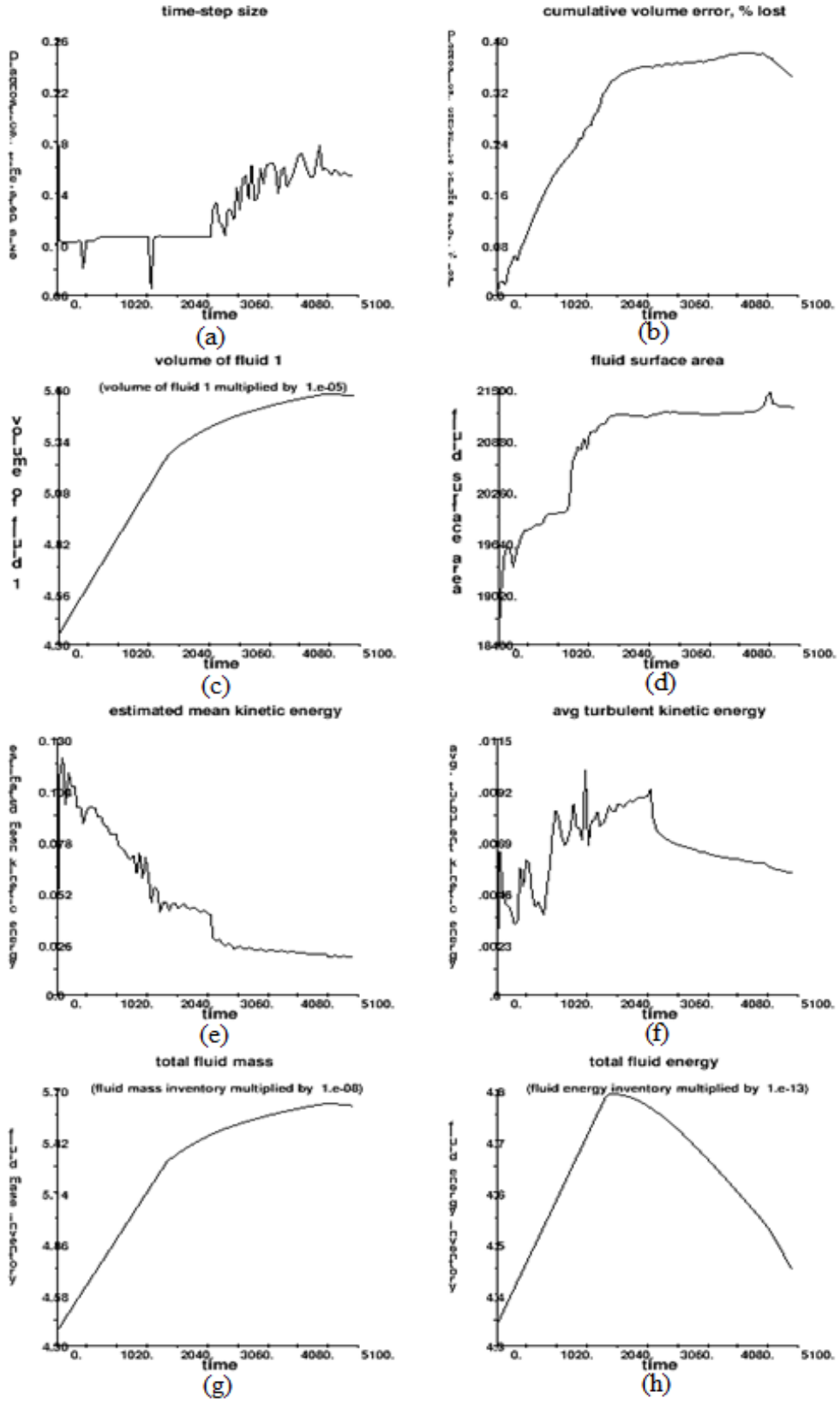

Figure A5: Simulation S5: a) time-step size, b) cumulative volume error (%), c) volume of fluid, d) fluid surface area, e) estimated mean kinetic energy, f) average turbulent kinetic energy, g) total fluid mass, h) total fluid energy.

S6

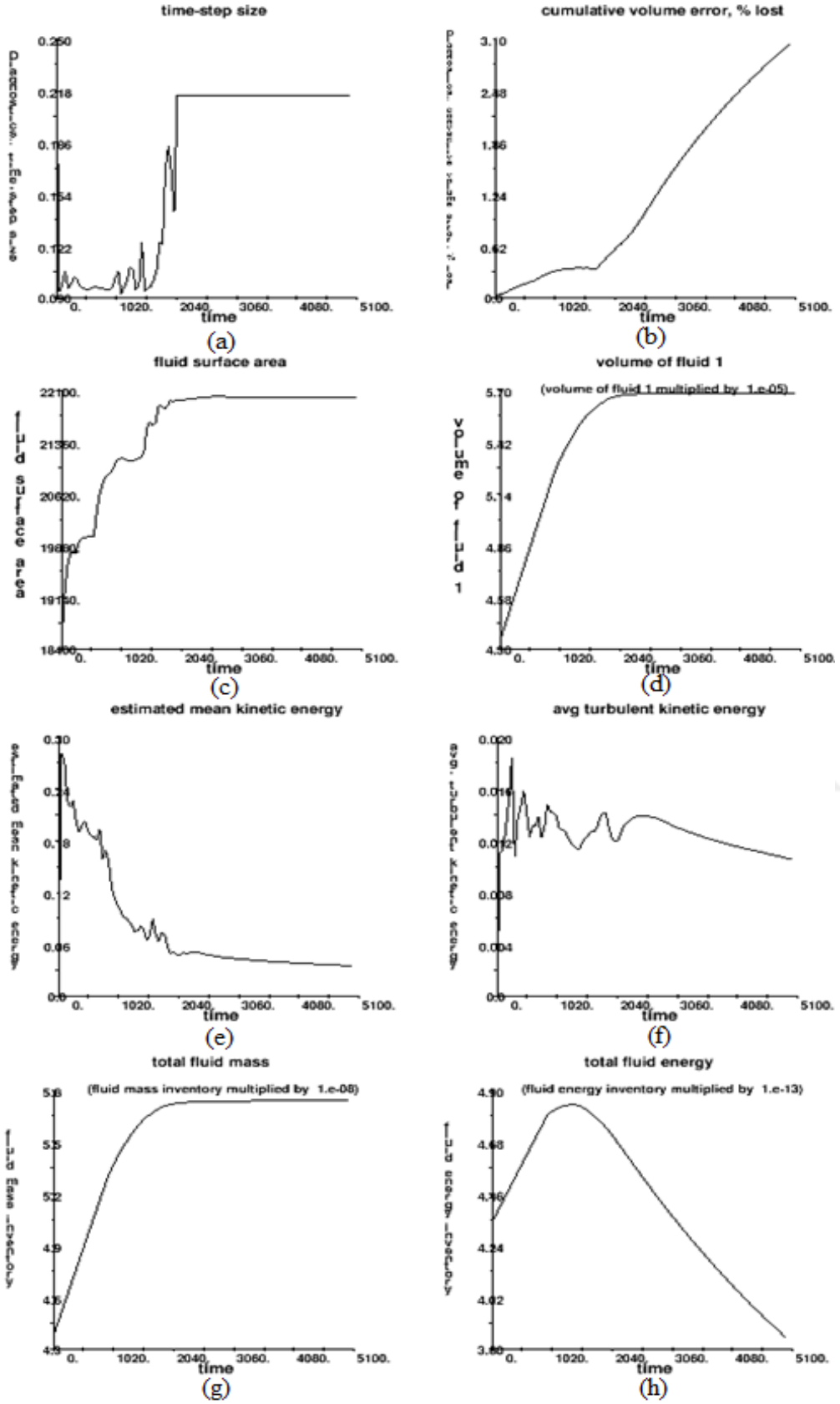

Figure A6: Simulation S6: a) time-step size, b) cumulative volume error (%), c) volume of fluid, d) fluid surface area, e) estimated mean kinetic energy, f) average turbulent kinetic energy, g) total fluid mass, h) total fluid energy.

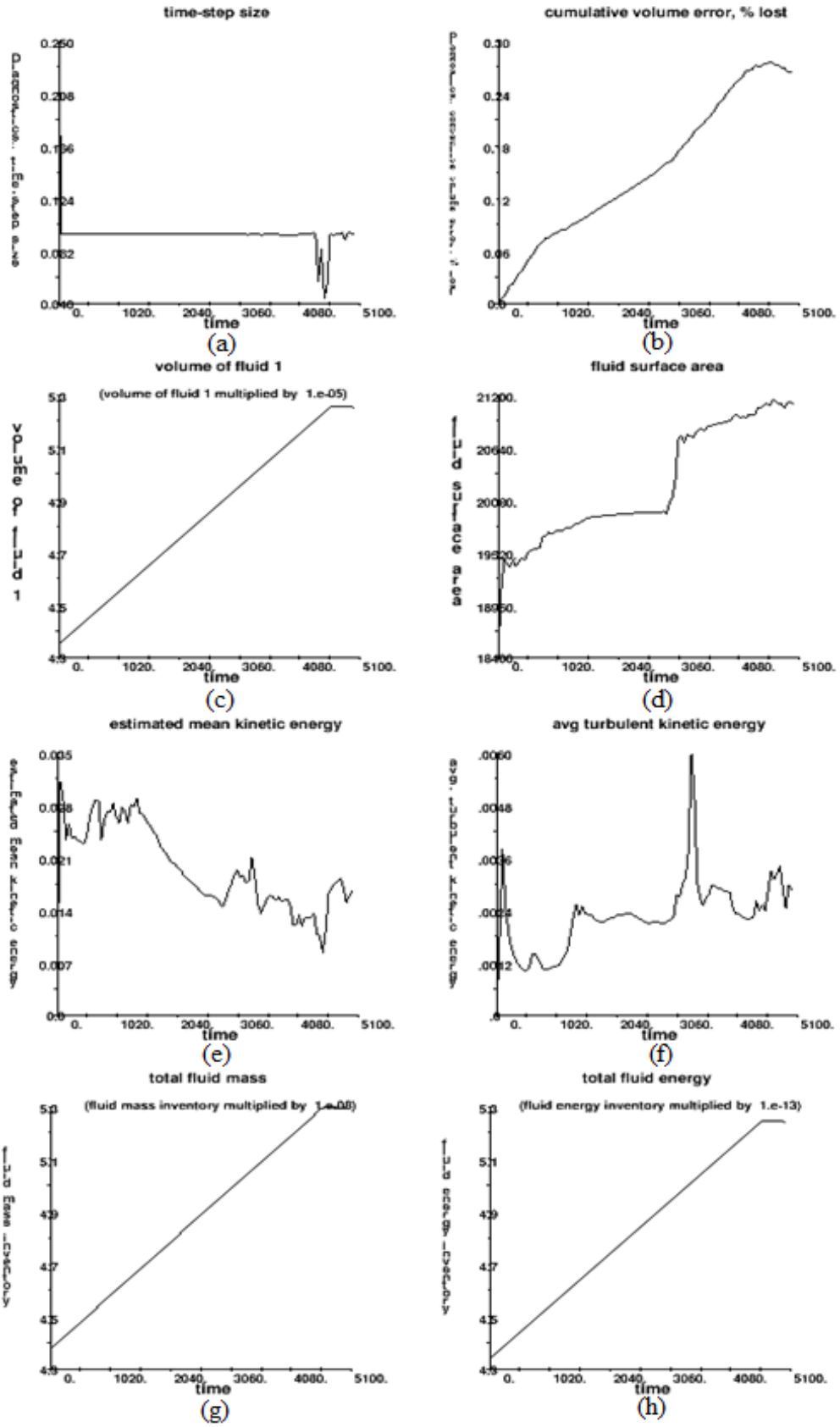

Figure A7: Simulation S7: a) time-step size, b) cumulative volume error (%), c) volume of fluid, d) fluid surface area, e) estimated mean kinetic energy, f) average turbulent kinetic energy, g) total fluid mass, h) total fluid energy.

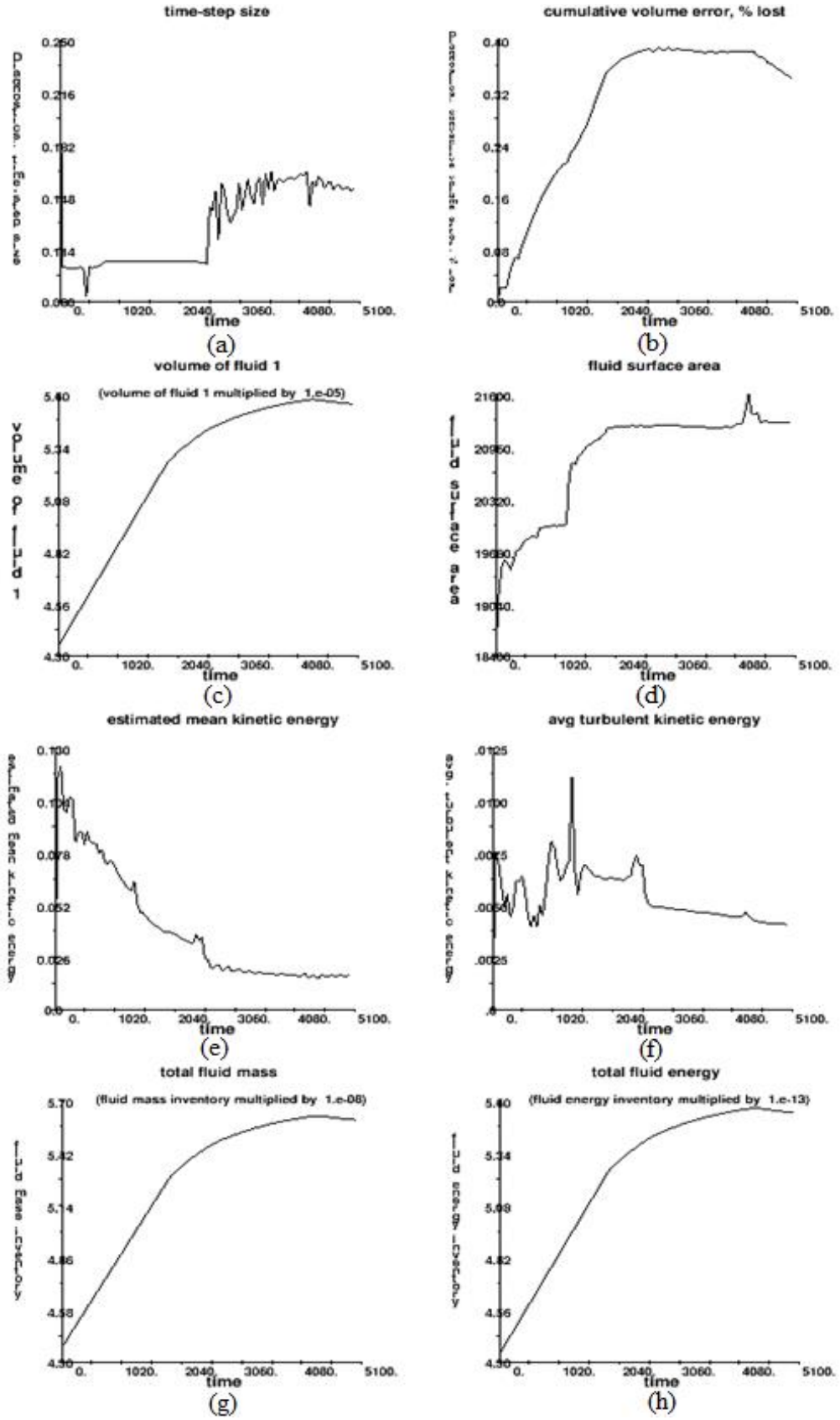

Figure A8: Simulation S8: a) time-step size, b) cumulative volume error (%), c) volume of fluid, d) fluid surface area, e) estimated mean kinetic energy, f) average turbulent kinetic energy, g) total fluid mass, h) total fluid energy.

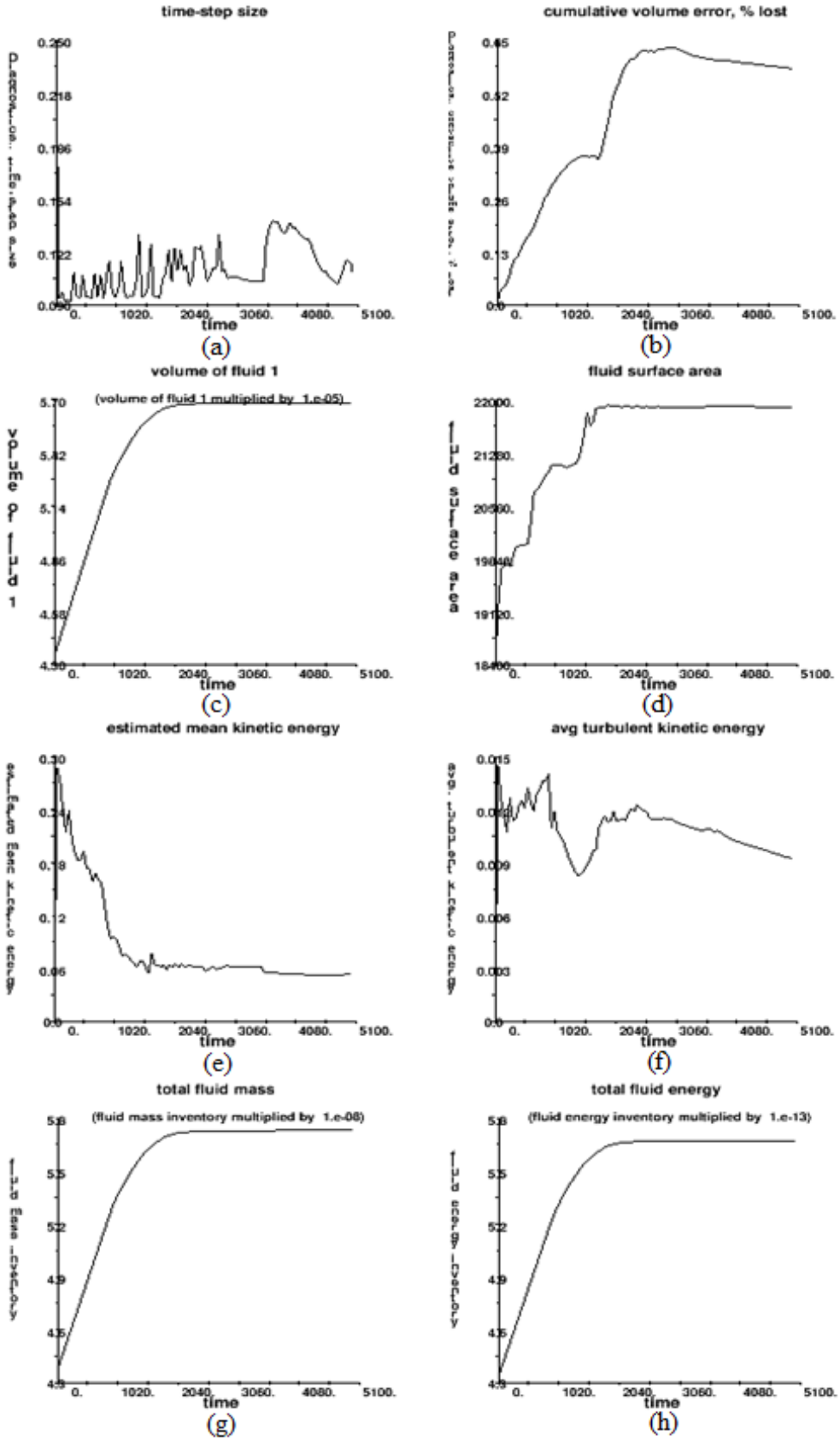

Figure A9: Simulation S9: a) time-step size, b) cumulative volume error (%), c) volume of fluid, d) fluid surface area, e) estimated mean kinetic energy, f) average turbulent kinetic energy, g) total fluid mass, h) total fluid energy.

S10

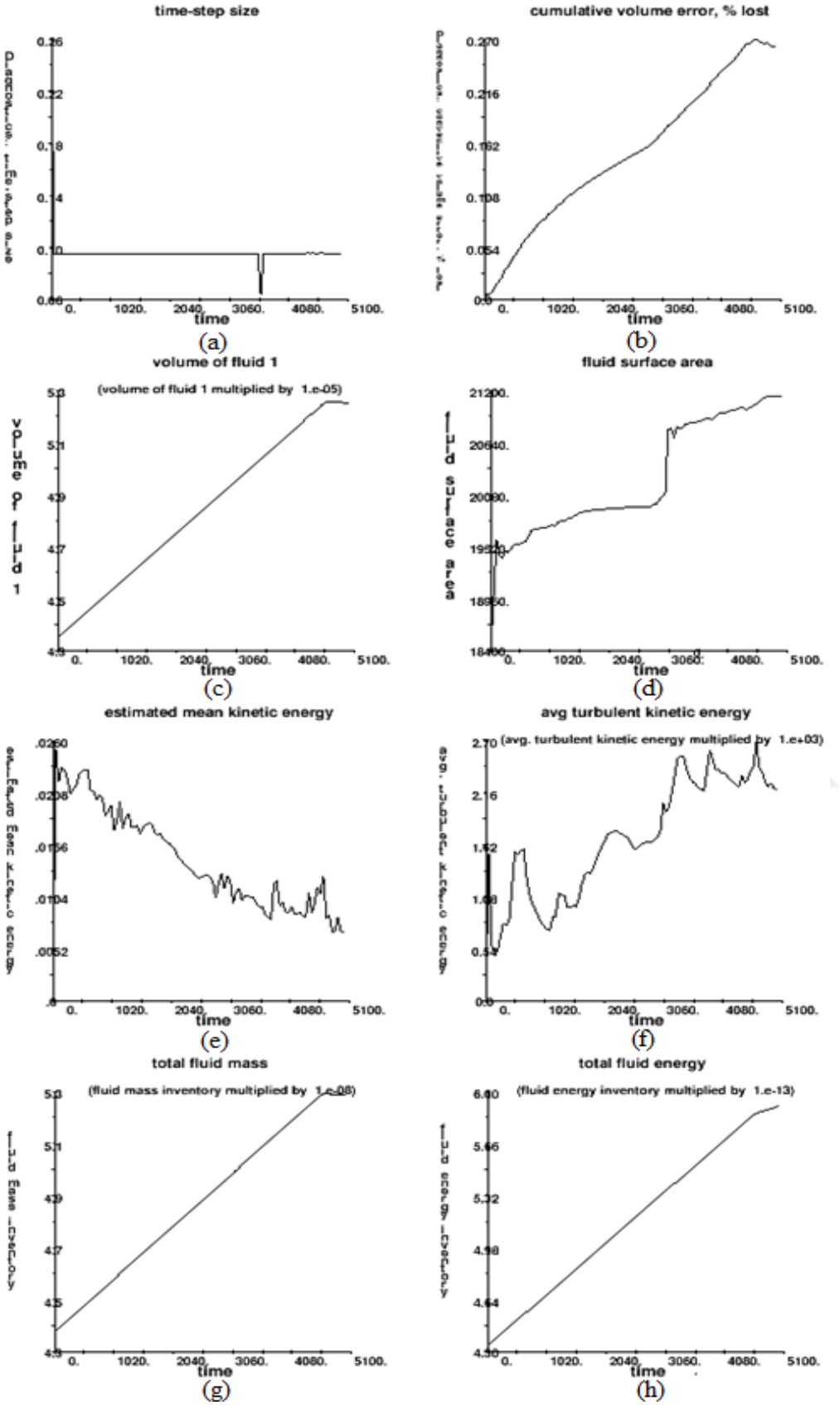

Figure A10: Simulation S10: a) time-step size, b) cumulative volume error (%), c) volume of fluid, d) fluid surface area, e) estimated mean kinetic energy, f) average turbulent kinetic energy, g) total fluid mass, h) total fluid energy.

S11

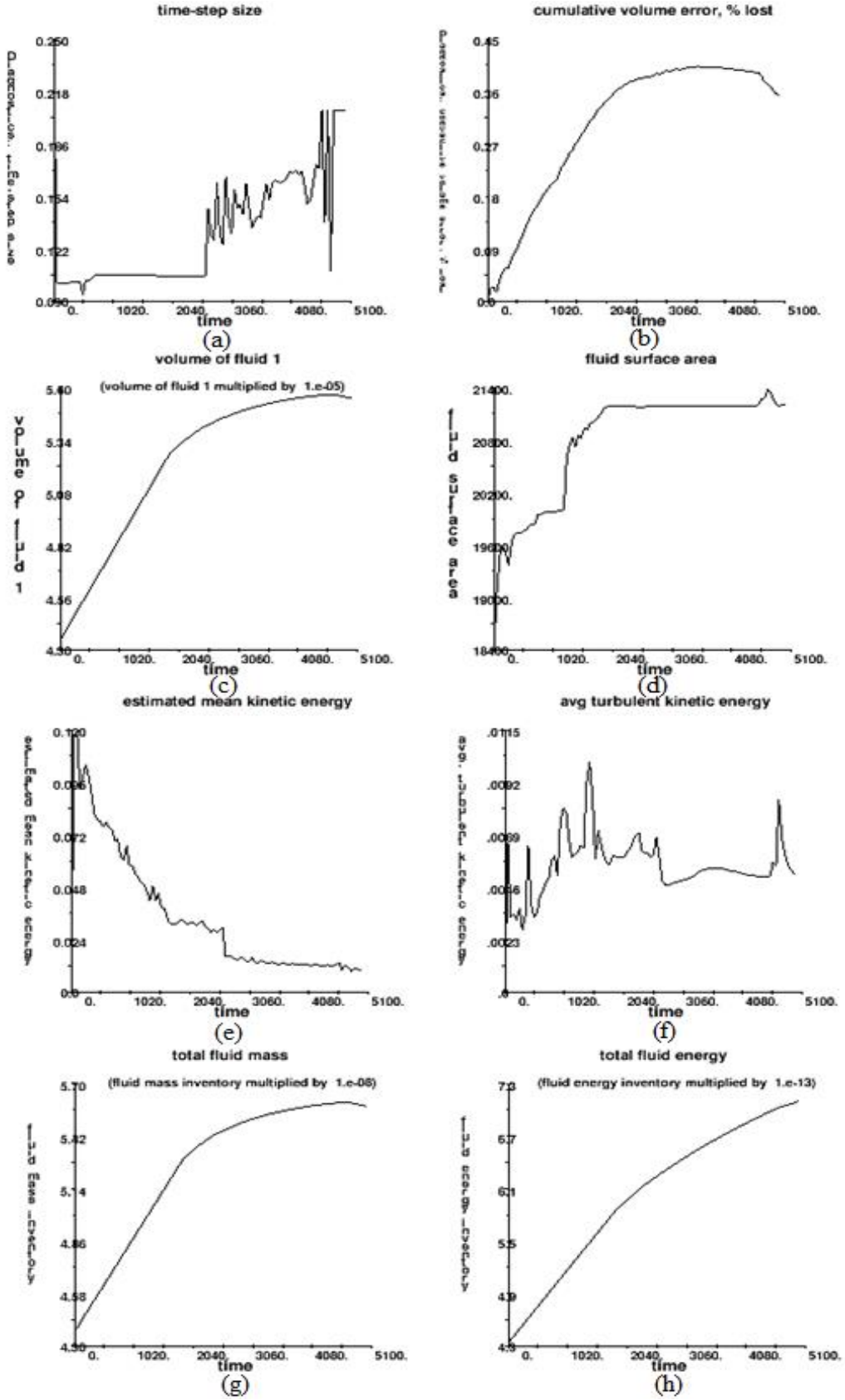

Figure A11: Simulation S11: a) time-step size, b) cumulative volume error (%), c) volume of fluid, d) fluid surface area, e) estimated mean kinetic energy, f) average turbulent kinetic energy, g) total fluid mass, h) total fluid energy.

S12

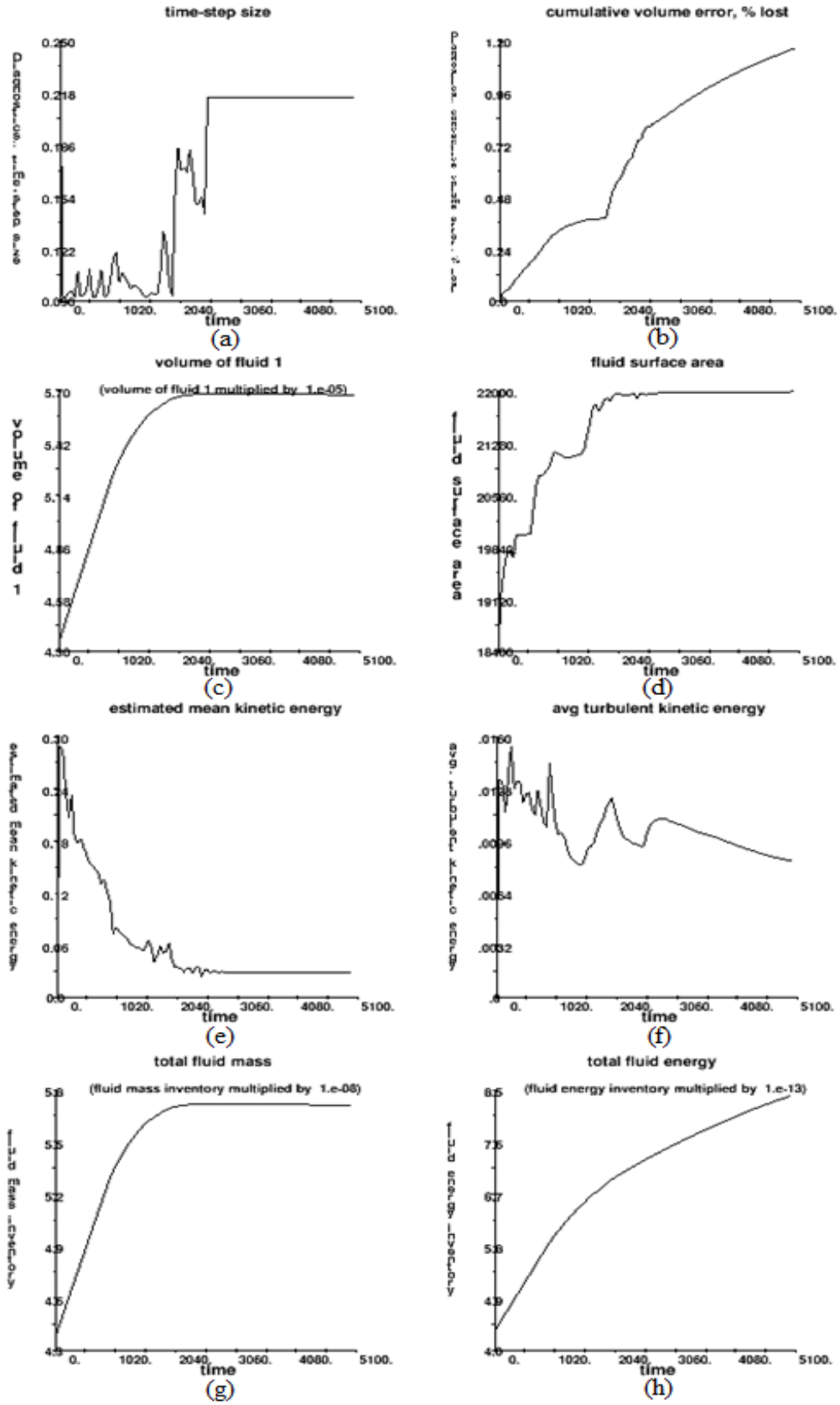

Figure A12: Simulation S12: a) time-step size, b) cumulative volume error (%), c) volume of fluid, d) fluid surface area, e) estimated mean kinetic energy, f) average turbulent kinetic energy, g) total fluid mass, h) total fluid energy.

S13

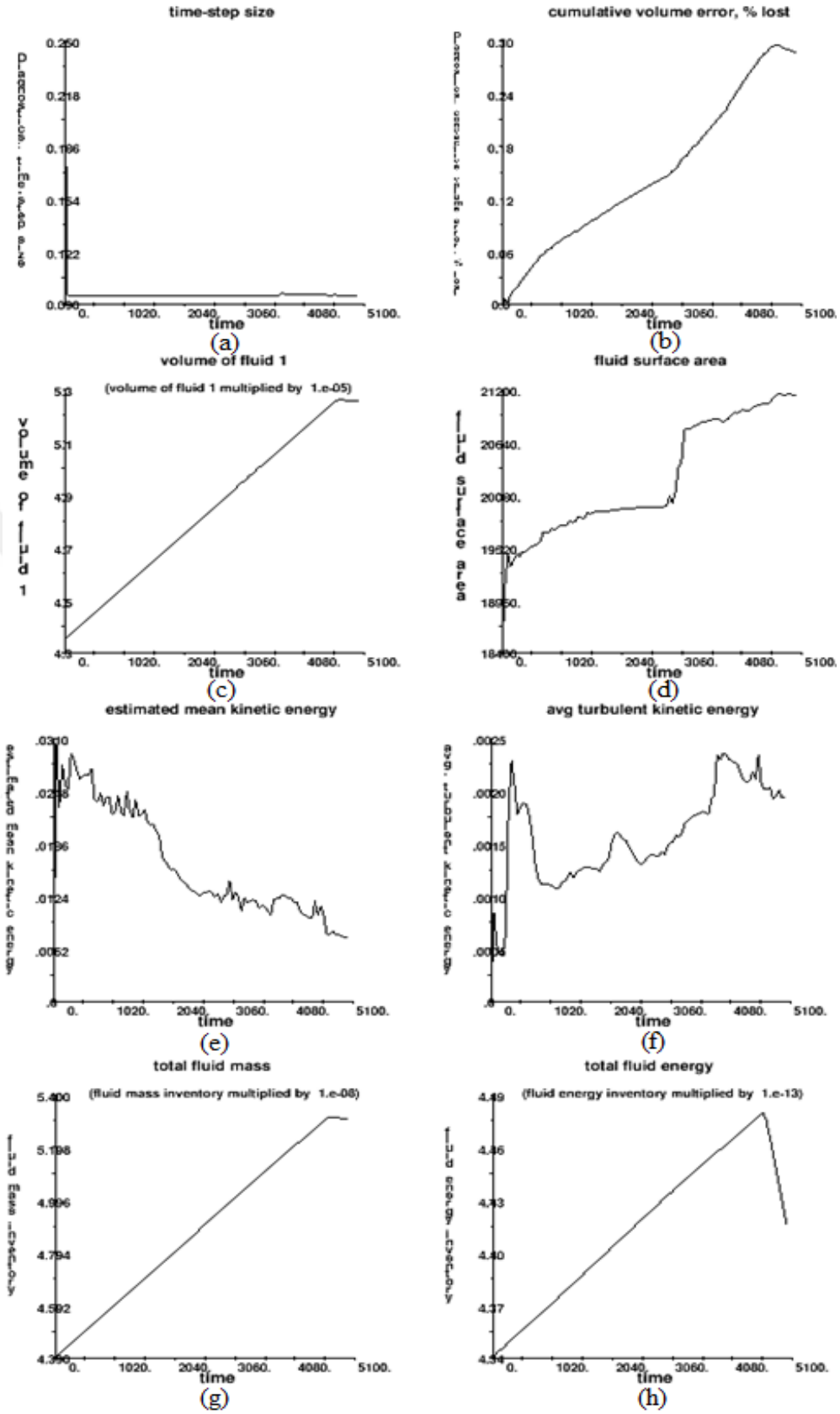

Figure A13: Simulation S13: a) time-step size, b) cumulative volume error (%), c) volume of fluid, d) fluid surface area, e) estimated mean kinetic energy, f) average turbulent kinetic energy, g) total fluid mass, h) total fluid energy.

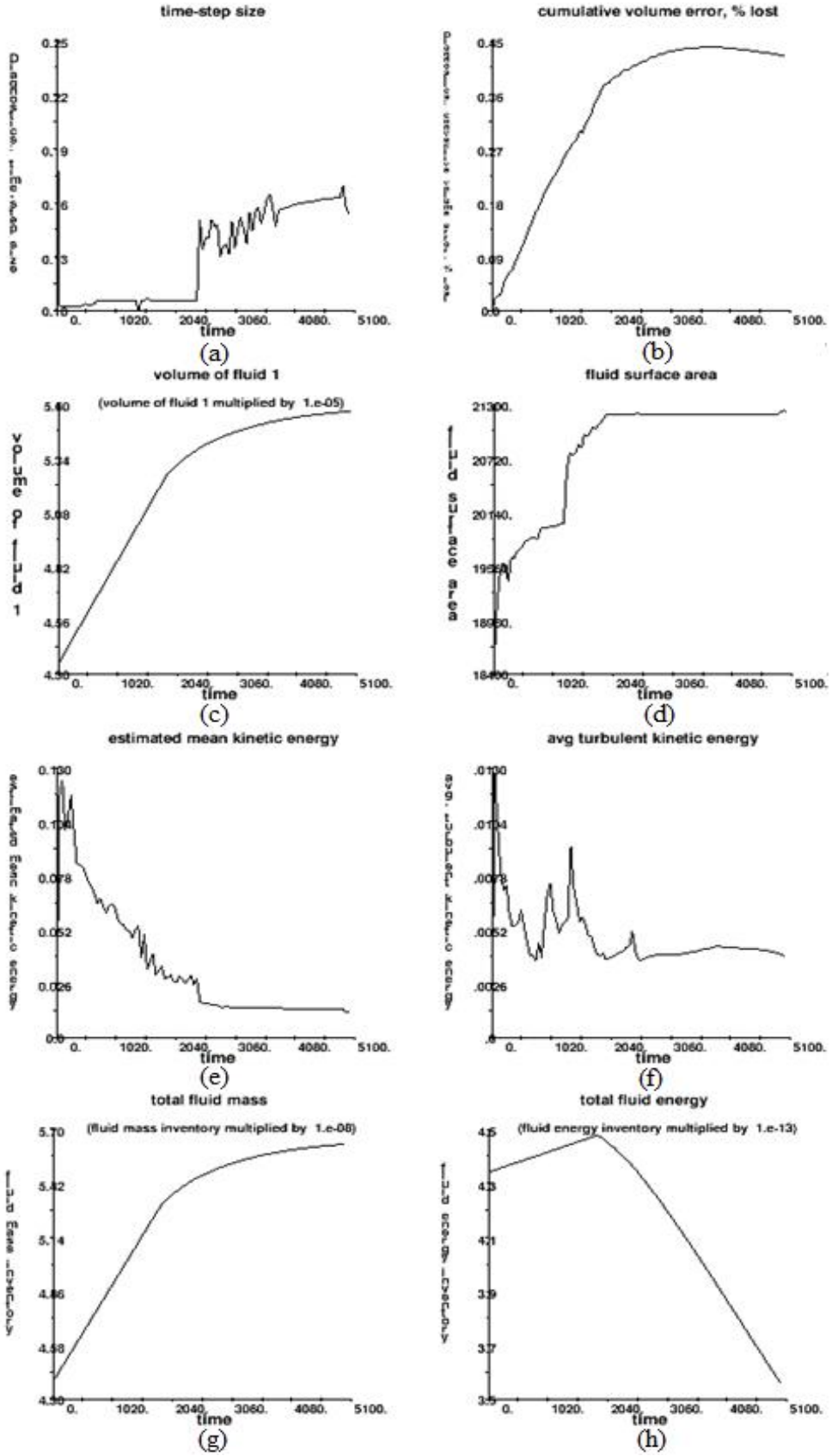

Figure A14: Simulation S14: a) time-step size, b) cumulative volume error (%), c) volume of fluid, d) fluid surface area, e) estimated mean kinetic energy, f) average turbulent kinetic energy, g) total fluid mass, h) total fluid energy.

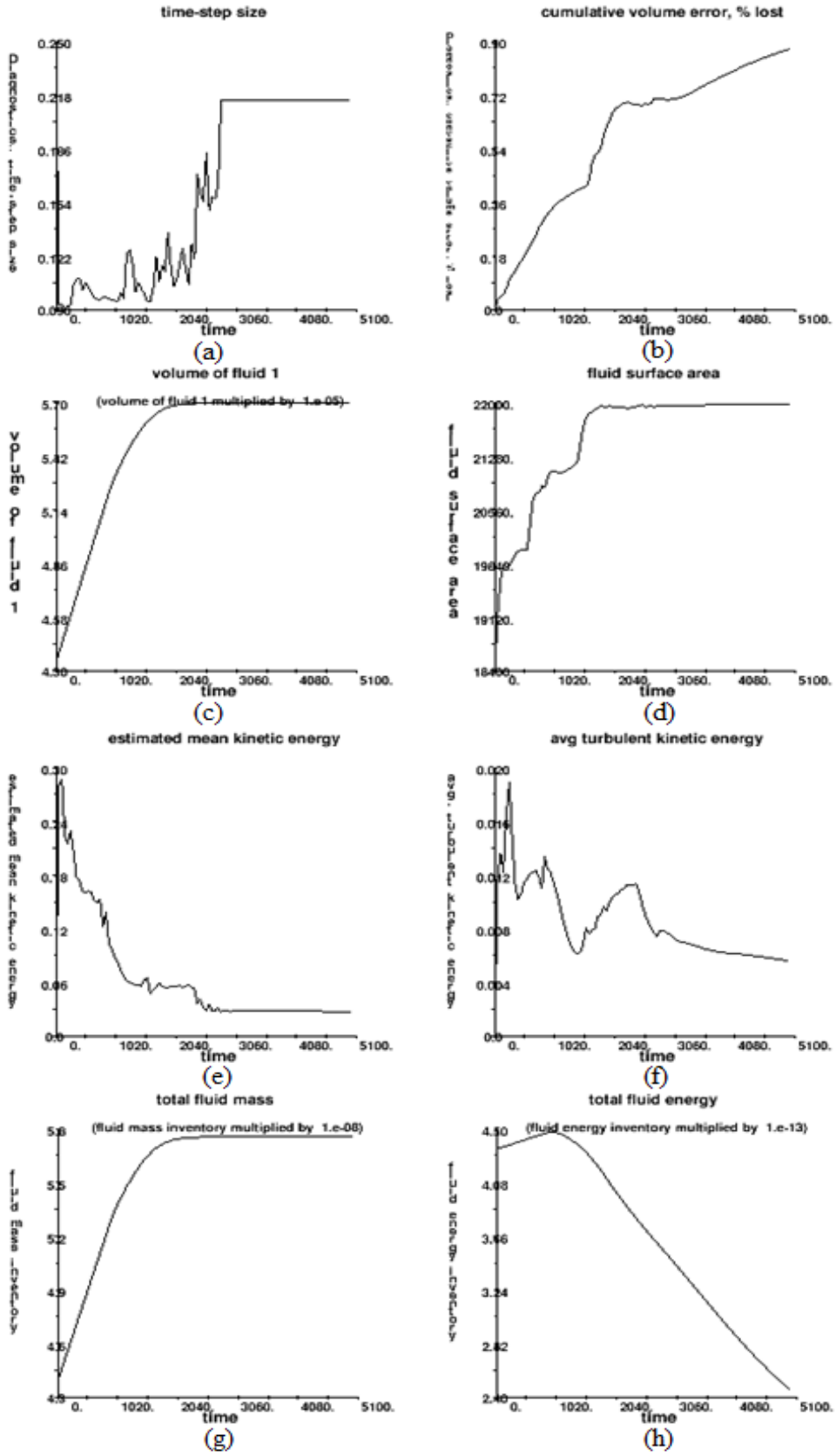

Figure A15: Simulation S15: a) time-step size, b) cumulative volume error (%), c) volume of fluid, d) fluid surface area, e) estimated mean kinetic energy, f) average turbulent kinetic energy, g) total fluid mass, h) total fluid energy.

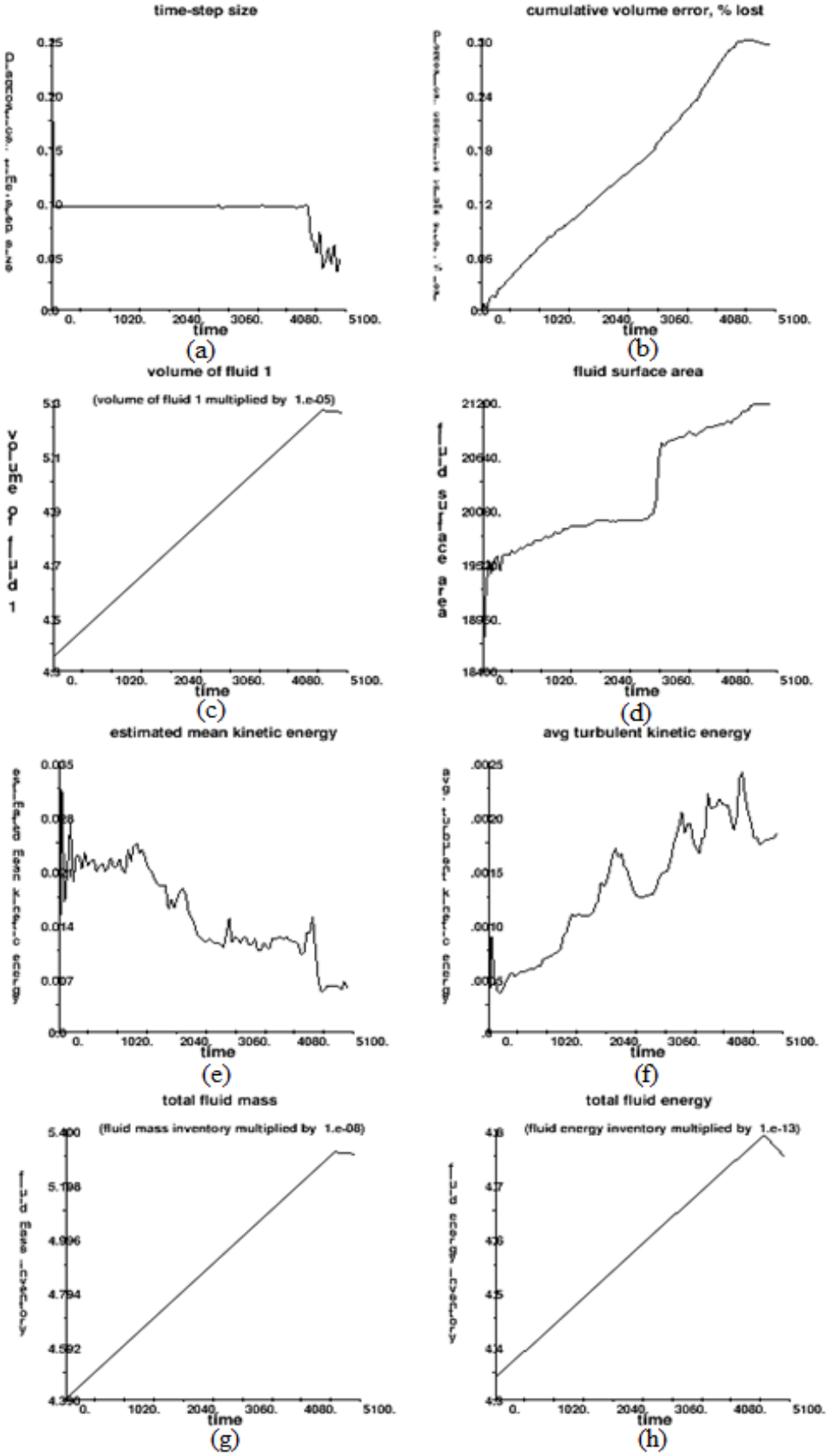

Figure A16: Simulation S16: a) time-step size, b) cumulative volume error (%), c) volume of fluid, d) fluid surface area, e) estimated mean kinetic energy, f) average turbulent kinetic energy, g) total fluid mass, h) total fluid energy.

S17

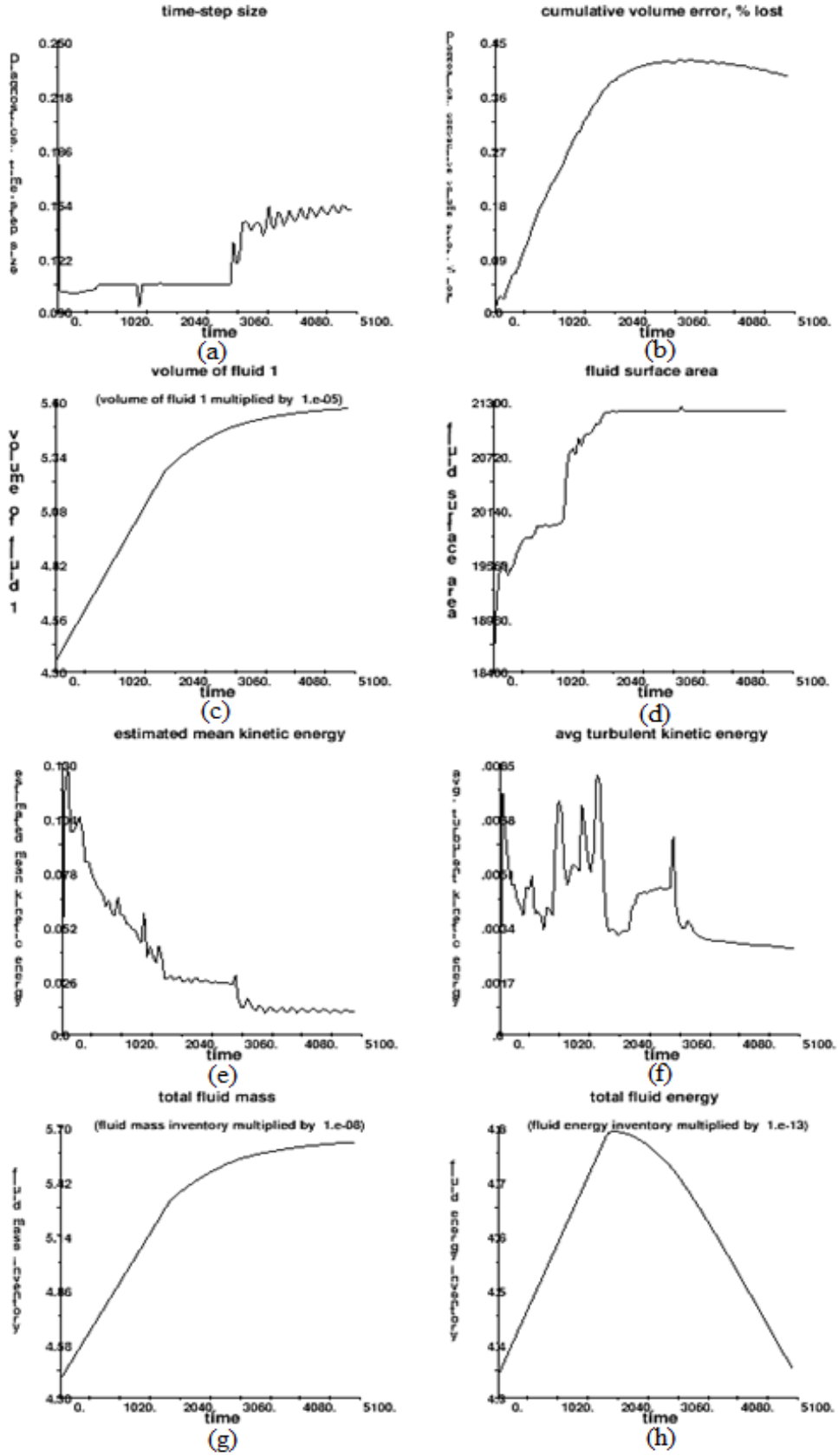

Figure A17: Simulation S17: a) time-step size, b) cumulative volume error (%), c) volume of fluid, d) fluid surface area, e) estimated mean kinetic energy, f) average turbulent kinetic energy, g) total fluid mass, h) total fluid energy.

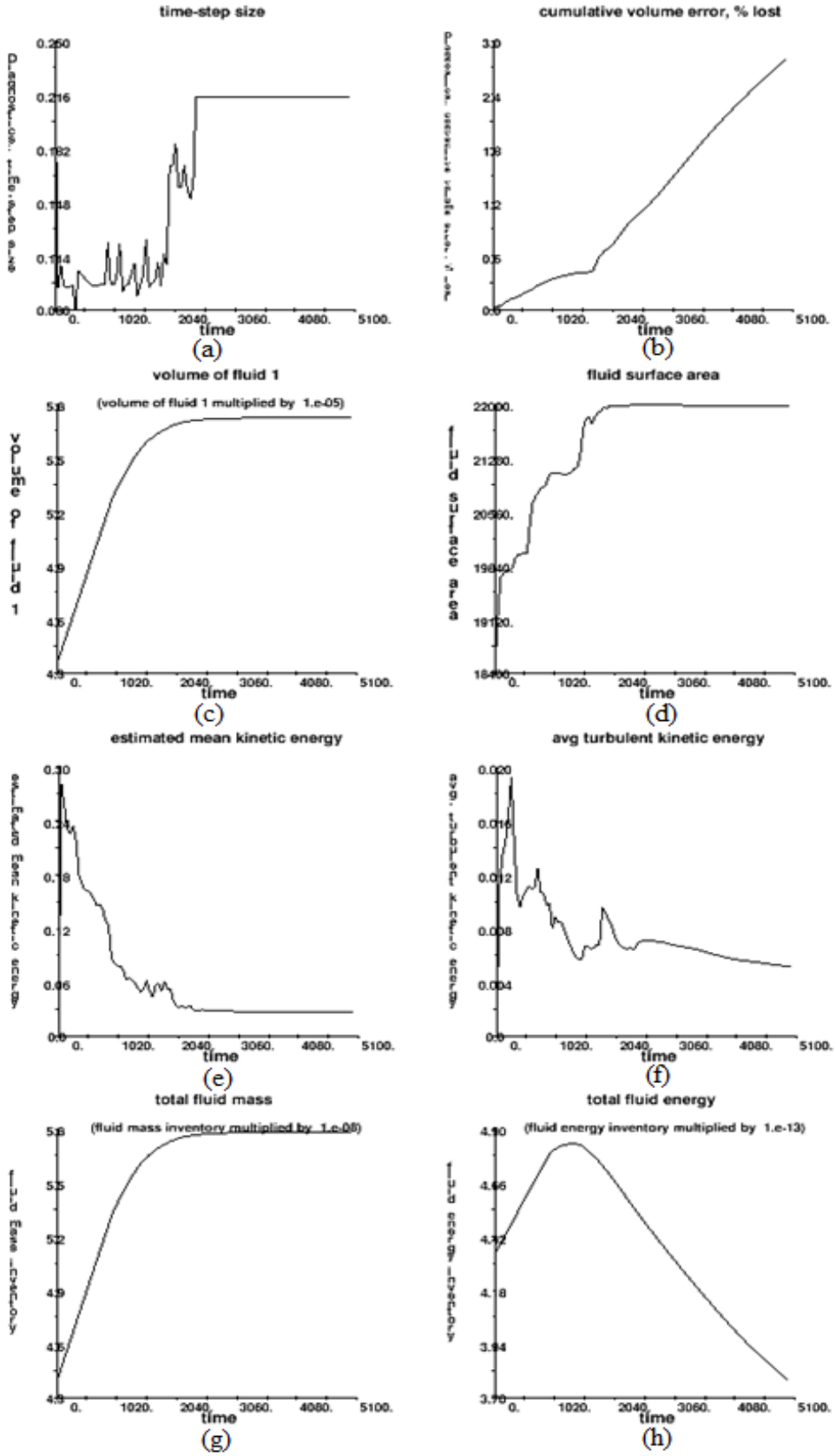

Figure A18: Simulation S18: a) time-step size, b) cumulative volume error (%), c) volume of fluid, d) fluid surface area, e) estimated mean kinetic energy, f) average turbulent kinetic energy, g) total fluid mass, h) total fluid energy.

S19

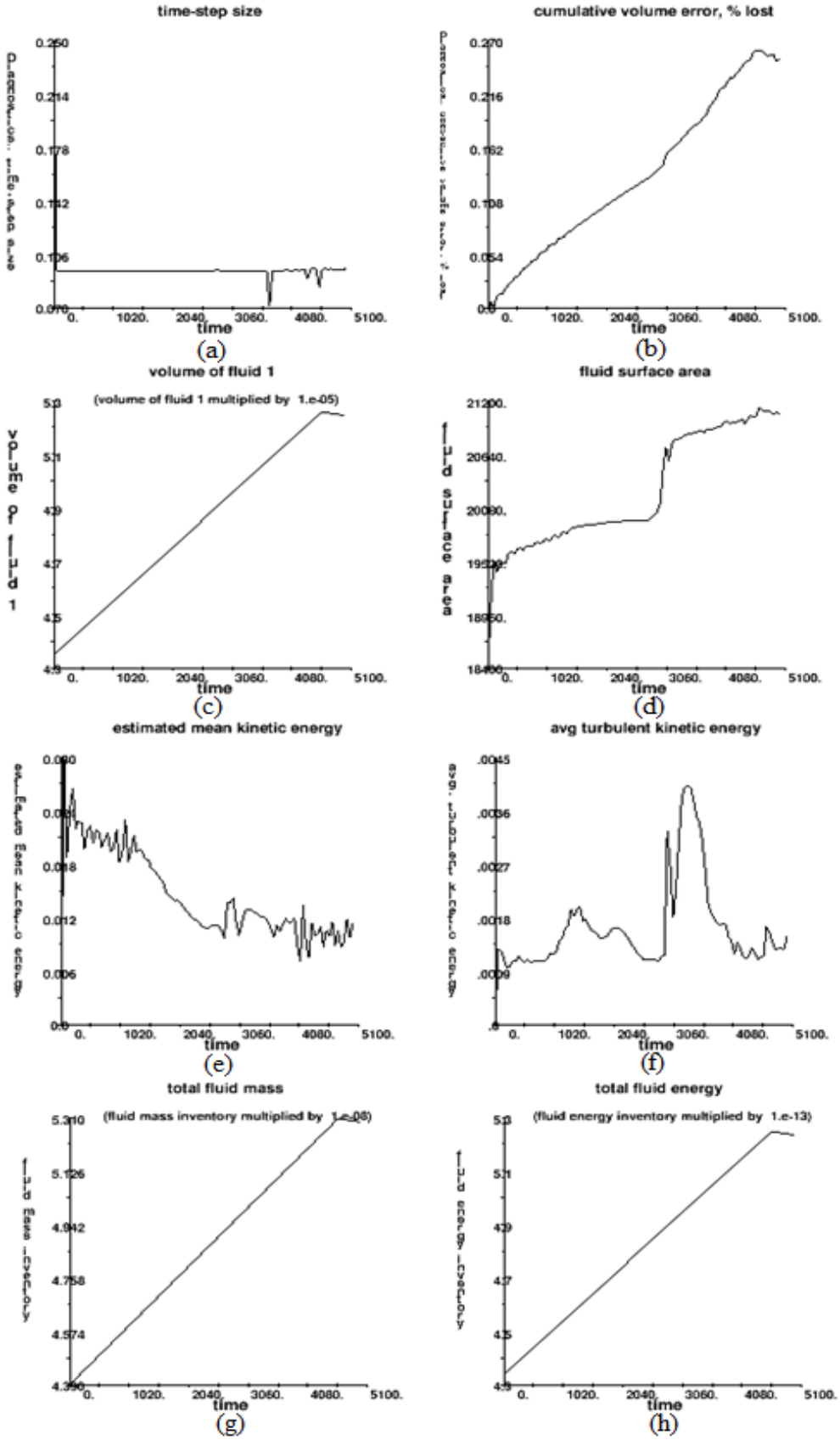

Figure A19: Simulation S19: a) time-step size, b) cumulative volume error (%), c) volume of fluid, d) fluid surface area, e) estimated mean kinetic energy, f) average turbulent kinetic energy, g) total fluid mass, h) total fluid energy.

S20

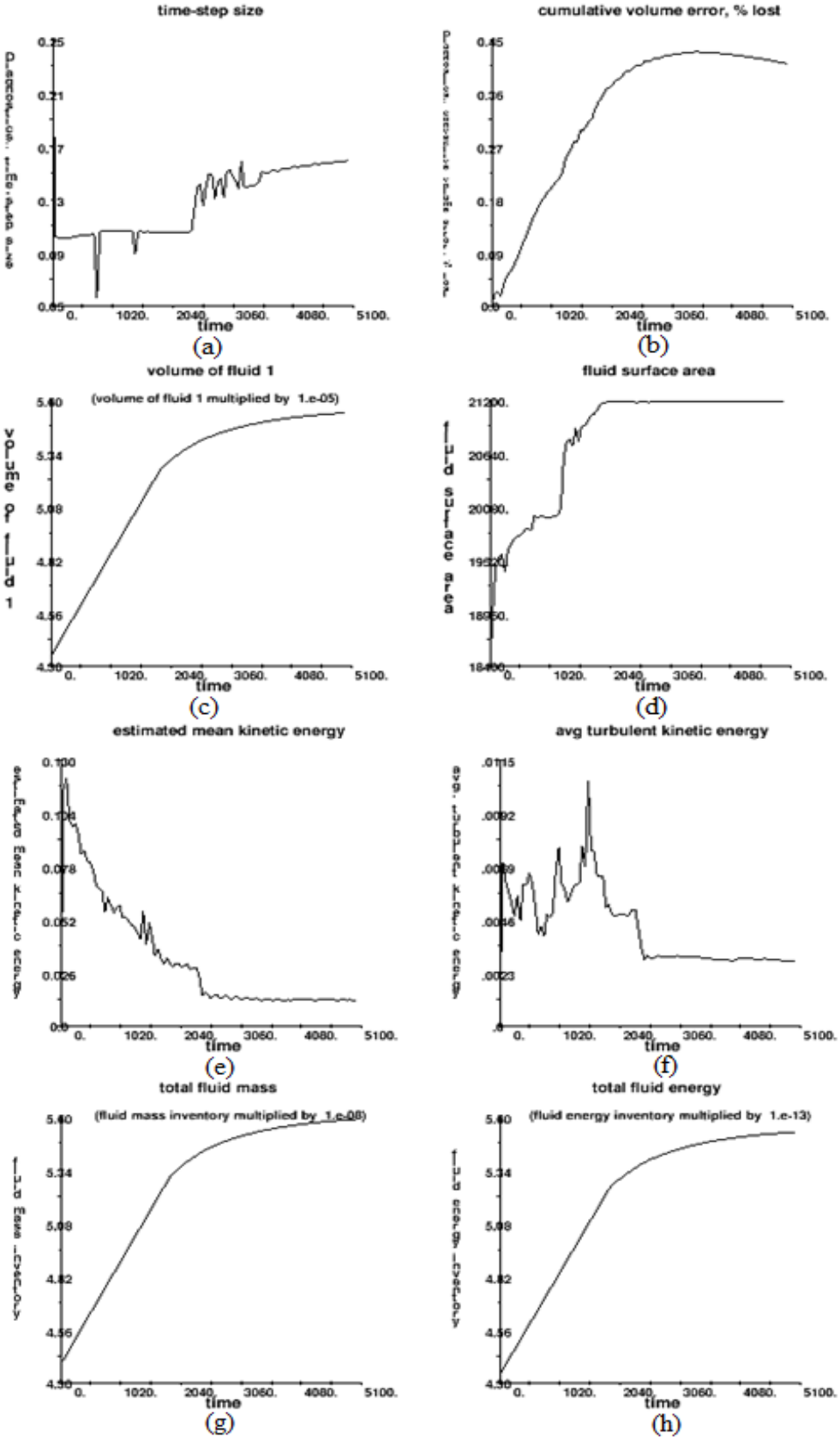

Figure A20: Simulation S20: a) time-step size, b) cumulative volume error (%), c) volume of fluid, d) fluid surface area, e) estimated mean kinetic energy, f) average turbulent kinetic energy, g) total fluid mass, h) total fluid energy.

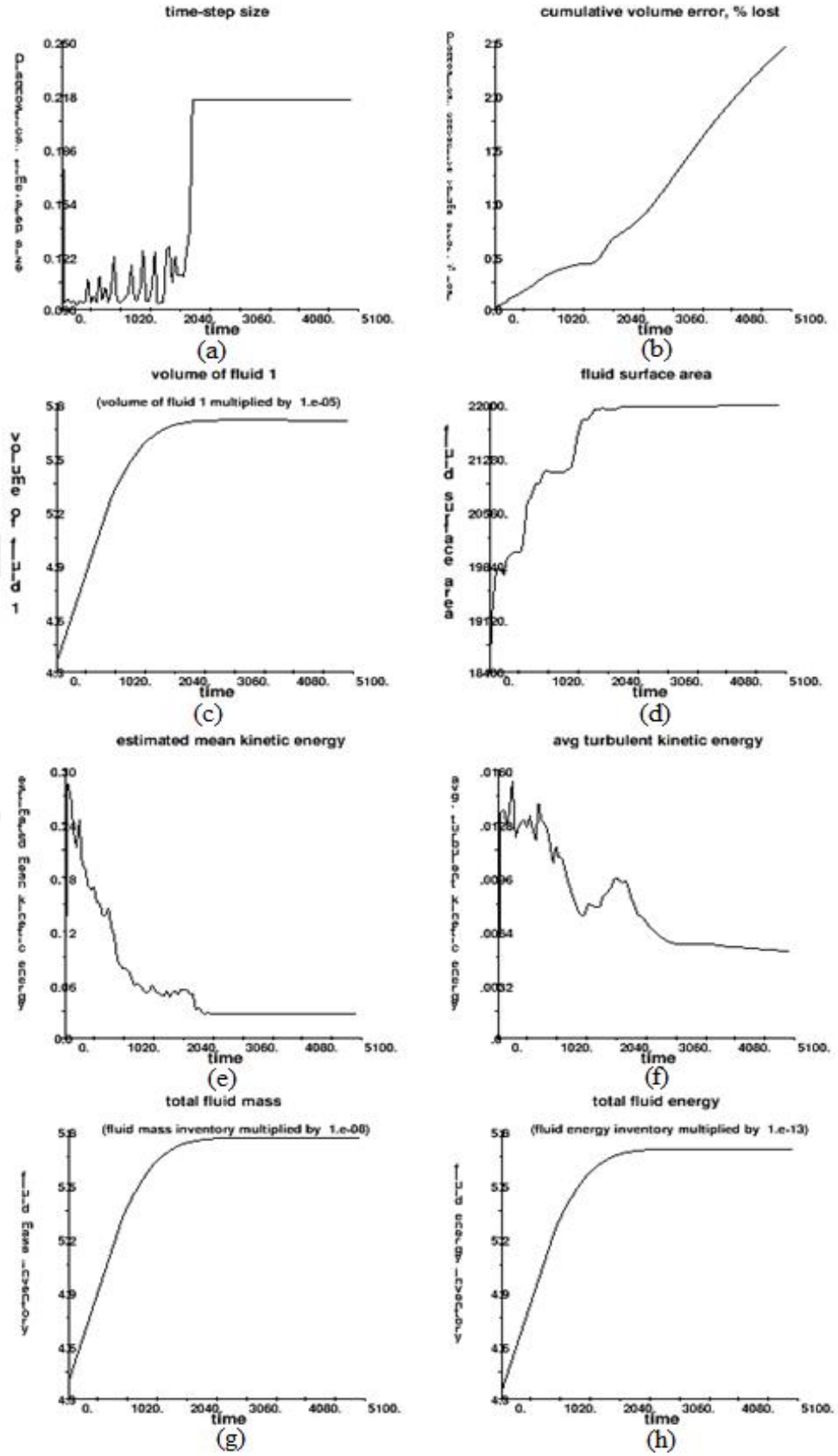

Figure A21: Simulation S21: a) time-step size, b) cumulative volume error (%), c) volume of fluid, d) fluid surface area, e) estimated mean kinetic energy, f) average turbulent kinetic energy, g) total fluid mass, h) total fluid energy.

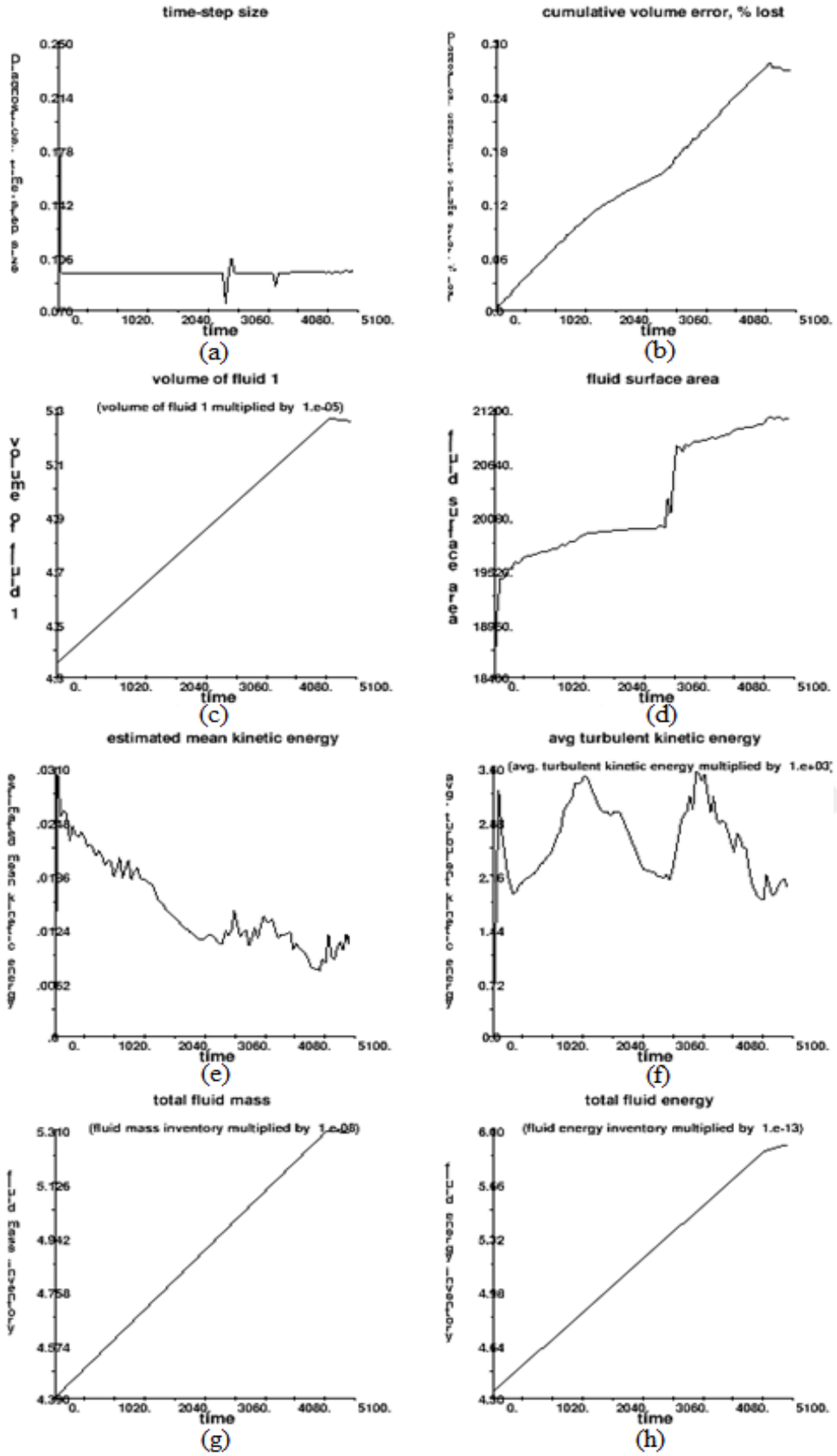

Figure A22: Simulation S22: a) time-step size, b) cumulative volume error (%), c) volume of fluid, d) fluid surface area, e) estimated mean kinetic energy, f) average turbulent kinetic energy, g) total fluid mass, h) total fluid energy.

S23

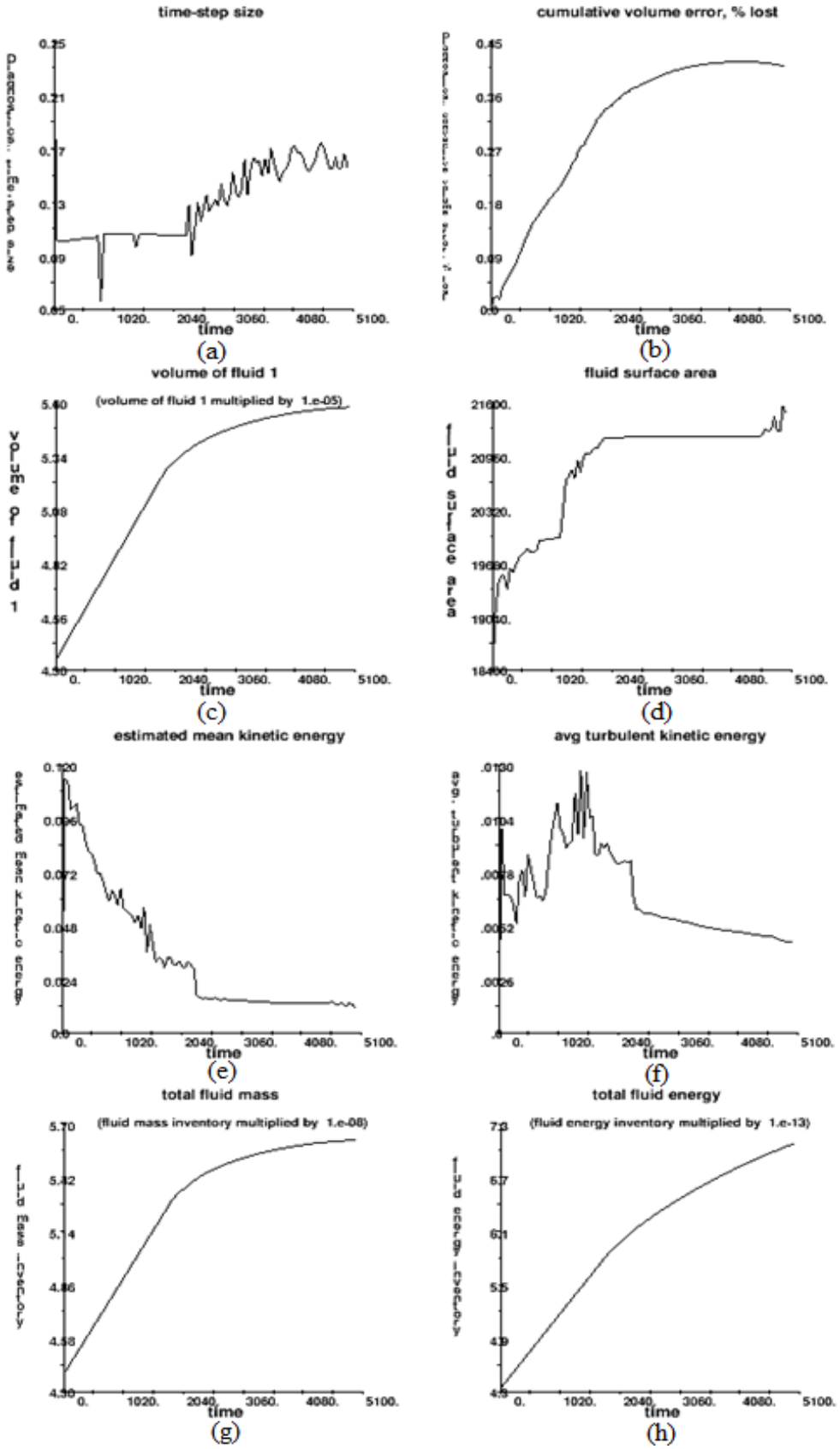

Figure A23: Simulation S23: a) time-step size, b) cumulative volume error (%), c) volume of fluid, d) fluid surface area, e) estimated mean kinetic energy, f) average turbulent kinetic energy, g) total fluid mass, h) total fluid energy.

S24

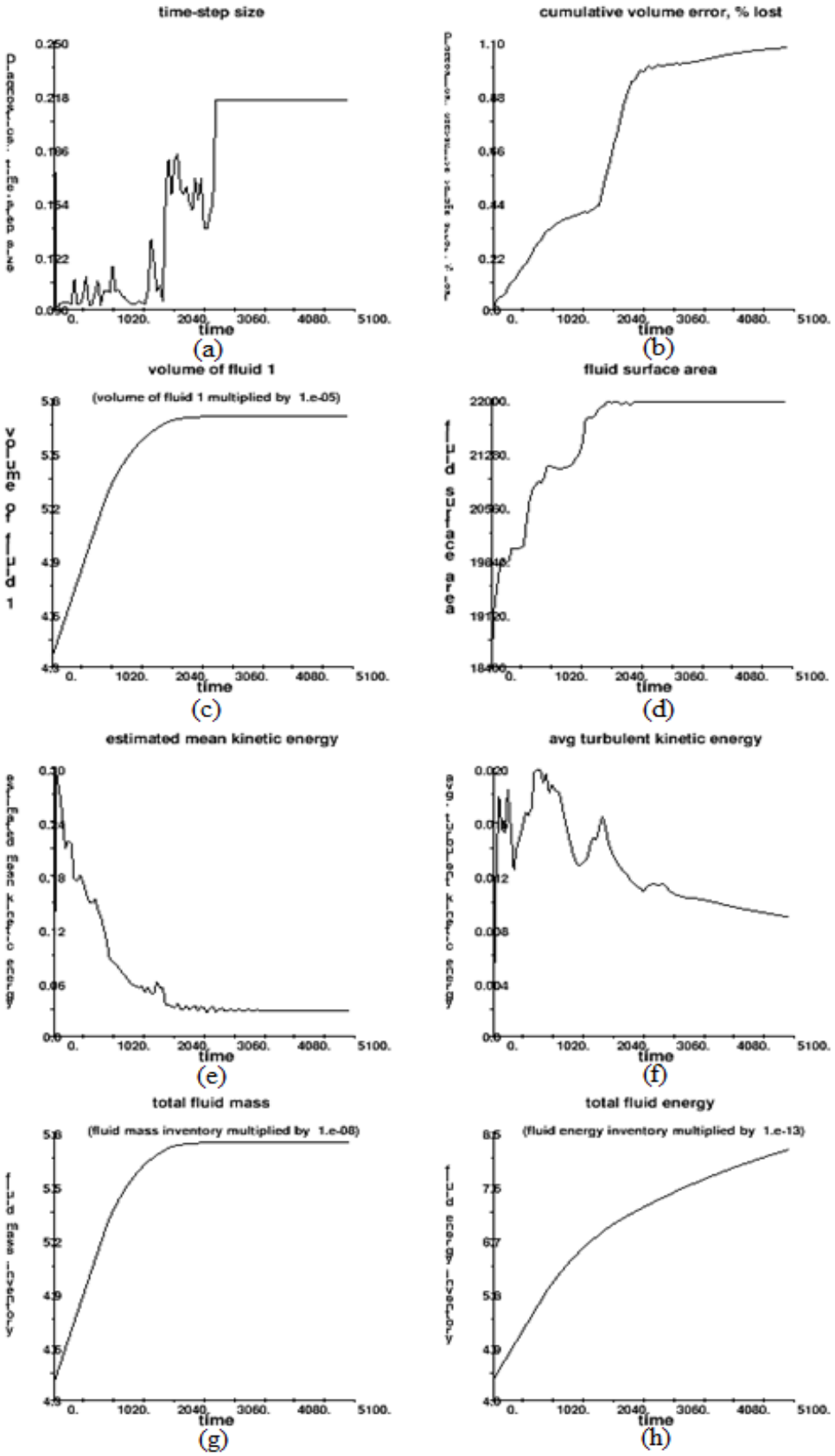

Figure A24: Simulation S24: a) time-step size, b) cumulative volume error (%), c) volume of fluid, d) fluid surface area, e) estimated mean kinetic energy, f) average turbulent kinetic energy, g) total fluid mass, h) total fluid energy.

B1

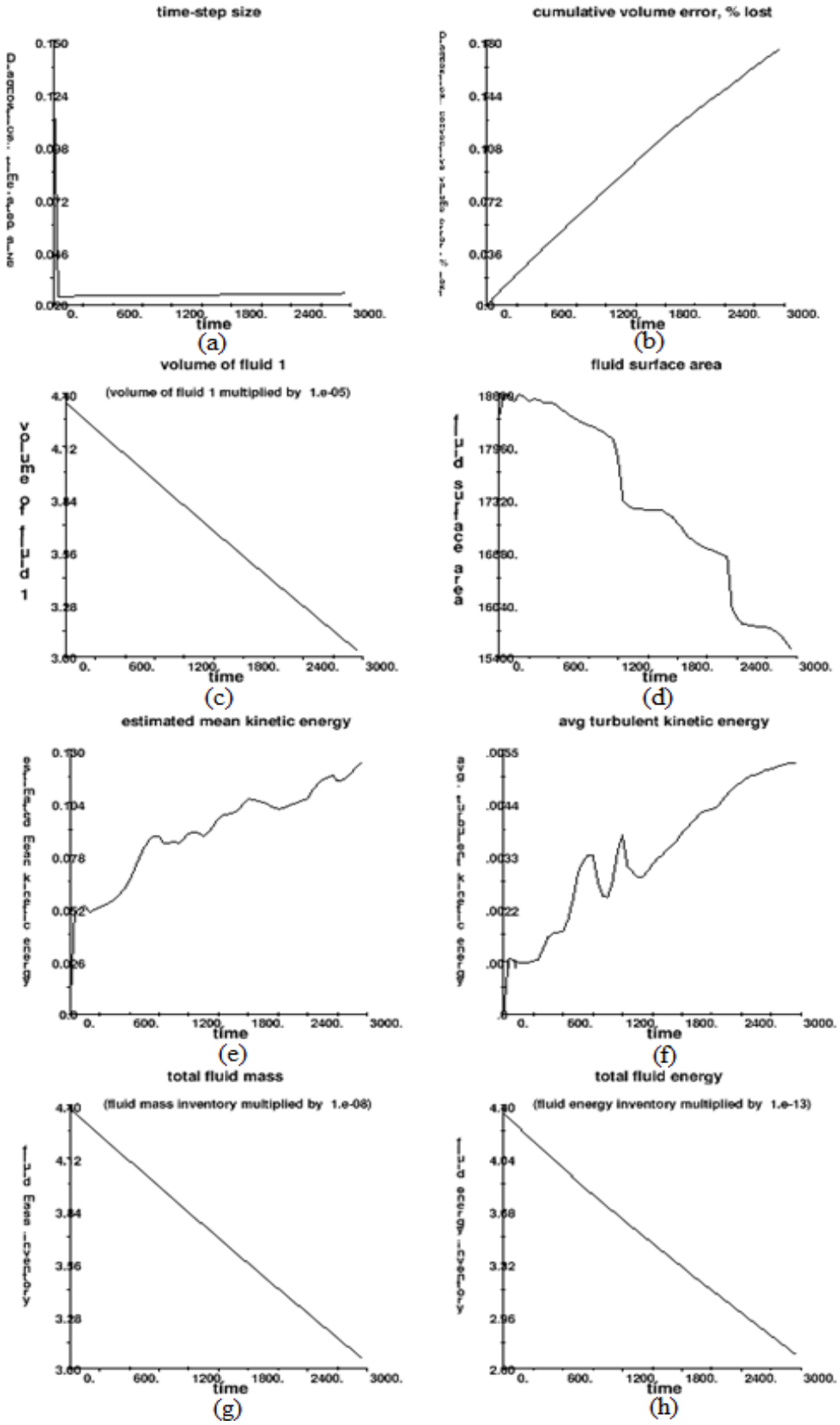

Figure A25: Simulation B1: a) time-step size, b) cumulative volume error (%), c) volume of fluid, d) fluid surface area, e) estimated mean kinetic energy, f) average turbulent kinetic energy, g) total fluid mass, h) total fluid energy.

B2

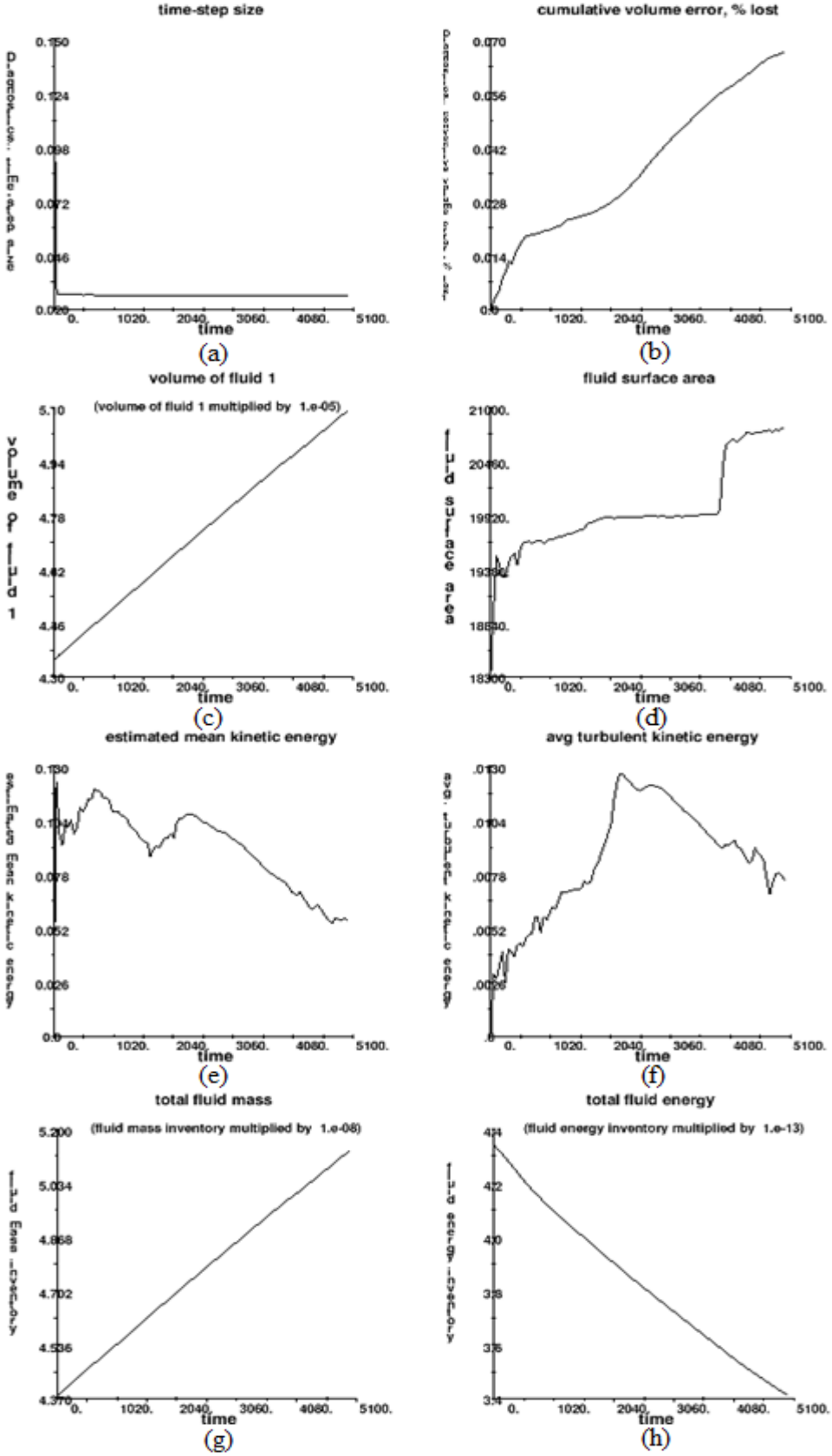

Figure A26: Simulation B2: a) time-step size, b) cumulative volume error (%), c) volume of fluid, d) fluid surface area, e) estimated mean kinetic energy, f) average turbulent kinetic energy, g) total fluid mass, h) total fluid energy.

B3

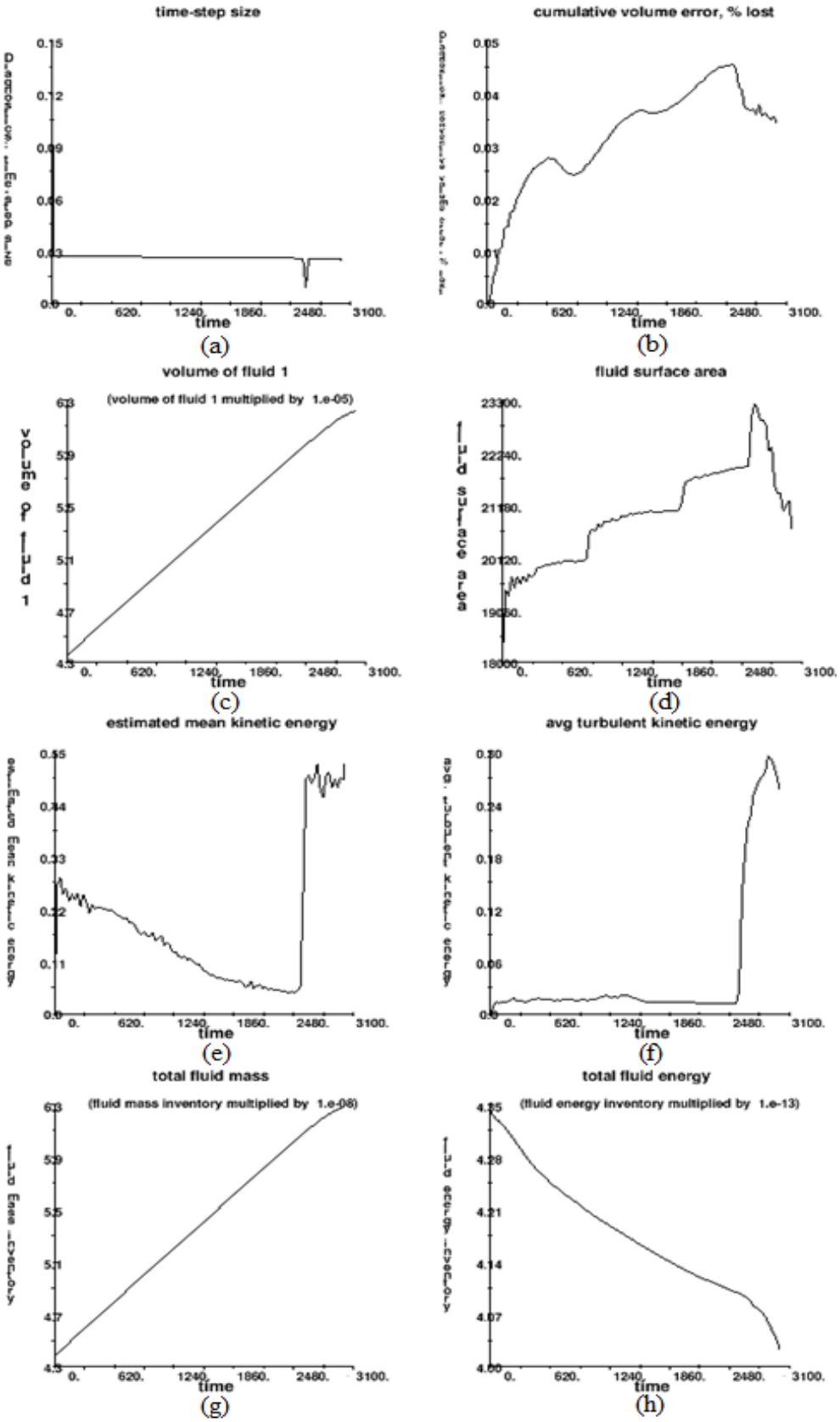

Figure A27: Simulation B3: a) time-step size, b) cumulative volume error (%), c) volume of fluid, d) fluid surface area, e) estimated mean kinetic energy, f) average turbulent kinetic energy, g) total fluid mass, h) total fluid energy.

B4

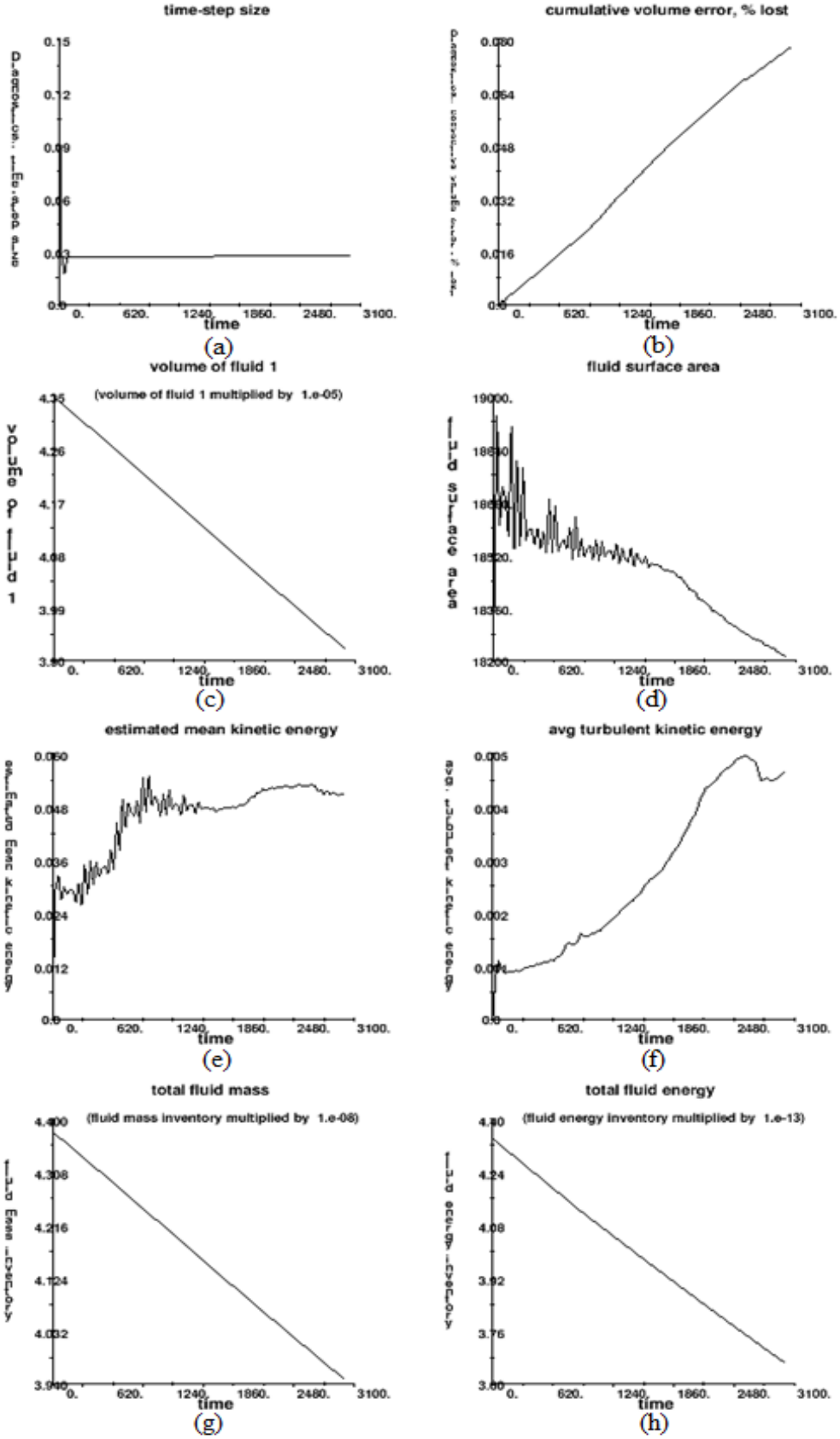

Figure A28: Simulation B4: a) time-step size, b) cumulative volume error (%), c) volume of fluid, d) fluid surface area, e) estimated mean kinetic energy, f) average turbulent kinetic energy, g) total fluid mass, h) total fluid energy.

B5

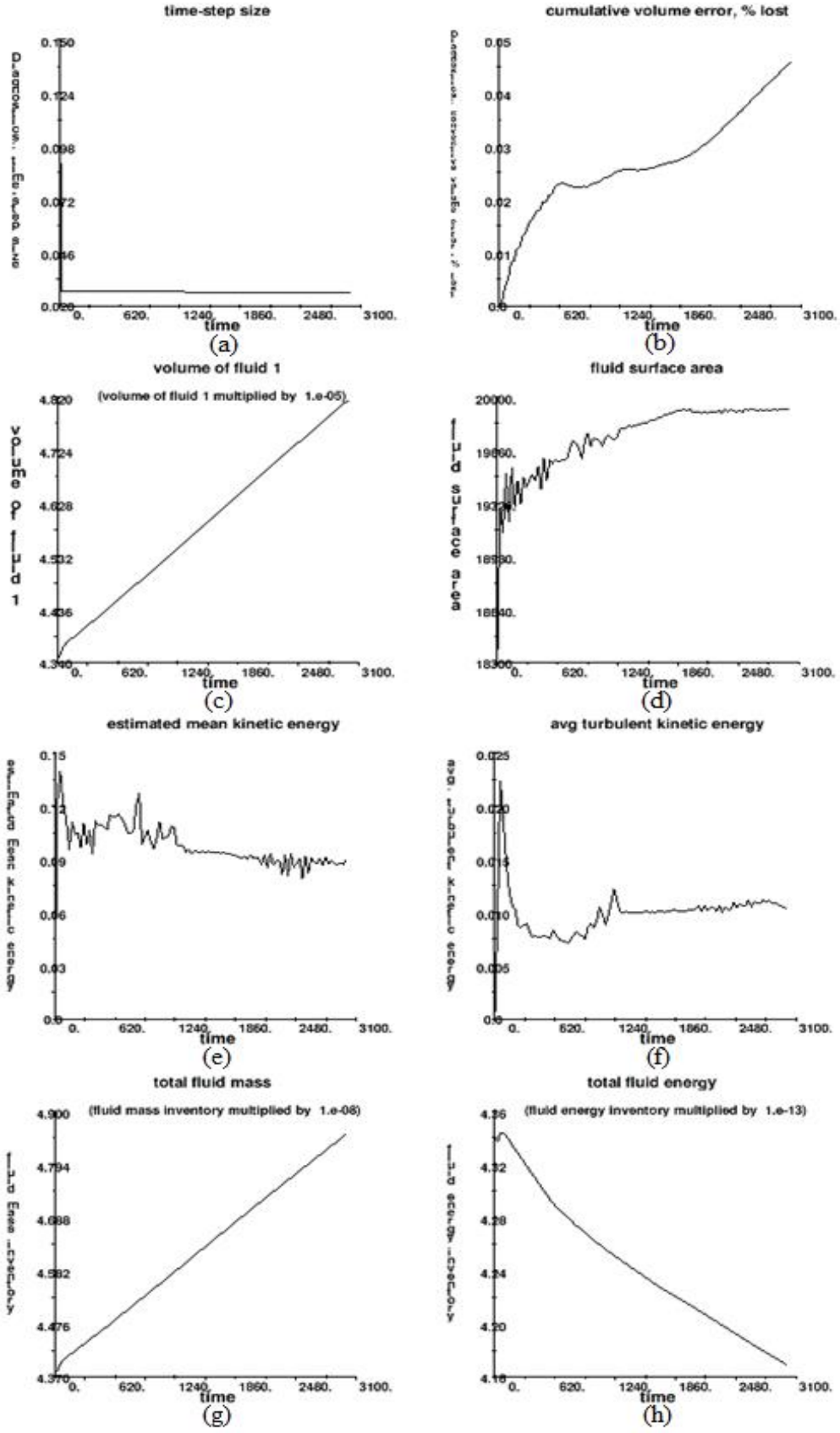

Figure A29: Simulation B5: a) time-step size, b) cumulative volume error (%), c) volume of fluid, d) fluid surface area, e) estimated mean kinetic energy, f) average turbulent kinetic energy, g) total fluid mass, h) total fluid energy.

B6

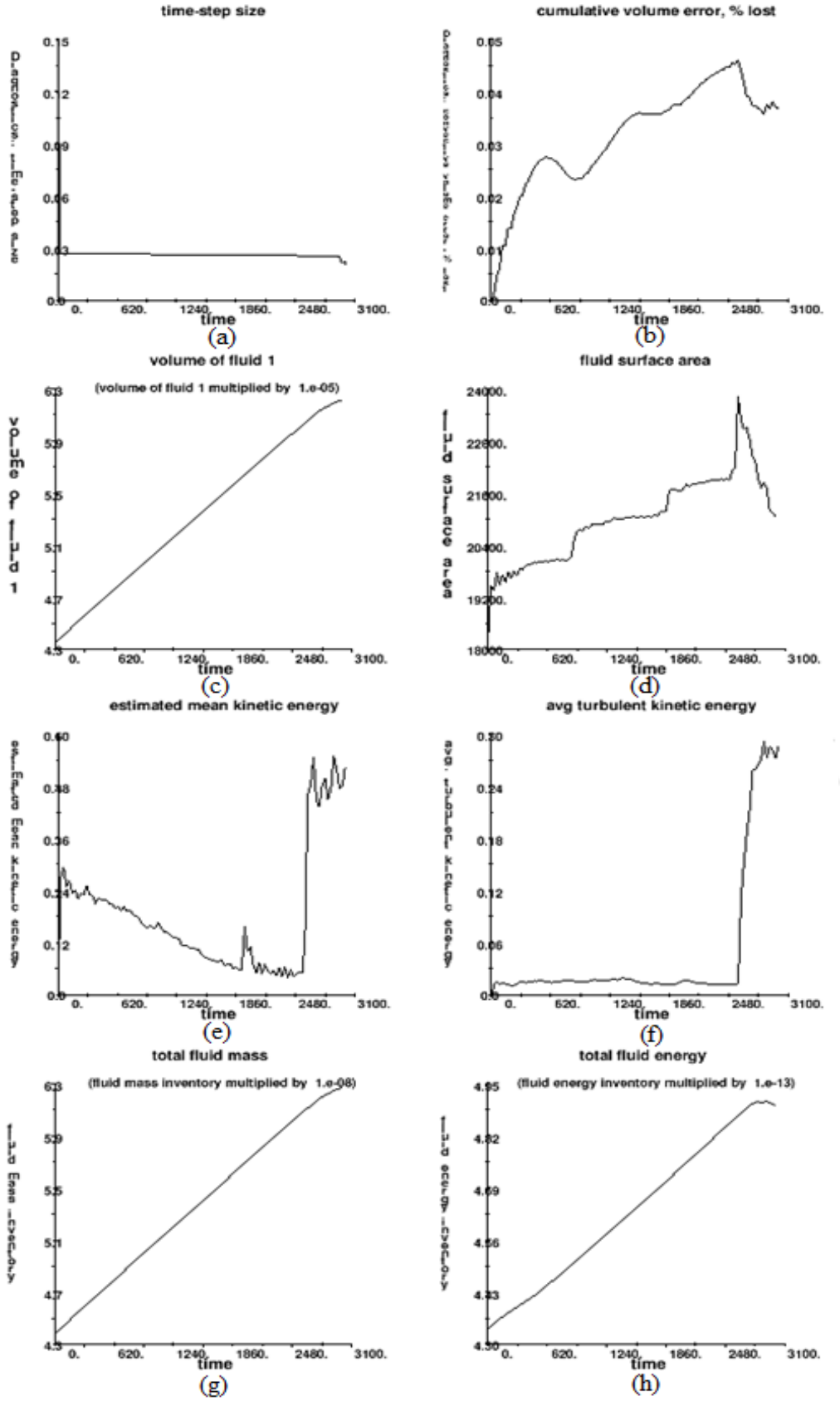

Figure A30: Simulation B6: a) time-step size, b) cumulative volume error (%), c) volume of fluid, d) fluid surface area, e) estimated mean kinetic energy, f) average turbulent kinetic energy, g) total fluid mass, h) total fluid energy.

B7

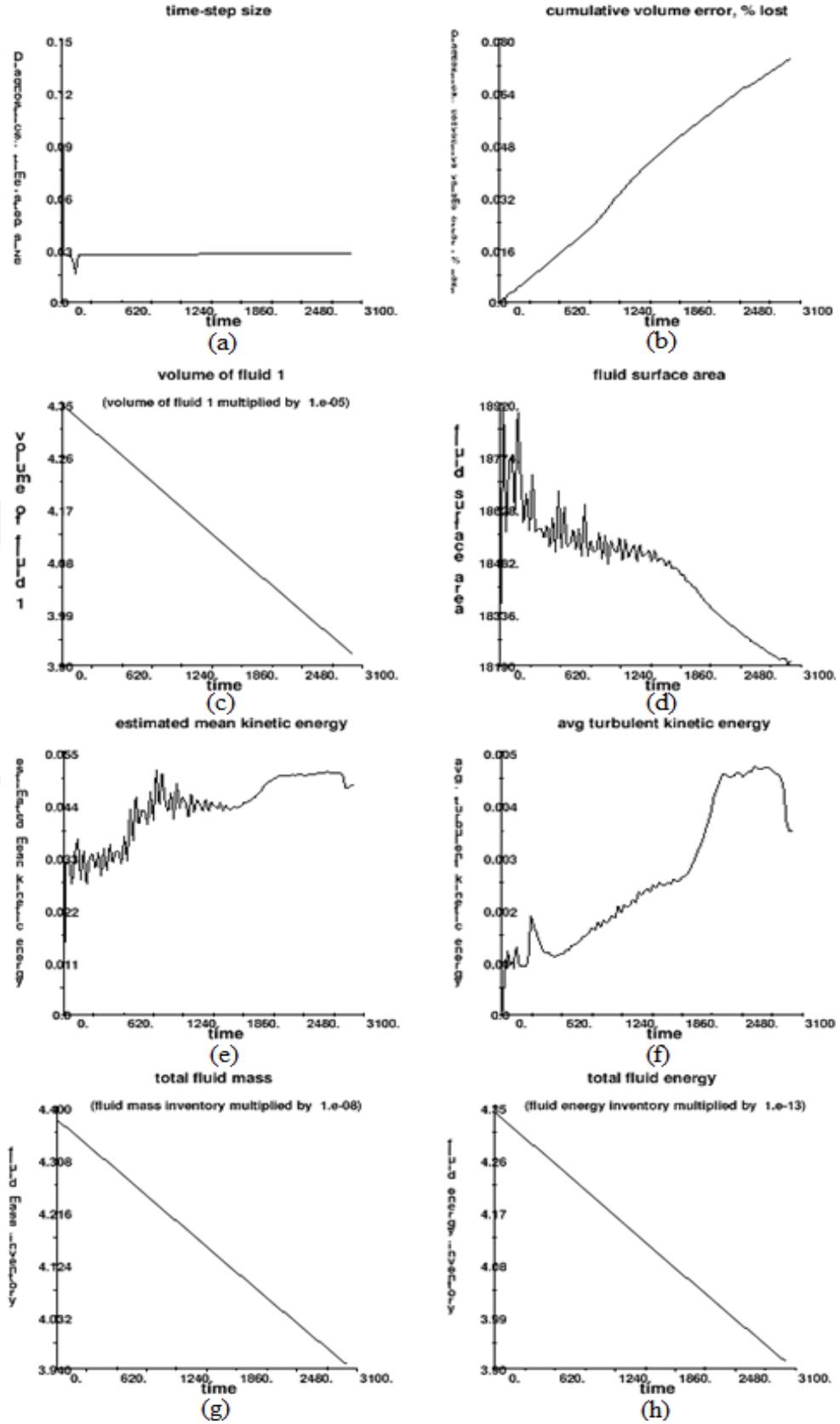

Figure A31: Simulation B7: a) time-step size, b) cumulative volume error (%), c) volume of fluid, d) fluid surface area, e) estimated mean kinetic energy, f) average turbulent kinetic energy, g) total fluid mass, h) total fluid energy.

B8

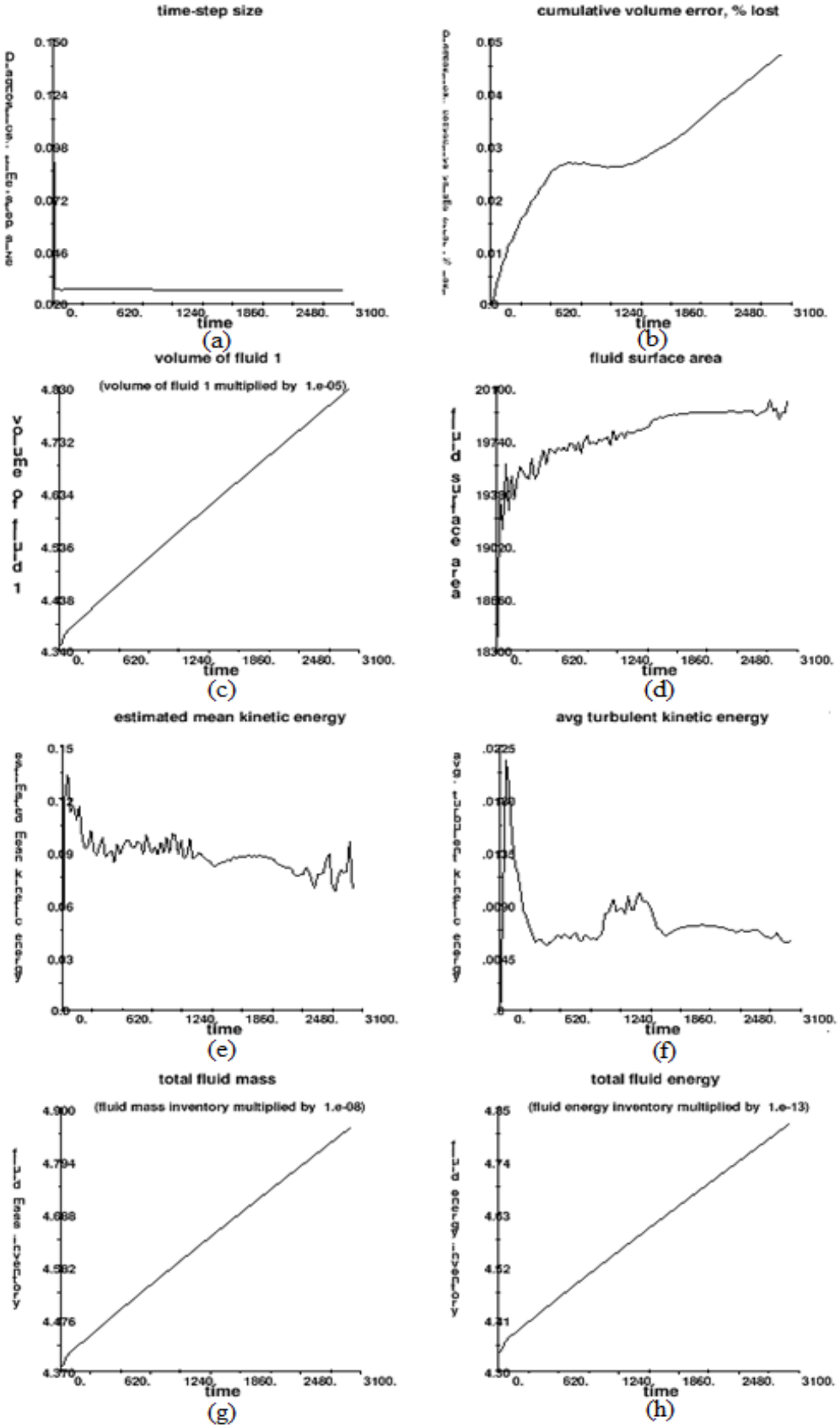

Figure A32: Simulation B8: a) time-step size, b) cumulative volume error (%), c) volume of fluid, d) fluid surface area, e) estimated mean kinetic energy, f) average turbulent kinetic energy, g) total fluid mass, h) total fluid energy.

B9

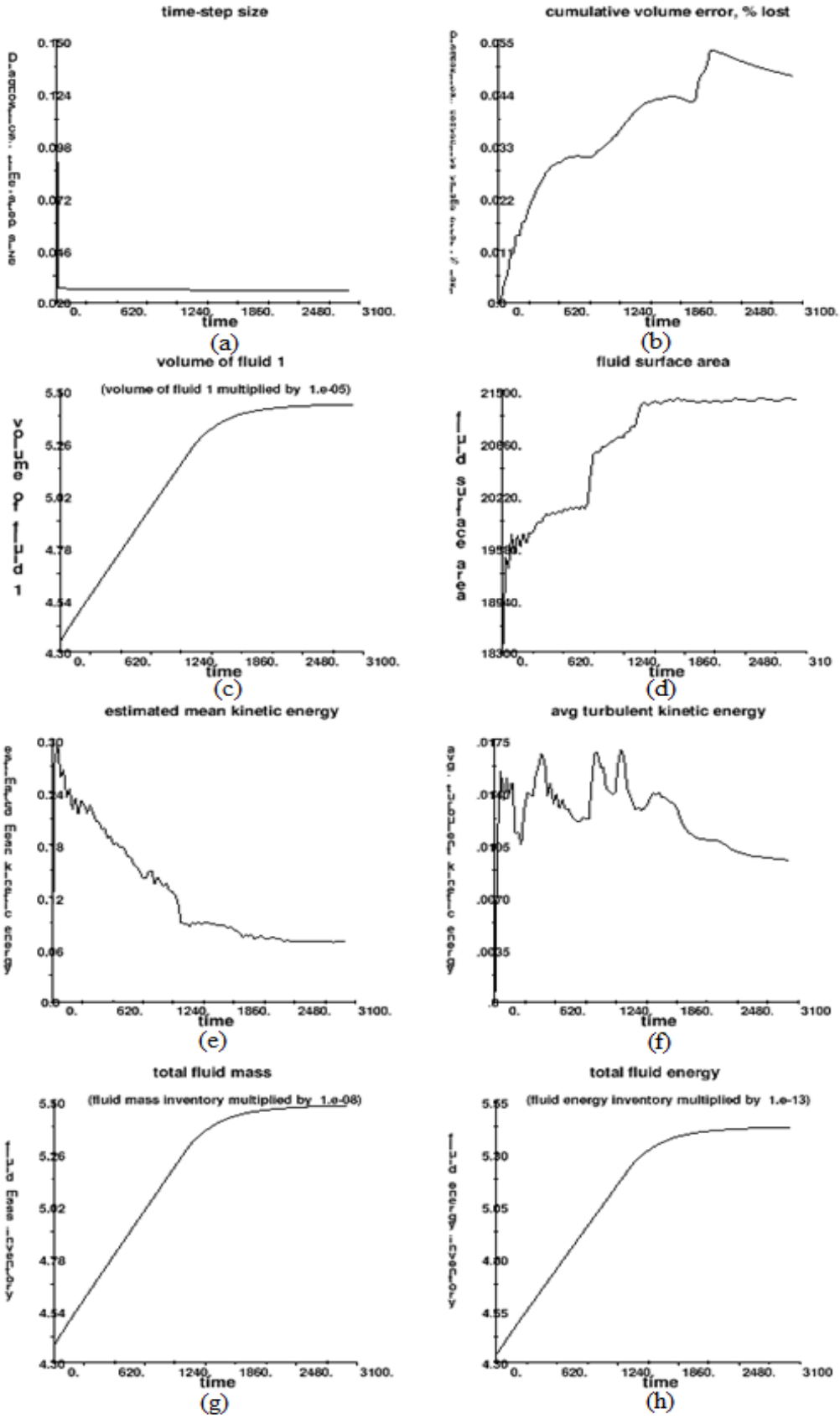

Figure A33: Simulation B9: a) time-step size, b) cumulative volume error (%), c) volume of fluid, d) fluid surface area, e) estimated mean kinetic energy, f) average turbulent kinetic energy, g) total fluid mass, h) total fluid energy.

B10

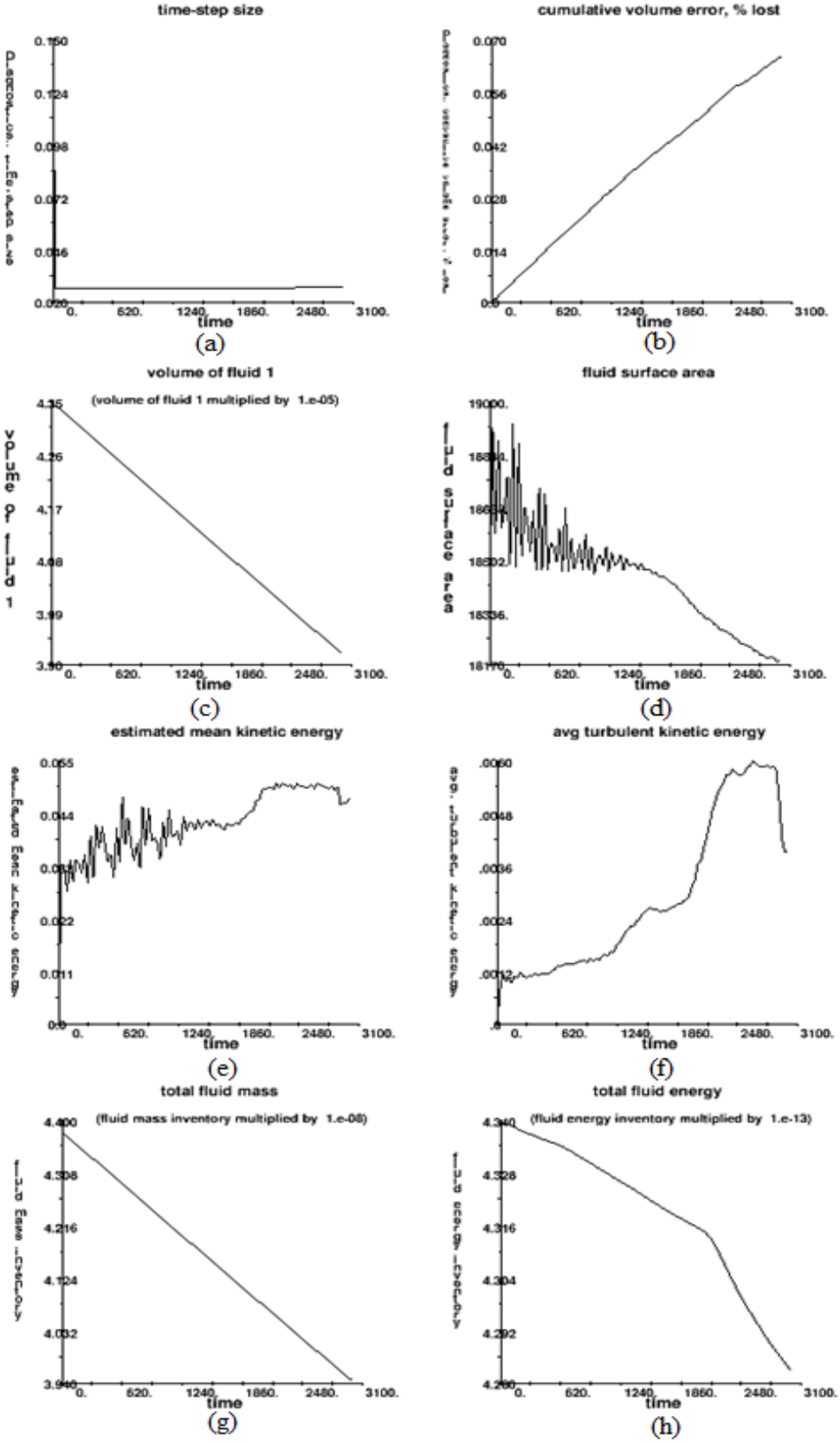

Figure A34: Simulation B10: a) time-step size, b) cumulative volume error (%), c) volume of fluid, d) fluid surface area, e) estimated mean kinetic energy, f) average turbulent kinetic energy, g) total fluid mass, h) total fluid energy.

B11

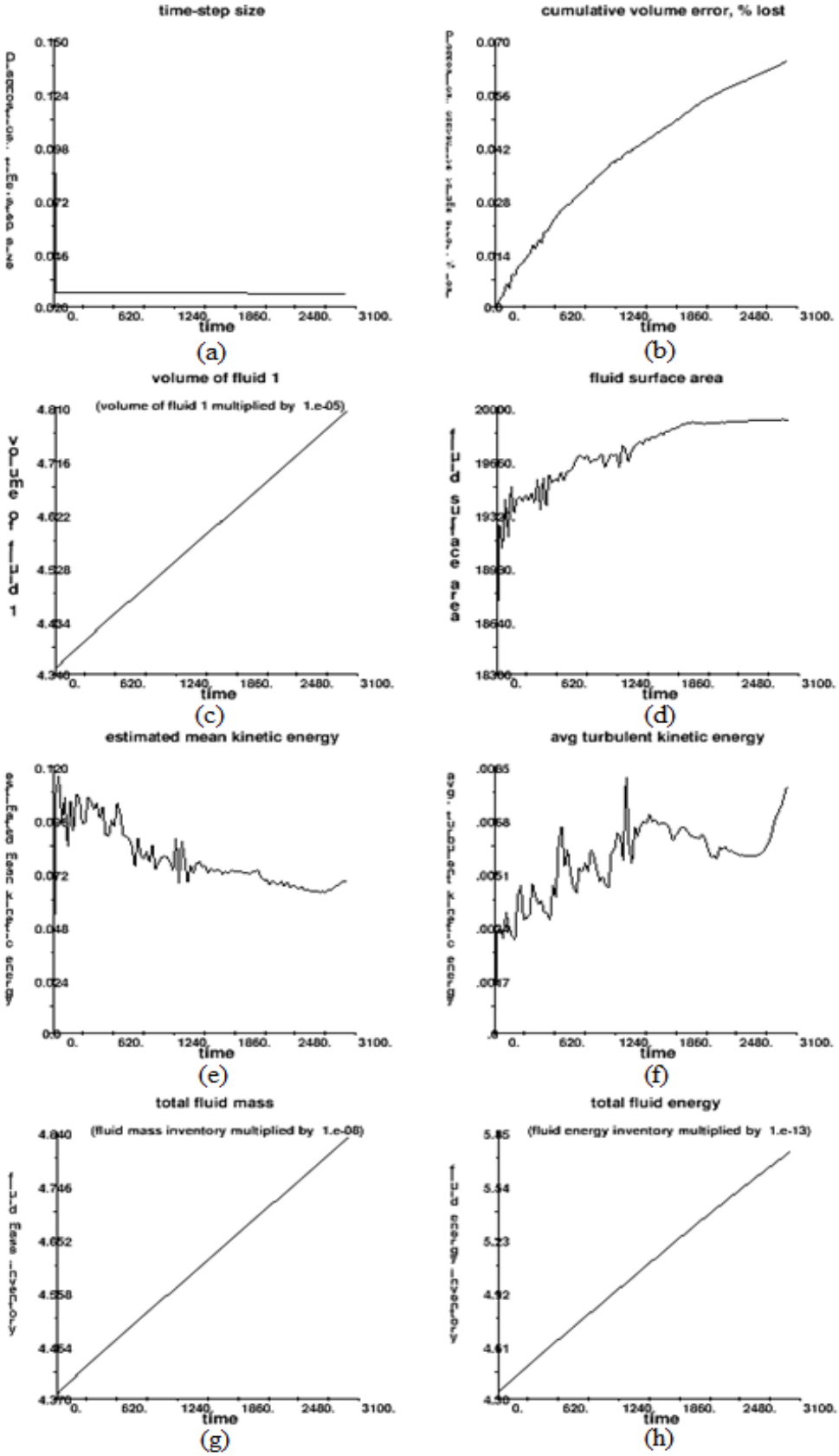

Figure A35: Simulation B11: a) time-step size, b) cumulative volume error (%), c) volume of fluid, d) fluid surface area, e) estimated mean kinetic energy, f) average turbulent kinetic energy, g) total fluid mass, h) total fluid energy.

B12

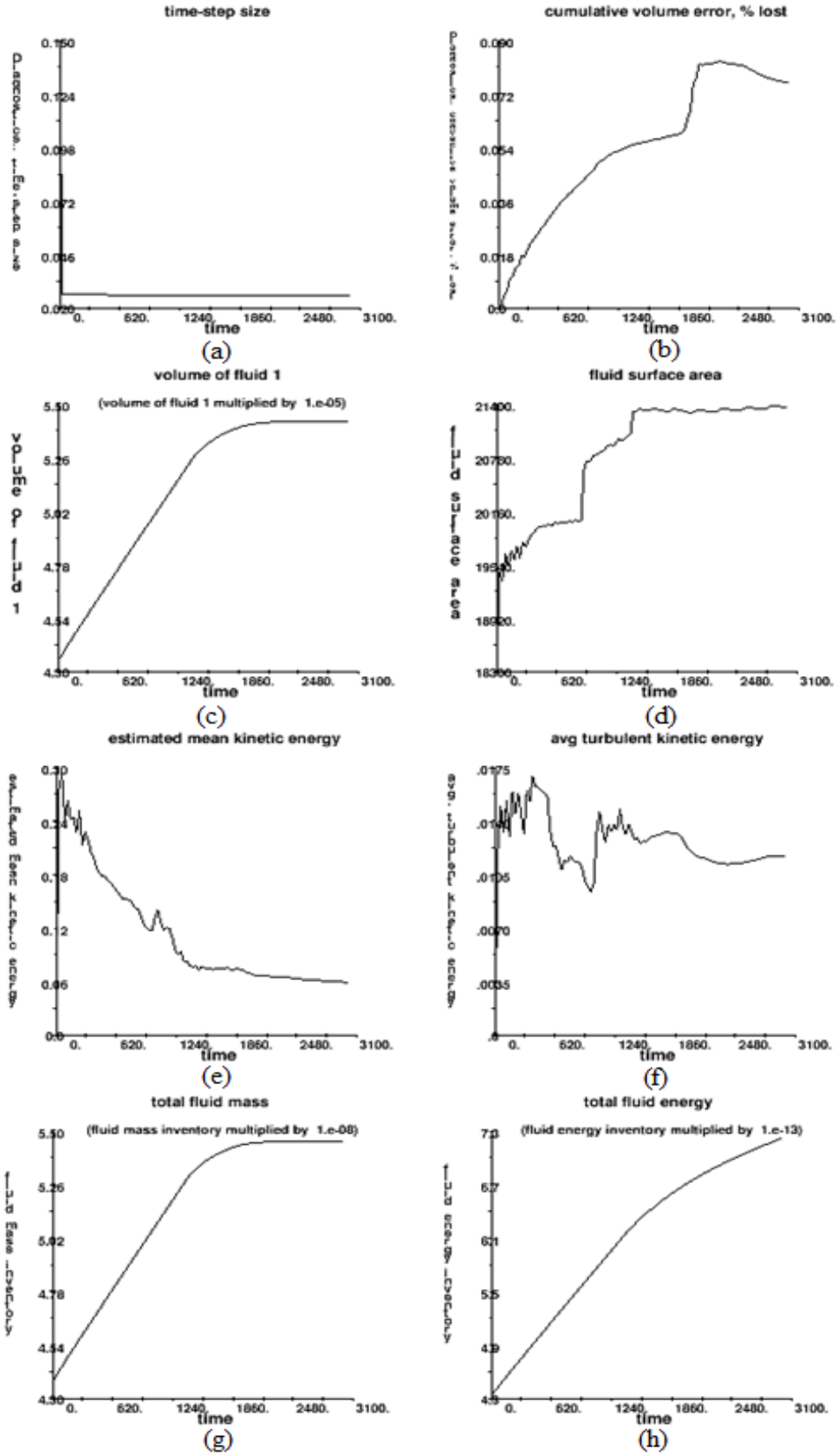

Figure A36: Simulation B12: a) time-step size, b) cumulative volume error (%), c) volume of fluid, d) fluid surface area, e) estimated mean kinetic energy, f) average turbulent kinetic energy, g) total fluid mass, h) total fluid energy.

B13

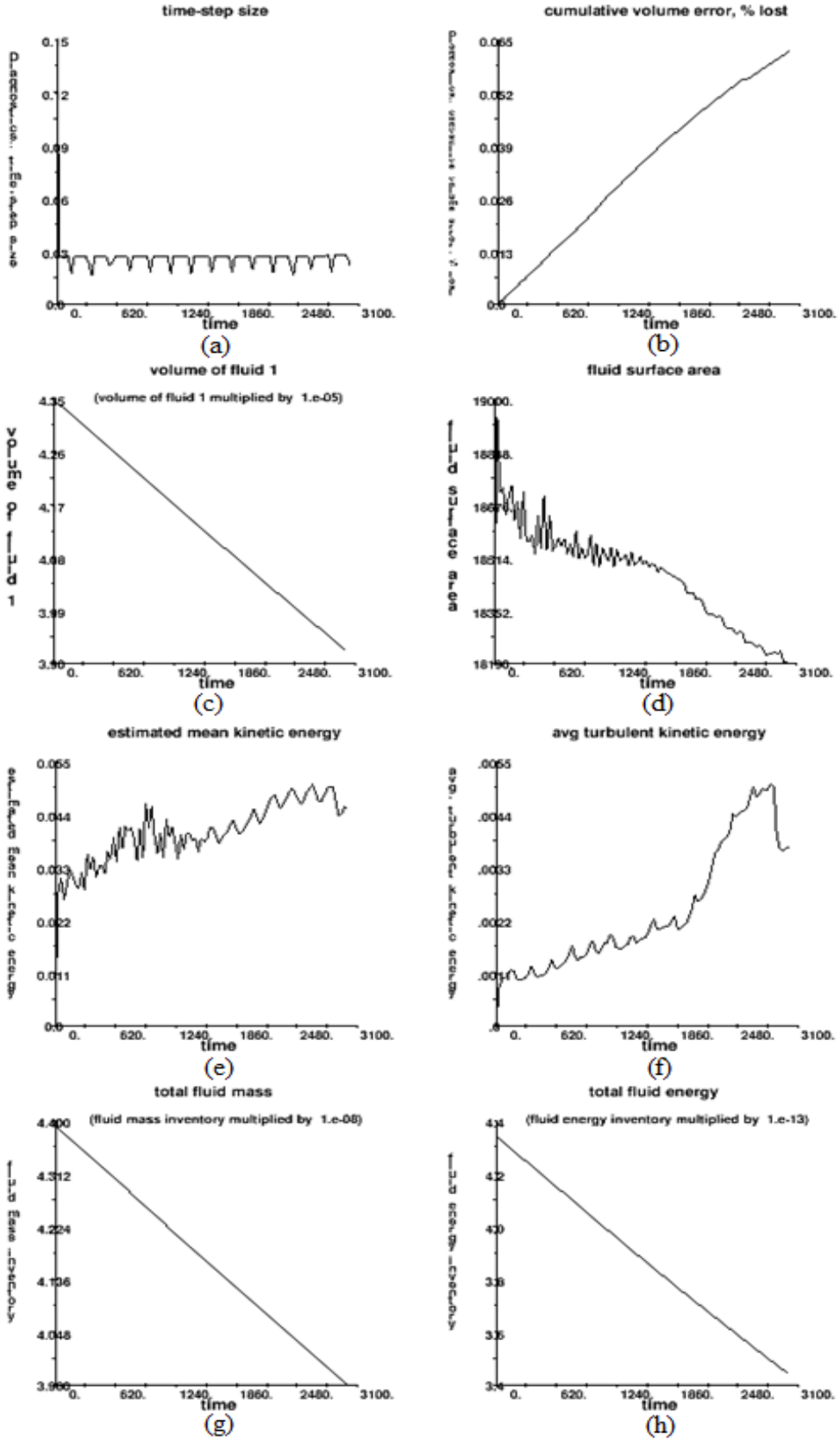

Figure A37: Simulation B13: a) time-step size, b) cumulative volume error (%), c) volume of fluid, d) fluid surface area, e) estimated mean kinetic energy, f) average turbulent kinetic energy, g) total fluid mass, h) total fluid energy.

B14

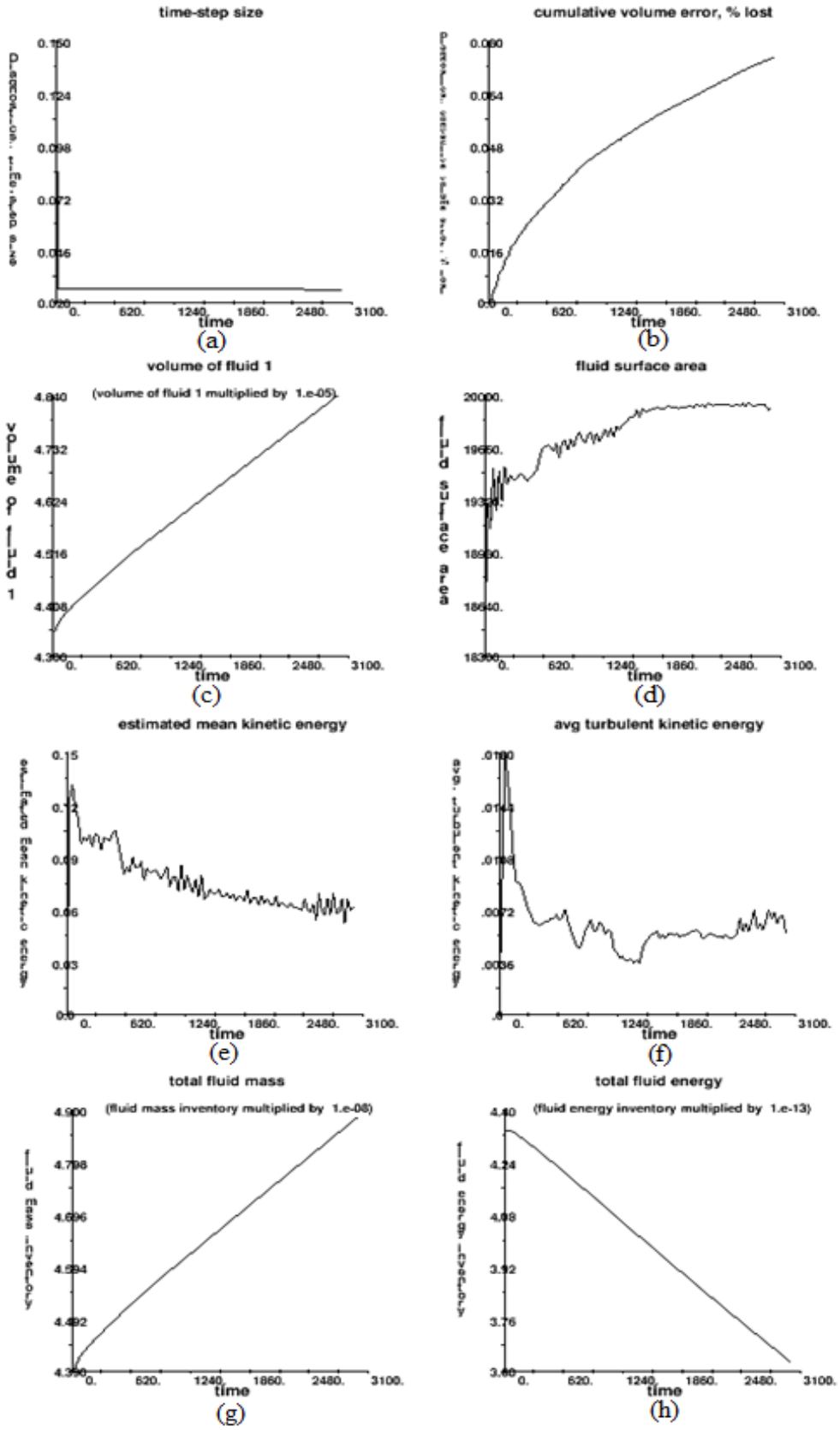

Figure A38: Simulation B14: a) time-step size, b) cumulative volume error (%), c) volume of fluid, d) fluid surface area, e) estimated mean kinetic energy, f) average turbulent kinetic energy, g) total fluid mass, h) total fluid energy.

B15

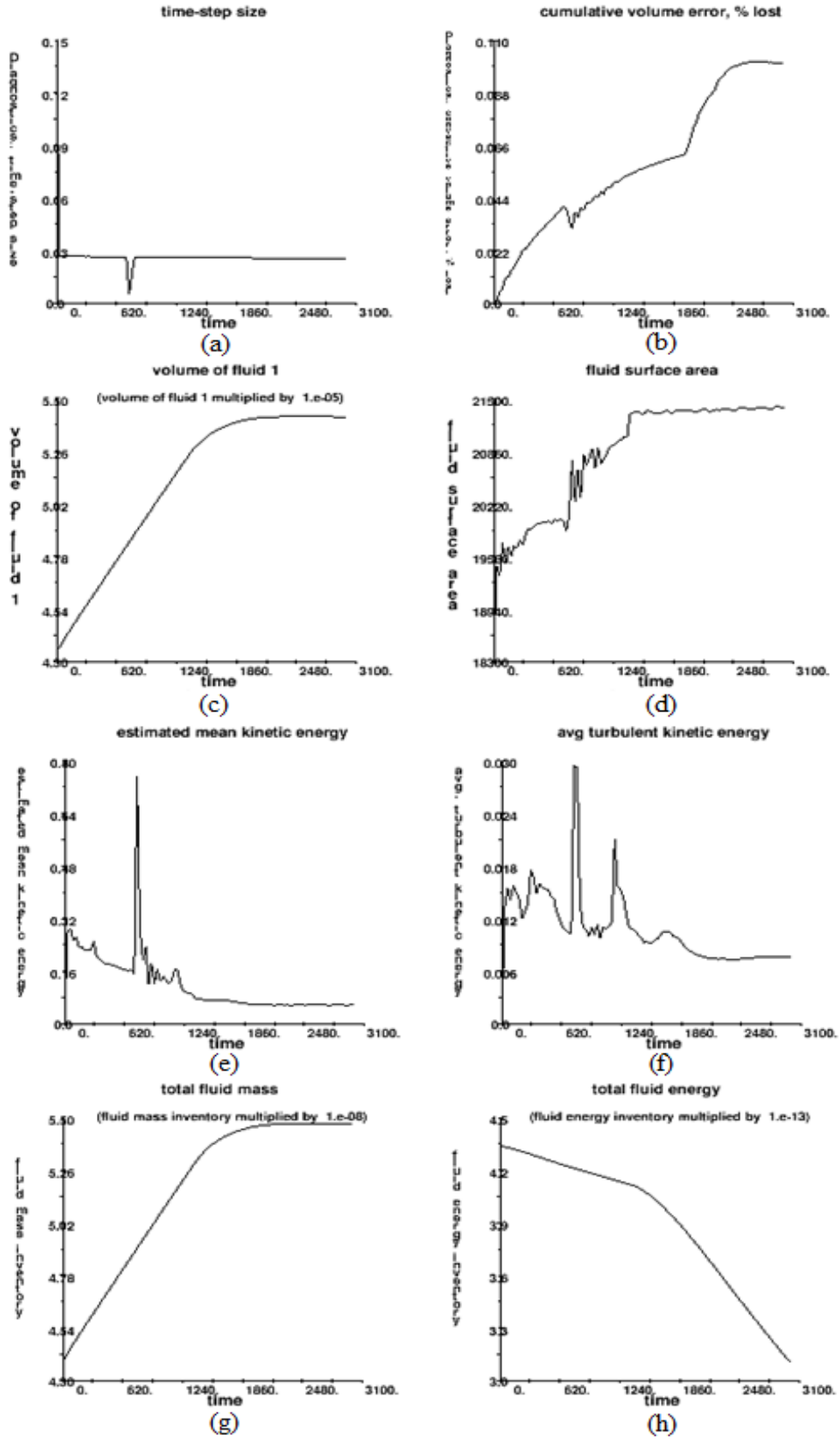

Figure A39: Simulation B15: a) time-step size, b) cumulative volume error (%), c) volume of fluid, d) fluid surface area, e) estimated mean kinetic energy, f) average turbulent kinetic energy, g) total fluid mass, h) total fluid energy.

B16

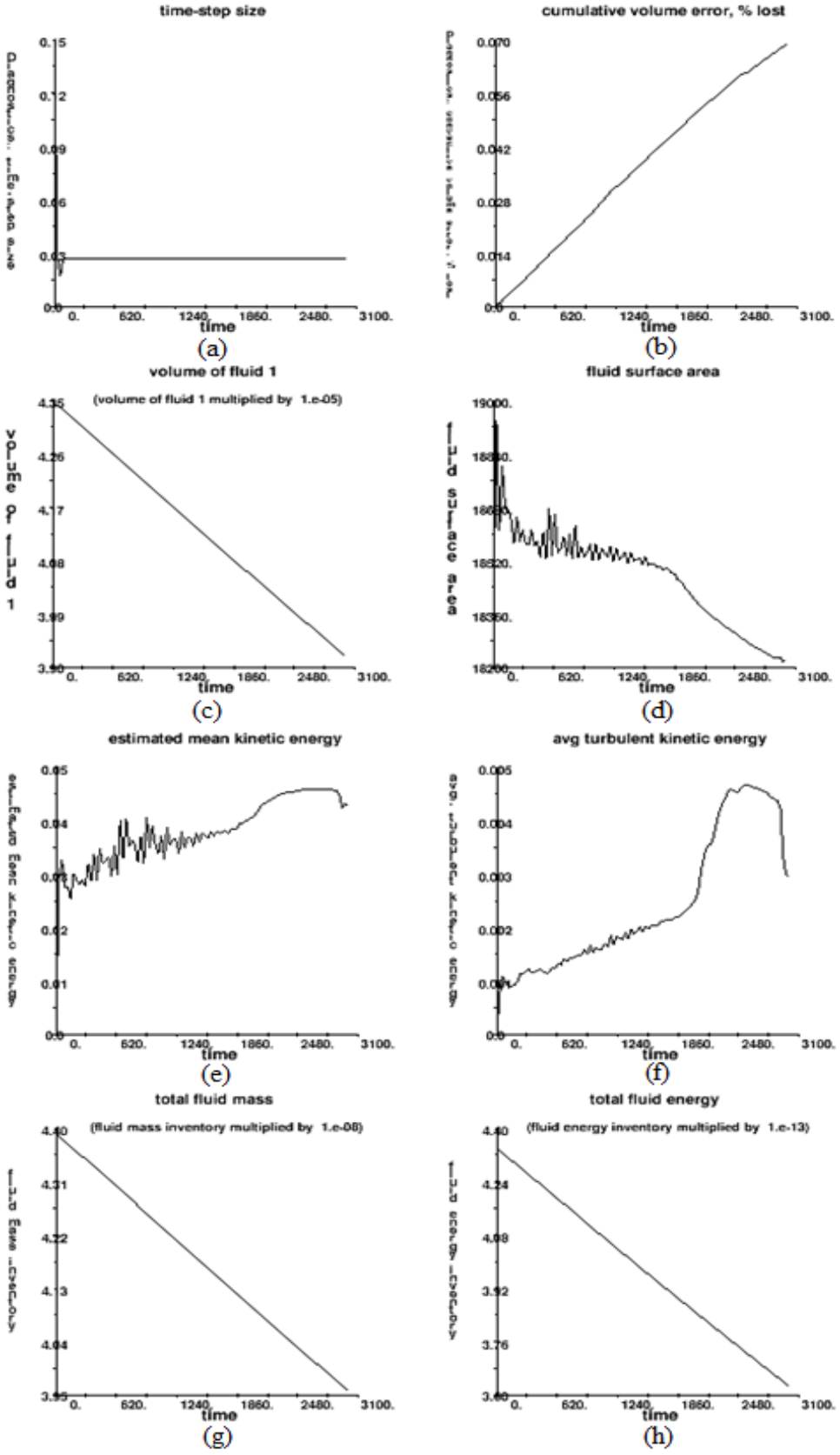

Figure A40: Simulation B16: a) time-step size, b) cumulative volume error (%), c) volume of fluid, d) fluid surface area, e) estimated mean kinetic energy, f) average turbulent kinetic energy, g) total fluid mass, h) total fluid energy.

B17

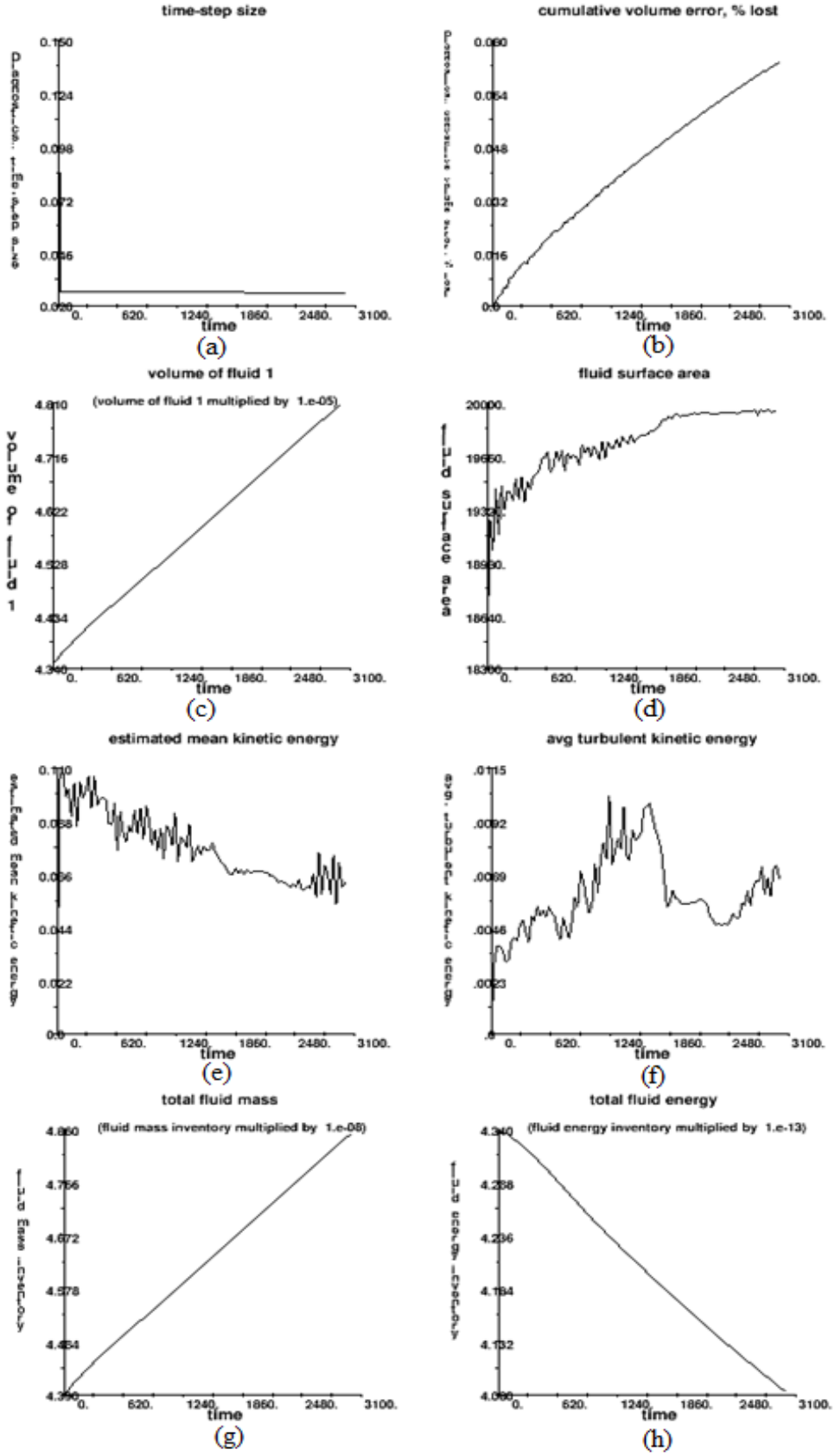

Figure A41: Simulation B17: a) time-step size, b) cumulative volume error (%), c) volume of fluid, d) fluid surface area, e) estimated mean kinetic energy, f) average turbulent kinetic energy, g) total fluid mass, h) total fluid energy.

B18

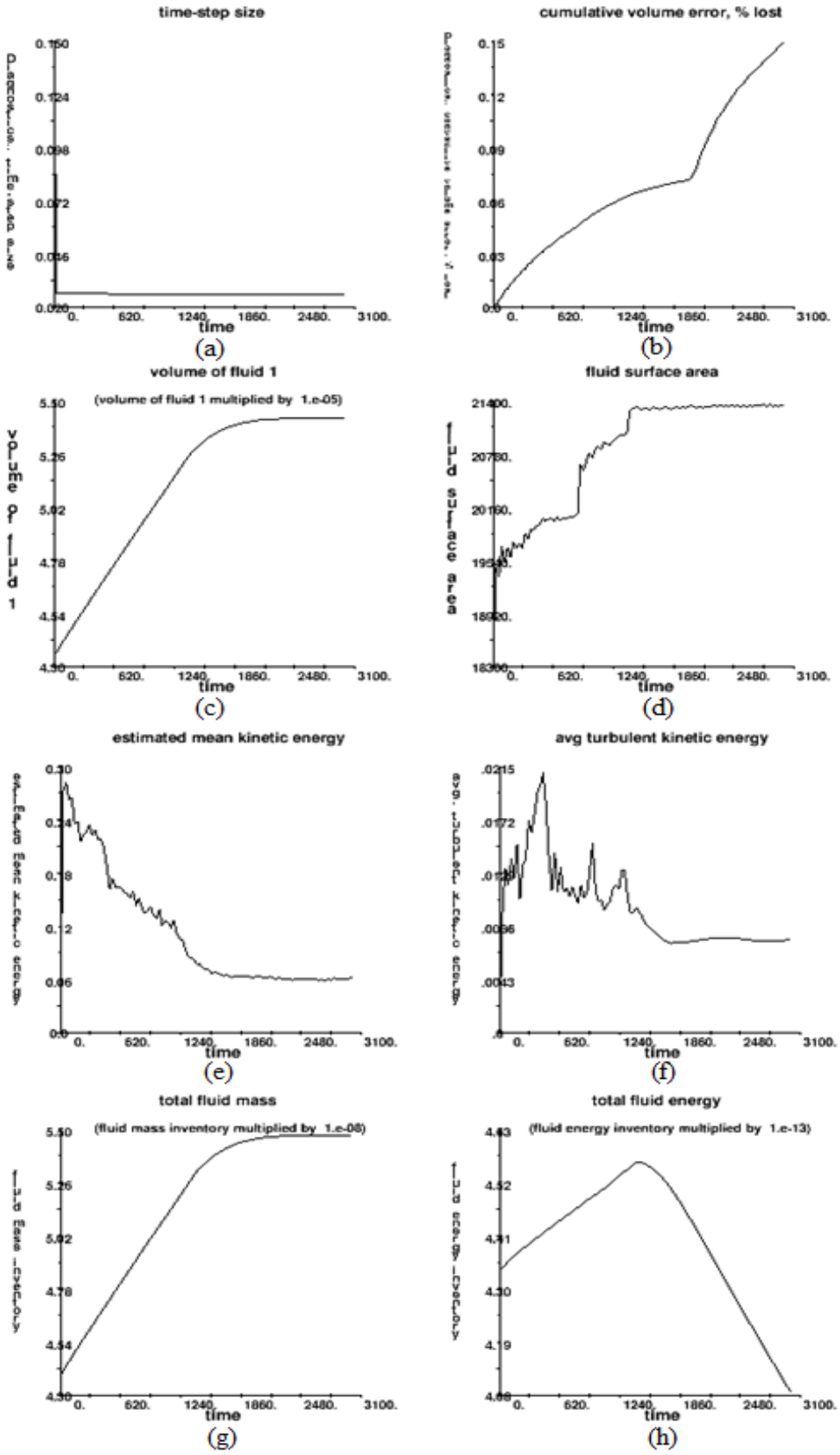

Figure A42: Simulation B18: a) time-step size, b) cumulative volume error (%), c) volume of fluid, d) fluid surface area, e) estimated mean kinetic energy, f) average turbulent kinetic energy, g) total fluid mass, h) total fluid energy.

B19

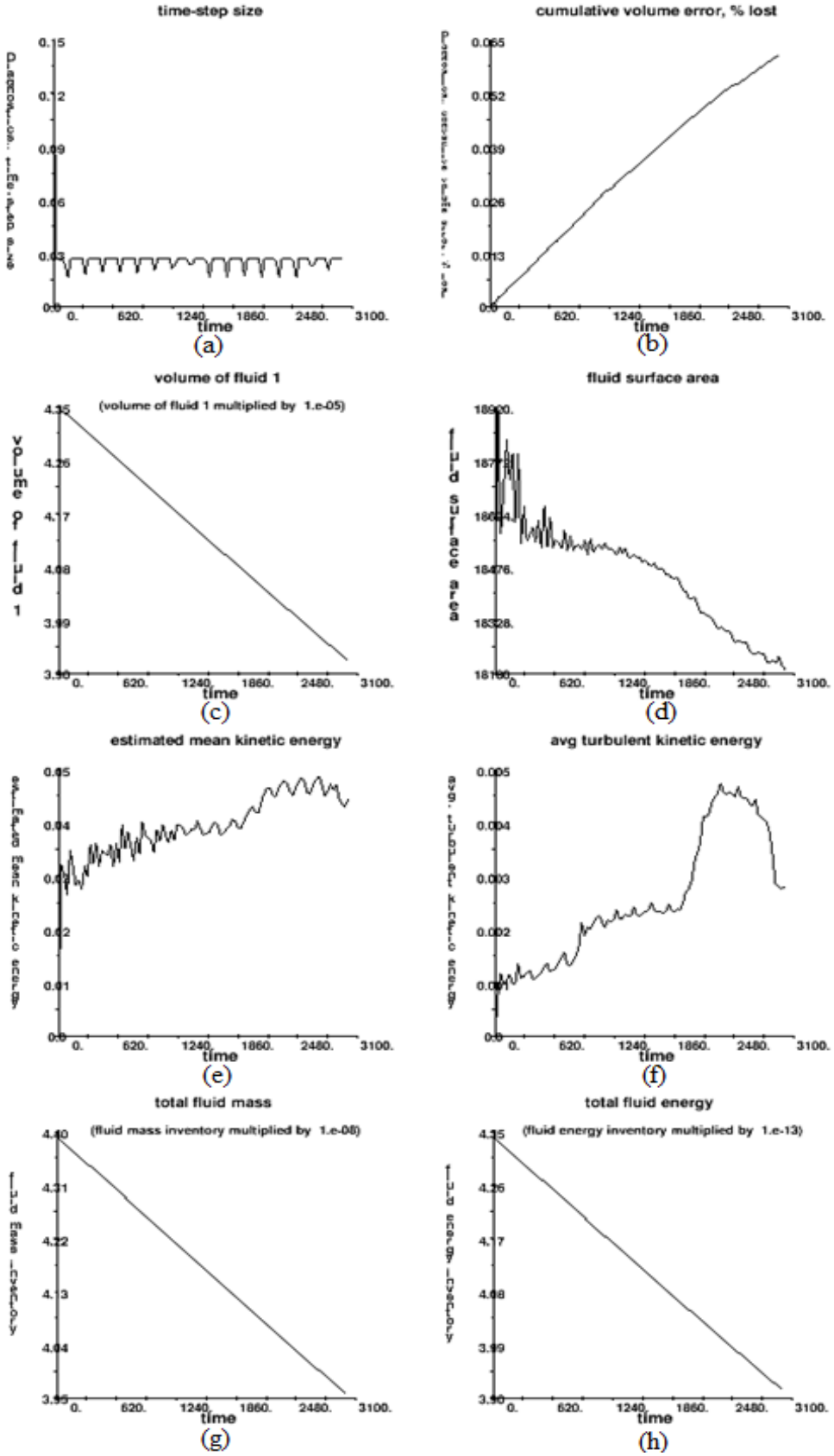

Figure A43: Simulation B19: a) time-step size, b) cumulative volume error (%), c) volume of fluid, d) fluid surface area, e) estimated mean kinetic energy, f) average turbulent kinetic energy, g) total fluid mass, h) total fluid energy.

B20

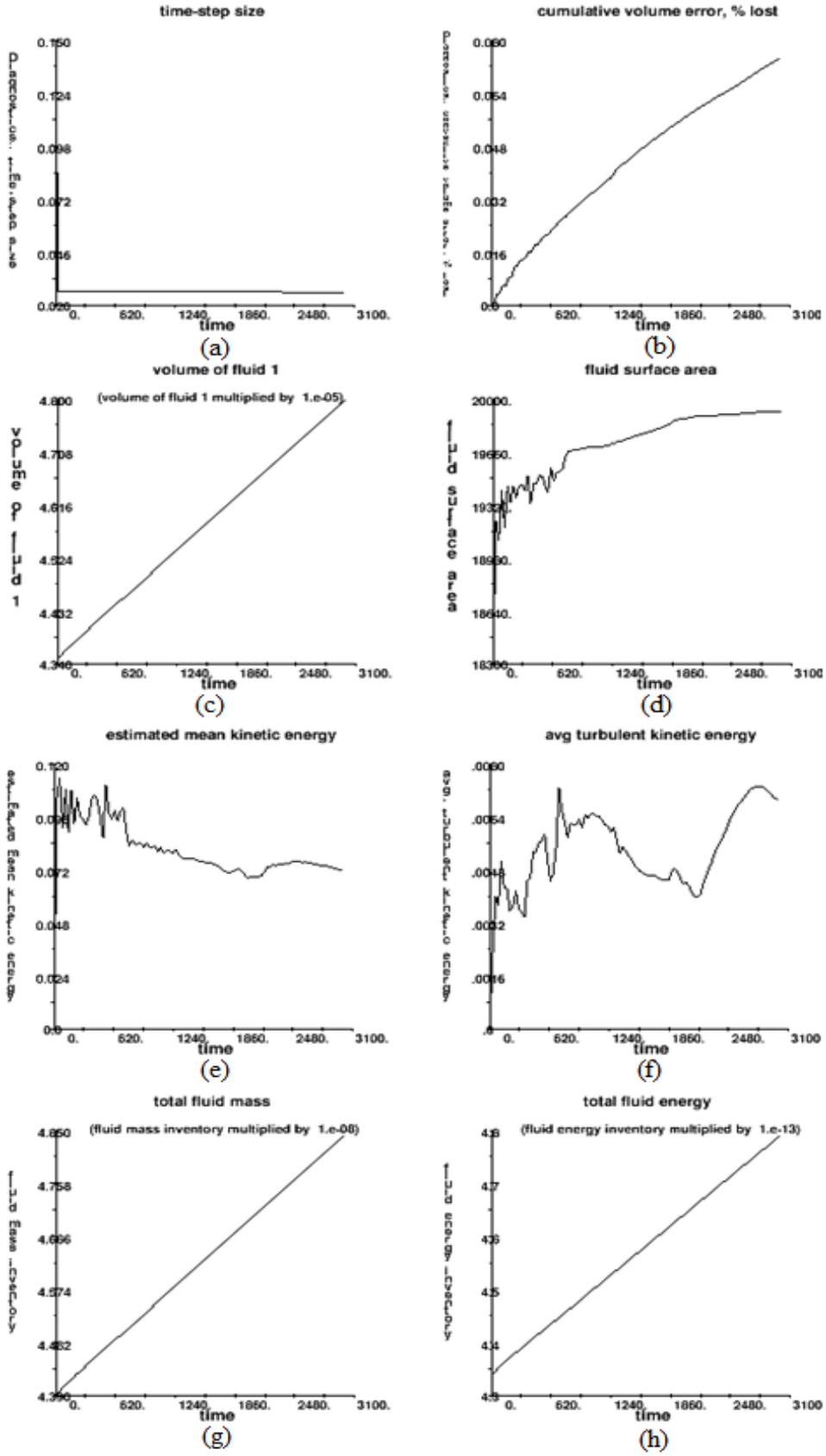

Figure A44: Simulation B20: a) time-step size, b) cumulative volume error (%), c) volume of fluid, d) fluid surface area, e) estimated mean kinetic energy, f) average turbulent kinetic energy, g) total fluid mass, h) total fluid energy.

B21

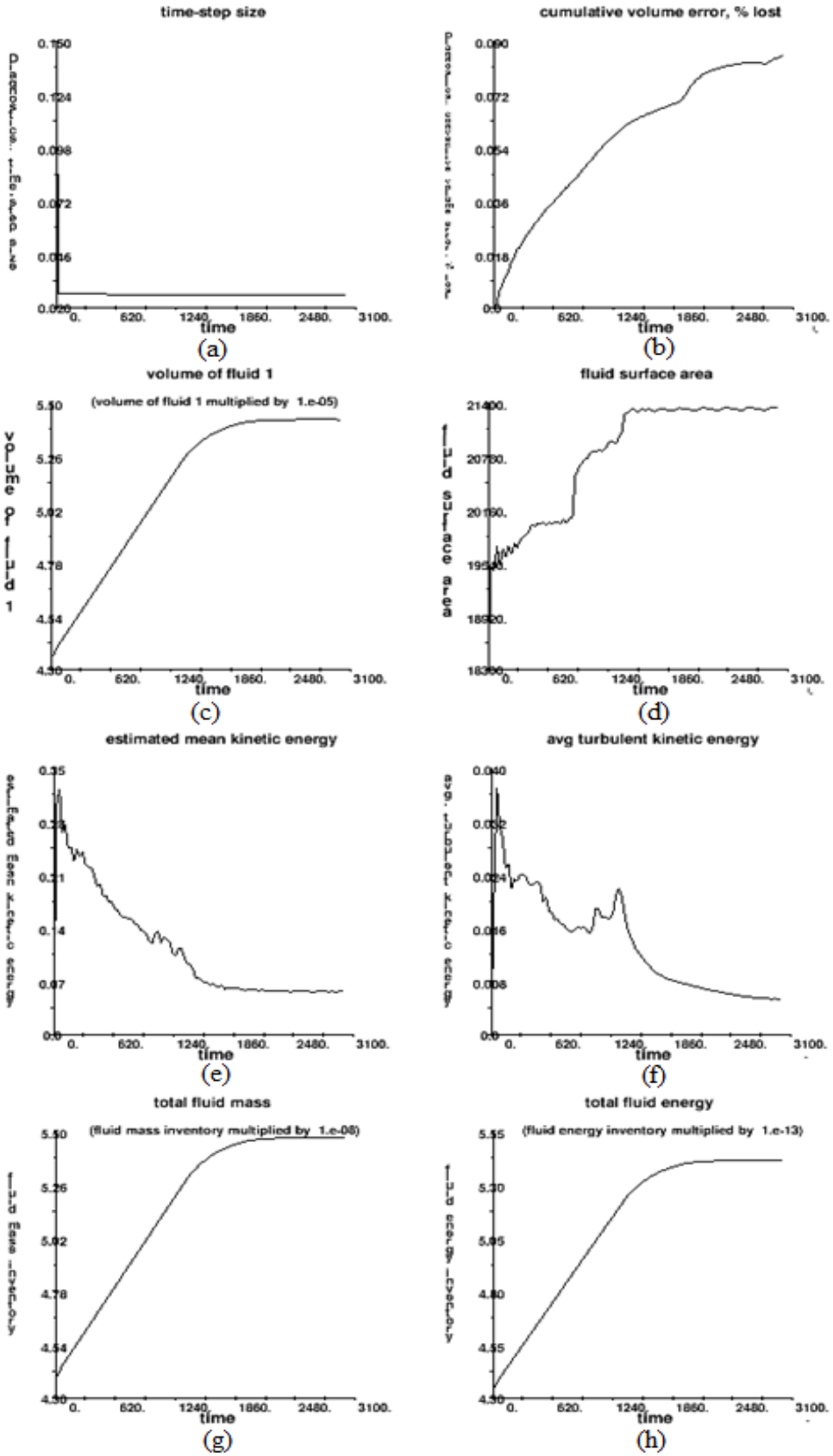

Figure A45: Simulation B21: a) time-step size, b) cumulative volume error (%), c) volume of fluid, d) fluid surface area, e) estimated mean kinetic energy, f) average turbulent kinetic energy, g) total fluid mass, h) total fluid energy.

B22

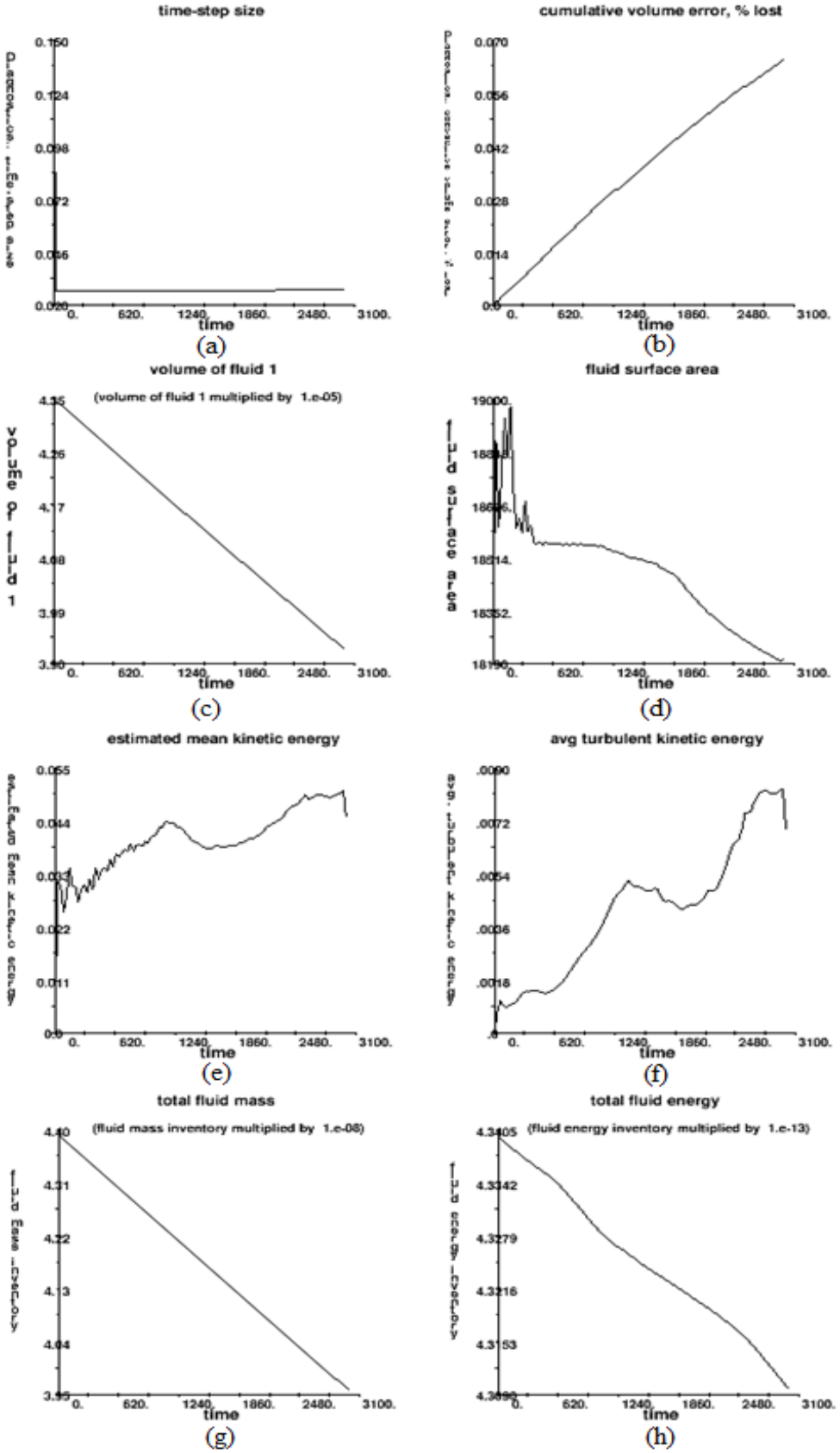

Figure A46: Simulation B22: a) time-step size, b) cumulative volume error (%), c) volume of fluid, d) fluid surface area, e) estimated mean kinetic energy, f) average turbulent kinetic energy, g) total fluid mass, h) total fluid energy.

B23

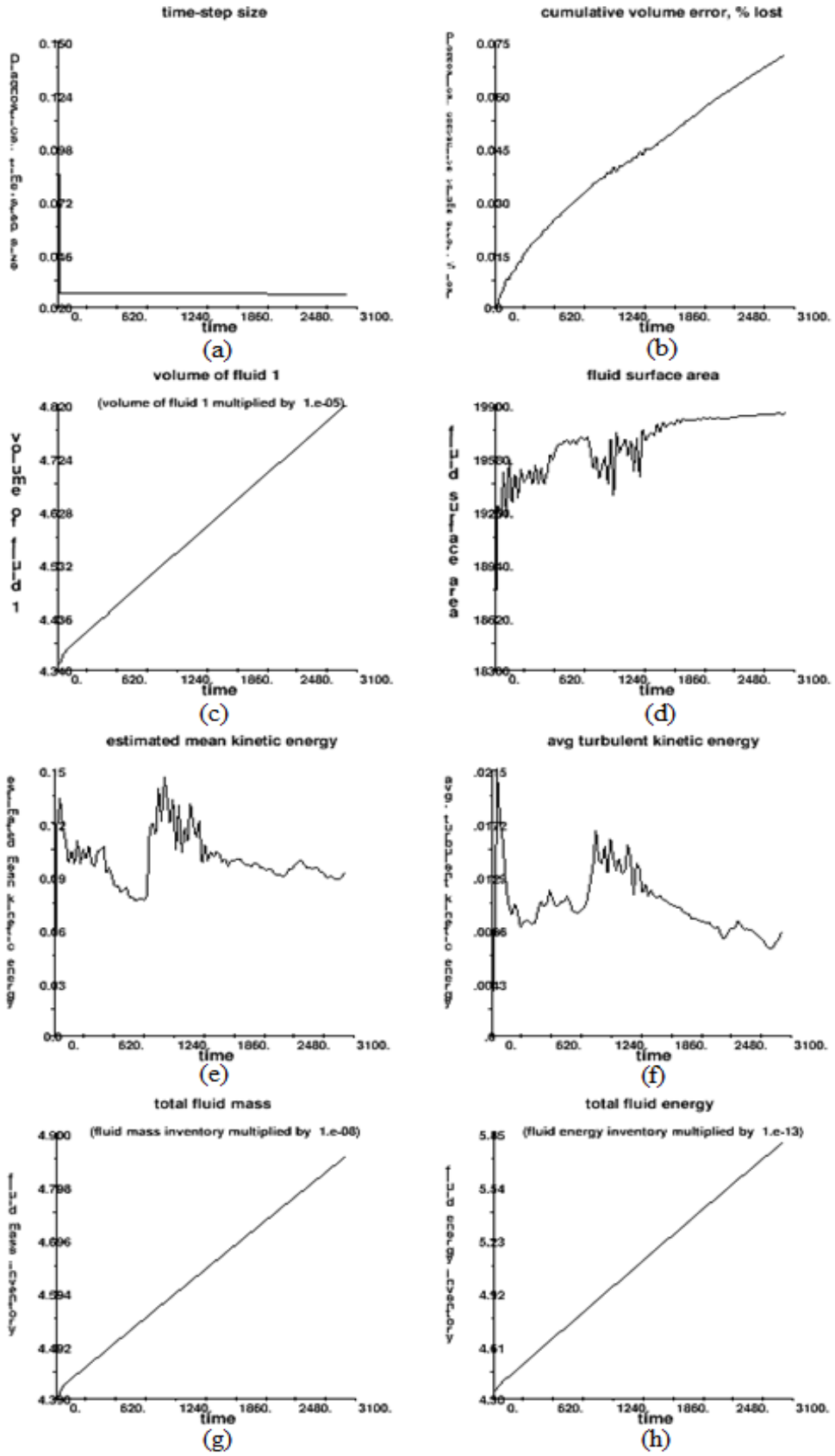

Figure A47: Simulation B23: a) time-step size, b) cumulative volume error (%), c) volume of fluid, d) fluid surface area, e) estimated mean kinetic energy, f) average turbulent kinetic energy, g) total fluid mass, h) total fluid energy.

B24

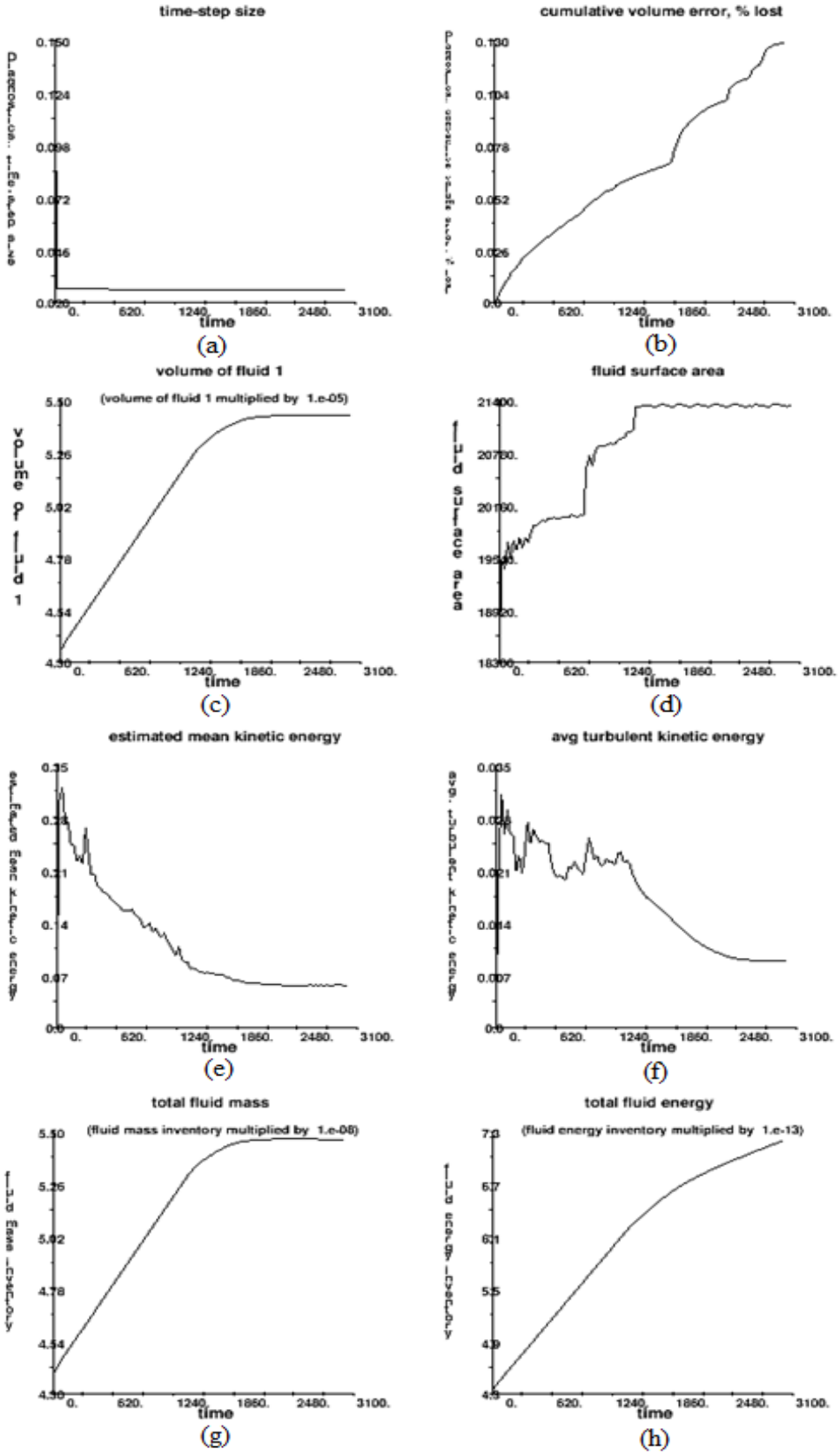

Figure A48: Simulation B24: a) Time-step size, b) cumulative volume error (%), c) volume of fluid, d) fluid surface area, e) estimated mean kinetic energy, f) average turbulent kinetic energy, g) total fluid mass, h) total fluid energy.

APPENDIX B: Wentworth Grain Size Chart from United States Geological Survey.

Figure B1: Wentworth grain size chart from united states geological survey.